

Isocyanide-Based Multicomponent Reactions and Polymerizations to Achieve Molecular and Supramolecular Chirality

Doctoral Thesis

Jinxiu Zhou

Donostia/San Sebastián

eman ta zabal zazu



Universidad
del País Vasco

Euskal Herriko
Unibertsitatea

ACRONYMS AND ABBREVIATIONS

μL	Microliter
Å	Angstrom
Abs	Absorbance
AFM	Atomic Force Microscopy
AO	Atomic Orbital
Asy Ugi-4CR	Asymmetric Ugi four component reaction
Bn	Benzyl
BTC	Bis(trichloromethyl)carbonate, also named triphosgene
C	Concentration
°C	Degree Celsius
ca.	Circa, means about
cat.	Catalyst
CD	Circular Dichroism
CDA	Chiral Dicarboxylic Acids
CE	Capillary Electromigration
CHL	Chloroform, also written as CHCl_3
CIP	Cahn-Ingold-Prelog priority rules
COSY	Correlation Spectroscopy
CPA	Chiral Phosphoric Acid
CPL	Circularly Polarized Light
CSP	Chiral Stationary Phase
d	Doublet (NMR)
D-	Dexter
DCM	Dichloromethane
dd	Double doublet (NMR)
de.	Diastereoisomeric excess
deg	Degree, °
DFT	Density Functional Theory
DIBAL	Diisobutylaluminium hydride
DIPAMP	1,2-Bis((R)-(2-methoxyphenyl)(phenyl)phosphino)ethane

ABBREVIATIONS AND ACRONYMS

DLS	Dynamic Light Scattering
DMF	<i>N, N</i> -dimethyl formamide
DMSO	Dimethyl sulfoxide
DNA	Deoxyribonucleic acid
DOSY	Diffusion-Ordered Spectroscopy
dr.	Diastereoisomeric ratio
E	Electric field
ECD	Electronic Circular Dichroism
ee	Enantiomeric excess
Et ₃ N	Triethylamine
EPC	Enantiomerically Pure Compounds
eq.	Equivalent
EtOAc	Ethyl acetate
EtOH	Ethanol
FC	Flash Column
FMO	Fragment Molecular Orbital Method
FTIR	Fourier Transform Infrared Spectroscopy
g	Gram
GC	Gas Chromatography
GPC	Gel Permeation Chromatography
h	Hour
HMBC	Heteronuclear Multiple Bond Correlation
HPLC	High-Performance Liquid Chromatography
HRMS	High-Resolution Mass Spectrometry
HSQC	Heteronuclear Single Quantum Coherence
ⁱ BU	Iso-Butyl
ⁱ Pr	Iso-Propyl
IR	Infrared
IUPAC	International Union of Pure and Applied Chemistry
J	Coupling constant
kDa	Polymer molecular weight unit, 1 kDa=1000 g/mol
L-	Laevus
L*	Chiral ligand

LC	Liquid Chromatography
LCPL	Left-handed Circular Polarized Light
m	Multiplet (NMR)
MCRs	Multicomponent Reactions
mdeg	Millidegree
Me	Methyl
MeCN	Acetonitrile
MeOH	Methanol
mg	Milligram
min	Minute
mL	Milliliter
MM-MC	Molecular Mechanical Monte Carlo calculation
mmol	Millimol
Mn	Number average molecular weight
MO	Molecular Orbital
mPEG	Methoxypolyethylene glycol
MS	Mass Spectrometry
MS (4Å)	Molecular Sieves
Mw	Weight average molecular weight
N/A	Not available
NC	Isocyanide
N _D	<i>endo-D</i>
N _L	<i>endo-L</i>
NMP	<i>N</i> -methyl-2-pyrrolidone
NMR	Nuclear Magnetic Resonance
OPLS	Optimized Potentials for Liquid Simulations
OR	Optical Rotation
ORD	Optical Rotatory Dispersion
ORTEP	Oak Ridge Thermal-Ellipsoid Plot Program
PCM	Polarizable Continuous Model
PDI	Polydispersity Index
PFP	Pentafluorophenyl
Ph	Phenyl

ABBREVIATIONS AND ACRONYMS

PMMA	Polymethylmethacrylate
PPM	Post Polymerization Modification
ppm	Unit of chemical shift in NMR, δ
QTOF	Quadrupole-Time Of Flight
R	Arbitrary substituent
RCPL	Right-Handed Circular Polarized Light
Rh	Hydrodynamic radius
RNA	Ribonucleic Acid
ROA	Vibrational Raman Optical Activity
rt	Room temperature
s	Singlet (NMR)
S	Strong (FTIR)
SFC	Supercritical Fluid Chromatography
SNR	Signal-to-Noise Ratio
t	Triplet (NMR)
T	Temperature
TA	Tartaric acid
^t Bu	Tert Butyl
TEA	Triethylamine
TFA	Trifluoroacetic acid
THF	Tetrahydrofuran
TLC	Thin Layer Chromatography
Ugi-4CR	Ugi 4 Component Reaction
UV-VIS	Ultraviolet-Visible
VCD	Vibrational Circular Dichroism
wt%	Percentage by weight
X _D	<i>exo</i> -D
X _L	<i>exo</i> -L

This thesis dissertation has been carried out in the Department of Organic Chemistry I of the Chemistry Faculty at the University of the Basque Country, in Donostia-San Sebastián, under the supervision of Dr Iván Rivilla de la Cruz and Prof. Fernando P. Cossío Mora, and tutored by Dr. Haritz Sardon.

Financial support has been provided by the China Scholar Council “National Construction High-Level Graduate Program” and Donostia International Physics Center (DIPC).

This Dissertation is divided into three main chapters. Chapter I is a general introduction focused on chirality. Chapter 2 describes a newly designed 4-isocyanide benzaldehyde spacer for helix poly(isocyanides), synthesizing new chiral and achiral isocyanide monomers. Chapter 3 discloses the asymmetric synthesis of Ugi four-component reaction and polymerization by using chiral aldehydes, including the chiral characterization of the Ugi adducts.

INDEX

Acronyms and abbreviations	i
Chapter I Introduction	1
1.1 Scales of chirality	3
1.1.1 Molecular chirality and supramolecular chirality.....	4
1.1.2 Analytical methods for chirality	7
1.1.3 Methodology to obtain enantiomerically pure compounds	14
1.2 Polyisocyanide with helical structure	19
1.2.1 Chemical feature of isocyanide and involved domain.....	19
1.2.2 Methodologies of polymerization of poly(isocyanides).....	23
1.2.3 Structure and characterization	30
1.2.4 The future of poly(isocyanides).....	32
1.3 Isocyanide-based asymmetric Ugi 4 component reaction	32
1.3.1 Ugi multicomponent reactions	32
1.3.2 Asymmetric Ugi 4 component reactions	34
1.3.3 Ugi 4 component reactions in the polymerization.....	36
Chapter II Helix sense controlled poly(isocyanides) via Coordinate Polymerization....	39
2.1 Objectives	41
2.2 Densely substituted prolines as monomers.....	41
2.2.1 Synthesis of ferrocenyl-proline EhuPhos catalysts	43
2.2.2 Chemical synthesis of chiral γ -isocyano-prolines	47
2.3 4-Isocyanide benzaldehyde as a spacer in the synthesis of poly(isocyanides)....	53
2.3.1 Isocyanide monomer synthesized from 4-isocyanide benzaldehyde spacer .	56
2.4 Polymerization of 4-substituted phenyl isocyanides	59
2.4.1 Optimization of the polymerization reaction of imino isocyanides 31	59
2.4.2 Polymerization of achiral and chiral imino isocyanides 31	64

INDEX

2.5 Helix sense control polymerization of isocyano- <i>N</i> -methylated pentasubstituted prolines	68
2.6 Mechanistic studies	74
2.7 Conclusions	84
Chapter III Ugi four-component reaction and polymerization processes.....	85
3.1 Objectives	87
3.2 Asymmetric Ugi reaction	87
3.2.1 Synthesis of chiral aldehydes	88
3.2.2 Asymmetric Ugi reaction with chiral aldehydes	89
3.2.3 Reaction mechanism and origins of stereocontrol	93
3.2.4 Kinetic study.....	96
3.3 Ugi polymerization.....	99
3.4 Conclusions	103
Annexes	105
I General Information	107
II Analytical methods	107
III Synthetic procedures and analytical data.....	109
IV NMR spectra	129
V HPLC data	196
VI Crystal XRD.....	204

CHAPTER I
INTRODUCTION

1.1 SCALES OF CHIRALITY

Chirality is an intrinsic characteristic of matter and, in particular, all living things.¹ In general, chirality was a concept initially proposed for structures that failed to coincide with their mirror symmetry image through spatial and rotational translation.

Chirality can be found at all scales in the universe, from neutrinos and chiral atoms (caused by the interaction between the weak force interact and electrons),² to chiral molecules, such as amino acids, helix supramolecular structures (prepared by self-assembly or by polymerization),³ chiral biomacromolecules (such as DNA and proteins), microorganisms (helix-shaped bacteria),⁴ macroscopic biological systems (grapevine⁵ and seashells), neutron stars, and galaxies (Figure 1).

A minor scale ($<10^{-11}$ m) of chirality is defined as “chiral symmetry”, which can be observed at the fundamental particle level. At this scale, chirality was used to describe particles that possess “Left-handed” and “Right-handed” spins.⁶

At a larger scale ($\approx 10^{-10}$ m), numerous chemical compounds can be found in natural systems showing “Molecular chirality”. The molecule turns to be chiral when its mirror image cannot coincide with itself through spatial translation or rotation. This means that sp^3 carbon can be considered chiral when the four attaching atoms or groups are of different types. The two types of molecules are named enantiomers and show opposite optical rotation power.⁷

At the supramolecular level (10^{-9} – 10^{-7} m), most biological macromolecules or supramolecular systems possess intrinsic chirality as they are composed of chiral building blocks. The polypeptides and proteins are condensed of natural L-amino acids and can arrange to form α -helix, β -sheet, or random coil structures.⁸ Moreover, the left-handed double helix framework of DNA or RNA are generated from the D form of deoxyribose or ribose.⁹ However, chiral supramolecules can also be obtained from achiral building blocks. For instance, the helix poly(isocyanides) and poly(diphenylacetylene)s can be

¹ Avalos, M. N.; Babiano, R.; et al. *Tetrahedron: Asymmetry*. **2000**, *11*, 2845-2874.

² Hegstrom, R. A.; Kondepudi, D. K. *Sci. Am.* **1990**, *262*, 108-115; Bouchiat, M.A.; Pottier, L. *J. Sci. Am.* **1984**, *250*, 100-111.

³ Yanagawa, H.; Ogawa, Y.; et al. *J. Am. Chem. Soc.* **1989**, *111*, 4567-4570.

⁴ Norris, C. R.; Marks, S. L.; et al. *J. Clin. Microbiol.* **1999**, *37*, 189-194.

⁵ Smyth, D. R. *Development*. **2016**, *143*, 3272-3282.

⁶ Griffiths, D. *Introduction to elementary particles*, John Wiley & Sons, **2020**.

⁷ Alden Mead, C. *Permutation groups symmetry and chirality in molecules*, Springer, **1974**, 1-88.

⁸ Lippmann, D.; Dix, J. *Advances in biochirality*, Elsevier, Amsterdam, **1999**.

⁹ Bonner, W. A. *Origins of life and evolution of the biosphere*. Springer. **1991**, *21*, 59-111.

optically active without chiral carbons in the main chain.¹⁰ The chirality of these polymers is produced by a regular but nonsymmetric arrangement of each repeat unit and thus makes the main chain accumulate in a helical conformation. Moreover, chiral artificial supramolecular structures achieved by self-assembly and polymerization come out with potential applications such as chiral recognition, chiroptical switches, catalysts, circularly polarized luminescence (CPL), and biological applications.

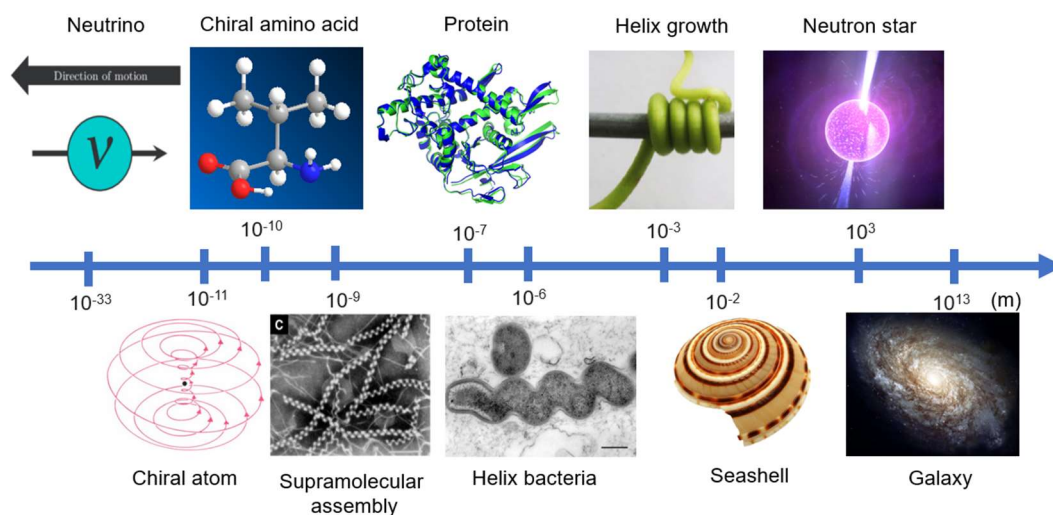


Figure 1. Various scales of chiral architectures.

The emergence of chirality on a larger scale includes the helix virus or bacteria, the chiral growth of green plants such as vines, and the rotating stars and galaxies.

In conclusion, chirality has its manifestations and definitions in each scale of matter. In this Thesis, molecular and supramolecular chirality will be discussed.

1.1.1 Molecular chirality and supramolecular chirality

Chirality is inextricably linked with our lives. Trace back to the evolution of life on Earth, in which only one-handedness was selected by nature. As a result, L-amino acids and D-sugars were chosen as the main components of proteins/enzymes and DNA/RNA. The doubt of how this preference was raised and amplified from initial racemic reactions still requires a solid answer. The hypothesis of evolutionary advantage, chiral physical interaction, and Earth's magnetic field could be part of the answer.¹¹

¹⁰ Tarrío, J. J.; Rodríguez, R.; et al. *Angew Chem.* **2022**, *134*, e202115070.

¹¹ a) Huck Nina, P. M.; Jager Wolter, F.; et al. *Science.* **1996**, *273*, 1686-1688. b) Thiemann, W. "Speculations and facts on the possible inductions of chirality through earth magnetic field.". *Origins of life.* Springer. **1984**, *14*, 421-426.

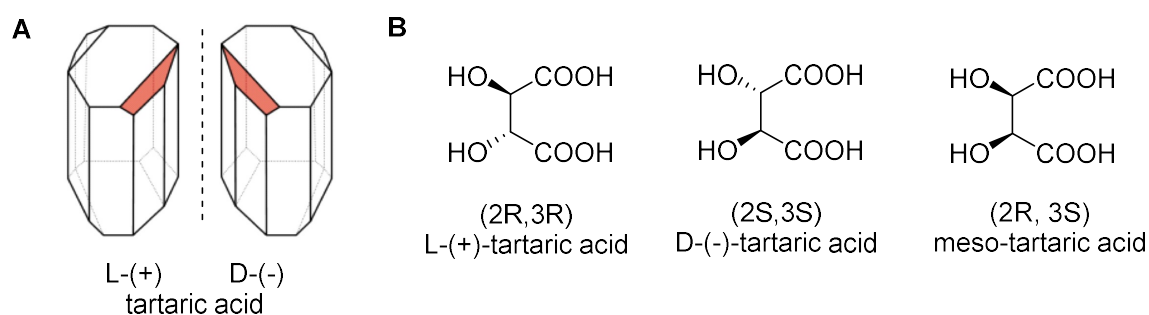


Figure 2. (A) Pasteur's drawing of the enantiomorph crystals of sodium ammonium tartrate and (B) Three different configurations for tartaric acid.

Even though chiral compounds have already existed for billions of years, it was not until 18th century that chemists began to be aware of the chirality in molecules. In 1848, *Louis Pasteur* (1822-1895) compared the sodium ammonium salt of tartaric acid (TA) to study its unknown structure. Surprisingly, two crystal types were found in optically inactive TA samples. One was identical to optically active (+)-TA samples obtained from fermented grape juice during the wine-making process. Another one was the mirror image of the first one (Figure 2).¹² His discovery of two enantiomorph crystal types of tartaric acid has led to the establishment and development of molecular chirality theory.

The classification of chirality is mainly focused on molecular and supramolecular scales. For molecular chirality, it is a common understanding that any molecule that contains an asymmetric carbon is chiral. However, asymmetric carbon is not a necessary condition for chirality. Molecular chirality can also be obtained from other possibilities. Thus, molecular chirality can be essentially classified as point, plane, axis, and helical chirality (Figure 3).¹³ At the supramolecular level, chirality commonly appears as helical types such as helix ribbons and twist ribbons, or helical assemblies consisting of nanospheres, nanoparticles, columns, double helix structures, and twisted bundles from the binding of multiple helix chains.

Given that chirality appears in various levels and types, the descriptors of two chiral configurations are complex. The absolute configuration of a few chiral conventions is depicted in Figure 3 and is described below.

c) Pasteur, L. *Séances Acad. Sci.* **1848**, 26, 535-538. d) Schulz, G. E.; Schirmer, R. H. *Principles of protein structure*, Springer Science & Business Media, **2013**.

¹² Brown, C. J.; Bergman, R. G.; et al. *J. Am. Chem. Soc.* **2009**, 131, 17530-17531.

¹³ Gal, J. *Chirality*. **2011**, 23, 647-659.

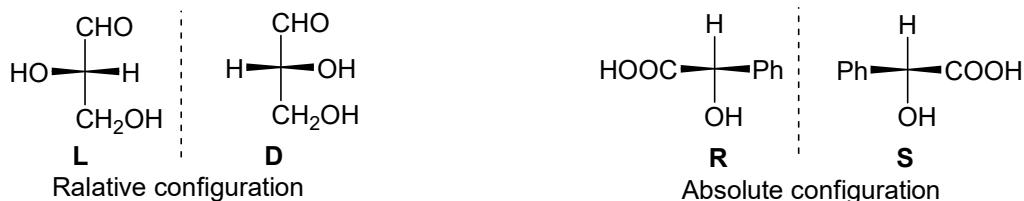
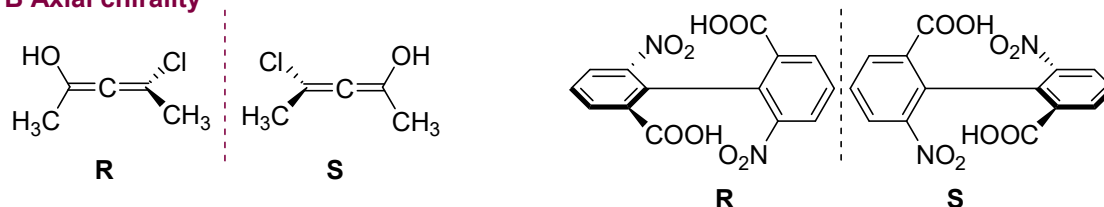
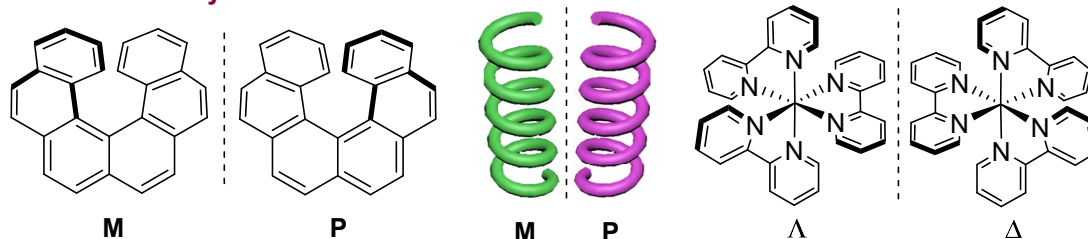
A Point Chirality**B Axial chirality****C Helical chirality**

Figure 3. The classification of molecular chirality as point, plane, and axis chirality with certain chiral conventions.

D & L system.

Derived from the Latin terms *laevus* (left-hand) and *dexter* (right-hand) and referred from the enantiomers of glyceraldehyde. In general, this system has been used to name naturally occurring substances such as α -amino acids and sugars, as well as their derivatives.

(+) & (-), [also named as (d) & (l)] system.

Measured from a polarimeter and unrelated with D/L system, (+) & (d) describe dexter (right) turn of polarization plane with a positive optical rotation, and (-) & (l) described laevus (left) turned.

R & S system.

For a specified chiral carbon, the lowest priority group point to the back of the plane, according to the Cahn-Ingold-Prelog priority rules (CIP). If the sequence

of the other groups runs in a counterclockwise direction, the chiral carbon was S (sinister) configuration. Otherwise, it is denoted as R (rectus).

M & P system.

Commonly refer to helical systems such as supramolecular assemblies, helix ribbons, and twisted ribbons. Focus the sight along the axis of the helix structure when a clockwise screwing motion of the helix is away from the observer. It is a P helix configuration (right-handed helix). Otherwise, it is an M helix configuration (left-handed helix).

Λ & Δ system.

They are used in coordination compounds with Λ for a left-handed propeller twist described by the ligands and Δ for a right-handed twist.

1.1.2 Analytical methods for chirality

Chiral molecules are identical to their enantiomers in general chemical and physical properties. This is the reason why chirality cannot be identified by general characterization methods such as Fourier-Transform Infrared (FTIR) or Nuclear Magnetic Resonance (NMR). However, in biochemistry, the characterization of chiral compounds is relevant as many chiral drugs have different pharmacology behavior depending on their different configurations. For instance, Thalidomide (Figure 4), Ibuprofen, Naproxen, and Ofloxacin are pharmacologically active in one of the configurations but harmful or with off-target side effects when present in another configuration.¹⁴

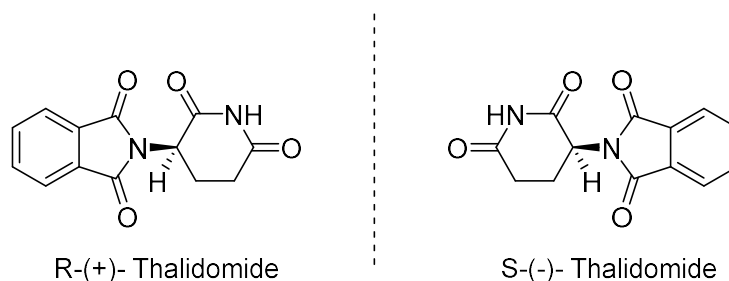


Figure 4. (R)- and (S)-enantiomers of Thalidomide. The (R)-form is responsible for sedative effects, and the (S)-form is responsible for immunomodulatory effects.

¹⁴ Yu, X. Y.; Chau, C. M.; et al. *Anal. Chem.* **2018**, *90*, 4089–4097.

The bioactivity difference between enantiomers has promoted fields like “Chiral analysis” and “Strategies for the synthesis of Enantiopure Compounds (EPC)”. The chiral analysis mainly included optical and chromatographic methods. Chiral analysis has attracted a growing interest in various pharmaceutical, environmental, and food fields.

1.1.2.1 Chiroptical spectroscopic methodologies

Light, in its wave description, consists of the regular propagation in time and space of in-phase magnetic and electric fields. As far as interaction with organic molecules is concerned, the electric field is more relevant. In general, the oscillation plane of the electric field vector points to all directions, thus statistically appearing unpolarized. Through a polarizer, natural light can be transformed into three kinds of polarized light in Figure 5.

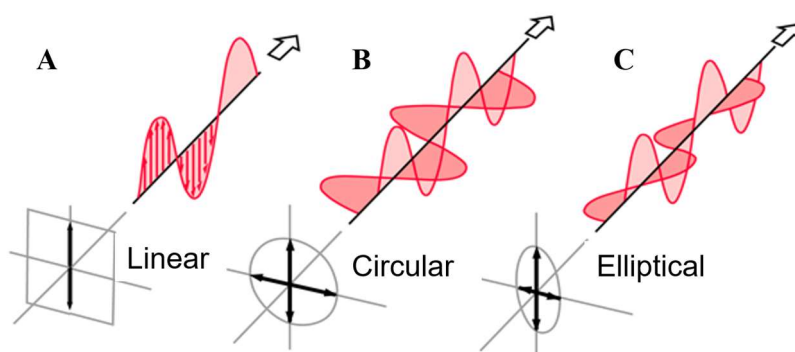


Figure 5. Classification of polarization. It is reproduced from ref 15.¹⁵

(A) Linear/plane polarization. The electric field vector vibrates and propagates alternately vertically up and down with the polarization plane and perpendicular to the wave travel direction;

(B) Circular polarization. Circularly Polarized Light (CPL) is composed of two planes of polarized light of equal amplitude and differing in phase by $\pi/2$;

(C) Elliptical polarization. Two planes of polarized light of circular polarization differing in amplitude, arranged in other phases rather than $\pi/2$.

¹⁵ Sardela, M. *Practical Materials Characterization*. 2014, Springer, New York, 43-92.

This polarized light is utilized in standard chiroptical methods, including Specific Optical Rotation (OR), Optical Rotatory Dispersion (ORD), Electronic Circular Dichroism (ECD), Vibrational Circular Dichroism (VCD), and vibrational Raman optical activity (ROA)¹⁶ to characterize the optical activities and properties of chiral samples (OR and CD methods are shown in Figure 6).

Specific optical rotation (OR) is the measured value from a polarimeter at T (K) and polarization wavelength at λ (nm), calculated according to the following formula:

$$[\alpha]_{\lambda}^T = \frac{\alpha_{obs}}{c \times l} \quad (1)$$

where α_{obs} ($^{\circ}$, deg) is the observed optical rotation degree from the polarimeter, c (g/mL) represents concentration, and l (dm) is the path length of the cell.¹⁷

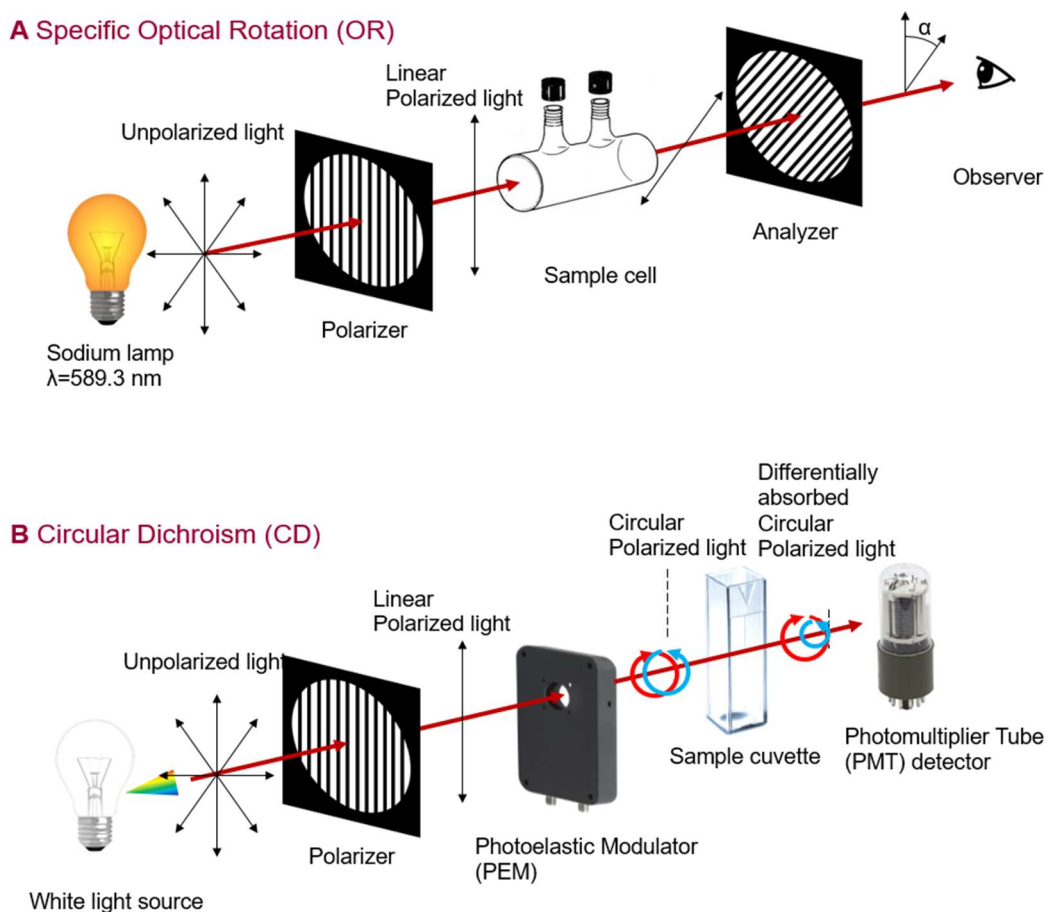


Figure 6. Schematic representation of OR (A) and CD (B).

¹⁶ Polavarapu, P. L. *Chiroptical spectroscopy: fundamentals and applications*, Crc Press, **2016**.

¹⁷ Soares, J. A. N. T. in *Introduction to Optical Characterization of Materials*, (Ed. M. Sardela), Springer, NY, **2014**, 43-92.

This method was used to characterize the abilities of a chiral sample to deflect a linear/plane-polarized light. First, a generated unpolarized light is transformed into linear polarized light through a polarizer. Then, it is passed through a cell containing the sample to be tested. If the sample is chiral, it would deflect the polarizing angle of the incident light, and this deflection is observed from the analyzer, facing the direction of polarized light propagation. If the deflection is clockwise, the value of the specific rotation is positive. This compound can be characterized as *dexter* (*d*) and named after an enantiomeric prefix descriptor (+); otherwise, the compound is *laevus* (*l*) and described after (-). For facile comparison, the polarimeter always uses a sodium lamp with a specific wavelength ($\lambda = 589.3 \text{ nm}$).

Optical rotatory dispersion (ORD) is the dispersion of rotation degrees measured from polarization with a series of different wavelengths. The curve in the ORD spectrum across an electronic absorption always appears as S shapes, called the Cotton effect (Figure 8).

In the absorption region of ORD, the two components of polarized light are absorbed differently by the optically active substance, so the emergent light is elliptically polarized (Figure 6 and 7). This phenomenon is called Circular Dichroism (CD).¹⁸

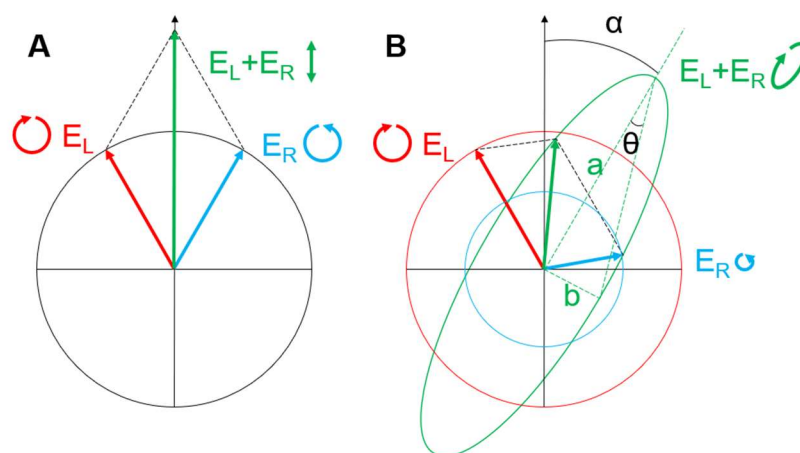


Figure 7. Schematic diagram of CD. E_L , red, left-hand circular polarized light; E_R , blue, right-hand circular polarized light; $E_R + E_L$, green, linearly polarized light. α refers to the optical rotation, and θ refers to the ellipticity.

In Figure 7, super-imposed incidence of two CPL (electric field vector E_L shown in red and E_R in blue) whose electric vector is equal in value but opposite in direction result in

¹⁸ Eyring, H.; Liu, H.C.; et al. *Chem. Rev.* **1968**, *68*, 525-540.

oscillating linearly polarized light ($E_R + E_L$, green). CD is caused when right-handed circular polarized light (RCPL) experiences a refractive index ($n > 1.0$) or absorption ($\epsilon > 0$), and left-handed circular polarized light (LCPL) is neither polarized nor absorbed. This behavior causes elliptical emergent light by an angle α with respect to the incident light (observed in OR or ORD), and ellipticity ($\theta = \tan^{-1}(b/a)$) recorded as the wavelength of CPL changes (Figure 8, a and b).

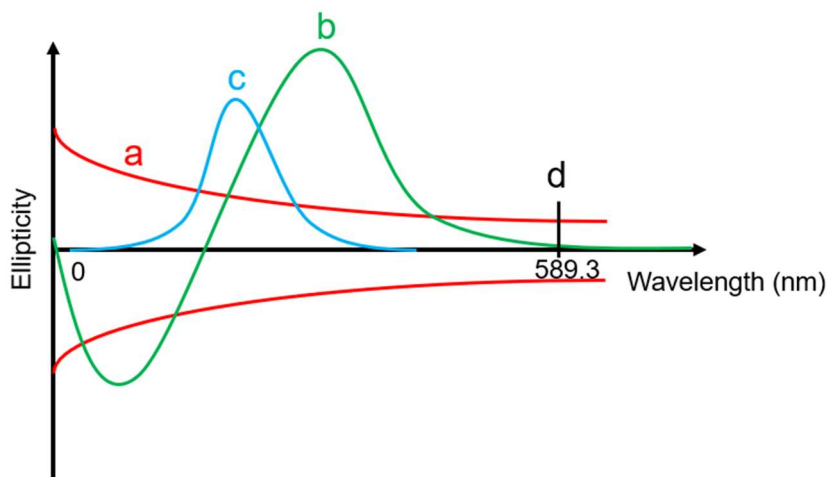


Figure 8. Typical chiroptical curves. (a) Plain ORD curve; (b) ORD curve with a single Cotton effect; (c) CD curve with a single Cotton effect curve and a maximum positive corresponding to (b); (d) Sodium D line measured from polarimeter at $\lambda = 589.3$ nm.

As the individual contributions to the ORD would be complicated to resolve, the utilization of the CD method in chirality characterization is in general, more convenient than ORD.¹⁹ The distinction between ECD and VCD relies on the length of the incident light, with ECD operating in the UV-Visible spectral region (~ 190 - 600 nm) and VCD in the IR region (4000 - 900 cm^{-1}). The collaborative combination of ECD and VCD can provide a more comprehensive understanding of the chiral structure. According to CD measurements, several physical quantities used in calculation and comparison are shown in Table 1.

¹⁹ Purdie, N. and Swallows, K. A., *J. Anal. Chem.* **1989**, *61*, 77-89.

Table 1. Physical quantities and their conversion relationships. C stands for concentration in g/L, M is the average molecular weight (g/mol), and L is the path length of the cell (cm). Their units are 1. Absorbance (Abs). 2. Milli-absorbance (mAbs). 3. A•L/mol•cm. 4. degrees (°). Five millidegrees (m°). 6. Units are deg•cm²/dmol

From ↓ To→	Abs ¹	Milliabsorbance ²	Molar Extinction ³	Degrees ⁴	Millidegrees ⁵	Molar Ellipticity ⁶
(A)	A	A×1000	$\frac{A \times M}{C \times L}$	A×32.98	A×32980	$\frac{A \times M \times 3298}{C \times L}$
(mA)	$\frac{mA}{1000}$	mA	$\frac{A \times M}{C \times L \times 1000}$	mA×0.03298	mA×32.98	$\frac{mA \times M \times 3.298}{C \times L}$
(ε)	$\frac{\epsilon \times C \times L}{M}$	$\frac{\epsilon \times C \times L \times 1000}{M}$	ε	$\frac{\epsilon \times C \times L \times 32.98}{M}$	$\frac{\epsilon \times C \times L \times 32980}{M}$	ε×329
(°)	$\frac{^\circ}{32.98}$	$\frac{^\circ}{0.03298}$	$\frac{^\circ \times M}{C \times L \times 32.98}$	°	°×1000	$\frac{^\circ \times M \times 100}{C \times L}$
(m°)	$\frac{m^\circ}{32980}$	$\frac{m^\circ}{32.98}$	$\frac{m^\circ \times M}{C \times L \times 32980}$	$\frac{m^\circ}{1000}$	m°	$\frac{m^\circ \times M}{C \times L \times 10}$
[Θ]	$\frac{[\Theta] \times C \times L}{M \times 3298}$	$\frac{[\Theta] \times C \times L}{M \times 3.298}$	$\frac{[\Theta]}{3298}$	$\frac{[\Theta] \times C \times L}{M \times 100}$	$\frac{[\Theta] \times C \times L \times 10}{M}$	[Θ]

In general, CD data are recorded as ellipticity (θ), which is related to absorbance ($\theta = 32.98 \Delta \text{Abs}$) and reported in a thousandth of degrees (mdeg or m°) in the CD spectrum. Molar ellipticity and molar extinction (ϵ) are ellipticity corrected for concentration and molecular weight, and generally used to characterize polymers or supramolecules with high molecular weight. The transformation of these physical quantities are shown in Table 1.

For optically active materials, CD intensity is related to many factors, including concentration effects, solvent effects, and temperature. A higher concentration of the sample would result in a higher ellipticity value, but it also binds to a higher signal-to-noise ratio (SNR) and can make the result unreliable. For convenience, the measurement usually goes under a widely accepted concentration such as 0.5 mg/mL. In addition, these values can vary greatly depending on other factors, such as the solvent or the temperature (Figure 9).

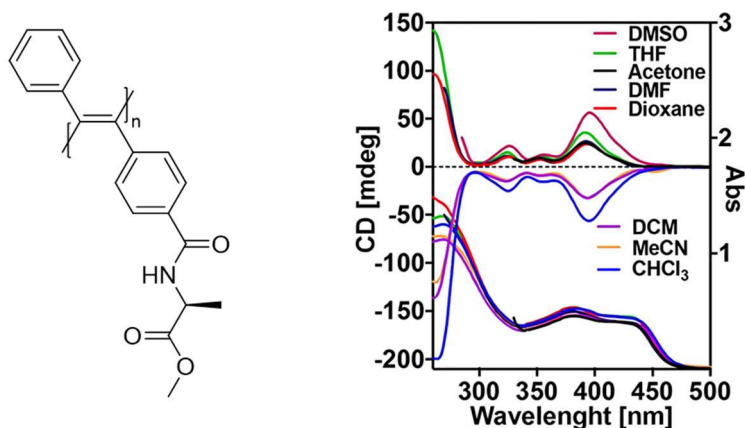


Figure 9. CD and UV spectra of poly-(S)-2 (Poly(diphenylacetylene)) in different solvents. Reproduced from ref. 10.

In contrast to CD, ROA is related to a scattering phenomenon instead of absorption. It consists of differential Raman scattering obtained when chiral substances are excited with a circularly polarized laser, or different intensities of Raman shifted scattered right and left circularly polarized light components when chiral samples are excited with linear and unpolarized laser incident light (Figure 10).

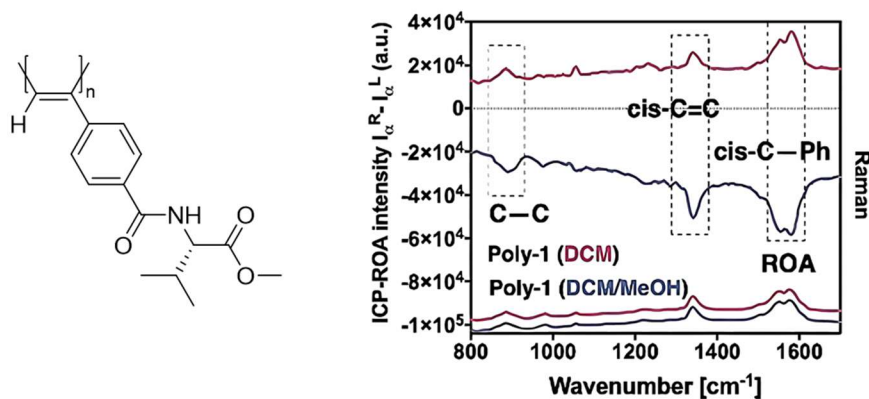


Figure 10. ROA spectra of Poly(phenylacetylene)s. Reproduced from ref. 20.²⁰

1.1.2.2 Chromatographic methodologies

Chiral chromatography is an effective strategy for chiral analysis and chiral resolution. The first Gas Chromatographic (GC) separation of enantiomers was performed by Gil-Av et al. in 1966, with a chiral stationary phase (CSP) obtained from amino acids

²⁰ Palomo, L.; Rodríguez, R.; et al. *Angew. Chem. Int. Ed.* **2020**, *59*, 9080-9087.

derivatives.²¹ On the other hand, the 1980s were a turning point in enantiomer separation, in which many new and improved CSPs were introduced.

General chiral chromatographic methodologies include GC, Liquid chromatography (LC), High-Performance Liquid Chromatography (HPLC), Supercritical fluid chromatography (SFC),²² and Capillary electromigration (CE) techniques.²³ The separation mechanism based on GC, LC, and HPLC, is mainly based on the multiple surface interactions between enantiomers and the CSP.²⁴ These interactions include hydrogen bonding, dispersion forces, dipole-dipole and steric interactions, among others, shown in Table 2.

Table 2. Electronic interactions among CSP and chiral analytes in LC.

Type of interactions	Strength	Direction	Distance dependency
Coulombic	Very strong	Attractive/Repulsive	Inverse square of the distance
Hydrogen bonding	Very strong	Attractive	Long range
Steric hindrance	Weak-very strong	Repulsive	Short range
π - π interaction	Strong	Attractive	Medium range
Ion-dipole	Strong	Attractive	Short range
Dipole-dipole	Intermediate	Attractive	Inverse cube of the distance
Dipole-induced dipole	Weak	Attractive	Inverse sixth power of distance
Dispersion forces	Very weak	Attractive	Inverse sixth power of distance

1.1.3 Methodology to obtain enantiomerically pure compounds

According to IUPAC,²⁵ asymmetric synthesis is a traditional term used for stereoselective synthesis of chiral compounds. This latter concept is defined as “a chemical reaction (or

²¹ Gil-Av, E.; Feibush, B.; et al. *Tetrahedron Lett.* **1966**, 7, 1009-1015.

²² Gere Dennis, R. *Science.* **1983**, 222, 253-259.

²³ Cifuentes, A. *J. Electroch.* **2006**, 27, 283-303.

²⁴ Berthod, A.; Li, W.; et al. *J. Anal. Chem.* **1992**, 64, 873-879.

²⁵ PAC, Basic terminology of stereochemistry, **1996**, 68, 2193..

reaction sequence) in which one or more new elements of chirality are formed in a substrate molecule and which produces the stereoisomeric (enantiomeric or diastereoisomeric) products in unequal amounts". Strategies for the synthesis of enantiopure compounds (EPC, EPC-synthesis, Figure 11) were described by Prof. Seebach in 1980 to meet the demand from organic chemistry of a) high enantiomeric excess and chemical yield; b) facile separation from chiral auxiliaries or reagents; c) economic recovery of chiral auxiliaries without racemization.²⁶

Resolution of racemates (also named racemic or chiral resolution) allows the separation of racemic mixtures that consist of two enantiomers by adequate physical or chemical methods. For instance, crystallization,²⁷ kinetic,²⁸ or chromatographic resolution (See chapter 1.1.2.2 Chromatographic methodologies).²⁹ The racemic resolution was widely used in substance preparation at industrial scale, especially in drug production.³⁰ However, its prospect is not optimistically considered due to the intrinsic drawback of being costly in time, materials, and energy.

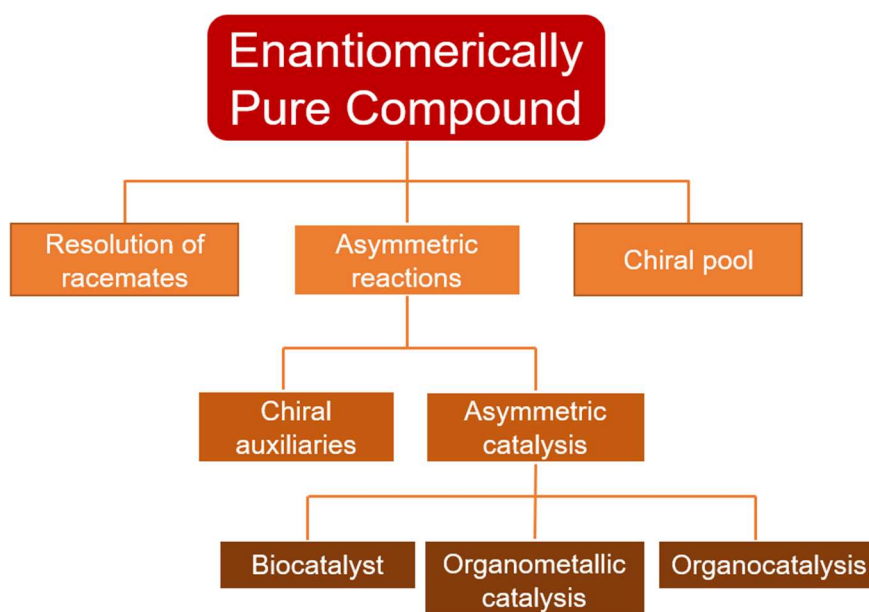


Figure 11. Strategies for the synthesis of Enantiomerically Pure Compounds.

²⁶ Scheffold, R. *Modern synthetic methods*. New York: Wiley. **1983**, 355.

²⁷ Anderson, N. G. *Org. Process Res. Dev.* **2005**, 9, 800-813.

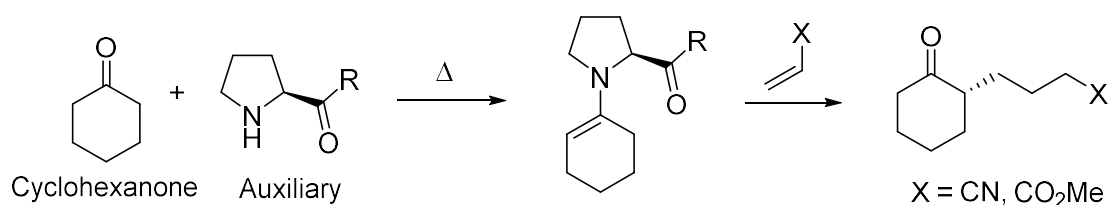
²⁸ Ros, A.; Magriz, A.; et al. *Org. Lett.* **2006**, 8, 127-130.

²⁹ Miller, L.; Potter, M. J. *J. Chromatogr. B.* **2008**, 875, 230-236.

³⁰ Mane, S. *Analytical Methods*. **2016**, 8, 7567-7586

The chiral pool method was named as a sequence of chemical transformations to produce the final products whose chirality was inherited and independent from the raw material (usually carbohydrates, amino acids, hydroxy acids, and terpenes).³¹ The limited availability of natural resources and reaction conditions that would lead to racemization have hindered the general application of this technology.

Chiral auxiliaries have been widely used in the synthesis of EPCs.³² Most of the available chiral auxiliaries are derived from compounds of natural origin similar to the chiral pool. However, the inner logic is indeed different. Chiral auxiliaries are molecules capable of temporarily binding the raw material, thus inducing chirality to the final products through one or more synthetic steps, followed by detaching and recovering.³³



Scheme 1. Synthesis of chiral ketones through chiral auxiliaries derived from L-proline.

The rules of choosing an appropriate chiral auxiliary for each asymmetric reaction involves considering factors such as a) a mild condition for the introduction and removal of the auxiliary, b) a high chemical yield, and c) high diastereoselectivity for chiral transfer steps or excellent enantioselectivity to get the final product. So far, the chiral auxiliary is one of the most popular methods in the asymmetric synthesis of biologically active compounds. Auxiliary systems such as those developed by Evans, Corey, Yamada, Enders, Oppolzer, and Kunz have significantly improved asymmetric synthesis in the last decades and continue bringing advances nowadays.³⁴

1.1.3.1 Asymmetric catalysis

Asymmetric catalysis is a type of catalysis in which a chiral catalyst directs the formation of a chiral compound such that the formation of a particular stereoisomer is favored.³⁵

³¹ Torrero, L. I.; Vinardell, M. H.; et al. *Recent Advances in Pharmaceutical Sciences V*, Research Signpost, **2015**.

³² Christmann, M.; Bräse, S. *Asymmetric synthesis II: more methods and applications*, John Wiley & Sons, **2013**.

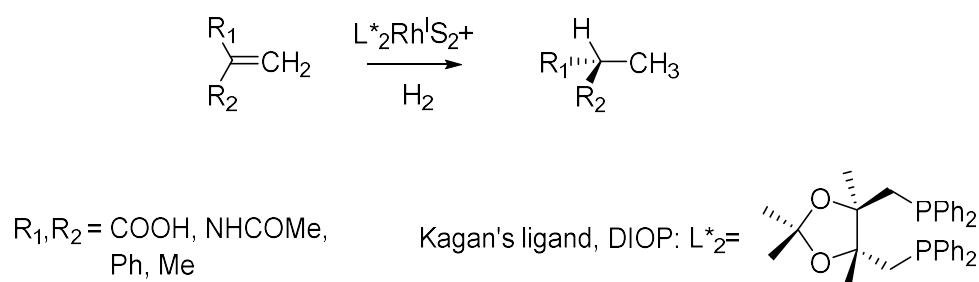
³³ Heravi, M. M.; Zadsirjan, V.; et al. *RSC. Adv.* **2016**, *6*, 30498-30551.

³⁴ Diaz-Muñoz, G.; Miranda, I. L.; et al. *Chirality*. **2019**, *31*, 776-812.

³⁵ List, B. *Chem. Rev.* **2007**, *107*, 5413-5415

Depending upon the nature of the asymmetric catalyst, biocatalysis, organometallic catalysis, and organocatalysis can be distinguished. Biocatalysts such as enzymes usually exhibit exquisite selectivity to catalyze reactions with excellent enantiomeric, diastereomeric and regio-selectivities.³⁶ Owing to its salient features of high specificity for the substrate and catalyst features derived from the cell's physiology, the exploitation of biocatalysts is quite different from conventional chemical processes. Biocatalysts have led to the development of a range of industrial products such as polymers, fragrances and flavors, pharmaceuticals, fine chemicals, biopharmaceuticals, and food.³⁷ So far, the employment of biocatalysts for the synthesis of many bioactive molecules is experiencing increasing widespread due to the readily accessible source from nature and the gradual improvement of the entire industrial processes.³⁶

In most cases, asymmetric synthesis achieved by organometallic catalyst was conducted with the cooperation of chiral ligands.



Scheme 2. Asymmetric hydrogenation of olefins by hydridorhodium(I) and DIOP complexes.

In this sense, in 1970, Henri Kagan described the first enantioselective asymmetric reaction catalyzed by an organometallic catalyst.³⁸ He used a Rh (I) catalyst bearing his chelating chiral C₂-asymmetric ligand, DIOP, to carry out this reaction, thus increasing the enantiomeric excess from 22% to 80%.

Afterwards, many other bidentate ligands were described to promote enantioselective reactions. For instance, BINAP was described by Noyori in 1980 and was found to have successful applications in several asymmetric reactions.³⁹ The most famous example was the Takasago synthesis of menthol. As one of the rare chiral ligands with good potential in industrial production, the modification of BINAP has become a popular area. So far, a family of BINAP catalysts has been synthesized and demonstrated to obtain excellent

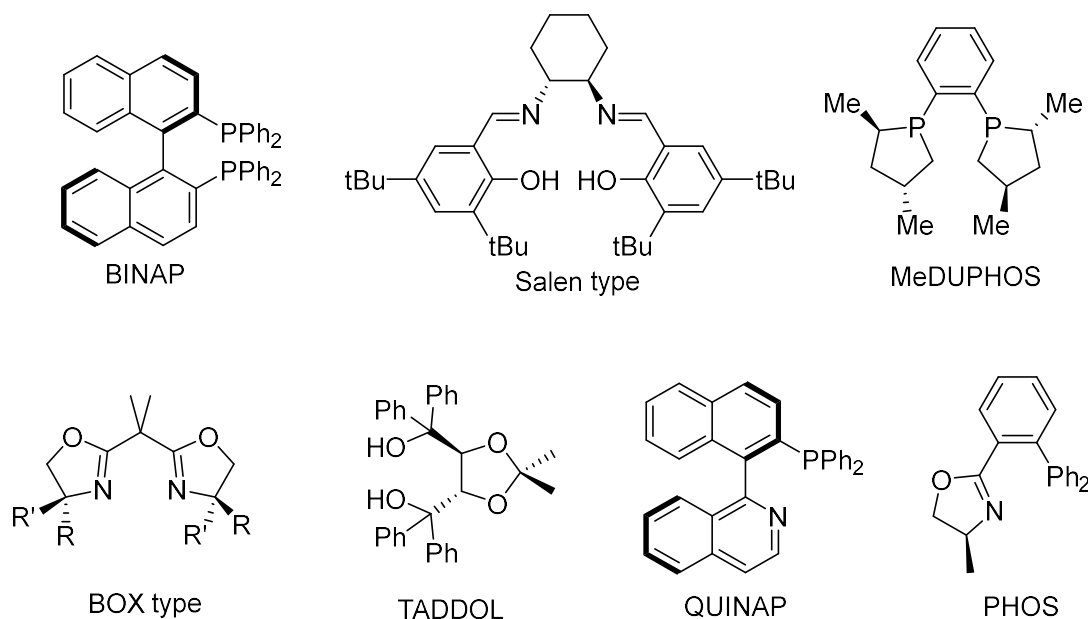
³⁶ Schmid, A.; Dordick, J. S.; et al. *Nature*. **2001**, *409*, 258-268

³⁷ Bell, E. L.; Finnigan, W.; et al. *Nat. Rev. Dis. Primers*. **2021**, *1*, 46.

³⁸ Kagan, H. B.; Dang, T.-P. *J. Am. Chem. Soc.* **1972**, *94*, 6429-6433.

³⁹ Miyashita, A.; Yasuda, A.; et al. *J. Am. Chem. Soc.* **1980**, *102*, 7932-7934.

efficiency (turnover) and selectivity (ee).⁴⁰ Apart from BINAPs, other chiral ligands such as QUINAP,⁴¹ MeDUPHOS,⁴² TADDOL,⁴³ Evans' bisoxazolines,⁴⁴ Salen type,⁴⁵ and phosphine-oxazolines⁴⁶ (Scheme 3) have also been developed.



Scheme 3. General bidentate ligands used in organometallic catalysis. BINAP: 2,2'-diphenylphosphino-1,1'-binaphthyl; MeDUPHOS: 1,2-bis(phospholano)benzene; BOX: bisoxazolines; TADDOL: α, α', α' - Tetraaryl-1,3-dioxolane-4,5-dimethanol; QUINAP: 1-(2-Diphenylphosphino-1-naphthyl)isoquinoline; PHOS: phosphine-oxazolines.

Ferrocene was discovered in 1951 and possess unique structures and ideal properties such as low cost, thermal stability, and high tolerance to many reagents.⁴⁷ The diastereoselective ortho lithiation of *N,N*-dimethyl-1-ferrocenylethylamine reported by Ugi was significant, it allows the preparation of various 1,2-disubstituted ligands by a considerable number of electrophiles reacting with lithiated species (Scheme 4).⁴⁸ The resulting ferrocenyl bidentate ligands were capable of promoting several enantioselective reactions.

⁴⁰ Berthod, M.; Mignani, G.; et al. *Chem. Rev.* **2005**, *105*, 1801-1836.

⁴¹ Alcock, N. W.; Brown, J. M.; et al. *Tetrahedron Asymmetry.* **1993**, *4*, 743-756.

⁴² Burk, M. J.; Stammers, T. A.; et al. *Organic Letters.* **1999**, *1*, 387-390.

⁴³ Seebach, D.; Beck, A. K.; et al. *Org. Lett.* **2001**, *40*, 92-138.

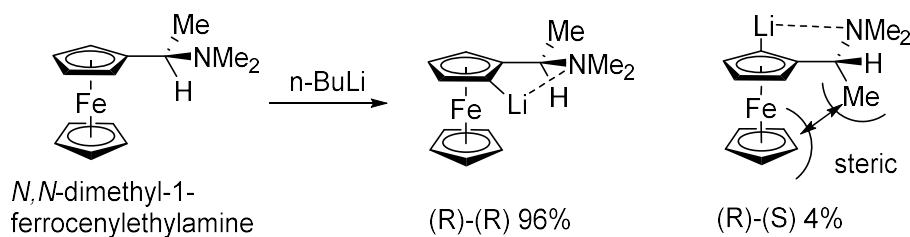
⁴⁴ McManus, H. A.; Guiry, P. J. *Chem. Rev.* **2004**, *104*, 4151-4202

⁴⁵ Katsuki, T. J., *Chem. Soc. Rev.* **2004**, *33*, 437-444.

⁴⁶ Schönleber, M.; Hilgraf, R.; et al. *Adv. Synth. Catal.* **2008**, *350*, 2033-2038.

⁴⁷ Kealy, T. J.; Pauson, P. L. *Nature.* **1951**, *168*, 1039-1040.

⁴⁸ Marquarding, D.; Hoffmann, P.; et al. *J. Am. Chem. Soc.* **1970**, *92*, 1969-1971.



Scheme 4. Diastereoselective ortho-lithiation of (R)-*N,N*-dimethyl-1-ferrocenylethylamine.

1.2 POLYISOCYANIDE WITH HELICAL STRUCTURE

1.2.1 Chemical feature of isocyanide and involved domain

Isocyanide (also named isonitrile or carbylamine, written as R-NC) is a functional group in which a nitrogen atom is bonded to two carbon atoms, the terminal one being a formal carbene with an empty valence orbital (Figure 12). This particular arrangement results in two resonance forms: one neutral structure with the carbene unit and one zwitterionic form⁴⁹ in which the nitrogen atom possesses a formal positive charge and the terminal carbon atom exhibits a formal charge of -1. Interestingly, the hybridization of both atoms is sp^2 for the neutral form, with a formal C-N-C angle of ca. 120 deg., and sp for the zwitterionic form, that it is usually associated with a C-N-C angle of ca. 180 deg. When the linear triple bond form is considered, an isocyanide can act as a nucleophile to attack electrophiles. If the carbenoid is considered, isocyanide can behave as a radical acceptor, as a carbene in many multicomponent reactions.

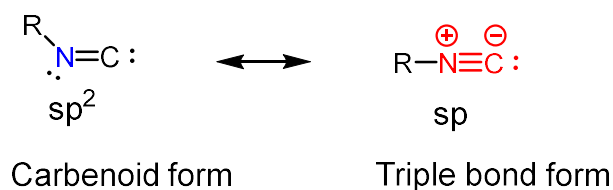


Figure 12. Isocyanide resonance of carbenoid form (left) and triple bond form (right).

Though isocyanides have been found in nature for years, it was not until the discovery of the Ugi reaction that isocyanides gradually entered synthetic chemistry and achieved the status of an essential reactive functional group.⁵⁰

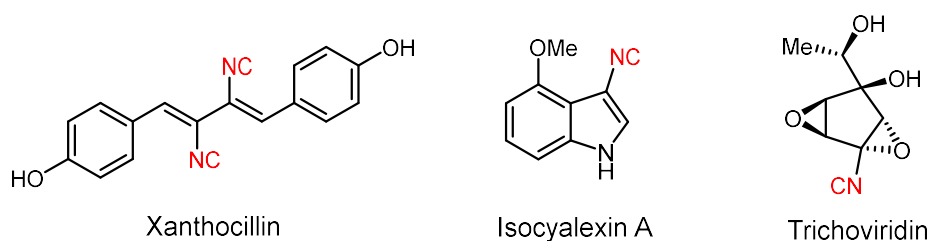
Isocyanides have a similar spatial size and dipole moment that nitriles (methyl isocyanide: 1.158 nm, 3.83 D; and acetonitrile: 1.157 nm, 3.92 D). Isocyanide molecules are

⁴⁹ Massarotti, A.; Brunelli, F.; et al. *Chemical Reviews*. **2021**, *121*, 10742-10788.

⁵⁰ Patil, P.; Ahmadian-Moghaddam, M.; et al. *Green Chem.* **2020**, *22*, 6902-6911

lipophilic, but due to the significant dipole moment, isocyanides are strong chelators in metal complexes. In addition, the strong coordinating properties of isocyanides make it preferable to bind with the metalloproteins, which was suggested as the source of the vile and atrocious odor.⁵¹

Isocyanide is a bioactive compound found in natural products; the identification of natural isocyanide could be traced back to the fifties. For example, the identification of Xanthocillin,⁵² Isocyaalexin A⁵³ and Trichoviridin⁵⁴ (Scheme 5), which are isocyanide-containing molecules isolated in vivo, shows the potential application in medical treatments. Also, isocyanoterpenes⁵⁵ synthesized by a special kind of sponge, constitute an interesting example.



Scheme 5. Bioactive isocyanides in nature.

Though both its nitrogen and carbon atoms can act as π -hole acceptors, the coordination of isocyanides with a metallic center is generally provided by the carbon atom. The interaction of the metallic atom and the nitrogen atom of isocyanide is more electrostatic than the carbon atom, while the carbon atom of isocyanide requires a shorter distance to favor the $n - \pi^*$ electron transition. Compared to carbon monoxide, isocyanides are better σ -donors and weaker π -acceptors in forming metallic complexes in different oxidation states. If the substituted group is aromatic, an additional conjugation would provide the back-donating electrons with a better delocalization, thus increasing the π -acceptor abilities of the isocyanide ligand. It has been reported that nitrogen and carbon could be engaged with one or two metal atoms to form metal isocyanide bond interactions (Scheme 6).

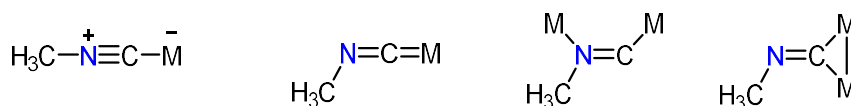
⁵¹ Turin, L. *Chem. Senses*. **1996**, *21*, 773-791.

⁵² Hübner I.; Shapiro J A.; et al. *ACS Cent. Sci.* **2021**, *7*, 488-498.

⁵³ Pedras, M. S. C. and Yaya, E. E., *Org. Biomol. Chem.* **2012**, *10*, 3613-3616.

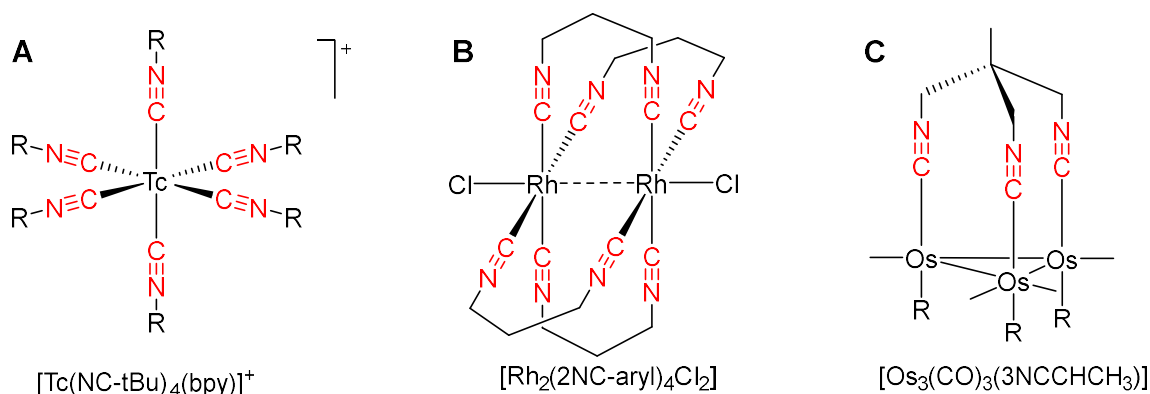
⁵⁴ Baldwin, J. E.; Adlington, R. M.; et al. *Chem. Commun.* **1996**, 41-42.

⁵⁵ Thompson, J. E.; Walker, R. P.; et al. *Tetrahedron*. **1982**, *38*, 1865-1873.



Scheme 6. Metal-isocyanide bonding interaction types. (M=Metal atom/ion)

In organometallic and coordination chemistry, the multidentate isocyanide ligands (Scheme 7) play an essential role in the topology of these compounds.⁵⁶ Compared to a single functional isocyanide, multidentate isocyanide metal bonding interactions are more stable and robust. Therefore, it can be employed to obtain important metal complexes with novel applications. For example, the coordinated isocyanides can transform into carbene and thus form a C-C bond between each ligand, so the multidentate complex could be used to promote polycarbene (polyisocyanide).



Scheme 7. Metal-isocyanide complexes. (A) Hexaisocyanide complexes of the monochromatic gamma emitter ^{99m}Tc for radiological diagnoses;⁵⁷ (B) Bridged Rh(I)-Rh(I) complex with 1,3-propane diisocyanide;⁵⁸ (C) Bridge tri-Os planes with tripodal isocyanide ligands.⁵⁹

Isocyanide is a significant member in multicomponent reactions,⁶⁰ insertion reactions,⁶¹ and cyclization reactions. Relevant examples of these processes are discussed in Figure 13.

⁵⁶ Hahn, F. E. *Angew. Chem. Int. Ed.* **1993**, *32*, 650-665.

⁵⁷ O'Connell, L. A.; Dewan, J.; et al. *Inorg. Chem.* **1990**, *29*, 3539-3547.

⁵⁸ Lewis, N. S.; Mann, K. R.; et al. *J. Am. Chem. Soc.* **1976**, *98*, 7461-7463

⁵⁹ Constable, E. C.; Johnson, B. F. G.; et al. *J. Organomet. Chem.* **1991**, *403*, C15-C18.

⁶⁰ Dömling, A. *Chem. Rev.* **2006**, *106*, 17-89.

⁶¹ Qiu, G.; Ding, Q.; et al. *Chem. Soc. Rev.* **2013**, *42*, 5257-5269.

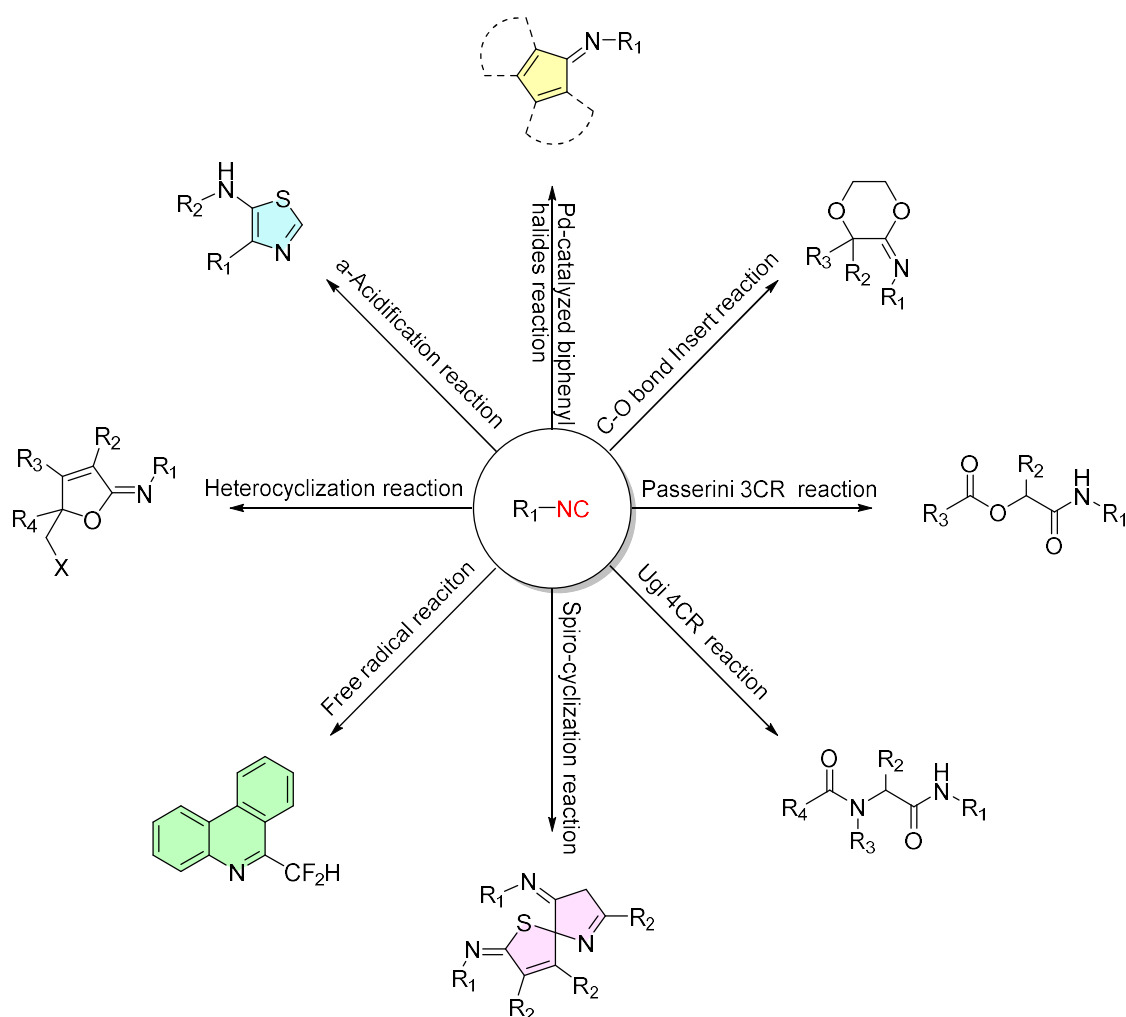


Figure 13. Isocyanides in various organic reactions, including Multicomponent reaction (Passerini 3CR reaction & Ugi 4CR reaction), insertion reactions (C-O bond insertion reaction, Pd-catalyzed biphenyl halides reaction, and free radical reactions), cyclization reaction (spiro-cyclization reaction & heterocyclization reaction), and others (α -acidification reaction).

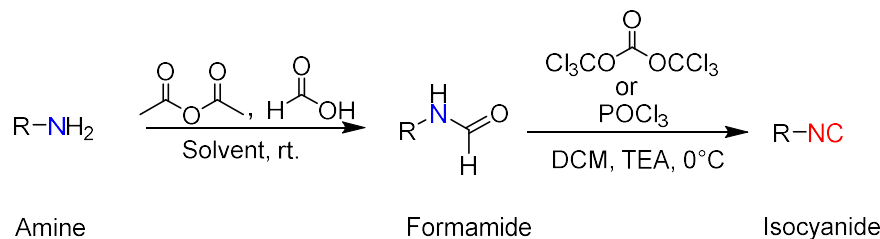
In the original procedure, isocyanides are obtained from amines via dichlorocarbene (Hofmann) or alkyl iodide via silver cyanide (Gautier).⁶² However, these methods are neither easy to operate nor suitable for the preparation of large quantities. Thanks to more controllable methods proposed by Ivar Ugi⁶³ and Hagedorn⁶⁴, which start from formamide via dehydrating agents such as phosphorus oxychloride, bis(trichloromethyl)carbonate (BTC), PPh₃/iodine, and p-TsCl (Scheme 8), over 26,000

⁶² a) Gokel, G. W.; RP, W.; et al. "Phase-transfer Hofmann carbylamine reaction: tert-butyl isocyanide." **1976**. b) Gautier, A. *Ann. Chim.* **1869**, *17*, 103-107.

⁶³ Ugi, I. Meyr, R. J. A. C. *Angew. Chem.* **1958**, *70*, 702-703.

⁶⁴ Hagedorn, I.; Eholzer, U.; et al. *Chem. Ber.* **1960**, *93*, 1584-1590.

isocyanides have been synthesized and described. So far, more than 3,000 isocyanides are commercially available.



Scheme 8. General steps to obtain isocyanide now.

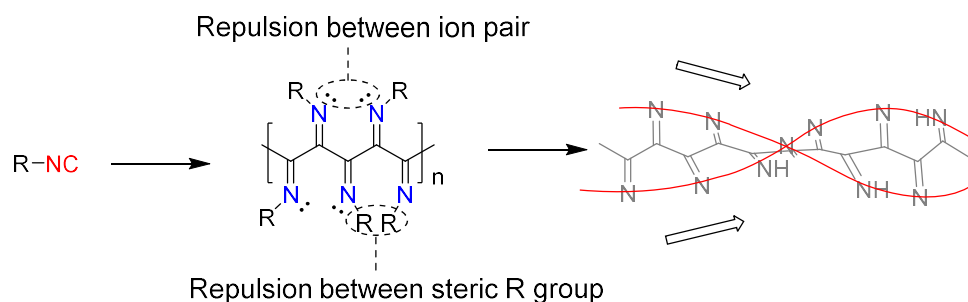
Most isocyanides are relatively unstable, and the reaction time, temperature, acidity, and storage conditions would affect the quality of the products and yields. Alexander designed novel preparation methods to improve the synthesis that meet large-scale synthesis demand, ease of operation, and high conversion.⁵⁰ The technique simplifies Ugi's method and work-up procedure by implementing the reaction in the flash column, allowing the preparation of many highly sensitive isocyanides in efficient ways.

1.2.2 Methodologies of polymerization of poly(isocyanides)

Isocyanide is easily polymerized into linear polymers, researchers have realized the possibilities of the secondary structure of polyisocyanide considering the repulsion among substituents along the polymeric chain.⁶⁵ Computational calculations proposed repulsions mainly in two cases. While a small side chain is contained in the polymer, an electronic repulsion occurs between the N ion pairs (Scheme 9). Alternatively, when the side chain is bulky enough, steric repulsion between the R groups occurs. Both cases can force the backbone of polyisocyanide to adopt a non-planar conformation, which means that the plane of the chain would twist itself and result in a helical conformation or a twisted band. This arrangement was confirmed by CD analysis of poly(*tert*-Butyl isocyanide).⁶⁶

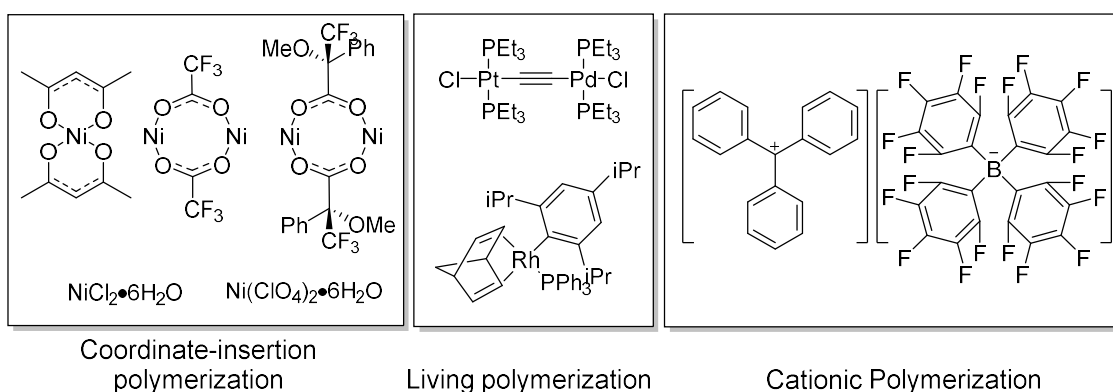
⁶⁵ Schwartz, E.; Koepf, M.; et al. *Polym. Chem.* **2011**, *2*, 33-47.

⁶⁶ Van Beijnen, A.; Nolte, R.; et al. *Tetrahedron.* **1976**, *32*, 2018-2019



Scheme 9. Electronic and steric repulsion force the chain to adopt a twisted band and helix formation.

The polymerization of isocyanides can be generalized into three mechanisms: coordination-insertion polymerization, cationic polymerization, and living polymerization. Each mechanism has similar initiators, propagation pathways, and methodologies to control the polymer's helix sense. Commonly used catalysts and/or initiators for the preparation of poly(isocyanides) according to three mechanisms are gathered in Scheme 10.



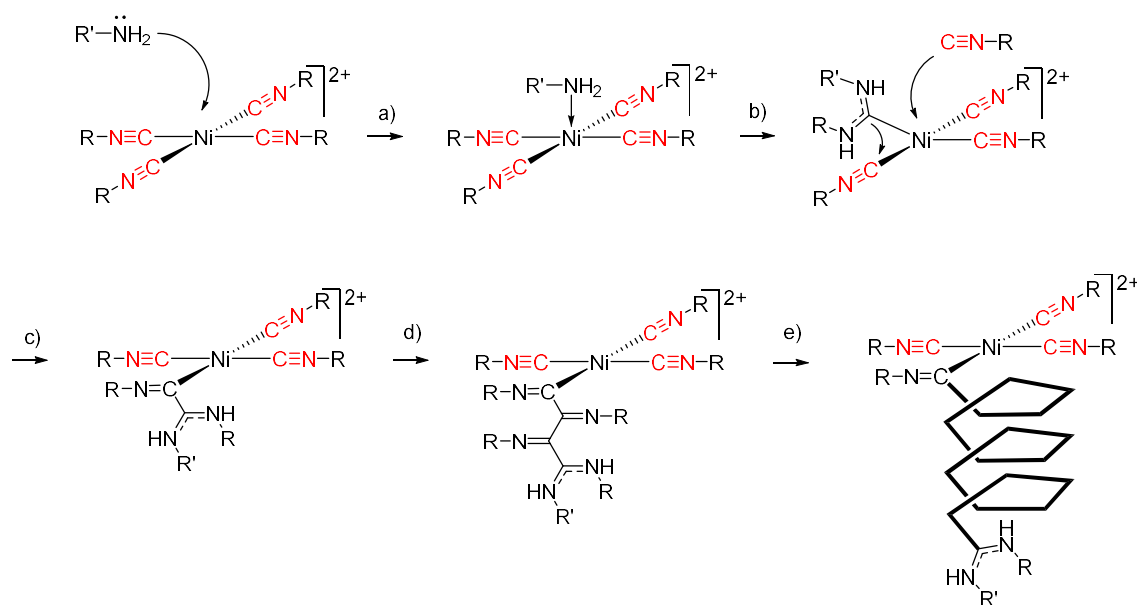
Scheme 10. Various types of catalysts for the polymerization of isocyanides.

Helical poly(isocyanides) have stable helix conformations since the helix inversion barrier exceeds approximately 85 kJ/mol, depending on the sidechain.⁶⁶ However, compared to the other helical polymers, poly(isocyanides) do not have a chiral center in each repeating unit; if the side groups are not bulky, there will not be enough repulsion to stabilize the conformation of the backbones against various environments. Therefore, poly(isocyanides) are also considered as dynamic helical structures. To increase the stability of the helix conformation, common standard methods were used, such as introducing bulkier side groups or building interactions such as hydrogen bonds between side groups.

1.2.2.1 Coordination-insertion polymerization

Ni(II) complexes constitute the most common metallic salts to conduct this polymerization for its economical, easily accessible, and robust reaction condition.

The initiation and propagation stages of Ni(II) catalyzed polyisocyanide formation is similar to other polymerization mechanisms catalyzed by metallic complexes. The “Merry-go-round” mechanism was proposed by Cornelissen, J et al. as a suitable model to study the kinetics of the whole process.⁶⁷ The initiation step of the polymerization starts from Scheme 11, (a) a square-planar Ni(II) isocyanide complex attaches to a nucleophile on the nickel center; (b) The nucleophile then migrates to the isocyanide of the complex to form a carbene-like intermediate that initiates the polymerization; (c) The carbene intermediate reacts with one of its two neighbor isocyanide ligands, and therefore thus giving rise to the imine backbone. Then, the resulting vacant coordinate position is occupied by the insertion of a new isocyanide monomer; (d) The imine located at the end of the chain reacts with its neighbor isocyanide continuously to propagate the polymer chain, and this process is repeated until the Ni(II) species entirely lose its activity; (e) Meanwhile, the imine backbone would twist and arrange itself in a helical conformation.

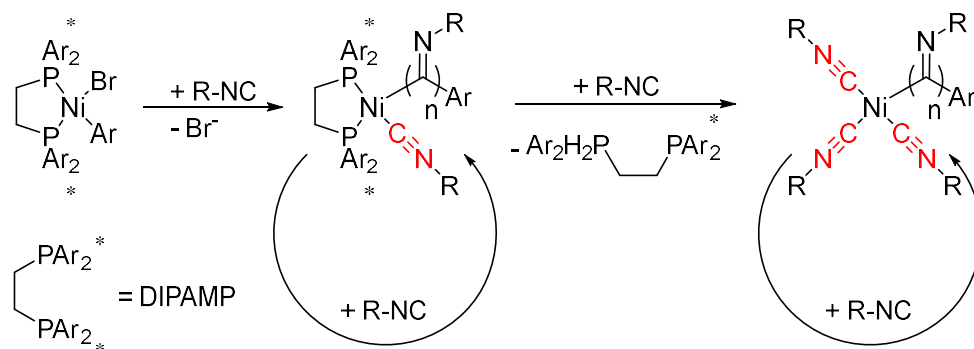


Scheme 11. Ni(II) catalyzed “Merry-go-round” mechanism in the polymerization of isocyanide

⁶⁷ Cornelissen, J. J. L. M.; Rowan, A. E.; et al. *Chem. Rev.* **2001**, *101*, 4039-4070.

The helix sense control of a coordination-insertion polyisocyanide was performed by a chiral nucleophile (chiral initiator or catalyst), chiral monomer, chiral auxiliary, and post-processing.

According to the step (b) depicted in Scheme 11, a chiral nucleophile (R') and an achiral monomer (R) were selected to get an asymmetric initiation.⁶⁸ The obtained chiral carbene could selectively react with one of the two neighbors and affect the imine backbone to arrange selectively as M-helix or P-helix, which is similar to the “Sergeants and Soldiers” rules in stereochemistry.⁶⁹ Alternatively, the chiral initiation can start from other achiral nucleophile with the presence of a chiral ligand.⁷⁰ The catalyst would attach by means of the nickel center (the insertion of the isocyanide is asymmetric) until it is replaced by an isocyanide monomer attached to the nickel center.



Scheme 12. $[(L_2)Ni(Ar)Br]$ catalyzed helix sense controlled poly(vinyl phenyl isocyanide).

An example of a chiral nickel catalyst was described by Frank Pammer et al. In this study, a type of chiral nickel pre-catalyst $[(L_2)Ni(Ar)Br]$ ($L_2 = RR/SS$ - DIPAMP, $Ar = \text{ortho-anisyl}$) was described, which promoted the helix sense-controlled poly(vinyl phenyl isocyanide) in high molecular weights ($M_n = 50 - 100$ kDa, $1 \text{ kDa} = 1000 \text{ g/mol}$) and high CD signal.⁷¹ The ^{31}P -NMR technique was used to monitor the polymerization, and free DIPAMP signal appeared in five minutes. This means that chiral ligand L_2 lost its attachment with the nickel center, and an isocyanide monomer occupied the position. In the discussion about the kinetics, two routes of propagation were proposed. Firstly, the isocyanide monomer was initiated with the aromatic substituted ligand DIPAMP (Scheme 12) in an asymmetric way. Then, the other isocyanide was attached to the nickel center

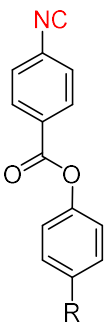
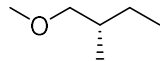
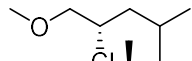
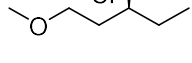
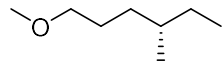
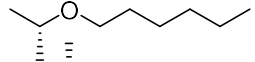
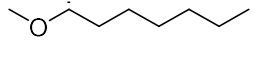
⁶⁸ Tang, Y.; Zhao, S.Q.; et al. *Polymer*. **2018**, *142*, 52-60.

⁶⁹ Prins, L. J.; Timmerman, P.; et al. *J. Am. Chem. Soc.* **2001**, *123*, 10153-10163.

⁷⁰ Kamer, P. C. J.; Nolte, R. J. M.; et al. *J. Am. Chem. Soc.* **1988**, *110*, 6818-6825.

⁷¹ Schraff, S.; Krienborg, N. M. et al. *J. Polym. Sci.* **2020**, *58*, 2221-2233.

and replaced the bromide ion. As isocyanides are stronger ligands than phosphines,⁷² the displacement of chiral DIPAMP ligand would occur with the propagation is going. After several rounds, the route turns like the ‘‘Merry-go-round’’ mechanism. In this research, even if the chiral source has been removed after the initiation, the helix sense could still be maintained in the propagation to obtain a controlled helix polymer.

A		R=	Monomer configuration	Polymer helix sense
			S	M
			S	M
			S	P
			S	None
			R	M
			R	M

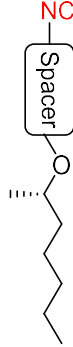
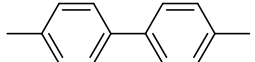
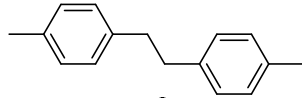
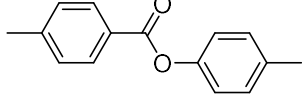
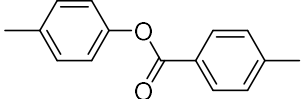
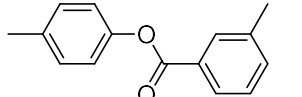
B		Spacer=	Polymer $\Delta\epsilon_{363}$
			+0.52
			0
			+3.05
			+0.90
			-1.51

Figure 14. A) Handedness of the poly(isocyanides) and the mesophases induced by the formamide precursors to them; B) Various lengths of the spacer between the (R)-octyloxy chain and the reactive group and the CD values of the polymer.⁷³

In general, the chiral monomer is a more general method to control the helix sense in the polymerization. Since the discovery of poly(isocyanides), most of these helical polymers

⁷² Harvey, P. D. *Coord. Chem. Rev.* **2001**, 219-221, 17-52.

⁷³ Amabilino, D. B.; Serrano, J.-L., *J Polym Sci A Polym Chem.* **2006**, 44, 3161-3174.

were obtained by means of this methodology.⁷⁴ Therefore, compared with a chiral initiator or catalyst, a chiral monomer is a more efficient way to control the helix sense. However, the monomer structure corresponds to the helix sense (Figure 14), to obtain an optically pure monomer is a must and has a high cost.

The chiral auxiliary is also a costly method to obtain helix sense control. This method conducts the polymerization in the presence of a chiral solvent or enriched chiral auxiliary solution, which requires the utilization of a large amount of chiral reagent. In addition, even though the dynamic helix sense of polyisocyanide was usually considered a defect property, it allowed modifying its helix structure in post-processing steps, such as dissolving in acid/base media, different solvents, or miscible with chiral reagents.

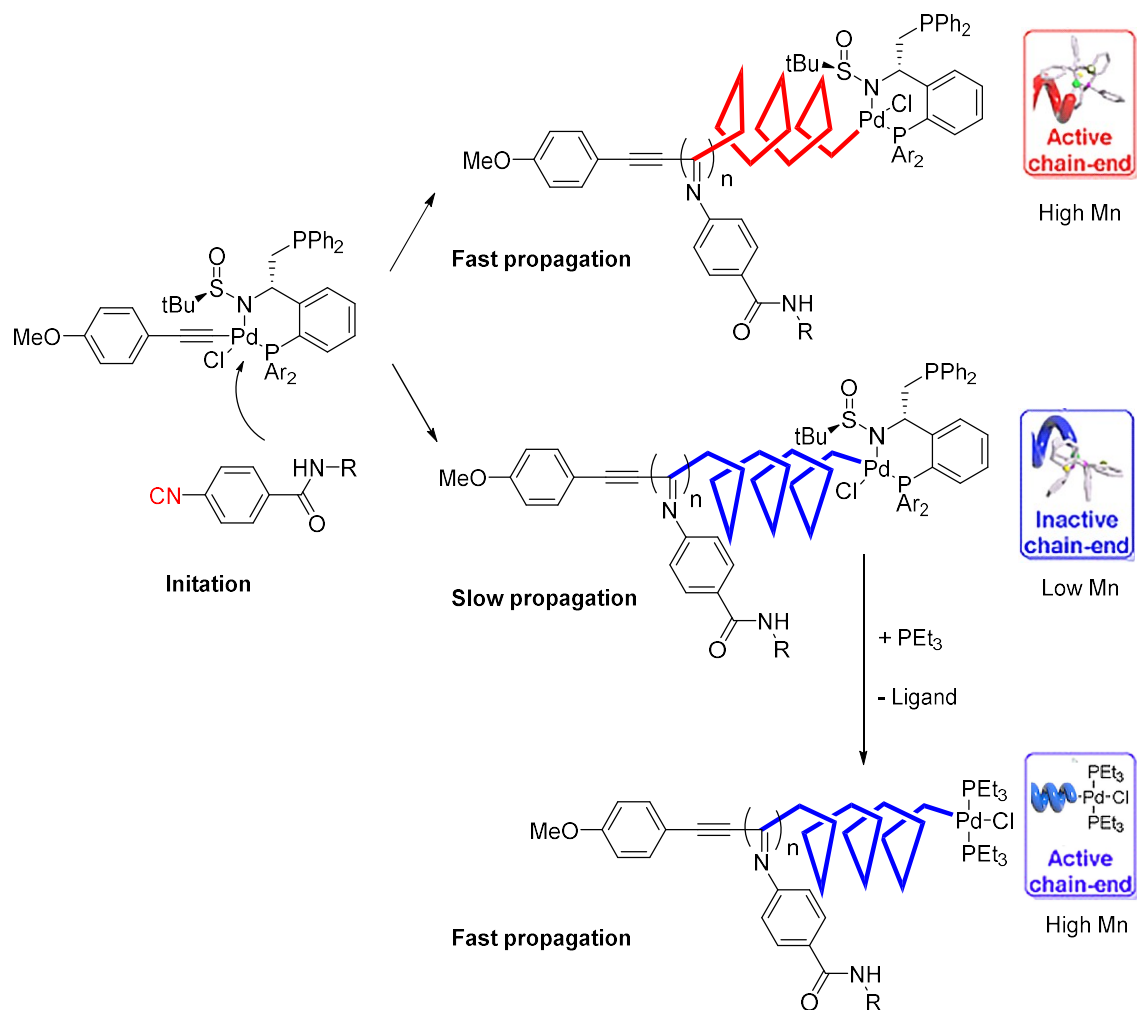
1.2.2.2 Living polymerization

Recently, poly(isocyanides) obtained via Pd(II)-catalytic system have attracted increasing researchers interest, and many new helical polyisocyanide have been synthesized by this method.⁷⁵ Living polymerization is an efficient tool to obtain a polymer with controllable properties. Moreover, palladium complexes have many optional chiral and achiral ligands. Despite using chiral monomers, employing chiral Pd(II) catalysts has functional advantages in controlling helix sense. Zong-Quan Wu⁷⁶ et al. reported a Pd(II)-(L*)-Cl catalyst (Scheme 13), which could promote the helix sense in a selective polymerization of achiral peptide isocyanide monomers.

⁷⁴ a) Cornelissen, J. J. L. M.; Graswinckel, W. S.; et al. *J Polym Sci A Polym Chem.* **2001**, *39*, 4255-4264.; b) Kajitani, T.; Okoshi, K.; et al. *J. Am. Chem. Soc.* **2006**, *128*, 708-709; c) Dama, M.; Berger, S. *Org. Lett.* **2012**, *14*, 241-243.

⁷⁵ a) Jiang, Z.-Q.; Zhao, S.Q.; et al. *Macromolecules.* **2018**, *51*, 737-745. b) Yang, L.; Tang, Y.; et al. *Macromolecules.* **2016**, *49*, 7692-7702. c) Su, Y.-X.; Xu, L.; et al. *Macromolecules.* **2020**, *53*, 3224-3233. d) Hayashi, H.; Kikuchi, R.; et al. *J. Mater. Chem. C.* **2019**, *7*, 7442-7453. e) Pomarico, S. K.; Lye, D. S.; et al. *Polym. Chem.* **2018**, *9*, 5655-5659. f) Zhao, S.-Q.; Hu, G.; et al. *ACS Macro Lett.* **2018**, *7*, 1073-1079.

⁷⁶ Zhou, L.; Xu, X. H.; et al. *Angew. Chem.* **2021**, *133*, 819-825.



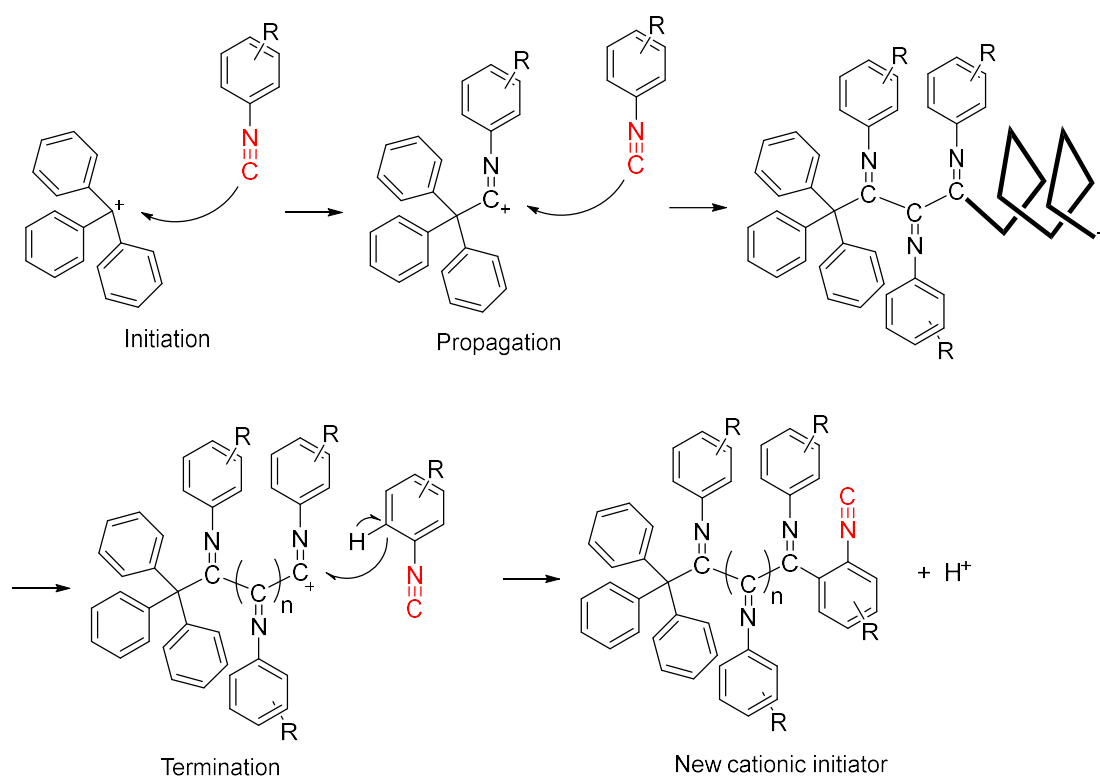
Scheme 13. Synthesis of single-handed helical polyisocyanide via Pd(II)-(L*)-Cl catalyst in living polymerization. Left-hand helix, red and right-hand helix, blue.

Pd(II) induced initiation is similar to that associated with Ni(II). However, in the propagation steps, the Pd(II) species was active when the chain was in a favorable helix conformation, and the propagation rate was faster than that observed from the chain with an unfavorable helix. This results in the different Mn values of the two types of helix structures. Interestingly, the inactive Pd(II) species with unfavorable helix sense could be activated by replacing the chiral ligand with an achiral ligand, which was considered as a strong evidence to support this mechanism.

As a reliable tool to get a controllable poly(isocyanides), the Pd(II) complex catalyst was confronted with the high cost in synthetic steps and the strict polymerize conditions. The solution of these drawbacks could make this tool more useful in the near future.

1.2.2.3 Cationic polymerization

Poly(isocyanides) obtained from coordination insertion or living polymerization usually contains metal ions which are complex and costly to remove in the workup. Alternatively, polyisocyanide could be obtained via protonic acids or Lewis acids in a cationic mechanism.⁷⁷ However, cationic polymerization usually gets low molecular weight polymers, around 10^3 g/mol, compared to other mechanisms. So far, Yuping Dong and Xiaofang Li et al. have described a metal-free initiator $[\text{Ph}_3\text{C}]^+[\text{B}(\text{C}_6\text{F}_5)_4]^-$ (Scheme 14) to carry out the polymerization of aromatic isocyanide to obtain helical polymers with higher molecular weight up to 1.2×10^7 g/mol.⁷⁸



Scheme 14. $[\text{Ph}_3\text{C}]^+[\text{B}(\text{C}_6\text{F}_5)_4]^-$ catalyzed cationic mechanism in the polymerization of aromatic isocyanide.

1.2.3 Structure and characterization

In general, the screw sense of polyisocyanide could be determined by techniques such as CD and AFM (Atomic Force Microscopy). A cylindrical helix model was generated from computational calculations by comparing the CD spectrum with theoretical predictions.

⁷⁷ a) Millich, F.; Baker, J. K.; et al. *Macromolecules*. 1969,2,122–128. b) Stackman, R. W. *J. Macromol. Sci. Part A*. **1968**, 2, 225–236.

⁷⁸ Yan, X.; Zhang, S.; et al. *Angew. Chem.* **2018**, 57, 8947-8952.

The energy eigenstates of the coupled oscillator system were considered to find out where is the active region in CD and predict the helix sense from the positive or negative sign of the calculated value (Figure 15).

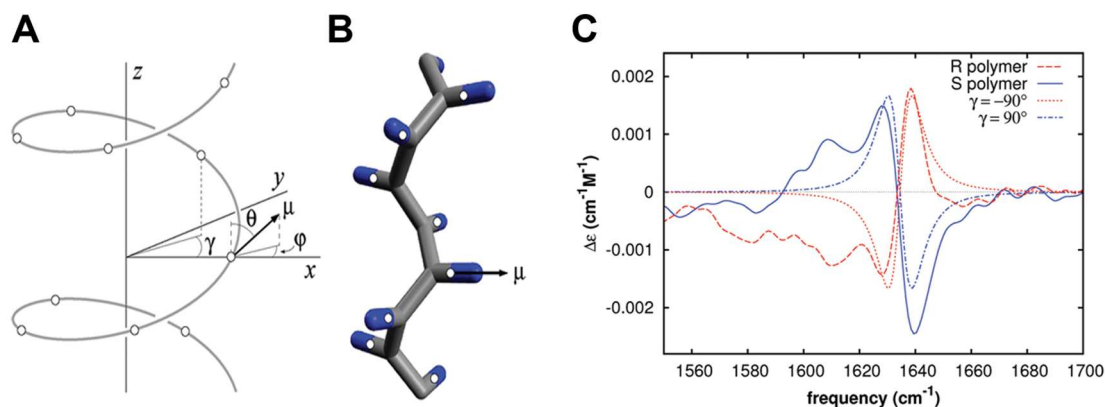


Figure 15. (A) Helix model and framework (B) for theoretical calculation of a helical chain. (C) Comparison of experimental VCD of R&S polymer and their calculated VCD. In the model, the side C=N bond point to the direction of μ with θ degrees to the axis Z and ϕ degrees to the axis X. The θ and ϕ define the direction of the transition dipole moments. Reproduced from ref. 78.

Microscopy methodologies could also characterize the helicoidal structure and helix sense. For example, the height, radius, and helix angle θ of the secondary structure can be obtained from AFM images and verified with the theoretically predicted helix structure (Figure 16).

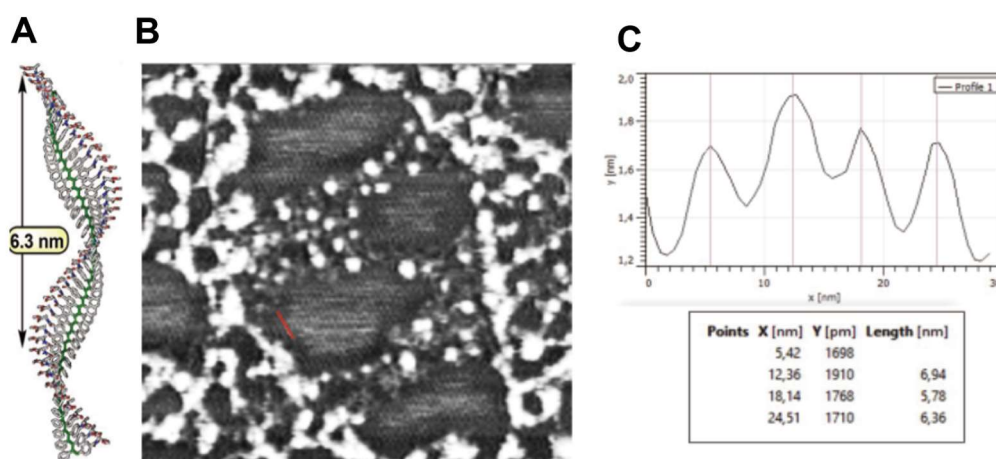


Figure 16. The Helix structure of Chiral Poly(diphenylacetylene)s determined by AFM images. (A) Schematic representation (B) AFM image. (C) Distinguish by nanoscope processing software.

Reproduced from ref. 10.

1.2.4 The future of poly(isocyanides)

Various helical poly(isocyanides) have been synthesized and researched over the years.⁶⁵ It is now possible to acquire polymers with a wide range of properties thanks to the development of new monomers and targeted catalysts. However, there is room for further improvements. Emergent preparation and characterization techniques in the future could provide additional advances in this field.

Due to the polymers' unique nature, poly(isocyanides) have flourished since their discovery and probably will continue in the future.⁶⁵ For example, the well-defined polymer backbone can work as chiral catalysts or nanowires along with its excitons can readily travel. Consequently, it is anticipated that poly(isocyanides) will keep attracting the interest of (bio)chemists and physicists.

1.3 ISOCYANIDE-BASED ASYMMETRIC UGI 4 COMPONENT REACTION

Multicomponent Reactions (MCRs) are one-pot reactions that use more than two starting materials in which most of the atoms from the beginning elements are incorporated into the final product. MCRs are frequently a helpful substitute for sequential multistep synthesis because of their different tags, such as atomic economical, efficient, and convergent.⁷⁹ Many fundamental MCRs are name reactions, for example, Passerini, Ugi, van Leusen, Hantzsch, Strecker, Biginelli, or one of their numerous versions.⁸⁰ In this Thesis, Ugi 4 component reactions (Ugi-4CRs) will be discussed.

1.3.1 Ugi multicomponent reactions

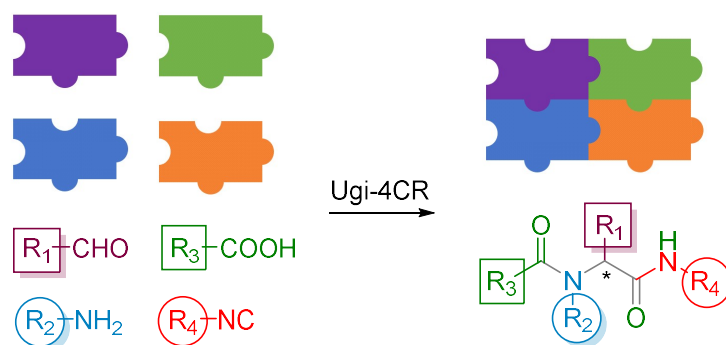
The Ugi multicomponent reaction (Ugi-4CR) is one of the most important synthetic tools in organic chemistry. This reaction was described by Ivar Ugi in 1959.⁸¹ It allows easy production of α -acylaminoamide derivatives (also called α -acetoamido carboxamides, or peptoids) in a single synthetic step by combining an aldehyde, an amine, a carboxylic acid, and an isocyanide (Scheme 15). So far, many articles have described various characteristics, catalysts, conditions, effects, and diversity-oriented syntheses of Ugi-4CR.⁸²

⁷⁹ Tietze, L. F. *Chem. Rev.* **1996**, *96*, 115-136.

⁸⁰ Ugi, I.; Dömling, A.; et al. *Endeavour.* **1994**, *18*, 115-122.

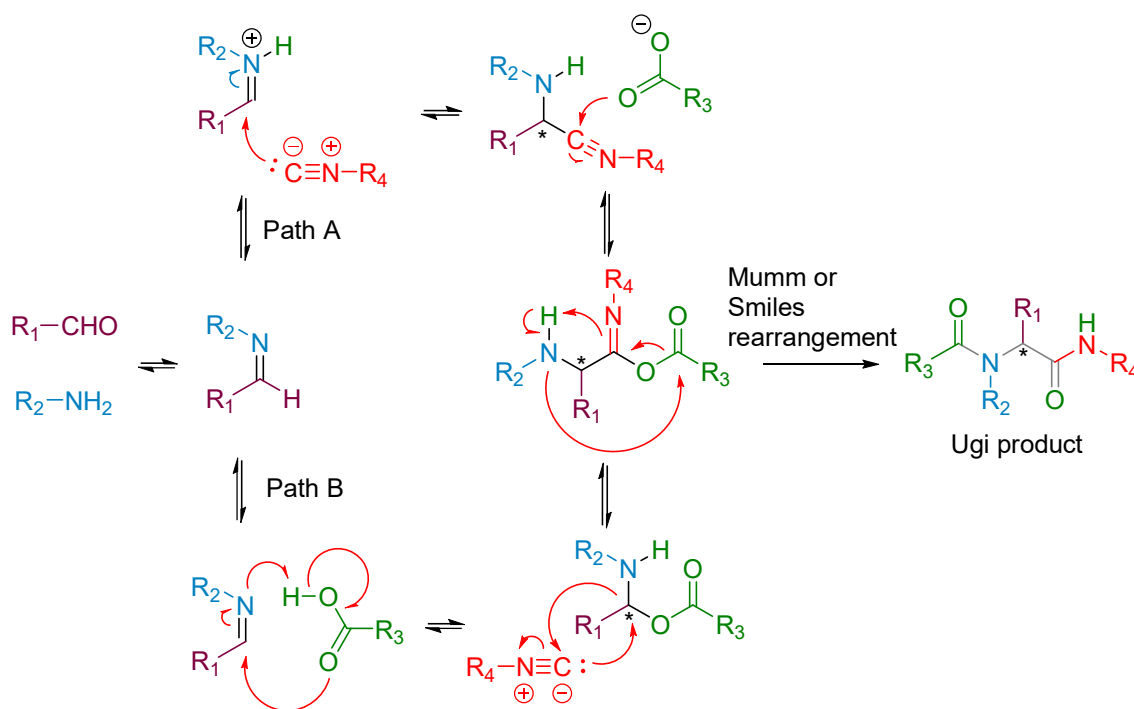
⁸¹ Ugi, I. *Angew. Chem. Int. Ed.* **1959**, *71*, 386-386.

⁸² Rocha, R. O.; Rodrigues, M. O.; et al. *ACS Omega.* **2020**, *5*, 972-979.



Scheme 15. Ugi 4 component reaction.

In general, the Ugi-4CRs are facile to conduct, but a complete understanding of the mechanisms is highly complex. This is mainly due to the possibility that several kinetic pathways may run concurrently in the same sequence. When the complexity of the multi-component system and newly generated stereo-centers are also considered, the efforts to identify the crucial parameters that will influence this MCR could be a significant challenge. This phenomenon is also general in other MCRs.⁸³



Scheme 16. Current two proposed reaction pathways observed for the Ugi-4CRs.

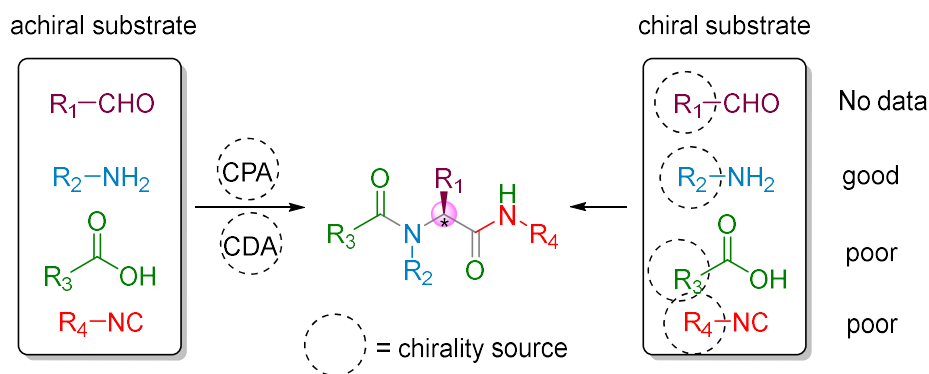
⁸³ Alvim, H. G. O.; da Silva Júnior, E. N.; et al. *RSC Adv.* **2014**, *4*, 54282-54299.

It has been proposed that the Ugi reaction has more than one reaction pathway for its transformation. Currently, the general view agrees that two mainly competitive reaction pathways can determine the direction of the Ugi-4CR (Scheme 16).⁸⁴

Both reaction pathways start from the imine generated from the condensation between the aldehyde and amine components. The imine is then activated by forming a hydrogen-bonded complex with the acidic substrate. The activated imine plays an essential role since two options could happen: either the isocyanide addition (classical view), which would produce the nitrilium ion, or the carboxylic acid insertion, which was hypothesized a few years ago and would produce the hemiaminal intermediate. Both proposals lead to the same intermediate, which proceeds through the Mumm rearrangement or Smiles rearrangement and led the final Ugi adduct.

1.3.2 Asymmetric Ugi 4 component reactions

It could be observed from Scheme 16 and 17 that the final Ugi product has a new chiral center. The challenge for effective chiral induction and control in Ugi-4CRs is considerable as well as in other MCRs.



Scheme 17. Asymmetric Ugi 4 component reactions. CPA: Chiral Phosphoric Acid; CDA: Chiral Dicarboxylic Acids.

The methodology of asymmetric control in Ugi-3CR was achieved by chiral isocyanides, which leads to a high enantiomeric excess (ee) of the corresponding product.⁸⁵ However, the attempt of chiral isocyanides or carboxylic acid in Ugi-4CR results in poor

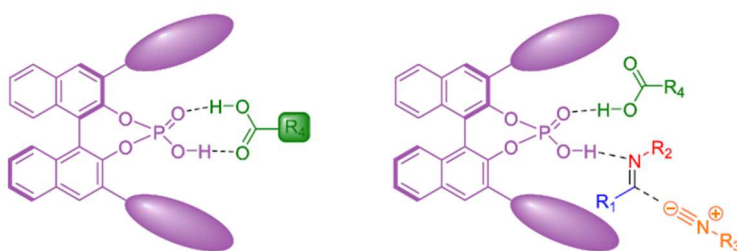
⁸⁴ a) Medeiros, G. A.; da Silva, W. A. et al. *Chem. Commun.* **2014**, 50, 338-340. b) Chéron, N.; Ramozzi, R.; et al. *J. Org. Chem. Res.* **2012**, 77, 1361-1366.

⁸⁵ Bock, H.; Ugi, I. *J. Prakt. Chem.* **1997**, 339, 385-389.

stereocontrol. The other approach from chiral amines, such as α -methylbenzylamines,⁸⁶ α -ferrocenylethylamines,⁸⁷ and α -aminoesters⁸⁸ usually yield a moderate stereoselectivity at room temperature, which can be higher at around -70 °C. Since the condensed product of enantiopure amine and aldehyde would inherit the chirality from amine. Optical active imines were also investigated as an excellent chiral auxiliary to promote the asymmetric Ugi 3 component reaction⁸⁹ and Ugi-4CR.

Besides those chiral substrate materials, asymmetric Ugi-4CR (Asy Ugi-4CR) could also be achieved by introducing chiral ligands. For instance, CPA (Chiral Phosphoric Acid)⁹⁰ found by Zhang et al and CDA (Chiral Dicarboxylic Acids)⁹¹ were two newly discovered catalysts to yield high enantioselectivity from achiral substrates.

In the case that uses CPA as a chiral catalyst, the enantiomer excess of the Ugi outcomes could reach 99% ee in the S configuration and 96% ee in the R configuration. DFT(Density Functional Theory) calculations supported the results. It was emphasized the significance of noncovalent interactions in the transition state for effective chiral transmission and transformation success.



Scheme 18. (Left) A proposed heterodimerization method for activating carboxylic acids using CPAs. (Right) A heterotrimer complex is produced by imide activation from the heterodimer generated between the CPA and the carboxylic acid reagent.⁹²

⁸⁶ Kelly, C. L.; Lawrie, K. W. M.; et al. *Tetrahedron Lett.* **2000**, *41*, 8001-8005.

⁸⁷ Demharter, A. Ugi, I. *J. Prakt. Chem.* **1993**, *335*, 244-254.

⁸⁸ Sung, K.; Chen, F.L.; et al. *Mol. Divers.* **2003**, *6*, 213-221.

⁸⁹ Banfi, L.; Basso, A.; et al. *Tetrahedron Lett.* **2004**, *45*, 6637-6640.

⁹⁰ Zhang, Y.; Ao, Y. F.; et al. *Angew. Chem. Int. Ed.* **2016**, *55*, 5282-5285.

⁹¹ Hashimoto, T.; Kimura, H.; et al. *Angew. Chem.* **2012**, *124*, 7391-7393.

⁹² Zhang, J.; Yu, P., *Science*. **2018**, *361*, eaas8707.

1.3.3 Ugi 4 component reactions in the polymerization

Ugi 4-CRs could be a feasible method in polymer chemistry according to three possibilities: monomer synthesis,⁹³ polycondensation, and Post-Polymerization Modification (PPM).⁹⁴

As a type of step-growth polymerization, polycondensation is the direct utilization of Ugi-4CRs as a binding reaction for monomers to join together and lose one equivalent of water. The first approach to the synthesis of a variety of substituted Ugi-type polypeptoids via Ugi-4CR was achieved by Meier et al. in 2014.⁹⁵

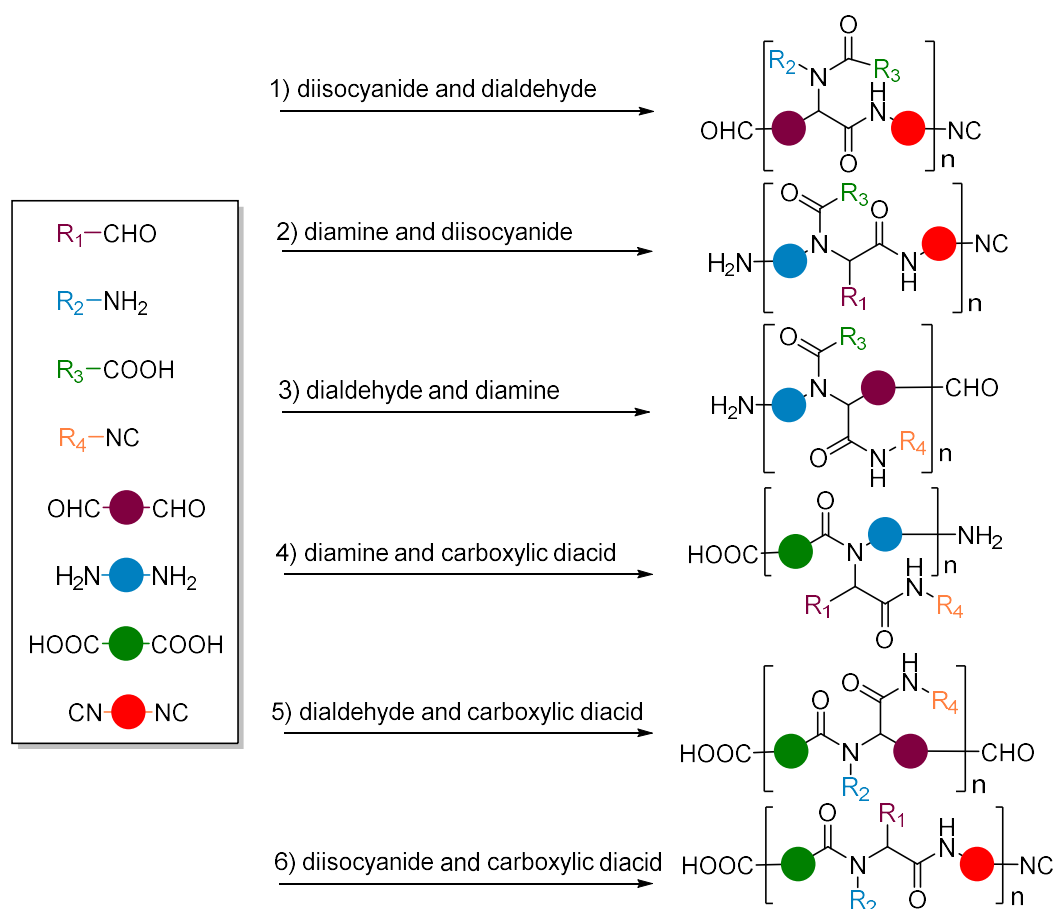


Figure 17. Six possible monomer combinations of linear Ugi-4CR polymerizations.

In this research, the goal was focused on the preparation of linear polypeptoids using Ugi-4CR. Only two bifunctional AA-type components and two monofunctional components were considered as the monomer, which resulted in six possible monomer combinations: 1) diisocyanide and dialdehyde (+ amine + carboxylic acid); 2) diamine and diisocyanide;

⁹³ Robotham, C. V.; Baker, C.; et al. *Mol. Divers.* **2003**, *6*, 237-244.

⁹⁴ Yang, B.; Zhao, Y.; et al. *Polym. Chem.* **2014**, *5*, 2704-2708.

⁹⁵ Schlinger, A.; Dannecker, P.-K.; et al. *Macromolecules.* **2014**, *47*, 2774-2783.

3) dialdehyde and diamine; 4) diamine and carboxylic diacid; 5) dialdehyde and carboxylic diacid; 6) diisocyanide and carboxylic diacid (Figure 17).

To ensure a smooth Ugi reaction and the solubility of the resulting polymers, a mixture of methanol and tetrahydrofuran were used to produce Ugi-type condensed polypeptoids with molecular weights of up to 18 kDa. Notably, the aldehyde component must have a blocked position to prevent the Ugi reaction's byproducts and obtain polymers with high molecular weights. In addition, since water was reported to accelerate the reaction, *N*-methyl-2-pyrrolidone (NMP) was used as a solvent to conduct the Ugi-4CR polymerization in the presence of water.⁹⁶ As a variant, Ugi five-component condensation (Ugi-5CC) yielding *N*-(alkoxycarbonyl) amino amides by reacting carbon dioxide with an alcohol (usually methanol), an isocyanide, an oxo-component (aldehyde or ketone), and a primary amine, has also been tested in polycondensation reactions to produce Ugi-type polypeptoids with a molecular weight around 20 kDa.⁹⁷

The high efficiency of Ugi-4CRs makes it possible to be a candidate for Click reaction and be employed in the PPM (Figure 18). Tao et al.⁹⁴ applied the Ugi-4CRs to the polymer conjugation process and prepared functional block copolymers from two pre-synthesized polymers: a benzaldehyde terminated polymethylmethacrylate (PMMA) and an aniline-terminated methoxypolyethylene glycol (mPEG). The NMR and GPC results show that fluorescent or other reactive groups in the middle chain have been successfully introduced.

⁹⁶ Gangloff, N.; Nahm, D.; et al. *Polym. Chem.* **2015**, *53*, 1680-1686.

⁹⁷ Sehlinger, A.; Schneider, R.; et al. *Macromol. Rapid Commun.* **2014**, *35*, 1866-1871.

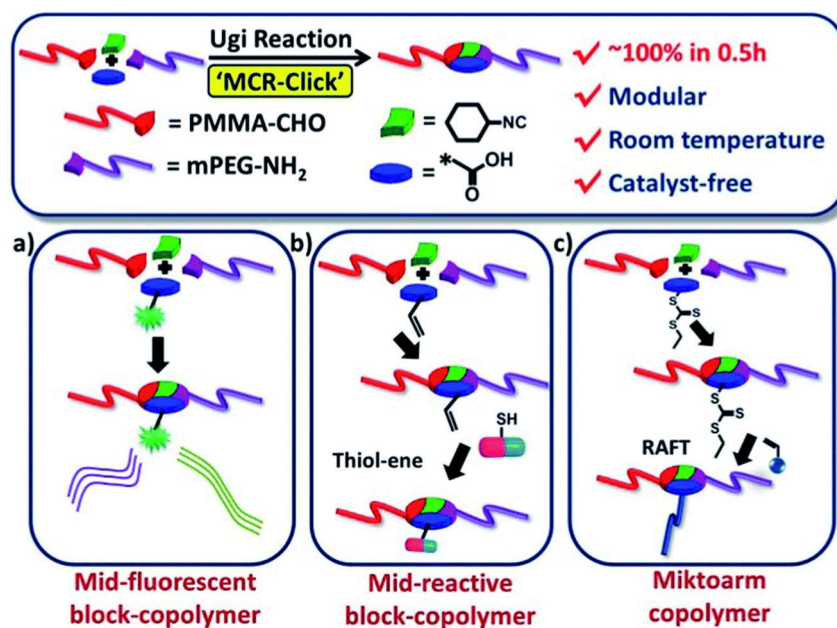


Figure 18. Ugi-4CR polymerizations and its Click features. (a) Block copolymer that is mid-fluorescent. (b) Modification of a mid-reactive block copolymer using the thiol-ene click reaction. (c) Miktoarm star copolymer was created through the union of raft polymerization with Ugi-type polymer conjugation, reproduced from ref 94.

In conclusion, multi-functional polymers can be easily synthesized by applying Ugi-4CR polymerizations.⁹⁴ Though the study has just started, the increasing action of Ugi-4CRs and other MCRs applications in macro molecules or polymer areas has paved an innovative approach for creating a new class of polymers that might not be achievable by other reactions in a straightforward way.

CHAPTER II
HELIX SENSE CONTROLLED
POLY(ISOCYANIDES) VIA COORDINATE
POLYMERIZATION

2.1 OBJECTIVES

The main objectives of the first part of the present PhD project have been the following:

- i*) To generate poly(isocyanides) possessing helical chirality by introducing unnatural proline derivatives. To this end, the following items have been synthesized:
 - i-1*) Enantioselective synthesis of densely substituted prolines via (3+2) cycloadditions between imines (as azomethine ylide precursors) and nitroalkenes (as π -deficient dipolarophiles).
 - i-2*) Synthesis of enantiopure isocyanides incorporating the unnatural proline derivatives synthesized in (*i-1*).
 - i-3*) Synthesis of poly(isocyanides) in Ni(II) catalyzed polymerization of monomer obtained as indicated in (*i-2*).
- ii*) To determine the structure-chirality relationship according to the *endo* or *exo* structure of the (3+2) cycloadditions indicated in (*i-1*), (*i-2*) and (*i-3*).

2.2 DENSELY SUBSTITUTED PROLINES AS MONOMERS

Densely substituted prolines have been described by our research group as effective asymmetric organocatalysts to promote many enantioselective reactions and polymerizations. For example, aldol reaction between cyclohexanone and aromatic aldehydes,⁹⁸ Michael additions of ketones to nitroalkenes,⁹⁹ and ring-opening polymerization of *rac*-Lactide.¹⁰⁰

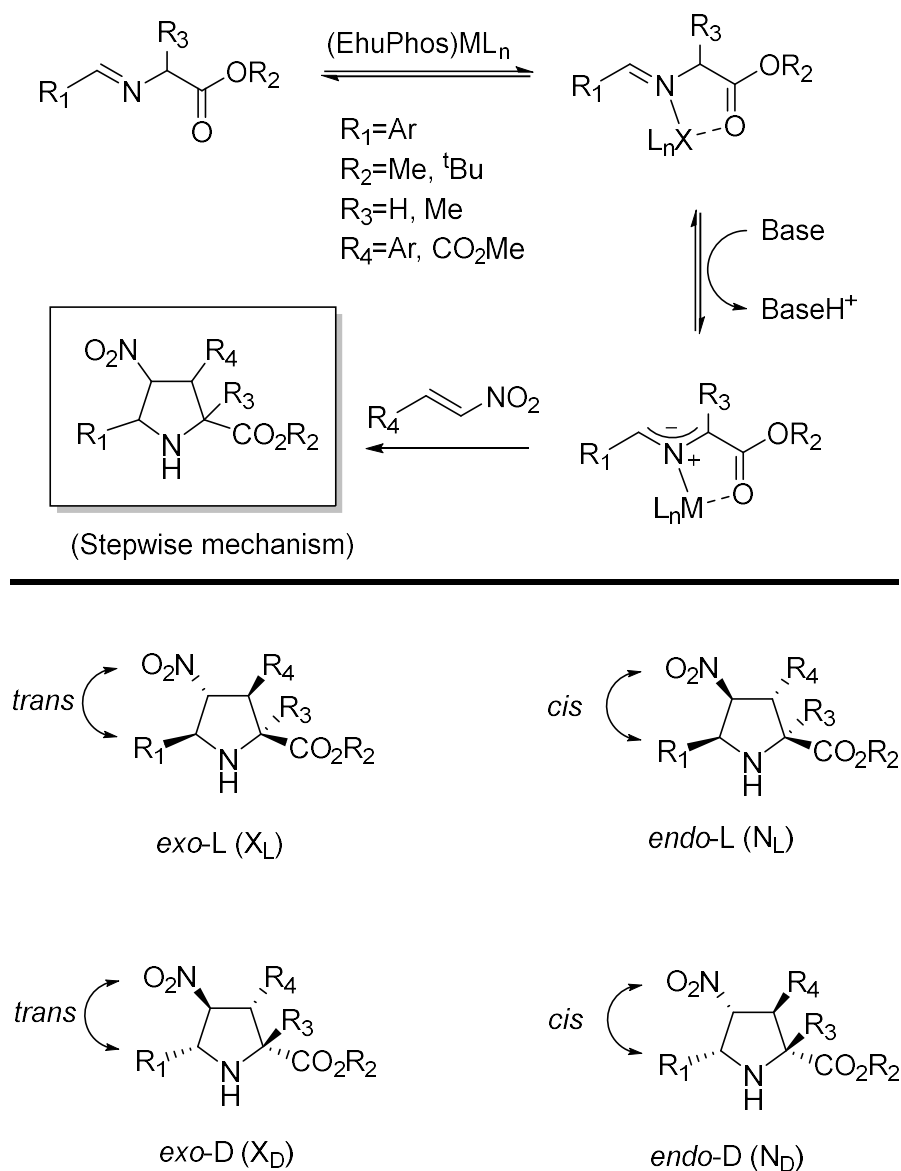
These unnatural prolines are obtained by means of a family of catalysts termed EhuPhos (from Euskal Herriko Unibertsitatea) and can yield at will *endo* or *exo* (3+2) cycloadducts belonging to the L- and D-series (Scheme 19).

In *endo* (3+2) cycloadducts, the nitro and R₁ groups are in a *trans* relationship, whereas in the *endo* cycloadducts these substituents are *cis* to each other.

⁹⁸ Conde, E.; Bello, D.; de Cózar, A.; Sánchez, M.; Vázquez, M. A.; Cossío, F. P. *Chem. Sci. J.* **2012**, *3*, 1486-1491.

⁹⁹ Ruiz-Olalla, A.; Retamosa, M. D. G.; & Cossio, F. P. *J. Org. Chem.* **2015**, *80*, 5588-5599.

¹⁰⁰ Sanchez-Sanchez, A.; Rivilla, I.; Agirre, M.; Basterretxea, A.; Etxeberria, A.; Veloso, A.; Cossio, F. P. *J. Am. Chem. Soc.* **2017**, *139*, 4805-4814.

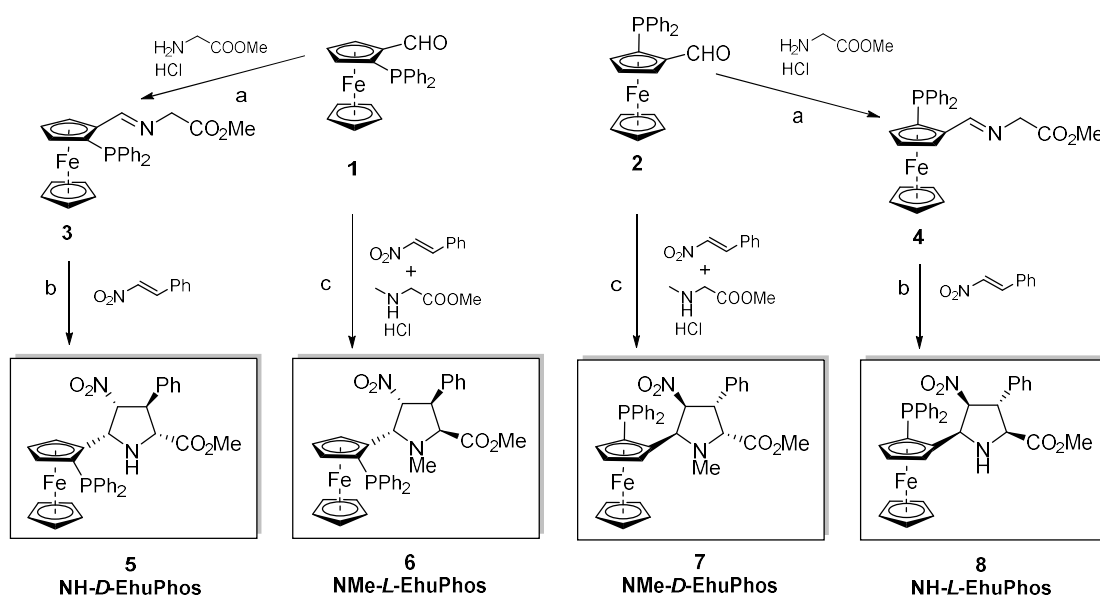


Scheme 19. Synthesis of densely substituted prolines via (3+2) cycloaddition and *exo/endo* – D/L naming rules.

2.2.1 Synthesis of ferrocenyl-proline EhuPhos catalysts

The synthetic procedure of ferrocenyl-proline catalysts, prolines, and modified prolines will be discussed in this subsection. The chemical synthesis of the different EhuPhos catalysts has been previously described in our research group.¹⁰¹ Ultimately, these synthesis rely on the two enantiomers of phosphinoferrocenyl aldehyde (**1** and **2**), obtained according to the method developed by Kagan et al.¹⁰²

Four different configurations of densely substituted prolines, four types of chiral ferrocene-prolines: **NH-D-EhuPhos** (**5**), **NMe-L-EhuPhos** (**6**), **NMe-D-EhuPhos** (**7**), and **NH-L-EhuPhos** (**8**) should be introduced as the chiral ligand.



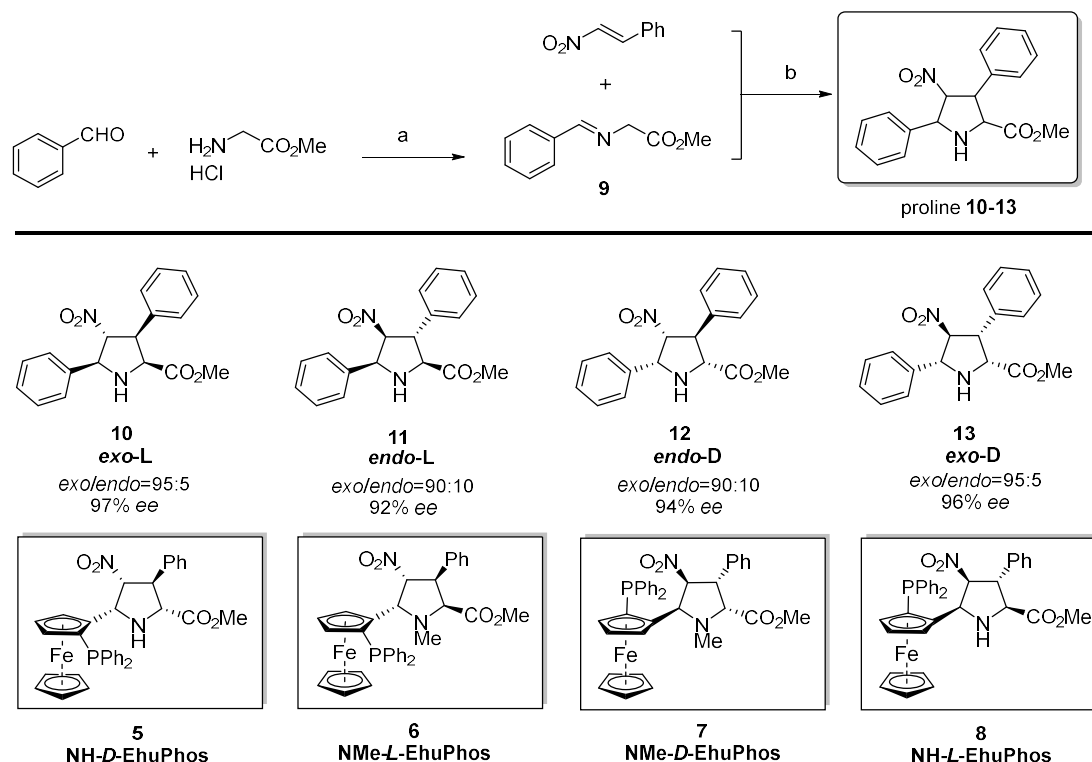
Scheme 20. Synthesis of chiral EhuPhos catalysts **5-8** from chiral aldehydes **1** and **2**. Reagents and conditions: a) glycine methyl ester hydrochloride (0.38 g, 3.0 mmol), MgSO_4 , Et_3N (0.4 mL, 3.0 mmol), dry DCM (10 mL), aldehyde **1** or **2** (1.00 g, 2.5 mmol), rt, 20 h; b) imine **3** or **4** (0.49 g, 1.0 mmol), trans- β -nitrostyrene (0.18 g, 1.2 mmol), Et_3N (0.14 mL, 1.0 mmol), LiBr (0.14 g, 1.6 mmol), dry THF (10 mL), rt, 2 h 45 min; c) aldehyde **1** or **2** (0.52 g, 1.3 mmol), sarcosine methyl ester hydrochloride (0.24 g, 1.7 mmol), trans- β -nitrostyrene (0.25 g, 1.7 mmol), Et_3N (0.24 mL, 1.7 mmol), MgSO_4 , toluene (20 mL), reflux, 7 h.

From chiral aldehydes **1**, ferrocenyl-proline catalyst **5** was synthesized through two step route. Firstly, imine intermediate **3** was isolated after condensation of (*R*)-1-(diphenylphosphino)-2-formylferrocene **1** with glycine methyl ester hydrochloride.

¹⁰¹ Retamosa, M. de G.; Ruiz-Olalla, A.; Agirre, M.; de Cózar, A.; Bello, T.; & Cossío, F. P. *Chem. Eur. J.* **2021**, *27*, 15671-15687.

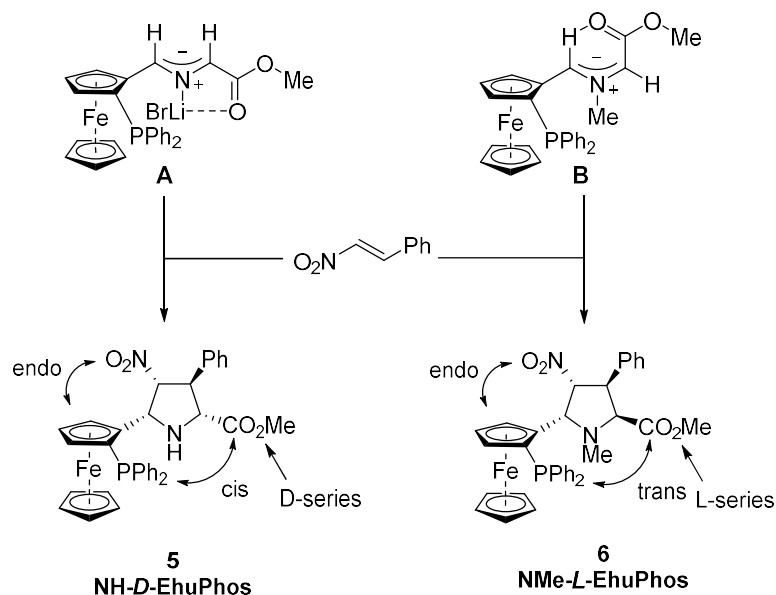
¹⁰² Riant, O.; Samuel, O.; Flessner, T.; Taudien, S.; & Kagan, H. B. *J. Org. Chem. Res.* **1997**, *62*, 6733-6745.

Subsequently, (3+2) cycloaddition reaction of intermediate imine **9** with trans- β -nitrostyrene was conducted in the presence of LiBr (Scheme 20).



Scheme 21. Synthesis of four types of densely substituted prolines via chiral EhuPhos catalysts. Reaction conditions: a) Glycine methyl ester hydrochloride (3.0 mmol, 376.6 mg), Et₃N (3.0 mmol, 420 μ L), MgSO₄, dry DCM (5 mL), benzaldehyde (2.3 mmol, 234 μ L), rt, 16 h. b) Ferrocene-proline ligand **5** - **8** (0.015 mmol, 9.27 mg), Cu(CH₃CN)₄PF₆ (5.2 mg, 0.014 mmol), Et₃N (0.023 mmol, 3.2 μ L), imine **9** (0.45 mmol, 80 mg), trans- β -nitrostyrene (0.50 mmol, 75 mg), dry THF (3 mL), temperature (-20°C for proline **10** and **13**, -80°C for proline **6** and **7**), 48 h.

EhuPhos catalyst **6**, the **NMe-L-EhuPhos** (Scheme 21), was prepared from a three-component reaction of the same chiral ferrocene aldehyde **1** with methyl ester hydrochloride and trans- β -nitrostyrene.



Scheme 22. Formation of NH-D and NMe-L EhuPhos catalysts.

Formation of catalyst **NH-D-EhuPhos** is consistent with the formation of azomethine ylide **A**, in which the phosphinoferrocenyl and the methoxy carbonyl groups are in a *cis* relationship generated by the C=O---Li stabilizing interaction. In contrast, formation of **NMe-L-EhuPhos** stems from azomethine ylide **B**. In this latter case, the steric clash between the *N*-methyl and methoxycarbonyl groups generate a *trans* configuration that is preserved in the final cycloadduct. Using the same reaction condition but changing the ferrocene aldehyde configuration to (1*S*)-1-(Diphenylphosphino)-2-formylferrocene, two more ferrocene-prolines **7** and **8** were obtained via the same synthetic route.

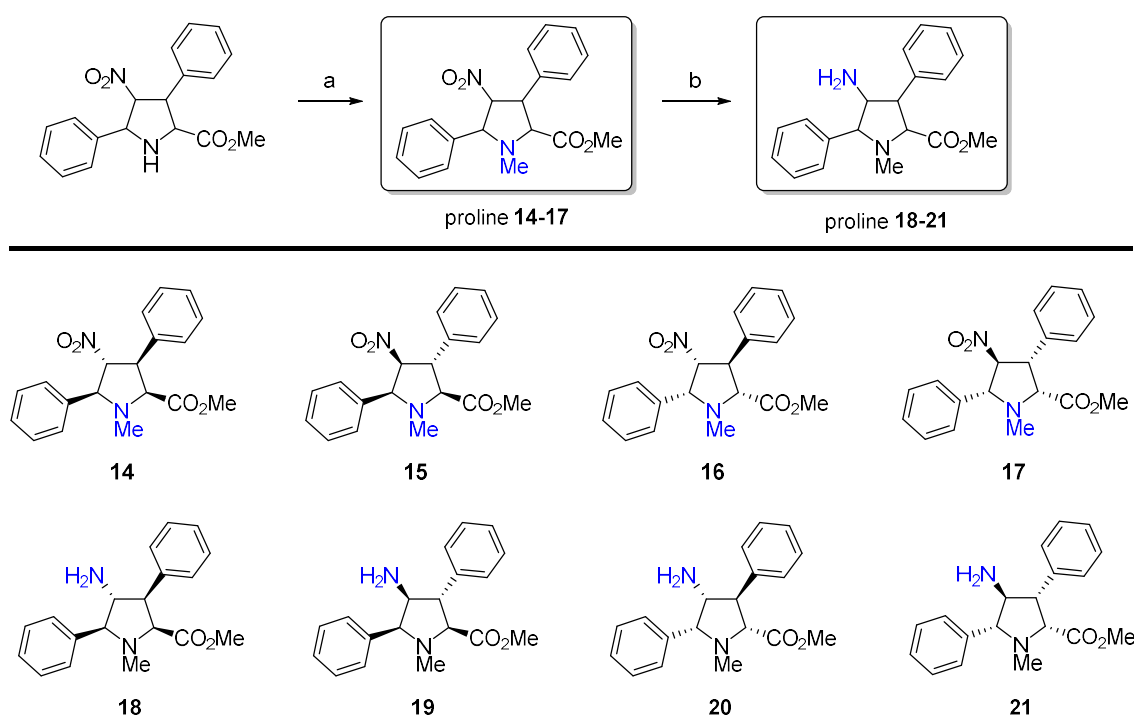
These ferrocenyl-prolines were able to catalyze asymmetric synthesis reactions such as heterocyclic substrates in the reaction with ethyl diazoacetate.¹⁰³ Owing to the significant steric hindrance, the four types EhuPhos catalysts show excellent enantioselectivity in the asymmetric (3+2) cycloaddition of olefins with imines in the presence of [Cu(CH₃CN)₄]PF₆ as a metallic salt catalyst. Therefore, the EhuPhos [Cu(CH₃CN)₄]PF₆ system was introduced to synthesize densely substituted unnatural prolines.

Imine **9** (Scheme 21) was obtained by condensation between benzaldehyde and glycine methyl ester hydrochloride as a starting material. This imine was consumed in the following (3+2) cycloaddition with *trans*- β -nitrostyrene. The ferrocenyl-proline [Cu(CH₃CN)₄]PF₆ systems were employed in this cycloaddition, and four kinds of

¹⁰³ Lacambra, A. *Novel methods for stereocontrolled cycloaddition/dearomatization reactions under catalytic conditions*. 2017. Doctoral Thesis, Université de Bordeaux.

densely substituted prolines were obtained respectively in high yields and optical purity. As described in the previous articles, the asymmetric catalytic activity raised from the steric hindrance brought by methyl ester and phenyl groups. After this cycloaddition, the γ -nitro group was functionalized to proceed with the subsequent steps.

These modifications started from the secondary amine protection with a methyl group to prevent the possible formamidation in the two nitrogens. As described in the literature,⁹⁸ the methylation reaction was carried out with trioxane, triethyl silane, and trifluoroacetic acid in DCM. After this general process, the isolated methylated prolines **14-17** were obtained.



Scheme 23. Modifications of densely substituted prolines. Reaction conditions: a) Densely substitute prolines **10 - 13** (1 mmol, 326 mg), 1,3,5-trioxane (3 mmol, 270 mg), TFA (10 mmol, 0.77 mL), Et_3SiH (10 mmol, 1.60 mL), DCM (1.6 mL), rt, 48 h. b) H-Cube[®] Pro hydrogenation flow reactor, Raney Nickel (batch number N0618, product ID THS-01112), prolines **14 - 17**, 4 mg/mL in MeOH, flow rate: 1 mL/min, 40 °C, 20 bar.

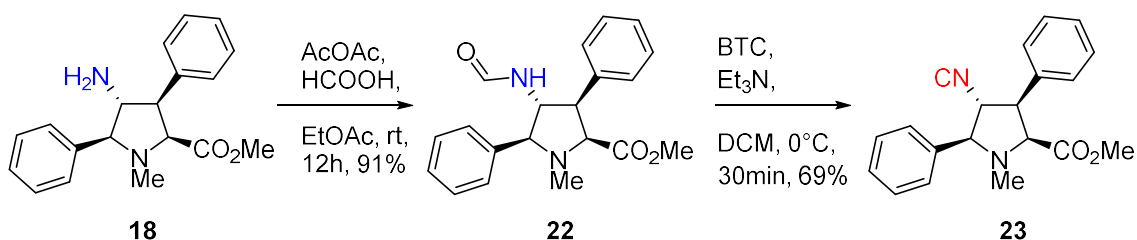
In order to obtain the desired isocyanide monomers, two transformations of γ -nitroprolines were required (Scheme 23). First, *N*-methylation of the NH secondary amine moiety was carried out in the presence of trifluoroacetic acid and triethylsilane. The resulting γ -nitro- *N*-methyl prolines were reduced to the corresponding primary amines by hydrogenation (H_2 , 20 bar) in the presence of Raney Nickel as heterogeneous catalyst

in methanol at 40 °C under flow conditions (1 mL/min). Under these smooth reaction conditions, no noticeable isomerization of the starting γ -nitro-*N*-methyl proline ester was observed.

2.2.2 Chemical synthesis of chiral γ -isocyano-prolines

We adopted the general synthetic route, consisting of formamidation from the starting amine group and subsequent dehydration. In the first step, only *exo*-L proline **18** was utilized as an example to verify the feasibility of this method. The formamide proline derivatives could be obtained from either the condensation of amine with formic acid or the transesterification of formate. Both methods were tried out in order to optimize the formamidation. In the condensation with formic acid all the starting materials were consumed after 12 hours of mixing at room temperature.

In contrast, the transesterification with methyl formate resulted in poor conversion. Furthermore, pre-mixing the formic acid and acetic anhydride neat at 60 °C, followed by addition to the reaction mixture, promoted the formamidation reaction with a high yield of 91%. The optimized formamidation procedure yielded in proline **22** as a white solid without further purification (Scheme 24).



Scheme 24. Synthetic route from amine formed proline **18** to isocyanide formed proline **23**.

From the $^1\text{H-NMR}$ spectrum shown in Figure 20, the formamide proton (marked as green) could be observed at 8.05 ppm, indicating that the formamidation had been successfully conducted. Interestingly, the $^1\text{H-NMR}$ spectrum of γ -formamide **22** is split in two ensembles of signals, most likely associated with the coexistence of two rotamers distributed about the formamide group. Monte Carlo simulations using the MMFF94 force field¹⁰⁴ showed different conformers depending on (i) the rotamery of the formamide group; (ii) envelope of half-chair conformation of the pyrrolidine ring. These

¹⁰⁴ a) Halgren, T. A. *J. Comput. Chem.* **1999**, *20*, 720-729. b) Halgren, T. A. *J. Comput. Chem.* **1996**, *17*, 490-519.

different conformation result in different positions of the *N*-methyl and methoxycarbonyl groups, as well as those of the phenyl group and the C-H groups at C1-C4 (Figure 19).

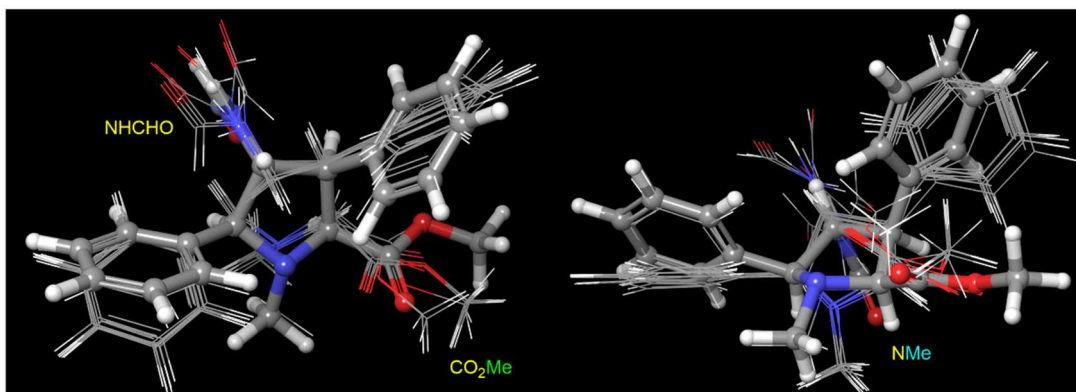


Figure 19. Monte Carlo conformer distribution of γ -formylpyrrolidine **22**, computed with the MMFF94 Molecular Mechanics force field. Among the 400 conformations explored, those within 4kJ/mol are shown. The differences in formyl, ester, phenyl and half-chair/envelope conformations are highlighted.

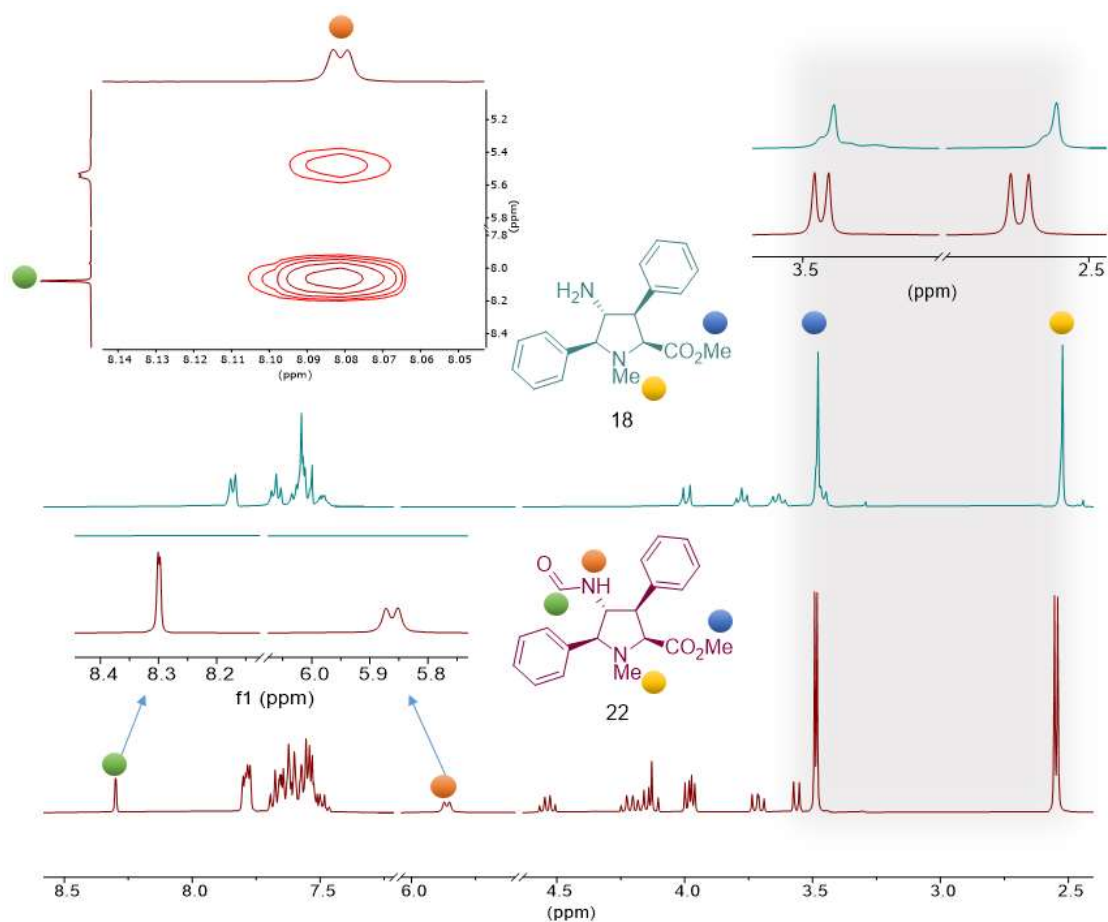
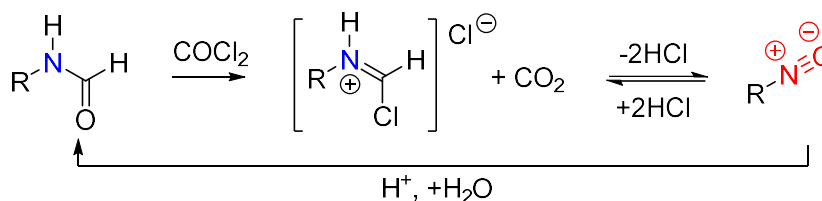


Figure 20. $^1\text{H-NMR}$ and COSY spectra of γ -amino proline **18** and γ -formamide derivative **22** in CDCl_3 . The split of the protons corresponds to the two methyl groups in both cases, and the proton of the aldehyde group in compound **22**, could be observed.

Three phosgene molecules were generated by decomposition reaction of BTC under basic conditions in DCM. The phosgene is a very active electrophile that could initiate electrophilic substitution with the formamide and result in iminium and CO₂. Under these conditions, the proton and chloride from the iminium were deprived, and nitrogen and the terminal carbon atom were left to form the corresponding isocyanide. After a series of workup and purification procedures, the product was obtained and characterized by ¹H-NMR, ¹³C-NMR, MS and FTIR. The strong and clear peak at 2150 cm⁻¹ corresponds to the vibration of the -C≡N bond, which confirmed the successfully installation of the isocyanide group in the proline ring.

According to our experience, the isocyanide product was a sensitive and toxic compound with an irritating odor. For some small molecular isocyanides, the low boiling point may cause the odor to be even stronger, so the total synthesis process should go under ventilation. Even though it was obtained from the dehydration of formamide, the isocyanide is quite stable in water under basic or neutral conditions, but was unstable under acidic conditions, as the reverse reaction to form the iminium salt would take place in acid media (Scheme 25). Fortunately, the purification in an acid silica column would not cause too much loss of isocyanide in most cases. If the products were susceptible to acid environments, a neutral aluminum column could be used to purify them.



Scheme 25. Reaction mechanisms of formamide to isocyanide under phosgene type dehydration.

The isocyanate proline **23** was a white crystal, unlike the amino-type proline or formamide-type proline. We then sent the crystal for analysis by X-ray diffraction. As can be seen in Figure 21, the oak ridge thermal-ellipsoid plot program (ORTEP) diagram for compound **23** shows a bond angle close to 180°, which corresponds to the geometry of a triple bond. This kind of straight C-C≡N bond has also been reported in another isocyanide compounds.¹⁰⁵

¹⁰⁵ Yamamoto, Y.; Aoki, K.; et al. *Inorg. Chem.* **1979**, *18*, 1681–1687.

Besides, the distance between nitrogen and carbon was 1.14 Å. The bond length of the isocyanide proline **23** is shorter compared to another isocyanide (methyl isocyanide: 1.158 Å), which is compatible with stronger interaction between nitrogen and carbon.

Density Functional Theory (DFT, B3LYP-D3BJ/6-31+G* level of theory),¹⁰⁶ calculations showed a geometry for **23** compatible with the X-ray structure. In particular, the linear arrangement between the isocyanide group and the C-4 atom indicated that the zwitterionic resonance bond is largely the most important one (Figure 21, A). Moreover, analysis of the electrostatic potential projected on the electron density (Figure 21, C) showed a considerable negative potential energy on the terminal carbon atom of the isocyanide group, as well as a positive charge on the formally sp hybridized nitrogen atom.

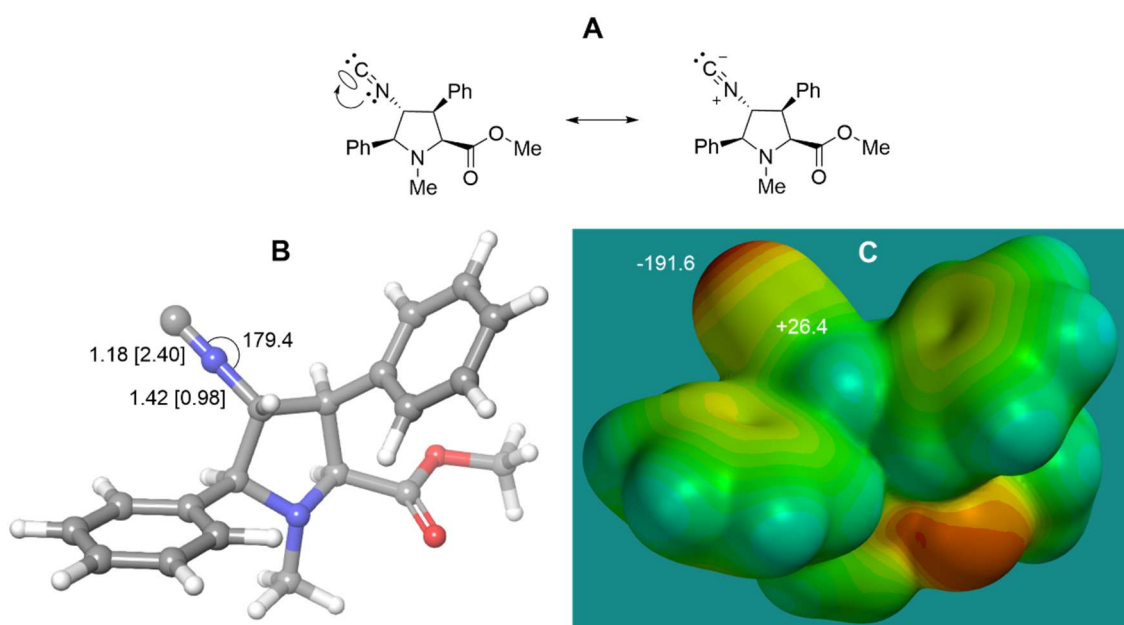


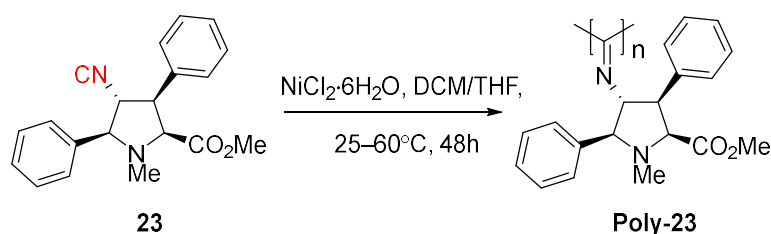
Figure 21. Electronic analysis of isocyanide **23**. (A) Main resonance forms. (B) Chief geometric features computed at the B3LYP-D3BJ/6-31+G* level of theory. Bond distances and angle are given in Å and deg., respectively. Wiberg bond indexes, computed in the Natural Atomic Orbitals basis (in atomic units) are shown in brackets (see Crystal XRD structure in annexes VI). (C) Electrostatic map projected onto electron density (isovalue: 0.02 e/bohr³). Potential energy values are given in kJ/mol.

The isocyano proline **23** was then used in the polymerization reaction. Considering the three types of polyisocyanide mechanisms, the coordination-insertion mechanism is the

¹⁰⁶ a) Becke, A. D. *J. Chem Phys.* **1993**, *98*, 5648-5652. b) Lee, C.; Yang, W.; Parr, R. G. *Phys. Rev. B.* **1988**, *37*, 785-789. c) Vosko, S. H.; Wilk, L.; Nusair, M. *Can. J. Phys.* **1980**, *58*, 1200-1211. d) Stephens, P. J.; Devlin, F. J.; Chabalowski, C. F.; Frisch, M. J. *J. phys. Chem.* **1999**, *98*, 11623-11627. e) Grimme, S.; Ehrlich, S.; Goerigk, L. *J. comput. Chem.* **2011**, *32*, 1456-1465.

easiest to implement: the initiator of the cationic process mechanism is commercially available, whereas the catalyst of living polymerization requires a long synthetic route. Thus, coordination-insertion cationic methods were chosen. In particular, $\text{NiCl}_2 \cdot 6\text{H}_2\text{O}$ was selected as the catalyst for coordination insertion polymerization. Alternatively, $[\text{Ph}_3\text{C}][\text{B}(\text{C}_6\text{F}_5)_4]$ was checked as the initiator of cationic polymerization. As far as the Ni(II)-catalyzed reaction is concerned, several researchers have reported that oxygen could accelerate the polymerisation as O_2 could keep the nickel center fixed in +2 oxidation state, whereas the excess amount of isocyanide could reduce it to Ni(I).⁶⁵ In order to test this hypothesis, we pre-set both argon and atmosphere environments for the nickel polymerization.

Table 3. Ni(II)-catalyzed polymerization of isocyanide proline **23** under different conditions.



entry	Solvent	T (°C)	Mn (g/mol)	Mw (g/mol)	PDI ^a
1 ^b	DCM	25	1792	4225	2.4
2 ^c	DCM	25	1647	4278	2.6
3 ^c	THF	25	<1000	<1000	NA
4 ^c	THF	60	<1000	<1000	NA
5 ^c	MeOH	25	<1000	<1000	NA

^a Mn and Mw were measured by GPC with toluene as standard and THF as eluent. Mn is referred to number average molecular weight and Mw weight averaged molecular weight. The polymer dispersity index (PDI) is a value of Mw/Mn. When a polymer material is under reasonable control in its polymerization, the chain tends to generate the same length, in this case, the value of Mn and Mw would be similar, and the PDI would be close to 1. Reaction conditions: ^b under Ar atmosphere. ^c Under air. Catalyst: $\text{NiCl}_2 \cdot 6\text{H}_2\text{O}$; 48 h.

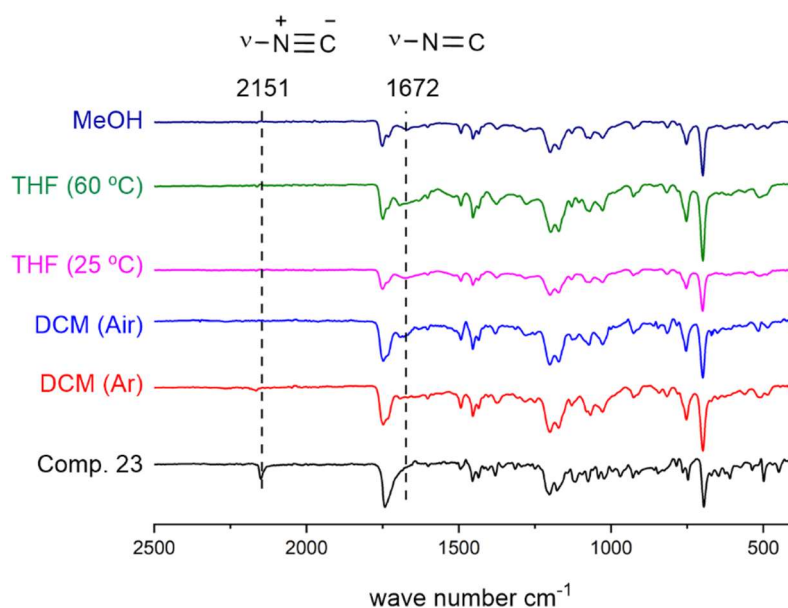
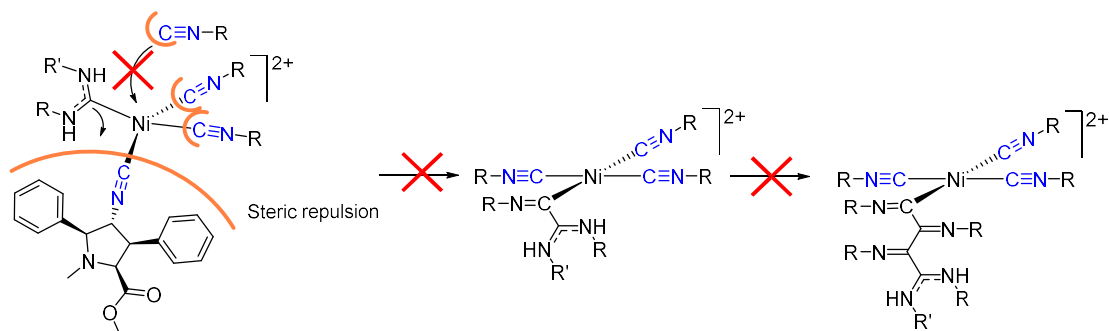


Figure 22. FTIR spectrum of **poly-23** obtained from under several reaction conditions.

The different polymerization experiments were carried out at room temperature and under stirring for over 48 hours to reach the highest possible conversion. In the infrared spectrum (Figure 22), we can observe that the peak corresponding to the isocyanide group at 2150 cm^{-1} was displaced by a peak at 1682 cm^{-1} in $\text{NiCl}_2 \cdot 6\text{H}_2\text{O}$ catalyzed polymerization, which corresponds to the stretching vibration of iminic $\text{C}=\text{N}$ bond. The polymerization reaction did not proceed in solvents different to DCM, such as THF and methanol (Table 3). In contrast, no polymerization reaction was observed by FTIR and NMR when $[\text{Ph}_3\text{C}][\text{B}(\text{C}_6\text{F}_5)_4]$ was used to initiate the process.

Then, GPC was used to get more information about the obtained polymers. However, though almost all the isocyanide was converted in the reaction, only oligomers with five or six repeating units were obtained. After checking the structure of monomeric isocyanoproline **23**, we concluded that the highly congested structure of the pyrrolidine ring close to the isocyanide moiety could be responsible for the low efficiency of the polymerization process, which did not progress beyond a few oligomeric products. According to the “Merry-go-round” mechanism, the propagation steps required new insertion of isocyanide monomer. However, the steric clash in isocyanoproline **23** caused significant resistance for the insertion of monomer. Therefore, the polymerization stopped at the initial steps, and only a penta-isocyanide nickel complex was formed (Scheme 26), which could be confirmed by the molecular weight obtained from GPC (calculated: 1660.64,

measured: 1792, 1647). In the other case, from entries 3-5, the reaction was not working under these reaction conditions.

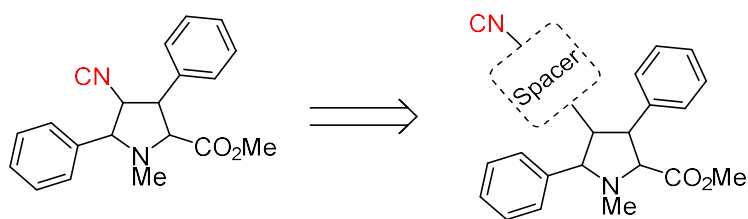


Scheme 26. The prohibition of propagation caused by the steric hindrance by the bulky substituted proline.

In conclusion, the isocyano-densely substituted proline was successfully obtained and characterized through the formamidation-dehydration sequence. The polymerization of enantiopure isocyanide **23** was attempted under Ni(II) catalysis. Our results indicate that the initiation was successful, but the propagation steps were not able to proceed due to the significant steric hindrance among the densely substituted isocyanide **23** units. Moreover, in the cationic mechanism in the presence of $[\text{Ph}_3\text{C}][\text{B}(\text{C}_6\text{F}_5)_4]$, the polymerization was neither successfully initiated nor propagated.

2.3 4-ISOCYANIDE BENZALDEHYDE AS A SPACER IN THE SYNTHESIS OF POLY(ISOCYANIDES)

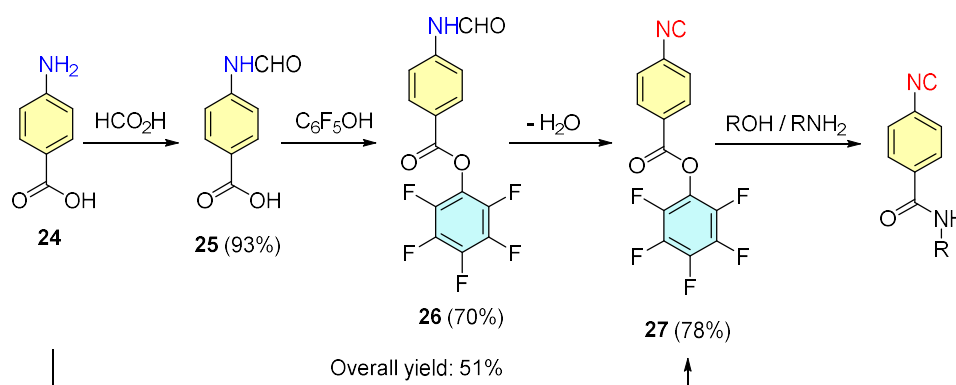
From the previous experimental result, we assumed that in the coordination polymerization of isocyanide **23**, the steric hindrance was the main reason that stopped the propagation. To attach the catalyst to the helical chain, a spacer between isocyanide group and the proline could be a suitable strategy to avoid steric repulsion (Scheme 27).



Scheme 27. A spacer introduced between isocyanide and proline substitute could reduce the steric repulsion.

In other reported examples, many researchers have adopted the 4-isocyanide benzoic acid as spacer and used it in a wide range of coordination-insertion living polymerizations, and cationic polymerizations.¹⁰⁷

According to the reported method, the preparation of this kind of spacer starts from 4-aminobenzoic acid **24**.¹⁰⁸ Formamidation of the amino group of **24** via formic acid to obtain 4-formamidobenzoic acid **25**. Then, pentafluorophenol (PFP) was used to yield pentafluorophenyl 4-formamidobenzoate **26** as an active ester. Subsequently, dehydration of **26** yields pentafluorophenyl 4-isocyanobenzoate **27** (Scheme 28). Therefore, this method introduces the active PFP group. In addition, this esterification can be carried out under mild conditions, which is more efficient than the direct condensation, and also prevents the possible racemization if chiral substituents were included.



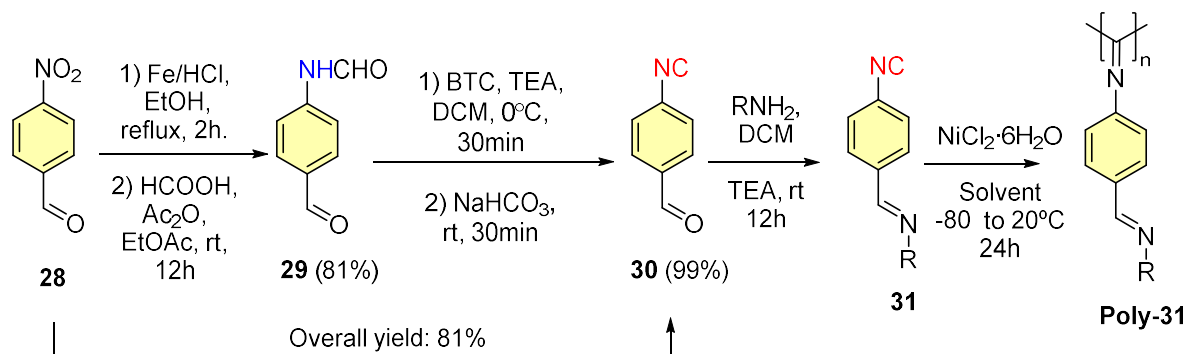
Scheme 28. Methods to introduce 4-isocyanide benzoic acid as a spacer to conduct isocyanide monomer.¹⁰⁸

However, spacer **27** required three steps, including an additional step to install the PFP group. This led to a global yield of 51%. To develop a more convenient spacer, a new method which encompasses simplicity and atom economy was envisaged. This method consists of preparing 4-isocyanide benzaldehyde **30** by means of the route gathered in Scheme 29. Thus, reduction of the nitro group of aldehyde **28** followed by reaction with formic acid yielded 4-formamidobenzaldehyde **29** in quantitative yield. Dehydration of the formamide group of this latter compound with BTC gave isocyanide **30** with 81% overall yield. Condensation of 4-isocyanobenzaldehyde with the corresponding amine led

¹⁰⁷ a) Deming, T. J. and Novak, B. M., *Macromolecules*. **1991**, *24*, 326-328. b) Su, M.; Liu, N., *Macromolecules*. **2016**, *49*, 110-119. c) Xu, A.; Hu, G., *Chem. Asian J.* **2013**, *8*, 2003-2014

¹⁰⁸ a) Zubia, A.; Mendoza, L., *Angew. Chem. Int. Ed.* **2005**, *44*, 2903-2907. b) Ramírez-Fernández, J.; Botubol, J. M., *Nat. Prod. Commun.* **2011**, *6*, 1934578X1100600404

to imines **31**, where Ni (II)-catalyzed polymerization reaction should give rise the corresponding polyisocyanide structure, denoted in Scheme 29 as **poly-31**.

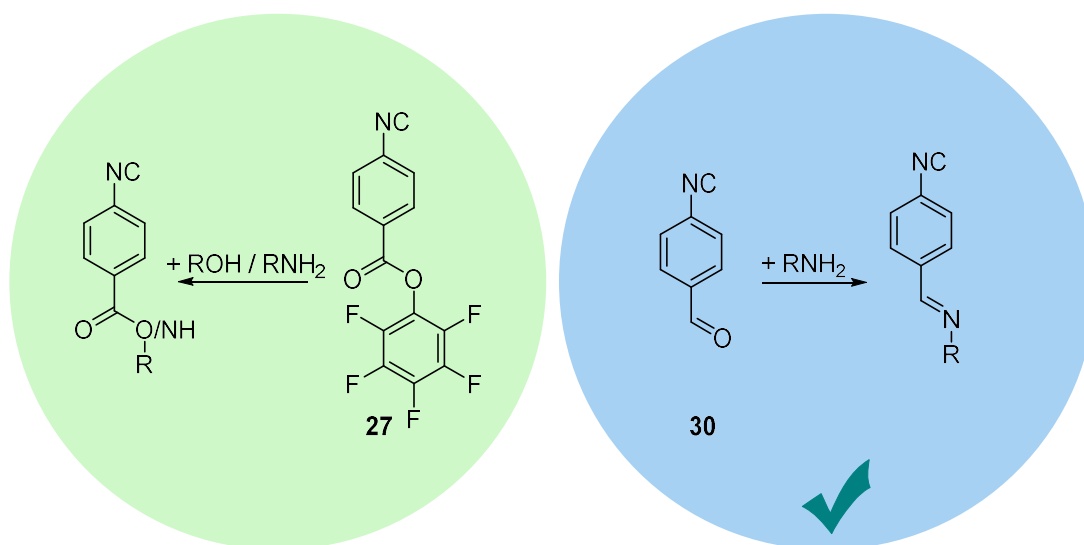


Scheme 29. Method to introduce 4-isocyanide benzaldehyde as a spacer to conduct polyisocyanide.

Therefore, according to our results, this method is superior to the previous one (Figure 23), the desired starting imine being obtained in ca. 81% overall yield, since the condensation step leading to imines **31** can be considered as quantitative.

4-isocyano benzoic acid spacer **27**

4-isocyano benzaldehyde spacer **30** (this work)



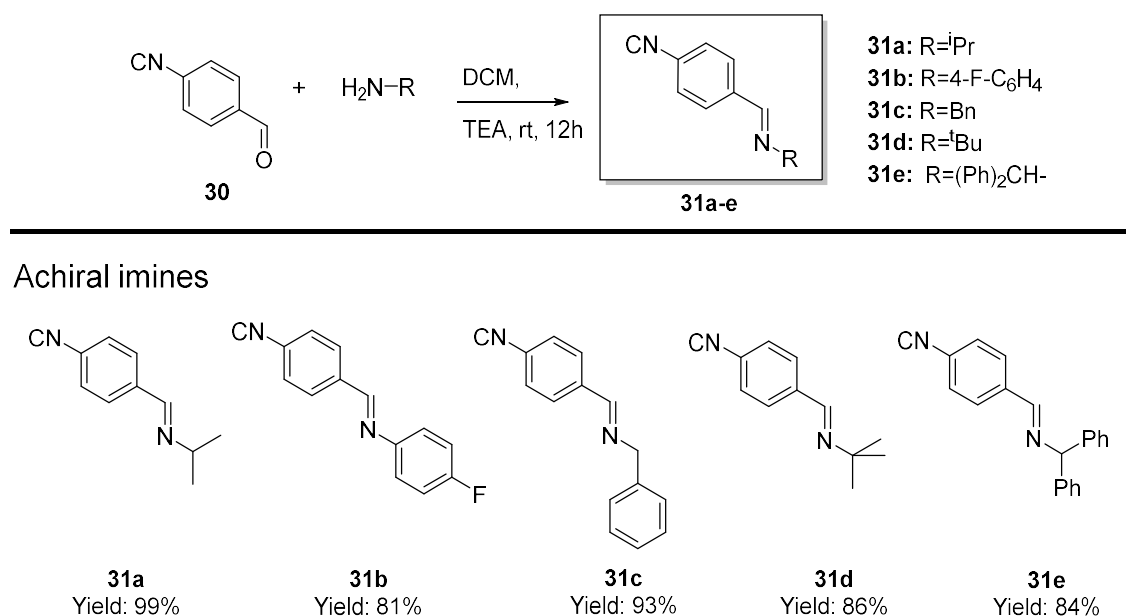
3 steps in preparation and 51% global yield 2 steps in preparation and 81% global yield

Figure 23. Comparison between 4-isocyano benzoic acid spacer **27**¹⁰⁸ and 4-isocyano benzaldehyde spacer **30**.

The obtained 4-isocyanide benzaldehyde **30** was a transparent light yellow crystal. After several preparations of this product, we found that it was unstable when store at room temperature. However, the ¹H-NMR analysis did not show remarkable differences after being kept in the freezer for one year.

2.3.1 Isocyanide monomer synthesized from 4-isocyanide benzaldehyde spacer

The previously prepared spacer was then utilized in different condensation reactions with commercially available amines to study the scope of the reaction. As indicated below (Scheme 30), achiral amines such as isopropylamine, 4-fluoroaniline, benzylamine, tert-butylamine, and benzhydrylamine were selected. The corresponding imines were obtained in good yields and purity after workup. Therefore, these imino isocyanide monomers **31a-e** could be directly used in the subsequent polymerization reaction. However, all our attempts to synthesize the imines **31** derived from aniline, tritylamine and α -benzylphenethylamine went with no success. In the case of the reaction with aniline, the $^1\text{H-NMR}$ spectrum showed an ensemble of broad signals, whilst the spectra of the crude reaction mixtures after reaction with tritylamine and α -benzylphenethylamine showed no significant conversion.



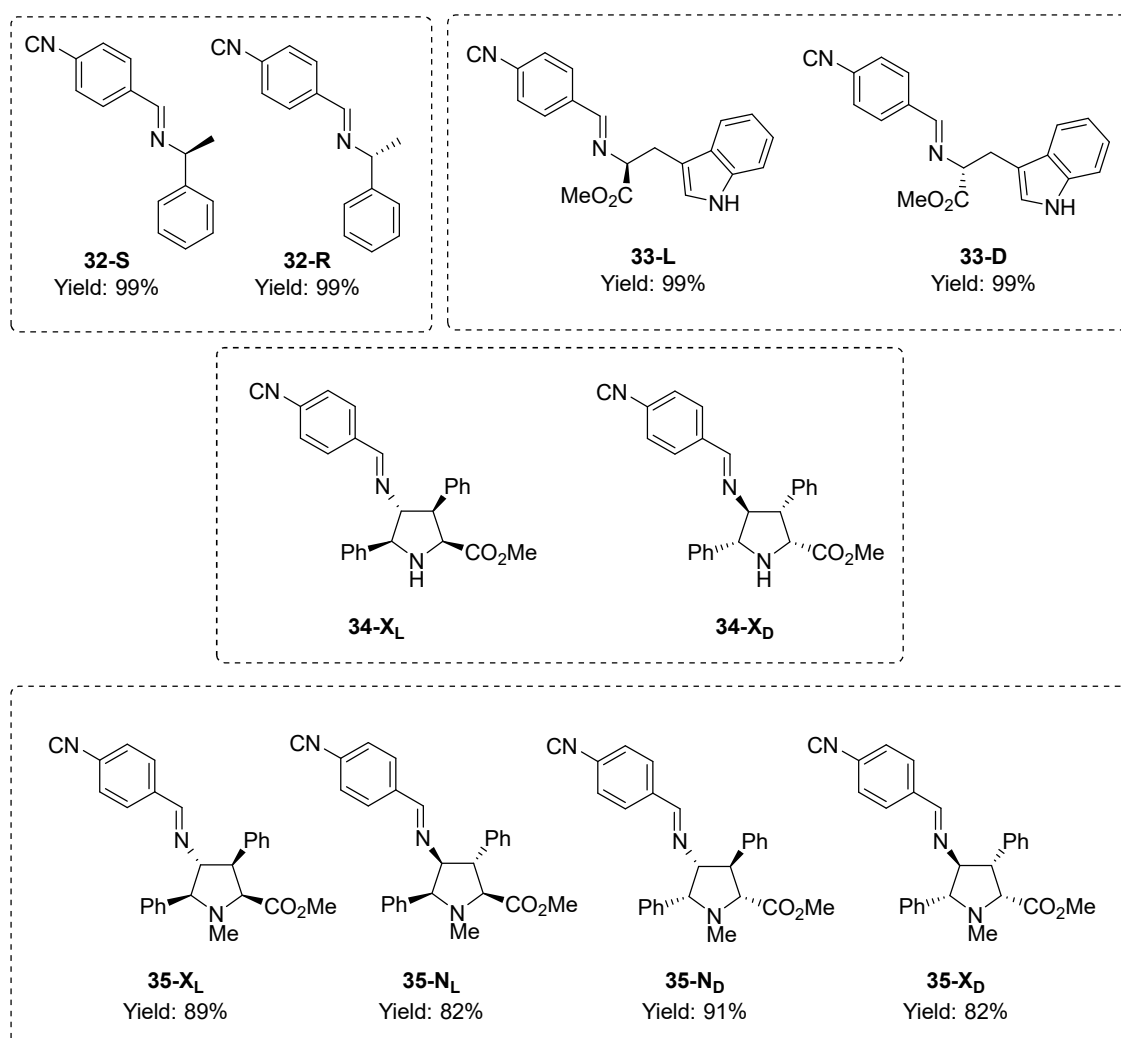
Scheme 30. Condensation between 4-isocyanobenzaldehyde and achiral amines.

After obtaining these results from achiral amines, we expanded the scope of the reaction by introducing chiral amines such as *S*- and *R*- α -methyl-benzylamine, *D*- and *L*-tryptophan methyl ester, and the previously synthesized (Scheme 23) *L*- and *D*-prolines in both their NH and *N*-methylated forms. The isocyanide imines **32-35** thus prepared are gathered in Scheme 31, together with the corresponding yields of pure isolated products.

Due to the conjugated isocyanophenyl system, the nucleophilic addition of amines to the aldehyde moiety of **30** was favored. The reactions in methanol were in high conversion

without the necessity of adding dehydration agents. However, the purification of the obtained products by flash column, was unsuccessful, since the imines were not stable in a weak acid environment. To get the high-quality isocyanide monomer, the amine formed prolines **31-35** were used in 1.2:1 equivalent ratio to consuming all the isocyno aldehyde. The excess amount of amine could be removed by washing it with water and brine. ¹H-NMR characterization of the isocyanide monomers **31-35** showed the signal corresponding to the H-C=N-R proton indicating successful condensation. The obtained new series of isocyanides were stored in the fridge for polymerization under the previously optimized conditions.

Chiral imines



Scheme 31. Condensation between 4-isocyanobenzaldehyde and chiral amines.

Almost all the prepared isocyanide imines were dark brown oils. The exception was the isocyanide **35** series, for which amorphous foamed solid forms were obtained.

Subsequent recrystallization of these solid products was successfully accomplished in DCM. In this case, a crystal structure was obtained which was analyzed by X-ray diffraction techniques, as indicated in Figure 24.

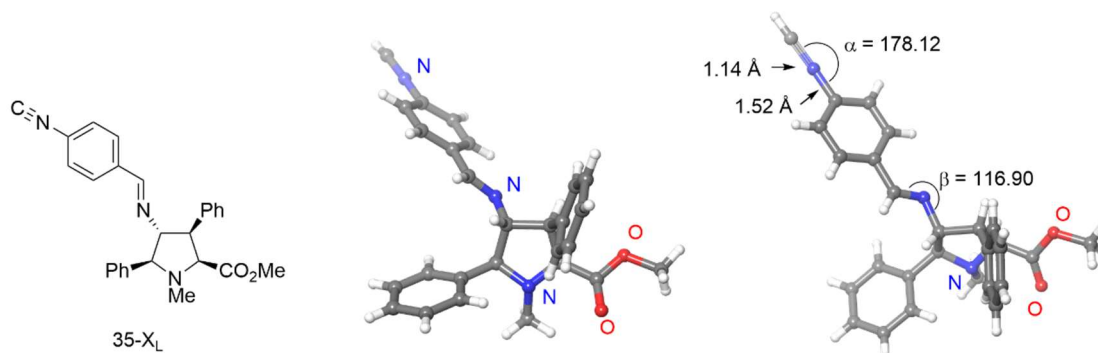


Figure 24. Ball and stick representation for the isocyanide derivative **35-X_L** (to see the ORTEP diagram, visit chapter VI).

In the crystal structure of **35-X_L**, we can observe that the 4-isocyanide phenyl and imine moieties lie in the same plane, showing the existence of π - π conjugation between the imine and the para-substituted phenyl ring. The bond angle of isocyanide is 178° , similar to the isocyanoproline **23** (Figure 21), indicating that in both cases, the major resonance type of isocyanide is in triple bond form. The N=C bond length of **36-X_L** is 1.14 Å, the same found as in isocyanoproline **23**, which declares that the same chemical environment was between isocyanoproline **23** and its spacer congener **35-X_L**.

The chiroptical analysis of chiral imines **32-35** was conducted. The chiral imines were dissolved in chloroform (CHL or CHCl₃) at a specific concentration in the sample cell, which allowed a 589.3 nm light source from a sodium lamp to pass through. According to Table 4, all the chiral imines exhibit weak and negative optical rotation. This was unusual, and we suggested that the weak signal may be due to the imine moiety.

Table 4 Specific optical rotation of chiral imines

Chiral monomer	$[\alpha]_{589.3}^a$	Chiral monomer	$[\alpha]_{589.3}$
32-S	-1.7	35-X_L	-10.1
32-R	-18.0	35-N_L	-10.5
33-L	-8.1	35-N_D	-9.4
33-D	-4.4	35-X_D	-32.2

^a Specific optical rotation measured at 20°C, CHCl₃, 1 mg/mL

2.4 POLYMERIZATION OF 4-SUBSTITUTED PHENYL ISOCYANIDES

2.4.1 Optimization of the polymerization reaction of imino isocyanides **31**

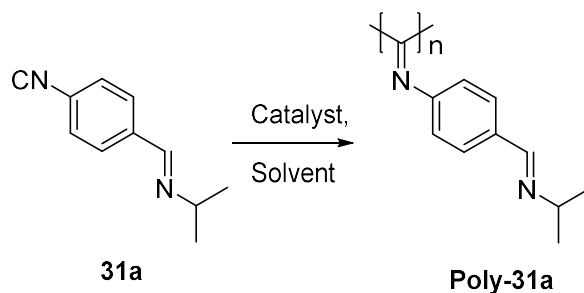
We first arranged a model polymerization series of experiments for the new spacer system to study its response to various reaction conditions. The model polymerizations were implemented with 4-isocyanophenyl-*N*-isopropyl-methanimine **31a** derived from 4-isocyanide benzaldehyde **30** and isopropylamine. In these experiments, different catalysts, catalyst loadings, solvents and reaction times were considered.

As far as the catalyst is concerned, only nickel (II) salts (Table 5, entries 1-3) were studied (vide infra). Thus, NiCl₂, Ni(acac)₂, and Ni(ClO₄)₂ were implemented in the polymerization experiments. The obtained results showed significant differences depending upon the catalyst used (Table 5). In Ni(acac)₂ cases, the obtained polymer was in low molecular weight (14.3 kDa in Mn). In addition, the high polydisperse index showed that this catalyst is highly uncontrollable. When Ni(ClO₄)₂ was used, the polydisperse index decreased, but the molecular weight did not meet the minimum requirements for polymers. Finally, only nickel chloride hexahydrate yielded high molecular weights in the corresponding polymers, although the PDI was still too high for an acceptable polymerization reaction.

In a second series of experiments, several catalytic loadings were compared (Table 5, entries 1, 4 and 5). The obtained results permitted to conclude that a catalytic loading larger than 1% (entry 4) led to lower Mn values, whereas a lower catalytic loading (entry 5) did not represent a significant improvement. Then different solvents were analyzed (entries 6-13). The obtained results showed that methanol did not significantly improve the results of the polymerization reaction in terms of either Mn, Mw repeating units and PDI values. In a final series of experiments (Table 5, entries 14-18) the solvent (including

concentration), catalytic loading and reaction time were re-analyzed, thus, refining the reaction conditions. We concluded that the best reaction conditions corresponded to entry 17, with THF, 3% mol catalytic loading and a reaction time of 2 hours. This value led to reasonable Mn and Mw values, with the lowest PDI dispersion parameters.

Table 5. Optimized polymerization conditions of **Poly-31a**.



Entry	catalyst	Load (mol%)	Solvent	Mn (kDa)	Repeating units	Mw (kDa)	PDI ^a
1	NiCl ₂ ^b	1	DCM 1ml	100.6	585	378.4	3.77
2	Ni(acac) ₂	1	DCM 1ml	14.3	84	44.7	3.13
3	Ni(ClO ₄) ₂	1	DCM 1ml	27.5	160	73.8	2.69
4	NiCl ₂	5	DCM 1ml	16.7	97	36.4	2.18
5	NiCl ₂	0.5	DCM 1ml	101.5	590	378	3.73
6	NiCl ₂	1	DCM 5ml	131	761	512.4	3.92
7	NiCl ₂	1	DCM 0.5ml	56.7	330	158.2	2.8
8	NiCl ₂	1	MeOH 1ml	21	122	90.3	4.3
9	NiCl ₂	1	THF 1ml	124.4	723	332.1	2.67
10	NiCl ₂	1	THF 0.75ml	128.2	745	283.5	2.22
11	NiCl ₂	1	THF 0.5ml/DCM 0.25ml	123.1	715	290.2	2.36
12	NiCl ₂	1	THF 0.25ml/DCM 0.5ml	105.7	614	414.3	3.92
13	NiCl ₂	1	Toluene 1ml	77.9	453	239.8	3.08
14 ^c	NiCl ₂	1	THF 0.75ml	114.7	666	316.1	2.76
15 ^d	NiCl ₂	1	THF 0.75ml	126.2	733	426.8	3.39
16 ^e	NiCl ₂	1	DCM 1ml	119.1	692	612.2	5.15
17	NiCl ₂	3	THF 0.75ml	72.8	423	121.7	1.68
18	NiCl ₂	1.5	THF 0.75ml	93.1	541	216.9	2.33

^a Mn, Mw and PDI measured from waters 717 plus GPC system with THF as eluent and polystyrene as standard. ^b Used in NiCl₂·6H₂O. ^c Reaction time 0.5h. ^d Reaction time 1h. ^e Reaction time 20 h.

Polymerization reaction in the presence of a chiral ligand

Additionally, in the first optimization, the temperature was not considered because the temperature also influences helix sense control. In asymmetric synthesis, low temperature always has better stereocontrol. And in the polymerization of helical sense-controlled polyisocyanide, the same trend was observed. The helix sense-controlled polymerization of 4-isocyanophenyl-*N*-isopropyl-methanimine was performed with chiral ligand *exo*-L **10**.

Our initial hypothesis was that interaction of square-planar $[\text{Ni}(\text{CN-R})_4]^{2+}$ with pyrrolidine **10** should lead to a complex as shown in Figure 25, A. This interaction should introduce a chiral discrimination factor that could induce chiral helicity in the polymer (Figure 25, A).

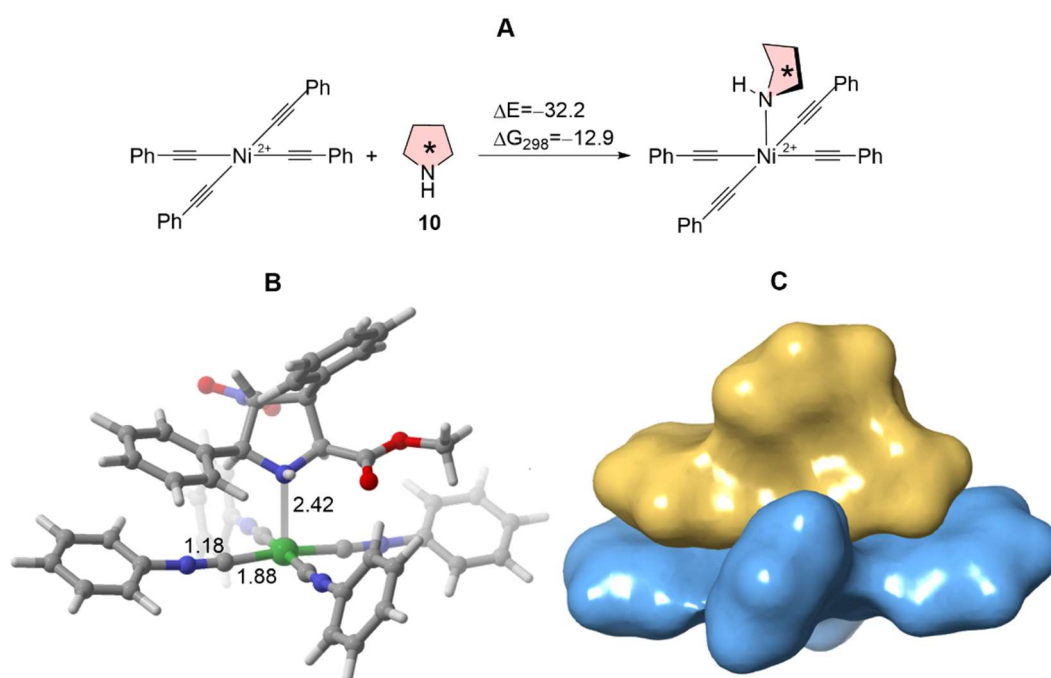
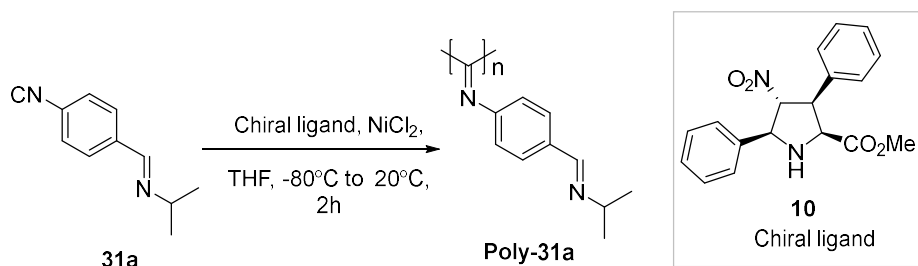


Figure 25. Description of the interaction between model $[\text{Ni}(\text{CNPh})_4]^{2+}$ complex and X_L proline **10** at the $\omega\text{B97xD}/6\text{-31G}^*(\text{C,N,O,H})\&\text{LanL2DZ}(\text{Ni})$ level of theory. (A) Internal (ΔE) and Gibbs (ΔG , at 298 K) reaction energies, in kcal/mol, associated with the interaction process. (B) Chief geometric features of the $[\text{Ni}(\text{CNPh})_4]^{2+}$ -**10** complex. Bond distances are given in Å. (C) Van der Waals surfaces of pyrrolidine **10** (in yellow) and $[\text{Ni}(\text{CNPh})_4]^{2+}$ (in blue), with 0.14 Å probe radius, showing the close interaction between both components.

Table 6. Optimized temperature to a polymerization reaction of **Poly-36**.

Entry	T(°C)	Mn (g/mol)	Repeating unit	Mw (g/mol)	PDI ^a
1	20	15210	89	20844	1.37
2	0	9192	53	13194	1.44
3	-20	8313	47	11768	1.41
4	-50	6475	37	8811	1.36
5	-80	863	4	907	1.05

Reaction conditions: *exo*-L (3%); NiCl₂·6H₂O (3%). ^a Mn, Mw and PDI measured from waters 717 plus GPC system with THF as eluent and polystyrene as standard.

According to Table 6, the helix sense-controlled polymerizations were carried out at a series of temperatures ranging from 20°C to -80°C. At 20°C, the Mn was 15.2 kDa, and PDI was 1.37. Compared to the result without chiral ligand at 20°C (72.8 kDa), the Mn has decreased by almost 80%. In addition, the Mn reduction indicated that the chiral ligand should participate in the polymerization process. We speculate that the interaction of the proline nitrogen with Ni(II) should hinder, at least partially, the insertion of a new isocyanide monomer (*vide infra*). Actually, a DFT study at the ω B97xD/6-31G* & LanL2DZ level of theory¹⁰⁹ showed a weak, but noticeable interaction between chiral ligand **10** and the starting [Ni(CNPh)₄]²⁺ complex, in which the pyrrolidine nitrogen atom interacts with the metallic center thus generating a complex via an exergonic process (Figure 25, B), in which there is an important crowding that must hinder the evolution of the system along the polymerization process.

The hindrance may lead to a low helix sense control or a reduction in initiation and propagation reaction rates.

¹⁰⁹ a) Chai, J. D.; Head-Gordon, M. *Phys. Chem. Chem. Phys.* **2008**, *10*, 6615-6620. b) Hay, P. J.; Wadt, W. R. *J. Chem. Phys.* **1985**, *82*, 299-310.

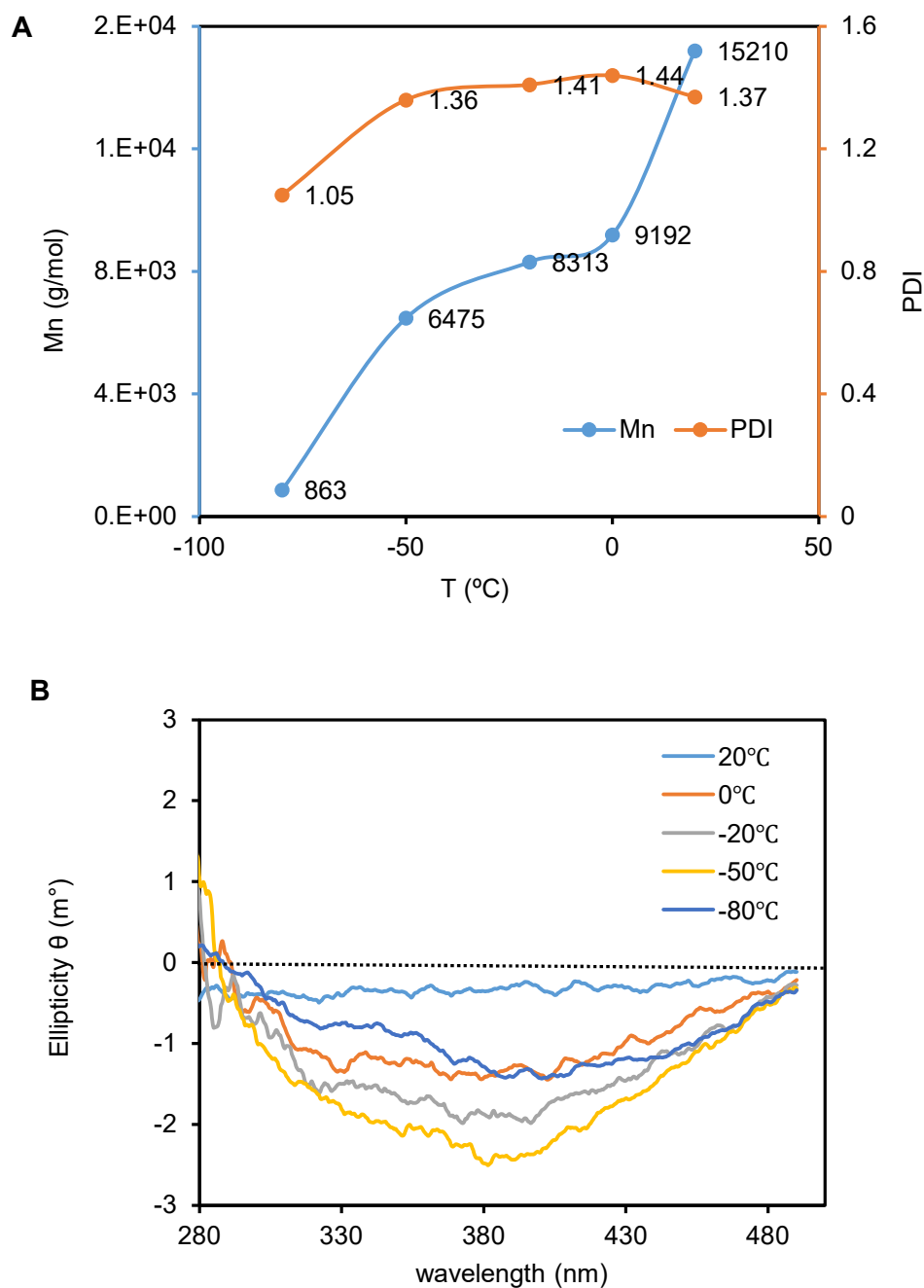


Figure 26. A. The molecular weight and CD spectrum of **Poly-31a**. B. CD was measured at CHCl_3 in 0.5 mg/ml.

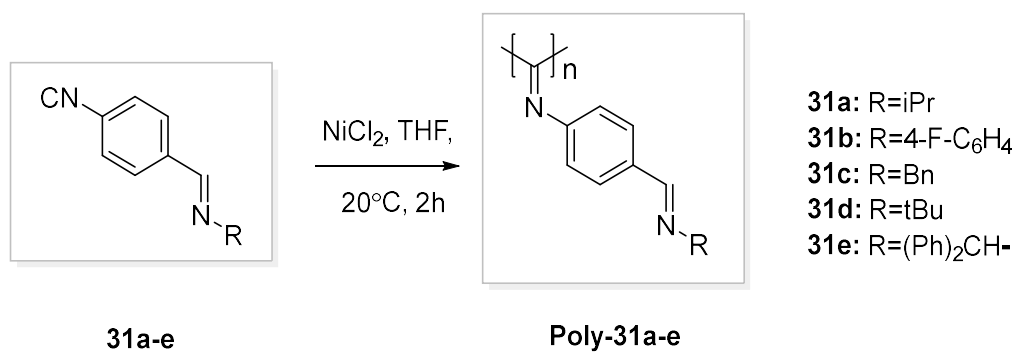
In addition, the Mn values showed a significant influence with the temperature. When the temperature gradually decreased from 20 °C to -80 °C, the average molecular weight decreased from 15 kDa to less than 1 kDa. However, even though the helix sense control was not good, we can conclude the best temperature for this kind of helix sense controlled polymerization due to the trend of the change of CD value and Mn. According to Figure 26 at -20 °C, the Mn was close to the average value and CD intensity was slightly less

than the best value. In summary, -20 °C was considered the best temperature for this helix sense-controlled polymerization.

2.4.2 Polymerization of achiral and chiral imino isocyanides **31**

Five isocyanide imine monomers were obtained through the condensation reaction between 4-isocyanide benzaldehyde and the corresponding achiral amine. Each monomer **31**, obtained as a brown oil, was dissolved in THF and the corresponding polymerization reaction was initiated by nickel chloride to the corresponding polymers (Table 7).

Table 7. Polymerization of achiral (4-Isocyanophenyl)-*N*-substituted methanimines.



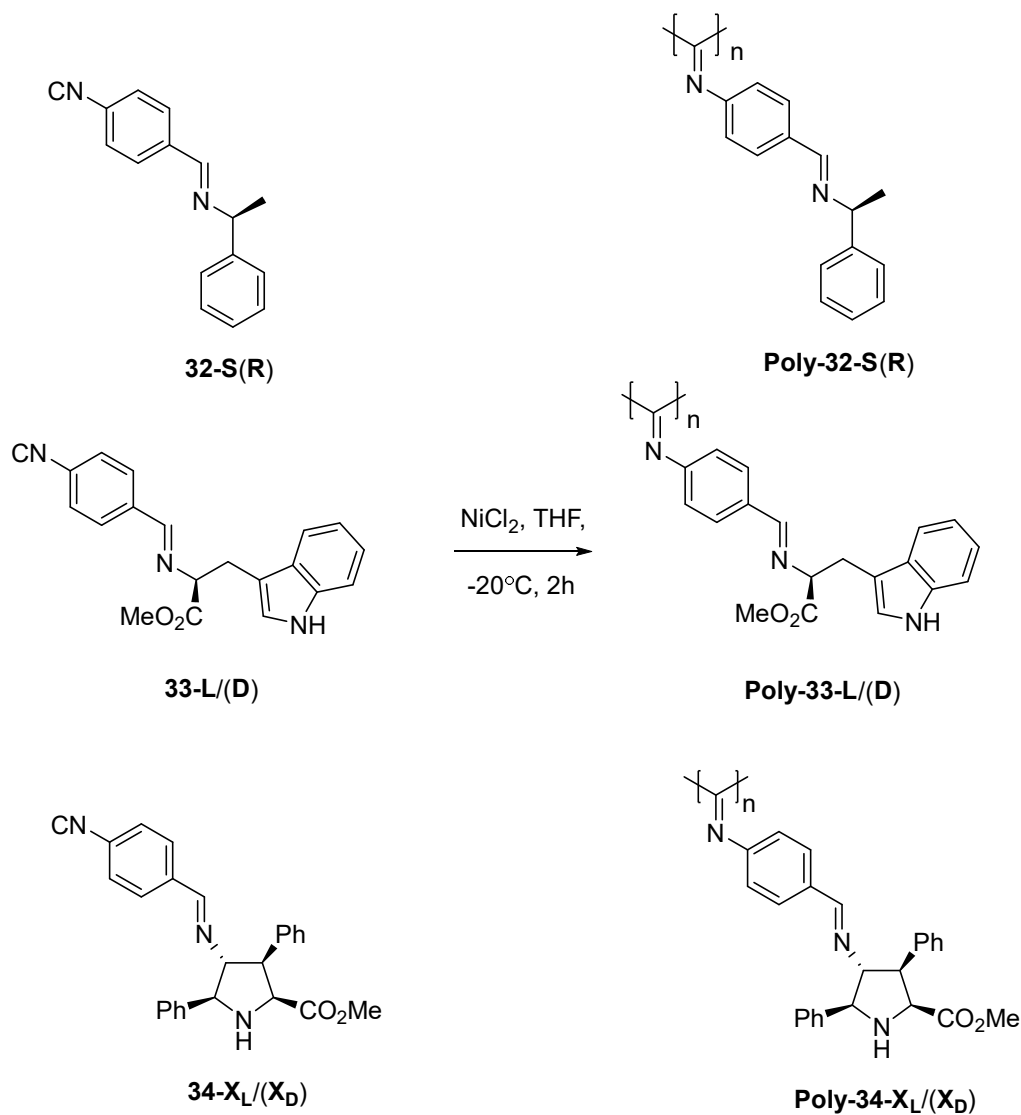
Entry	Description	R	Mn (kDa)	repeating unit	Mw (kDa)	PDI	Rh (nm)
1	31a	ⁱ Pr	72.8	423	121.7	1.68 ^a	N/A ^c
2	31b	4-F-C ₆ H ₄	134.7	601	152.9	1.13 ^b	7.0
3	31c	Bn	122.0	554	140.5	1.15 ^b	7.8
4	31d	^t Bu	57.0	306	65.4	1.14 ^b	5.6
5	31e	(Ph) ₂ CH-	39.3	133	43.2	1.10 ^b	3.3

Reaction conditions: temperature: 20 °C; NiCl₂·6H₂O (3%). ^a Mn, Mw and PDI measured from waters 717 plus GPC system with THF as eluent and polystyrene as standard. ^b Measured from Agilent 1200 HPLC-DLS (high performance liquid chromatography-dynamic light scattering) system with THF as eluent and polystyrene as standard. ^c Not available. Hydrodynamic radius (Rh) is a parameter obtained by DLS to describe the size of a macromolecule.

According to the molecular weight data obtained by GPC, **Poly-31a**, **Poly-31b** and **Poly-31c** with a substituted group of isopropylamine, 4-fluoro aniline, and benzylamine have the highest Mn value of 119.1 kDa, 134.7 and 122 kDa, respectively. The repeating unit in **Poly-31a**, **Poly-31b** and **Poly-31c** have reached 423, 601 and 554, respectively, **Poly-31d** with the tert-Butyl group has a moderate Mn of 57 kDa and 306 repeating unit value

and **Poly-31e** have the lowest Mn of 39.3 kDa among all the poly(isocyanides) prepared from achiral monomers.

Table 8. Polymerization of chiral (4-Isocyanophenyl)-*N*-substituted methanimines.



Entry	Description	Mn (kDa)	repeating unit	Mw (kDa)	PDI	Rh (nm)
1	32-S	81.4	348	98.4	1.2 ^a	6.7
2	32-R	98.9	422	117.7	1.2 ^a	7.4
3	33-L	9.3	28	10.2	1.1 ^b	1.3
4	33-D	11.9	36	13.4	1.2 ^b	N/A
5	34-X_L	24.1	59	37.1	1.5 ^b	2.6
6	34-X_D	41.8	102	58.1	1.4 ^b	3.8

Reaction conditions: temperature: -20°C ; $\text{NiCl}_2 \cdot 6\text{H}_2\text{O}$ (3%). ^a Measured from Agilent 1200 HPLC system with THF as eluent and polystyrene as standard. ^b Measured from Agilent 1200 HPLC-DLS system with

THF (1% TFA) as eluent and polystyrene as standard. Hydrodynamic radii (R_h) is a parameter obtained by DLS to describe the size of a macromolecule.

We speculated that, according to these results, a small quantity of active coordinative Ni(II)-isocyanide-nucleophile complex were generated at the beginning of the reaction, but they could consume the rest of the monomer and obtain large chains. Considering that most of the samples' PDI values ranged from 1.1 to 1.5, we conclude the chain transfer reaction was not favored in this way.

When chiral monomers were introduced in the reaction, the results were somewhat different. In the polymerization of chiral isocyanide monomer prepared from α -methyl benzylamine, which was used in the optimization of solvent effect in the measurement of CD analysis (vide infra) the results were excellent. **Poly-32-S** and **Poly-32-R** have M_n values of 81.4 kDa and 98.9 kDa and PDI of 1.2, respectively (Table 8). The repeat units for the two configurations are 348 for the (S)-monomer and 422 for its (R)-congener.

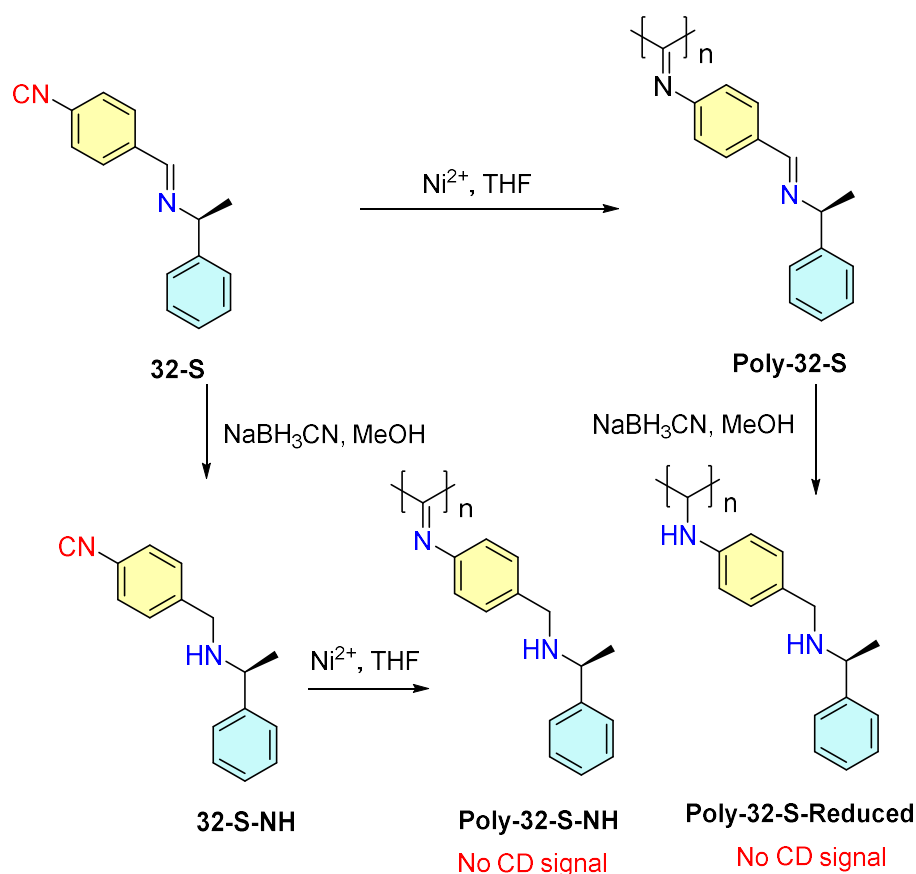
However, these polymers have smaller molecular weights than **Poly-32-S/(R)** for isocyanide monomers derived from **33** and **34** monomers. Thus **Poly-33-L**, **Poly-33-D**, **Poly-34-X_L**, and **Poly-34-X_D** exhibit M_n values of 9.3 kDa, 11.9 kDa, 24.1 kDa and 41.8 kDa, respectively. In principle, the decrease in M_n should be due to the secondary amine and not to the methyl ester serie. The secondary amine may bind the Ni(II) that should have been acting as the initiator in the polymerization and cause a lack of initiating species, resulting in a low M_n (see Figure 25). When the secondary amine was methylated, the M_n increased to 99.7 kDa (**Poly-35-X_L**, Table 9, entry 1).

The insolubility of the poly(isocyanides) in THF may also cause the decrease of the M_n . We observed that **Poly-33-D/(L)** was not soluble in THF, and **Poly-34-X_L/(X_D)** were not soluble in all common organic solvents. We assumed that the polymer's structure caused the great difference in solubility between monomers and polymers. In order to verify this hypothesis, 1% TFA was added to THF. **Poly-33-D/(L)** and **Poly-34-X_L/(X_D)** resulted to be soluble in the acid media. However, the THF-1% TFA mixture could not be used in the polymerization since isocyanides are incompatible with acids.

NMR was used to characterize the chemical structure **Poly-32-S** and **Poly-35-X_L**. Broad signals were observed in the $^1\text{H-NMR}$ spectra, as expected for this kind of macromolecules. The imine functional group can produce mixtures of *E* and *Z* isomers. To improve the structural stability of these polymers, we intended to reduce the imine to

amine with NaBH_4 , thus eliminating the E/Z configurational dichotomy. Two reaction routes were designed as shown in Scheme 32. The first route consisted of a direct reduction of the polymer. In this way, both imine groups in **Poly-32-S** would be reduced to form the corresponding secondary amine in **Poly-32-S-reduced** (see Scheme 32).

Another one was the reduction of the monomer; using one equivalent of sodium cyanoborohydride, **32-S** was reduced into amine **32-S-NH** according to $^1\text{H-NMR}$, and IR. In particular the FTIR spectrum showed that the isocyanide: $:\text{C}=\text{N}^- \leftrightarrow (-)\text{C}\equiv\text{N}(+)-$ was preserved at 2120 cm^{-1} . The polymer obtained from **32-S-NH** has one amine and one imine group in each unit. However, the CD analysis (vide infra) showed that both reduced polymers have no helicity left in the chain. The structure of the product on the reaction condition may destroy the helicity in the first case. In the second case, the hydrogen bond between the unit may prevent the side chain from arranging itself into a stable structure. Since the reduction would break the helix structure, these routes were abandoned.



Scheme 32. Reduction of **32-S** to obtain polymers with amine structure.

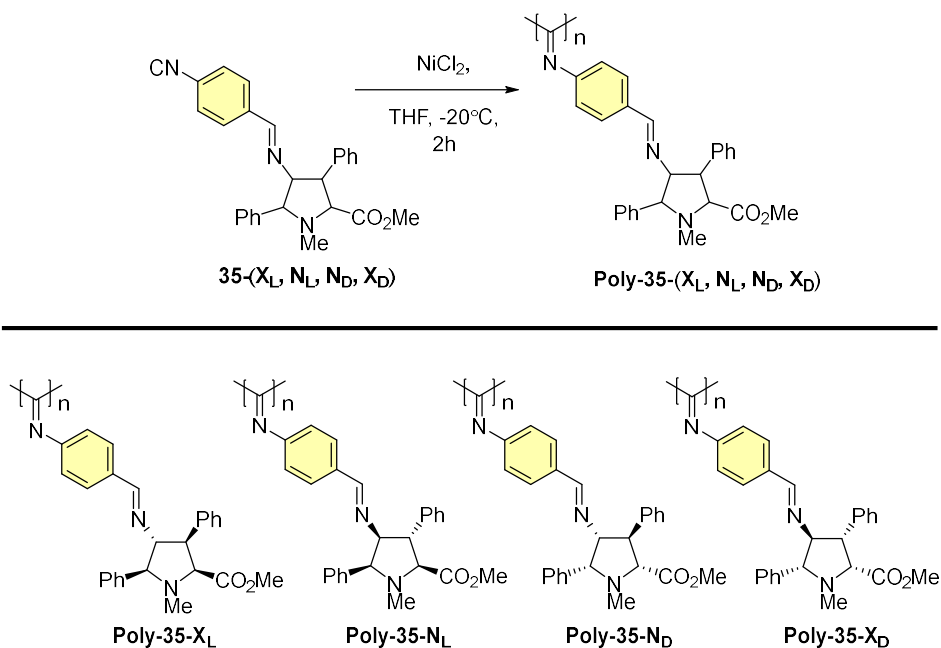
2.5 HELIX SENSE CONTROL POLYMERIZATION OF ISOCYANO-*N*-METHYLATED PENTASUBSTITUTED PROLINES

The polymerization of enantiopure (4-Isocyanophenyl)-*N*-(proline) methanimines were conducted in dry THF at -20 °C. To this reaction mixture, the nickel catalyst was injected as a solution of NiCl₂·6H₂O in MeOH (0.2 mol/L, 3%). Compared to the volume of THF (0.75 mL), MeOH (0.060 mL) that was used in the reaction mixture was less than 10%. However, MeOH can act as the nucleophile to initiate the “Merry-go-round” polymerization (*vide infra*).

The obtained proline polymers prepared via the optimized conditions were in high molecular weight, as it can be seen by inspection of the data gathered in Table 9.

We determined that the Mn values of the polymers were distributed from 70 kDa to 100 kDa, and the polymeric materials were in nearly perfect PDI (1.16 – 1.08), indicating completely stereocontrolled isocyanide polymerization.

Table 9. Polymerization of (4-Isocyanophenyl)-*N*-(proline) methanimines.



Entry	Description	Mn (kDa)	Repeating unit	Mw (kDa)	PDI	Rh (nm)
1	X _L	99.7	274	115.8	1.16	5.9
2	N _L	70.9	184	77.7	1.09	5.2
3	N _D	61.5	160	76.0	1.23	4.4
4	X _D	70.2	180	76.1	1.08	4.5

Reaction conditions: temperature: $-20\text{ }^{\circ}\text{C}$; $\text{NiCl}_2\cdot 6\text{H}_2\text{O}$ (3%). Mn was measured from Agilent 1200 HPLC-DLS system with THF as eluent and polystyrene as standard. Hydrodynamic radius (Rh) is a parameter obtained by DLS to describe the size of a macromolecule.

The metal residual was a significant index for consideration of the material's applications in biochemistry or medicinal chemistry. The metal residue should be removed as it would cause protein denaturation in further studies. Since 3% equivalent of nickel metal ion were present in the crude reaction mixture the polymer was treated with an aqueous ammonium solution (2 mol/L in water) as soon as the reaction was finished.

Assuming that all the nickel ion remained in the product, the calculated percentage of nickel residue should be 4.14 mg/g (0.4% in wt%). The experimental value of nickel residue measured by Inductively Coupled Plasma Mass Spectrometry (ICP-MS) was 3.72 mg/g (0.37% in wt%), which result was consistent with that calculated before treatment. After being treated with the ammonium solution, the content of nickel residue in the polymer decreased to 0.0572 mg/g (0.006% in wt%). Therefore, the nickel residue was reduced by two orders of magnitude, which indicated that the nickel was efficiently removed from the polymer through only one simple workup procedure (Figure 27).

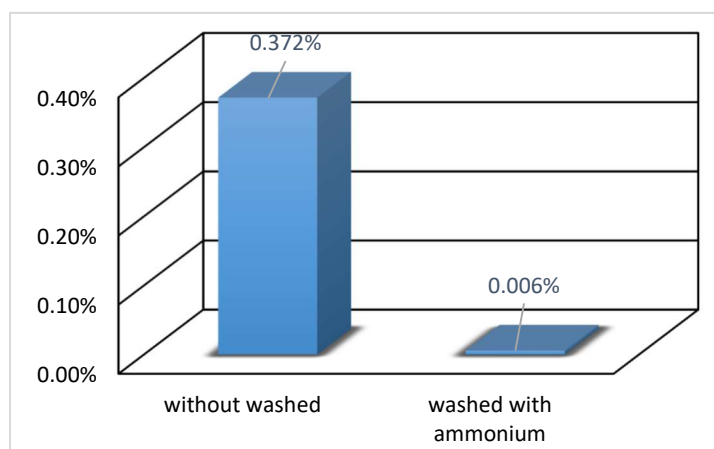


Figure 27. Comparison of nickel ion percentage of **Poly-35-X_L** before and after washing with ammonium solution.

CD measurements

The solvent has a strong effect in the measurement of CD value, as the polymer solvent effect can determine the conformation of the polymer, thus modulating the ability to rotate the circularly polarized light beam. First, we compared the CD values of the polymers

with the corresponding monomer (Figure 28). As can be seen in the plot, the intensity of ellipticity and the maximum wavelength value increase in the case of polymer compared with the monomer. This behavior may be due to a regular rearrangement of the chiral repeating units of **32** (**S** or **R** monomer) in the polymer chain that generates the helicity.

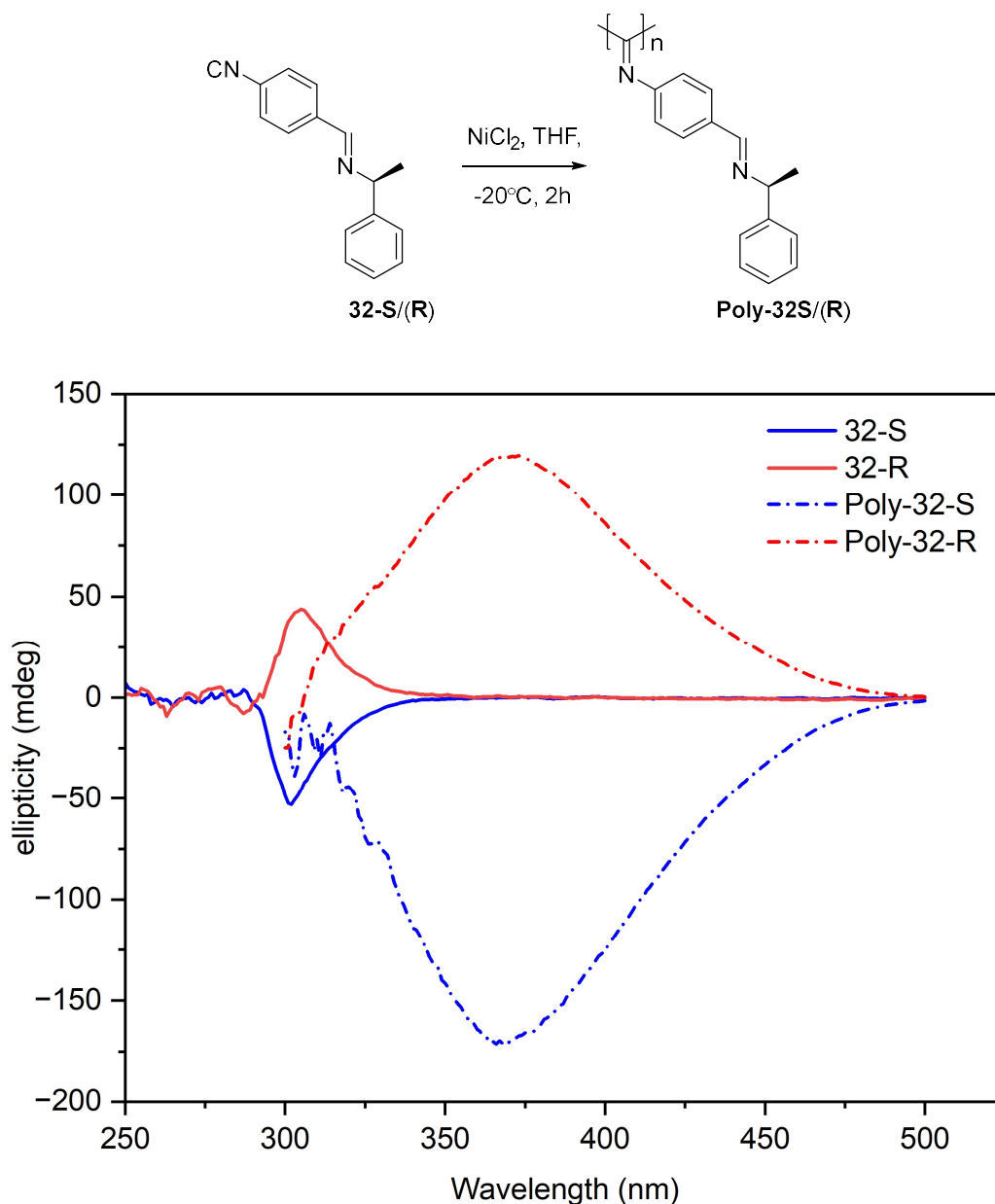


Figure 28. CD spectra of **Poly-32-S** and **R** and the corresponding monomer **32-S** and **R** in DCM.

Poly-32S and **Poly-32R** were used to study the solvent effect in CD measurements. Both polymers were dissolved in chloroform, dichloromethane (DCM), dimethyl sulfoxide (DMSO), acetonitrile (MeCN), methanol, and tetrahydrofuran (THF) at 0.5 mg/ml to conduct the CD measurements. In Figure 29, we can observe that in solvents such as

DCM, THF, and CHCl_3 the polymers showed very high negative or positive results from 300 nm to 500 nm. In MeCN and DMSO, no noticeable ellipticity was observed. Finally, methanol showed a very weak opposite effect.

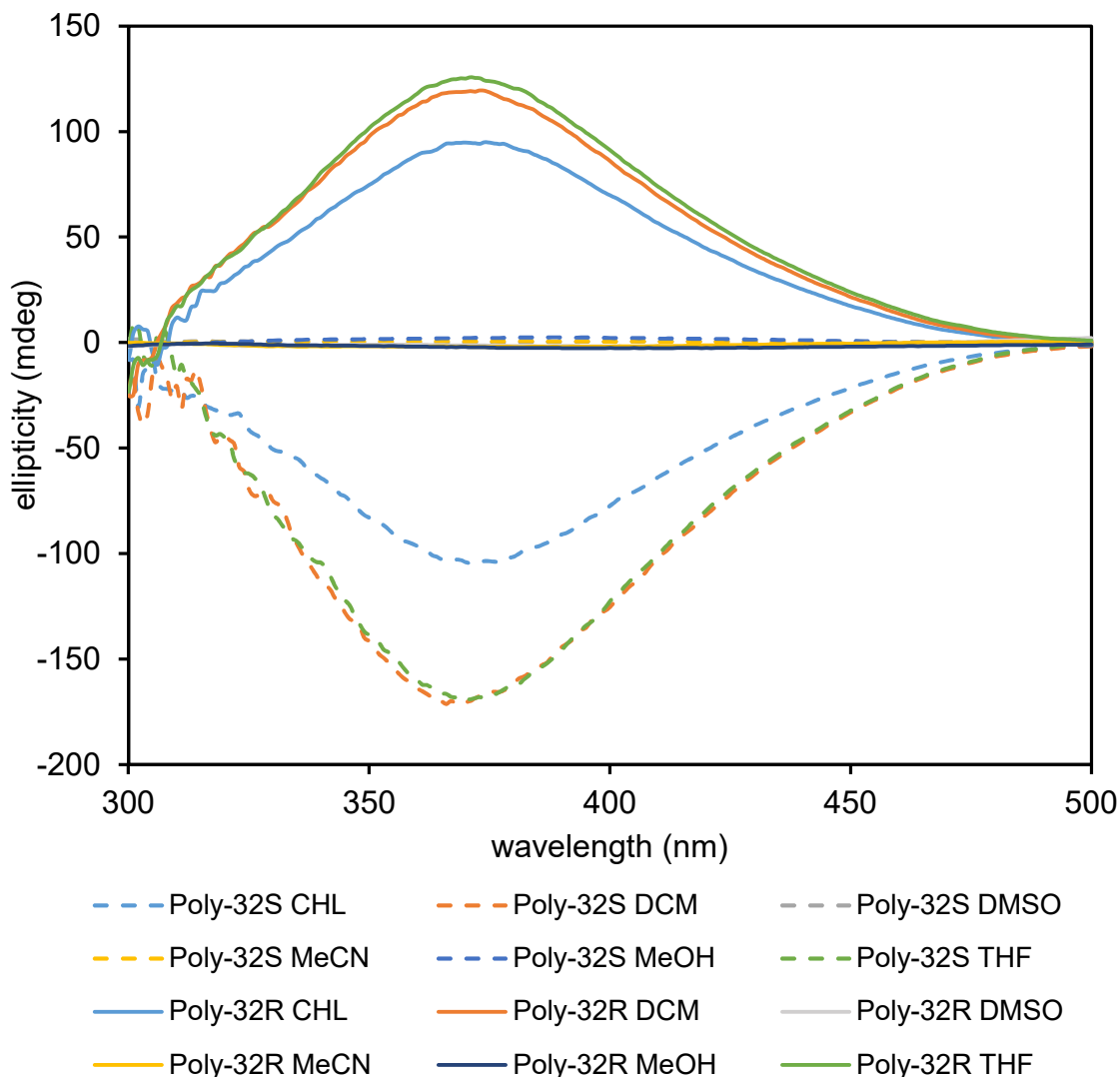


Figure 29. Measurement CD of **Poly-32S** and **Poly-32R** at various solvents at 0.5 mg/ml.

It could be observed from the data of this figure that **Poly-32S** always shows higher ellipticity values than **Poly-32R**. We propose that this difference was due to the different M_n of these two samples. According to Table 8, **Poly-32S** has an M_n value of 98.4 kDa, whereas in the case of **Poly-32R** is 117.7 kDa. A longer chain would create more quantities of regularly arranged sidechains, thus inducing a stronger ability to absorb a specific circular polarized light in CD measurements. We, therefore, concluded that DCM and THF were the two best solvents for the 4-isocyano-imine polymers. In addition,

considering the convenience of sample recovery, the DCM was the best one because of its lower boiling point.

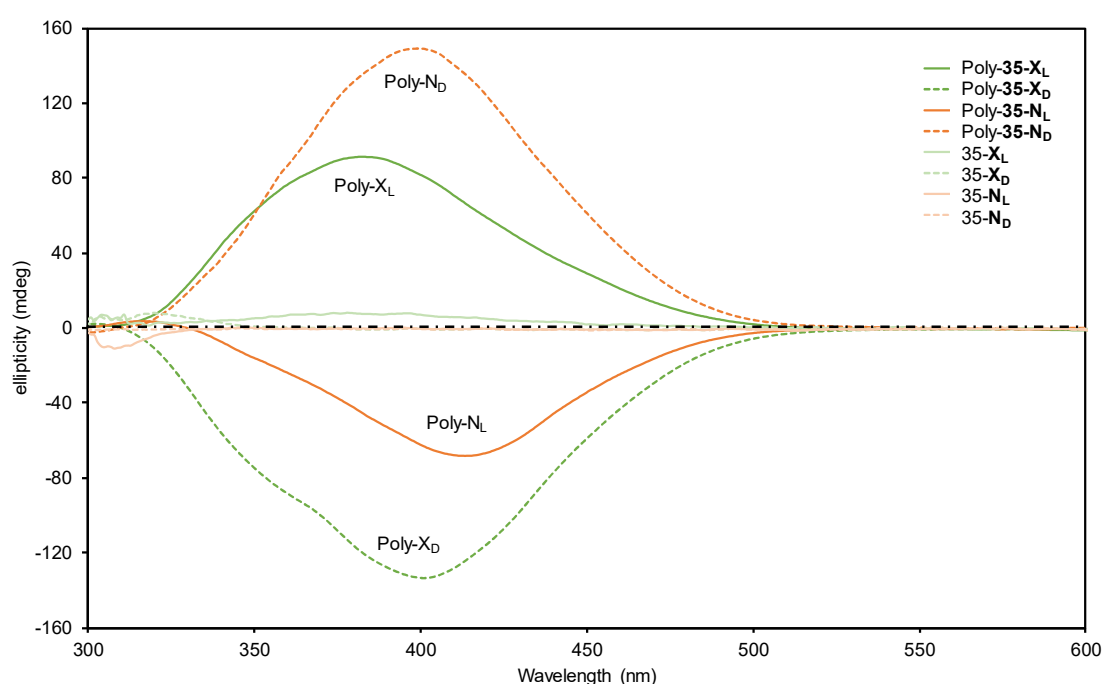
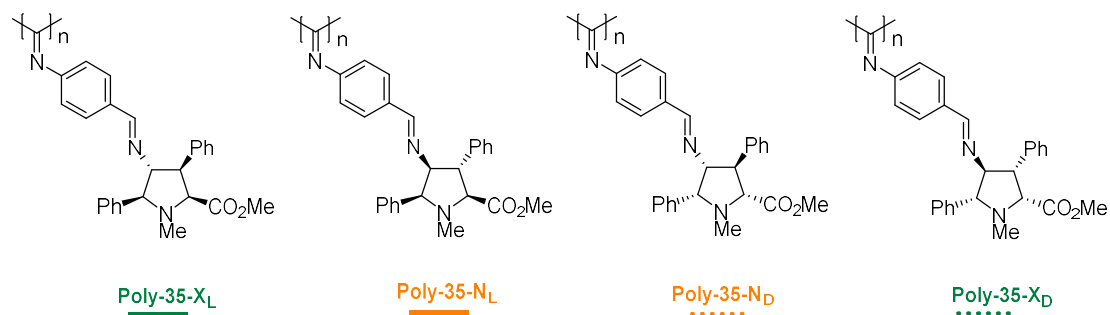


Figure 30. CD spectra of **Poly-35-X_L**, **X_D**, **N_L** and **N_D** and the corresponding monomers **35-X_L**, **X_D**, **N_L** and **N_D**.

Besides polymer properties, the characterization of the secondary structure of the polymer has also been studied. The CD spectra were recorded from 250 nm to 650 nm in DCM to identify the helical structure. All samples were tested at a concentration of 0.5 mg/mL. In all cases, very high CD signals were observed. Among the four helical polymers, **Poly-35-X_D** and **Poly-35-N_D** exhibit the highest ellipticity up to 149 mdeg and -133 mdeg, respectively at 400 nm; **Poly-35-X_L** shows peak ellipticity of 92 mdeg at 385 nm and **Poly-35-N_L** reaches its ellipticity maximum of -69 mdeg at 415 nm. It could be found that the handedness of the polymers are opposite according to the enantiomeric D or L

form of the substituted prolines. **Poly-35-X_D** and **Poly-35-N_D** exhibited an opposite curve, whilst **Poly-35-X_L** and **Poly-35-N_L** follow the same trend.

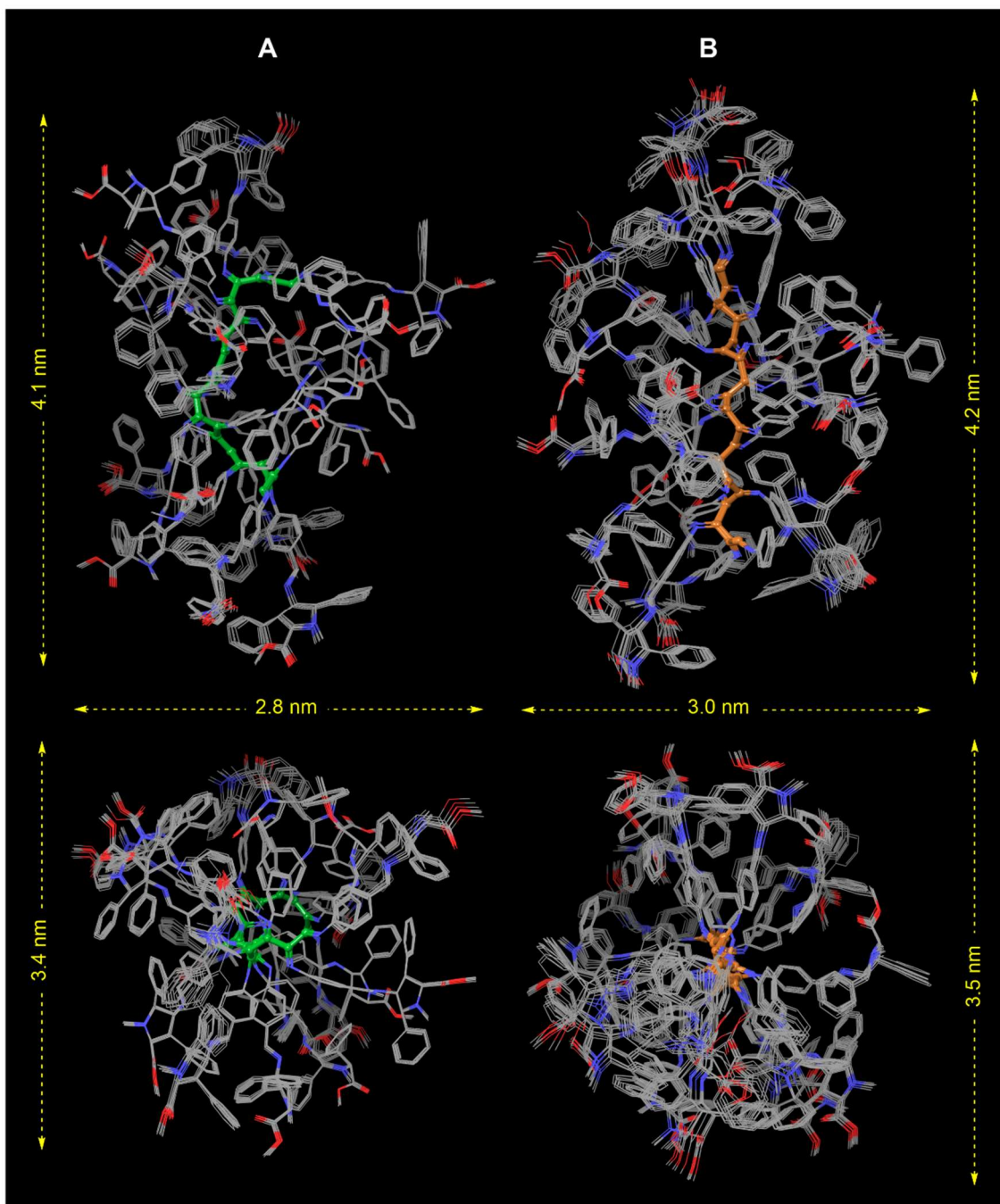


Figure 31. Longitudinal (upper panels) and axial (lower panels) views of MM-MC calculations (OPLS3e force field, in chloroform as solvent, OPLS: optimized potentials for liquid simulations) showing the 10 preferred conformations within 8.7 kJ/mol (A) and 6.8 kJ/mol (B) of 20-mer isonitrile polymers corresponding to the **Poly-35-X_L** (A) and **Poly-35-N_L** (B) series. The central carbon chains are represented as ball-and-stick draws for the **Poly-35-X_L** (A, in green) and **Poly-35-N_L** (B, in orange) series. The approximate dimensions (in nm) of the respective 20-mer units are shown.

It is important to note that the CD curves of monomeric isocyano prolines showed much less intense CD curves, almost negligible in some cases (Figure 28 and 30). Therefore, we conclude that the behavior of polymeric species stems from the special geometric features of the respective macromolecules.

In order to get a better understanding of the behavior of these chiral polymers, we performed Molecular Mechanics Monte Carlo (MM-MC) simulations using the OPLS force field¹¹⁰ as implemented in MacroModel and Maestro, Schrödinger, LLC, New York, NY 2021. In order to assess the structural features of these polymers at a reasonable computational cost, we carried out the MM-MC simulations with 20-mer repeating units of **Poly-35-XL** and **Poly-35-NL**. Among the 4000 structures generated, only the ten most stable structures within 8.7 kJ/mol of **(35-XL)₂₀** and 6.8 kJ/mol of **(35-NL)₂₀** structures were selected and merged in Figure 31.

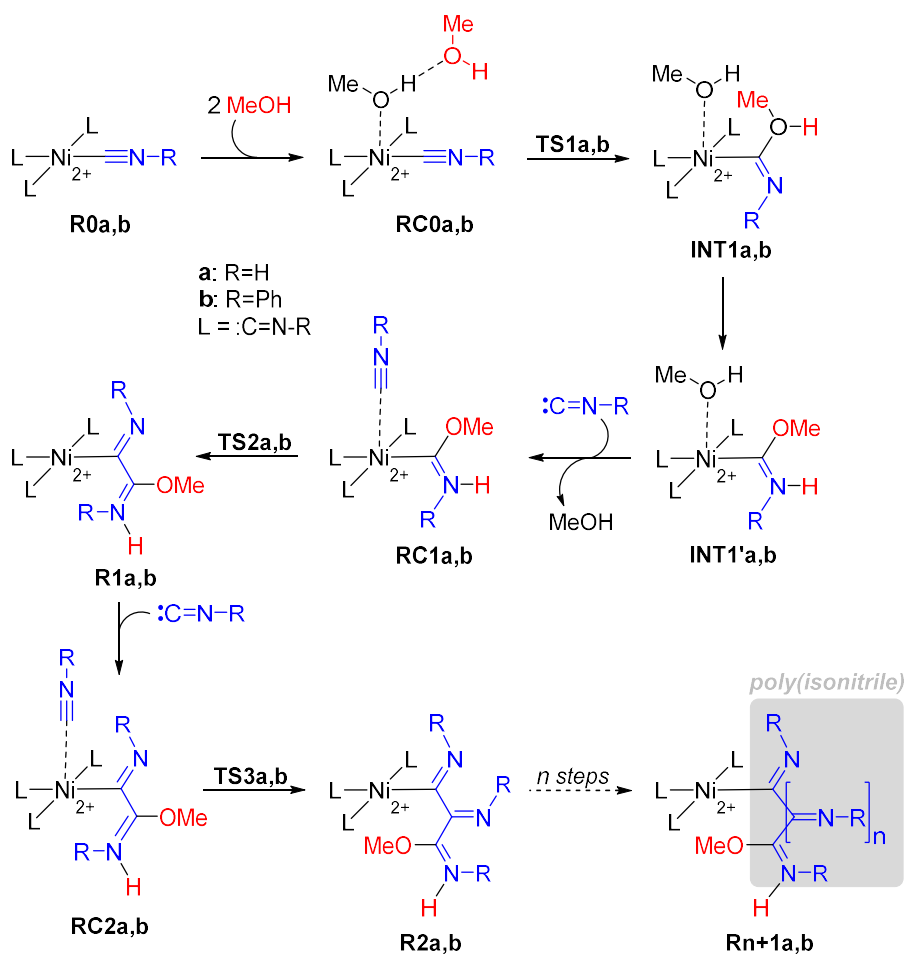
In this Figure, the preferred conformations of **(35-XL)₂₀** (A) and **(35-NL)₂₀** (B) are shown in longitudinal (upper panels) and axial (lower panels) views. The radius/length of **(35-XL)₂₀** and **(35-NL)₂₀** were 2.8/3.0 nm and 3.5/4.2 nm, which are close to the Rh (hydrodynamic) radius obtained from DLS (dynamic light scattering, 5.2-5.9 nm). The backbones in the main chain were marked (green for **(35-XL)₂₀** and orange for **(35-NL)₂₀**, the same color type used in Figure 30). A noticeable difference in the backbone could be seen for **(35-XL)₂₀** and **(35-NL)₂₀**. The green carbon chain in **(35-XL)₂₀** is of spiral staircase type, and the orange one was a nearly straight wavy zig-zag line. The previous CD spectra indicated that the maximum ellipticity of the two polymers was neither in the same value nor in the same wavelength, a result compatible with the substantial structural differences for both **XL** and **NL** repeating units.

2.6 MECHANISTIC STUDIES

DFT calculations as the ω B97xD/6-31G* (C, H, N, O) & LanL2DZ (Ni) level of theory were conducted in order to get a better understanding of the Ni (II)-catalyzed polymerization processes discussed in the previous paragraphs. We selected two series of calculations that incorporate the main geometric and structural features of these experiments. In the a-series, the simplest isocyanide CNH was coordinated to a Ni(II)

¹¹⁰ Roos, K. ; Wu, C.; Damm, W.; Reboul, M.; Stevenson, J. M.; Lu, C.; Dahlegren, M. K.; Mondal, s.; Chen, W.; Wang, W.; Wang, L.; Abel, R.; Friesner, R. A.; Harder, E. D. *J. Chem. Theory Comput.* **2019**, *15* 1863-1874.

cation in a square planar geometry. The b-series describes the same reaction in the presence of CN-Ph. The possible reaction paths generated by the ‘‘Merry-go-round’’ mechanism are shown in Scheme 33.



Scheme 33. General view of ‘‘Merry-go-round’’ Mechanism initiated by MeOH.

Since the Ni(II) catalyst was added by injection of $\text{NiCl}_2 \cdot 6\text{H}_2\text{O}$ salt in MeOH solution (0.2 mol/L), so in the reaction mixture, the MeOH content was much higher than H_2O , which was brought in by nickel hydrate. Thus, we assumed that MeOH was the nucleophile that initiates the polymerization with Ni(II). The computational study was carried out on the gas phase environment, and the free energy of the starting material was set to 0 kcal/mol.

The reaction starts with the coordination of the square planar $[\text{Ni}(\text{CNH})_4]^{2+}$ complex **R0a** with two molecules of methanol, connected by a $\text{O-H} \cdots \text{H}$ hydrogen bond (Figure 32, Scheme 33). This leads to the formation of the reactive complex **RC0a**, in which a O-Ni interaction is generated. This step is quite exergonic, although the O-Ni interaction

involves four electrons, resulting from the combination of the dz^2 atomic orbital (AO) of the Ni(II) center with the π^* molecular orbital (MO) of the methanol units, which results in two-electron populated σ and σ^* MO's (Figure 33).

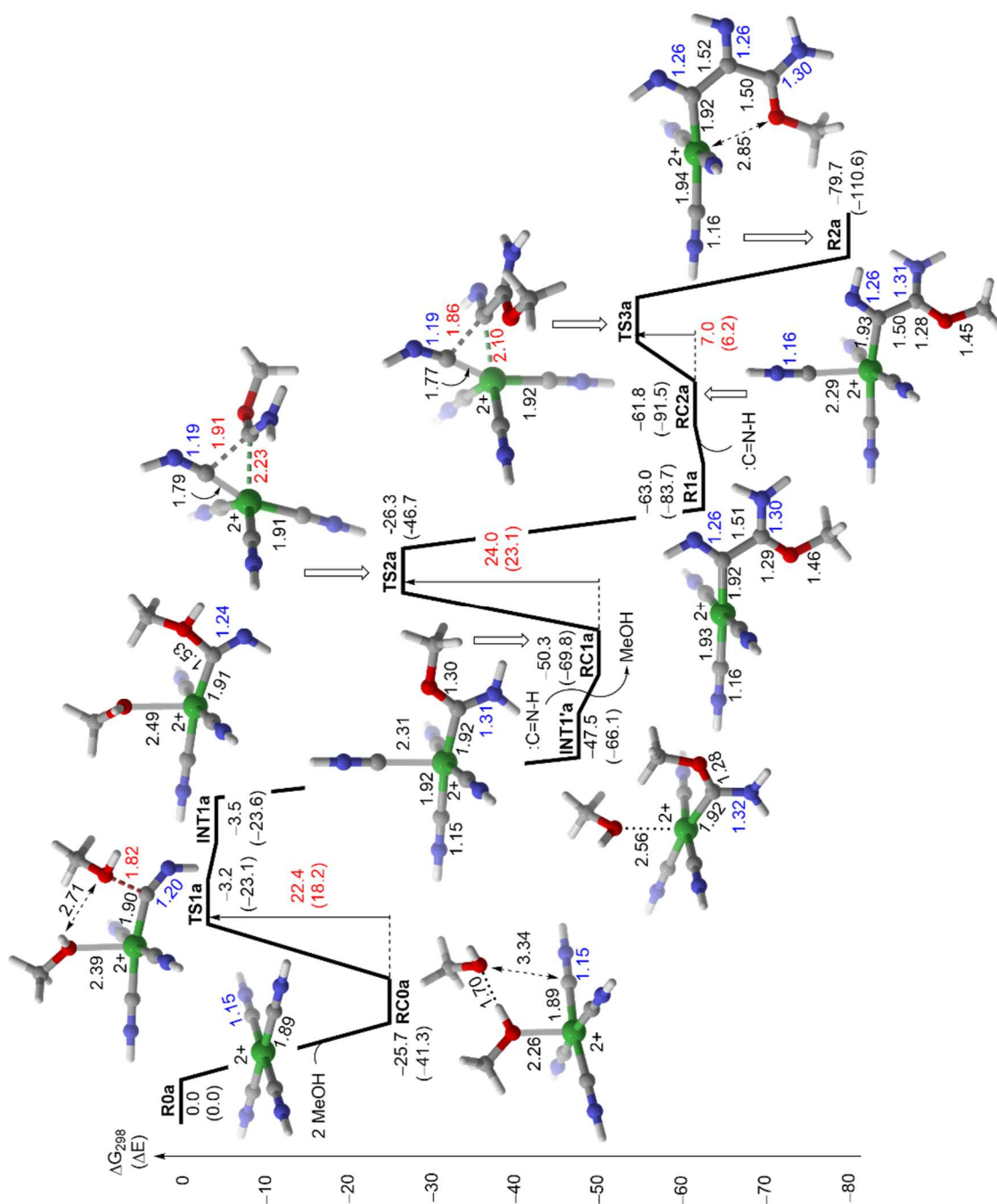


Figure 32. Reaction profile calculated for the a-series (R=H, Scheme 33) at the ω B97xD/6-31G*(C, H, O, N)&LanL2DZ(Ni) level of theory. Numbers close to the stationary points (reactants, intermediates transition structures and products) correspond to the relative Gibbs energies, in kcal/mol, calculated at 298.15 K. Numbers in parentheses are the relative total (electronic and nuclear) energies, including zero-

point vibrational corrections, also in kcal/mol. Bond distances and internuclear distances are given in Å. Color code: gray, C; white, H, blue, N; red, O; green, Ni.

From **RC0a**, one MeOH molecule adds to the isocyanide carbon atom via **TS1a**, to give rise to the highly stabilized complex **INT1'a**, resulting from a prototropy of **INT1a** from the oxygen to the nitrogen atom of the isocyanide ligand.

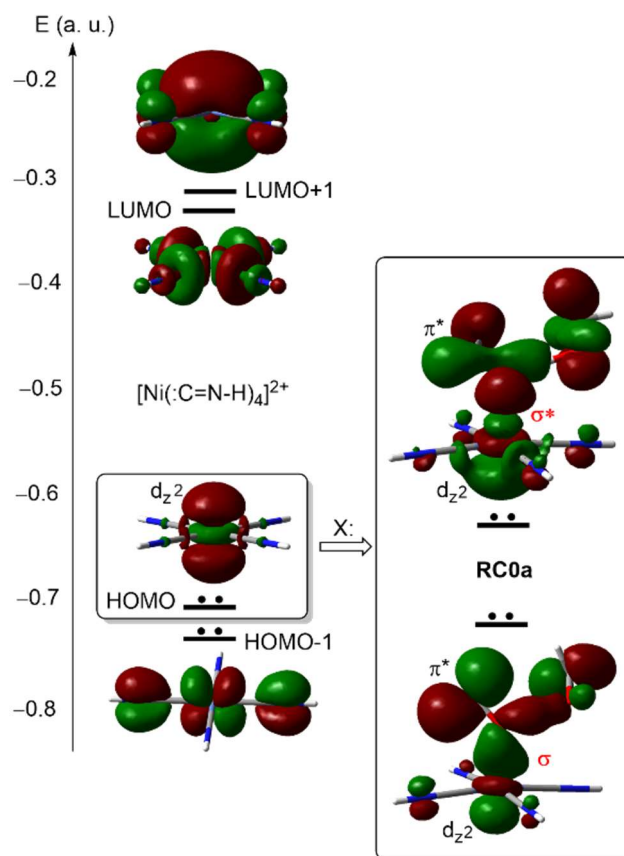


Figure 33. Relevant Kohn-Sham orbitals of **R0a** ($[\text{Ni}(:\text{C}=\text{N}-\text{H})_4]^{2+}$) and **RC0a** ($[\text{Ni}(:\text{C}=\text{N}-\text{H})_4]^{2+} \cdot 2\text{MeOH}$) complexes, computed at the $\omega\text{B97xD}/6-31\text{G}^*(\text{C},\text{H},\text{O},\text{N})$ & $\text{LanL2DZ}(\text{Ni})$ level of theory with an isovalue of 0.02 atomic units.

The apical MeOH of intermediate **INT1'a** is substituted by one isocyanide molecule to yield reactive complex **RC1a**, which exhibits a strong C-Ni interaction resulting from the interaction between the d_z^2 and d_{yz} AOs of the Ni(II) center and the π_{yz} MO of the isocyanide, the perpendicular π_{xz} MO of this ligand remaining unaffected, as it is shown in Figure 34.

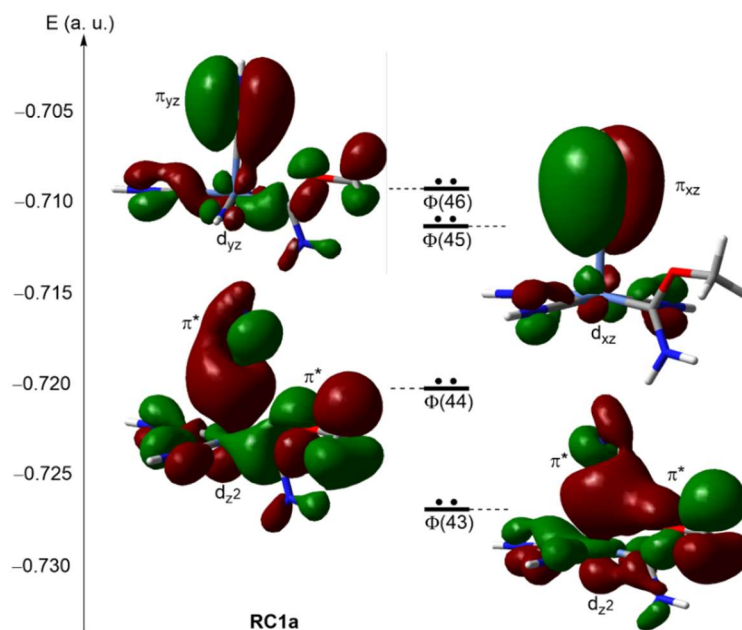


Figure 34. Relevant Kohn-Sham orbitals of reactive complex **RC1a**, computed at the ω B97xD/6-31G*(C,H,O,N)&LanL2DZ(Ni) level of theory with an isovalue of 0.02 atomic units.

This latter reactive complex initiates the propagation steps via reaction with the ligand resulting from the interaction with the previous isocyanide-MeOH moiety. This step leads to the addition of intermediate **R1a** via transition structure **TS2a**, with an activation energy of ca. 24 kcal/mol. As it can be seen by inspection of the FMOs of Figure 35, this latter saddle point combines the σ (Ni-C) component with the σ^\ddagger (C \cdots C) interaction along a symmetry-allowed process.

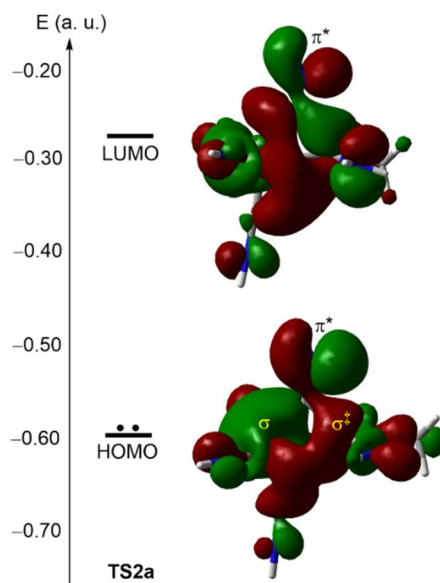


Figure 35. Relevant Kohn-Sham orbitals of transition structure **TS2a**, computed at the ω B97xD/6-31G*(C,H,O,N)&LanL2DZ(Ni) level of theory with an isovalue of 0.02 atomic units.

From intermediate **R1a**, the coordination-rearrangement process is repeated via **RC2a** and **TS3a** to yield **R2a**, which will coordinate an additional isocyanide molecule to continue with the polymerization process. Interestingly, this latter step proceeds with a significantly lower activation energy (ca. 7 kcal/mol), which is compatible with a large turnover catalytic cycle.

The next step in our research was to repeat the above discussed calculations in the b-series, in which the phenyl isocyanide ligand (R=Ph) is closer to the system used in our experimental studies. The reaction profile corresponding to the initiation steps are shown in Figure 36. As in the preceding case, the reaction starts with the coordination of two MeOH units to the square planar $[\text{Ni}(\text{CNH})_4]^{2+}$ complex **R0b**. This step is less exergonic than the equivalent calculated for the parent studies. Inspection of the MOs of **RC0b** (Figure 37) shows a more congested system, with closer filled MOs that suggest a higher Pauli repulsion in this initial complex.

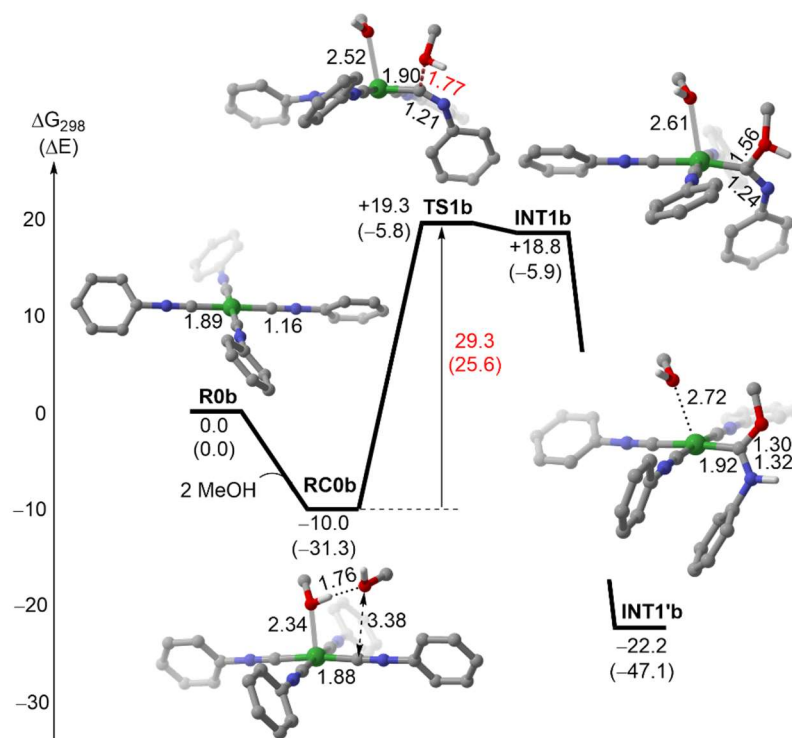


Figure 36. Reaction profile calculated for the initiation steps of b-series (R=Ph, Scheme 33) at the $\omega\text{B97xD}/6\text{-}31\text{G}^*(\text{C,H,O,N})\&\text{LanL2DZ}(\text{Ni})$ level of theory. Numbers close to the stationary points (reactants, intermediates transition structures and products) correspond to the relative Gibbs energies, in kcal/mol, calculated at 298.15 K. Numbers in parentheses are the relative total (electronic and nuclear) energies, including zero-point vibrational corrections, also in kcal/mol. Bond distances and internuclear distances are given in Å. Color code: gray, C; blue, N; red, O; green, Ni. Hydrogen atoms have been omitted for clarity.

The next steps of the initiation part of the mechanism follows the previously observed sequence for the a-series. Thus, one MeOH ligand migrates to the carbon atom of the adjacent phenyl isocyanide moiety, followed by a 1,3-prototropy from the oxygen to the nitrogen atom to give rise to intermediate **INT1'b**.

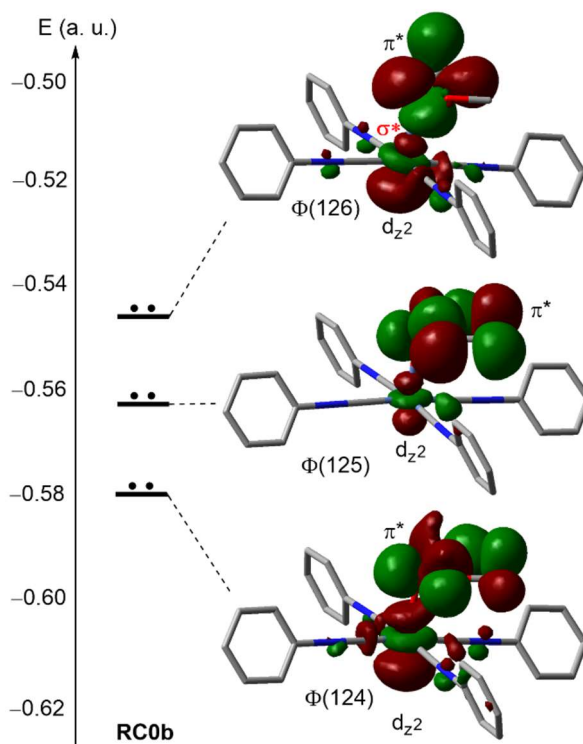


Figure 37. Relevant Kohn-Sham orbitals of reactive complex **RC0b**, computed at the ω B97xD/6-31G*(C,H,O,N)&LanL2DZ(Ni) level of theory with an isovalue of 0.02 atomic units.

The reaction profile corresponding to the first and second propagation steps of the b-series is gathered in Figure 38. As in the preceding case, intermediate **INT1'b** interexchanges with MeOH for the first CNPh isocyanide unit to be incorporated to one isocyanate of the Ni(II) complex. This occurs via transition structure **TS2b**, associated with a late three-center saddle point. This step leads to the 16-electron complex **R1b**, with a coordination position ready to incorporate the second CNPh isocyanide monomer to yield reactive complex **RC2b**, from which transition structure **TS3b**, structurally very similar to **TS2b** yields the active intermediate **R2b**. The electronic situation of this latter reactive complex is similar (but more complex to that found for its **RC2a** congener) with interaction between the π -MO of CNPh with the d_{xz} AO of the metallic center, and a σ^* MO associated with the carbenoid moiety and the d_{z^2} AO of Ni(II) (Figure 39).

Subsequent similar steps lead to the polymeric chain. Also, in this case, the barrier associated with the formation of the last 16-electron intermediate is significantly lower than that calculated for the previous step.

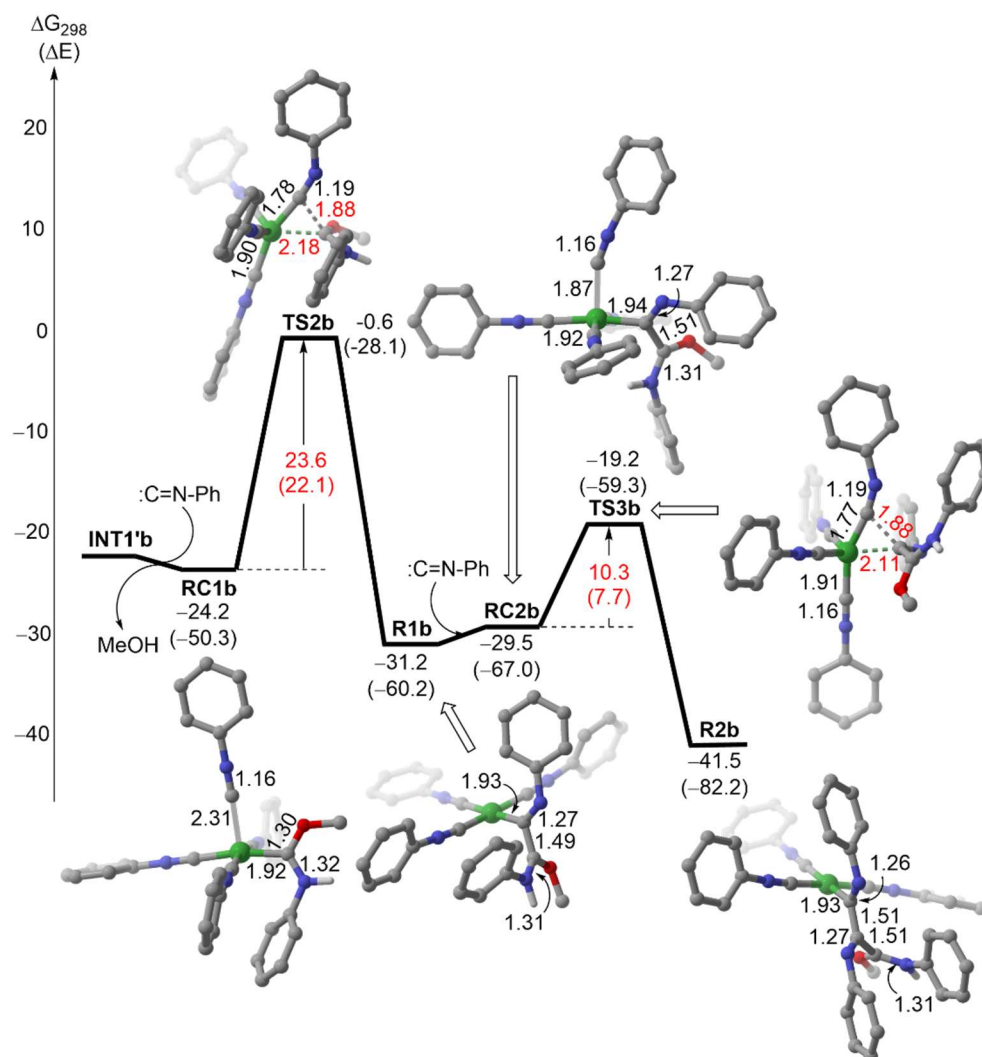


Figure 38. Reaction profile calculated for the propagation steps of b-series (R=Ph, Scheme 33) at the ω B97xD/6-31G*(C,H,O,N)&LanL2DZ(Ni) level of theory. Numbers close to the stationary points (reactants, intermediates transition structures and products) correspond to the relative Gibbs energies, in kcal/mol, calculated at 298.15 K. Numbers in parentheses are the relative total (electronic and nuclear) energies, including zero-point vibrational corrections, also in kcal/mol. Bond distances and internuclear distances are given in Å. Color code: gray, C; blue, N; red, O; green, Ni. Hydrogen atoms have been omitted for clarity.

In summary, our calculation show a global downhill polymerization process with decreasing activation energies as long as the polymerization process progresses. This is compatible with the efficient polymerization found experimentally. Other initiators like X_L chiral proline derivative (vide supra) result in much more congested initial

intermediates, which eventually can hamper the progression along the polymerization steps.

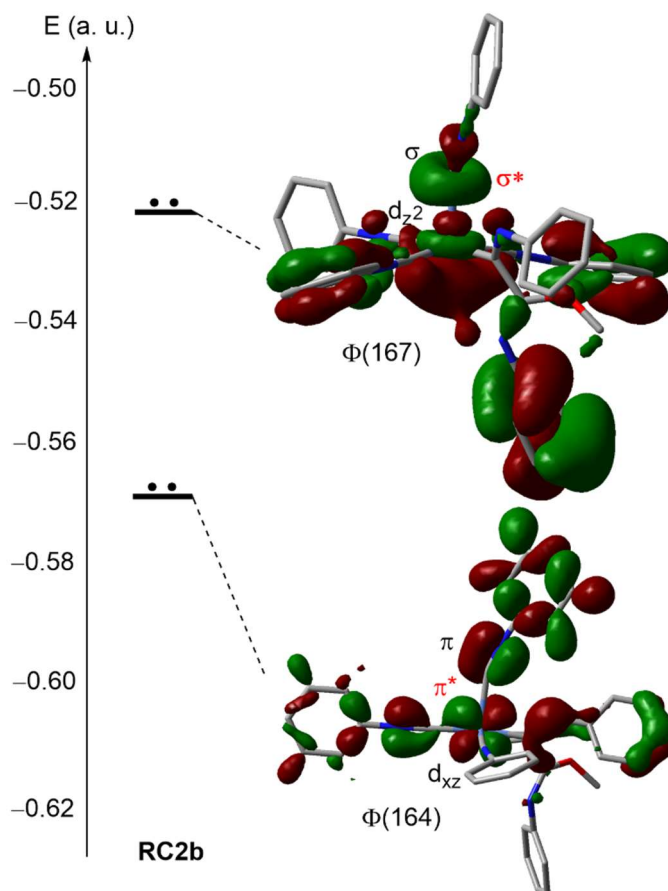
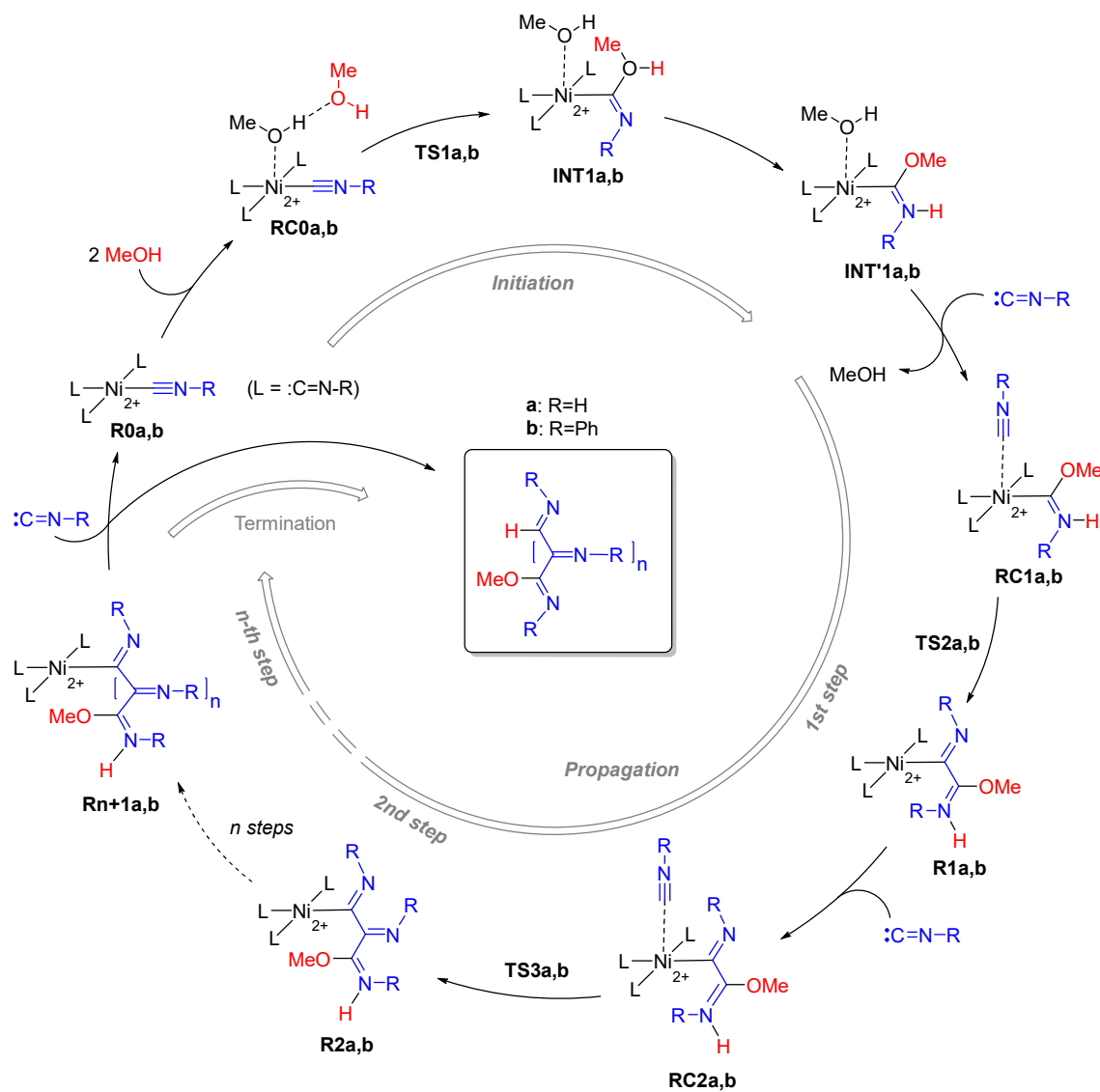


Figure 39. Relevant Kohn-Sham orbitals of reactive complex **RC2b**, computed at the ω B97xD/6-31G*(C,H,O,N)&LanL2DZ(Ni) level of theory with an isovalue of 0.02 atomic units.

On the basis of these DFT studies, we propose a refined version of the “Merry-go-round” mechanism depicted in Scheme 34. According to the cyclic mechanism, the initiation steps consist of the incorporation of two equivalents of Lewis base, such as methanol to the initial 16-electron square planar Ni(II) complex, followed by the addition of one equivalent of the Lewis base to the carbon atom of an adjacent isocyanide ligand. The unstable intermediate **INT1** is transformed in a more stable local minimum **INT’1** via 1,3-prototropy. The first step of the propagation phase consists of the substitution of the remaining basic ligand (MeOH in our case) by an additional isocyanide molecule to lead to intermediate **RC1**, which is therefore incorporated to the catalytic cycle, to form the next 16-electron complex **R1**, which incorporates the next isocyanide monomer to form the next reactive complex **RC2**. These propagation steps are repeated n-times until the **R_{n+1}** complex, instead of incorporating an additional isocyanide unit to the metallic

center, releases the final polymer with the concomitant recovery of the initial $[\text{Ni}(\text{CNR})_4]^{2+}$ R0 complex, thus reinitiating another catalytic cycle.



Scheme 34. Proposed cyclic mechanism for the polymerization of isocyanides catalyzed by Ni(II) salts.

2.7 CONCLUSIONS

From the studies carried out in this chapter, the following conclusions can be drawn:

1. Formation of isocyanide monomers from densely substituted γ -nitropolines by means of a hydrogenation-formylation-dehydration sequence can be conducted in an efficient manner. However, polymerization of these isocyanides in the presence of Ni(II) does not result in an efficient polymerization process.
2. An alternative design consisting of the elongation of the isocyanide chain by introduction of para-isocyano phenylimines results in an efficient polymerization process. Both achiral and chiral series of polymers have been obtained by this approach, with excellent stereocontrol.
3. In the case of isocyanide monomers incorporating terminal γ -amino prolines belonging to the *endo*- and *exo*- series, excellent helical chiralities have been observed. Very interestingly, the chiroptical properties of the *exo*- and *endo*-series are very different, which has been attributed to different arrangements in the respective polyisocyanide chains on the basis of Monte Carlo Molecular Mechanics Simulations.
4. DFT calculations have permitted to propose a model compatible with our experimental findings. This model constitutes a refinement of the previously proposed “Merry-go-round” mechanism and distinguishes the initiation process and different propagation steps. During the incorporation of successive monomeric units, the first addition is intrinsically different to the successive ones. Finally, the termination step releases the final polymeric chain, with concomitant regeneration of the initial $[\text{Ni}(\text{CNP})_4]^{2+}$ square-planar catalytic complex.

CHAPTER III
UGI FOUR-COMPONENT REACTION AND
POLYMERIZATION PROCESSES

3.1 OBJECTIVES

In this Chapter, on polymerization reactions in four component Ugi transformations, our general objectives have been the following uses:

1. To study the stereoselectivity induced in this reaction by chiral aldehydes possessing a good σ -attractor such as an alkoxy group.
2. To analyze the kinetics of this process in order to get a deeper knowledge of the processes that govern the four-component Ugi reaction.

A series of chiral aldehydes were designed and synthesized. Their influence in the multicomponent reaction was tested and verified by both variables experimental and computational methods, which would help to clarify the main kinetic variables that governs this process.

Furthermore, several polymerizations utilizing the chiral aldehydes in the formation of optically active polymers were conducted, and the potential of chiral monomeric units in the polymerization was examined.

3.2 ASYMMETRIC UGI REACTION

Chapter 1.3.2 has discussed how the Asy Ugi-4CR reaction could be accelerated in a stereocontrolled manner by an adequate catalyst or using chiral starting materials. In the latter case, chiral amines, acids, and isocyanides have been introduced in the reaction. In addition, the intermediate imine has also been used to improve the diastereomeric control. Regarding the other results, chiral amines and chiral imines always exhibited good enantiomer excesses of the Ugi-4CR products. This result indicates that the intermediate imine should be the key factor in controlling the configuration of the products. As shown in Figure 40, one of the possible reaction pathways was the isocyanide addition which could go through two different addition routes in the presence of the chiral substitutes. Depending on chiral substitutes R^1 or/and R^2 , the isocyanide addition could happen from the front or back side of the imine plane, which would consequently promote the corresponding adducts and the final product in opposite configurations.

Optically active imine could be prepared from commercially available chiral amines, where the R^2 substrate was chiral. However, the R^1 chiral center is closer to the asymmetric addition center and could induce better stereocontrol. Thus, we synthesized the chiral aldehydes to make R^1 a chiral substrate and promote the preferential isocyanide addition along a given prochiral face.

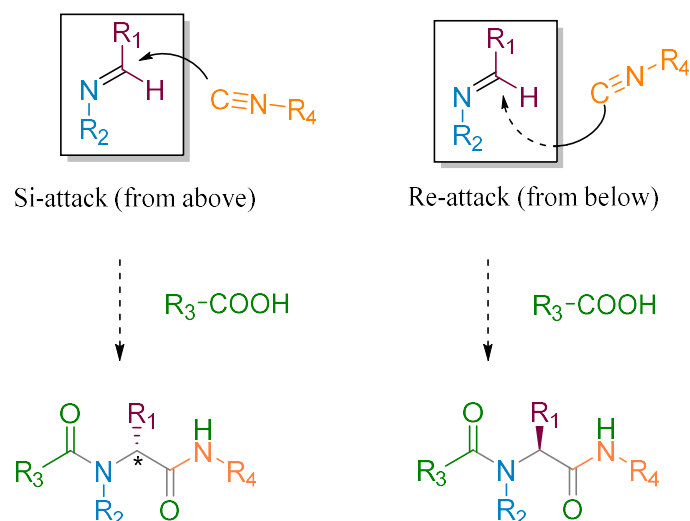
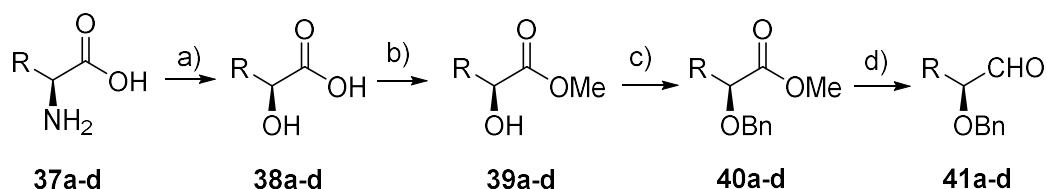


Figure 40. The attachment of isocyanide from the front side of the imine plane and the back side.

3.2.1 Synthesis of chiral aldehydes

To study the asymmetric Ugi-4CR with chiral aldehydes, we decided to follow the synthesis strategy from previous work in our group. The synthetic route started with the preparation from the readily available natural L-amino acids. L-Alanine, L-Valine, L-Leucine, and L-tert-Leucine were used in the synthesis of the required chiral aldehydes.

The amino group of the amino acid was first substituted with sodium nitrite to obtain the diazonium salt, followed by the hydrolysis of these unstable salts in a neutral environment to yield the corresponding 2-hydroxy acids **38** were obtained with retention of configuration. The obtained compounds were employed in the next step of methyl esterification under mild conditions. The esterification step required slight heating with corresponding alcohols in toluene to yield α -hydroxy esters **39**. Subsequently, the benzyl substitution to yield benzyloxy esters **40** was conducted via sodium hydride deprotonation of the hydroxy group. Finally, the reduction of the methyl ester group was considered to yield the corresponding α -benzyloxy aldehydes **41**, this was performed by controlled reactions with DIBAL (Scheme 35).



37-40a: R=Me; **37-40b:** R=ⁱPr; **37-40c:** R=ⁱBu; **37-40d:** R=^tBu

Scheme 35. Steps to prepare the chiral aldehydes **41**. a) **6** (1.0 equiv in 1 M H₂SO₄), NaNO₂ (1.5 equiv in H₂O), 0 °C, 24 h; b) DMP (1.0 equiv), TsOH·H₂O (0.007 equiv), MeOH, 45 °C, 24 h; c) **8** (1.0 equiv), NaH (1.0 equiv), anhydrous THF, 0 °C, 10 min, then benzyl bromide (1.2 equiv), RT, 24 h; d) **8** (1.0 equiv), DIBAL(1.5eq), anhydrous THF, -78 °C, 1 h. Me, Methyl; ⁱPr, isopropyl; ⁱBu, iso-butyl; ^tBu, tert-butyl.

The enantiomeric purity of the obtained aldehydes was determined by measuring optical rotation in chloroform at 589.3 nm and 0.1 g/L at 20 °C. All the chiral aldehydes prepared showed negative optical rotations in chloroform, as it can be seen in Table 10. Comparison of our results with those reported in the literature (when available) showed satisfactory results.¹¹¹

Table 10. Optical rotation of chiral aldehydes (CHCl₃, 1 g/100 mL, 589.3 nm, 20 °C). The optical rotation value described by other researchers were shown in brackets.

Aldehyde				
	41a	41b	41c	41d
[α]_{589.3}	-61° (ref: -60°)	-52°	-22° (ref: -22.8°)	-64°

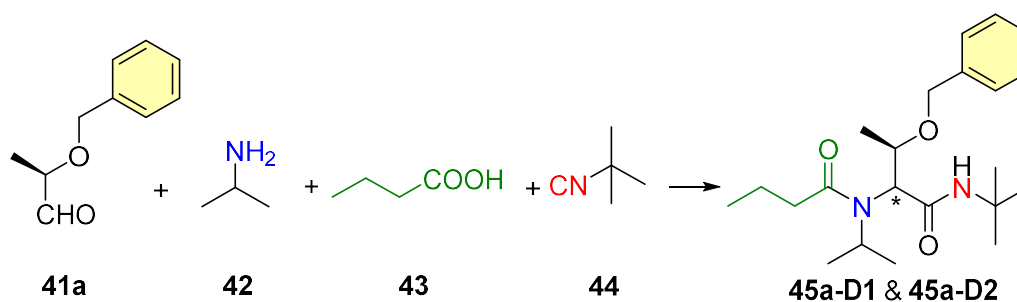
3.2.2 Asymmetric Ugi reaction with chiral aldehydes

The Ugi-4CRs were usually carried out in one flask by addition of the four substrates in a polar protic solvent such as methanol. Various methods were used to accelerate the condensation step corresponding to the formation of the imine, such as by molecular sieves (MS) or magnesium sulfate to remove the byproduct of water when the imine is difficult to form. However, the molecular sieves should be removed as soon as the imine was formed. Otherwise, the reaction did not work.

¹¹¹ Ramírez-Fernández, J.; Botubol, J. M.; Bustillo, A. J.; Aleu, J.; Collado, I. G.; Hernández-Galán, R. *Nat. Prod. Commun.* **2011**, *6*, 1934578X1100600404.

As previously reported, we found that the Ugi-4CRs were not sensitive to the atmosphere environment or the presence of water. Thus, for repeatability and accessibility considerations, we carried out the asymmetric Ugi-4CR under mild conditions without inert gas environment protection. To determine the optimal conditions, a model reaction of (S)-2-ethoxypropanal **41a**, isopropylamine **42**, butyric acid **43** and tert-butyl isocyanide **44** under various reaction conditions was investigated. The results are shown in Table 11.

Table 11. First optimization of asymmetric Ugi-4CR.



Entry	aldehyde	Solvent	Temperature (°C)	Diastereomer 1 (45a-D1, %) ^a	Diastereomer 2 (45a-D2, %) ^a	Total yield (%)
1	41a	MeOH	20	46	35	83
2	41a	DCM	20	42	38	80
3	41a	MeOH	0	47	41	88
4	41a	DCM	0	37	40	77

^a Diastereomer ratio, and the yields of **45a-D1** and **45a-D2** were obtained after purification by FC.

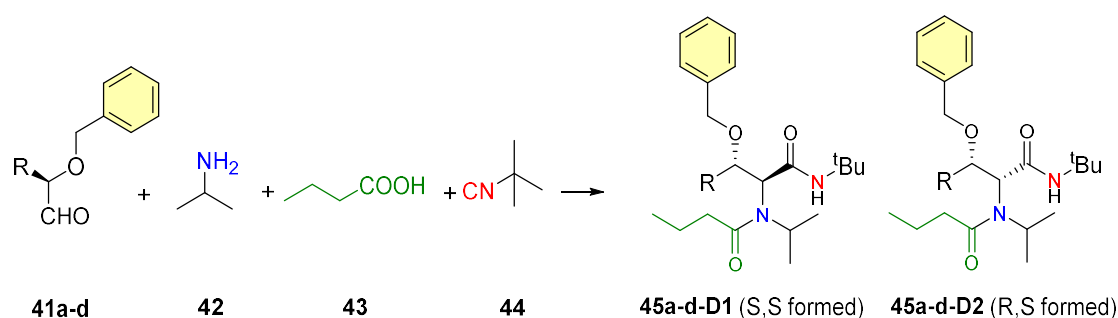
Our results indicated that methanol was more favorable than dichloromethane. This is in agreement with other studies, which indicated that the Ugi-4CR is more favorable in polar solvents. However, the temperature decrease did not give better diastereomeric control (Table 11, entries 3 and 4).

With the conditions obtained from the model reaction, the first step of the asymmetric Ugi-4CR was achieved by the synthesis of imine by mixing aldehyde **41a** with isopropylamine **42**, followed by the injection of butyric acid **43** and tert-butyl isocyanide **44**.

The chiral aldehydes and isopropylamine were mixed for at least one hour. This was to ensure the total formation of imine. In the following steps, the butyric acid was added to

protonate the imine to form an iminium intermediate. After addition of the acid for 10 min, the final reactant, tert-butyl isocyanide, was added to the resulting reaction mixture. The reaction was monitored by thin-layer chromatography. After a high conversion was reached, the reaction mixture was evaporated under reduced pressure and then purified by HPLC-UV-VIS with an achiral column to obtain two diastereomers, the corresponding α -acylaminoamide peptides were obtained in **45a-d** (S,R) and (R,R) forms respectively. The diastereomeric ratio (dr.) were determined by HPLC and $^1\text{H-NMR}$ (Table 12). It's interesting to indicate that two diastereomers were always in the form of a colorless oil and a crystal, which facilitated the separation of both diastereomers (See annexes III and V). In the case of Ugi adduct **45d-D1** the crystals could be resolved by X-ray diffraction analysis (Figure 41, see annexes VI for further details).

Table 12. Asy Ugi-4CR with chiral aldehydes.



Entry	aldehyde	R	dr ^a	Diastereomer 1	Diastereomer 2	Total yield (%) ^c
				45a-d-D1 (ee, %) ^b	45a-d-D2 (ee, %) ^b	
1	41a	Me	50:50	33	43	82
2	41b	ⁱ Pr	65:35	77	80	73
3	41c	^t Bu	60:40	50	25	72
4	41d	^t Bu	80:20	88	57	76

Reaction condition: MeOH, rt. ^a Diastereomer ratio refers to the corresponding diastereomer 1 (S,S formed): diastereomer 2 (R,S formed), Determined by HPLC with the achiral stationary phase. ^b Determined by HPLC with the chiral stationary phase (see annexes V), the exact structure of **45b-D1** and **45d-D1** was determined by crystal-XRD (see annexes VI). ^c Determined by FC with silica gel.

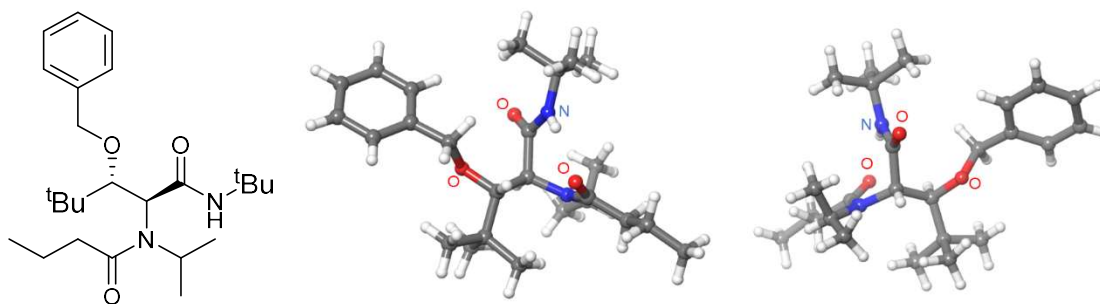


Figure 41. Ball and stick representation for the isocyanide derivative **45d-D1**. (to see the ORTEP diagram, visit annexes VI)

The results of the survey corresponding to the reaction of aldehydes **41a-d** are summarized in Table 12. In the original attempt, the asymmetric Ugi-4CR with (S)-2-ethoxy-propanal **41a** with a methyl group in the alkyl chain gave no diastereomer control and poor enantiomer control. It was concluded that the methyl group of **41a** is not bulky enough to induce any significant stereocontrol. Therefore, increasing the volume with a bulkier substituent could improve the diastereomeric ratio. Thus (S)-2-(benzyloxy)-3-methyl-butanal **41b** possessing an ⁱPr group was prepared. As supposed, the presence of the isopropyl in the α - position improved the stereomeric ratio. This result motivated us to test another bulky alkyl groups, such as the three isomers of the butyl group: sec-butyl, iso-butyl, and tert-butyl. However, as sec-butyl α -substituted aldehyde would introduce three chiral centers in the final products and would cause additional difficulties in the HPLC analyses, this option was finally abandoned. Therefore, (S)-2-(benzyloxy)-4-methylpentanal **41c** and (S)-2-(benzyloxy)-3,3-dimethylbutanal **41d** were prepared and used in asymmetric Ugi-4CRs (Table 12 entries 3 and 4).

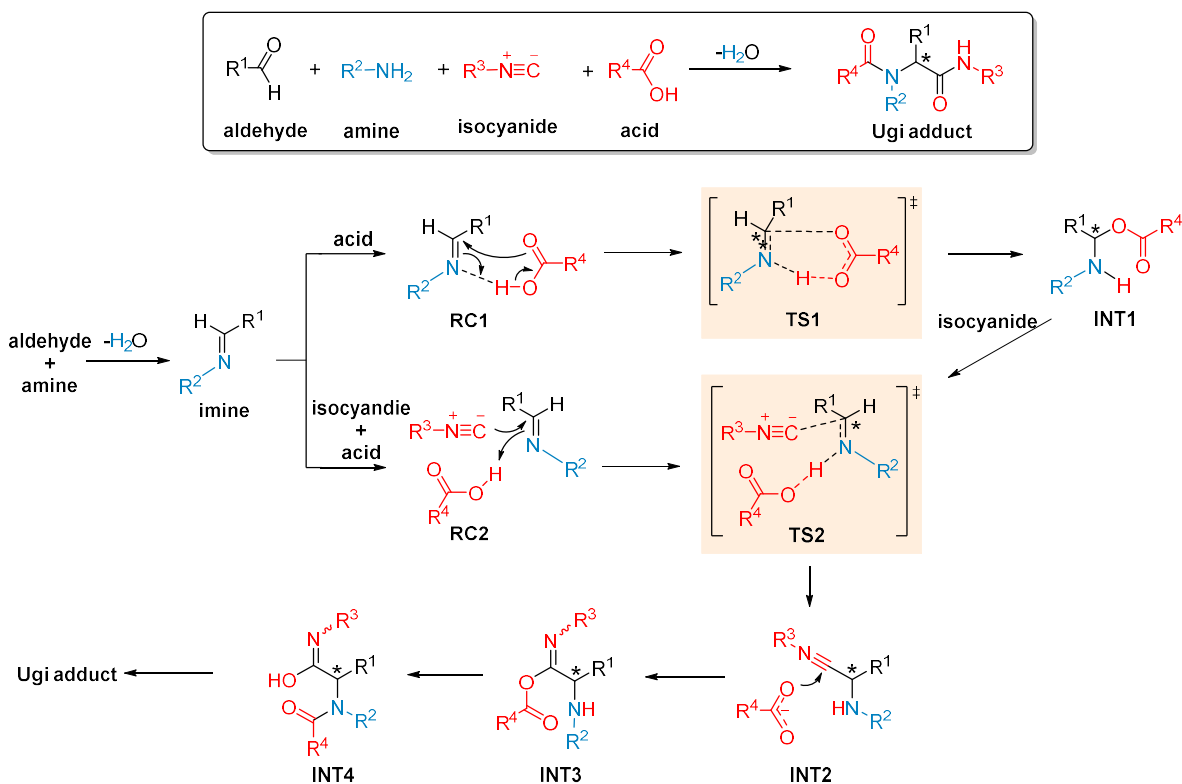
Though aldehyde **41c** with a sec-butyl group got the same result as **41b**, aldehyde **41d** with the tert-butyl group yielded a higher diastereomeric ratio of 80:20 of products **45d-D1:45d-D2**. This was attributed to the distance between the steric center and the nucleophilic addition site. For a sequence from methyl, isopropyl, iso-butyl to tert-butyl group, which enjoys the same distance between the steric center and the nucleophilic addition center, the one with more significant steric repulsion owns the best asymmetric control.

Another information that could be obtained from Table 12 is the racemization of the starting chiral aldehyde. According to entry 1, the chiral center of (S)-2-ethoxypropanal **41a** has undergone a kind of racemization process in the Ugi-4CR, which results in a low

enantiomer excess of S and R configuration in **45a-D1** (S,S-configuration) and **45a-D2** (R,S configuration). The acidic conditions may cause the racemization. These partial racemization processes were less extensive in the case of aldehyde **41b** and **41d** (diastereomer D1).

3.2.3 Reaction mechanism and origins of stereocontrol

In this study, we have proposed a slightly different reaction pathway. According to Scheme 36, the Ugi reaction required the union of an aldehyde, an amine, an isocyanide and a carboxylic acid to form the final Ugi adduct. The first steps of the reaction always start from the formation of an imine, achieved by the condensation of the aldehyde and the amine. The next step has two possible routes. One proceeds towards intermediate **INT1** with the protonation by the added carboxylic acid through reagent complex **RC1** and transition state **TS1**. The other route forms **INT2** via interaction with both isocyanide and carboxylic acid (Scheme 36). However, through DFT calculations, we observed (results not shown) that the intermediate **INT1** is a dead end and cannot evolve towards **INT2** via **TS2**. This means **INT2**, is the only viable intermediate that leads to the final Ugi adduct by the widely accepted rearrangement through **INT3** and **INT4**.



Scheme 36. Proposed reaction pathway for asy Ugi-4CRs.

In order to understand the behavior of the methyl and tert-butyl groups, we performed DFT studies of the transition structures associated with the *re* and *si* attacks of tert-butyl isocyanide **44** on the imines derived from aldehydes **41a** (R = Me) and **41d** (R = ^tBu). These calculations were performed using the M06-2X¹¹² hybrid functional and the 6-31+G* basis set. The solvent was tackled as a continuous with the Polarizable Continuous Model (PCM).¹¹³ The solvent introduced in the calculation was methanol, the same used in the experimental studies.

In principle, two possible stereochemistries can be considered in this kind of addition reactions. In the first one, the sigma bond being formed (σ^\ddagger) can be antiperiplanar respect to de σ -attractor. In this case, the antiperiplanar benzyloxy group, for which there is a two-electron stabilizing interaction between the σ^\ddagger orbital and the low-lying σ^* antibonding orbital of the C-O bond (Figure 42 model A). This is the Einstein-Felkin-Anh model.¹¹⁴ The alternative approach consists of the interaction between the antibonding σ_\ddagger^* orbital of the new bond being formed and the σ orbital associated with the antiperiplanar alkyl group (methyl and tert-butyl in our case). This corresponds to the Cieplak model¹¹⁵ and is represented in Figure 42, model B.

¹¹² Zhao, Y.;Truhlar, D. G. *Theor. Chem. Acc.* **2008**, *120*, 215-241.

¹¹³ Mennucci, B. *Wiley Interdiscip. Rev. Comput. Mol. Sci.* **2012**, *2*, 386-404.

¹¹⁴ a) Houk, K. N. *Theor. Chem. Acc.* **2000**, *103*, 330-331. b) Anh, N. T.; Eisenstein, O. *Nouv. J. Chim.* **1977**, *1*, 61-70.

¹¹⁵ a) Cieplak, A. S. *J. Am. Chem. Soc.* **1981**, *103*, 4540-4592. b) Alabugin, I. V.; Gimore, K. M.; Peterson, P. W. *Wiley Interdiscip. Rev. Comput. Mol. Sci.* **2011**, *1*, 109-141.

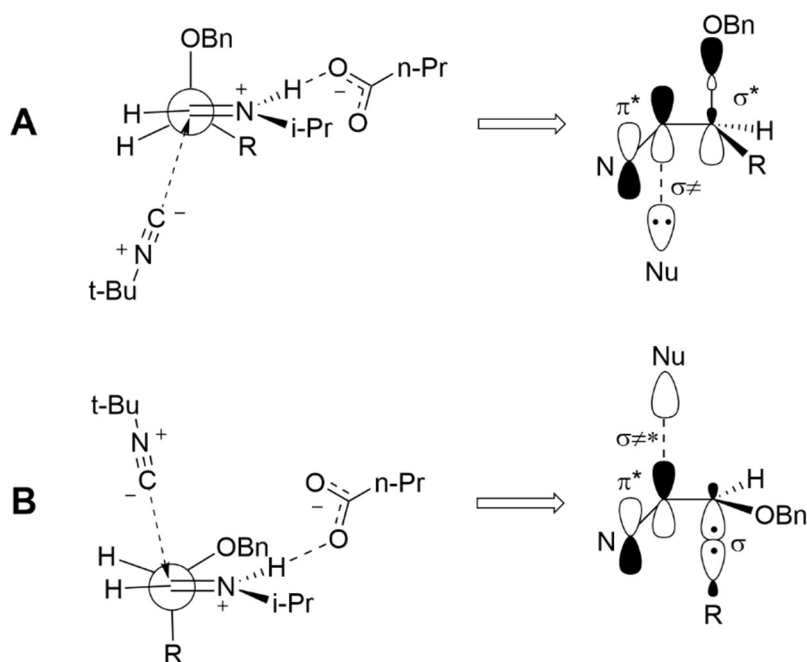


Figure 42. Two-electron interaction models between the nucleophilic isocyanide reactant and the intermediate electrophilic imine. (A) Einstein-Felkin-Anh. (B) Cieplak model.

Our calculations on the **TS2** transition structures (Scheme 36, Figure 43) associated with the nucleophilic attack of tert-butyl-isocyanide **44** to the imine formed in situ after the condensation between aldehydes **41a,d** and isopropylamine **42** activated with n-butyric acid **43** showed that in the case of aldehyde **41a** ($R = \text{Me}$) both *si* and *re* nucleophilic addition models A and B shown in Figure 42 are almost isoenergetic. In the case of aldehyde **41d** ($R = \text{tert-butyl}$), the Einstein-Felkin-Ahn model A of Figure 42 is the most favored one, probably because of the optimal trade-off between two-electron interaction and steric effects. This results in the preference for the *re*-attack in this latter case. Both computational results are in nice agreement with the experimental data reported in Table 12 and indicate that only a very bulky alkyl group can generate an efficient diastereocontrol in the Ugi reaction involving this kind of α -alkoxy aldehydes.¹¹⁶

¹¹⁶ Walsh, P. J.; Kozlowski, M. C. *Fundamentals of asymmetric catalysis*. 2009. University Science Books.

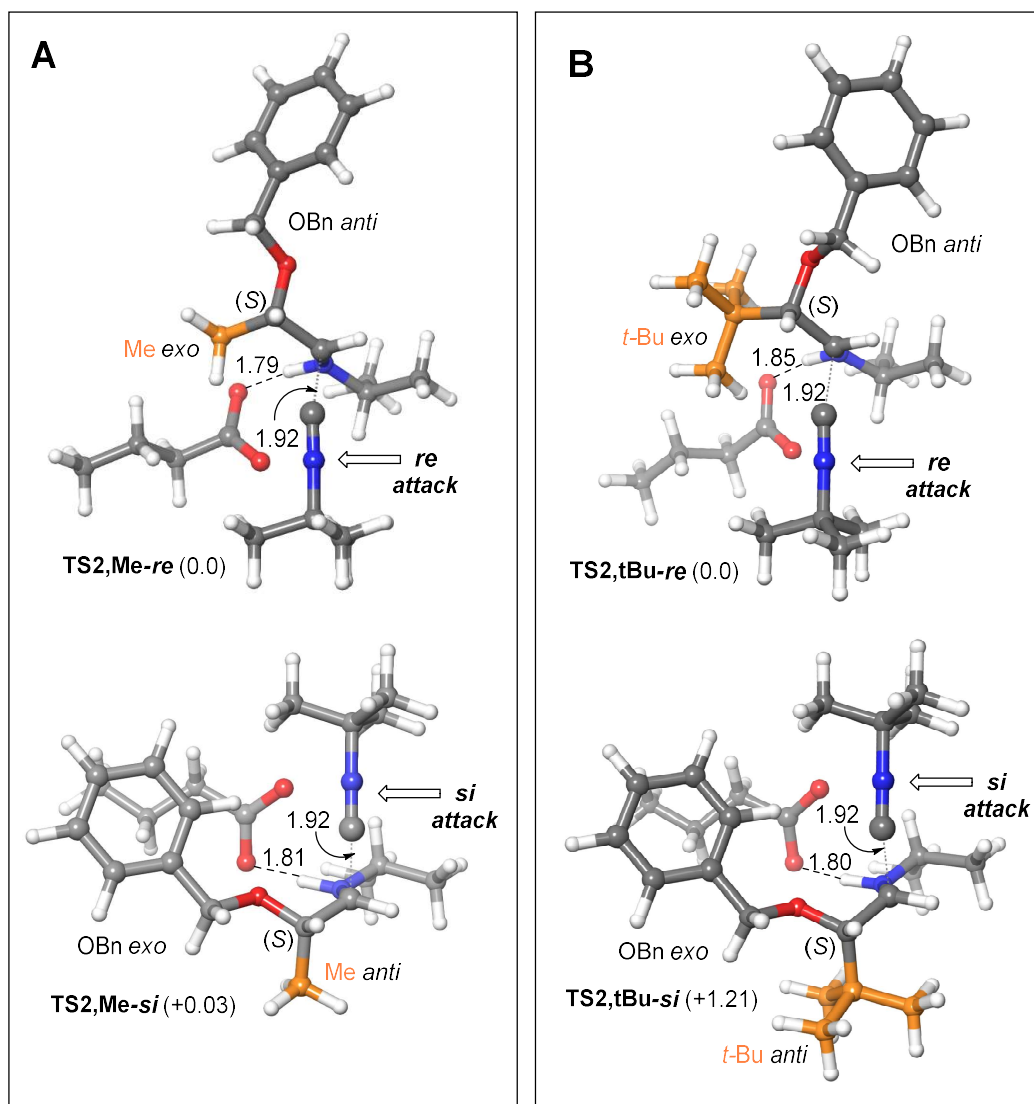


Figure 43. Transition structure (TS2, M06-2X(PCM solvent=methanol)/6-31+G(d,p) level of theory) corresponding to the stereochemistry-determining step of the Ugi reaction between butyric acid, tert-butyl isocyanide, isopropylamine, and aldehydes **41a** (A) & **41d** (B). Bond distances are given in Å. Numbers in parentheses are the relative free energies, in kcal/mol, computed at 298K.

The mechanism of the stereocontrolled Ugi-4CR is still under debate,¹¹⁷ as it has been discussed in the Introduction of this thesis.

3.2.4 Kinetic study

In order to get a deeper understanding of the reaction mechanism, we measured the evolution of the reaction mixtures by time-dependent NMR and FTIR. In this asymmetric Ugi-4CR, since the reaction includes a complex mixture of various compounds, it was

¹¹⁷ Banfi, L.; Basso, A.; Guanti, G.; Riva, R. *Asymmetric Isocyanide-based MCRs*. In *Multicomponent reactions*, Zhu, J. ; Bienaime, H.; Eds. Wiley-VCH; Weinheim, **2005**, pp1-10.

very difficult to find a signal to monitor the evolution of the reaction by NMR. Therefore, FTIR was used to determine the overall kinetic constant.

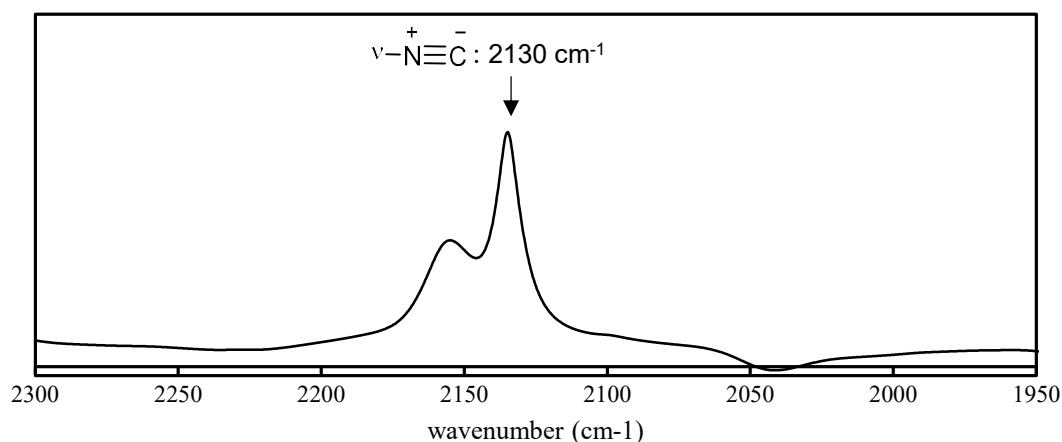


Figure 44. FTIR spectrum of asy-Ugi-4CR reaction mixture measure in KBr Liquid Cells with 20 scans after 1 hour reaction. Free isocyanide peak appears at 2130 cm^{-1} and the broad band corresponds to associated isocyanide-methanol aggregates.

In the IR spectra, the isocyanide signal corresponding to the 2130 cm^{-1} was clear and it was split because of the gaussian distribution of different hydrogen bonds formed by the anionic part of the isocyanide and the hydrogen atoms of the protic solvent¹¹⁸ (Figure 44). Therefore, the consumption rate of isocyanide could be used to calculate the reaction rate. The FTIR analyses were carried out in a KBr liquid cell with 20 scans every minute and the concentration of the isocyanide in the reaction mixture was calculated from the integral of the isocyanide peaks (from 2100 cm^{-1} to 2200 cm^{-1}).

First of all, a calibration experiment using different isocyanide solutions and IR integrals was conducted to assess the accuracy of this method. Five different concentrations of tert-butyl isocyanide in MeOH were prepared at 0.8 M, 0.9 M, 1.0 M, 1.1 M, and 1.2M. The IR integral of the isocyanide signal fits perfectly with the real concentration of $R^2 = 0.99$ (Figure 45). This result shows that time-dependent IR can be used to determine the global reaction constant.

¹¹⁸ a) Maj, M.; Ahn, C.; Błasiak, B.; Kwak, K.; Han, H.; Cho, M. *J. Phys. Chem. B.* **2016**, *120*, 10167-10180. b) Błasiak, B.; Ritchie, A. W.; Webb, L. J.; Cho, M. *Phys. Chem. Phys.* **2016**, *18*, 18094-18111. c) Maienschein-Cline, M. G.; & Londergan, C. H. *J. Phys. Chem. A.* **2007**, *111*, 10020-10025.

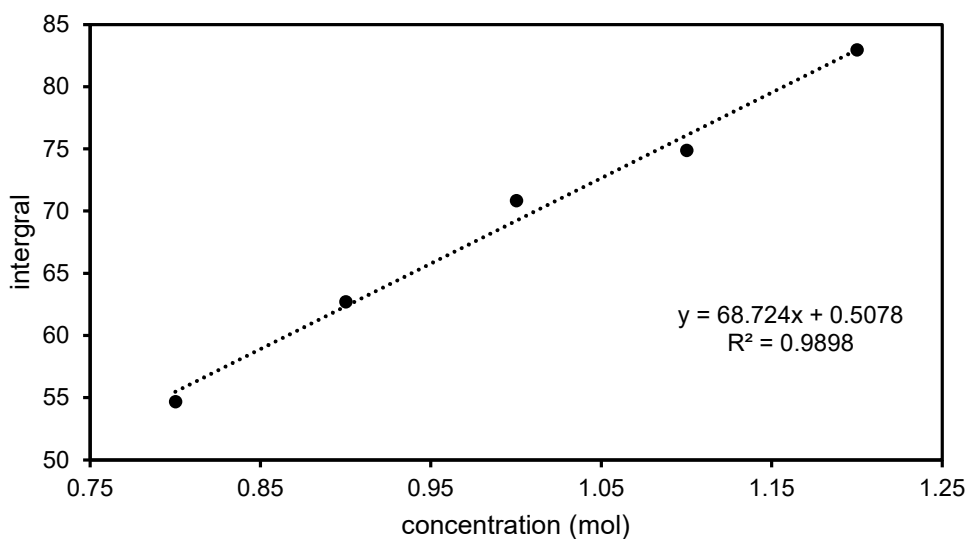


Figure 45. Calibration of IR isocyanide signals in MeOH solution at different concentrations.

Reaction half-lives method to determine the kinetic constant

The half-life method is one of the most popular methods to determine the order of a reaction. Considering that at $t = 0$, the initial value of $[B]$ is $[B]_0$, and that by definition at $t = t_{1/2}$, $[B]_t = [B]_0/2$, the reaction constant, k , and the reaction order, n , are connected by eq. (2).¹¹⁹

$$t_{\frac{1}{2}} = \frac{(2^{n-1} - 1)}{k(n-1)[B]_0^{n-1}} \quad (\text{eq. 2})$$

A logarithmic transformation of eq (2) yields the following linear expression:

$$\log t_{\frac{1}{2}} = \log \frac{(2^{n-1} - 1)}{k(n-1)} - (n-1) \log[B]_0 \quad (\text{eq. 3})$$

In this equation, $\log[B]_0$ and $\log t_{1/2}$ are linearly dependent. The slope and intercept can be calculated from a plotting line and used to calculate the reaction order and kinetic constant.

Thus, five plots were needed to carry out the calculation. Consequently, five reactions at different initial concentrations were conducted. We set up five Ugi-4CR in the following

¹¹⁹ Steinfeld, J. I., Francisco, J. S., & Hase, W. L. *Chemical kinetics and dynamics*. Upper Saddle River, NJ: Prentice Hall. 1999, 518.

initial concentrations: 0.8 M, 0.9 M, 1.0 M, 1.1 M, and 1.2 M. As a result, five curves of the evolution of isocyanide concentration with time were obtained. The five plots of $\log[B]_0$ with $\log t_{1/2}$ were used in Figure 46 to calculate the reaction order and reaction constant by linear fitting.

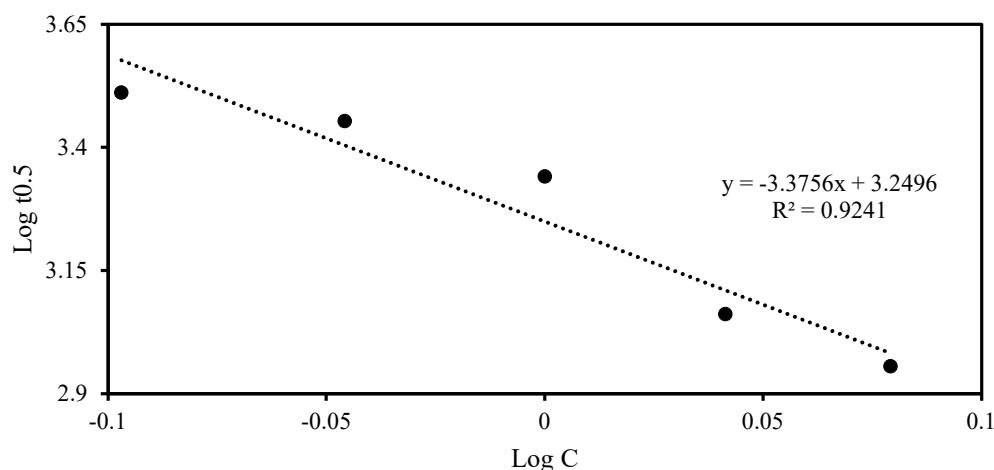


Figure 46. 5 plot fitting of asy Ugi-4CR by reaction half-life methods.

According to the fitting line, the slope of the line is 3.37 and the intercept is 3.24, which figures out the reaction order $n = 4.3 \cong 4$ and global reaction constant $k = 1.7 \cdot 10^{-3} \text{ mol} \cdot \text{L}^{-1}$. This result suggests that the four components required for the successive addition steps are relevant in the kinetics of these reactions.

3.3 UGI POLYMERIZATION

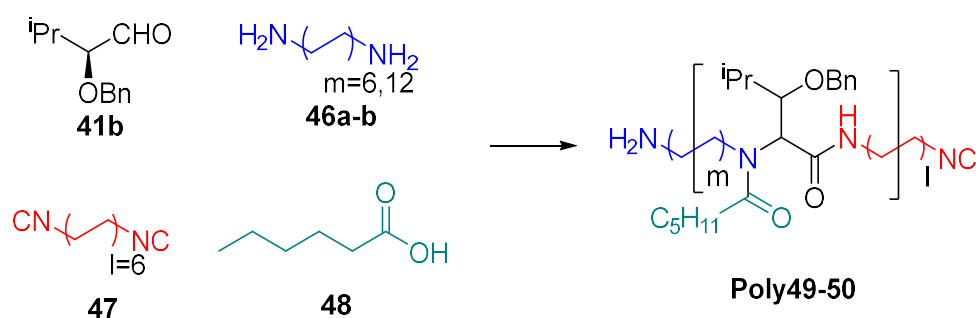
The extension of multicomponent reactions (MCRs) from small molecules to the field of polymer chemistry has accelerated the preparation of functional polymers with complex structures and special properties that have been recently appreciated in polymer science.

As one of the most significant members among MCRs, Ugi 4-component polymerization has been demonstrated to yield poly(peptide-peptoids), a biocompatible material that is being actively explored for biomedical application in an efficient and modular approach. However, polypeptoids obtained from ring-opening polymerization lack main-chain chirality, which should be attributed to the side chains appended to the amide nitrogen and the intermolecular and intramolecular hydrogen bondings are not strong enough.

Using asymmetric Ugi-4CR in polymerization would be a solution as it would generate a new controllable chiral center in the main chain, producing a polymer with both side chain and main chain chirality accessible.

Even though the Ugi-4CR exhibit high conversion in small molecules, Ugi 4-component polymerization always results in low efficiency and low M_n values, a common phenomenon among polymer materials. Our first Ugi-4CR polymerization attempt via diamine and diacid resulted in the formation of oligomers ($M_n < 1000$ g/mol). Michael et al.⁹⁵ investigated the non-chiral Ugi 4-component polymerization by combining two bifunctional and two monofunctional components. Overall, six combinations, diisocyanide and diamine have been suggested as the best combinations to yield a polymer with good properties ($M_n = 17800$ g/mol; PDI=2.23), and the other combination also results in a polymer M_n range from 9000 g/mol to 15000 g/mol.

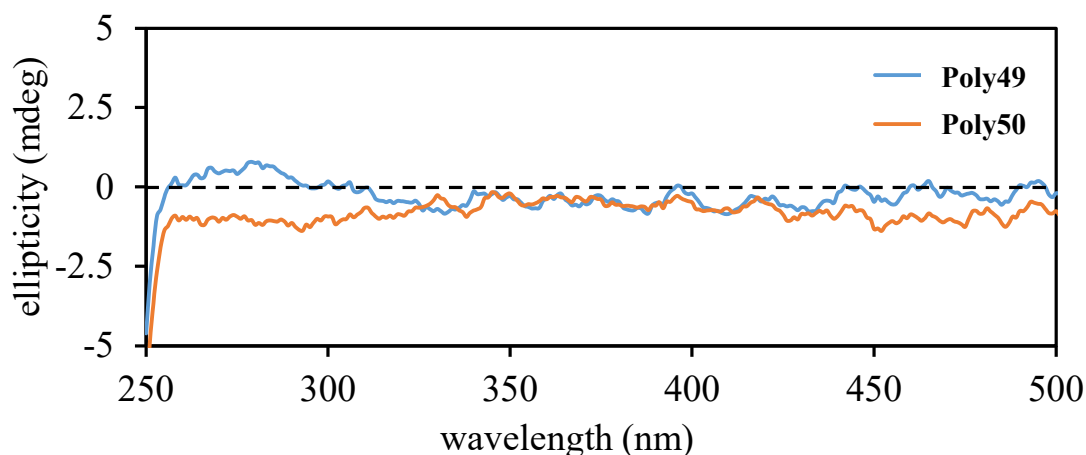
Chiral aldehyde with isopropyl substrate was used (derived from readily accessible L-Valine) to carry out the asymmetric polymerization because of its facile synthetic route and acceptable diastereomeric control. In the first attempt of our chiral Ugi polymerization, chiral aldehyde **41b**, ethane-1,2-diamine, glutaric acid, and tert-butyl isocyanide **44** were utilized in the preparation of the polymer. However, only oligomers with M_n values less than 1000 g/mol were obtained. This indicates that this method was not appropriate for the Ugi polymerization. So another reaction with bifunctional monomers were implemented.

Table 13. Asy Ugi-4CR polymerization conducted by diamine and diisocyanide.


Entry	Polymer	m	Mn (g/mol)	PDI	Repeating unit
1	Poly49	6	3600	1.30	4
2	Poly50	12	12800	1.28	14

Reaction conditions: T = 25 °C; MeOH/THF = 2/1 (v/v); 2 days.

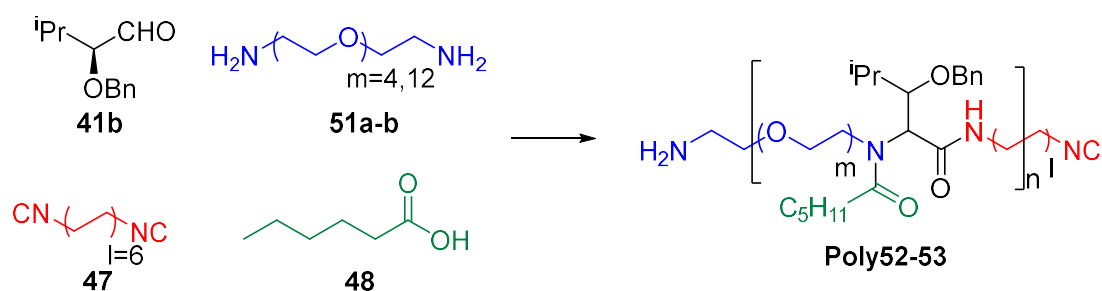
Hexamethylenediamine/1,12-Diaminododecane **46a**, 1,6-Diisocyanohexane **47** and hexanoic acid **48** were employed with chiral aldehyde **41b** to prepare **Poly-49** as the seconded attempt. The obtained results are reported in Table 13. The result obtained by GPC analysis shows that **Poly-49** was only an oligomer with 4 repeating units in its main chain. However, when the carbon atom in diamine was changed from 6 to 12 (diamine **46b**), the repeating unit increased to 14 and resulted in a Mn value of 12800 g/mol. The possible explanation for that should be derived from the reassembly steps. The reaction pathway proposed in Scheme 36 required a reassembly step from **INT3** to **INT4** to form a stable Ugi adduct. If the two neighboring polymer units were too close to each other, the reassembly might be restricted. Thus, when hexamethylenediamine **46a** was replaced by 1,12-Dodecanediamine **47b**, a much larger Mn **Poly50** was obtained.


Figure 47. CD spectrum of **Poly49** and **Poly50** in CHCl₃ at 20 °C (0.5 mg/mL).

Poly49 and **Poly50** were dissolved in chloroform to measure the CD intensity characterizing these two polymers' chirality (Figure 47). In our assumption, this peptoid-like polymer with chiral building blocks to form a similar structure as protein should exhibit helical chirality. However, the CD spectra indicates that the polymer has no chiral structure.

Aside diamines with long hydrocarbon chains, PEG-diamine was also included in the reaction in order to introduce more flexible part in the polymer chain. We reasoned that this could increase the activity of the backbone, thus permitting to arrange itself in a helical structure. In addition, we thought that the presence of PEG could increase the solubility of the polymer in water. Different PEG-diamines with four or twelve ethylene glycol units were assessed in the polymerization reaction. However, both **Poly52** and **Poly-53** obtained from the corresponding PEG-diamine **51a** and **51b** were oligomers with merely four repeating units (Table 14). This shows that the polymerization with PEG-diamine was not feasible.

Table 14. Asy Ugi-4CR polymerization conducted by PEG-diamine and diisocyanide.



Entry	Polymer	Diamine	m	Mn (g/mol)	PDI	Repeating unit
1	Poly52	51a	6	1900	1.19	4
2	Poly53	51b	12	2200	1.16	4

Reaction conditions: 25 °C, MeOH/THF = 2/1, 2day.

3.4 CONCLUSIONS

The following conclusions can be drawn from the asymmetric Ugi-4CR reaction, polymerization and mechanistic study.

1. A family of novel chiral aldehydes were prepared from natural amino acids in high yields via a series of reactions. The obtained aldehydes were characterized and showed high optical purities.
2. Asymmetric Ugi-4CR has been performed with previously prepared chiral aldehydes. The HPLC analyses denoted that when the substituted group in the α position of the chiral aldehydes were increased in size, both the diastereomer excess and enantiomer excess yielded better results. Computational studies showed that the stereochemical outcome is compatible with the Einstein-Felkin-Anh model when bulky substituents (ⁱPr and ^tBu) are considered.
3. Asymmetric Ugi, 4 component polymerizations, were carried out with different diamines and diisocyanides. The employment of 1,12-diaminododecane, 1,6-diisocyanohexane, hexanoic acid, and (S)-2-ethoxypropanal has permitted to obtain good Mn and PDI values. However, the desired chiral helical structure has been not been observed in the polymer material.

ANNEXES
PROCEDURES AND SPECTRA

I. GENERAL INFORMATION

All experiments requiring a dry atmosphere were performed using conventional vacuum lines and Schlenk techniques. The commercial reagents were purchased from Sigma MERK (Sigma-Aldrich), TCI (Tokyo Chemical Industry CO), abcr Gmbh and STREM and were used without further purification. Toluene and THF were purified by MBSPS 800 MBraun solvent purification system. EtOH (Ethanol, 96 %vol, VWR) MeOH (Methanol <0.1% water, VWR). Chloroform (stabilized with about 0,6 % of ethanol, MERCK), DMF (*N,N*-dimethylformamide, anhydrous 99,8%, MERCK). Hexane (95% alkanes mixture for synthesis, Panreac). EtOAc (Ethyl acetate ExpertQ® ACS, ISO, Reag., Scharlab). MeCN (Acetonitrile UVASOL® MERCK).

II. ANALYTICAL METHODS

Thin layer chromatographies (TLC) were performed on aluminium TLC plates (silica gel coated with fluorescent indicator F254), and visualized either by exposure to UV light or staining with potassium permanganate.

Flash column chromatographies were carried out with silica gel 60 (0.040- 0.063 mm), eluting with a gradient of polarity with ethyl acetate in a hexane mixture from 0% to 30%.

High performance liquid chromatographies were conducted on a e2695 Separations Module (Alliance, Waters) with chiral stationary phase and eluent of Hexane/Isopropanol.

Fourier Transform Infra-Red (FTIR) spectroscopy spectra were recorded on an FT-IR spectrometer equipped with a diamond detection and single-reflection ATR module; wavenumbers are given in cm^{-1} .

Nuclear Magnetic Resonance spectroscopy. ^1H -NMR, ^{13}C -NMR, g-COSY, HSQC, and HMBC spectra were recorded at 400 or 500 MHz and 101 or 126 MHz for ^{13}C -NMR, equipped with a z gradient BBOF probe, in Chloroform-d (CDCl_3), Actone-d₆, DMSO-d₆, or Methanol-d₄. The data are reported as s for singlet, d for doublet, dd for double doublet, t for triplet, m for multiplet or unresolved, coupling constant (J) in Hz, integration. The ^1H spectra were recorded using noesygppr1d sequence from Bruker's library at 500.13 MHz. A time domain of 64 k and a spectral width of 10000 Hz. Interpulse delay: 1 s. Acquisition time: 3 s. number of scans: 64. Mixing time: 0.01 s.

Mass spectrometry (MS) and high-resolution mass spectrometry (HRMS). High-resolution mass spectra (HRMS) were recorded on HPLC Agilent 1200 Series system coupled to a hybrid quadrupole-time of flight (LC-QTOF) mass spectrometer Agilent 6530 from Agilent Technologies (Santa Clara, CA, USA). Mobile phase was composed by 0.1 % formic acid in acetonitrile. Gas Temp. 325 °C; Drying gas: 5 l/min; Nebulizer: 40 psig; Shealt gas Temp. 375 °C; Shealt gas flow: 11 l/min. Vcap: 3500 V(+).

ICP-MASS were determined on Inductively Coupled Plasma Mass Spectrometer (ICP-MS) equipped with Laser Ablation System. The digestion was carried out using a Speedwave-four microwave-assisted digester (Berghof, serial no. 5304000), approximately 4 mg of sample, and 5 mL of 65% nitric acid applying a maximum of 200° (at 80% power). A quantitative analysis was carried out by ICP-MS (serial number SG19051122) using Ni to carry out the quantification and radio coma as an internal standard.

Optical rotation value was obtained from a Jasco P-2000 Digital Polarimeter. Samples were dissolved in chloroform and measured in a 100 mm sample cell with a light source of 589.3 nm. Specific optical rotation was calculated from observed optical rotation.

Circular dichroism spectroscopy. CD spectra were acquired on a J-1500 Circular Dichroism Spectrophotometer. Optically active samples were prepared in various organic solvents in a concentration of 0.5 mg / mL and scanned from 200 nm to 650 nm. The length of the sample cells was 1 cm.

Size-Exclusion Chromatography / Multi-Angle Light Scattering / Gel Permeation Chromatography (SEC/MALS) measurements were performed at 30 °C on an Agilent 1200 system equipped with PLgel 5µm Guard and PLgel 5µm MIXED-C columns, and triple detection: a differential refractive index (RI) detector (Optilab Rex, Wyatt), a multi-angle laser light scattering (MALS) detector (MiniDawn Treos, Wyatt), and a viscosimetric (VIS) detector (ViscoStar-II, Wyatt). Data analysis was performed with ASTRA Software (version 6.1) from Wyatt. THF was used as an eluent at a flow rate of 1 mL min⁻¹. A value of dn/dc = 0.185 was used (Polystyrene) for all the samples.

Single-crystal X-ray diffraction were carried out on Bruker D8 Advance. Operates with Theta-2Theta geometry with a Vario primary monochromator (CuKα1) and a 1-D LynxEye detector with 3 degrees of aperture and energy discrimination optimized for said radiation.

III. SYNTHETIC PROCEDURES AND ANALYTICAL DATA

The synthesis of chiral ferrocene aldehyde **1** & **2** has been described by Henri B. Kagan et al.¹⁰² and the synthesis of densely substituted prolins has been described by Cossío, F. P. et al.¹⁰⁰

α -(Diphenylphosphino)ferrocenecarboxaldehyde (1 & 2).¹⁰² Yield: 90%. ¹H NMR (400 MHz, Chloroform-d) δ 10.24 (s, 1H), 7.62 – 7.53 (t, 4H), 7.44 (d, 2H), 7.25 – 7.12 (t, 4H), 5.12 (s, 1H), 4.72 (s, 1H), 4.25 (s, 5H), 4.09 (s, 1H). ³¹P NMR (162 MHz, Chloroform-d) δ -22.91.

2-(Diphenylphosphino)-[(2-methoxy-2oxoethyl)-iminomethyl]ferrocene (3 & 4).¹⁰⁰ Yield: 85%. ¹H NMR (400 MHz, Chloroform-d) δ 8.51 (s, 1H), 7.59 (dt, J = 8.4, 4.4 Hz, 4H), 7.45 (q, J = 6.3, 5.8 Hz, 5H), 7.24 – 7.09 (m, 2H), 5.27 (s, 1H), 4.61 (s, 1H), 4.35 (d, J = 15.6 Hz, 1H), 4.19 (d, J = 4.1 Hz, 5H), 4.14 (d, J = 4.1 Hz, 1H), 3.96 (s, 1H), 3.77 (d, J = 3.7 Hz, 3H).

2-(Diphenylphosphino)ferrocenyl)-4-nitro-3-phenyl- pyrrolidine-2-carboxylate (5 & 8).¹⁰⁰ Yield: 60%. ¹H NMR (400 MHz, Chloroform-d) δ 7.61 (d, J = 4.3 Hz, 2H), 7.52 – 7.19 (m, 10H), 7.09 (d, J = 7.4 Hz, 2H), 4.99 (s, 1H), 4.51 (s, 1H), 4.38 (s, 1H), 4.29 – 4.15 (m, 5H), 4.05 (s, 2H), 3.94 – 3.82 (m, 5H). ³¹P NMR (162 MHz, Chloroform-d) -24.19.

1-Methyl-2-(diphenylphosphino)ferrocenyl)-4-nitro-3-phenyl- pyrrolidine-2-carboxylate (6 & 7).¹⁰⁰ Yield: 48%. ¹H NMR (400 MHz, Chloroform-d) δ 7.74 (m, J = 2.0 Hz, 2H), 7.49 – 7.36 (m, 5H), 7.27 (m, J = 16.9 Hz, 6H), 7.17 – 7.04 (m, 2H), 5.45 (dd, J = 8.1, 7.1 Hz, 1H), 5.23 (dd, J = 8.0, 4.9 Hz, 1H), 4.55 – 4.51 (m, 1H), 4.51 – 4.47 (m, 1H), 4.41 (s, 1H), 4.34 (q, J = 1.2 Hz, 1H), 4.29 – 4.25 (m, 1H), 3.87 (s, 5H), 3.36 (s, 3H), 2.95 (s, 3H). ³¹P NMR (162 MHz, Chloroform-d) δ -25.33.

(2S,3S,4R,5S)-Methyl 4-nitro-3,5-diphenylpyrrolidine-2-carboxylate (10 & 13).⁹⁹

Yield: 87%. ¹H NMR (400 MHz, Chloroform-d) δ 7.53 – 7.23 (m, 10H), 5.31 (dd, J = 6.5, 3.5 Hz, 1H), 4.95 (dd, J = 11.1, 6.5 Hz, 1H), 4.28 – 4.14 (m, 1H), 3.84 (s, 3H), 3.40 (dd, J = 11.1, 8.9 Hz, 1H).

(2S,3R,4S,5S)-Methyl 4-nitro-3,5-diphenylpyrrolidine-2-carboxylate (11 & 12).⁹⁹

Yield: 81%. ¹H NMR (400 MHz, Chloroform-d) δ 7.56 – 7.14 (m, 10H), 5.32 (dd, J = 6.6, 3.5 Hz, 1H), 4.95 (dd, J = 10.9, 6.5 Hz, 1H), 4.37 – 4.06 (m, 1H), 3.84 (s, 3H), 3.41 (d, J = 9.9 Hz, 1H).

Methyl (2S,3S,4R,5S)-1-methyl-4-nitro-3,5-diphenylpyrrolidine-2-carboxylate (14 & 17).¹⁰⁰

Yield: 75%. ¹H NMR (400 MHz, Chloroform-d) δ 7.64 – 7.18 (m, 10H), 5.03 (t, J = 6.9 Hz, 1H), 4.27 (dd, J = 9.3, 5.9 Hz, 1H), 3.97 (dd, J = 20.3, 8.7 Hz, 2H), 3.39 – 3.24 (m, 3H), 2.37 (d, J = 2.1 Hz, 3H).

Methyl (2S,3R,4S,5S)-1-methyl-4-nitro-3,5-diphenylpyrrolidine-2-carboxylate (15 & 16).¹⁰⁰

Yield: 67%. ¹H NMR (400 MHz, Chloroform-d) δ 7.52 – 7.22 (m, 10H), 5.35 – 5.24 (m, 1H), 4.58 (dd, J = 9.4, 6.5 Hz, 1H), 4.21 (d, J = 8.9 Hz, 1H), 3.79 (s, 3H), 3.49 (d, J = 9.3 Hz, 1H), 2.37 (s, 3H).

Methyl (2S,3R,4R,5S)-4-amino-1-methyl-3,5-diphenylpyrrolidine-2-carboxylate (18 & 21).¹²⁰

Yield: 95%. ¹H NMR (400 MHz, Chloroform-d) δ 7.66 – 7.54 (m, 2H), 7.43 (t, J = 7.3 Hz, 2H), 7.40 – 7.16 (m, 6H), 3.75 (d, J = 10.4 Hz, 1H), 3.53 (d, J = 8.4 Hz, 1H), 3.39 (dd, J = 10.3, 8.4 Hz, 1H), 3.28 – 3.17 (m, 4H), 2.29 (d, J = 3.1 Hz, 3H).

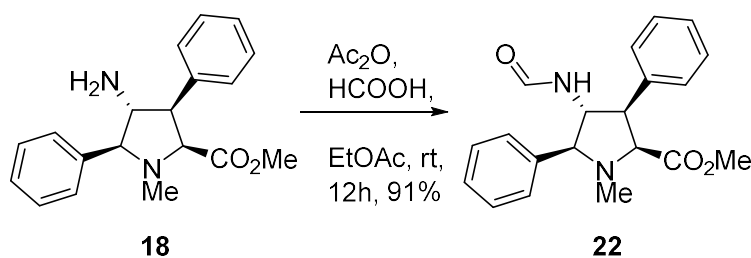
Methyl (2S,3S,4S,5S)-4-amino-1-methyl-3,5-diphenylpyrrolidine-2-carboxylate (19 & 20).¹²⁰

Yield: 89%. ¹H NMR (400 MHz, Chloroform-d) δ 7.43 (d, J = 8.4 Hz, 2H), 7.34

¹²⁰de Gracia Retamosa, M.; Ruiz Olalla, A.; et al. *Chem.Eur.J.* **2021**, *27*, 15671–15687

(d, $J = 6.4$ Hz, 2H), 7.32 – 7.21 (m, 6H), 4.01 (d, $J = 3.8$ Hz, 2H), 3.78 (s, 1H), 3.74 (s, 3H), 3.55 (d, $J = 9.4$ Hz, 1H), 2.40 (s, 3H).

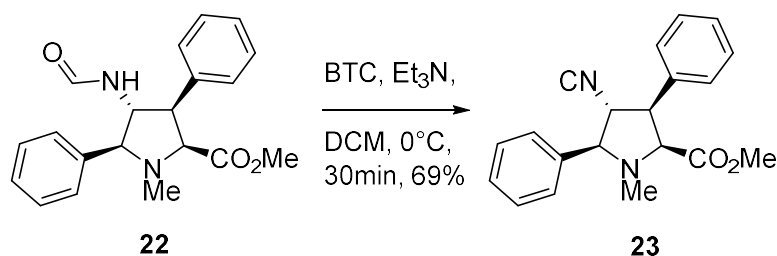
Synthesis of Methyl (2S,3R,4R,5S)-4-formamido-1-methyl-3,5-diphenylpyrrolidine-2-carboxylate (**22**)



To a solution of proline **18** (1.50 mmol, 465.6 mg) in EtOAc (10 mL) a mixture of formic acid (2.0 mmol, 0.189 mL) and acetic anhydride (3.0 mmol, 0.113 mL) were injected (formic acid and acetic anhydride were premixed neat at 60 °C for 1 h). The mixture was then stirred at r.t. for 12 h. Then water (20 mL) was added, and the mixture was extracted with EtOAc (3 × 20 mL). The combined organics were washed with sat. NaHCO₃ (2 × 20 mL) and brine (20 mL), dried (MgSO₄), filtered, and concentrated in vacuo to give crude formamide. Purification by flash column chromatography to yield colorless oil.

Yield: 91%. ¹H-NMR (400 MHz, Chloroform-d) δ 8.06 (d, 1H), 7.60 – 7.19 (m, 10H), 5.61 (d, 1H), 4.31 (dd, 1H), 3.99 (m, 1H), 3.72 (m, 1H), 3.47 (t, 1H), 3.24 (d, 3H), 2.31 (d, 3H). ¹³C-NMR (101 MHz, Chloroform-d) δ 171.31, 171.00, 164.17, 160.84, 139.26, 138.08, 138.00, 128.92, 128.66, 128.57, 128.51, 128.47, 128.42, 128.26, 128.14, 127.84, 127.79, 127.59, 127.25, 77.32, 77.00, 76.68, 76.00, 73.53, 71.62, 71.39, 66.90, 63.98, 52.72, 51.27, 51.18, 50.81, 39.71, 39.63.

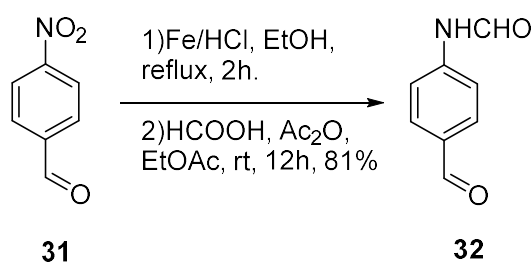
Synthesis of methyl (2S,3S,4R,5S)-4-isocyano-1-methyl-3,5-diphenylpyrrolidine-2-carboxylate (**23**)



Bis(trichloromethyl)carbonate (268 mg, 0.9 mmol) in DCM (3 ml) was added dropwise to a mixture of TEA (4.53 mmol) and the formamide **22** (510 mg, 1.51 mmol) in dry DCM (30 ml) over 30 min at 0 °C. The mixture was allowed to stir for 10 min before the addition of a saturated aqueous solution of NaHCO₃ (8 mL) and then the solution was stirred vigorously for 20 min. After washing successively with brine, the organic phase was collected and dried over MgSO₄. Purification by column chromatography afforded the monomer as a white crystal which was stored in fridge before usage.

Yield: 77.8%. ¹H-NMR (400 MHz, Chloroform-d) δ 7.65 – 7.58 (m, 1H), 7.51 – 7.23 (m, 10H), 4.05 (ddd, J = 8.6, 5.4, 1.9 Hz, 1H), 3.88 – 3.76 (m, 2H), 3.64 (d, J = 8.6 Hz, 1H), 3.25 (s, 3H), 2.32 (s, 3H). ¹³C-NMR (101 MHz, Chloroform-d) δ 158.91, 137.40, 128.94, 127.58, 75.90, 71.30, 65.55, 52.77, 51.36, 45.73, 39.29, 8.57. See crystal structure in Annexes VI.

Synthesis of N-(4-formylphenyl)formamide (**32**)¹²¹



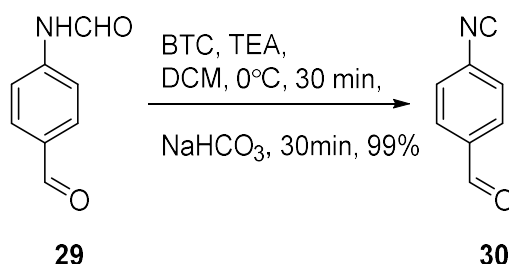
1) 4-nitrobenzaldehyde **31** (9.24 g, 60 mmol) was prepared in EtOH solution (500 mL of ethanol in 60 mL water) and Fe powder (12 g) was added subsequently. The mixture was stirred vigorously and conc. HCl (37 %, 1.2 mL) was injected in one portion. The reaction was then heated to reflux for 2 h. After the starting material was converted, the crude was filtered hot, and more quantity of water (200 mL) was added. Then EtOH was removed under vacuum and the mixture was diluted with sat. NaHCO₃ to set the pH to 8, then extracting with EtOAc (150 mL × 3). The organic phase was dried over MgSO₄ and concentrated to 200 mL to prevent the obtained 4-aminobenzaldehyde from self-polymerization and was soon used in solution in the next step without further purification.

2) A mixture of formic acid and acetic anhydride was prepared and stirred at 60 °C for 3 hours. Then the mixture was added into the solution 4-aminobenzaldehyde of the last steps and stirred at room temperature overnight. The reaction crude was washed with sat.

¹²¹ Zhang, Y.; Maverick, A.W. *Inorg. Chem.*, **2009**, 48, 10512-10518.

NaHCO₃ (200 mL × 3), dried under MgSO₄, and evaporated to obtain a white solid. Yield: 81%.

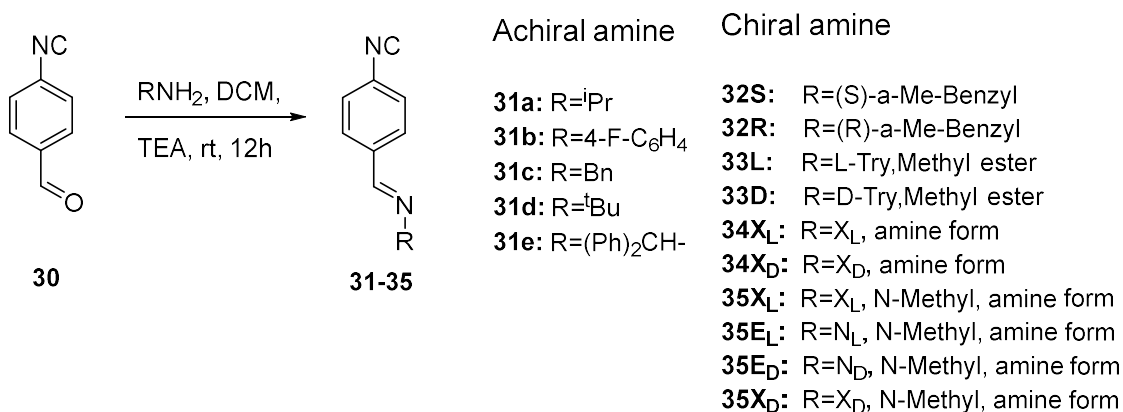
Synthesis of 4-isocyano benzaldehyde (30)



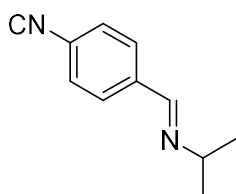
To a solution of N-(4-formylphenyl)formamide **29** (3.2 g, 21.45 mmol) in DCM (467 mL) was added Et₃N (8.92 mL, 64.35 mmol) and cooled to 0 °C. Bis(trichloromethyl)carbonate (3.78 g, 12.73 mmol) was dissolved in DCM and dropped slowly. The reaction was stirred for 30 min and then stirred with sat. NaHCO₃ for additional 30 min. When the reaction was finished, the mixture was washed with more quantities of sat. NaHCO₃ (150 mL × 3) and brine (100 mL × 1). The organic phase was concentrated and purified by flash column chromatography to get a transparent light brown crystal. The product was not stable neat at room temperature, and decomposed when delivered to MS.

Yield: 99%. ¹H-NMR (400 MHz, Chloroform-d) δ 10.07 (s, 1H), 7.97 (d, J = 8.5 Hz, 2H), 7.58 (d, J = 8.4 Hz, 2H). ¹³C-NMR (126 MHz, Chloroform-d) δ 189.79, 167.99, 136.32, 130.73, 127.19, 119.51. FTIR (cm⁻¹) 2123 (NC, ν_{C=N}), 1684 (CHO, ν_{C=O}), 1599 (Ar, ν_{C=C}), 827 (Ar, ν_{C-H}), 743 (Ar, ν_{C-H});

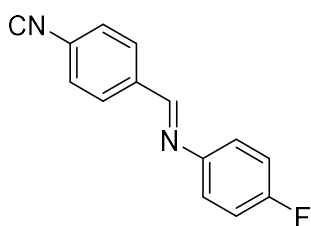
General procedure for preparing imine monomer with 4-isocyano benzaldehyde.



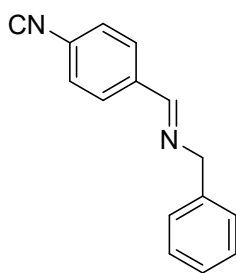
To a solution of amine (1.2 mmol) in MeOH (10 mL), 4-isocyanobenzaldehyde (1 mmol) and Et₃N (1 mmol) was added. The reaction mixture was stirred at room temperature overnight, The mixture was diluted with DCM (30 mL) and then washed with H₂O (30 mL × 3) and brine (30 mL). The crude was dried under MgSO₄ and evaporated under reduced pressure to obtain the products as coloured oils.



(E)-1-(4-isocyanophenyl)-N-isopropylmethanimine (31a). Brown oil, yield: 99%, from isopropylamine. ¹H-NMR (400 MHz, Chloroform-d) δ 8.32 (s, 1H), 7.79 (d, J = 8.5 Hz, 2H), 7.43 (d, J = 8.5 Hz, 2H), 3.67 – 3.50 (m, 1H), 1.29 (d, J = 6.4 Hz, 6H). ¹³C-NMR (126 MHz, Chloroform-d) δ 190.28, 167.99, 136.32, 130.73, 127.19, 119.51, 30.91, 22.26. FTIR (cm⁻¹) 2967(v_{C-H}), 2120 (NC, v_{C=N}), 1642 (imine, v_{C=N}), 1501 (Ar, v_{C=C}), 1378 (Me, v_{C-H}), 833 (Ar, v_{C-H}), LC/Q-TOF (m/z): [M]⁺ calcd. for C₁₁H₁₂N₂, 172,1000; found, 172,0999.

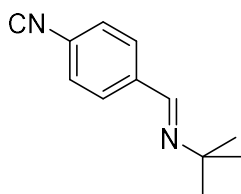


(E)-N-(4-fluorophenyl)-1-(4-isocyanophenyl)methanimine (31b). Brown oil, yield: 81, from 4-fluorophenylamine. ¹H-NMR (400 MHz, Chloroform-d) δ 8.47 (s, 1H), 8.00 – 7.90 (m, 2H), 7.54 – 7.47 (m, 2H), 7.25 (dd, J = 8.9, 4.9 Hz, 2H), 7.16 – 7.08 (m, 2H). ¹³C-NMR (126 MHz, Chloroform-d) δ 166.47, 162.86, 160.90, 157.83, 147.43, 137.13, 129.88, 127.11, 122.71, 116.38. FTIR (cm⁻¹) 2121 (NC, v_{C=N}), 1498 (Ar, v_{C=C}), 1216 (v_{C-F}), 832 (Ar, v_{C-H}), 734 (Ar, v_{C-H}). LC/Q-TOF (m/z): [M]⁺ calcd. for C₁₄H₉FN₂, 224,0750; found, 224,0754.



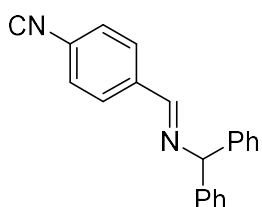
(E)-N-tert-butyl-1-(4-isocyanophenyl)methanimine (31c). Brown oil, yield: 93%, from benzylamine. ¹H-NMR (400 MHz, Chloroform-d) δ 8.41 (d, J = 1.5 Hz, 1H), 7.87 – 7.78 (m, 2H), 7.48 – 7.42 (m, 2H), 7.42 – 7.30 (m, 5H), 4.87 (d, J = 1.4 Hz, 2H). ¹³C-NMR (126 MHz, Chloroform-d) δ 165.95, 160.06, 138.95, 137.23, 130.99, 129.41, 128.83, 128.25, 127.45, 126.92, 65.29. FTIR (cm⁻¹) 2843(v_{C-H}), 2120 (NC, v_{C=N}), 1642 (imine, v_{C=N}), 1494 (Ar, v_{C=C}), 1448 (CH₂, v_{C-H}), 742

(Ar, ν_{C-H}), 696 (Ar, ν_{C-H}). LC/Q-TOF (m/z): $[M]^+$ calcd. for $C_{15}H_{12}N_2$, 220,1000; found, 220,1004.



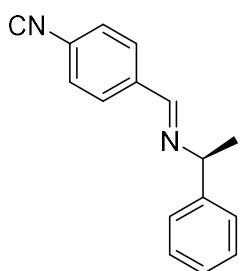
(E)-N-benzhydryl-1-(4-isocyanophenyl)methanimine (31d).

Brown oil, yield: 86%, from tertbutylamine. 1H -NMR (400 MHz, Chloroform-d) δ 8.27 (s, 1H), 7.79 (s, 1H), 7.44 (s, 1H), 1.32 (s, 11H). ^{13}C -NMR (126 MHz, Chloroform-d) δ 165.22, 153.16, 137.98, 128.77, 126.51, 126.19, 57.72, 29.52. FTIR (cm^{-1}) 2966(ν_{C-H}), 2119 (NC, $\nu_{C=N}$), 1638 (imine, $\nu_{C=N}$), 1501 (Ar, $\nu_{C=C}$), 1371 (Me, ν_{C-H}), 827 (Ar, ν_{C-H}). LC/Q-TOF (m/z): $[M]^+$ calcd. for $C_{12}H_{14}N_2$, 186,1157; found, 186,1158.



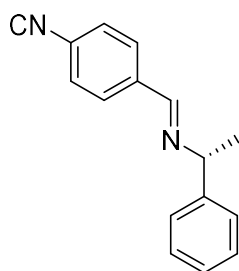
(E)-N-benzyl-1-(4-isocyanophenyl)methanimine (31e).

Brown oil, yield: 84%, from benzhydrylamine. 1H -NMR (400 MHz, Chloroform-d) δ 8.43 (s, 1H), 7.89 (s, 1H), 7.49 – 7.27 (m, 4H), 5.64 (s, 1H). ^{13}C -NMR (126 MHz, Chloroform-d) δ 165.69, 158.81, 144.84, 143.38, 137.07, 129.34, 128.52, 127.55, 127.17, 126.61, 77.92, 77.25, 77.00, 76.74. FTIR (cm^{-1}) 2843(ν_{C-H}), 2118 (NC, $\nu_{C=N}$), 1644 (imine, $\nu_{C=N}$), 1489 (Ar, $\nu_{C=C}$), 1449 (CH_2 , ν_{C-H}), 739 (Ar, ν_{C-H}), 694 (Ar, ν_{C-H}). LC/Q-TOF (m/z): $[M]^+$ calcd. for $C_{21}H_{16}N_2$, 296,1313; found, 296,1316.



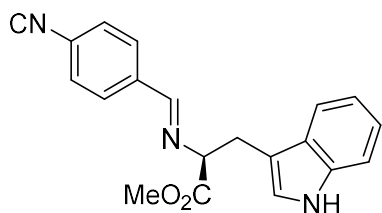
S-1-(4-isocyanophenyl)-N-(1-phenylethyl)methanimine (32-S).

Brown oil, yield: 99%, from S- α -Methyl benzylamine. 1H -NMR (500 MHz, Chloroform-d) δ 8.37 (s, 1H), 7.87 – 7.81 (m, 2H), 7.43 (dt, J = 6.9, 1.5 Hz, 3H), 7.37 (dd, J = 8.4, 6.8 Hz, 2H), 7.31 – 7.25 (m, 2H), 4.59 (q, J = 6.6 Hz, 1H), 1.61 (d, J = 6.6 Hz, 3H). ^{13}C -NMR (126 MHz, Chloroform-d) δ 165.85, 157.65, 144.92, 137.50, 129.41, 128.77, 127.31, 127.04, 126.86, 126.84, 70.13, 25.07. FTIR (cm^{-1}) 2120 (NC, $\nu_{C=N}$), 1641 (imine, $\nu_{C=N}$), 1492 (Ar, $\nu_{C=C}$), 1449 (Me, ν_{C-H}), 836 (Ar, ν_{C-H}), 759 (Ar, ν_{C-H}), 697 (Ar, ν_{C-H}); LC/Q-TOF (m/z): $[M]^+$ calcd. for $C_{16}H_{14}N_2$, 234,1157; found, 234,1157.



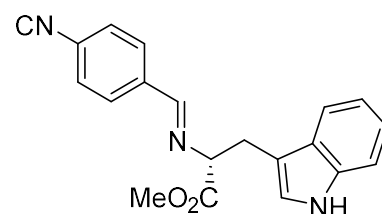
R-1-(4-isocyanophenyl)-N-(1-phenylethyl)methanimine (32-R).

Brown oil, yield: 99%, from R- α -Methyl benzylamine. $^1\text{H-NMR}$ (500 MHz, Chloroform- d) δ 8.38 (s, 1H), 7.87 – 7.81 (m, 2H), 7.46 – 7.40 (m, 4H), 7.37 (dd, J = 8.5, 6.8 Hz, 2H), 7.28 (d, J = 3.0 Hz, 2H), 4.59 (q, J = 6.7 Hz, 1H), 1.61 (d, J = 6.6 Hz, 4H). $^{13}\text{C-NMR}$ (126 MHz, Chloroform- d) δ 165.58, 157.39, 144.66, 137.24, 129.15, 128.71, 128.51, 127.54, 127.05, 126.60, 126.58, 126.02, 69.88, 51.53, 44.43, 24.81, 13.91, 13.71, 12.83. FTIR (cm^{-1}) 2119 (NC, $\nu_{\text{C}=\text{N}}$), 1641 (imine, $\nu_{\text{C}=\text{N}}$), 1492 (Ar, $\nu_{\text{C}=\text{C}}$), 1449 (Me, $\nu_{\text{C-H}}$), 836 (Ar, $\nu_{\text{C-H}}$), 760 (Ar, $\nu_{\text{C-H}}$), 698 (Ar, $\nu_{\text{C-H}}$). LC/Q-TOF (m/z): $[\text{M}]^+$ calcd. for $\text{C}_{16}\text{H}_{14}\text{N}_2$, 234,1157; found, 234,1158.



Methyl (S,E)-3-(1H-indol-3-yl)-2-((4-isocyanobenzylidene)amino)propanoate (33-L).

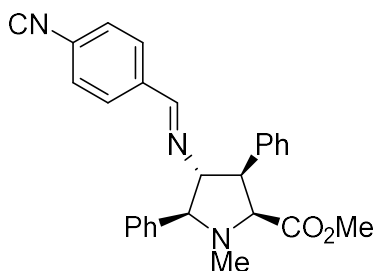
Brown oil, yield: 99%, from methyl L-tryptophanate. $^1\text{H-NMR}$ (500 MHz, Chloroform- d) δ 8.11 (s, 1H), 7.84 (s, 1H), 7.72 – 7.67 (m, 2H), 7.65 (dt, J = 7.9, 1.0 Hz, 1H), 7.38 (d, J = 8.2 Hz, 2H), 7.36 – 7.33 (m, 1H), 7.20 (ddd, J = 8.1, 7.0, 1.2 Hz, 1H), 7.12 (ddd, J = 8.0, 7.0, 1.0 Hz, 1H), 4.31 (dd, J = 8.8, 4.8 Hz, 1H), 3.80 (s, 3H), 3.58 (ddd, J = 14.5, 4.8, 0.9 Hz, 1H), 3.38 – 3.23 (m, 1H). $^{13}\text{C-NMR}$ (126 MHz, Chloroform- d) δ 172.48, 166.03, 161.68, 136.62, 136.37, 129.56, 127.43, 126.78, 123.64, 123.17, 123.16, 122.31, 119.70, 119.03, 111.41, 73.90, 52.55, 29.75. FTIR (cm^{-1}) 2121 (NC, $\nu_{\text{C}=\text{N}}$), 1731 ($\nu_{\text{C}=\text{O}}$), 1639 (imine, $\nu_{\text{C}=\text{N}}$), 1434 (Ar, $\nu_{\text{C}=\text{C}}$), 1163 ($\nu_{\text{C-O}}$), 740 (Ar, $\nu_{\text{C-H}}$). LC/Q-TOF (m/z): $[\text{M}]^+$ calcd. for $\text{C}_{20}\text{H}_{17}\text{N}_3\text{O}_2$, 331,1321; found, 331,1324.



Methyl (R,E)-3-(1H-indol-3-yl)-2-((4-isocyanobenzylidene)amino)propanoate (33-D).

Brown oil, yield: 99%, from methyl D-tryptophanate. $^1\text{H-NMR}$ (500 MHz, Chloroform- d) δ 8.09 (s, 1H), 7.84 (s, 1H), 7.72 – 7.67 (m, 2H), 7.67 – 7.64 (m, 1H), 7.38 (d, J = 8.2 Hz, 2H), 7.36 – 7.33 (m, 1H), 7.20 (ddd, J = 8.2, 7.0, 1.2 Hz, 1H), 7.12 (ddd, J = 8.0, 7.1, 1.0 Hz, 1H), 4.31 (dd, J = 8.8, 4.7 Hz, 1H), 3.80 (s, 3H), 3.58 (ddd, J = 14.5, 4.7, 0.8 Hz, 1H). $^{13}\text{C-NMR}$ (126 MHz, Chloroform- d) δ 172.22, 165.78, 161.42, 136.37,

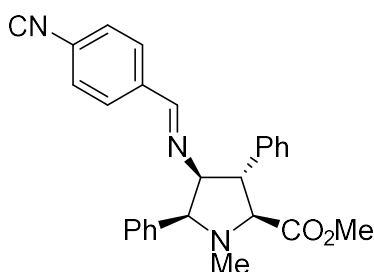
136.11, 129.31, 127.17, 126.53, 123.38, 122.89, 122.14, 122.07, 119.46, 118.78, 111.15, 73.65, 52.30, 29.50. FTIR (cm^{-1}) 2121 ($\text{NC}, \nu_{\text{C}=\text{N}}$), 1731 ($\nu_{\text{C}=\text{O}}$), 1640 (imine, $\nu_{\text{C}=\text{N}}$), 1434 ($\text{Ar}, \nu_{\text{C}=\text{C}}$), 1164 ($\nu_{\text{C}-\text{O}}$), 740 ($\text{Ar}, \nu_{\text{C}-\text{H}}$). LC/Q-TOF (m/z): $[\text{M}]^+$ calcd. for $\text{C}_{20}\text{H}_{17}\text{N}_3\text{O}_2$, 331,1321; found, 331,1324.



Methyl (2S,3R,4R,5S)-4-((4-isocyanobenzylidene)amino)-1-methyl-3,5-

diphenylpyrrolidine-2-carboxylate (35-XL). Light yellow solid, yield: 89%, from *exo*-L proline. $^1\text{H-NMR}$ (400 MHz, Chloroform- d) δ 7.63 (d, $J = 8.5$ Hz, 3H), 7.58 (s, 1H), 7.51 – 7.46 (m, 2H), 7.41 – 7.32 (m, 6H), 7.32 –

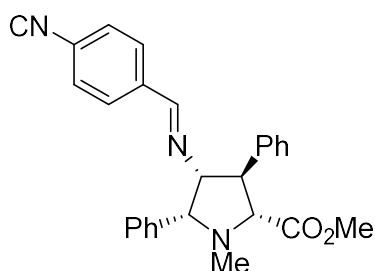
7.26 (m, 4H), 7.26 – 7.18 (m, 1H), 3.97 – 3.82 (m, 3H), 3.70 (dd, $J = 7.3, 3.8$ Hz, 1H), 3.26 (s, 3H), 2.35 (s, 3H). $^{13}\text{C-NMR}$ (101 MHz, Chloroform- d) δ 159.30, 128.68, 128.50, 128.10, 127.75, 126.62, 84.56, 72.37, 52.94, 50.71, 39.45. FTIR (cm^{-1}) 2120 ($\text{NC}, \nu_{\text{C}=\text{N}}$), 1747 ($\nu_{\text{C}=\text{O}}$), 1640 (imine, $\nu_{\text{C}=\text{N}}$), 1453 ($\text{Ar}, \nu_{\text{C}=\text{C}}$), 1170 ($\nu_{\text{C}-\text{O}}$), 750 ($\text{Ar}, \nu_{\text{C}-\text{H}}$), 699 ($\text{Ar}, \nu_{\text{C}-\text{H}}$). LC/Q-TOF (m/z): $[\text{M}]^+$ calcd. for $\text{C}_{27}\text{H}_{25}\text{N}_3\text{O}_2$, 423,1947; found, 423,1936.



Methyl (2S,3S,4S,5S)-4-((4-isocyanobenzylidene)amino)-1-methyl-3,5-

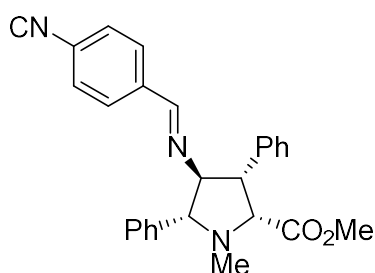
diphenylpyrrolidine-2-carboxylate (35-NL). Light yellow solid, yield: 82%, from *endo*-L proline. $^1\text{H-NMR}$ (400 MHz, Chloroform- d) δ 7.61 (s, 1H), 7.46 – 7.40 (m, 4H), 7.38 – 7.32 (m, 2H), 7.31 – 7.21 (m, 10H), 7.19 –

7.12 (m, 1H), 4.01 (d, $J = 3.9$ Hz, 2H), 3.83 – 3.77 (m, 1H), 3.74 (s, 3H), 3.55 (d, $J = 9.4$ Hz, 1H), 2.40 (s, 3H). $^{13}\text{C-NMR}$ (101 MHz, Chloroform- d) δ 156.55, 128.92, 128.54, 128.28, 127.73, 127.24, 125.92, 78.74, 74.57, 54.18, 50.40, 39.49. FTIR (cm^{-1}) 2120 ($\text{NC}, \nu_{\text{C}=\text{N}}$), 1747 ($\nu_{\text{C}=\text{O}}$), 1640 (imine, $\nu_{\text{C}=\text{N}}$), 1453 ($\text{Ar}, \nu_{\text{C}=\text{C}}$), 1170 ($\nu_{\text{C}-\text{O}}$), 750 ($\text{Ar}, \nu_{\text{C}-\text{H}}$), 699 ($\text{Ar}, \nu_{\text{C}-\text{H}}$). LC/Q-TOF (m/z): $[\text{M}]^+$ calcd. for $\text{C}_{27}\text{H}_{25}\text{N}_3\text{O}_2$, 423,1947; found, 423,1951.



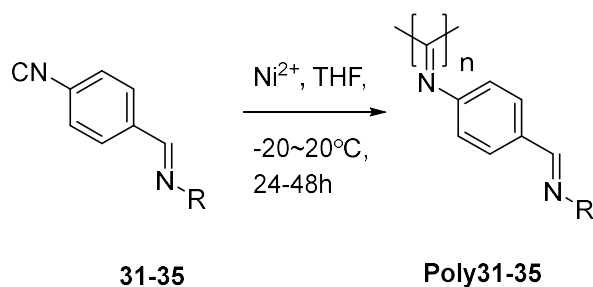
Methyl (2R,3R,4R,5R)-4-(((E)-4-isocyanobenzylidene)amino)-1-methyl-3,5-diphenylpyrrolidine-2-carboxylate (35-Nd).

Light yellow solid, yield: 91%, from *endo*-D proline. ¹H-NMR (500 MHz, Chloroform-d) δ 7.61 (s, 1H), 7.46 – 7.40 (m, 4H), 7.35 (dd, J = 8.0, 6.8 Hz, 2H), 7.27 (dt, J = 15.1, 7.3 Hz, 8H), 7.18 – 7.13 (m, 1H), 4.01 (d, J = 4.2 Hz, 2H), 3.83 – 3.78 (m, 1H), 3.74 (s, 3H), 3.55 (d, J = 9.3 Hz, 1H), 2.40 (s, 3H). ¹³C-NMR (126 MHz, Chloroform-d) δ 190.27, 172.53, 165.33, 157.97, 139.82, 137.77, 136.72, 130.74, 129.33, 128.96, 128.70, 128.15, 127.67, 127.21, 127.14, 126.33, 79.86, 76.68, 74.99, 55.83, 52.03, 39.89. FTIR (cm⁻¹) 2852 (ν_{C-H}), 2121 (NC, ν_{C=N}), 1742 (ν_{C=O}), 1637 (imine, ν_{C=N}), 1453 (Ar, ν_{C=C}), 1172 (ν_{C-O}), 740 (Ar, ν_{C-H}), 698 (Ar, ν_{C-H}). LC/Q-TOF (m/z): [M]⁺ calcd. for C₂₇H₂₅N₃O₂, 423,1947; found, 423,1952.



Methyl (2R,3S,4S,5R)-4-((-4-isocyanobenzylidene)amino)-1-methyl-3,5-diphenylpyrrolidine-2-carboxylate (35-Xd).

Light yellow solid, yield: 82%, from *exo*-D proline. ¹H-NMR (400 MHz, Chloroform-d) δ 7.67 – 7.61 (m, 2H), 7.58 (s, 1H), 7.51 – 7.44 (m, 2H), 7.40 – 7.32 (m, 6H), 7.32 – 7.26 (m, 4H), 7.25 – 7.19 (m, 1H), 3.96 – 3.81 (m, 3H), 3.73 – 3.66 (m, 1H), 3.26 (s, 3H), 2.35 (s, 3H). ¹³C-NMR (101 MHz, Chloroform-d) δ 159.30, 128.68, 128.51, 128.11, 127.76, 127.57, 127.29, 126.63, 126.11, 84.57, 72.37, 52.95, 50.71. FTIR (cm⁻¹) 2120 (NC, ν_{C=N}), 1747 (ν_{C=O}), 1640 (imine, ν_{C=N}), 1454 (Ar, ν_{C=C}), 1171 (ν_{C-O}), 750 (Ar, ν_{C-H}), 699 (Ar, ν_{C-H}). LC/Q-TOF (m/z): [M]⁺ calcd. for C₂₇H₂₅N₃O₂, 423,1947; found, 423,1952.

General procedure for polymerization.

Achiral amine

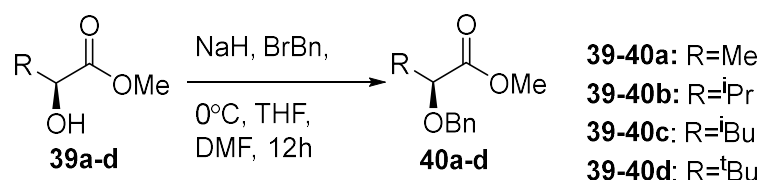
Chiral amine

31a: R=ⁱPr**32S:** R=(S)-*a*-Me-Benzyl**31b:** R=4-F-C₆H₅**32R:** R=(R)-*a*-Me-Benzyl**31c:** R=Bn**33L:** R=L-Try,Methyl ester**31d:** R=^tBu**33D:** R=D-Try,Methyl ester**31e:** R=(Ph)₂CH-**34X_L:** R=X_L, amine form**34X_D:** R=X_D, amine form**35X_L:** R=X_L, N-Methyl, amine form**35E_L:** R=N_L, N-Methyl, amine form**35E_D:** R=N_D, N-Methyl, amine form**35X_D:** R=X_D, N-Methyl, amine form

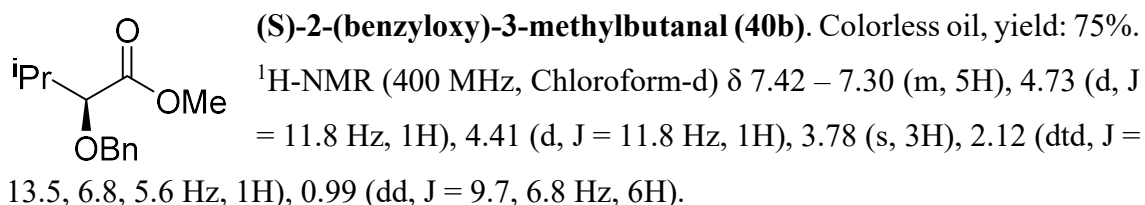
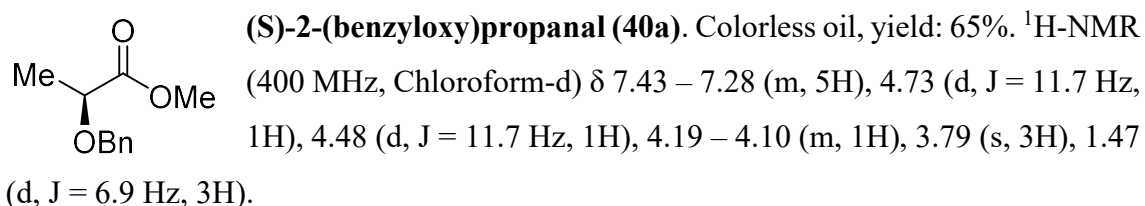
4-isocyanide monomer (0.4 mmol) was dissolved in THF (0.75 - 2 mL) and NiCl₂ • 6H₂O methanol solution (60.6 μL, 0.2 mmol / L in MeOH) was added. Then the mixture was stirred at 20 °C (20 °C for achiral monomer, -20 °C for chiral monomer) for 48 hours. The resulting polymer was precipitated in hexane, washed with ammonium solution (15 mL, 2 mol / L in water), and dried under vacuum to yield yellow to orange solid. The polymer samples were storage in the freezer to maintain the helix conformation.

Ugi reaction

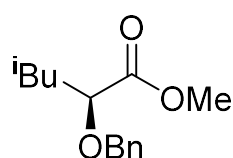
General procedure for the synthesis of 2-benzyloxy esters (**39a-d**) was previously described by Fernando et al.¹²²

Synthesis of methyl (R)-2-(benzyloxy)-2-substituted-acetate (40a-d**).**

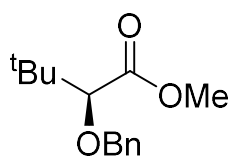
The prepared 2-hydroxyl esters (**39a-d**, 15.0 mmol) were dissolved in anhydrous tetrahydrofuran and slowly added into a mixture of anhydrous tetrahydrofuran (60 mL) and NaH (0.48 g, 20.0 mmol), under an inert atmosphere at 0°C. The mixture was stirred for 1 hour at r.t. Then benzyl bromide (20.0 mmol) was added dropwise at 0 °C, the mixture was allowed to reach room temperature. The reaction was monitored by TLC. When the reaction was complete, the reaction mixture was diluted in ether (100 mL) and quenched with MeOH (20mL) before washed with water. The remaining organic layer was dried over anhydrous MgSO₄ and evaporated under reduced pressure, providing the crude product **40a-d**, which was purified by flash column chromatography as a colorless oil. These esters have already been described.



¹²² Zubia, A; Mendoza L. *Angew. Chem., Int. Ed.* **2005**, 44.19, 2903-2907.

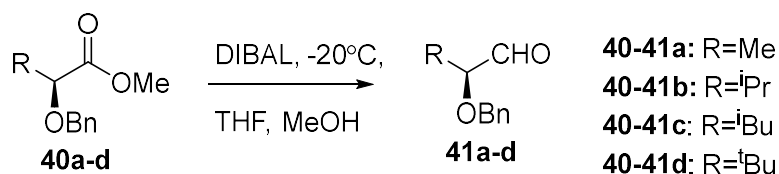


(S)-2-(benzyloxy)-4-methylpentanal (40c). Colorless oil, yield: 66%. ¹H-NMR (400 MHz, Chloroform-d) δ 7.43 – 7.29 (m, 5H), 4.72 (d, J = 11.6 Hz, 1H), 4.41 (d, J = 11.5 Hz, 1H), 4.01 (dd, J = 9.5, 4.1 Hz, 1H), 3.77 (s, 3H), 1.97 – 1.80 (m, 1H), 1.80 – 1.70 (m, 1H), 1.52 (ddd, J = 13.9, 8.9, 4.2 Hz, 1H), 0.94 (d, J = 6.5 Hz, 3H), 0.85 (d, J = 6.5 Hz, 3H).



methyl (S)-2-(benzyloxy)-3,3-dimethylbutanoate (40d). Colorless oil, yield: 54%. ¹H-NMR (400 MHz, Chloroform-d) δ 7.37 (d, J = 4.4 Hz, 5H), 4.67 (d, J = 11.8 Hz, 1H), 4.36 (d, J = 11.8 Hz, 1H), 3.76 (s, 3H), 3.63 (s, 1H), 1.01 (s, 9H).

Synthesis of (R)-2-(benzyloxy)-2-substituted-acetaldehyde (41a-d).



2-benzyloxy esters (**40a-d**, 10.0 mmol) were dissolved in THF (20 mL) and cooled to –20 °C under an inert atmosphere. DIBAL (1 M in hexane, 15.0 mmol, 15.0 mL) was added dropwise. After 5 min of stirring the reaction was quenched with MeOH (5 mL). Rochelle's salt solution (saturated potassium sodium tartrate tetrahydrate aqueous solution, 150 mL) was added, the mixture was stirred vigorously, and then extracted with hexane (3 × 50 mL). The organic layers were combined and dried over anhydrous MgSO₄ before evaporation. The obtained aldehydes were purified by flash column chromatography as a pale-yellow oil. It's should be noticed that the aldehyde should be stored under –20 °C and used in the Ugi reaction as soon as possible. The aldehyde would become totally racemic after 3 weeks at freezer.

$\text{H}_3\text{C}-\underset{\text{OBn}}{\underset{|}{\text{C}}}-\text{CHO}$ **(S)-2-(benzyloxy)propanal (41a)**.¹²³ Colorless oil, yield: 63%. ¹H-NMR (400 MHz, Chloroform-d) δ 9.70 (d, $J = 1.8$ Hz, 1H), 7.58 – 7.21 (m, 5H), 4.66 (q, $J = 11.7$ Hz, 2H), 3.93 (qd, $J = 6.9, 1.8$ Hz, 1H), 1.36 (d, $J = 7.0$ Hz, 3H). $[\alpha]_{589.3} = -61^\circ$, 1.00 g/100mL; Chloroform; 20 °C, (ref: -60°).

$\text{iPr}-\underset{\text{OBn}}{\underset{|}{\text{C}}}-\text{CHO}$ **(S)-2-(benzyloxy)-3-methylbutanal (41b)**.¹²⁴ Colorless oil, yield: 79%. ¹H-NMR (400 MHz, Chloroform-d) δ 9.70 (d, $J = 2.7$ Hz, 1H), 7.39 (d, $J = 4.4$ Hz, 5H), 4.72 (d, $J = 11.8$ Hz, 1H), 4.53 (d, $J = 11.8$ Hz, 1H), 3.51 (dd, $J = 5.8, 2.7$ Hz, 1H), 2.22 – 2.06 (m, 1H), 1.03 (t, $J = 7.1$ Hz, 6H). $[\alpha]_{589.3} = -52^\circ$, 1.00 g/100mL; Chloroform.

$\text{iBu}-\underset{\text{OBn}}{\underset{|}{\text{C}}}-\text{CHO}$ **(S)-2-(benzyloxy)-4-methylpentanal (41c)**.¹²⁵ Colorless oil, yield: 64%. ¹H-NMR (400 MHz, Chloroform-d) δ 9.68 (d, $J = 2.3$ Hz, 1H), 7.44 – 7.30 (m, 5H), 4.72 (d, $J = 11.6$ Hz, 1H), 4.54 (d, $J = 11.6$ Hz, 1H), 1.89 (ddtd, $J = 13.3, 8.7, 6.7, 5.4$ Hz, 1H), 1.70 – 1.59 (m, 1H), 1.45 (ddd, $J = 14.1, 8.7, 4.4$ Hz, 1H), 0.97 (d, $J = 6.7$ Hz, 3H), 0.89 (d, $J = 6.6$ Hz, 3H). $[\alpha]_{589.3} = -22^\circ$, 1.00 g/100mL; Chloroform; (ref: -22.8°)

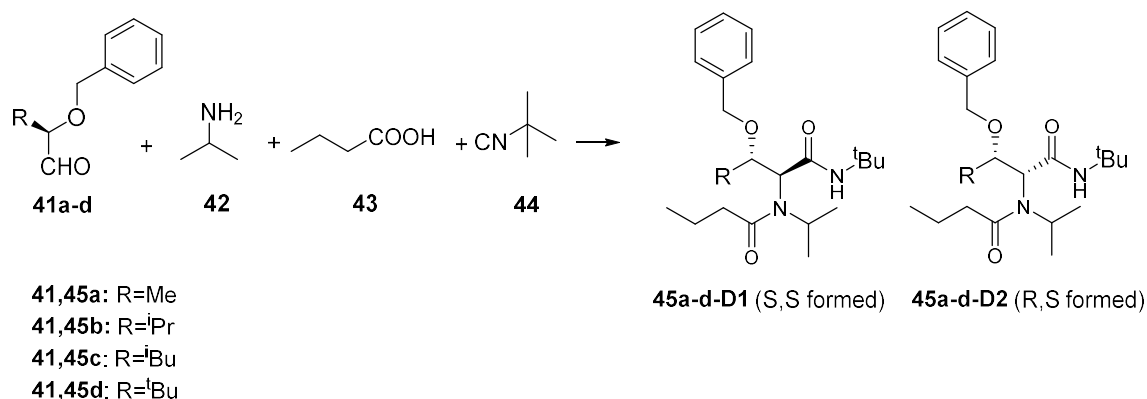
$\text{tBu}-\underset{\text{OBn}}{\underset{|}{\text{C}}}-\text{CHO}$ **(S)-2-(benzyloxy)-3,3-dimethylbutanal (41d)**. Colorless oil, yield: 71%. ¹H-NMR (400 MHz, Chloroform-d) δ 9.76 (d, $J = 3.4$ Hz, 1H), 7.42 – 7.28 (m, 5H), 4.68 (d, $J = 11.8$ Hz, 1H), 4.47 (d, $J = 11.9$ Hz, 1H), 3.31 (d, $J = 3.4$ Hz, 1H), 1.04 (s, 9H). ¹³C-NMR (126 MHz, Chloroform-d) δ 205.26, 137.53, 128.39, 127.90, 127.87, 90.47, 72.91, 26.07, 23.41. FTIR (cm^{-1}) 2958 (tBu, $\nu_{\text{C-H}}$), 2869 (CHO, $\nu_{\text{C-H}}$), 1728 (CHO, $\nu_{\text{C=O}}$), 1453 ($\nu_{\text{C-H}}$), 1365 ($\nu_{\text{C-H}}$), 1075 ($\nu_{\text{C-O}}$), 738 (Ar, $\nu_{\text{C-H}}$), 696 (Ar, $\nu_{\text{C-H}}$). $[\alpha]_{589.3} = -64^\circ$, 1.00 g/100mL; Chloroform.

¹²³ Ramírez-Fernández, J.; Botubol, J.M. *Nat. Prod. Commun.* **2011**, 6, 443-449.

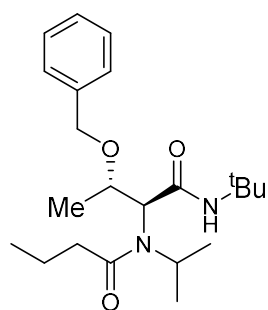
¹²⁴ Evans, D.A.; Cee, V. *J. Am. Chem. Soc.* **2006**, 128, 9433-9441.

¹²⁵ Hamada, C.; Usuki, Y. *Org. Lett.* **2019**, 21, 965-968

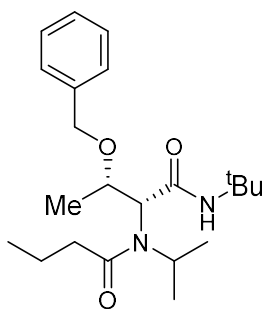
General procedure for asy Ugi-4CR



To a dry flask aldehyde (**41a-d**, 1.3 mmol), isopropylamine (1.3 mmol), and MeOH (1mL) were added. The resulting solution was stirred for 1 hour at r.t. After the imine was generated, butyric acid (1.0 mmol) was added to the mixture in one portion. After 10 min, tert-butyl isocyanide (1.2 mmol) was injected. Then the mixture was stirred for 12 h. When the reaction was complete, the reaction mixture was evaporated and purified directly by flash column chromatography to give 2 diastereomers as colorless oil. The HPLC data is shown in Annexes V.

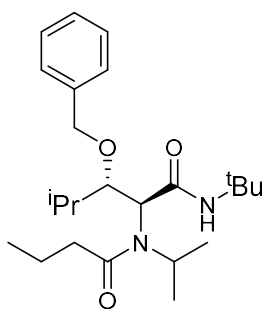


(2S,3S)-3-(benzyloxy)-N-(tert-butyl)-2-(N-isopropylbutanamide) butanamide (45a-D1). This compound was prepared from (S)-2-(benzyloxy)propanal **41a** as diastereomer 1 in 47% yield. ¹H-NMR (δ ppm, Chloroform-d) 8.38 (s, 1H), 7.33-7.26 (m, 5H), 4.72 (t, 1H, J=8.01 Hz), 4.56 (d, 1H, J=11.32 Hz), 4.33 (d, 1H, J=11.3 Hz), 4.04 (m, 1H), 3.44 (s, 1H), 2.41 (m, 1H), 2.24 (m, 1H), 1.64 (ddp, 2H, J=28.81 Hz, J'=14.51 Hz, J''=7.36 Hz), 1.35 (s, 1H), 1.31 (s, 9H), 1.28 (d, 3H, J=4.51 Hz), 1.23 (d, 3H, J=4.87 Hz), 1.15 (d, 3H, J=4.70 Hz), 0.97 (t, 3H, J=6.44 Hz); ¹³C-NMR (δ ppm, Chloroform-d) 174.50, 170.40, 138.90, 128.9, 127.51, 127.25, 71.19, 50.43, 36.88, 28.56, 21.36, 20.45, 18.90, 17.31, 13.86; FTIR (cm⁻¹) 3283 (ν_{N-H}), 2968 (ν_{C-H}), 2933 (ν_{C-H}), 2875 (ν_{C-H}), 1672 (ν_{C=O}), 1612 (ν_{C=O}), 1543 (Ar, ν_{C=C}), 1097 (ν_{C-O-C}), 732 (Ar, ν_{C-H}), 697 (Ar, ν_{C-H}); LC/Q-TOF (m/z): [M]⁺ calcd. for C₂₂H₃₆N₂O₃, 376.2726; found, 376,2731.



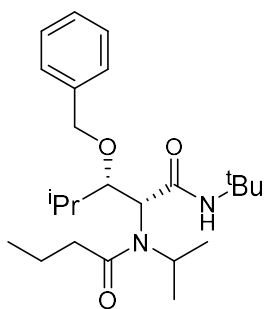
(2S,3R)-3-(benzyloxy)-N-(tert-butyl)-2-(N-isopropylbutyramido)-4,4-dimethylpentanamide (45a-D2).

This compound was prepared from (S)-2-(benzyloxy)propanal **41a** as diastereomer 2 in 35% yield. $^1\text{H-NMR}$ (δ ppm, Chloroform-d) 7.63 (s, 1H), 7.39-7.28 (m, 5H), 4.78 (t, 1H, $J=7.54$ Hz), 4.65 (d, 1H, $J=11.35$ Hz), 4.54 (d, 1H, $J=11.25$ Hz), 4.12 (m, 1H), 3.47 (s, 1H), 2.41 (m, 1H), 2.34 (m, 1H), 1.70 (dh, 2H, $J=14.14$ Hz, $J'=7.05$ Hz), 1.37 (s, 1H), 1.29 (s, 9H), 1.25 (t, 6H, $J=6.93$ Hz), 1.13 (d, 3H, $J=5.85$ Hz), 1.00 (t, 3H, $J=7.26$ Hz); $^{13}\text{C-NMR}$ (δ ppm, Chloroform-d) 174.02, 170.20, 138.21, 128.3, 127.81, 127.58, 75.40, 71.77, 64.94, 50.46, 49.65, 36.58, 28.66, 21.37, 20.99, 18.71, 17.28, 13.93; FTIR (cm^{-1}) 3292 ($\nu_{\text{N-H}}$), 2968 ($\nu_{\text{C-H}}$), 2930 ($\nu_{\text{C-H}}$), 2872 ($\nu_{\text{C-H}}$), 1673 ($\nu_{\text{C=O}}$), 1619 ($\nu_{\text{C=O}}$), 1544 ($\text{Ar}, \nu_{\text{C=C}}$), 1101 ($\nu_{\text{C-O-C}}$), 750 ($\text{Ar}, \nu_{\text{C-H}}$), 698 ($\text{Ar}, \nu_{\text{C-H}}$); LC/Q-TOF (m/z): $[\text{M}]^+$ calcd. for $\text{C}_{22}\text{H}_{36}\text{N}_2\text{O}_3$, 376.2726; found, 376.2730.

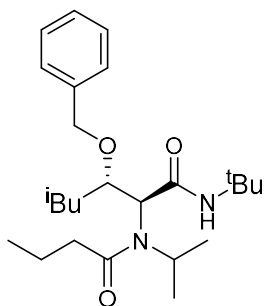


(2S,3S)-3-(benzyloxy)-N-(tert-butyl)-2-(N-isopropylbutyramido)-4-methylpentanamide (45b-D1).

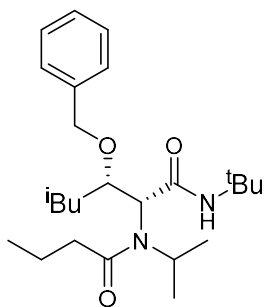
This compound was prepared from (S)-2-(benzyloxy)-3-methylbutanal **41b** as diastereomer 1 in 65% yield. $^1\text{H-NMR}$ (δ ppm, Chloroform-d) 8.48 (s, 1H), 7.38-7.20 (m, 5H), 4.59 (d, 1H, $J=11.6$ Hz), 4.48 (d, 1H, $J=11.5$ Hz), 4.03 (p, 1H, $J=6.7$ Hz), 3.64 (d, 1H, $J=10.3$ Hz), 2.40 (m, 1H), 2.20 (m, 1H), 1.92 (m, 1H), 1.71 (m, 1H), 1.61 (m, 1H), 1.32 (s, 9H), 1.24 (d, 6H, $J=6.8$ Hz), 1.11 (d, 3H, $J=6.6$ Hz), 1.07 (t, 6H, $J=6.7$ Hz), 0.99 (t, 3H, $J=7.4$ Hz); $^{13}\text{C-NMR}$ (δ ppm, Chloroform-d) 175.02, 170.86, 139.59, 128.32, 127.31, 127.23, 79.74, 74.78, 65.70, 50.94, 50.67, 37.25, 30.67, 28.72, 21.72, 21.38, 20.58, 19.06, 15.49, 14.17; FTIR (cm^{-1}) 3247 ($\nu_{\text{N-H}}$), 2962 ($\nu_{\text{C-H}}$), 2932 ($\nu_{\text{C-H}}$), 2874 ($\nu_{\text{C-H}}$), 1666 ($\nu_{\text{C=O}}$), 1604 ($\nu_{\text{C=O}}$), 1547 ($\text{Ar}, \nu_{\text{C=C}}$), 1067 ($\nu_{\text{C-O-C}}$), 743 ($\text{Ar}, \nu_{\text{C-H}}$), 697 ($\text{Ar}, \nu_{\text{C-H}}$); LC/Q-TOF (m/z): $[\text{M}]^+$ calcd. for $\text{C}_{24}\text{H}_{40}\text{N}_2\text{O}_3$, 404.3039; found, 404.3039.



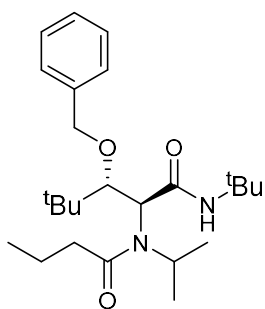
(2S,3R)-3-(benzyloxy)-N-(tert-butyl)-2-(N-isopropylbutyramido)-4-methylpentanamide (45b-D2). This compound was prepared from (S)-2-(benzyloxy)-3-methylbutanal **41b** as diastereomer 2 in 35% yield. ¹H-NMR (δ ppm, Chloroform-d) 7.38 (d, 2H, J=7.1 Hz), 7.32 (t, 2H, J=7.5 Hz), 7.28 – 7.24 (m, 1H), 4.81 (d, 1H, J=10.7 Hz), 4.58 (d, 1H, J=10.7 Hz), 4.12 (hept, 1H, J=6.9 Hz), 2.39 (dq, 2H, J=30.9, 7.5 Hz), 1.72 (q, 2H, J=7.4 Hz), 1.33 (s, 9H), 1.31 (d, 3H, J=6.9 Hz), 1.04 (d, 3H, J = 7.0 Hz), 1.00 (t, 3H, J=7.4 Hz), 0.91 (d, J=6.7 Hz, 3H). ¹³C-NMR (δ ppm, Chloroform-d) 175.13, 138.85, 128.14, 127.87, 127.32, 81.82, 75.59, 50.70, 37.31, 28.98, 28.60, 21.72, 21.51, 19.12, 15.27, 13.83; FTIR (cm⁻¹) 3282 (ν_{N-H}), 2963 (ν_{C-H}), 2868 (ν_{C-H}), 1665 (ν_{C=O}), 1617 (ν_{C=O}), 1557 (Ar,ν_{C=C}), 1066 (ν_{C-O-C}), 700 (Ar, ν_{C-H}); LC/Q-TOF (m/z): [M]⁺ calcd. for C₂₄H₄₀N₂O₃, 404,3039; found, 404,3042.



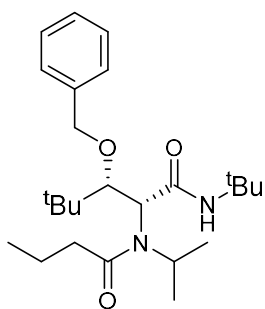
(2S,3S)-3-(benzyloxy)-N-(tert-butyl)-2-(N-isopropylbutyramido)-5-methylhexanamide (45c-D1). This compound was prepared from (S)-2-(benzyloxy)-4-methylpentanal **41c** as diastereomer 1 in 44% yield. ¹H-NMR (δ ppm, Chloroform-d) 8.40 (s, 1H), 7.34-7.26 (m, 5H), 4.73 (m, 1H), 4.58-4.46 (dd, 2H), 4.06 (p, 1H, J=6.73 Hz), 3.47 (m, 1H), 2.43 (m, 1H), 2.24 (m, 1H), 1.85 (m, 1H), 1.78-1.60 (m, 2H), 1.57 (m, 1H), 1.41 (m, 1H), 1.32 (s, 9H), 1.24 (d, 3H, J=6.72 Hz), 1.15 (d, 3H, J=6.61 Hz), 1.00 (t, 3H, J=7.38 Hz), 0.94 (t, 6H, J=6.27 Hz); ¹³C-NMR (δ ppm, Chloroform-d) 174.98, 170.58, 139.19, 128.43, 127.74, 127.57, 74.41, 73.69, 68.42, 50.70, 43.25, 37.29, 28.73, 24.86, 24.32, 22.21, 21.70, 20.69, 19.08, 14.18; FTIR (cm⁻¹) 3264 (ν_{N-H}), 2963 (ν_{C-H}), 2931 (ν_{C-H}), 2870 (ν_{C-H}), 1667 (ν_{C=O}), 1616 (ν_{C=O}), 1542 (Ar,ν_{C=C}), 1090 (ν_{C-O-C}), 696 (Ar, ν_{C-H}); LC/Q-TOF (m/z): [M]⁺ calcd. for C₂₅H₄₂N₂O₃, 418,3195; found, 418,3196.



(2S,3R)-3-(benzyloxy)-N-(tert-butyl)-2-(N-isopropylbutyramido)-5-methylhexanamide (45c-D2). This compound was prepared from (S)-2-(benzyloxy)-4-methylpentanal **41c** as diastereomer 2 in 28% yield. ¹H-NMR (δ ppm, Chloroform-d) 8.08 (s, 1H), 7.42-7.26 (m, 5H), 4.81 (m, 1H), 4.79 (d, 1H), 4.54 (d, 1H), 4.10 (p, 1H, J=6.72 Hz), 3.55 (s, 1H), 2.38 (m, 12H), 1.88 (m, 1H), 1.70 (m, 2H), 1.35 (s, 9H), 1.26 (dd, 6H, J=19.92 Hz, J'=6.71 Hz), 1.03 (m, 2H), 0.91 (dd, J=6.63 Hz, J'=3.73 Hz); ¹³C-NMR (δ ppm, Chloroform-d) 174.63, 171.88, 138.59, 128.69, 128.57, 127.87, 76.76, 74.37, 66.52, 50.90, 50.35, 43.03, 37.08, 31.18, 28.87, 24.52, 24.39, 21.75, 21.62, 21.30, 19.14, 14.21; FTIR (cm⁻¹) 3301 (ν_{N-H}), 2960 (ν_{C-H}), 2929 (ν_{C-H}), 2869 (ν_{C-H}), 1672 (ν_{C=O}), 1619 (ν_{C=O}), 1560 (Ar, ν_{C=C}), 1077 (ν_{C-O-C}), 752 (Ar, ν_{C-H}), 698 (Ar, ν_{C-H}); LC/Q-TOF (m/z): [M]⁺ calcd. for C₂₅H₄₂N₂O₃, 418,3195; found, 418,3196.



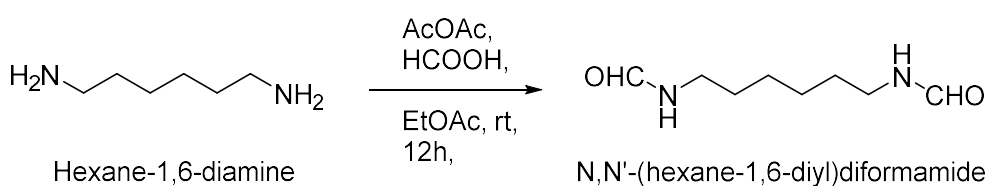
(2S,3S)-3-(benzyloxy)-N-(tert-butyl)-2-(N-isopropylbutyramido)-4,4-dimethylpentanamide (45d-D1). This compound was prepared from (S)-2-(benzyloxy)-3,3-dimethylbutanal **41d** as diastereomer 1 in 70% yield. ¹H-NMR (δ ppm, Chloroform-d) 8.56 (s, 1H), 7.33-7.25 (m, 5H), 4.59 (m, 2H), 4.33 (d, 1H, J=10.11 Hz), 4.01 (p, 1H, J=6.70 Hz), 3.73 (d, 1H, J=10.22 Hz), 2.36 (m, 1H), 2.16 (m, 1H), 1.70 (m, 1H), 1.62 (m, 1H), 1.31 (s, 9H), 1.25 (d, 3H, J=6.73 Hz), 1.10 (d, 3H, J=6.65 Hz), 1.09 (s, 9H), 0.99 (t, 3H, J=7.38 Hz); ¹³C-NMR (δ ppm, Chloroform-d) 174.89, 171.37, 139.68, 128.31, 127.16, 126.86, 83.74, 74.90, 65.17, 51.33, 50.79, 37.63, 37.28, 28.59, 26.89, 21.88, 20.69, 19.10, 14.19; FTIR (cm⁻¹) 3247 (ν_{N-H}), 2961 (ν_{C-H}), 2872 (ν_{C-H}), 1665 (ν_{C=O}), 1604 (ν_{C=O}), 1548 (Ar, ν_{C=C}), 1079 (ν_{C-O-C}), 742 (Ar, ν_{C-H}), 697 (Ar, ν_{C-H}); LC/Q-TOF (m/z): [M]⁺ calcd. for C₂₅H₄₂N₂O₃, 418,3195; found, 418,3192.



(2S,3R)-3-(benzyloxy)-N-(tert-butyl)-2-(N-isopropylbutyramido)-4,4-dimethylpentanamide (45d-D2).

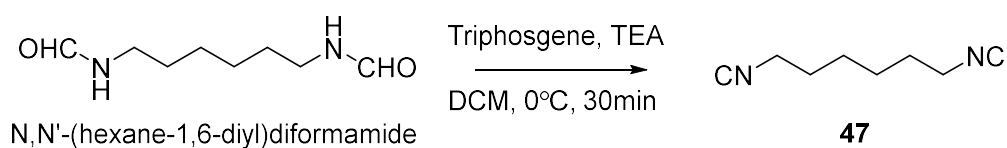
This compound was prepared from (S)-2-(benzyloxy)-3,3-dimethylbutanal **41d** as diastereomer 2 in 6% yield. ¹H-NMR (δ ppm, Chloroform-d) 7.40 (s, 1H), 7.30 (d, 2H, J=7.12 Hz), 7.22 (t, 2H, J=7.49 Hz), 7.15 (t, 1H, J=7.25 Hz), 4.90 (d, 1H, J=10.80Hz), 4.44 (d, 1H, J=10.83 Hz), 4.14 (d, 1H), 3.40 (d, 1H), 2.27 (m, 2H), 1.63 (m, 2H), 1.29 (dd, 6H, J=27.03 Hz, J'=6.85Hz), 1.16 (s, 9H), 0.94 (t, 3H, J=7.37 Hz), 0.91 (s, 9H); ¹³C-NMR (δ ppm, Chloroform-d) 175.93, 171.11, 139.13, 128.29, 127.73, 127.30, 83.83, 75.63, 63.43, 50.90, 50.56, 37.92, 37.69, 28.88, 26.69, 22.50, 21.74, 19.21, 14.26; FTIR (cm⁻¹) 3294 (ν_{N-H}), 2968 (ν_{C-H}), 2869 (ν_{C-H}), 1664 (ν_{C=O}), 1615 (ν_{C=O}), 1553 (Ar, ν_{C=C}), 1062 (ν_{C-O-C}), 759 (Ar, ν_{C-H}), 700 (Ar, ν_{C-H}); LC/Q-TOF (m/z): [M]⁺ calcd. for C₂₅H₄₂N₂O₃, 418,3195; found, 418,3195.

Synthesis of N,N'-(hexane-1,6-diyl)diformamide¹²⁶



To a solution of hexane-1,6-diamine (1.50 mmol, 174.3 mg) in EtOAc (10 mL) a mixture of formic acid (2.0 mmol, 0.189 mL) and acetic anhydride (3.0 mmol, 0.113 mL) were injected (formic acid and acetic anhydride were premixed neat at 60°C for 1 h). The mixture was then stirred at r.t. for 12 h. Then water (20 ml) was added, and the mixture was extracted with EtOAc (3 × 20 ml). The combined organics were washed with saturated NaHCO₃ (2 × 20 mL) and brine (20 ml), dried (MgSO₄), filtered, and concentrated in vacuo to give the crude. The crude product was purification by flash column chromatography to yield a light-yellow solid, 84%. ¹H-NMR (400 MHz, Methanol-d₄) δ 8.04 (s, 2H), 4.87 (s, 4H), 3.23 (t, J = 6.9 Hz, 4H), 1.54 (dd, J = 8.9, 4.8 Hz, 4H), 1.39 (dq, J = 7.5, 3.5 Hz, 4H).

¹²⁶ Prishchenko, A. A.; Alekseyev, R. S.; et al. *J. Organomet. Chem.* **2022**, 957, 122143.

Synthesis of 1,6-diisocyanohexane (47)¹²⁷

Triphosgene (268 mg, 0.9 mmol) in DCM (3 ml) was added dropwise to a mixture of TEA (4.53 mmol) and the N,N'-(hexane-1,6-diyl)diformamide (260 mg, 1.51 mmol) in dry DCM (30 ml) over 30 min at 0 °C. The mixture was allowed to stir for 10 min before the addition of a saturated aqueous solution of NaHCO₃ (8 mL) and then the solution was stirred vigorously for 20 min. After washing successively with brine, the organic phase was collected and dried over MgSO₄. Purification by column chromatography afforded the monomer as a colorless oil which was stored in fridge before use. Yield: 92%. ¹H-NMR (400 MHz, Chloroform-d) δ 3.43 (ddt, J = 6.6, 4.0, 2.0 Hz, 4H), 1.73 (dtd, J = 7.4, 5.2, 2.9 Hz, 4H), 1.52 (dq, J = 7.5, 3.5 Hz, 4H).

General procedure for polymerization

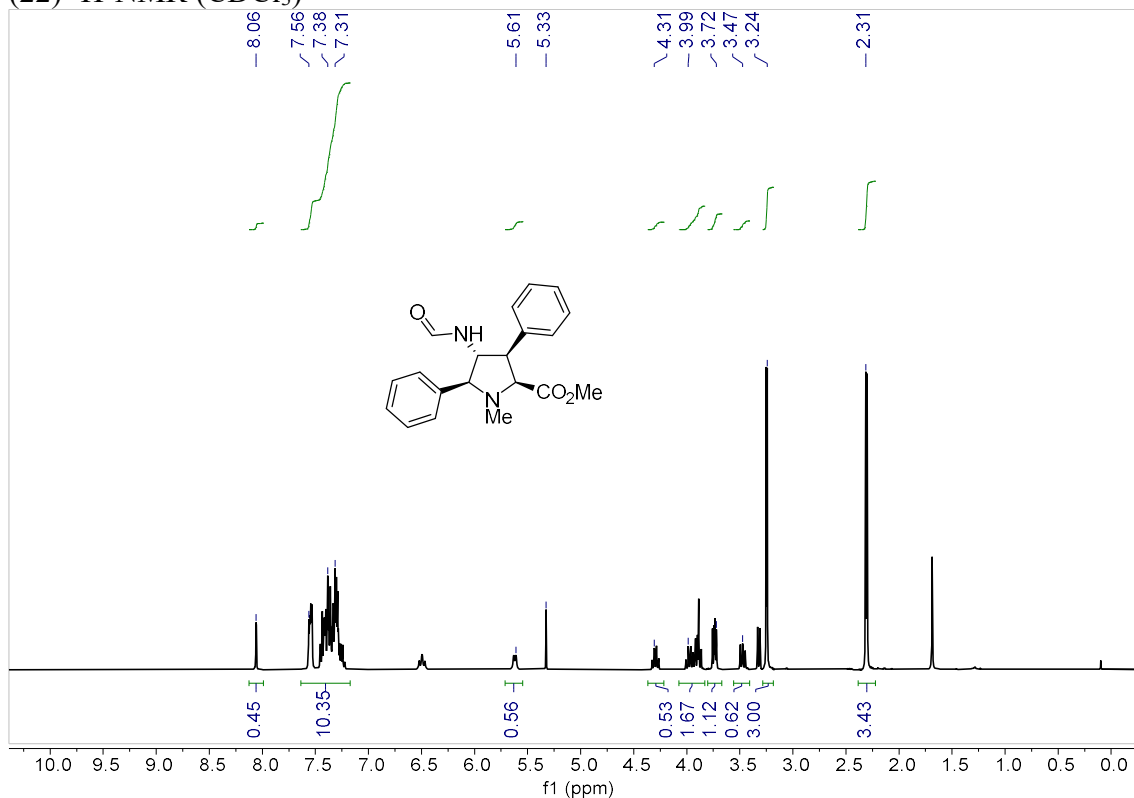
A solution of the (di)amine^a and (di)aldehyde in methanol (0.5 mL) was stirred at room temperature for 2 h then THF (1.0 mL), (di)isocyanide, and carboxylic (di)acid were injected. The resulting reaction mixture was stirred at room temperature for 48 h and then the solvent was removed in vacuo. The residue was precipitated in DCM and hexane mixture.

a) The equivalent for a di-functional reactant was 1 mmol, and for a single functional reactant was 2.2 mmol.

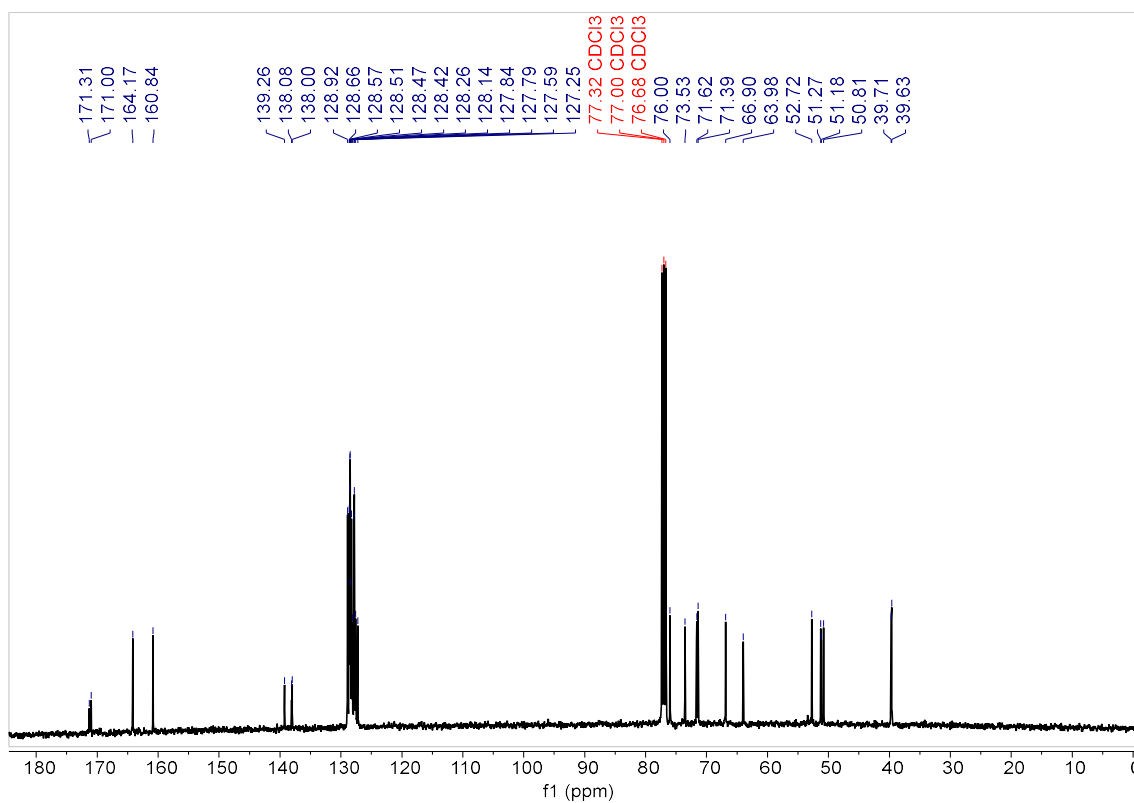
¹²⁷ Nickisch, R.; Conen, P.; et al. *Macromolecules*. **2022**, *55*, 3267-3275.

IV. NMR SPECTRA

Methyl (2S,3R,4R,5S)-4-formamido-1-methyl-3,5-diphenylpyrrolidine-2-carboxylate
(**22**) $^1\text{H-NMR}$ (CDCl_3)

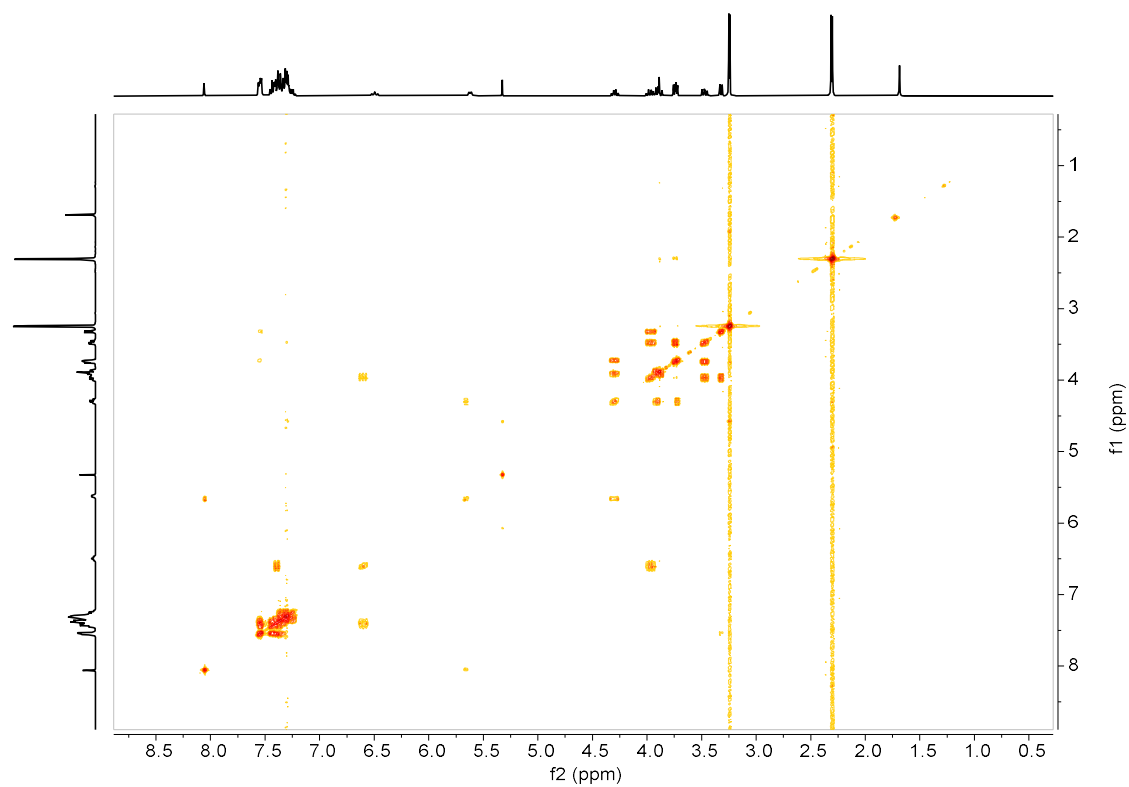


Methyl (2S,3R,4R,5S)-4-formamido-1-methyl-3,5-diphenylpyrrolidine-2-carboxylate
(**22**) $^{13}\text{C-NMR}$ (CDCl_3)

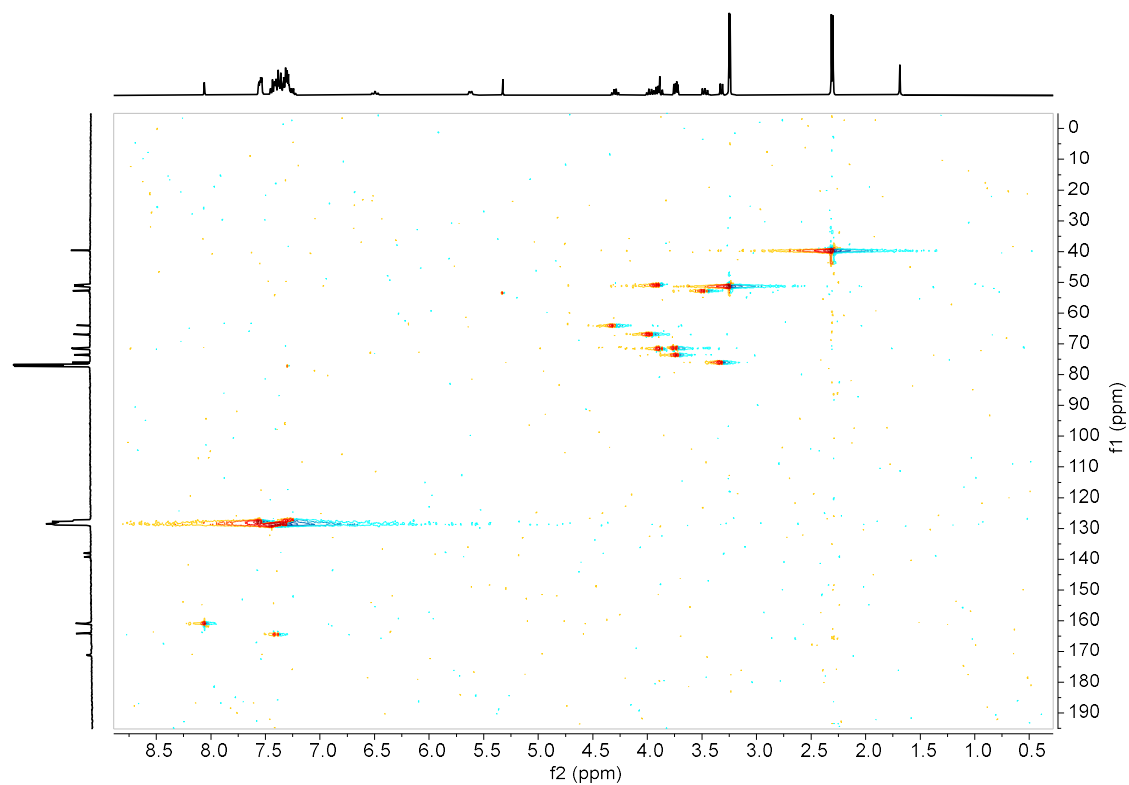


ANNEX IV

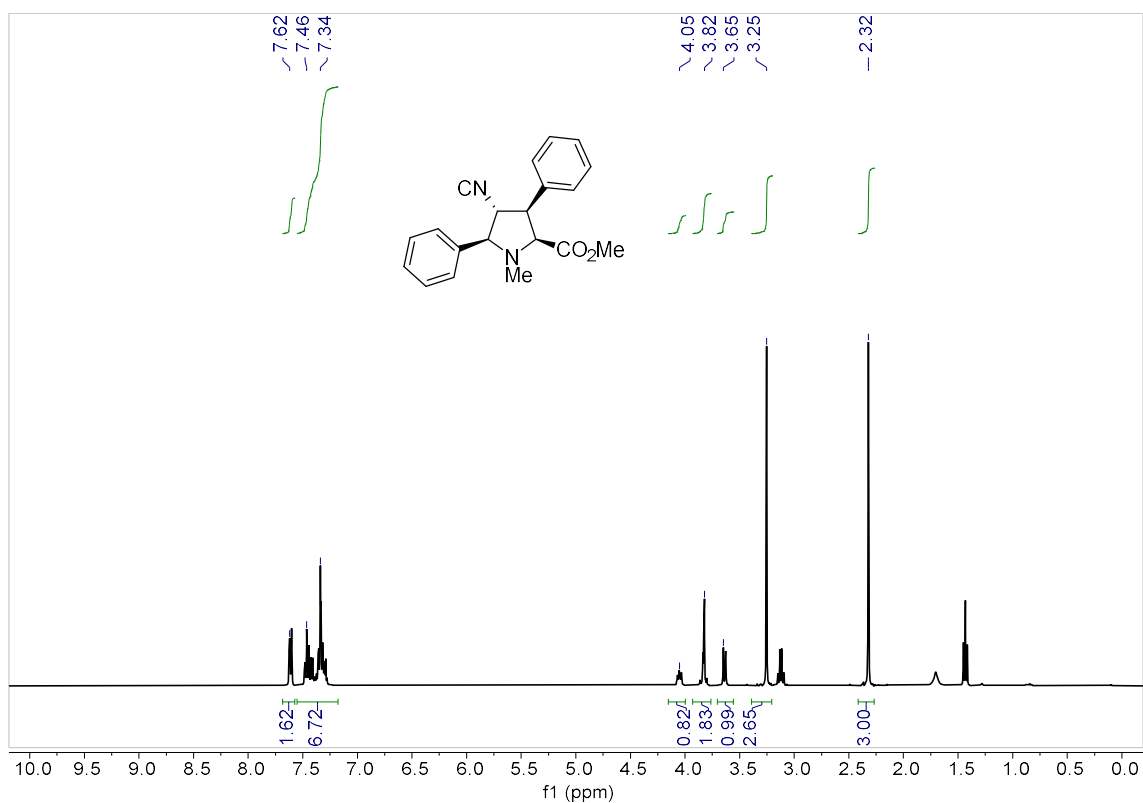
Methyl (2S,3R,4R,5S)-4-formamido-1-methyl-3,5-diphenylpyrrolidine-2-carboxylate
(**22**) g-COSY (CDCl₃)



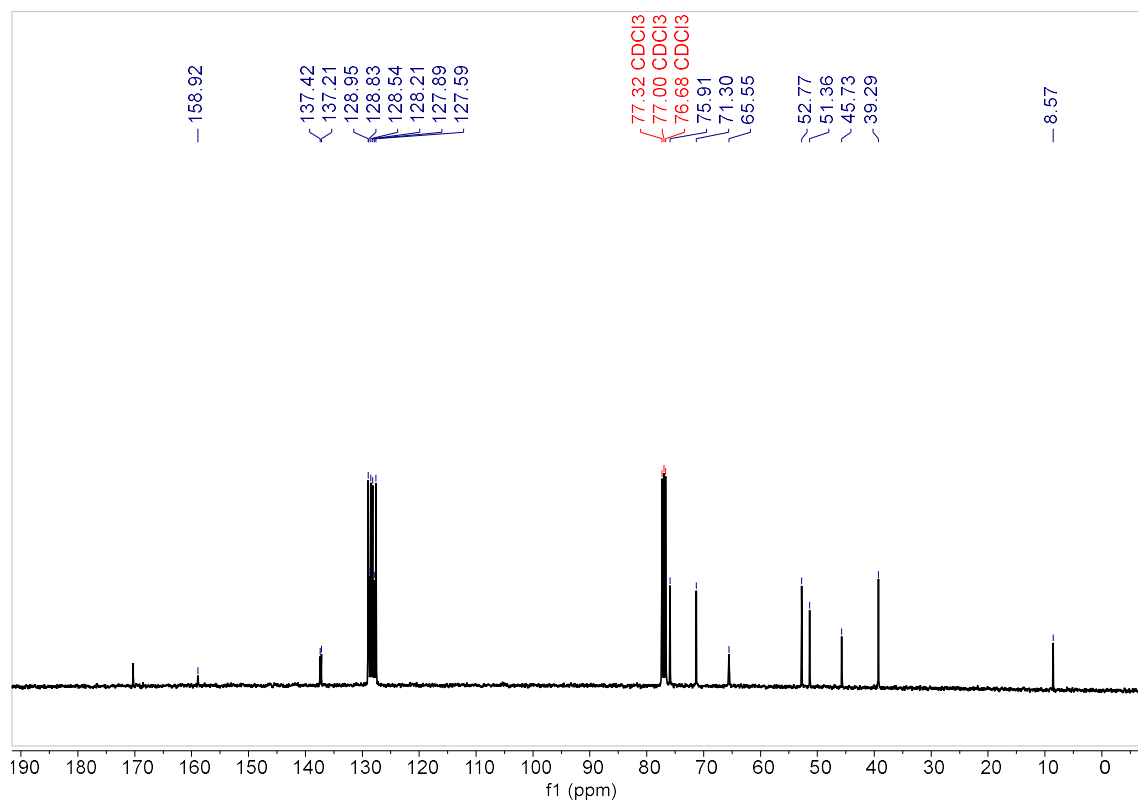
Methyl (2S,3R,4R,5S)-4-formamido-1-methyl-3,5-diphenylpyrrolidine-2-carboxylate
(**22**) g-HSQC (CDCl₃)



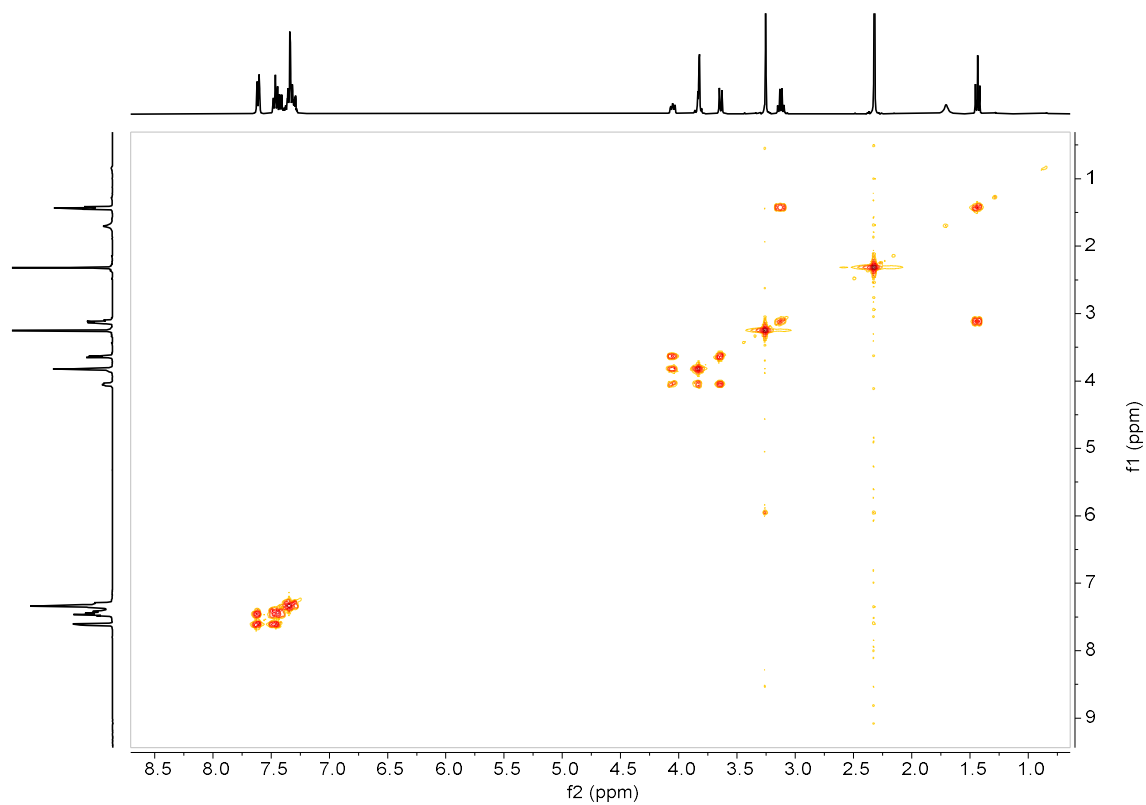
Methyl (2S,3S,4R,5S)-4-isocyano-1-methyl-3,5-diphenylpyrrolidine-2-carboxylate (**23**)
¹H-NMR (CDCl₃)



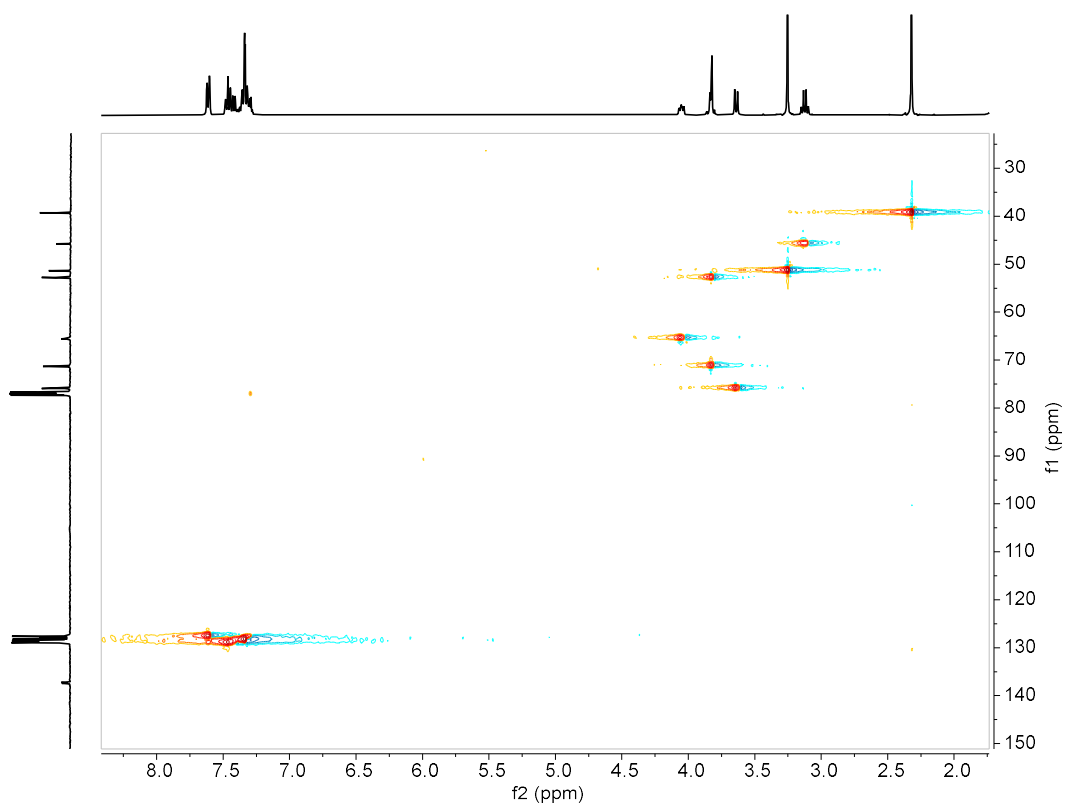
Methyl (2S,3S,4R,5S)-4-isocyano-1-methyl-3,5-diphenylpyrrolidine-2-carboxylate (**23**)
¹³C-NMR (CDCl₃)



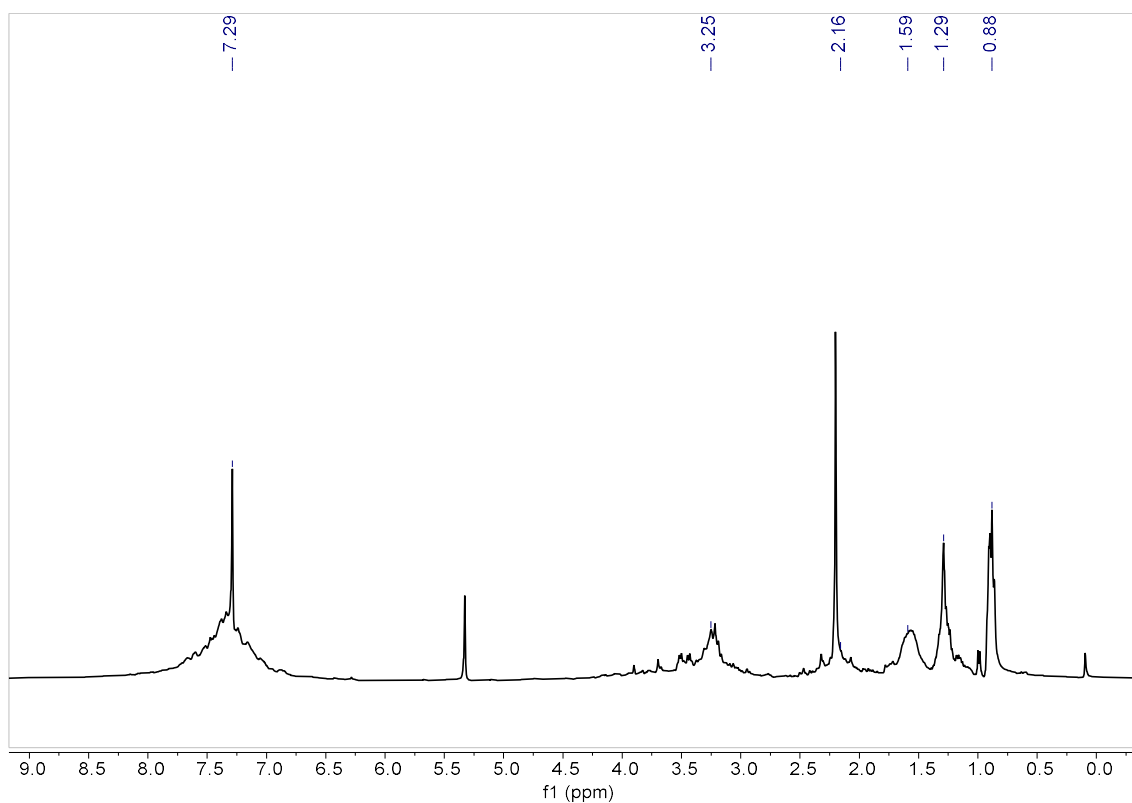
Methyl (2S,3S,4R,5S)-4-isocyano-1-methyl-3,5-diphenylpyrrolidine-2-carboxylate (**23**)
g-COSY (CDCl₃)



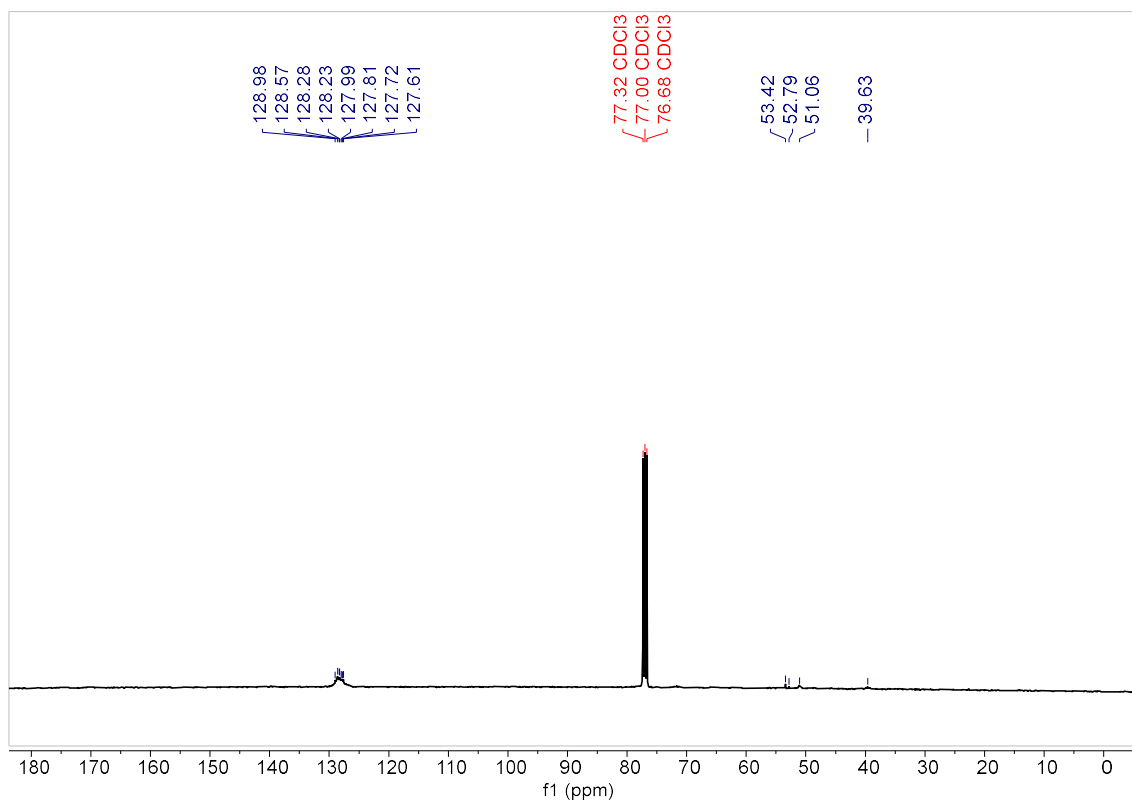
Methyl (2S,3S,4R,5S)-4-isocyano-1-methyl-3,5-diphenylpyrrolidine-2-carboxylate (**23**)
g-HSQC (CDCl₃)



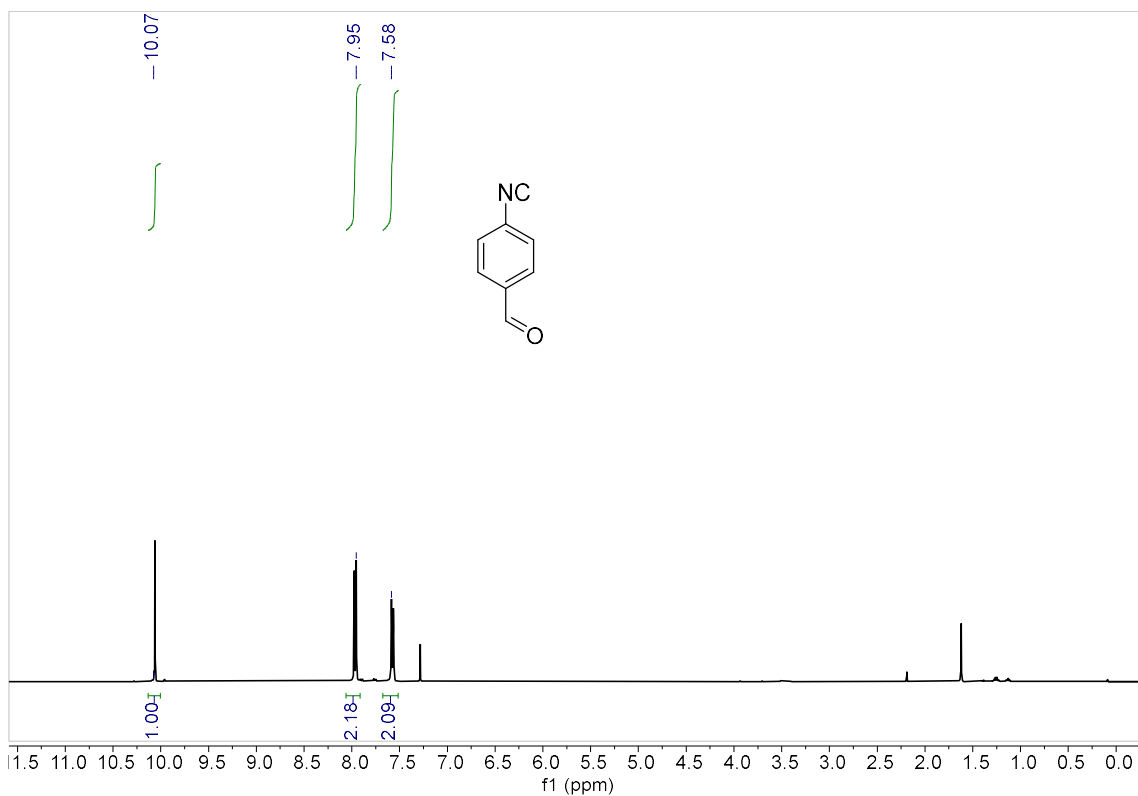
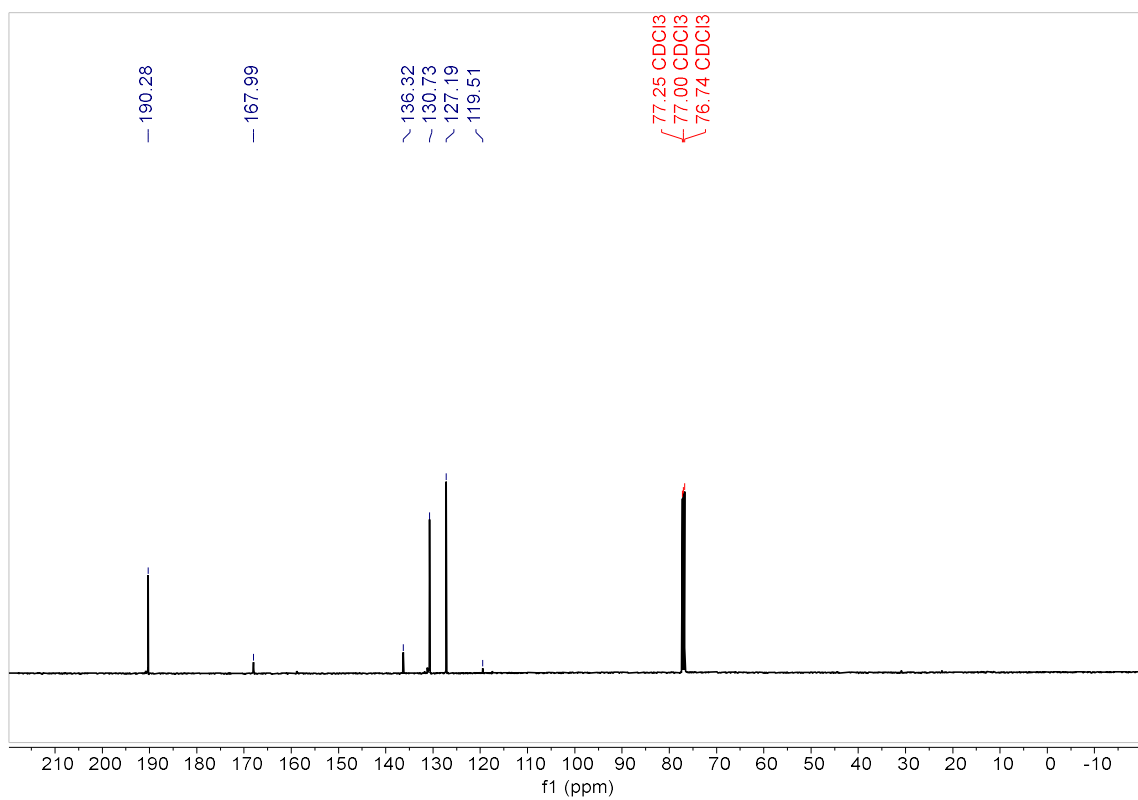
Poly[methyl (2S,3S,4R,5S)-4-isocyano-1-methyl-3,5-diphenylpyrrolidine-2-carboxylate] (**Poly-23**) $^1\text{H-NMR}$ (CDCl_3)

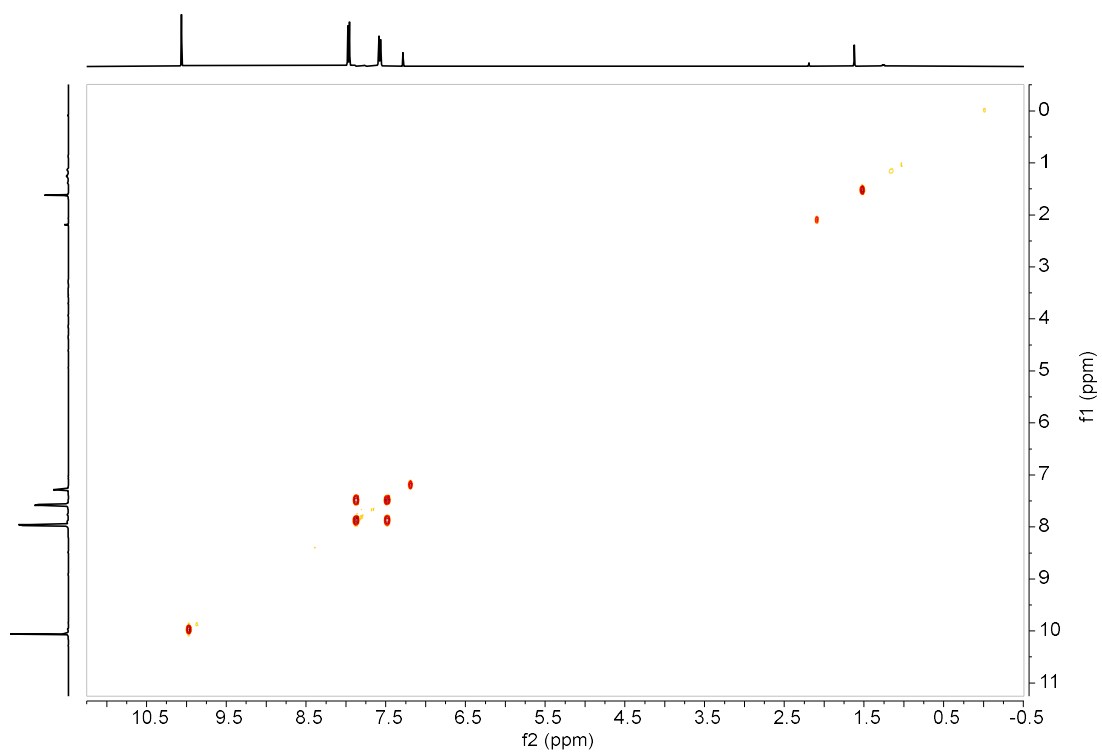
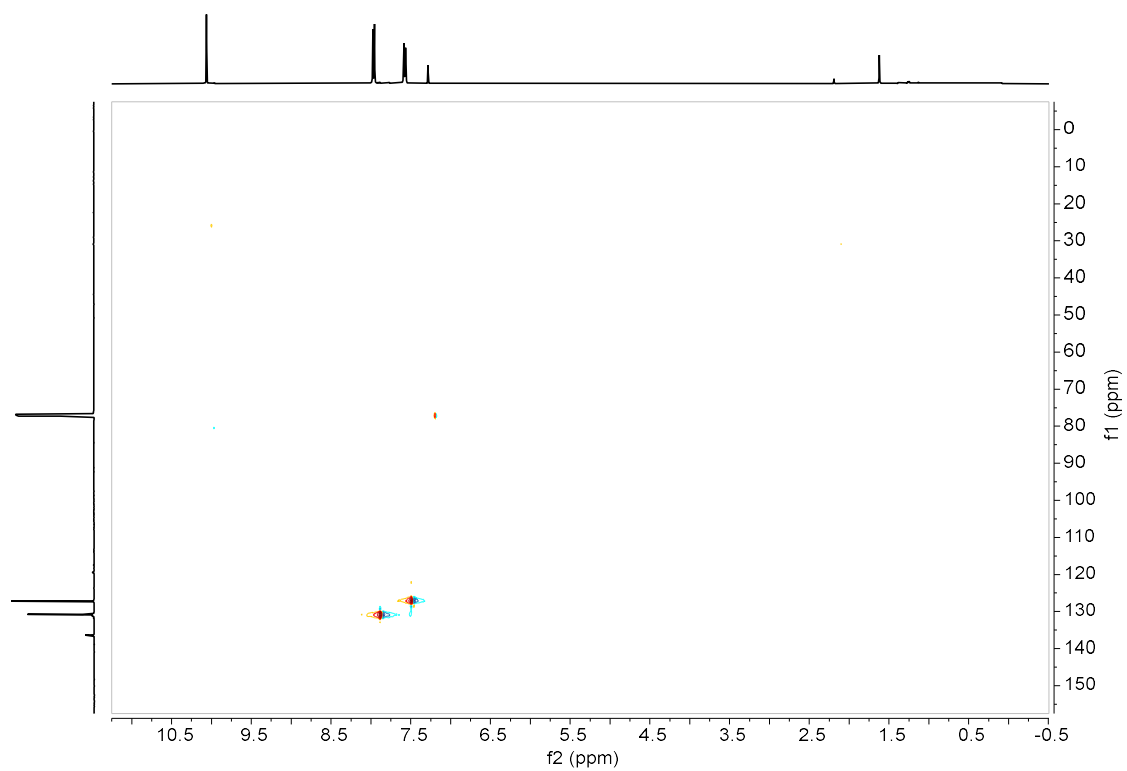


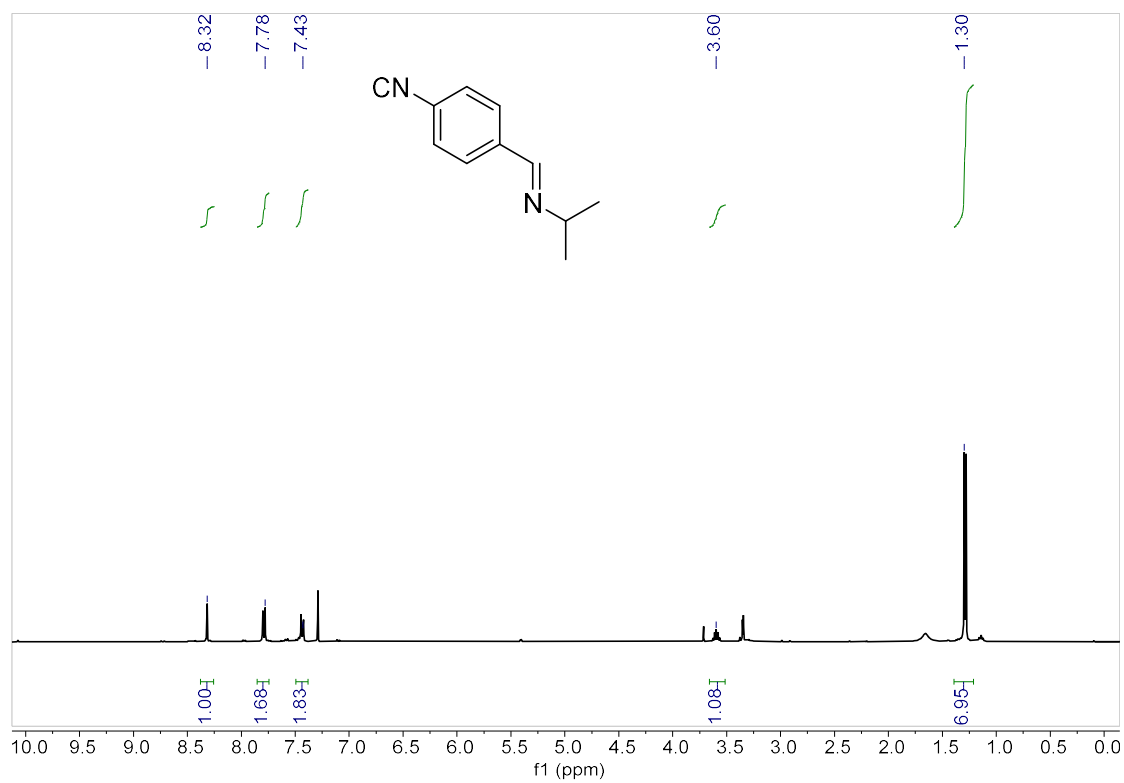
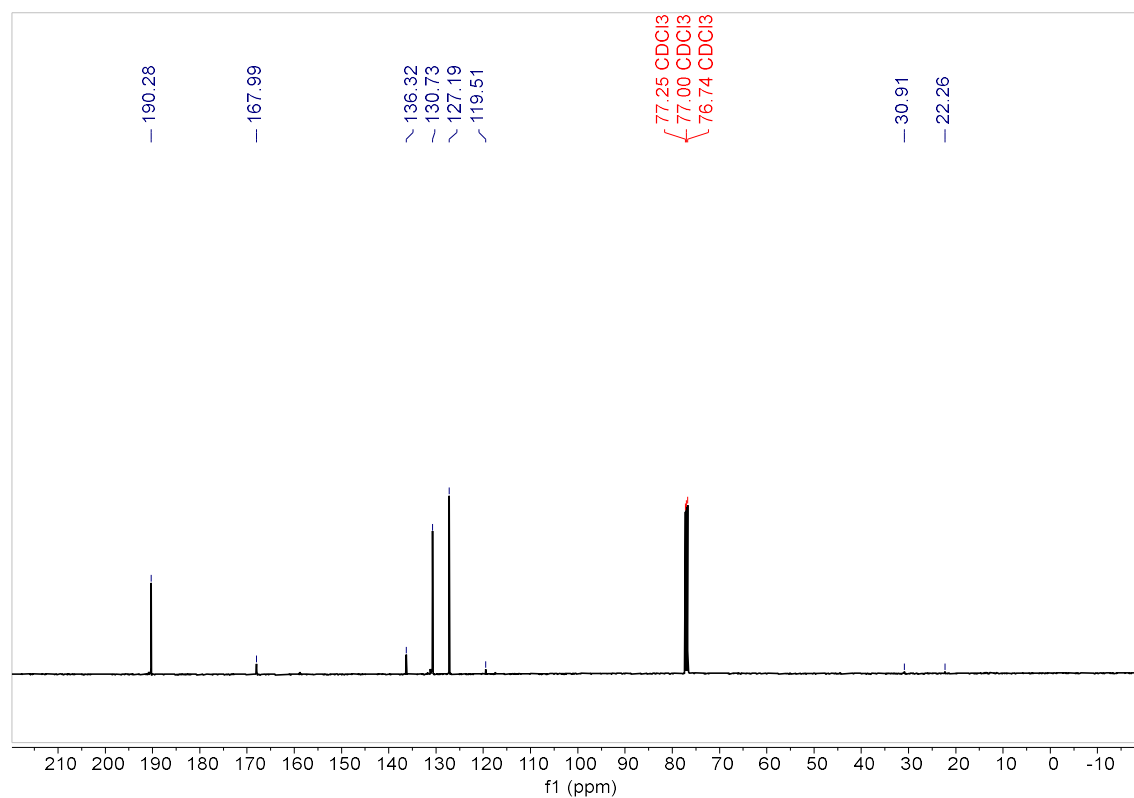
Poly[methyl (2S,3S,4R,5S)-4-isocyano-1-methyl-3,5-diphenylpyrrolidine-2-carboxylate] (**Poly-23**) $^{13}\text{C-NMR}$ (CDCl_3)

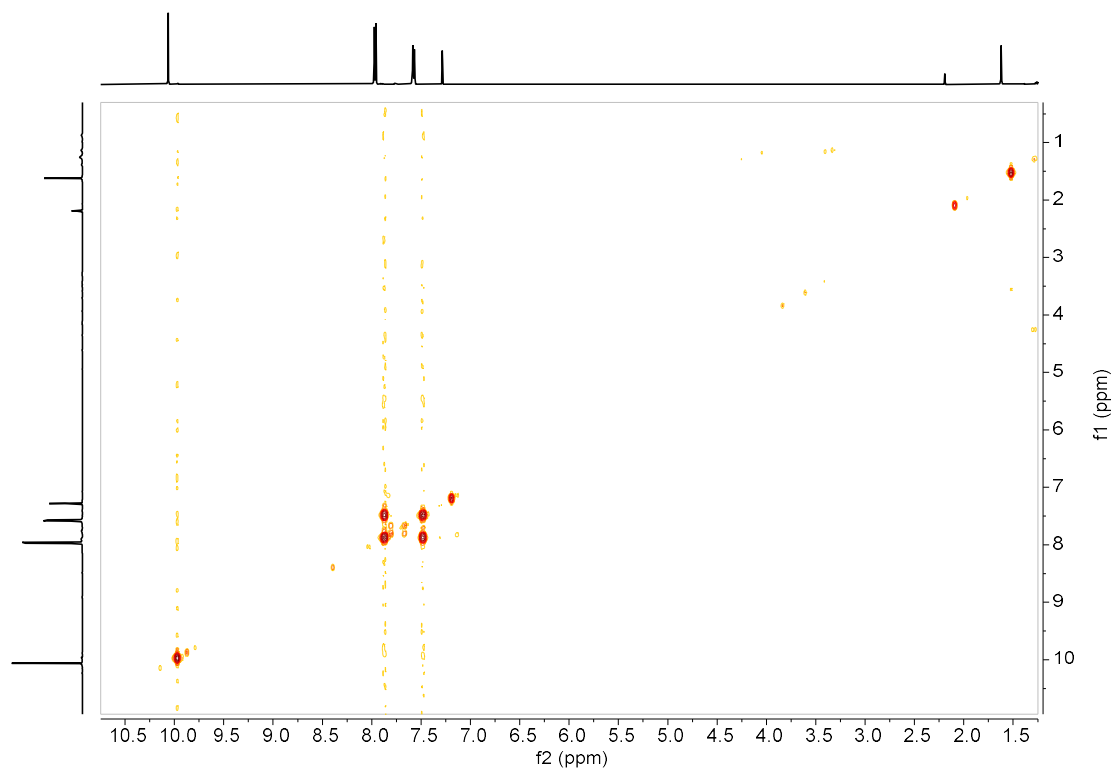
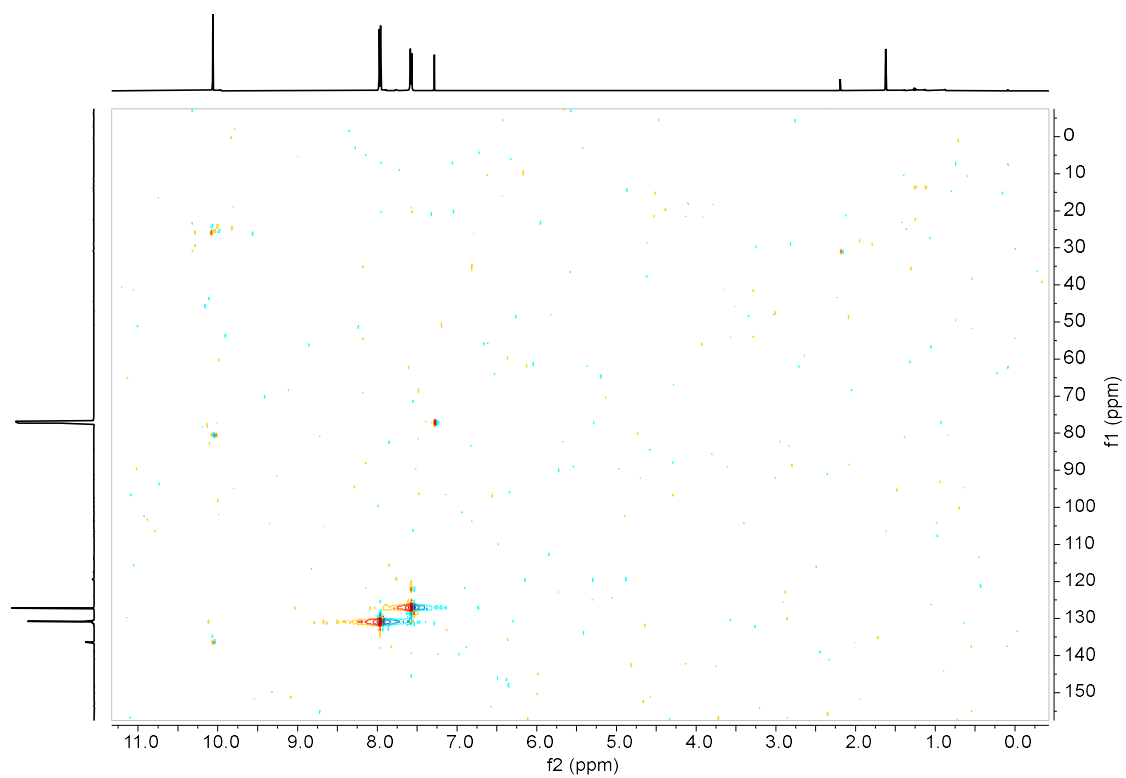


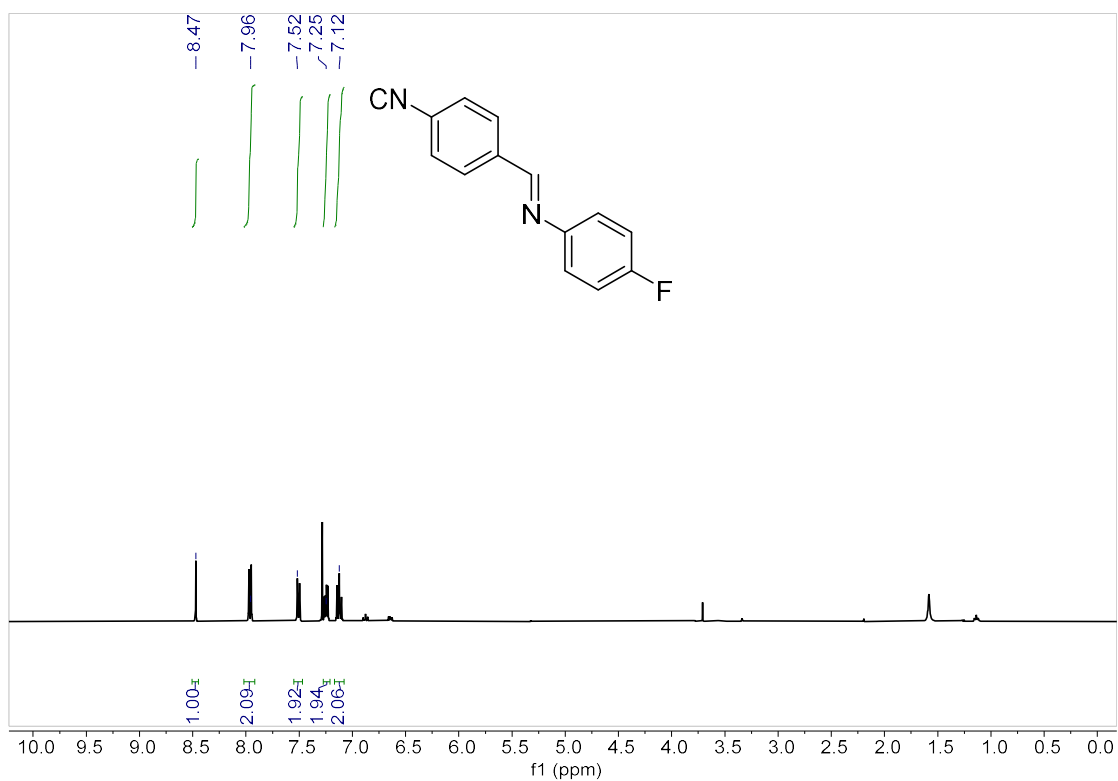
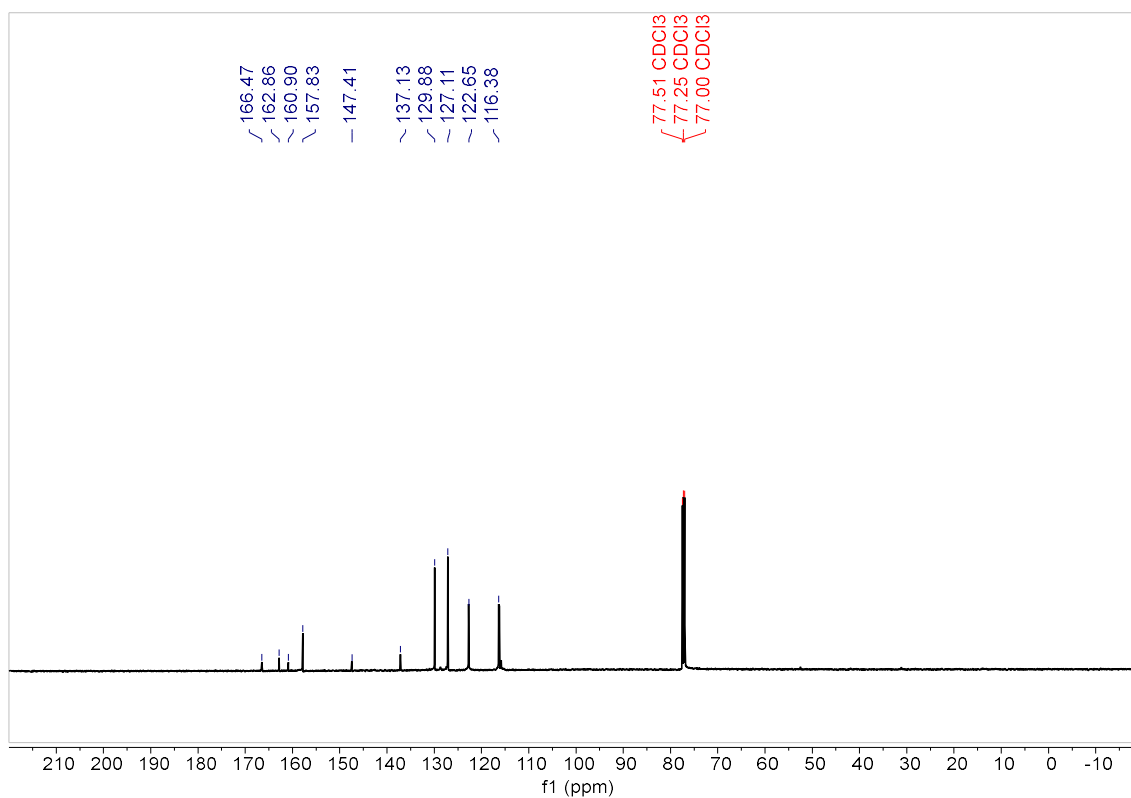
ANNEX IV

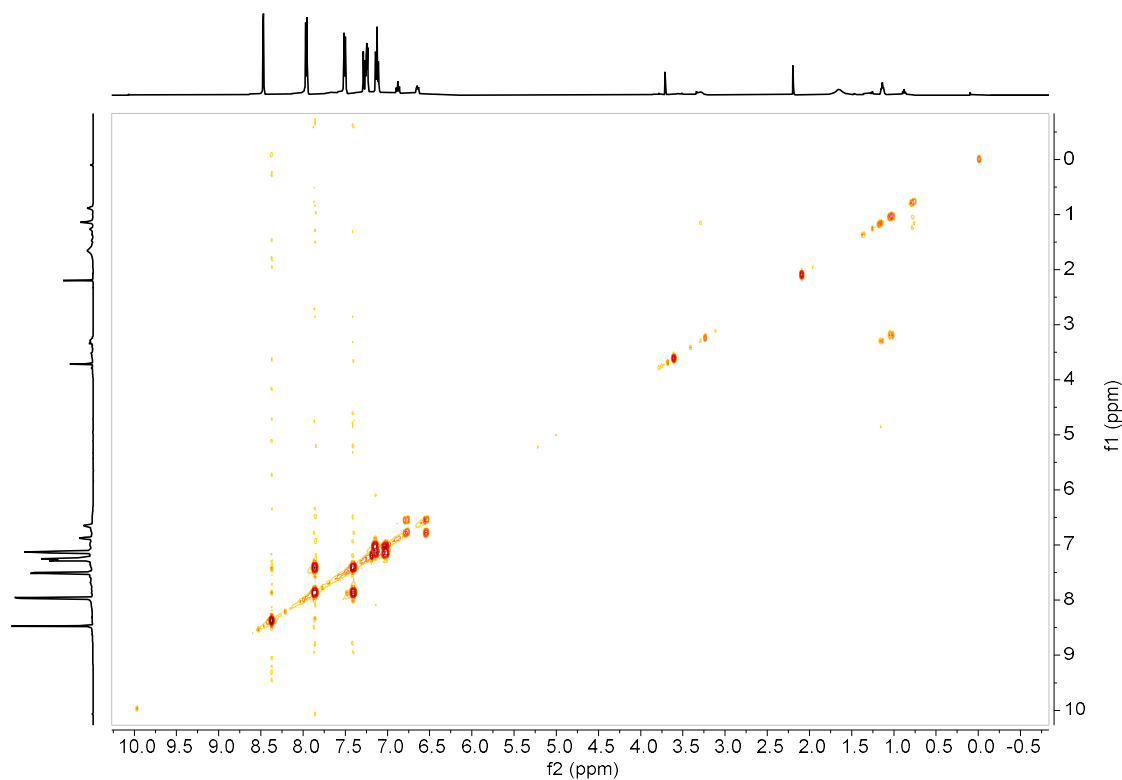
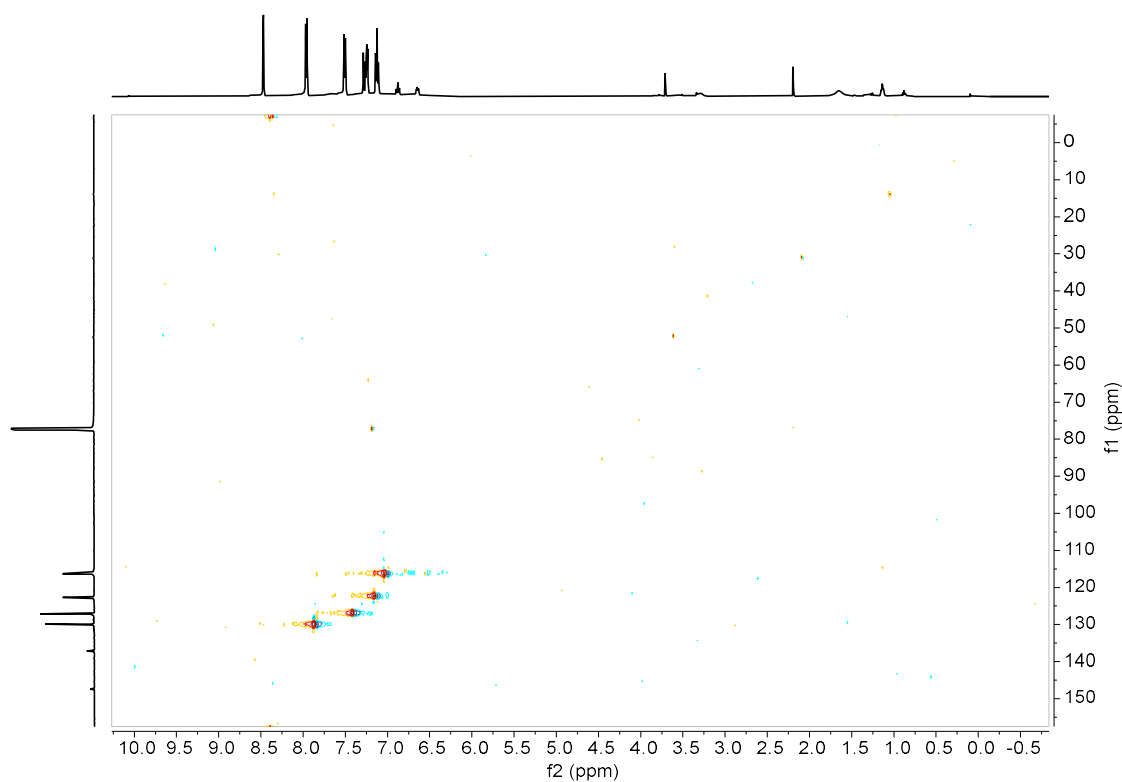
4-isocyano benzaldehyde (**30**) $^1\text{H-NMR}$ (CDCl_3)4-isocyano benzaldehyde (**30**) $^{13}\text{C-NMR}$ (CDCl_3)

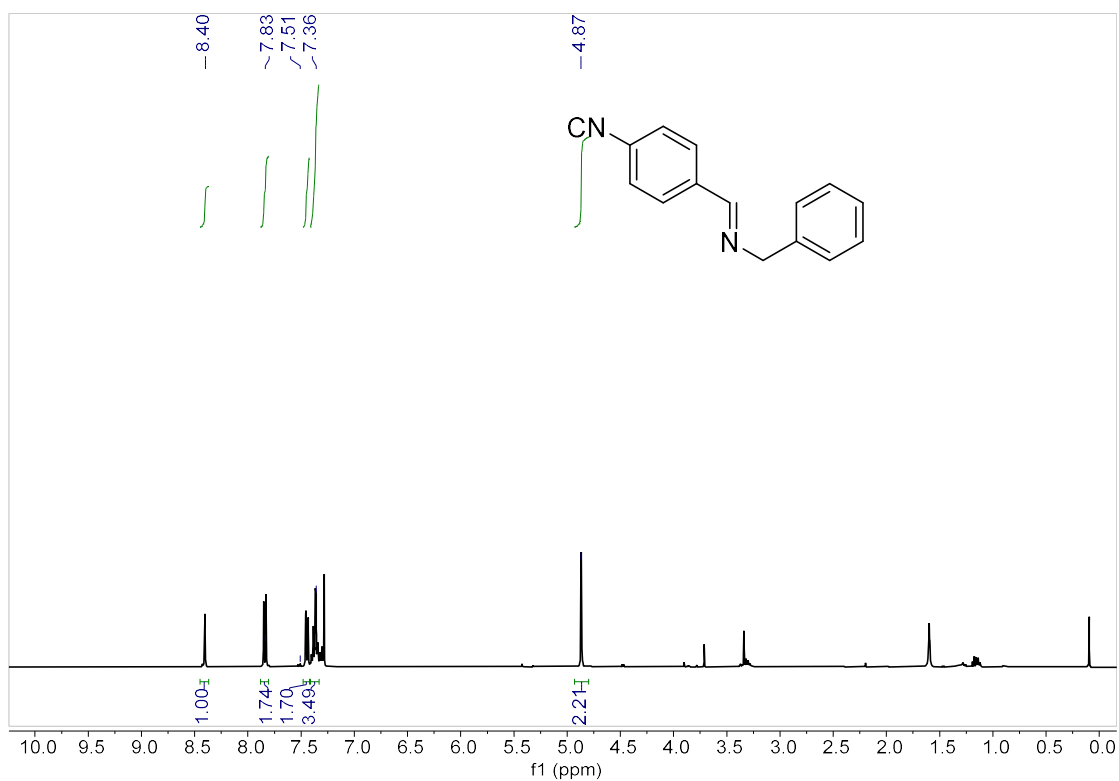
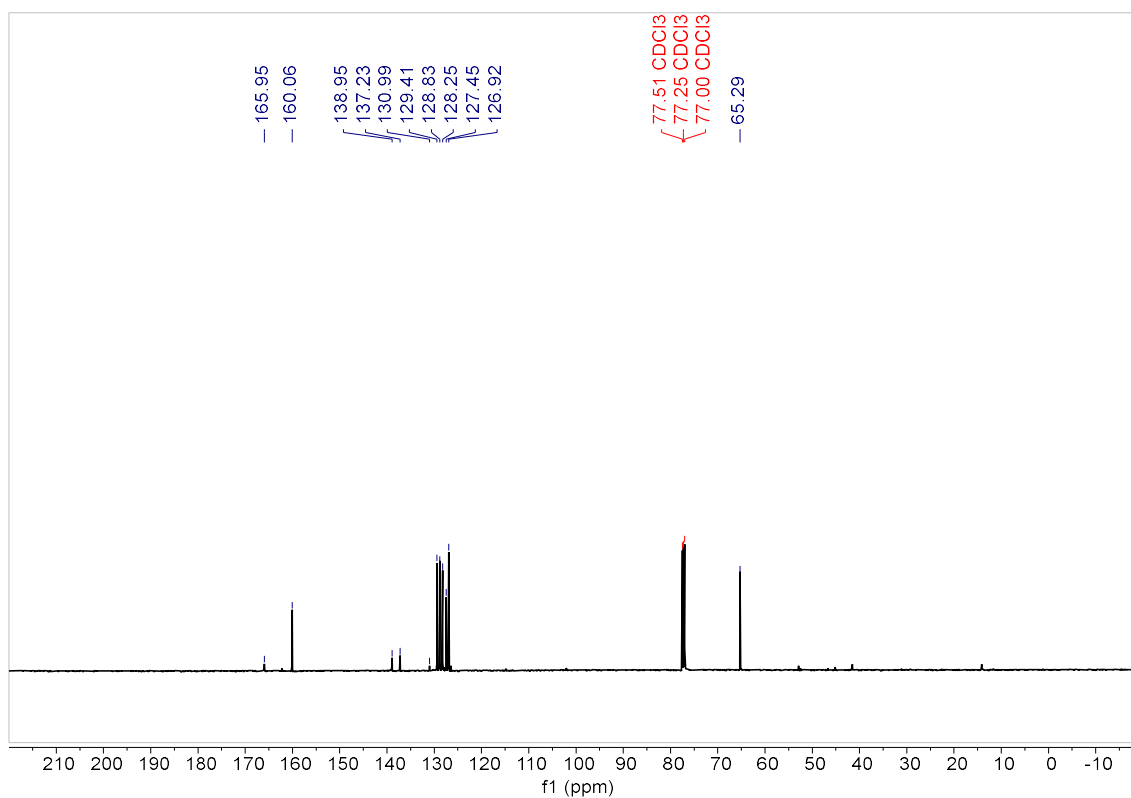
4-isocyano benzaldehyde (**30**) g-COSY (CDCl₃)4-isocyano benzaldehyde (**30**) g-HSQC (CDCl₃)

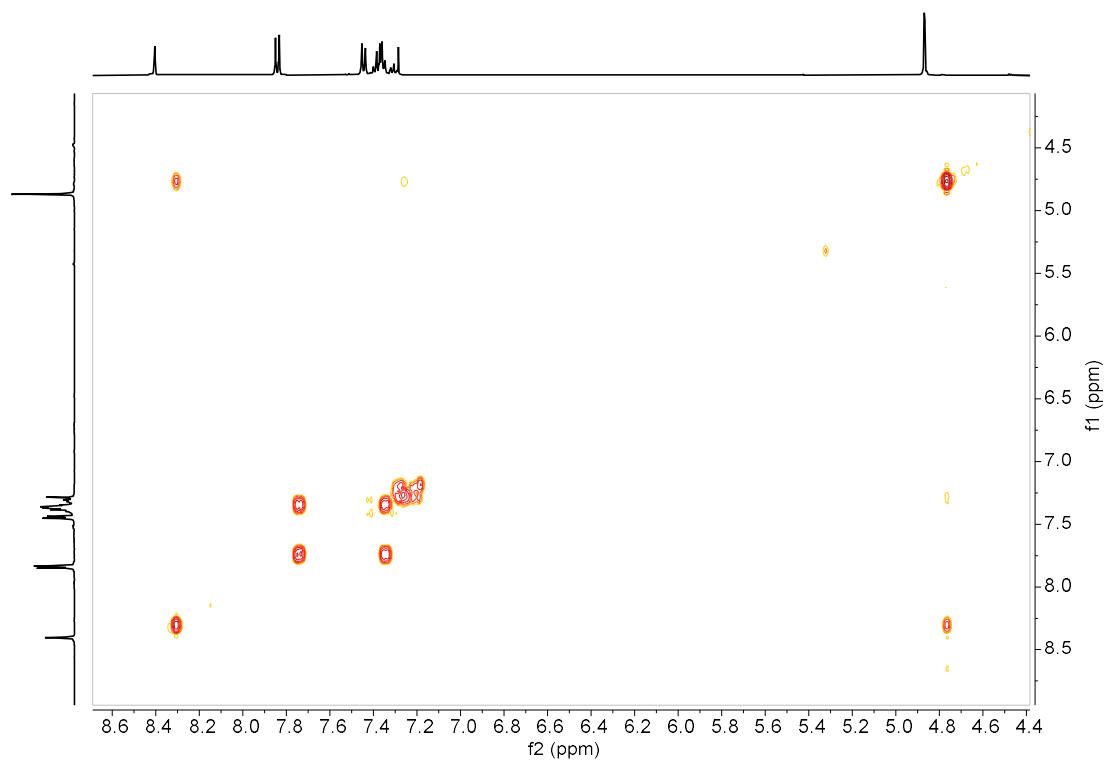
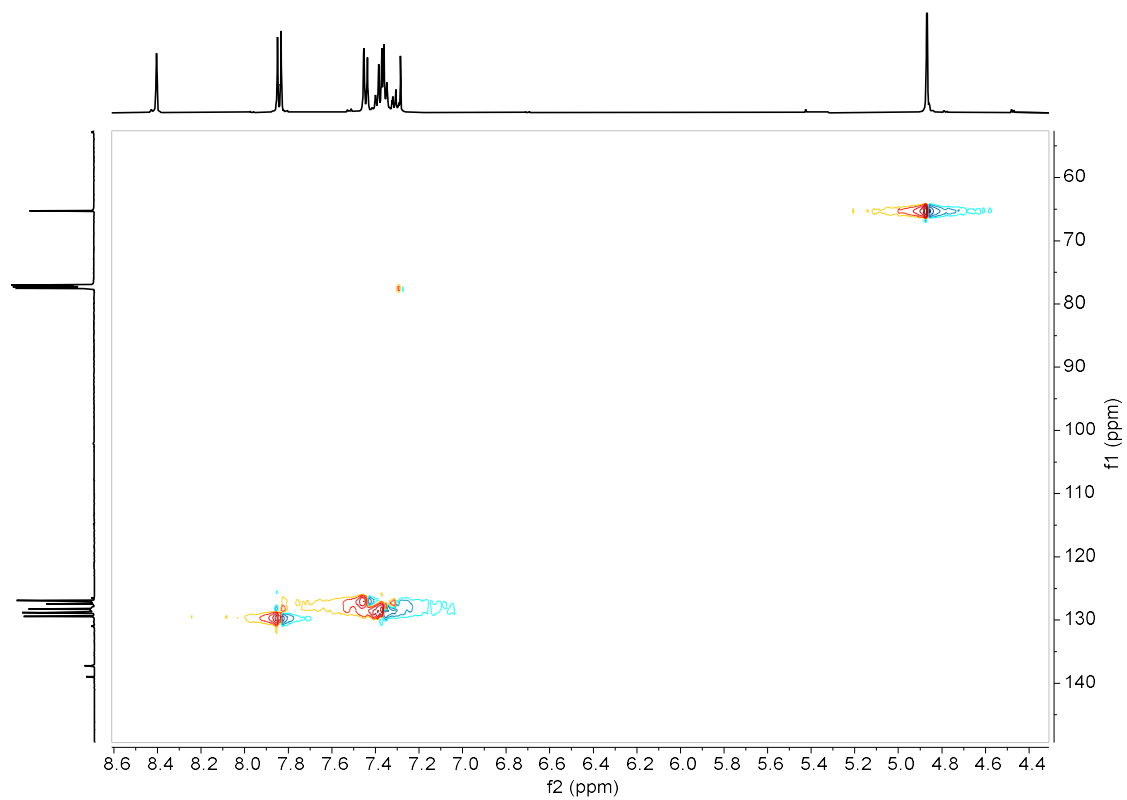
(E)-1-(4-isocyanophenyl)-N-isopropylmethanimine **31a**. $^1\text{H-NMR}$ (CDCl_3)(E)-1-(4-isocyanophenyl)-N-isopropylmethanimine **31a**. $^{13}\text{C-NMR}$ (CDCl_3)

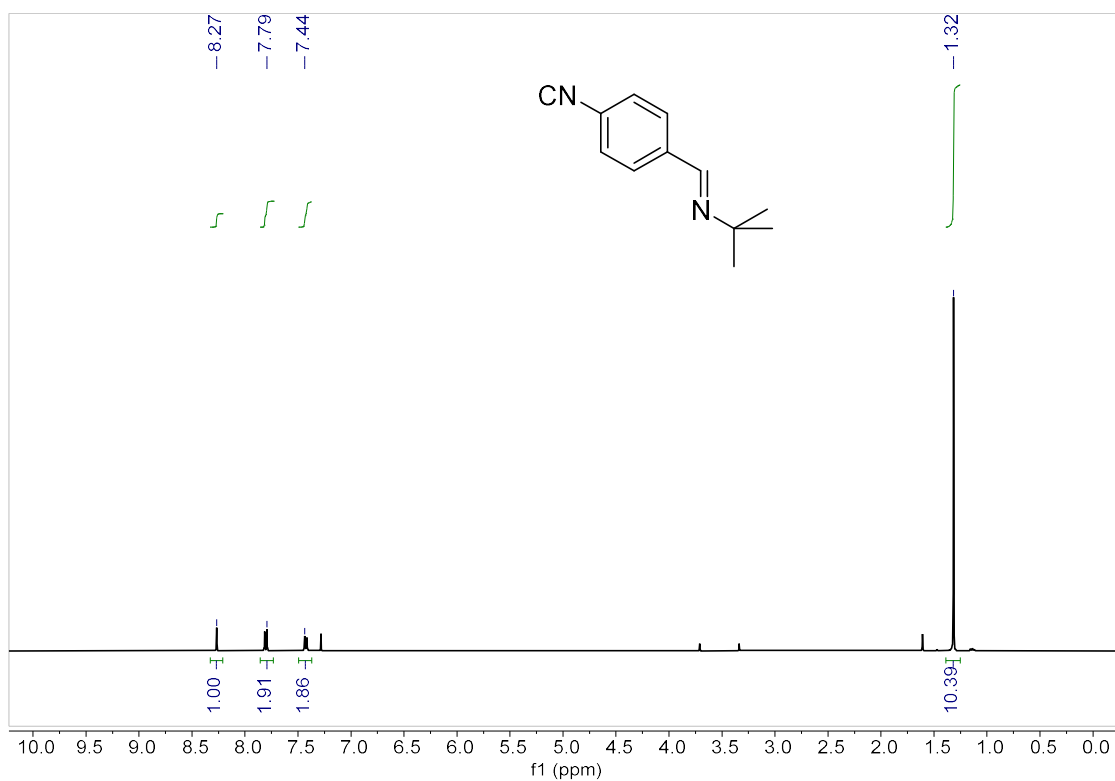
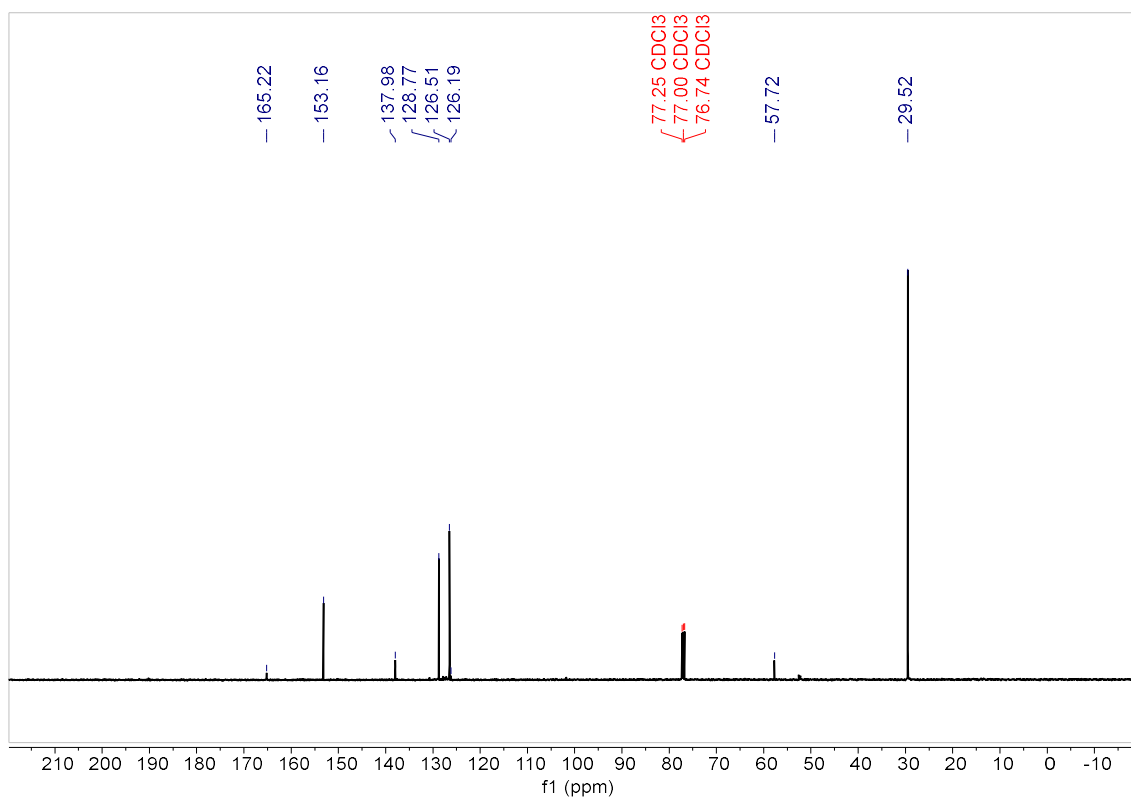
(E)-1-(4-isocyanophenyl)-N-isopropylmethanimine **31a**. g-COSY(CDCl₃)(E)-1-(4-isocyanophenyl)-N-isopropylmethanimine **31a**. g-HSQC(CDCl₃)

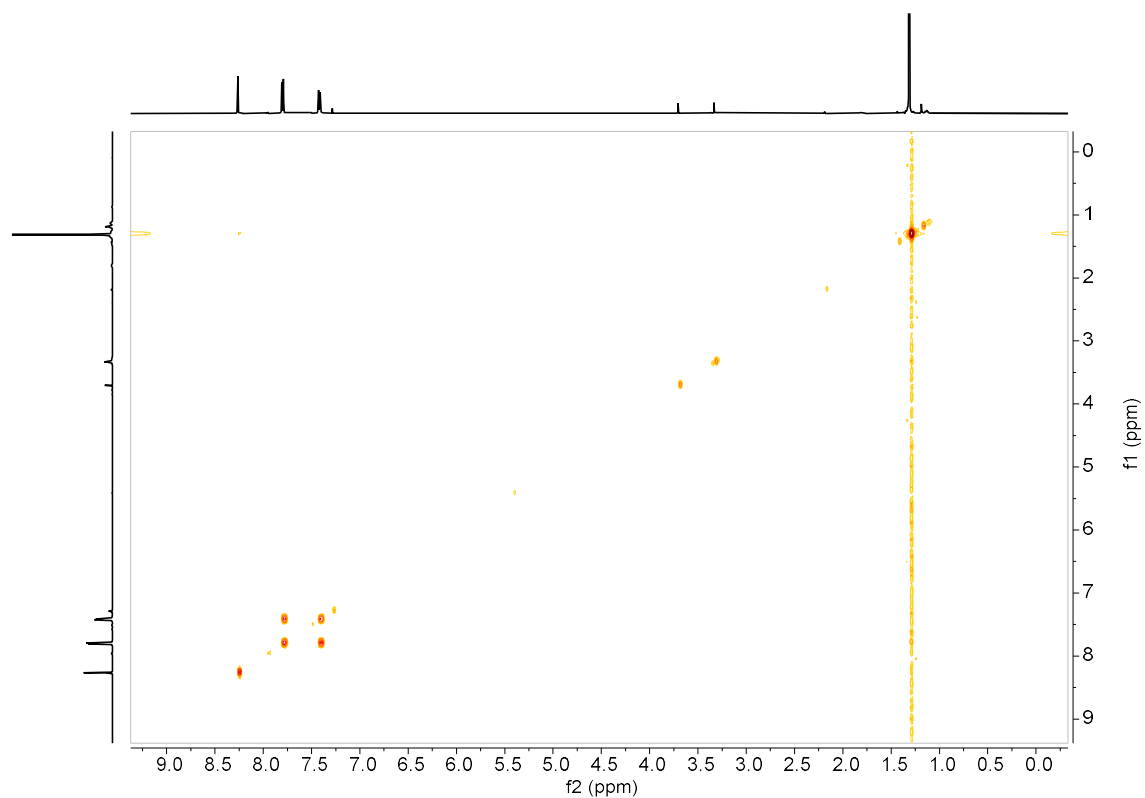
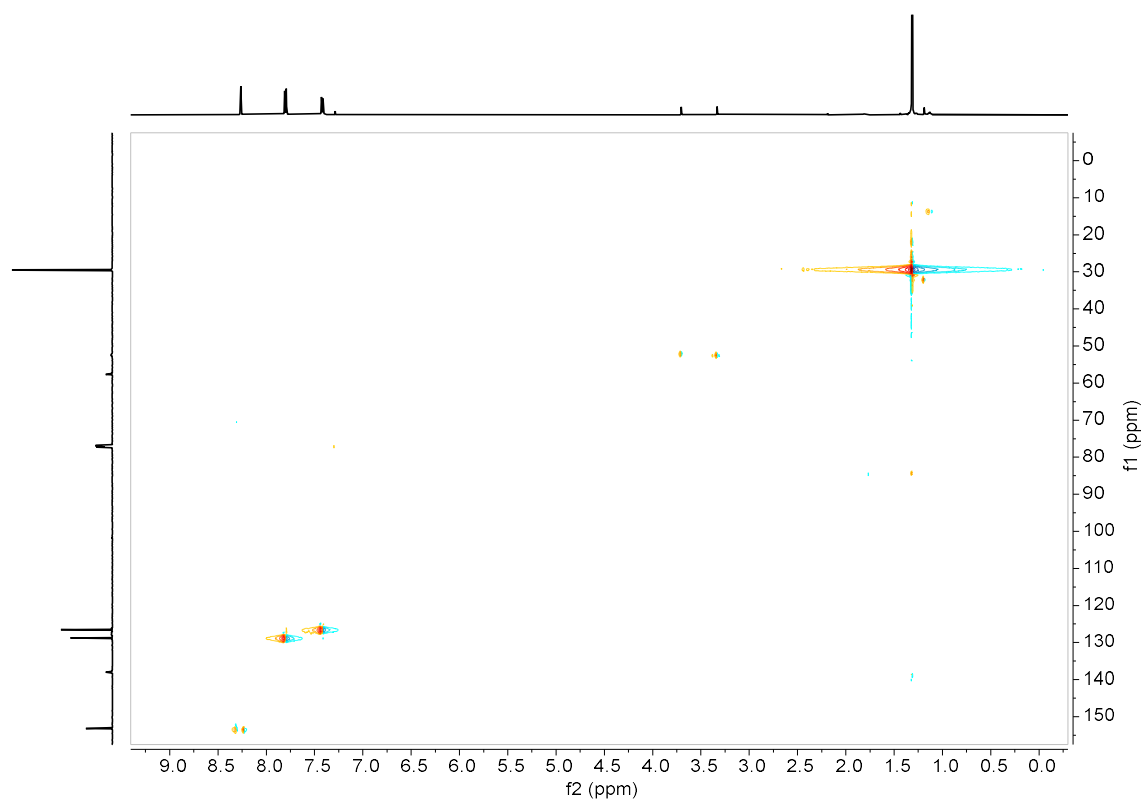
(E)-N-(4-fluorophenyl)-1-(4-isocyanophenyl)methanimine **31b**. $^1\text{H-NMR}$ (CDCl_3)(E)-N-(4-fluorophenyl)-1-(4-isocyanophenyl)methanimine **31b**. $^{13}\text{C-NMR}$ (CDCl_3)

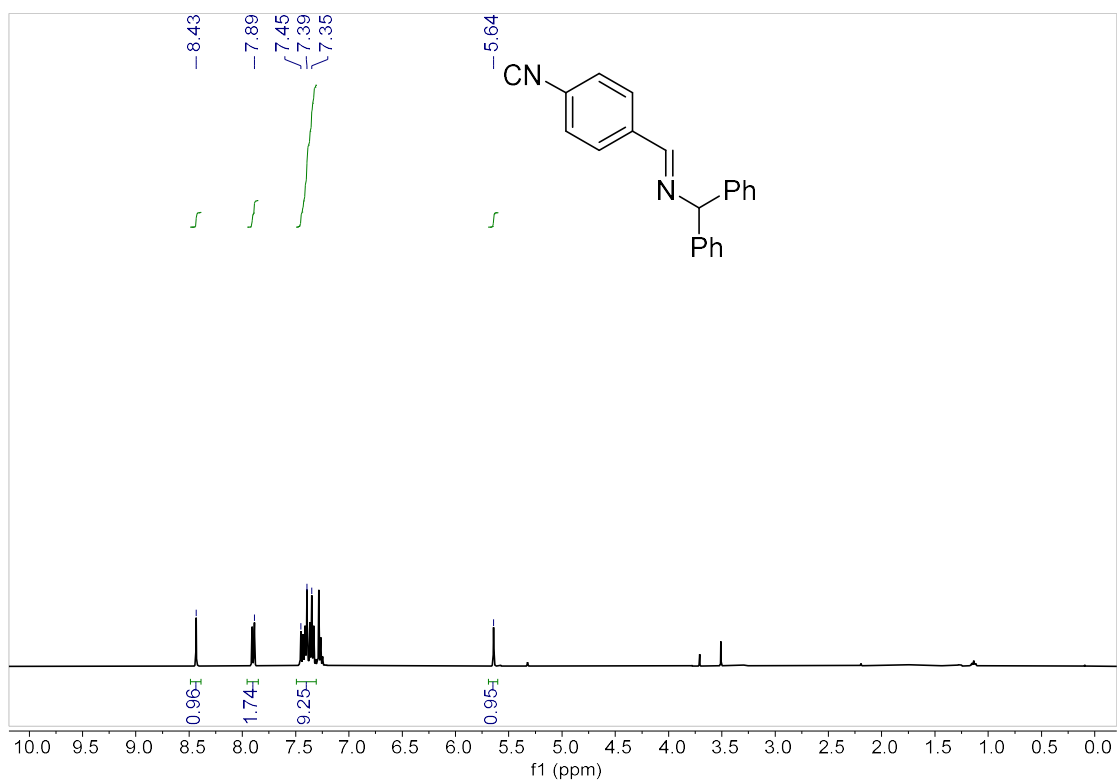
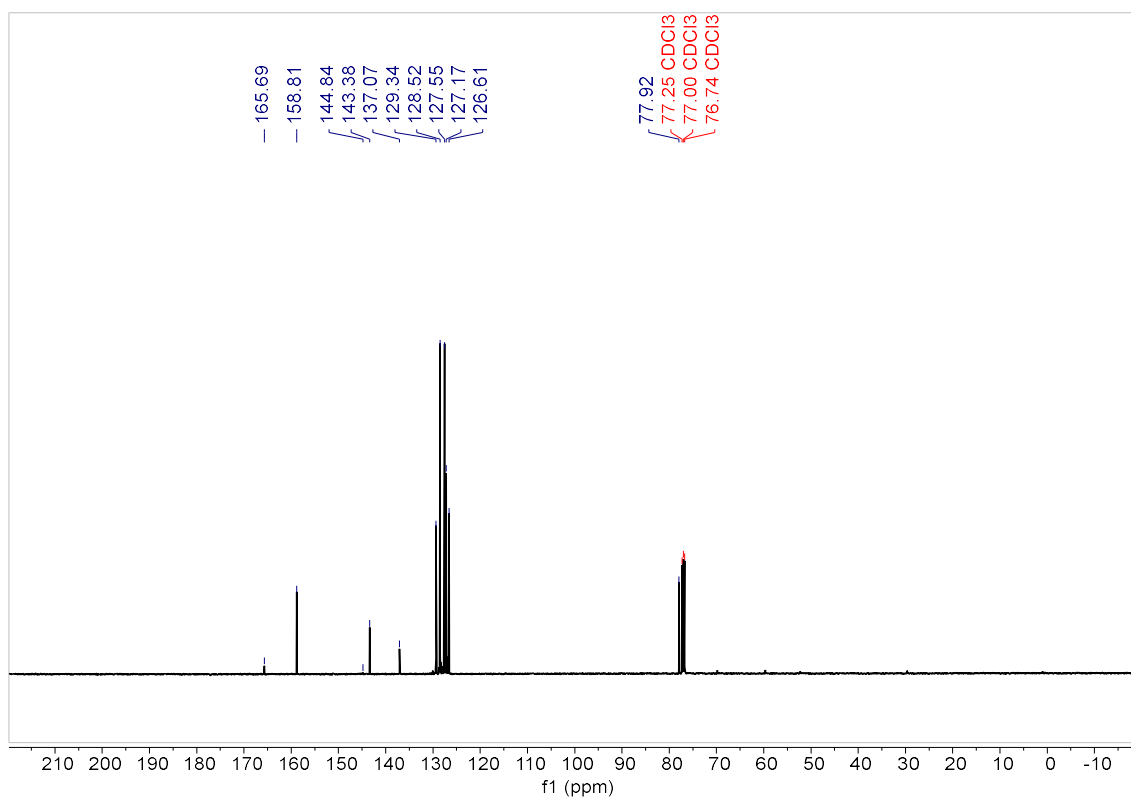
(E)-N-(4-fluorophenyl)-1-(4-isocyanophenyl)methanimine **31b**. g-COSY(CDCl₃)(E)-N-(4-fluorophenyl)-1-(4-isocyanophenyl)methanimine **31b**. g-HSQC(CDCl₃)

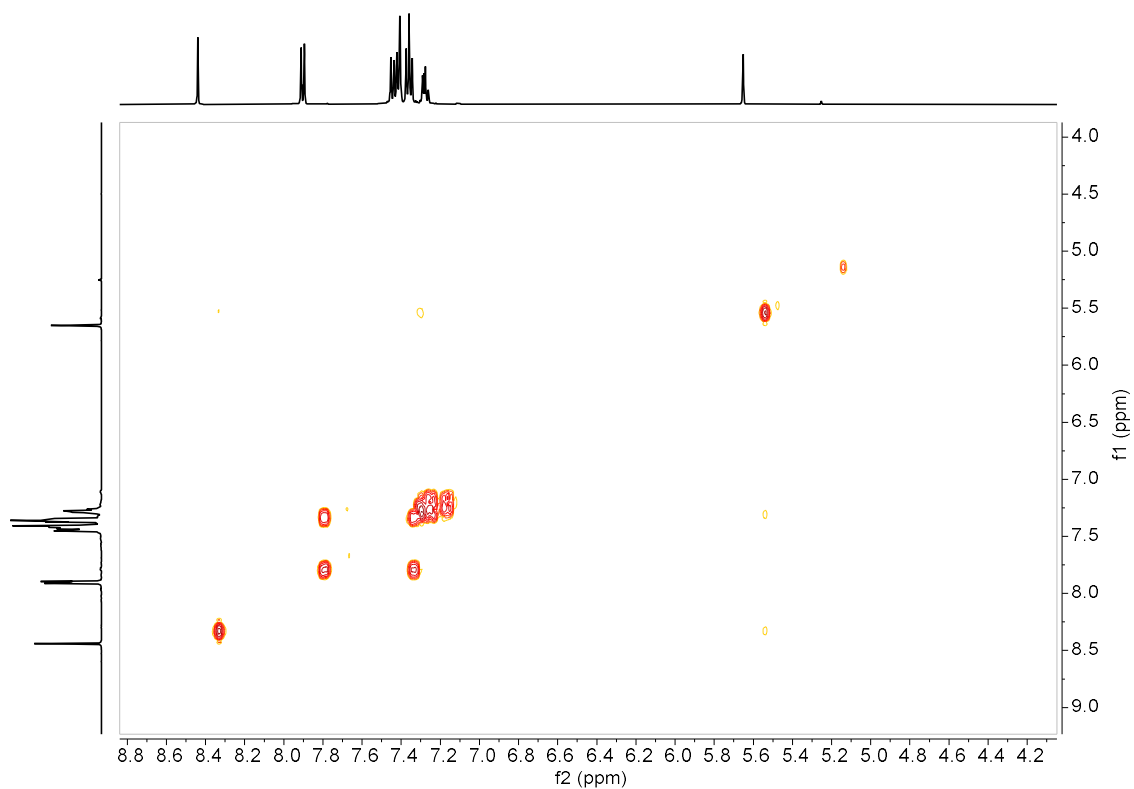
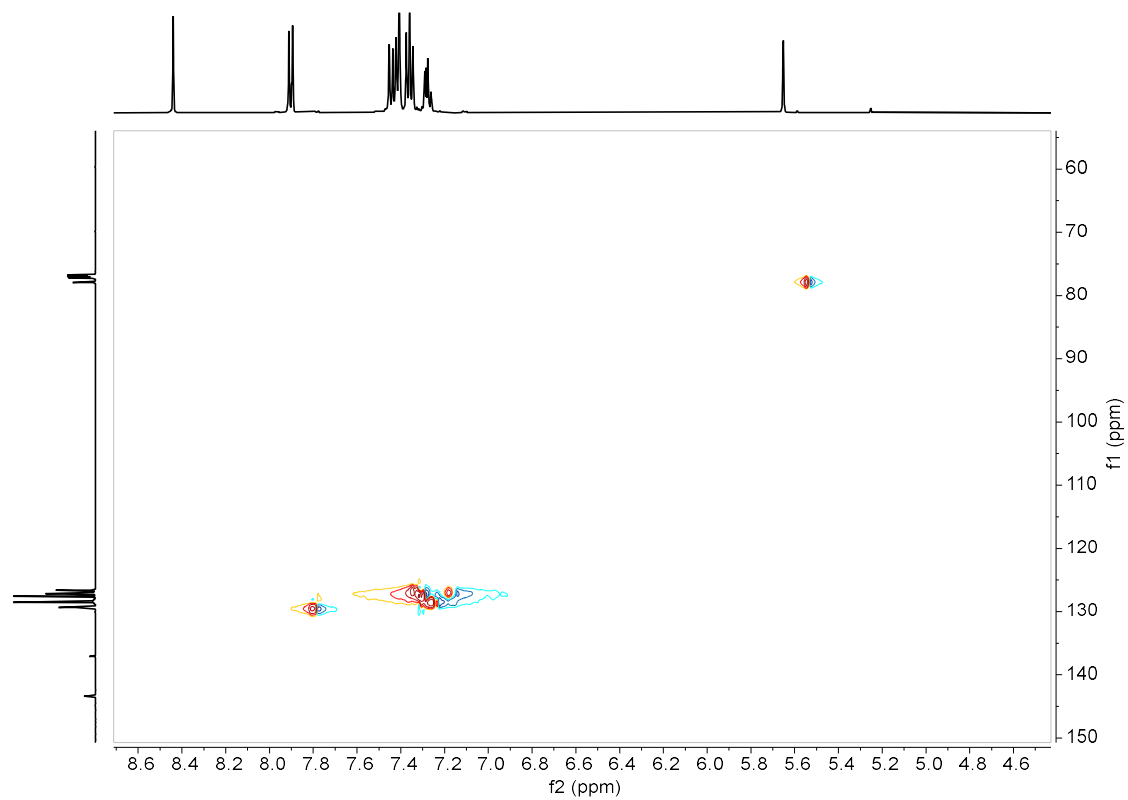
(E)-N-tert-butyl-1-(4-isocyanophenyl)methanimine **31c**. $^1\text{H-NMR}$ (CDCl_3)(E)-N-tert-butyl-1-(4-isocyanophenyl)methanimine **31c**. $^{13}\text{C-NMR}$ (CDCl_3)

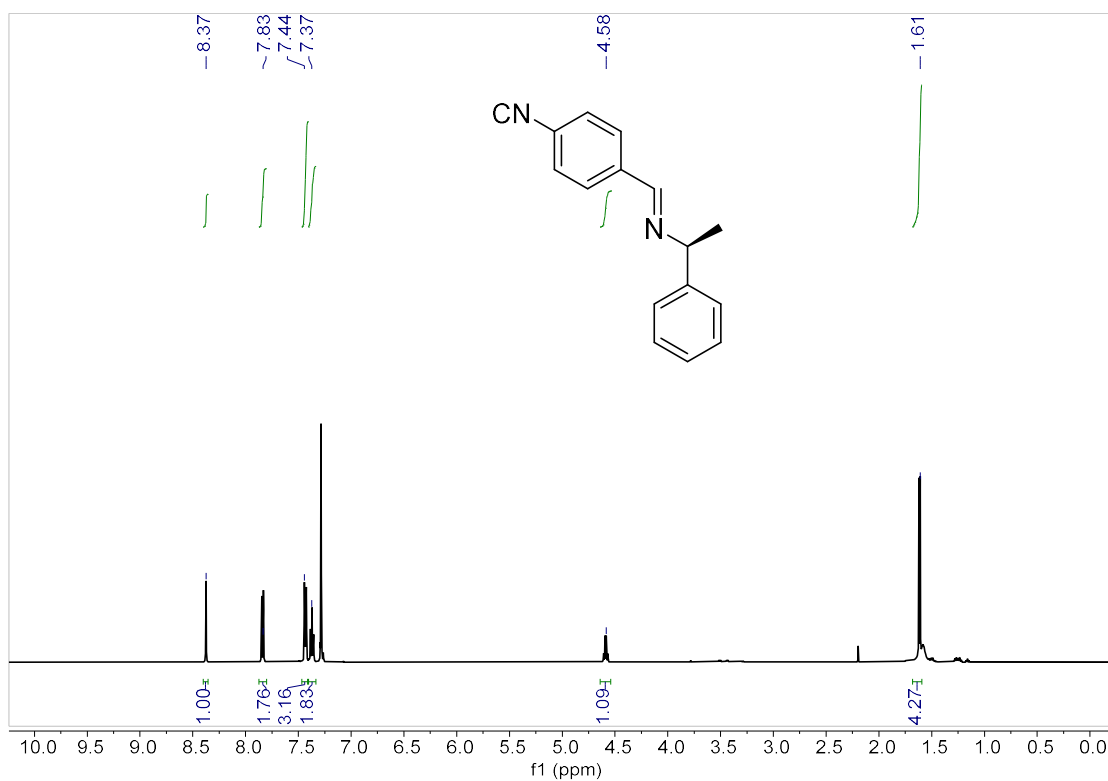
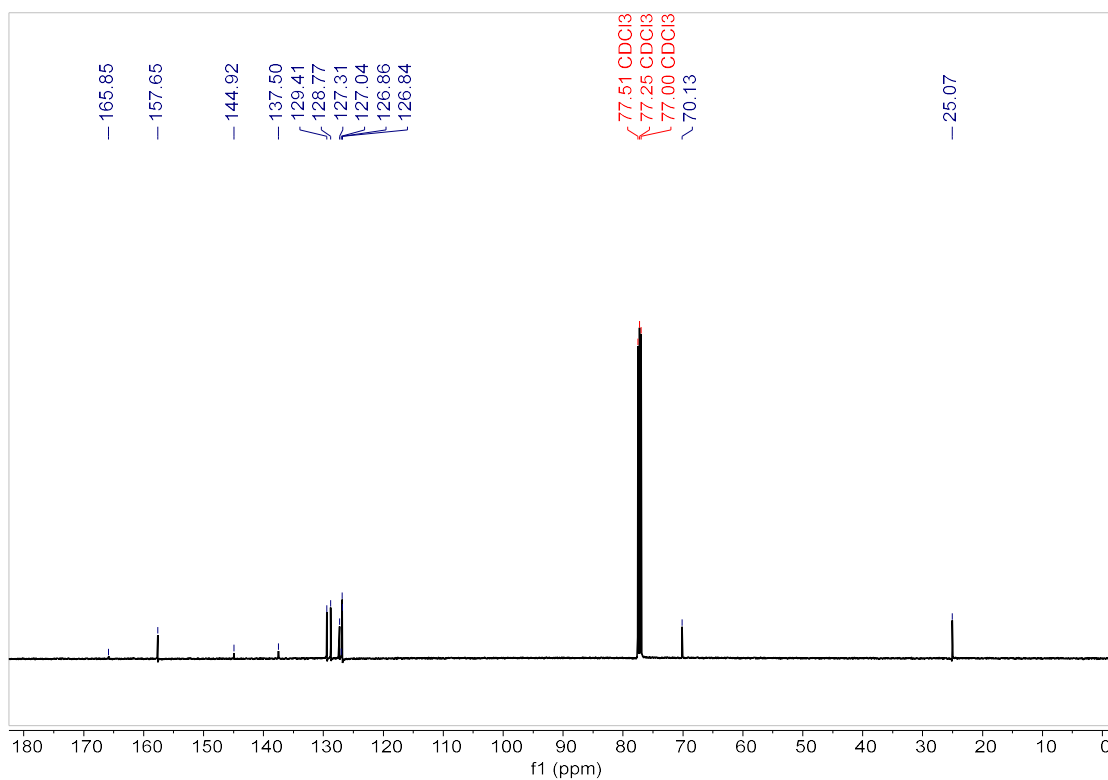
(E)-N-tert-butyl-1-(4-isocyanophenyl)methanimine **31c**. g-COSY (CDCl₃)(E)-N-tert-butyl-1-(4-isocyanophenyl)methanimine **31c**. g-HSQC (CDCl₃)

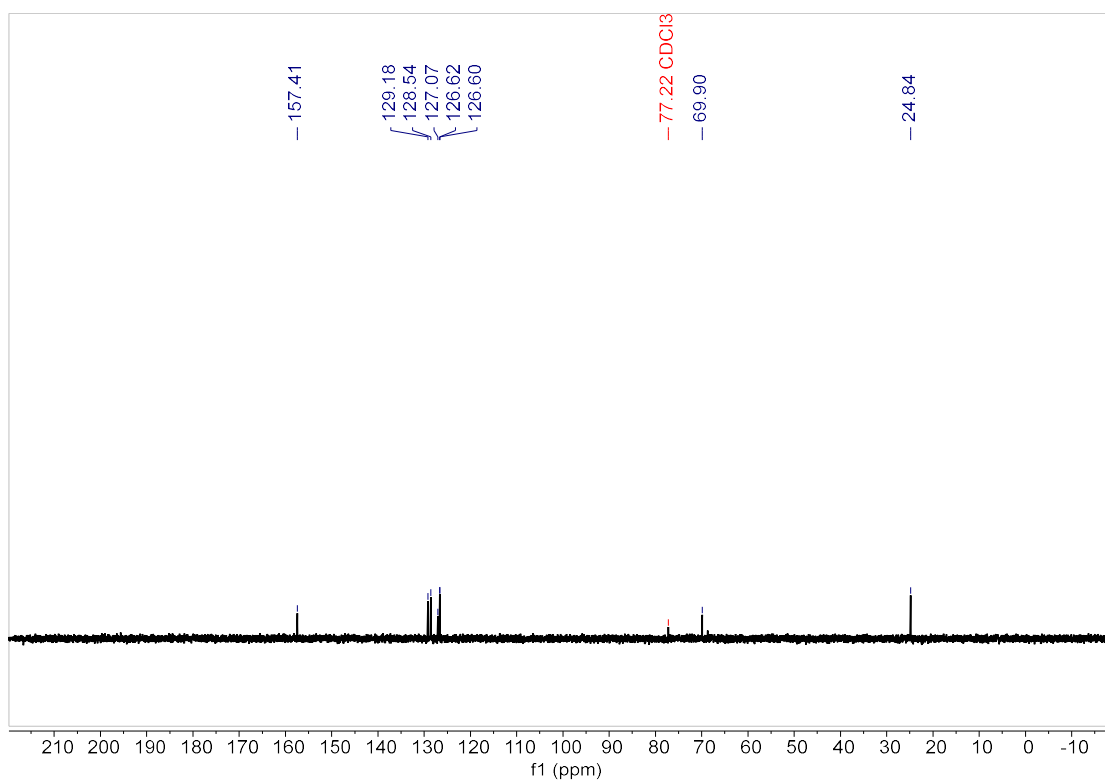
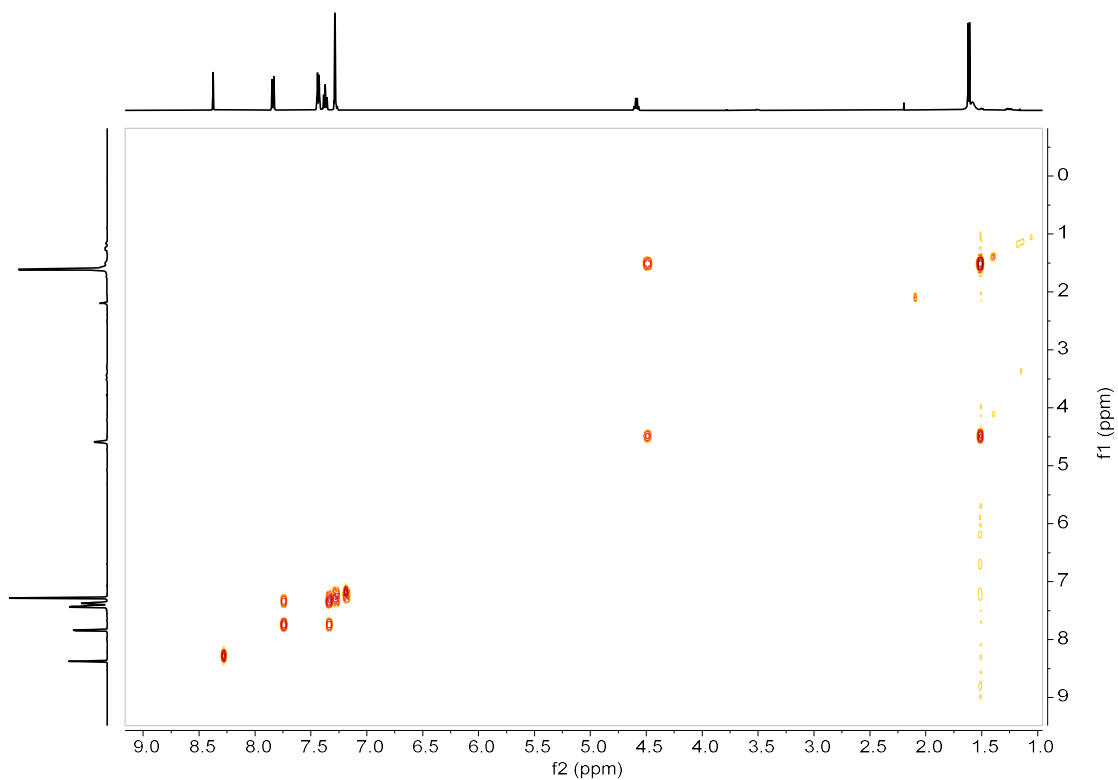
(E)-N-benzhydryl-1-(4-isocyanophenyl)methanimine **31d**. $^1\text{H-NMR}$ (CDCl_3)(E)-N-benzhydryl-1-(4-isocyanophenyl)methanimine **31d**. $^{13}\text{C-NMR}$ (CDCl_3)

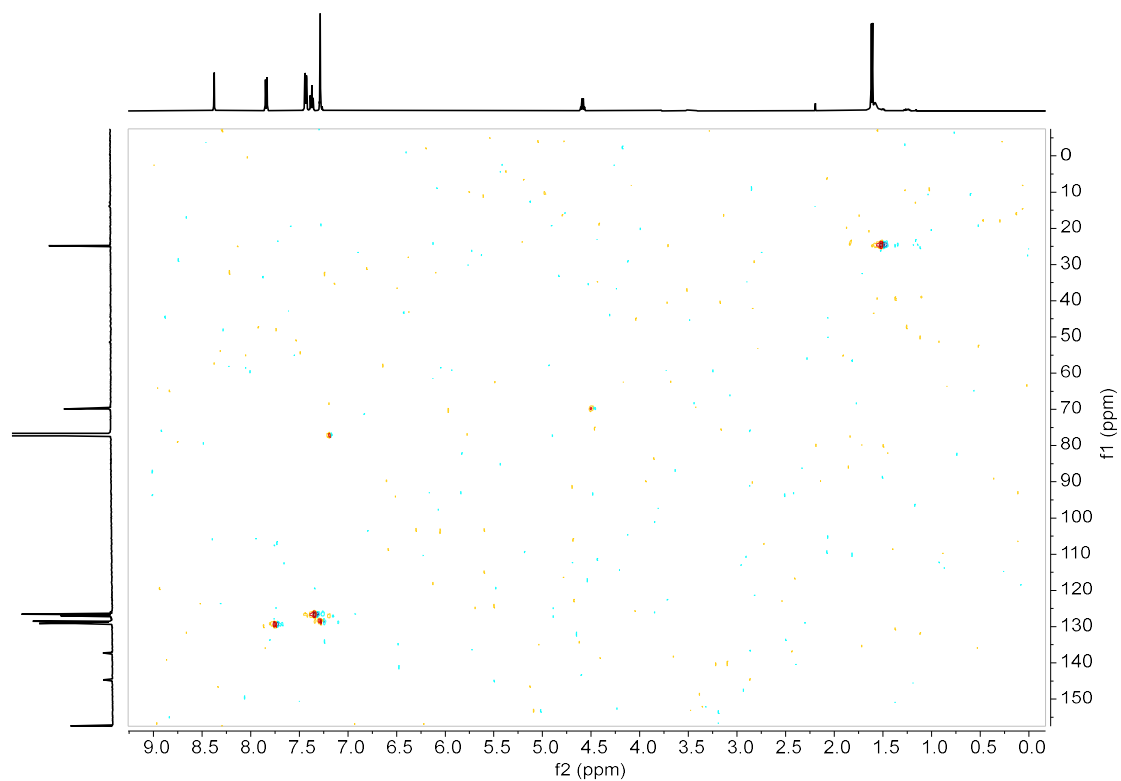
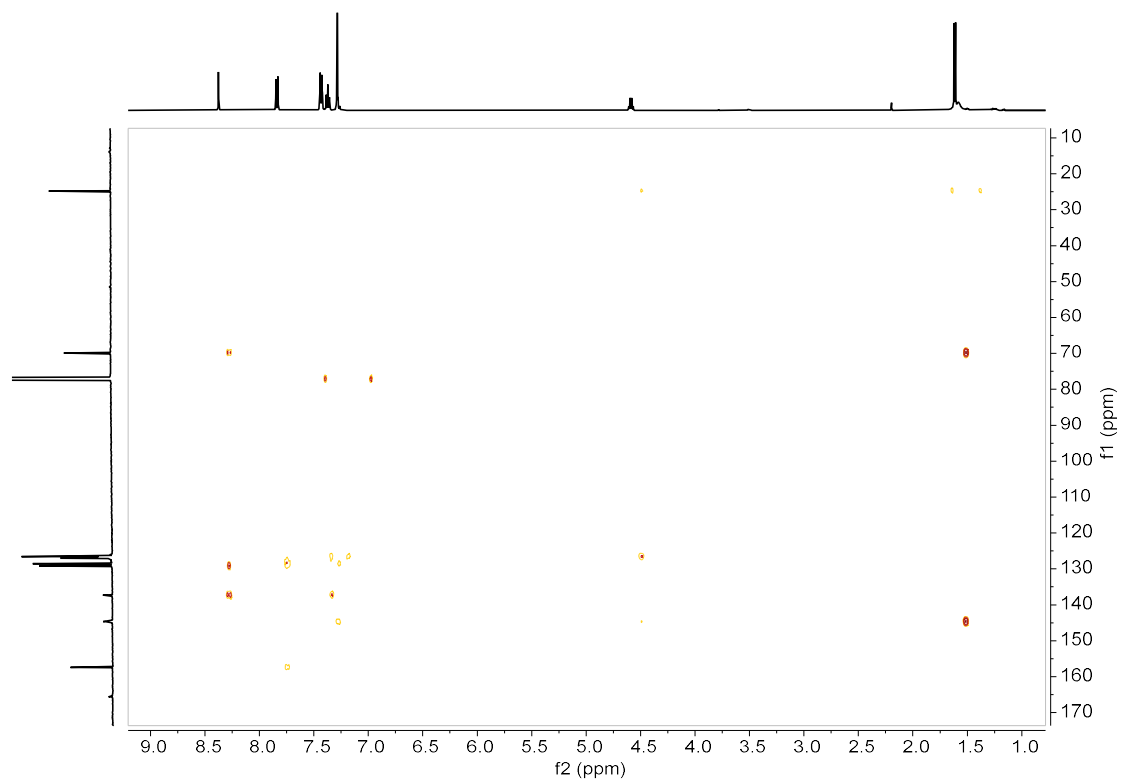
(E)-N-benzhydryl-1-(4-isocyanophenyl)methanimine **31d**. g-COSY (CDCl₃)(E)-N-benzhydryl-1-(4-isocyanophenyl)methanimine **31d**. g-HSQC (CDCl₃)

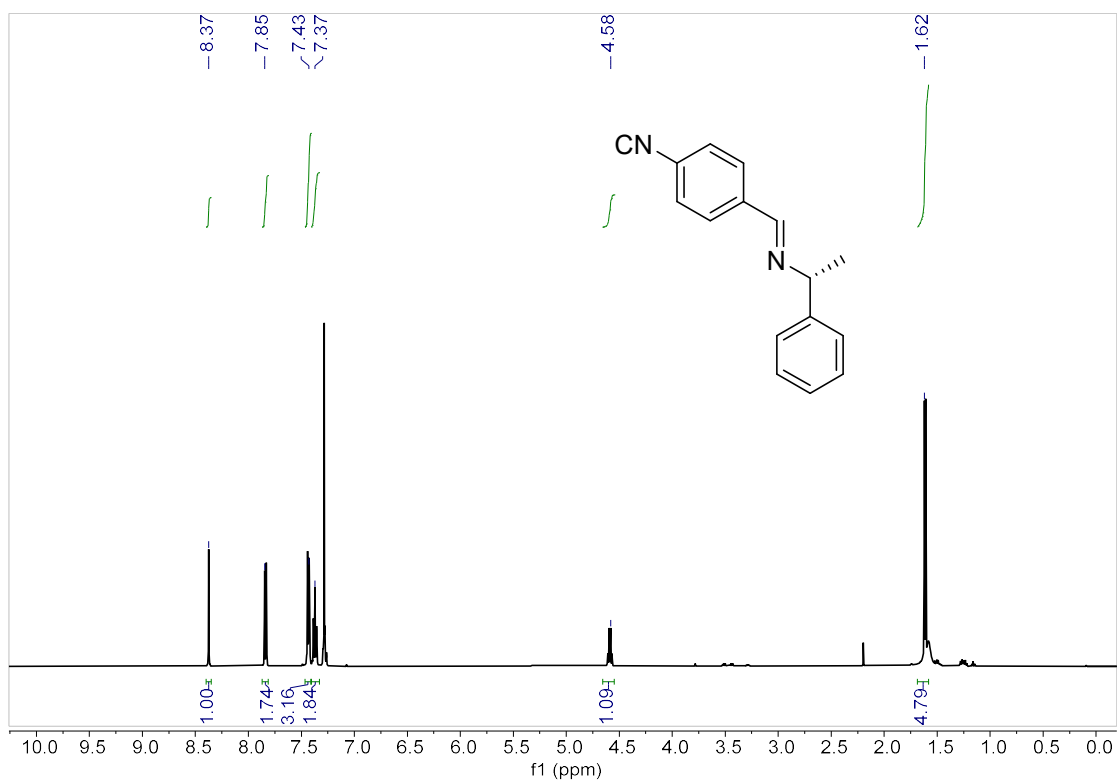
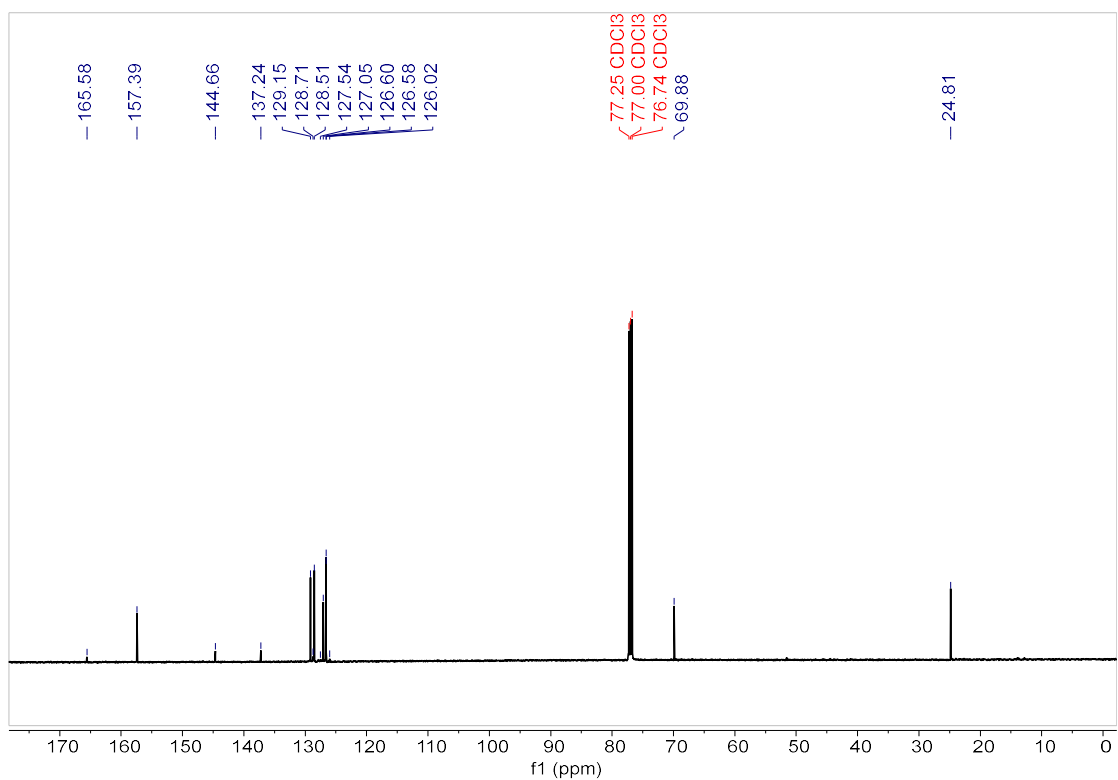
(E)-N-benzyl-1-(4-isocyanophenyl)methanimine **31e**. $^1\text{H-NMR}$ (CDCl_3)(E)-N-benzyl-1-(4-isocyanophenyl)methanimine **31e**. $^{13}\text{C-NMR}$ (CDCl_3)

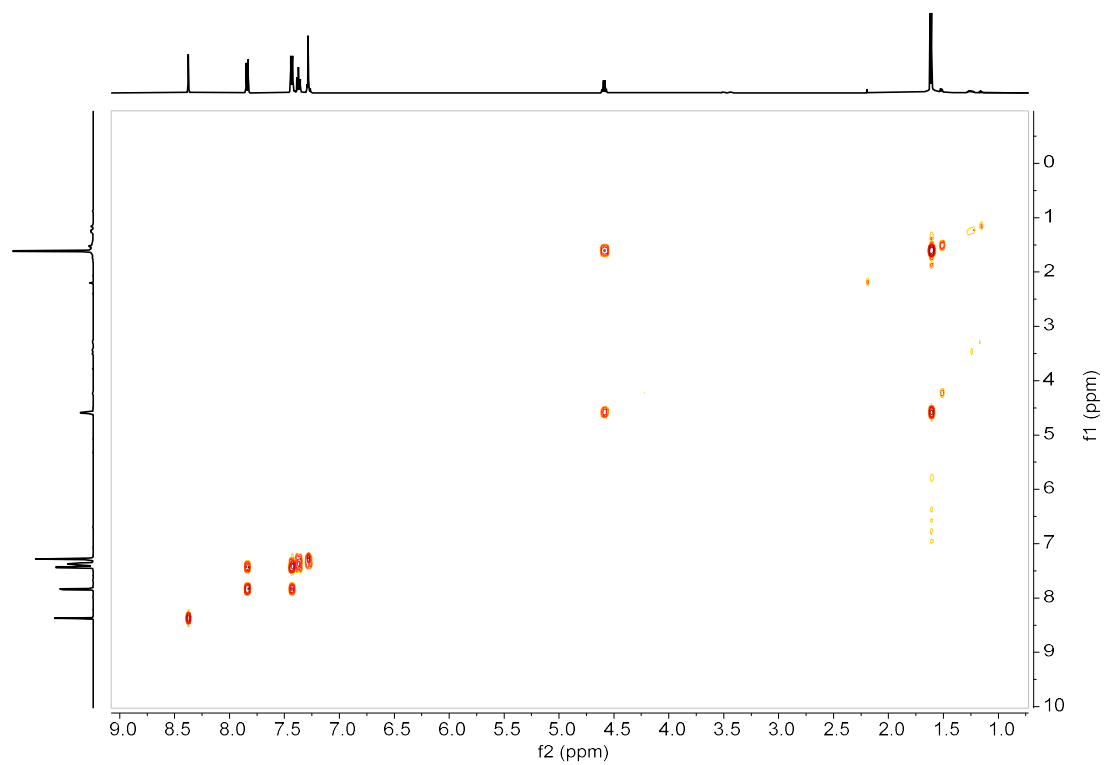
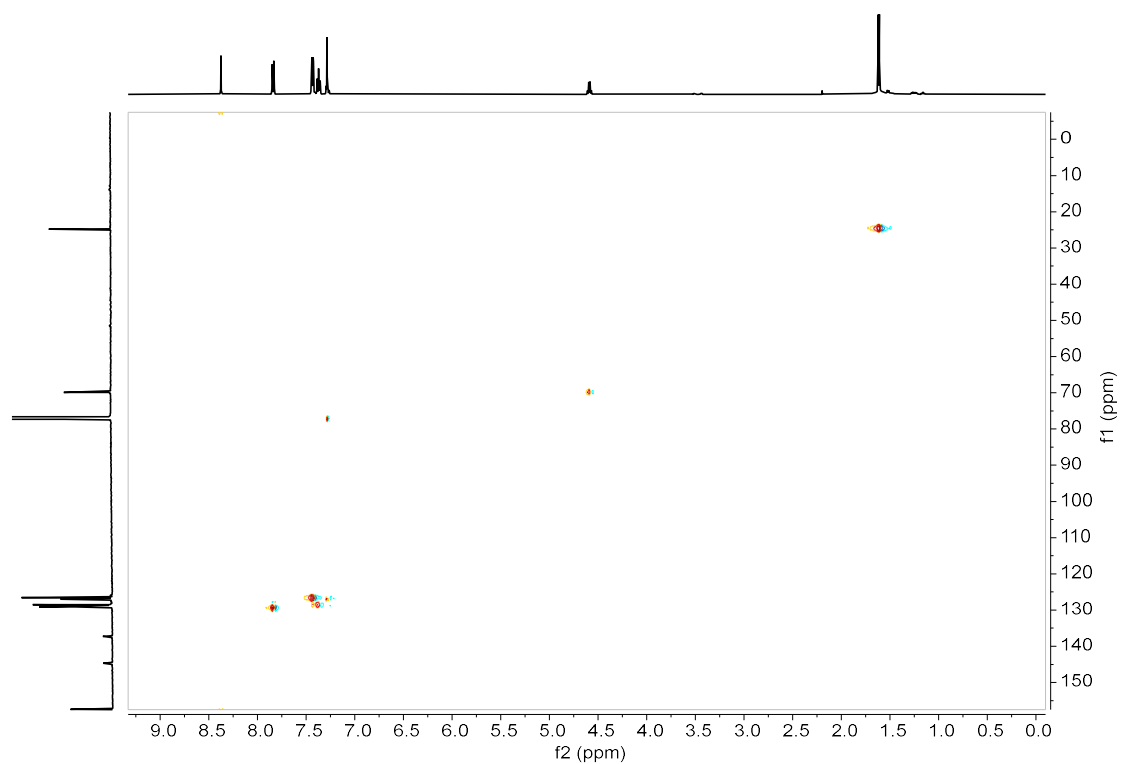
(E)-N-benzyl-1-(4-isocyanophenyl)methanimine **31e**. g-COSY (CDCl₃)(E)-N-benzyl-1-(4-isocyanophenyl)methanimine **31e**. g-HSQC (CDCl₃)

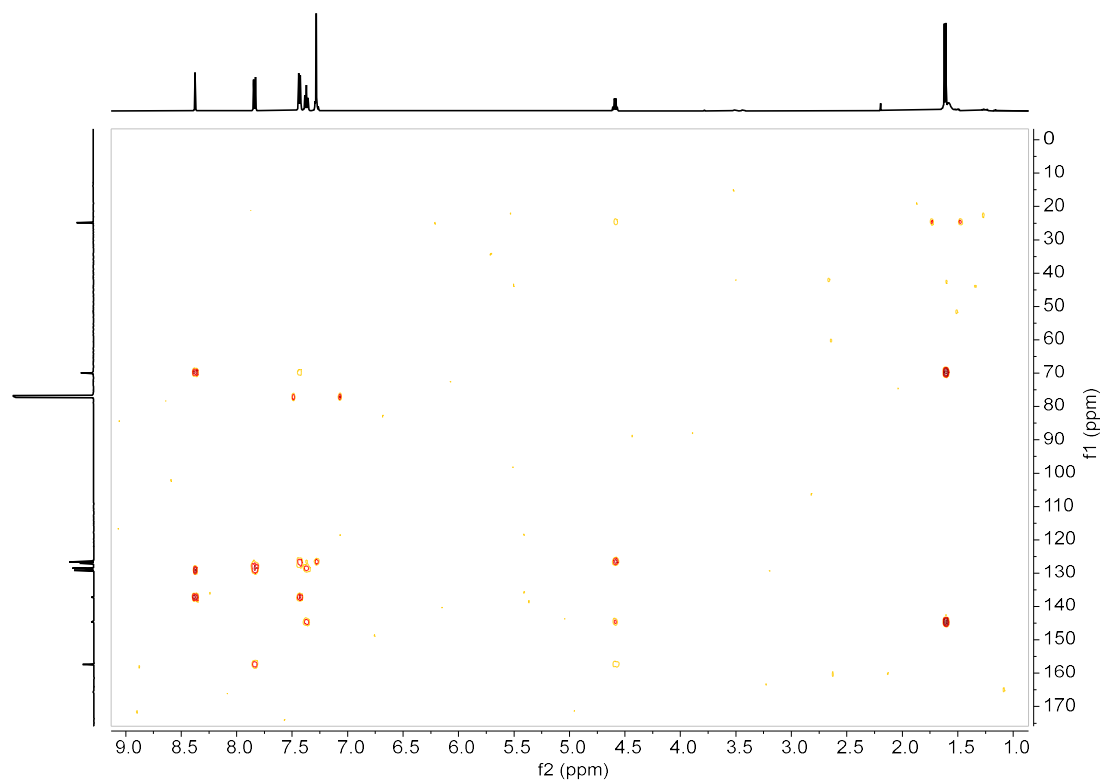
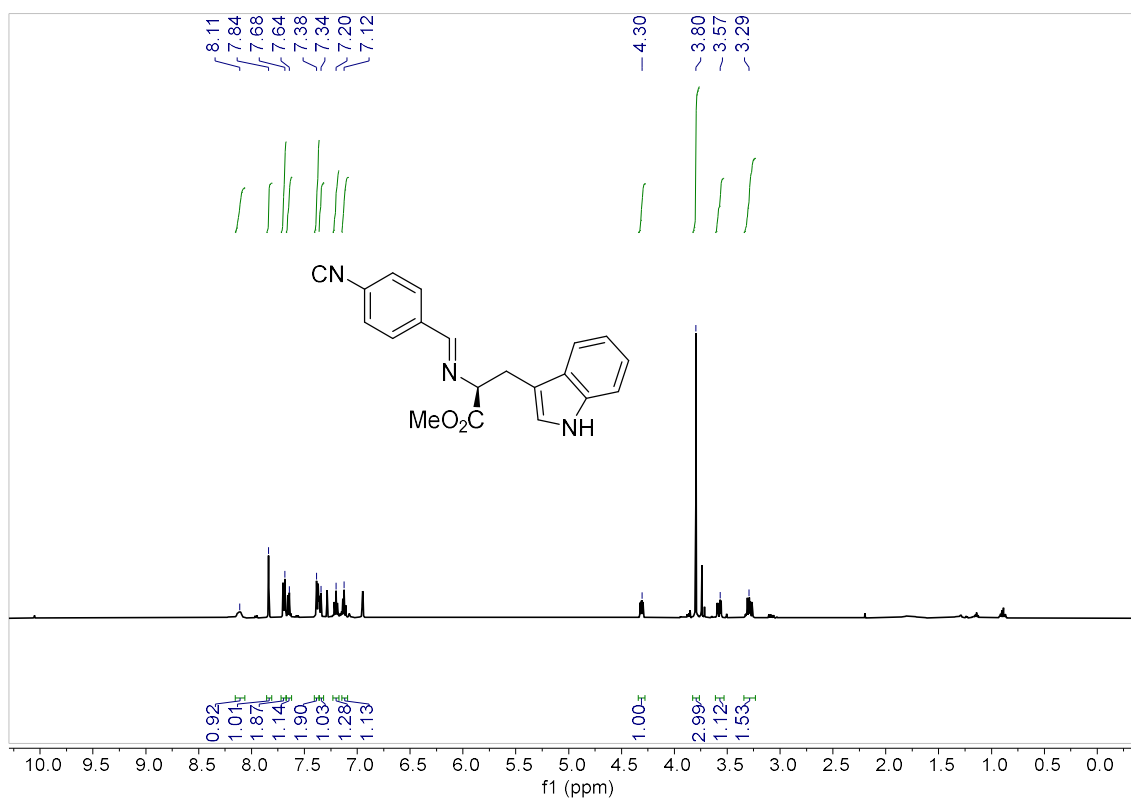
S-1-(4-isocyanophenyl)-N-(1-phenylethyl)methanimine **32-S**. $^1\text{H-NMR}$ (CDCl_3)S-1-(4-isocyanophenyl)-N-(1-phenylethyl)methanimine **32-S**. $^{13}\text{C-NMR}$ (CDCl_3)

S-1-(4-isocyanophenyl)-N-(1-phenylethyl)methanimine **32-S**. DEPT 135 (CDCl₃)S-1-(4-isocyanophenyl)-N-(1-phenylethyl)methanimine **32-S**. g-COSY (CDCl₃)

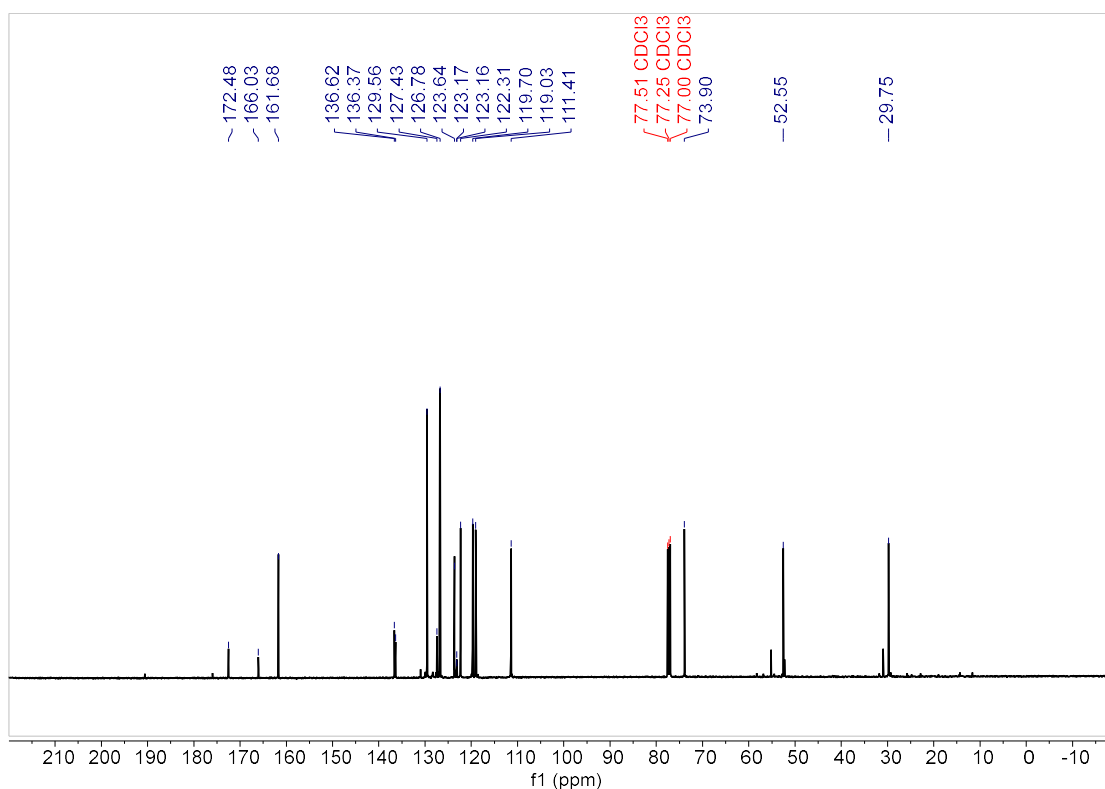
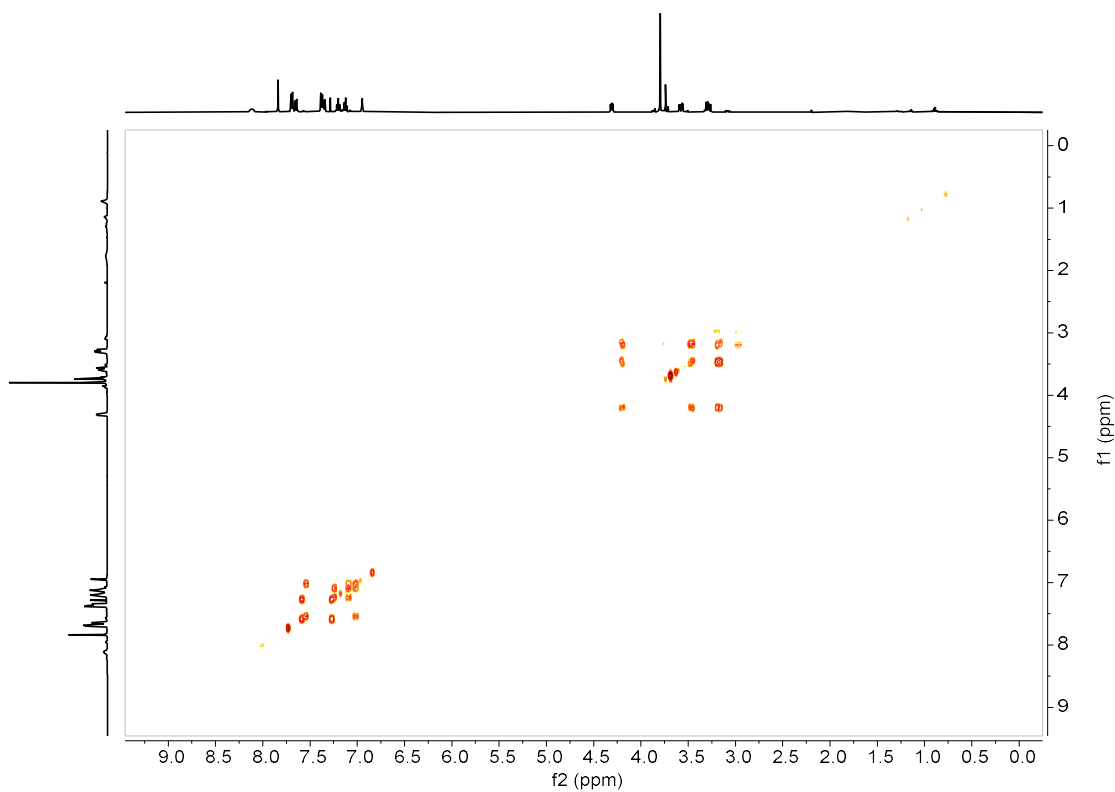
S-1-(4-isocyanophenyl)-N-(1-phenylethyl)methanimine **32-S**. g-HSQC (CDCl₃)S-1-(4-isocyanophenyl)-N-(1-phenylethyl)methanimine **32-S**. g-HMBC (CDCl₃)

R-1-(4-isocyanophenyl)-N-(1-phenylethyl)methanimine **32-R**. $^1\text{H-NMR}$ (CDCl_3)R-1-(4-isocyanophenyl)-N-(1-phenylethyl)methanimine **32-R**. $^{13}\text{C-NMR}$ (CDCl_3)

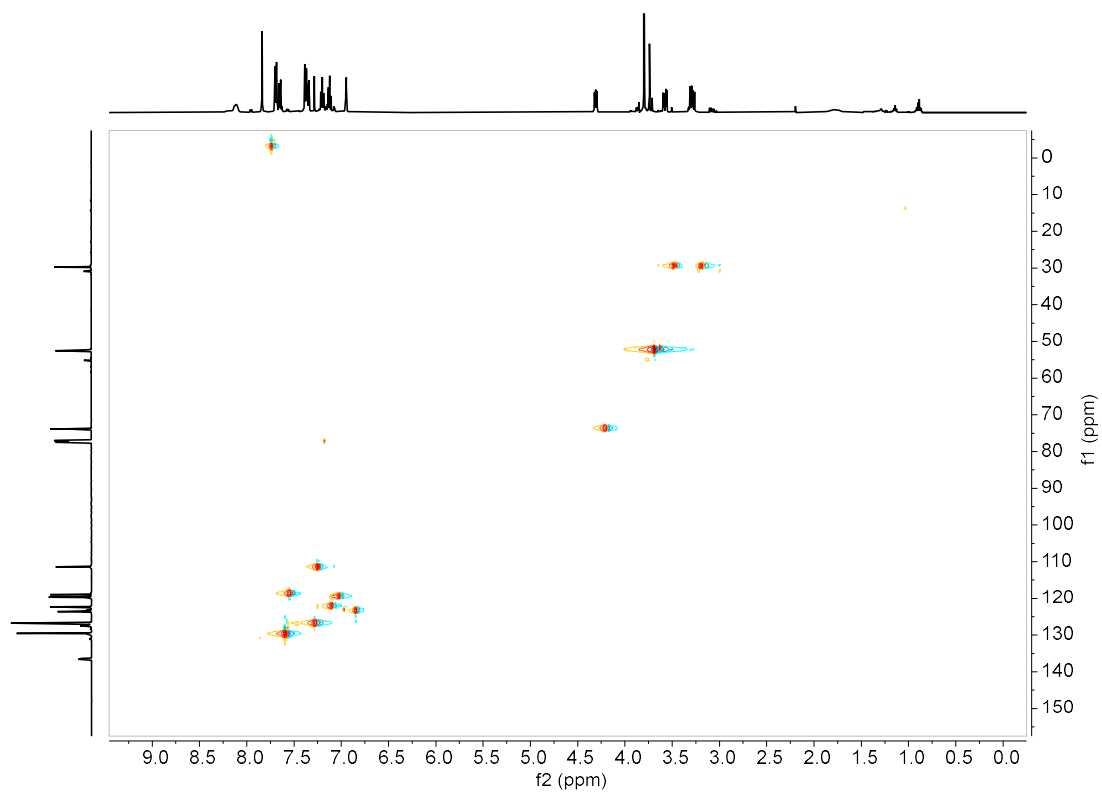
R-1-(4-isocyanophenyl)-N-(1-phenylethyl)methanimine **32-R**. g-COSY (CDCl₃)R-1-(4-isocyanophenyl)-N-(1-phenylethyl)methanimine **32-R**. g-HSQC (CDCl₃)

R-1-(4-isocyanophenyl)-N-(1-phenylethyl)methanimine **32-R**. g-HMBC (CDCl₃)Methyl (S,E)-3-(1H-indol-3-yl)-2-((4-isocyanobenzylidene)amino)propanoate (**33-L**).
¹H-NMR (CDCl₃)

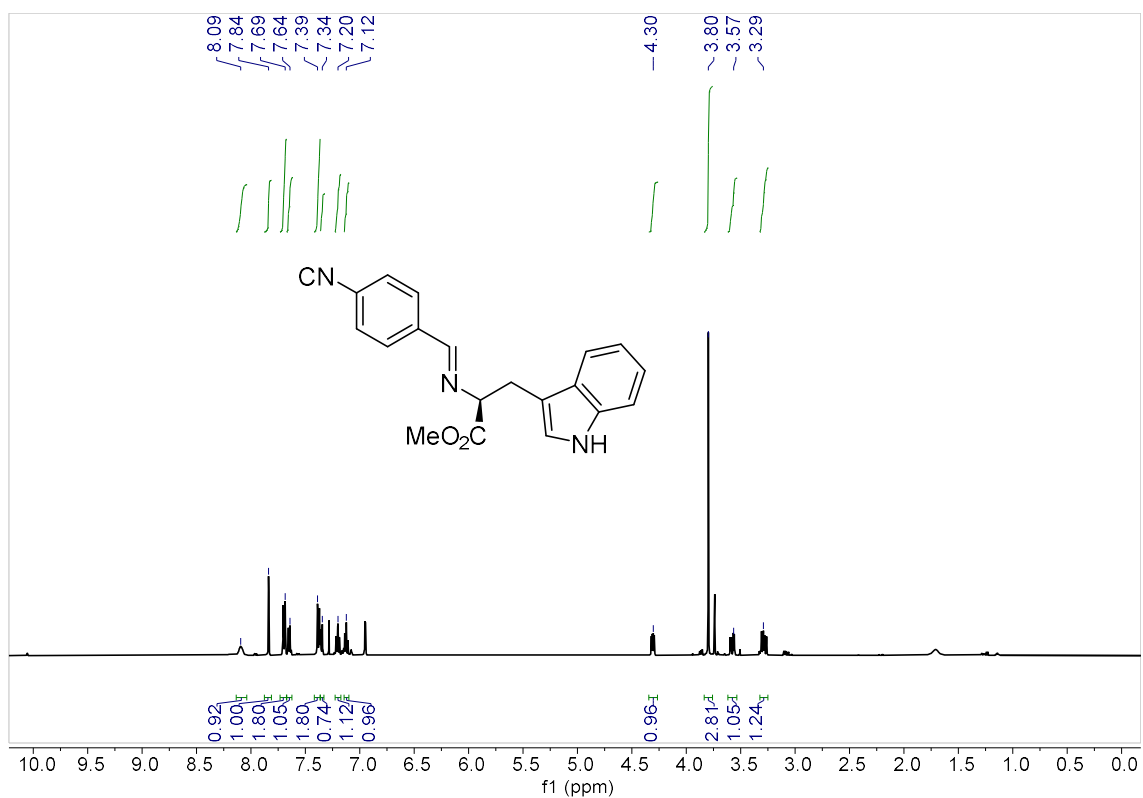
ANNEX IV

Methyl (S,E)-3-(1H-indol-3-yl)-2-((4-isocyanobenzylidene)amino)propanoate (**33-L**).
 ^{13}C -NMR (CDCl_3)Methyl (S,E)-3-(1H-indol-3-yl)-2-((4-isocyanobenzylidene)amino)propanoate (**33-L**). g-COSY (CDCl_3)

Methyl (S,E)-3-(1H-indol-3-yl)-2-((4-isocyanobenzylidene)amino)propanoate (**33-L**). g-HSQC (CDCl₃)

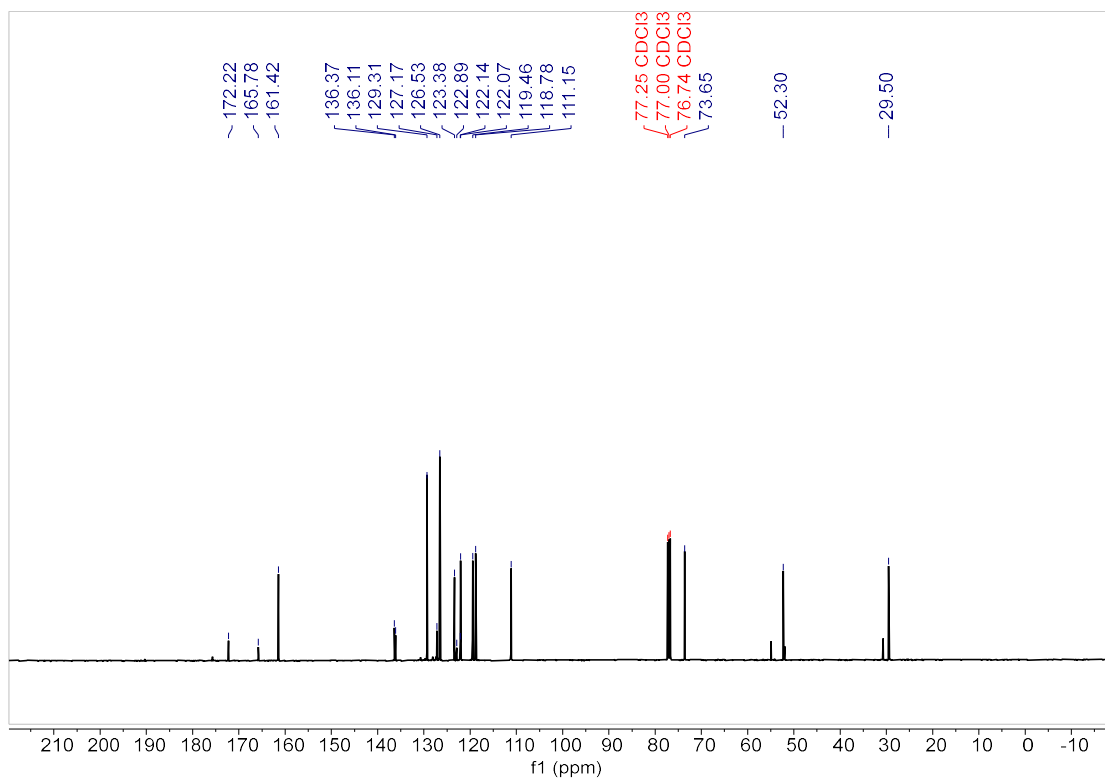


Methyl (R,E)-3-(1H-indol-3-yl)-2-((4-isocyanobenzylidene)amino)propanoate (**33-D**). ¹H-NMR (CDCl₃)

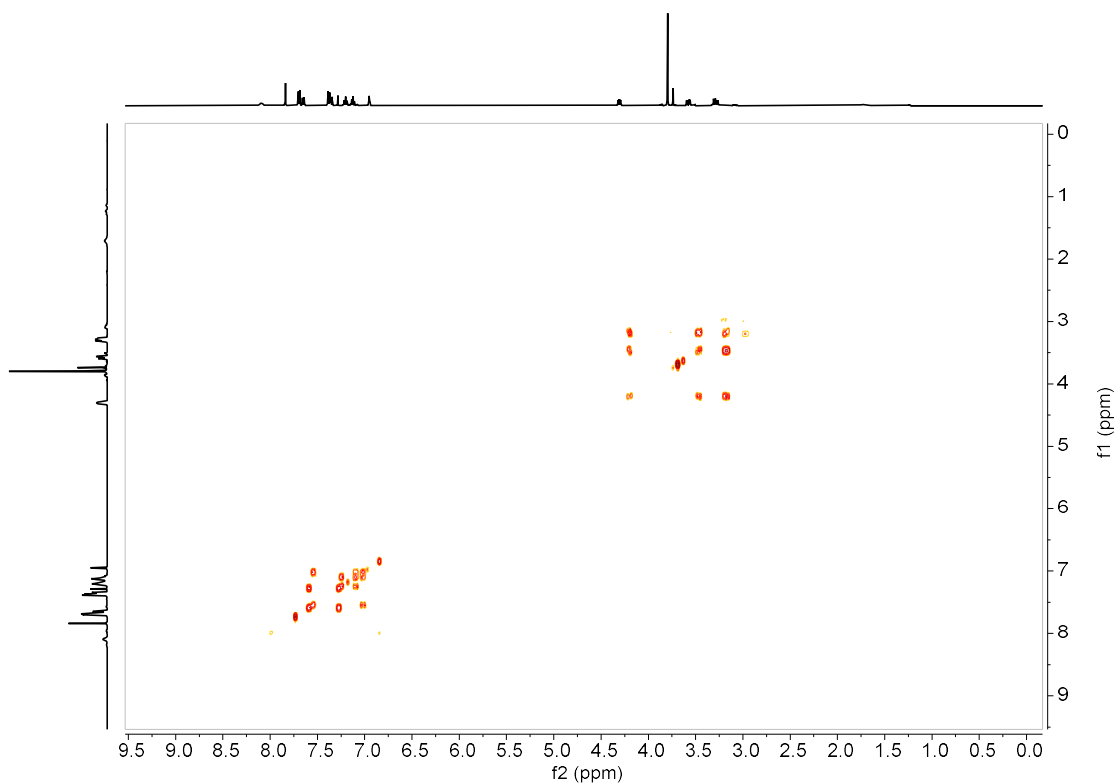


ANNEX IV

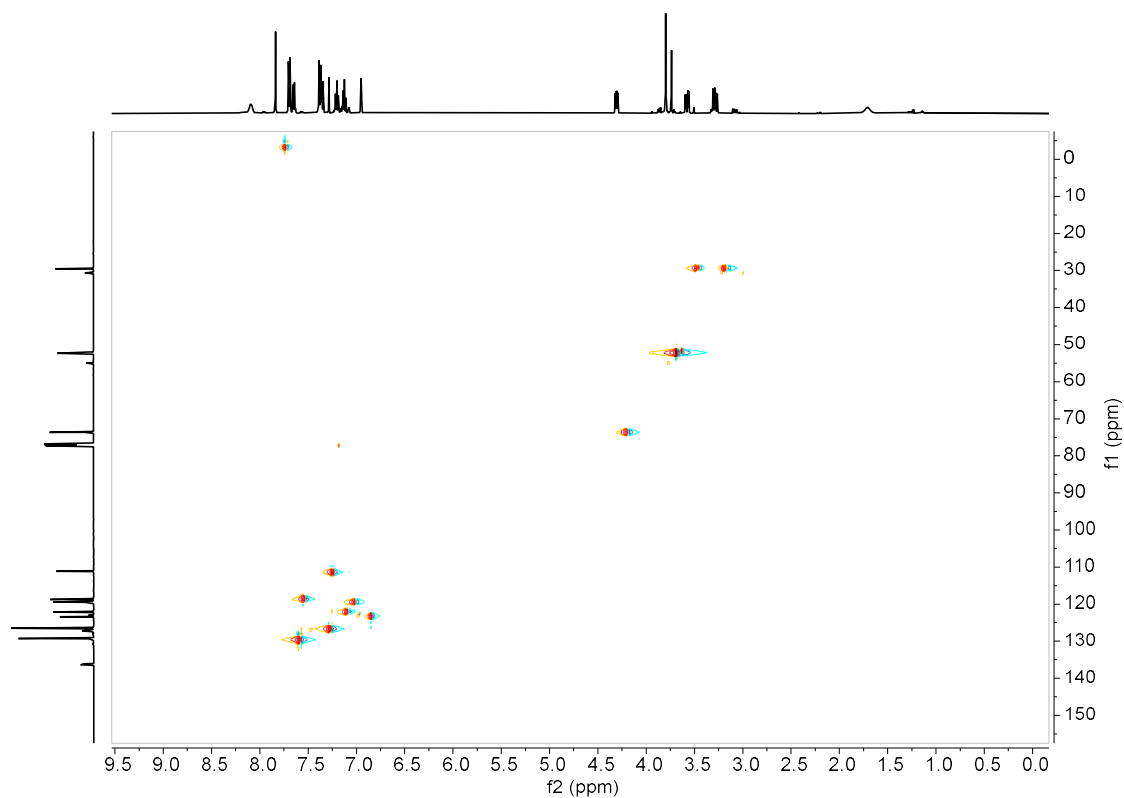
Methyl (R,E)-3-(1H-indol-3-yl)-2-((4-isocyanobenzylidene)amino)propanoate (**33-D**).
¹³C-NMR (CDCl₃)



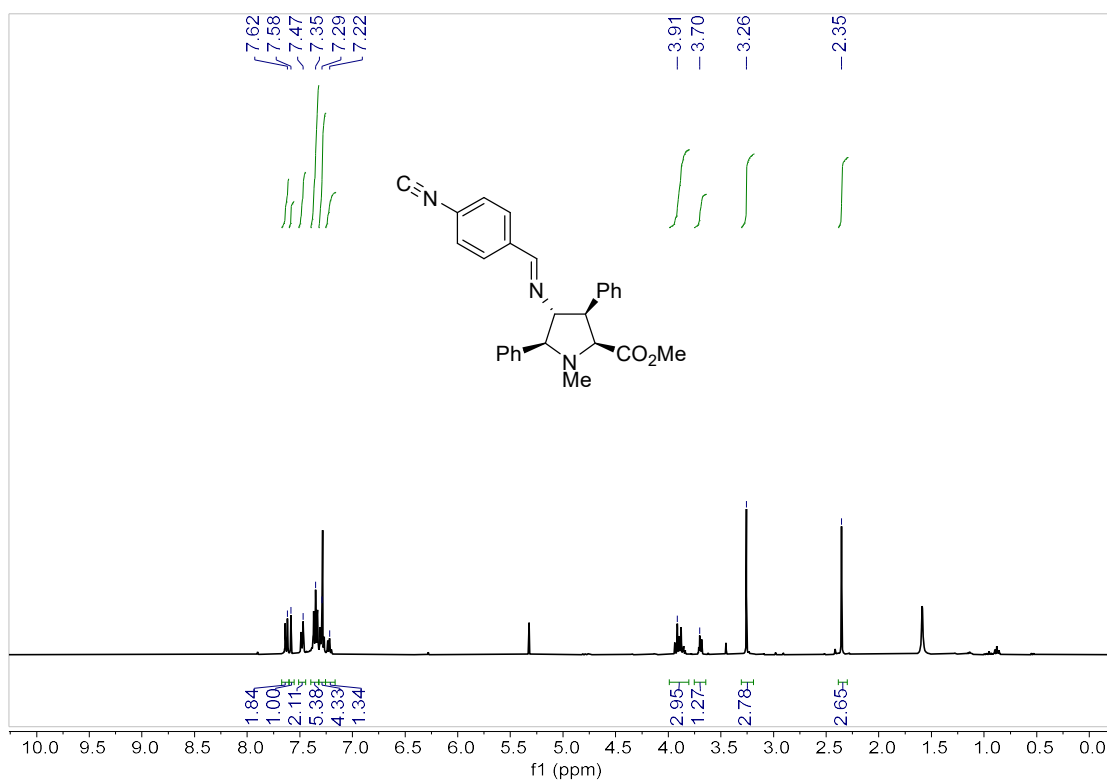
Methyl (R,E)-3-(1H-indol-3-yl)-2-((4-isocyanobenzylidene)amino)propanoate (**33-D**). g-COSY (CDCl₃)



Methyl (R,E)-3-(1H-indol-3-yl)-2-((4-isocyanobenzylidene)amino)propanoate (**33-D**). g-HSQC (CDCl₃)

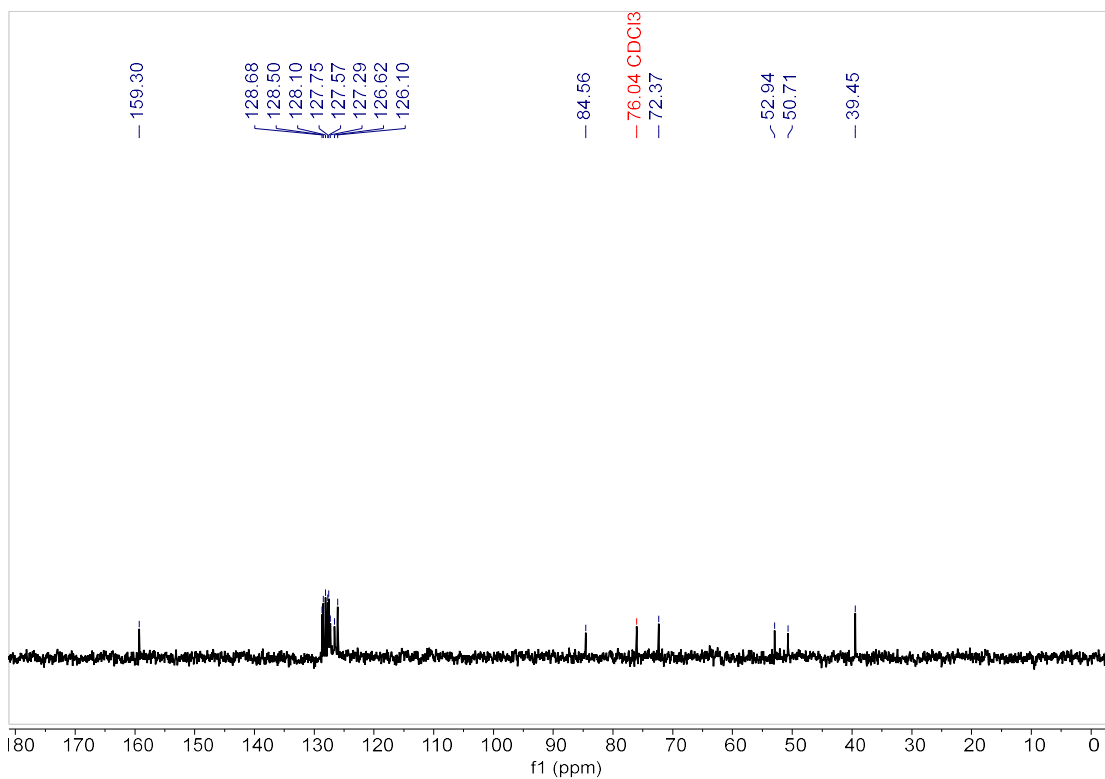


Methyl (2S,3R,4R,5S)-4-((4-isocyanobenzylidene)amino)-1-methyl-3,5-diphenylpyrrolidine-2-carboxylate (**35-XL**). ¹H-NMR (CDCl₃)

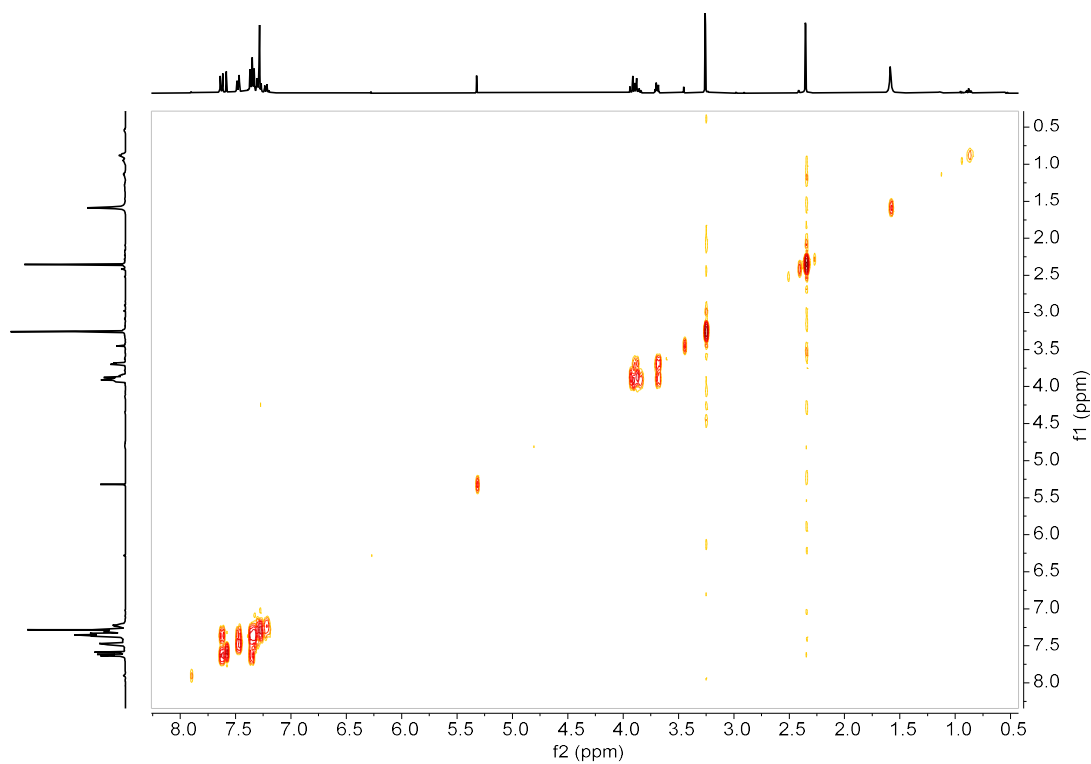


ANNEX IV

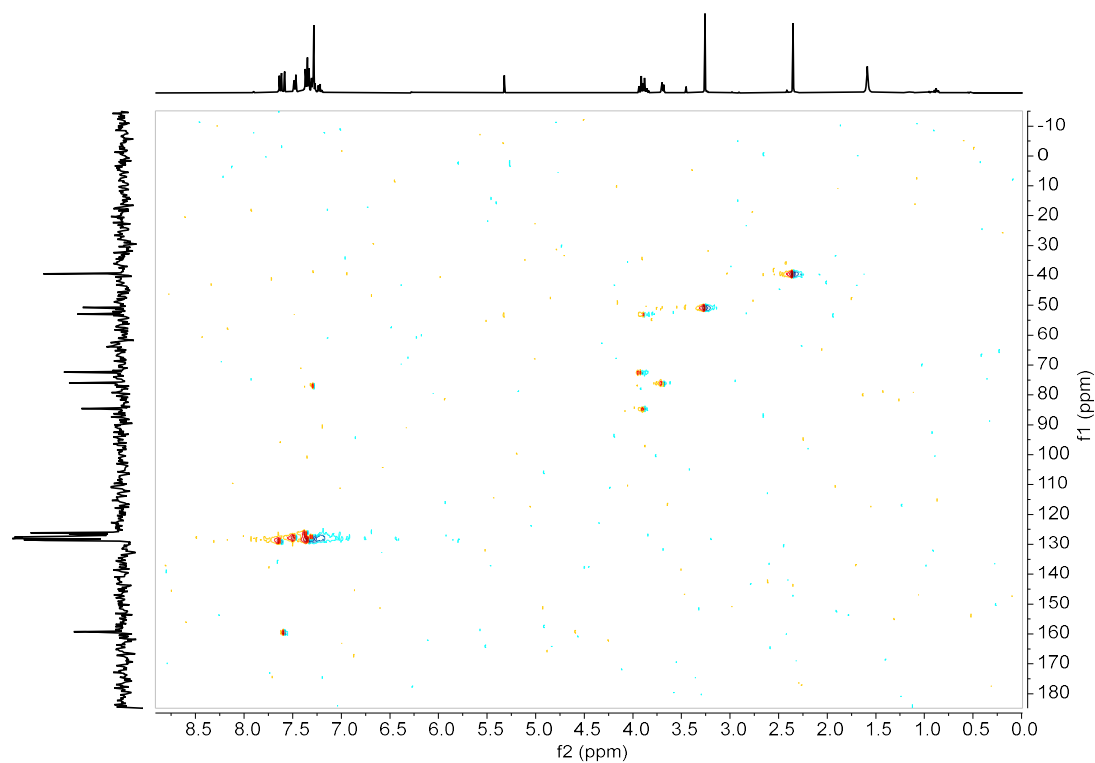
Methyl (2S,3R,4R,5S)-4-((4-isocyanobenzylidene)amino)-1-methyl-3,5-diphenylpyrrolidine-2-carboxylate (**35-XL**). $^{13}\text{C-NMR}$ (CDCl_3)



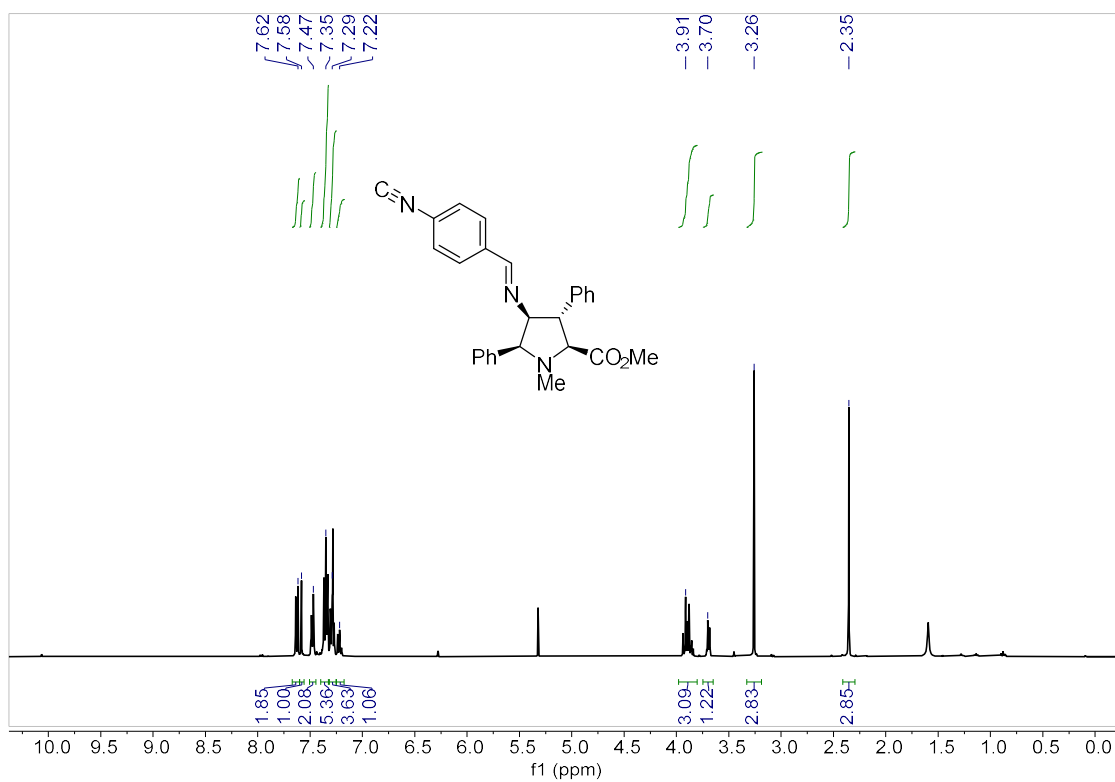
Methyl (2S,3R,4R,5S)-4-((4-isocyanobenzylidene)amino)-1-methyl-3,5-diphenylpyrrolidine-2-carboxylate (**35-XL**). g-COSY (CDCl_3)



Methyl (2S,3R,4R,5S)-4-((4-isocyanobenzylidene)amino)-1-methyl-3,5-diphenylpyrrolidine-2-carboxylate (**35-XL**). g-HSQC (CDCl₃)

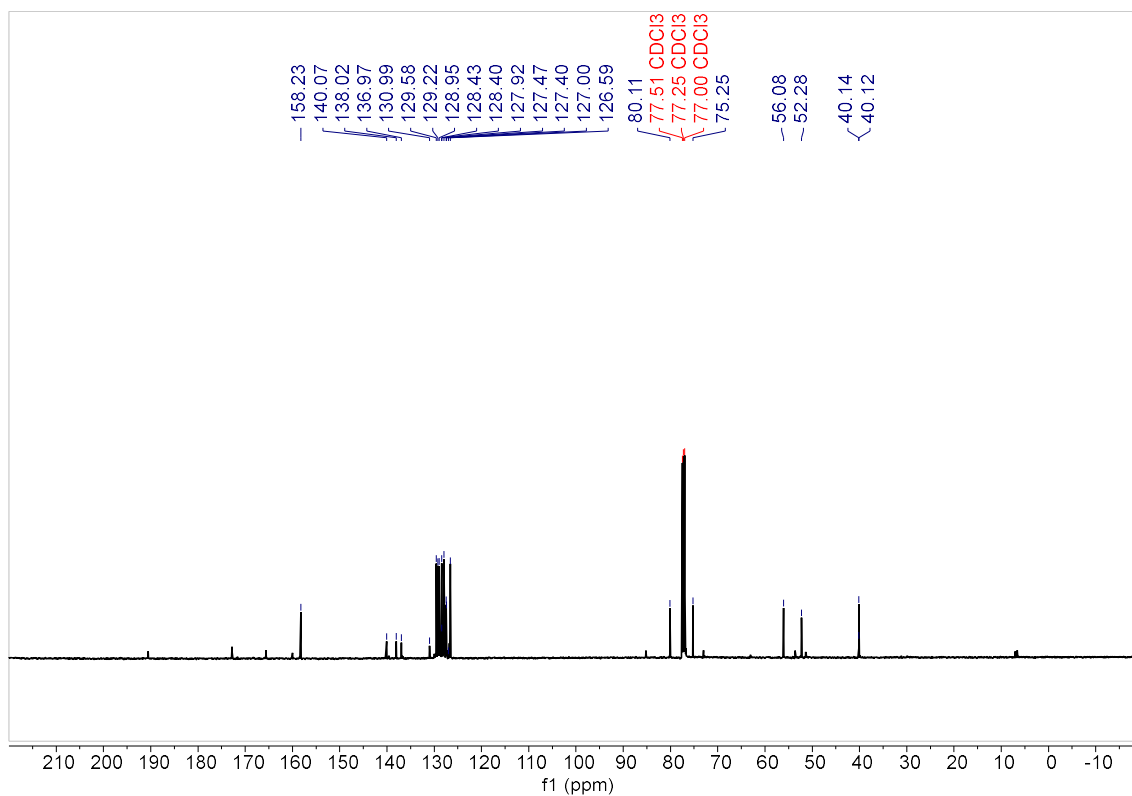


Methyl (2S,3S,4S,5S)-4-((-4-isocyanobenzylidene)amino)-1-methyl-3,5-diphenylpyrrolidine-2-carboxylate (**35-NL**). ¹H-NMR (CDCl₃)

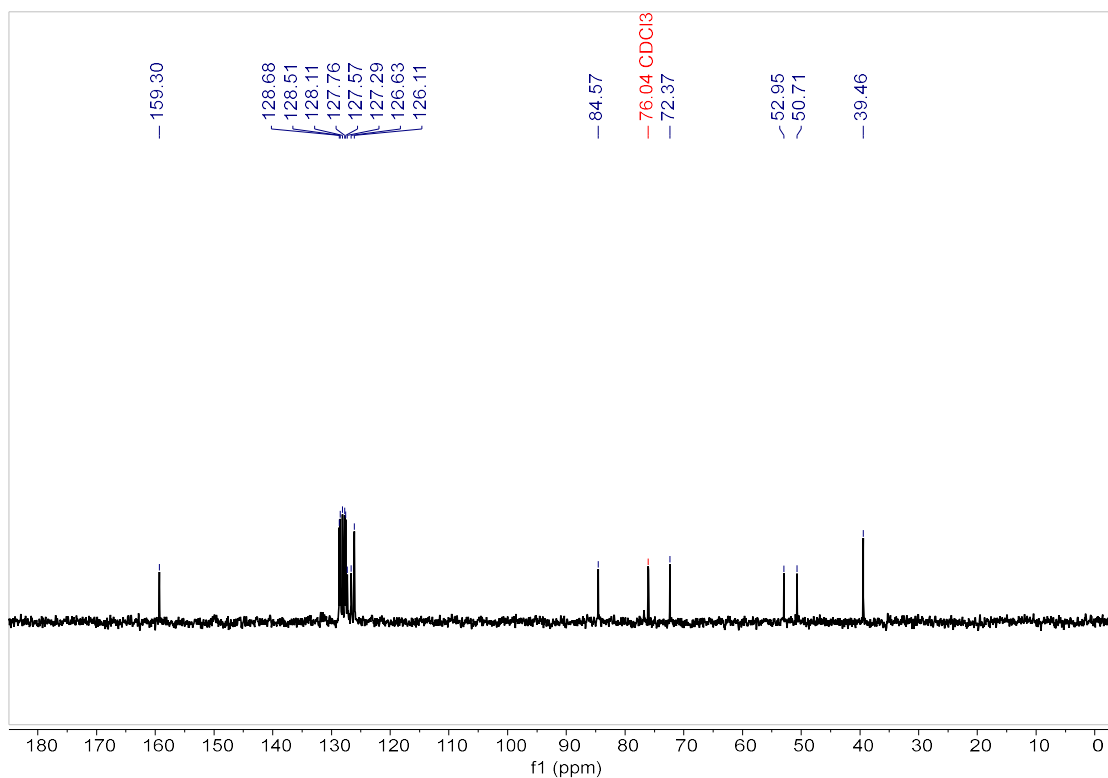


ANNEX IV

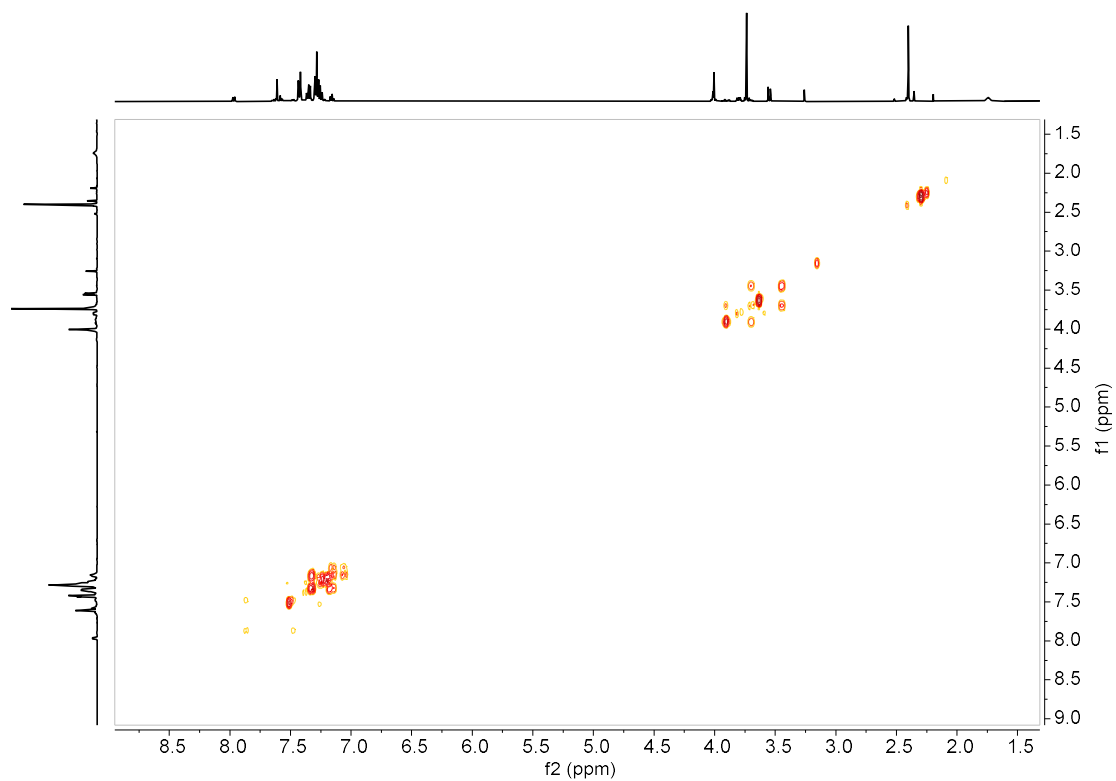
Methyl (2S,3S,4S,5S)-4-((-4-isocyanobenzylidene)amino)-1-methyl-3,5-diphenylpyrrolidine-2-carboxylate (**35-N_L**). ¹³C-NMR (CDCl₃)



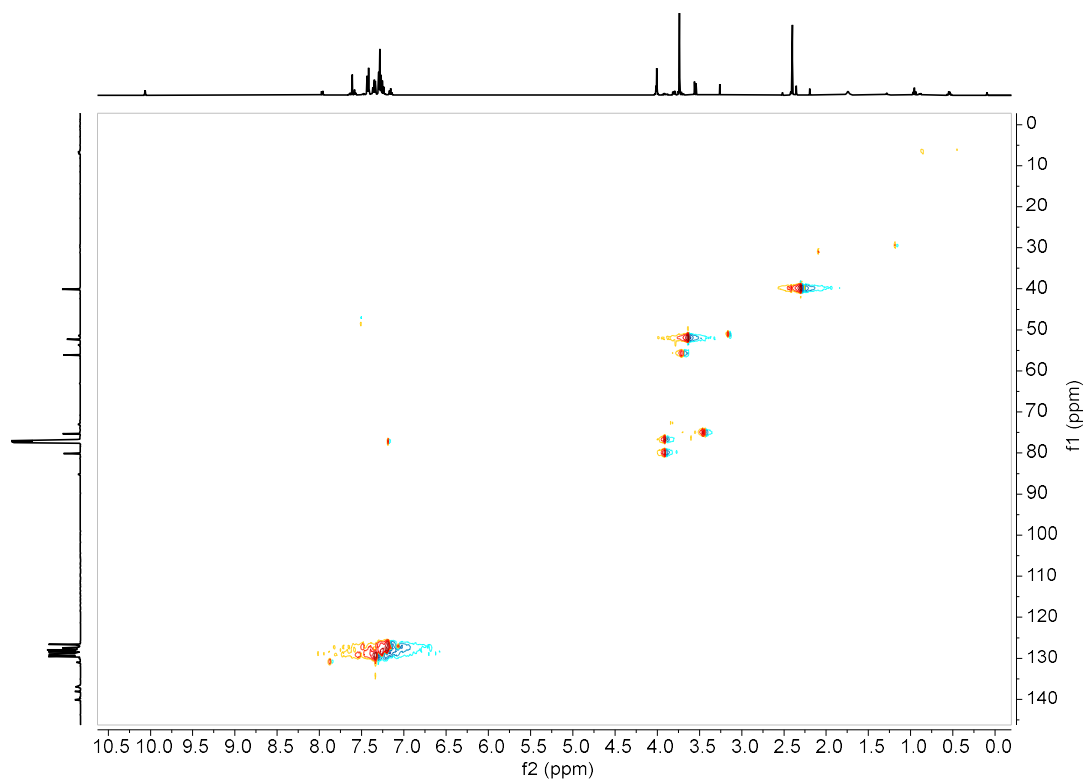
Methyl (2S,3S,4S,5S)-4-((-4-isocyanobenzylidene)amino)-1-methyl-3,5-diphenylpyrrolidine-2-carboxylate (**35-N_L**). DEPT135 (CDCl₃)



Methyl (2S,3S,4S,5S)-4-((-4-isocyanobenzylidene)amino)-1-methyl-3,5-diphenylpyrrolidine-2-carboxylate (**35-N_L**). g-COSY (CDCl₃)

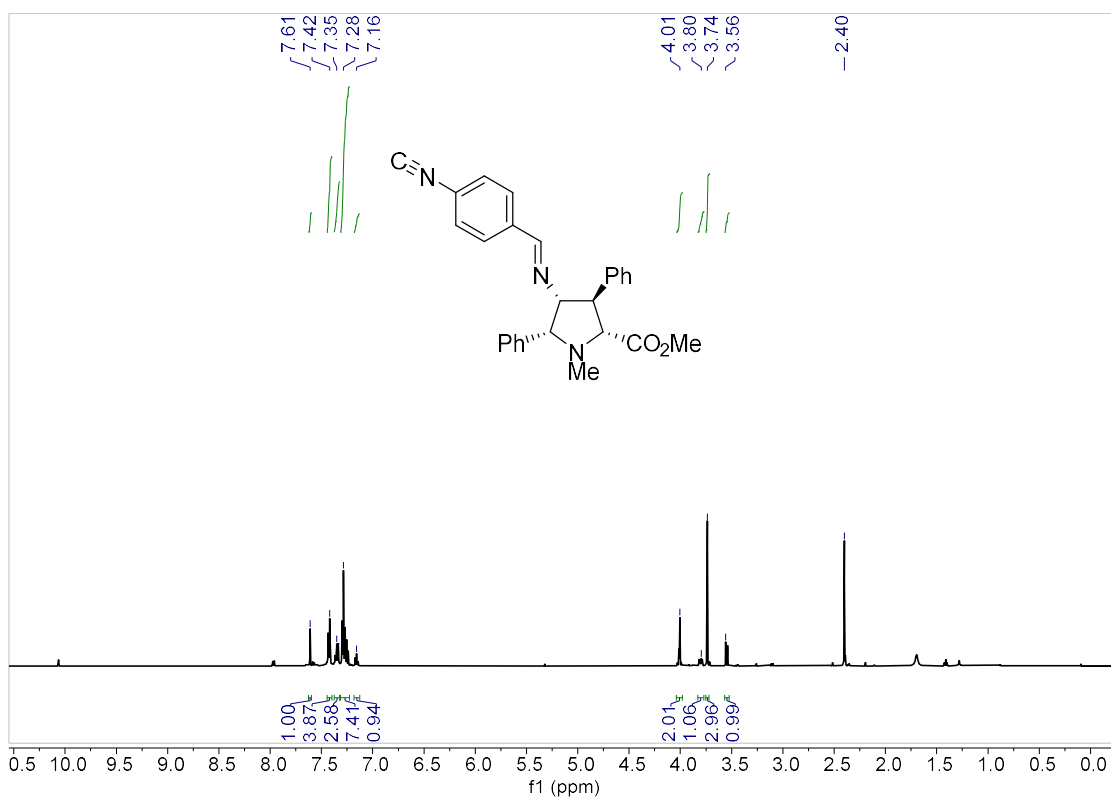


Methyl (2S,3S,4S,5S)-4-((-4-isocyanobenzylidene)amino)-1-methyl-3,5-diphenylpyrrolidine-2-carboxylate (**35-N_L**). g-HSQC (CDCl₃)

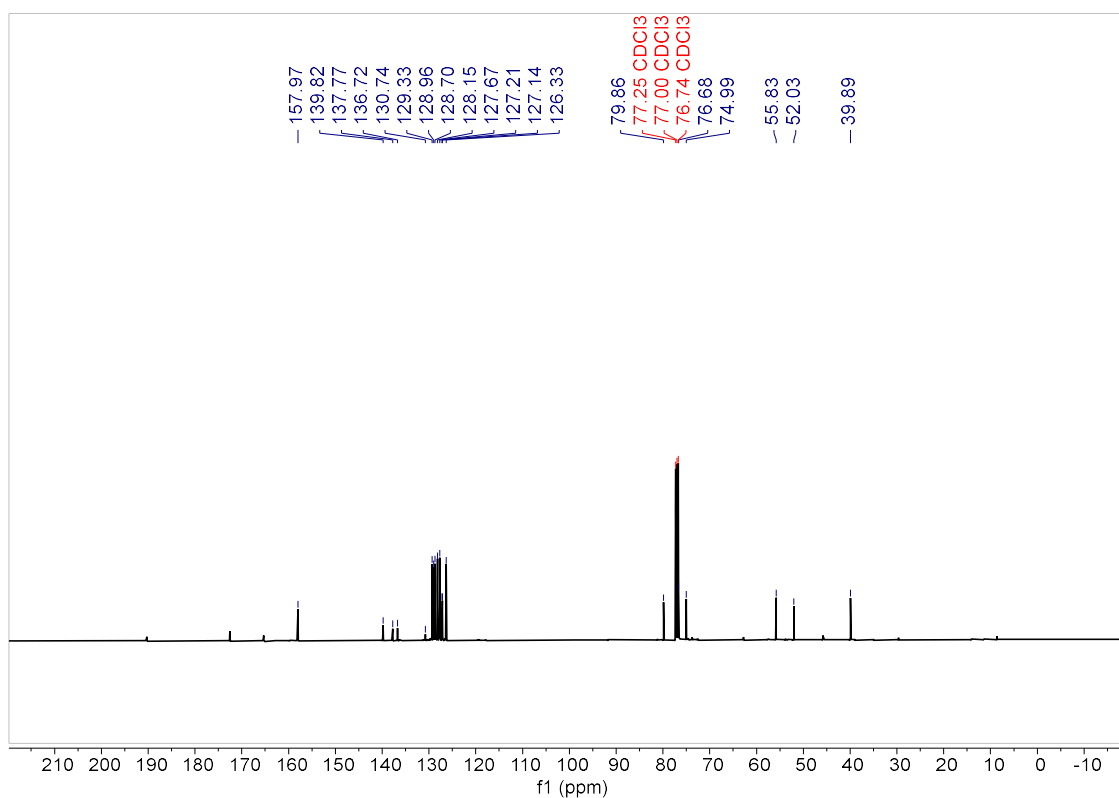


ANNEX IV

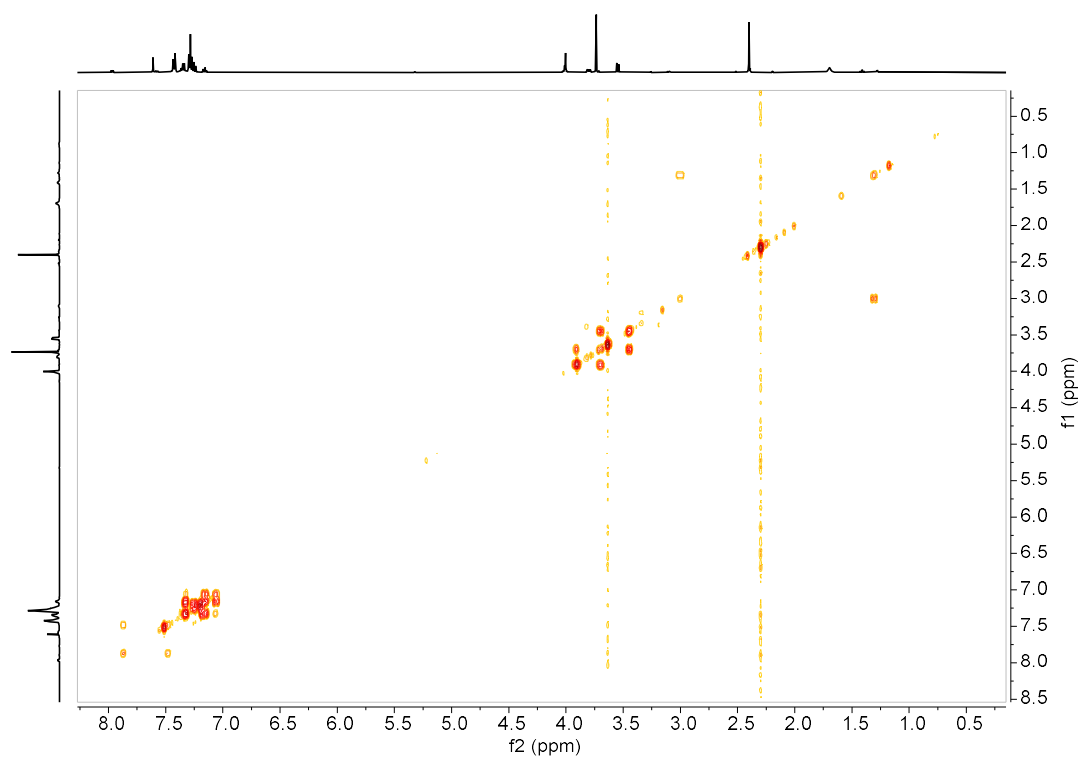
Methyl (2R,3R,4R,5R)-4-(((E)-4-isocyanobenzylidene)amino)-1-methyl-3,5-diphenylpyrrolidine-2-carboxylate (**N_D**). ¹H-NMR (CDCl₃)



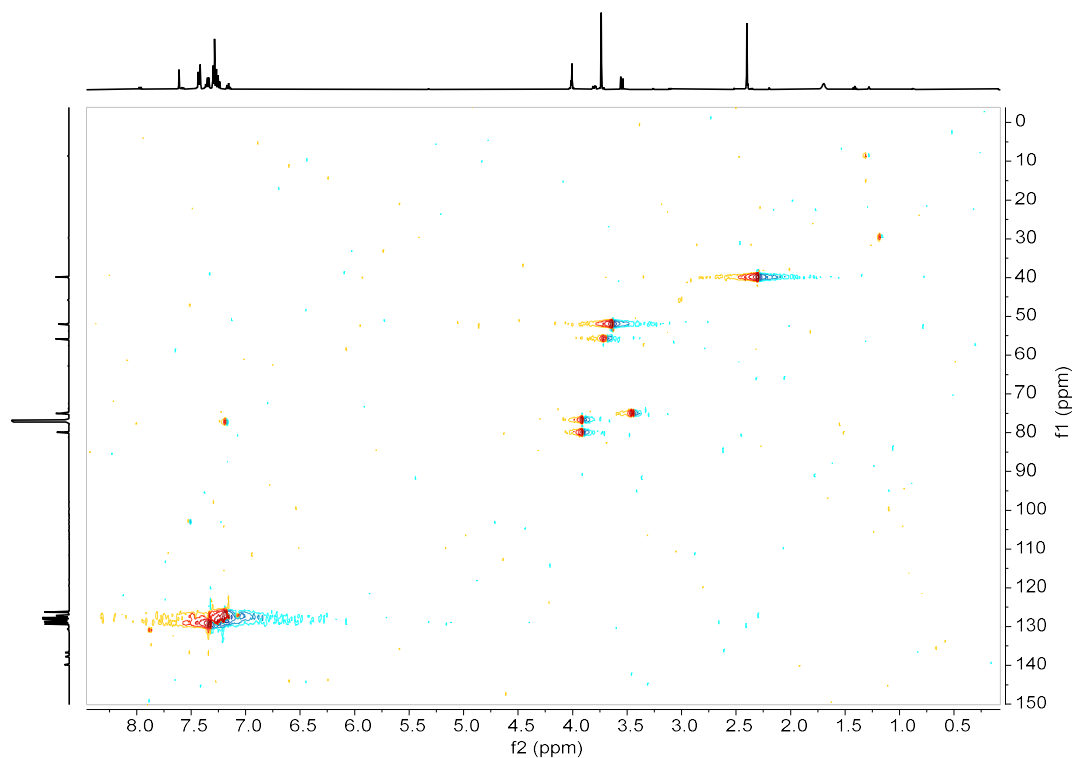
Methyl (2R,3R,4R,5R)-4-(((E)-4-isocyanobenzylidene)amino)-1-methyl-3,5-diphenylpyrrolidine-2-carboxylate (**N_D**). ¹³C-NMR (CDCl₃)



Methyl (2R,3R,4R,5R)-4-(((E)-4-isocyanobenzylidene)amino)-1-methyl-3,5-diphenylpyrrolidine-2-carboxylate (**N_D**). g-COSY (CDCl₃)

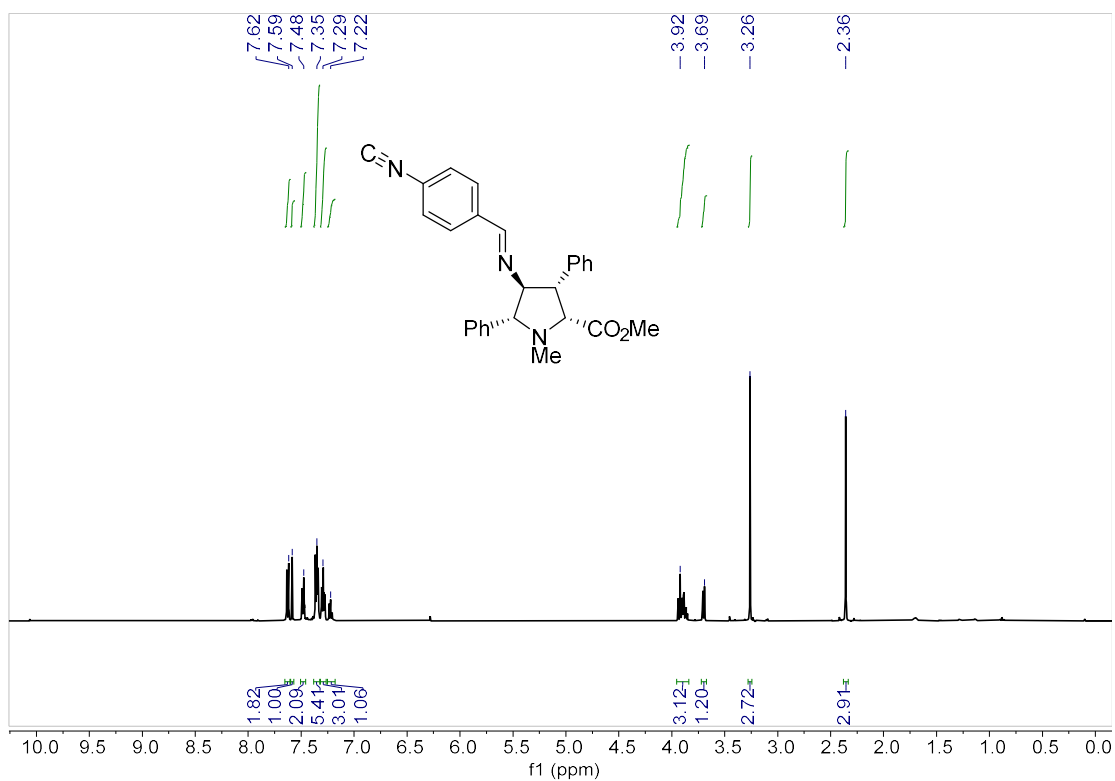


Methyl (2R,3R,4R,5R)-4-(((E)-4-isocyanobenzylidene)amino)-1-methyl-3,5-diphenylpyrrolidine-2-carboxylate (**N_D**). g-HSQC (CDCl₃)

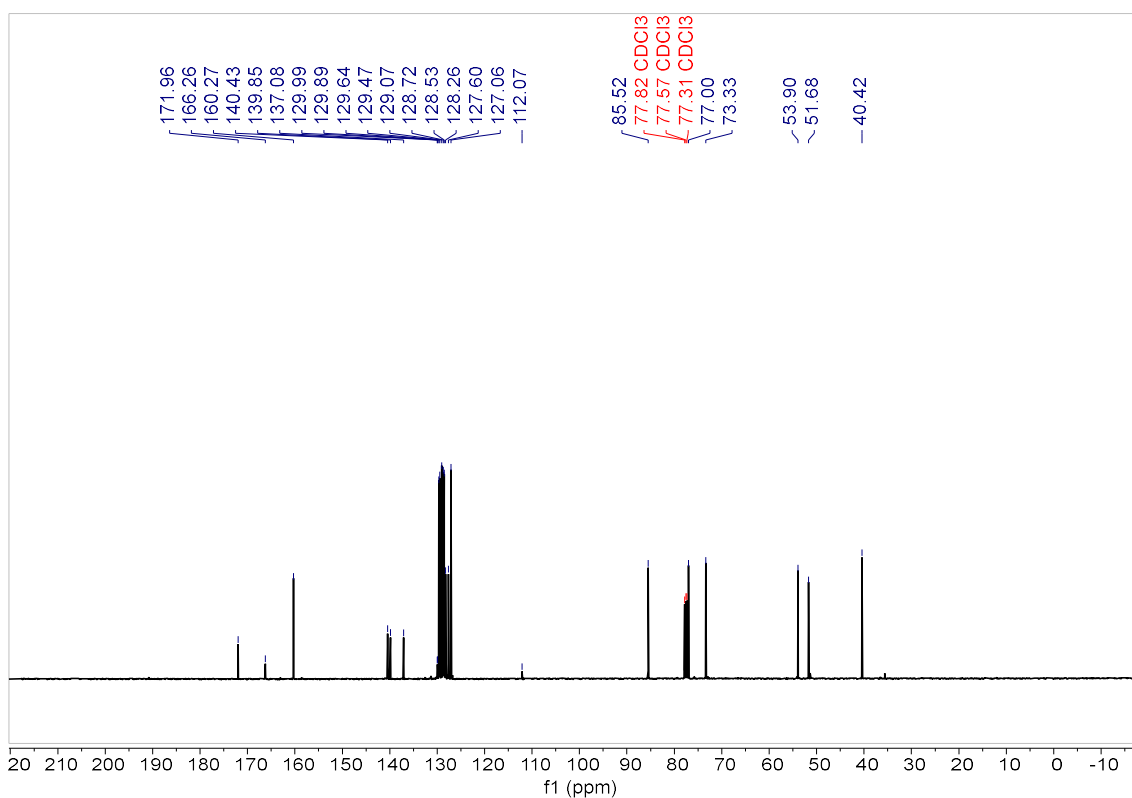


ANNEX IV

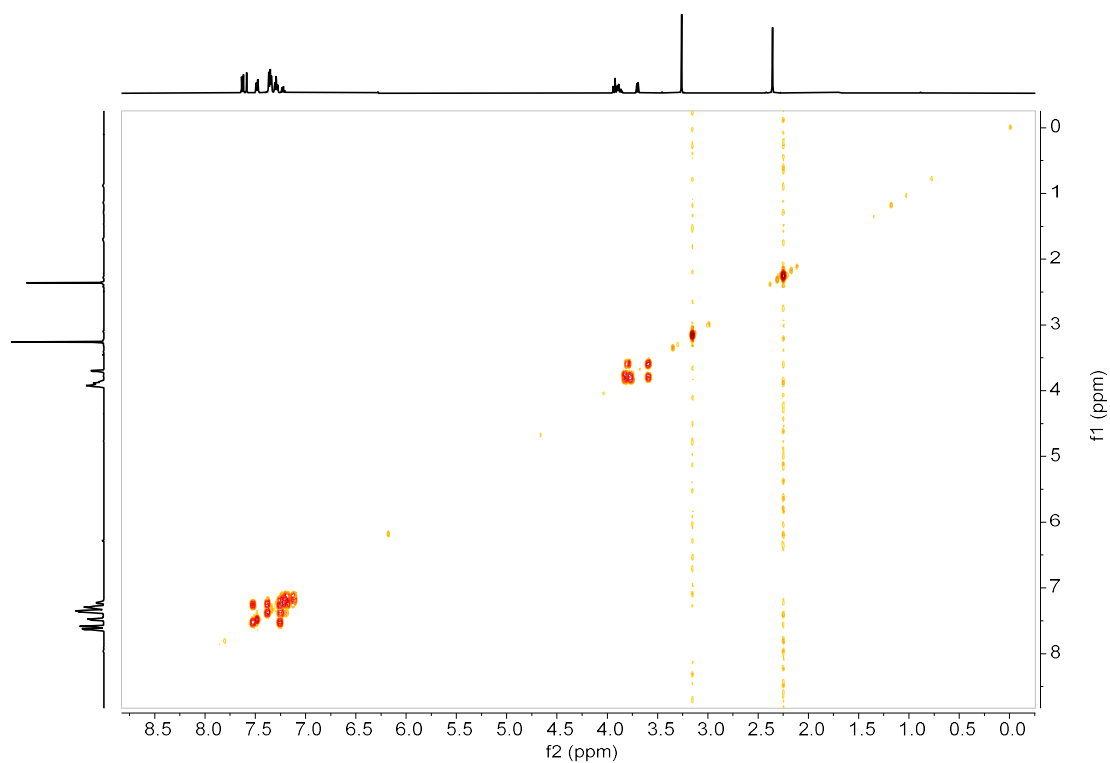
Methyl (2R,3S,4S,5R)-4-((-4-isocyanobenzylidene)amino)-1-methyl-3,5-diphenylpyrrolidine-2-carboxylate (**X_D**). ¹H-NMR (CDCl₃)



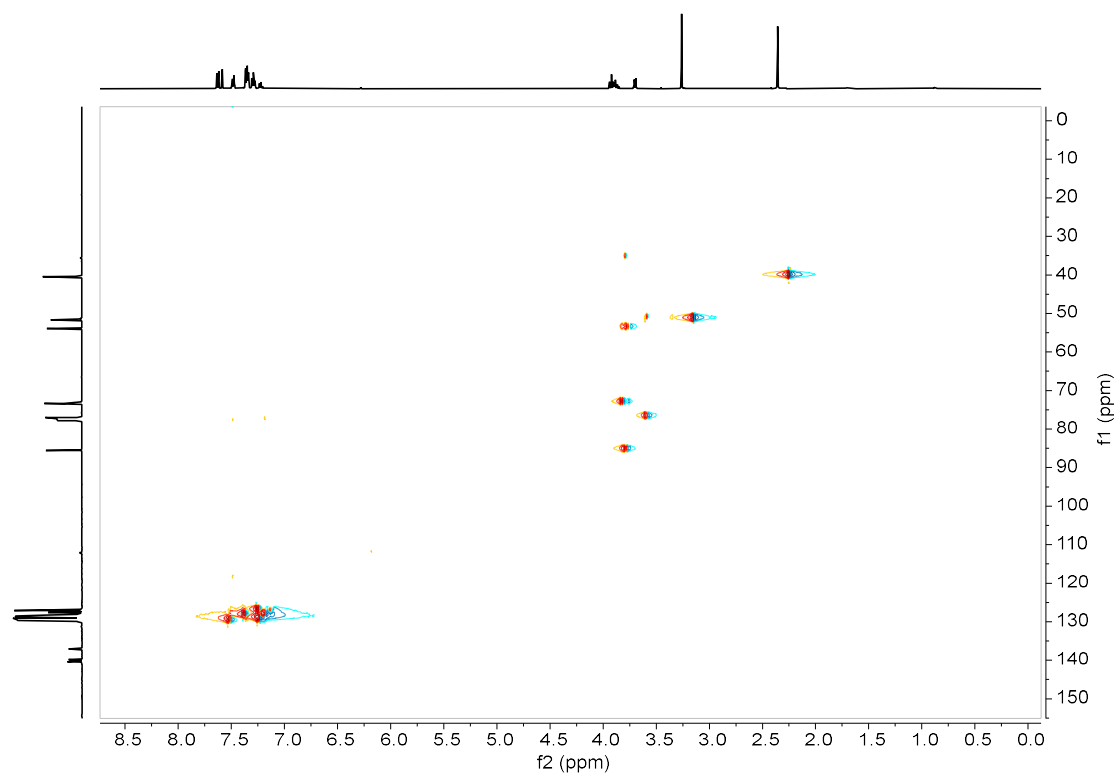
Methyl (2R,3S,4S,5R)-4-((-4-isocyanobenzylidene)amino)-1-methyl-3,5-diphenylpyrrolidine-2-carboxylate (**X_D**). ¹³C-NMR (CDCl₃)



Methyl (2R,3S,4S,5R)-4-((-4-isocyanobenzylidene)amino)-1-methyl-3,5-diphenylpyrrolidine-2-carboxylate (**X_D**). g-COSY (CDCl₃)

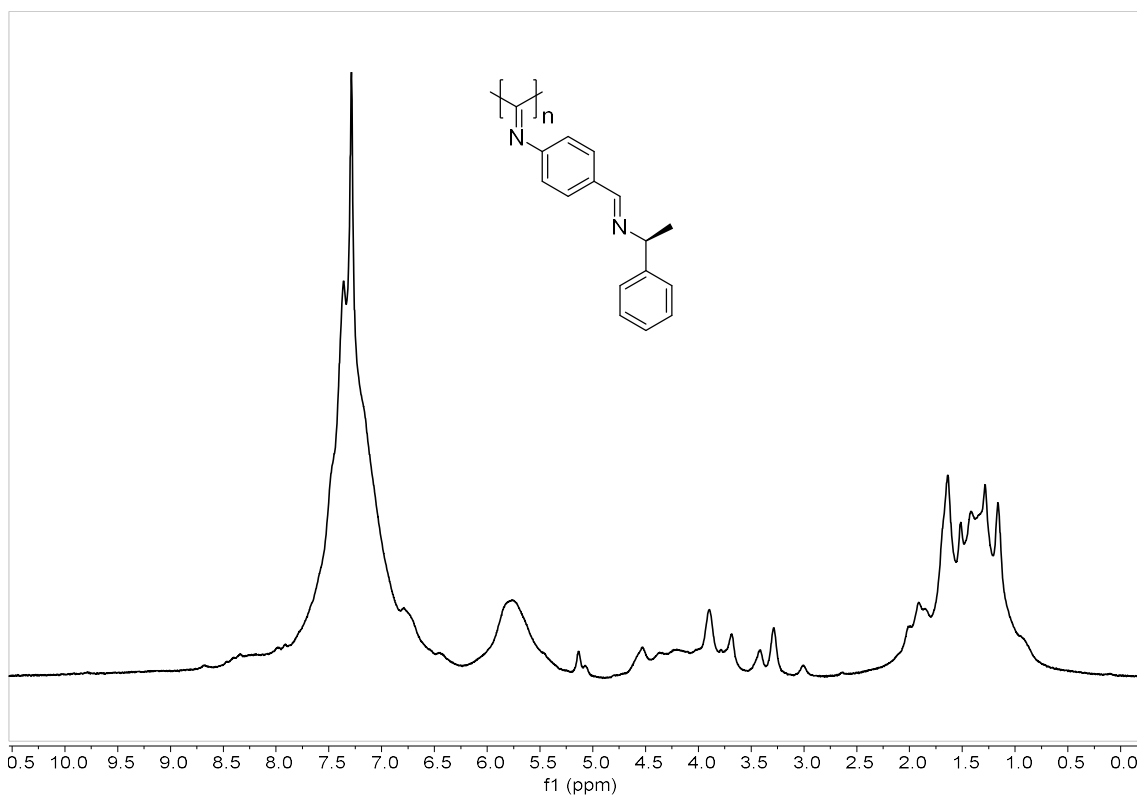


Methyl (2R,3S,4S,5R)-4-((-4-isocyanobenzylidene)amino)-1-methyl-3,5-diphenylpyrrolidine-2-carboxylate (**X_D**). g-HSQC (CDCl₃)

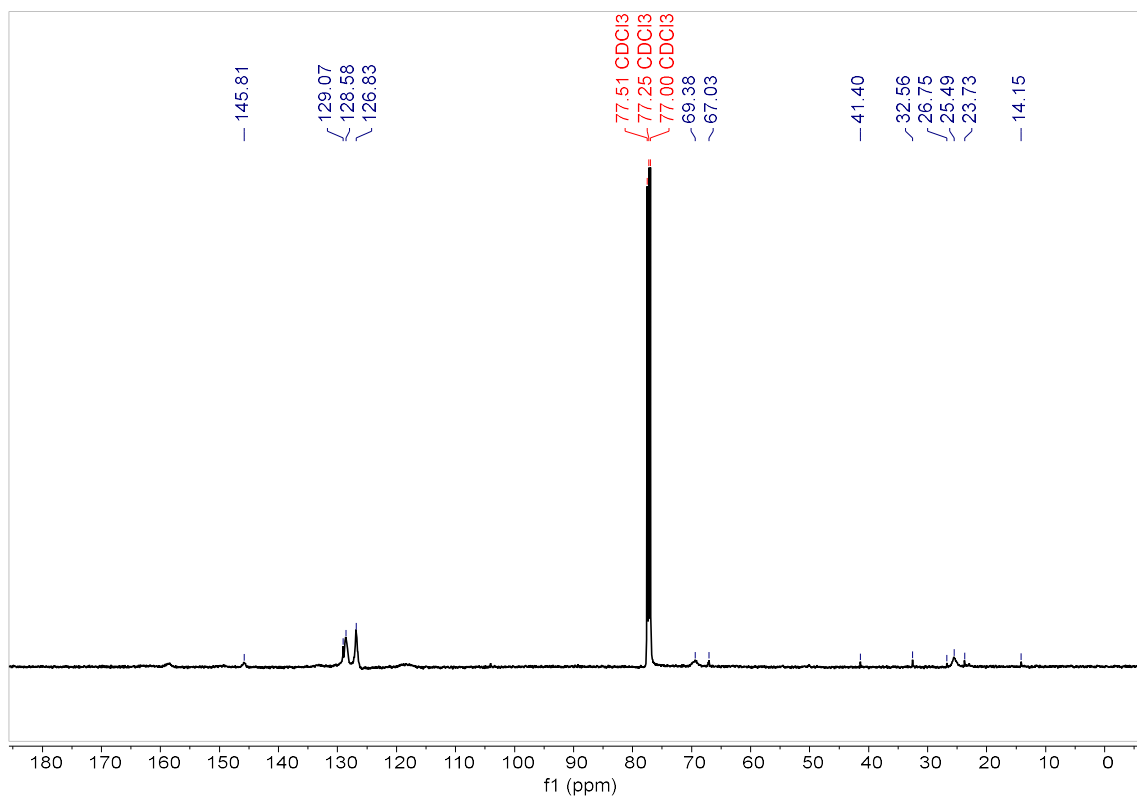


ANNEX IV

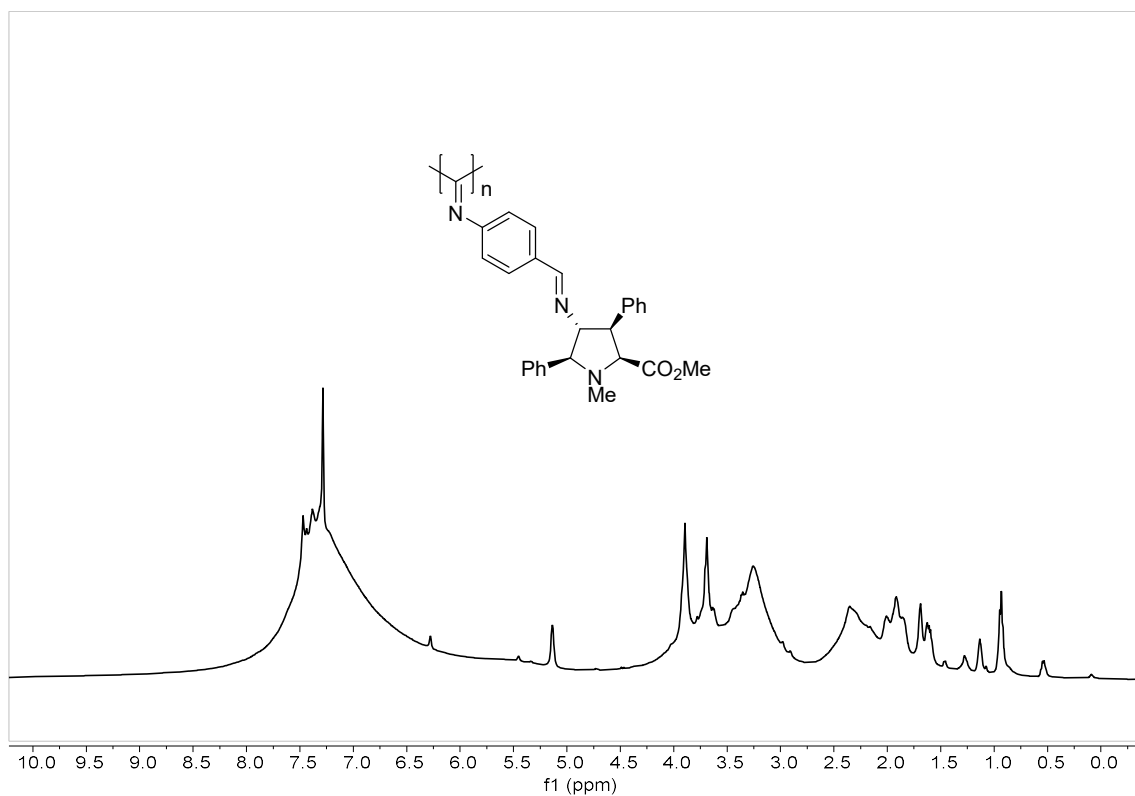
Poly-(S)-1-(4-isocyanophenyl)-N-(1-phenylethyl)methanimine (**poly-32S**). $^1\text{H-NMR}$ (CDCl_3)



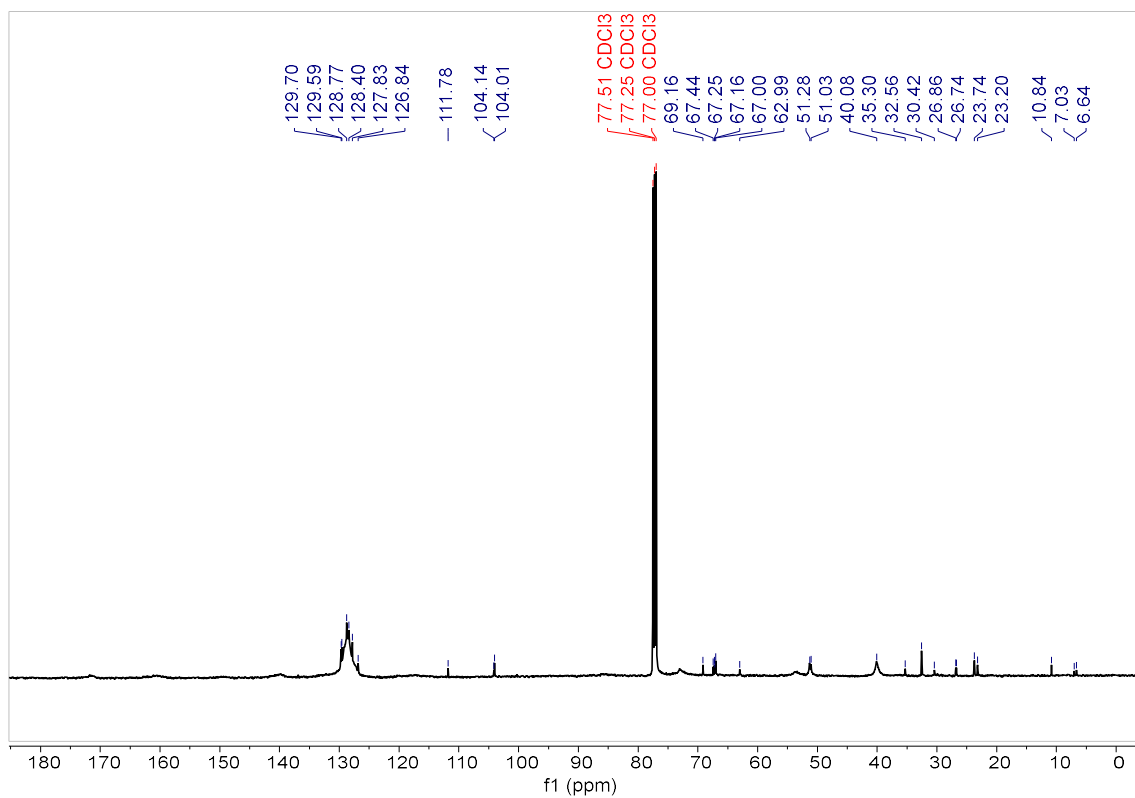
Poly-(S)-1-(4-isocyanophenyl)-N-(1-phenylethyl)methanimine (**poly-32S**). $^{13}\text{C-NMR}$ (CDCl_3)



Poly-(S)-1-(4-isocyanophenyl)-N-(1-phenylethyl)methanimine (**poly-35XL**). $^1\text{H-NMR}$ (CDCl_3)

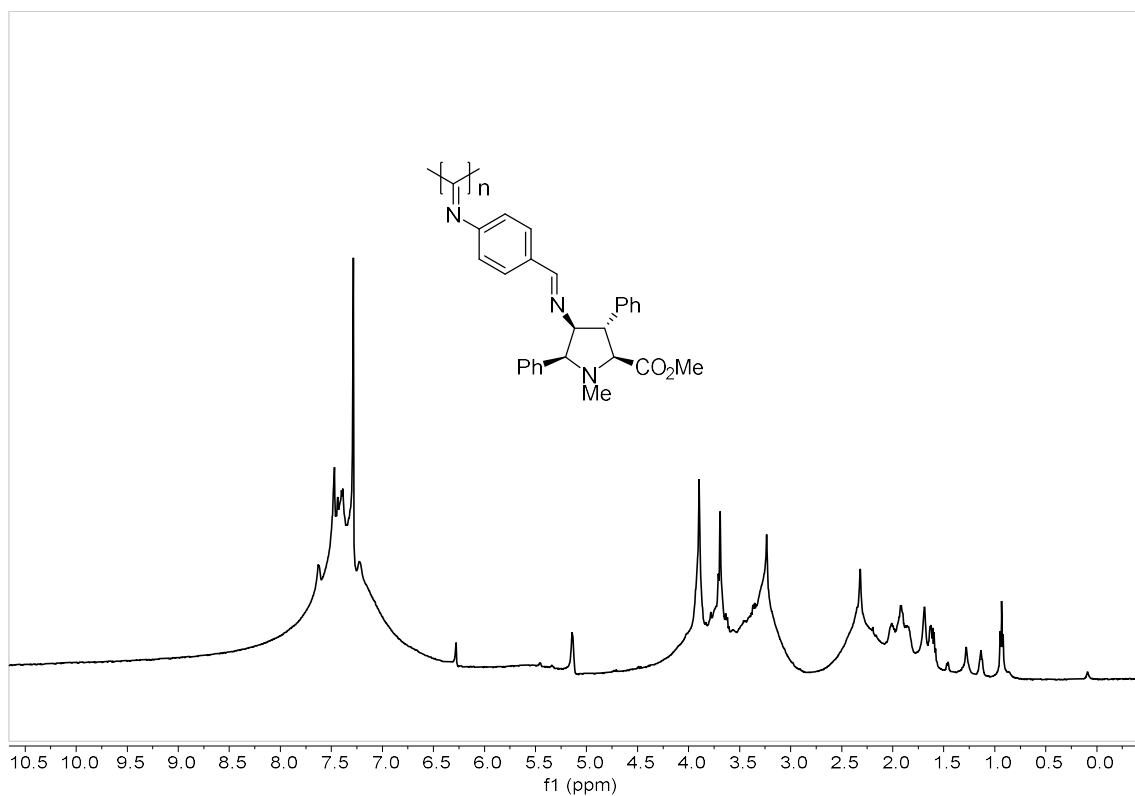


Poly-(S)-1-(4-isocyanophenyl)-N-(1-phenylethyl)methanimine (**poly-35XL**). $^{13}\text{C-NMR}$ (CDCl_3)

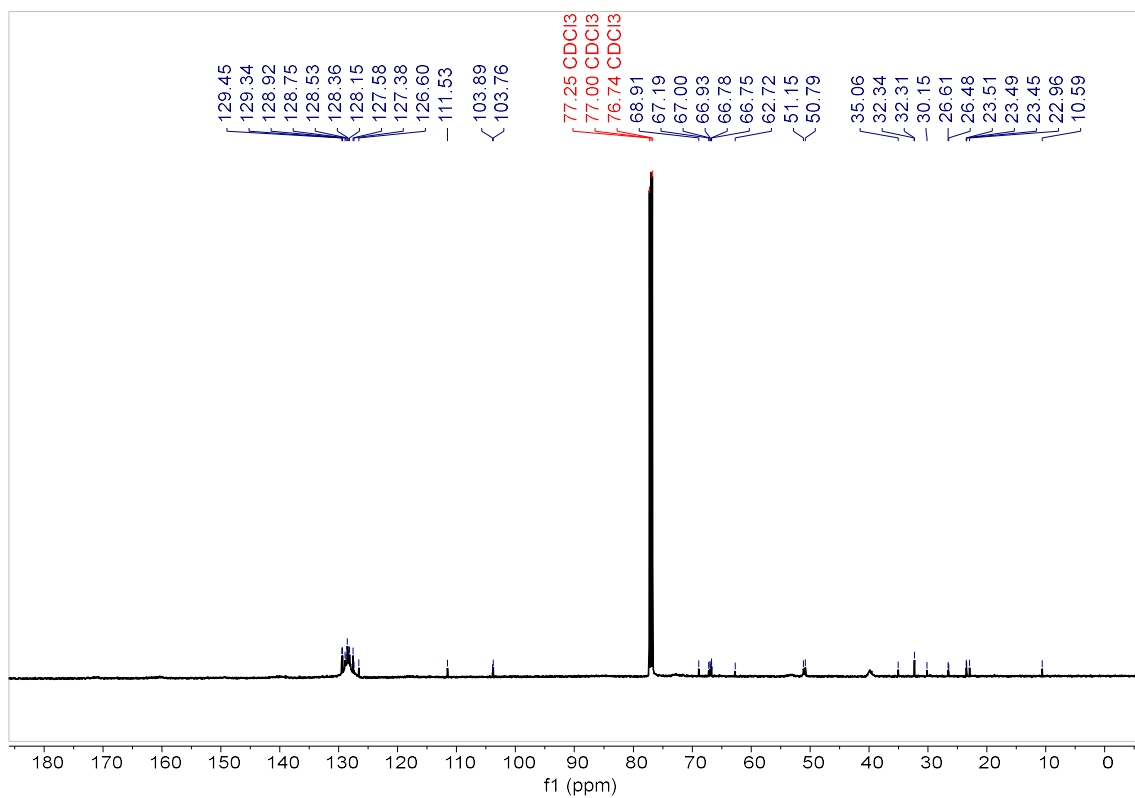


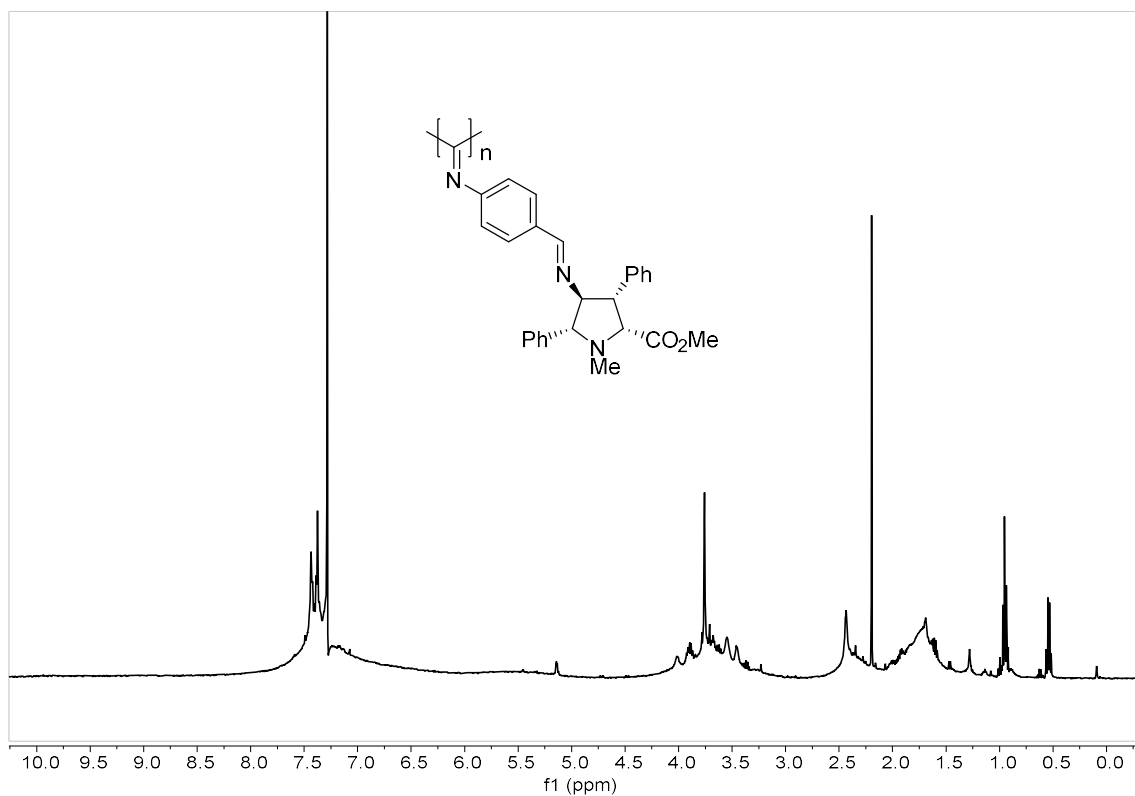
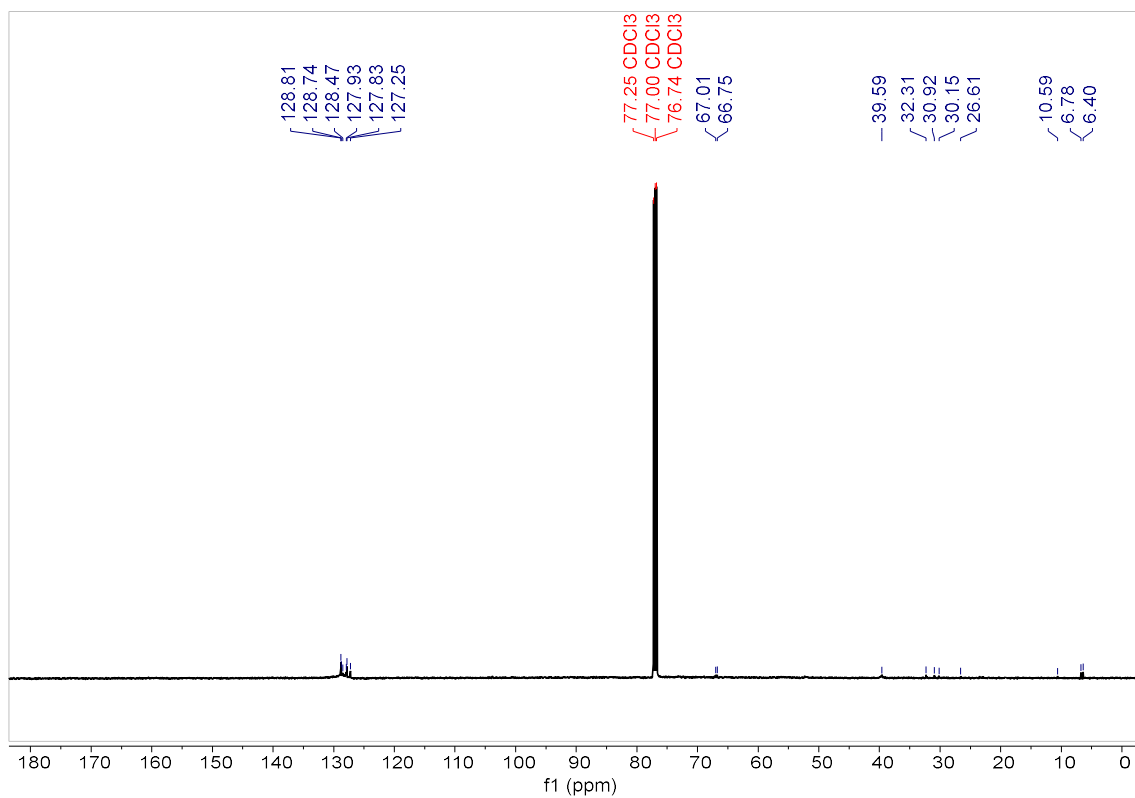
ANNEX IV

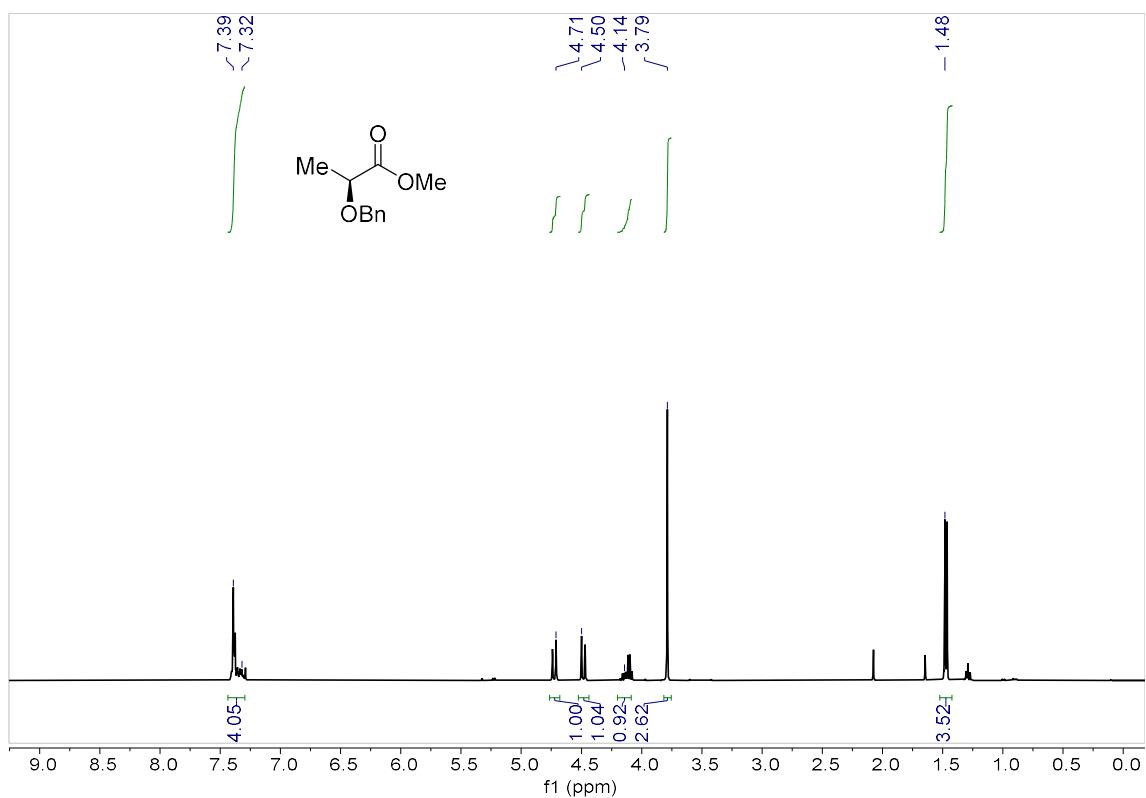
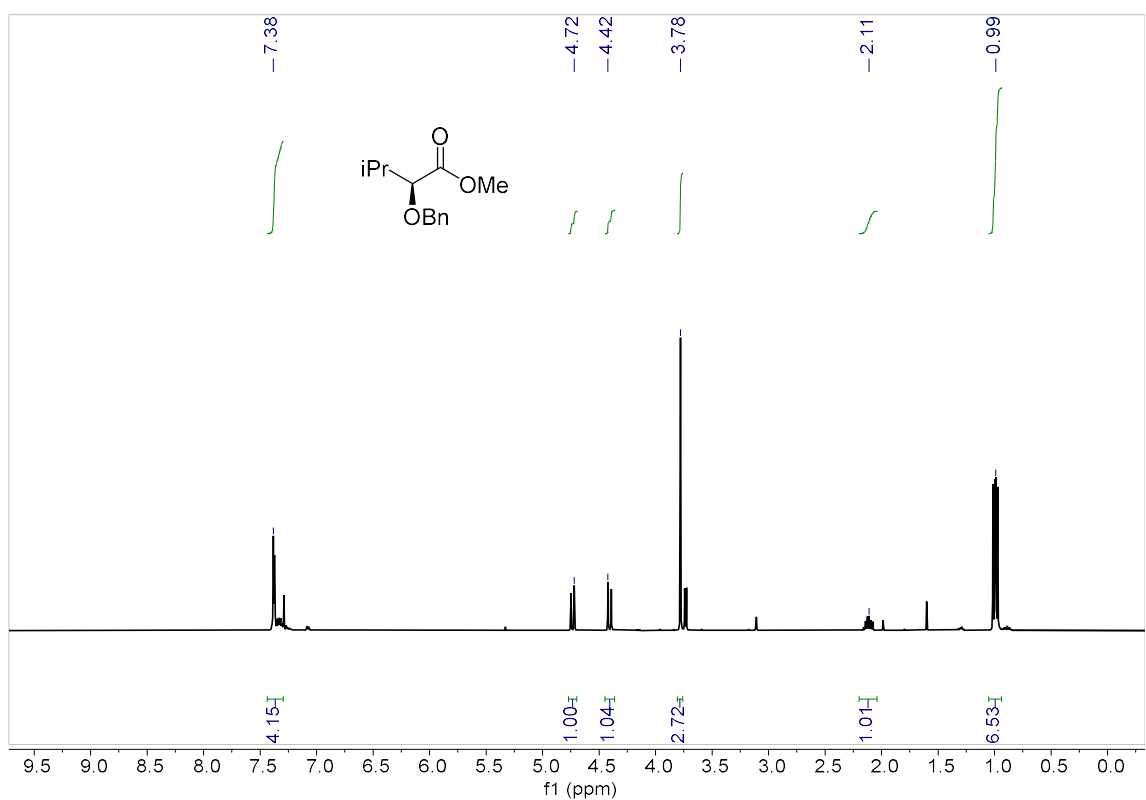
Poly-(S)-1-(4-isocyanophenyl)-N-(1-phenylethyl)methanimine (**poly-35NL**). $^1\text{H-NMR}$ (CDCl_3)

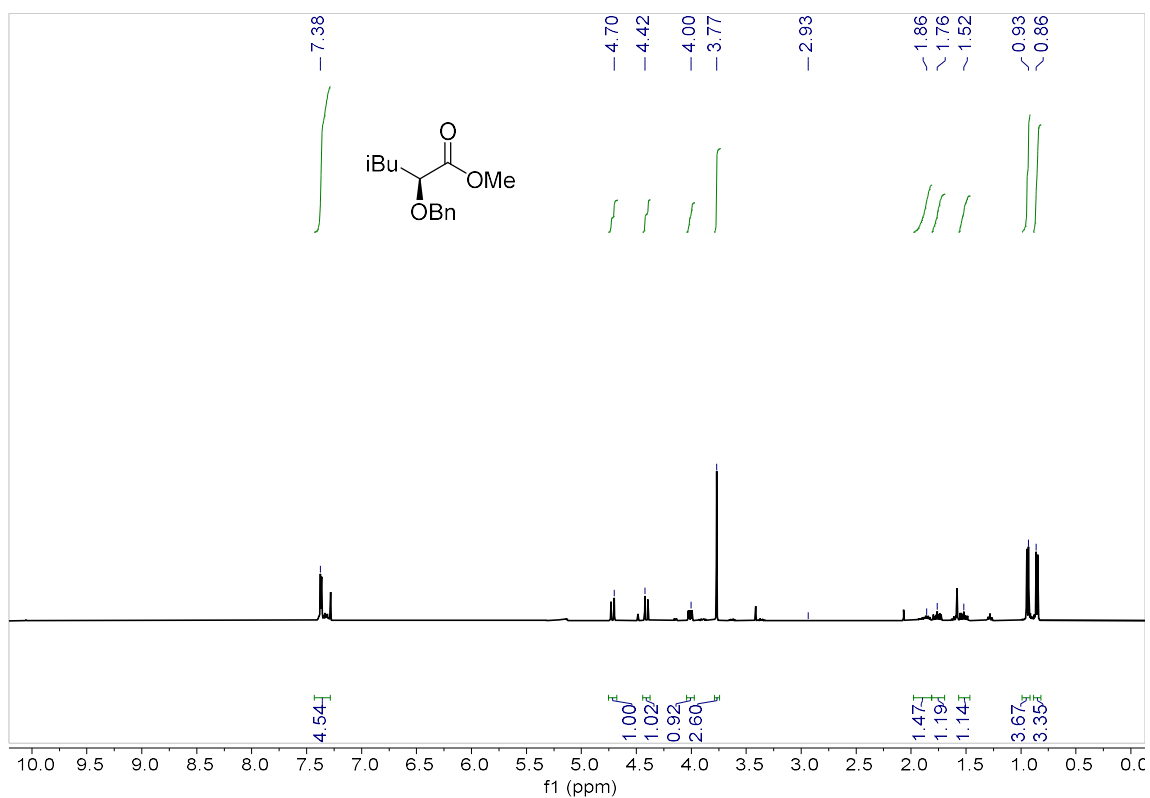
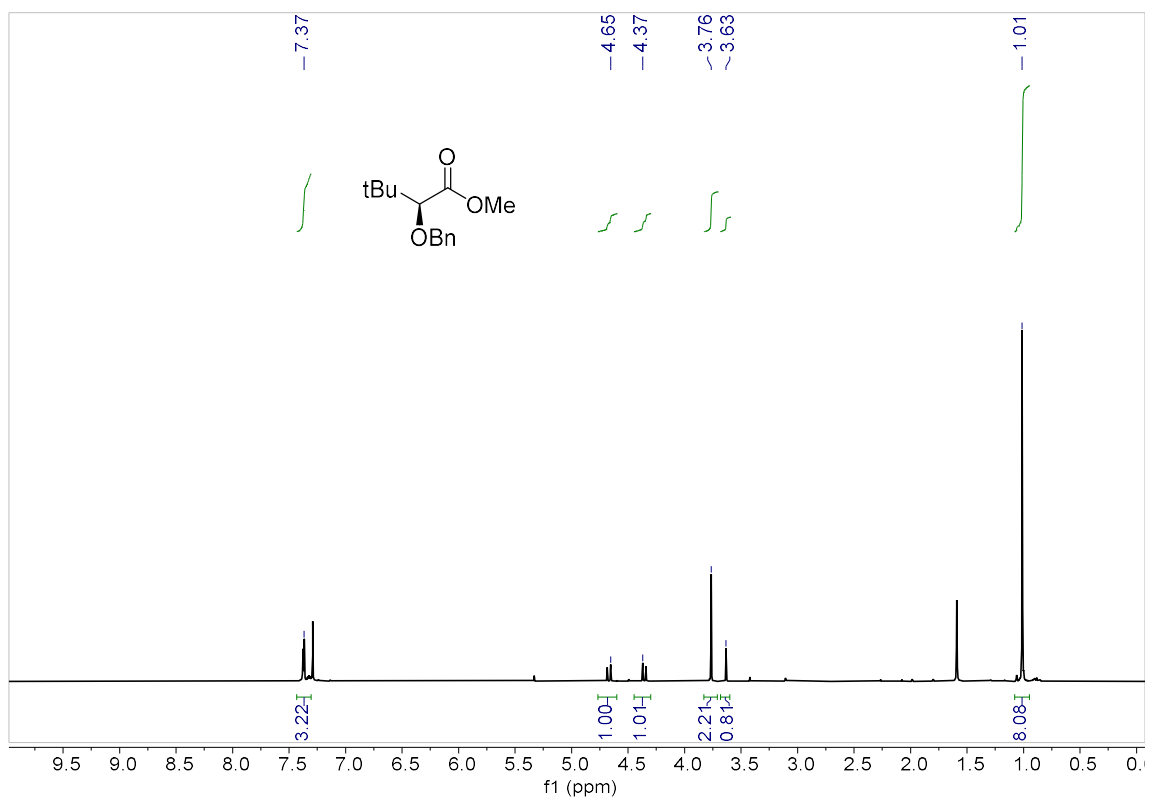


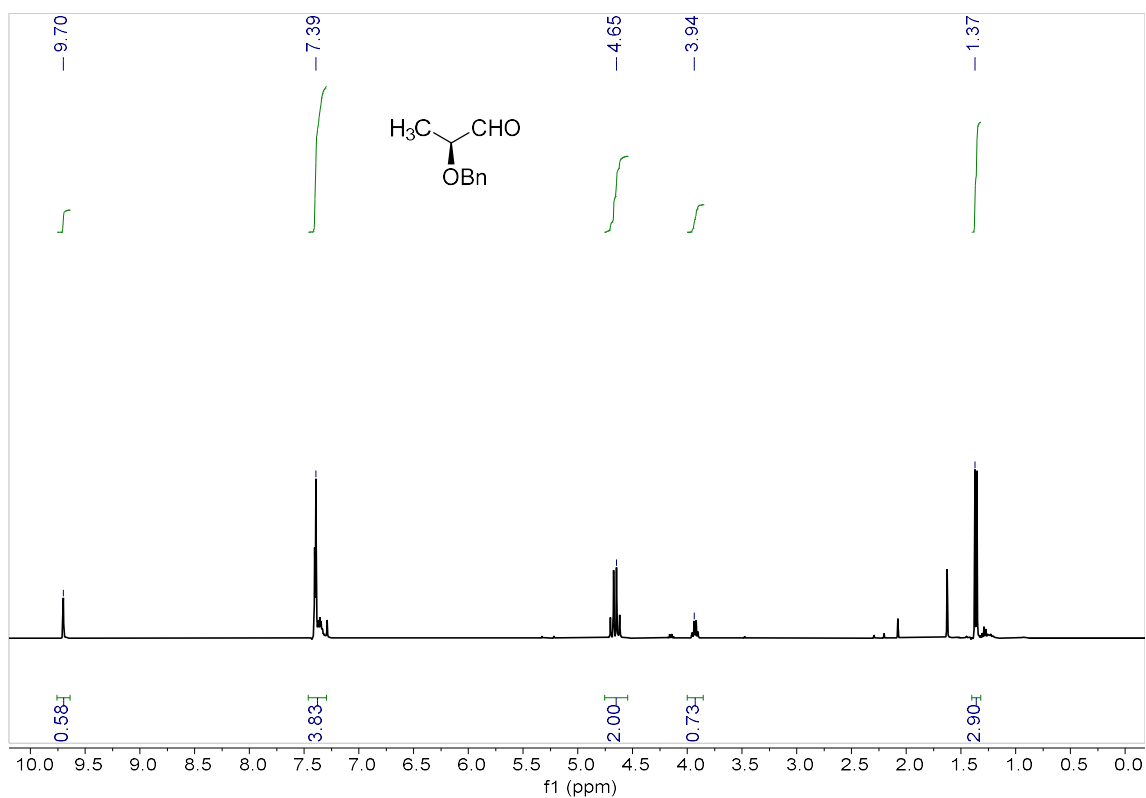
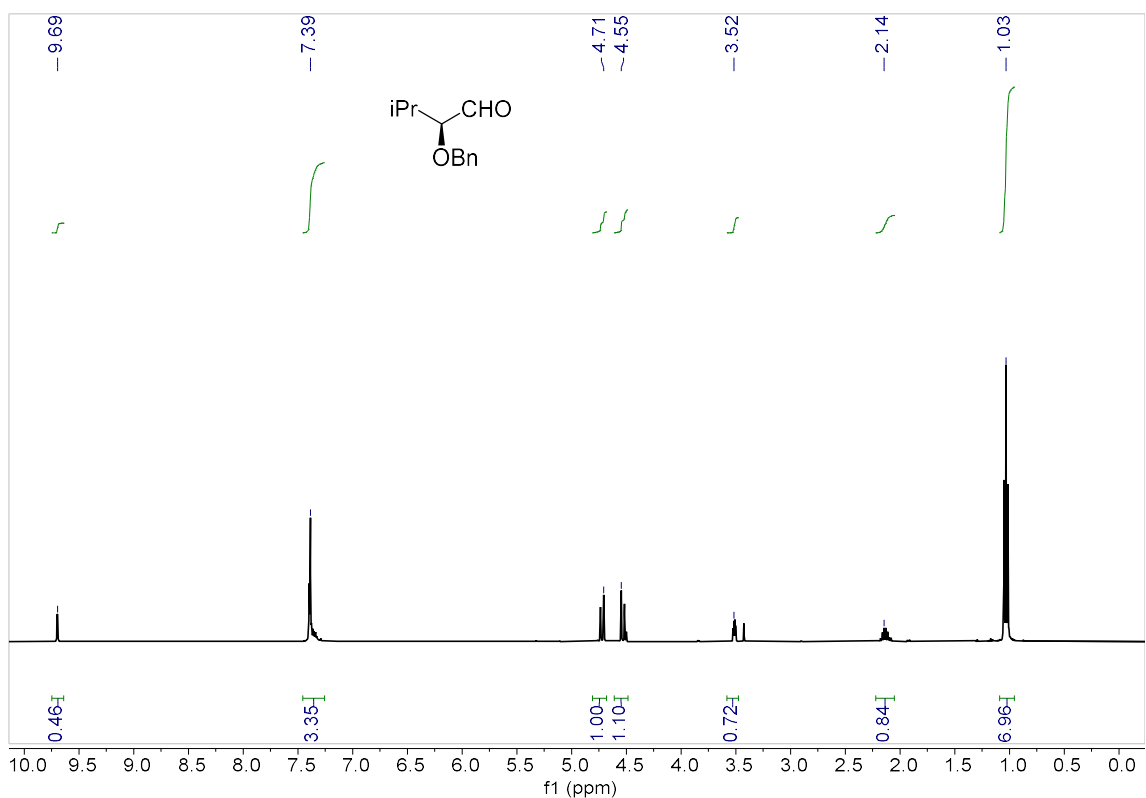
Poly-(S)-1-(4-isocyanophenyl)-N-(1-phenylethyl)methanimine (**poly-35NL**). $^{13}\text{C-NMR}$ (CDCl_3)

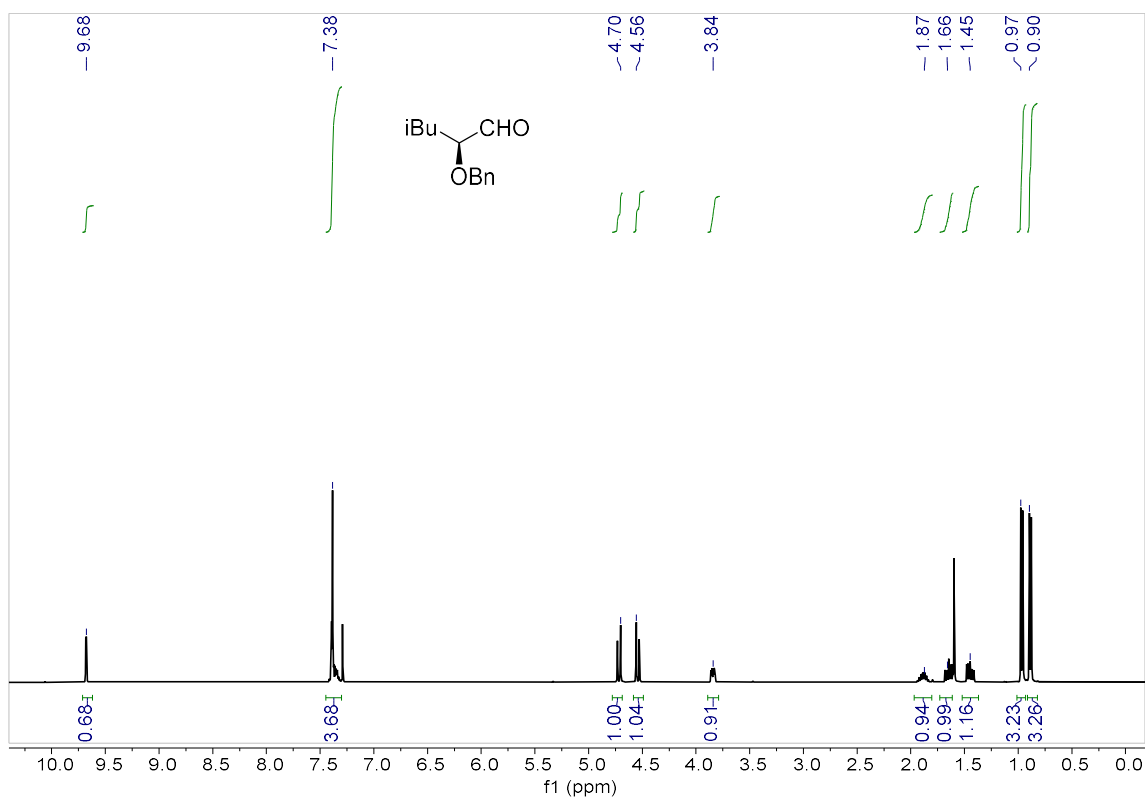
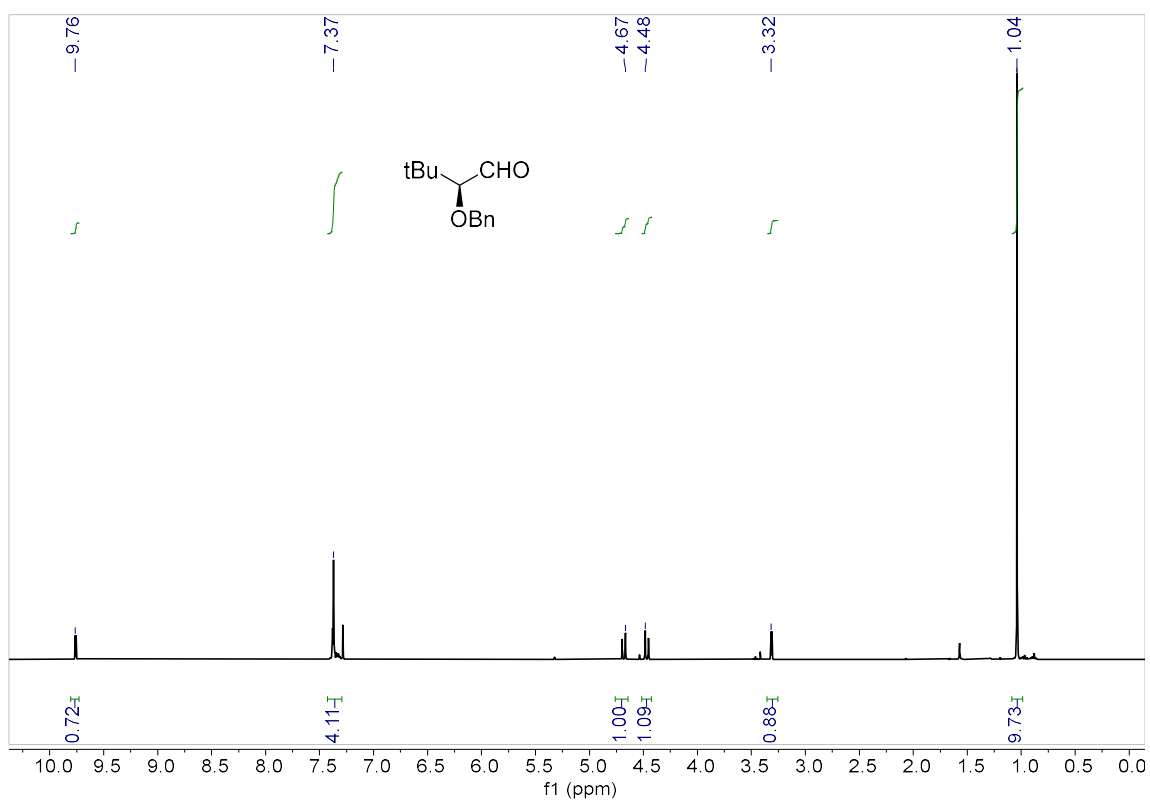


Poly-(S)-1-(4-isocyanophenyl)-N-(1-phenylethyl)methanimine (**poly-35Xd**). $^1\text{H-NMR}$ (CDCl_3)Poly-(S)-1-(4-isocyanophenyl)-N-(1-phenylethyl)methanimine (**poly-35Xd**). $^{13}\text{C-NMR}$ (CDCl_3)

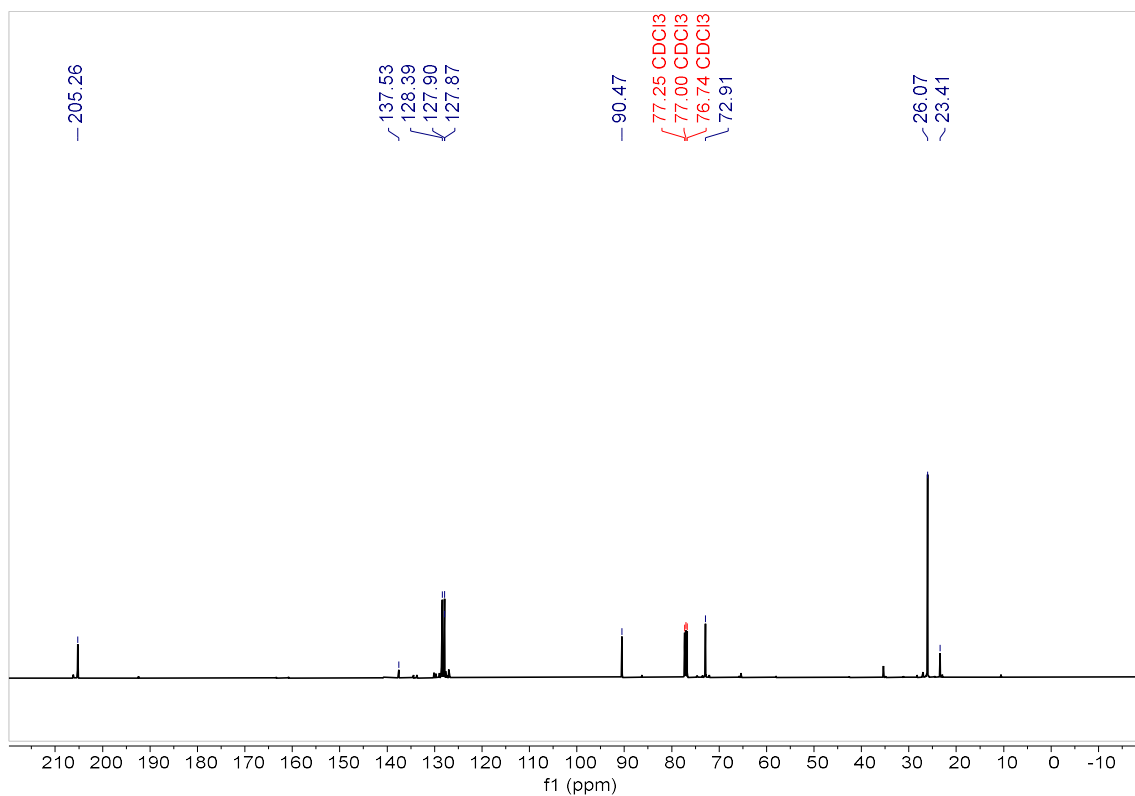
(S)-2-(benzyloxy)propanal (**40a**). $^1\text{H-NMR}$ (CDCl_3)(S)-2-(benzyloxy)-3-methylbutanal (**40b**). $^1\text{H-NMR}$ (CDCl_3)

(S)-2-(benzyloxy)-4-methylpentanal (**40c**). $^1\text{H-NMR}$ (CDCl_3)methyl (S)-2-(benzyloxy)-3,3-dimethylbutanoate (**40d**). $^1\text{H-NMR}$ (CDCl_3)

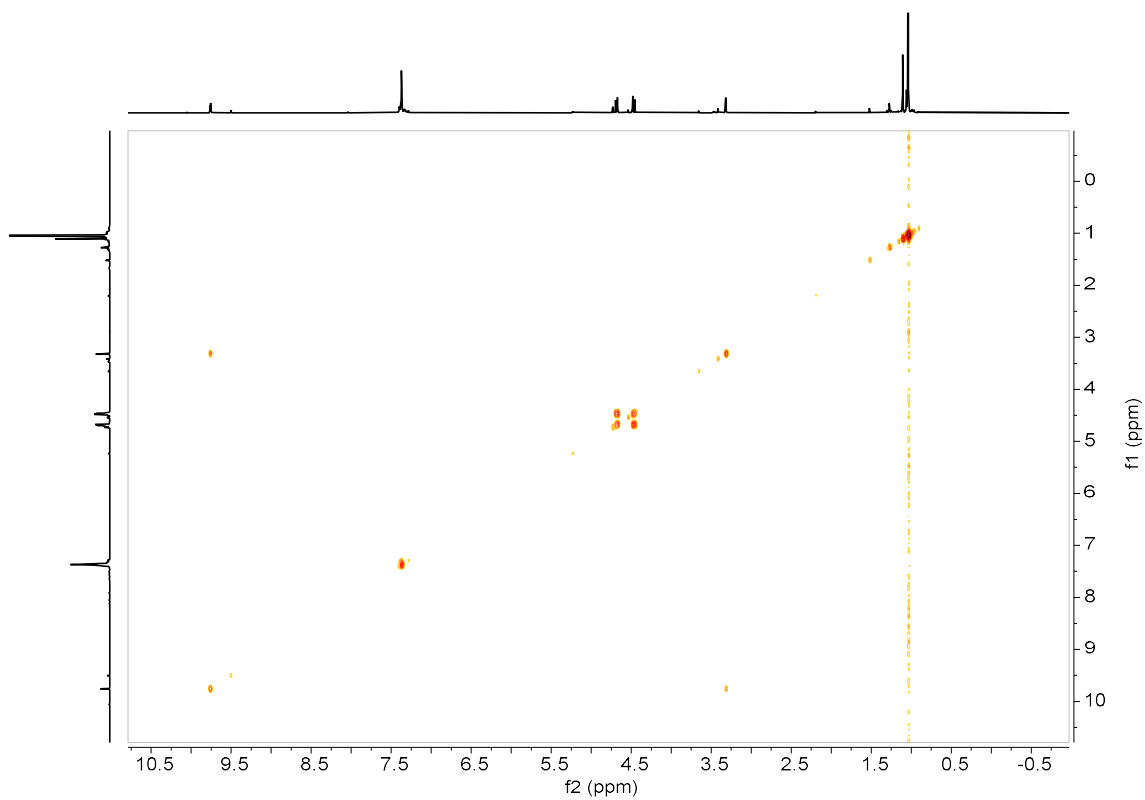
(S)-2-(benzyloxy)propanal (**41a**). $^1\text{H-NMR}$ (CDCl_3)(S)-2-(benzyloxy)-3-methylbutanal (**41b**). $^1\text{H-NMR}$ (CDCl_3)

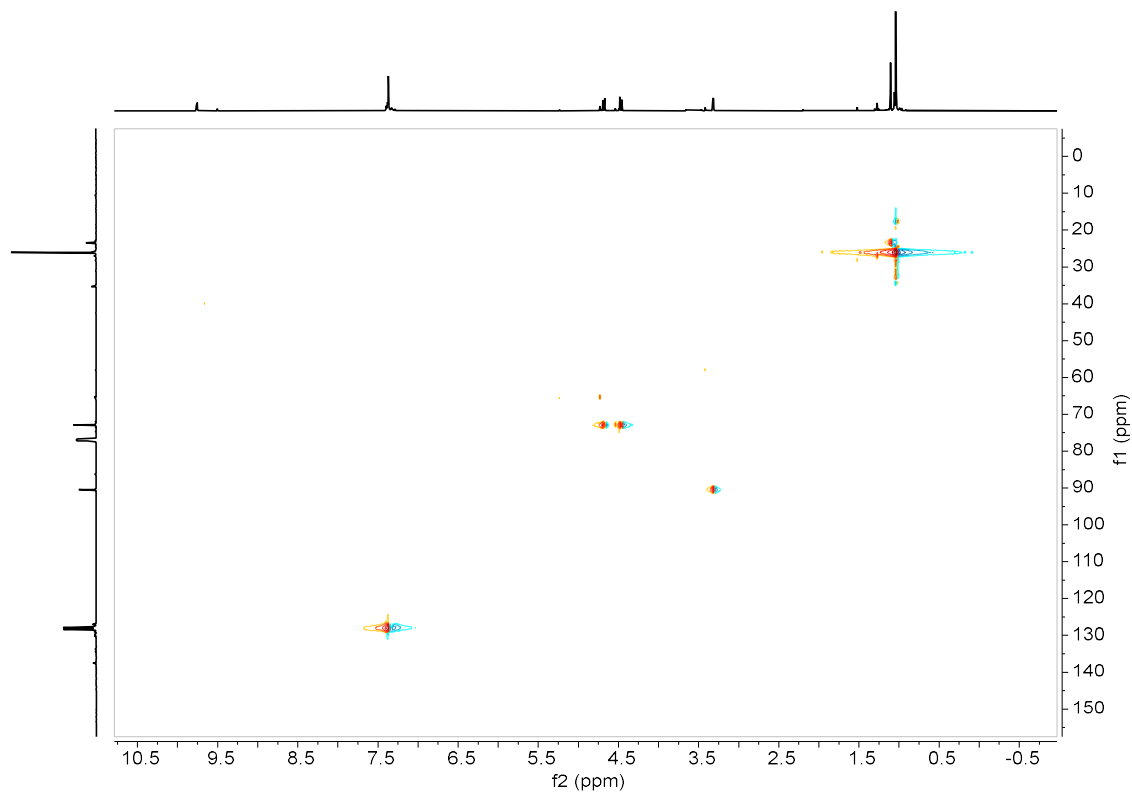
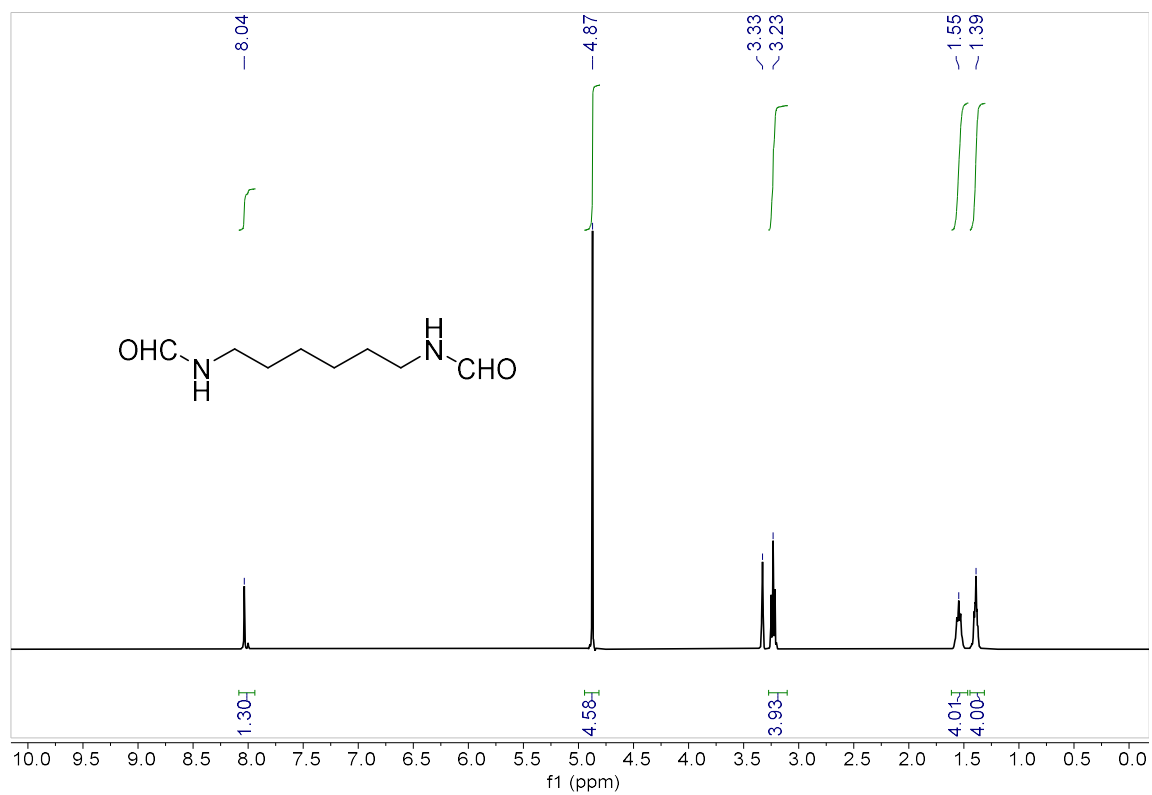
(S)-2-(benzyloxy)-4-methylpentanal (**41c**). $^1\text{H-NMR}$ (CDCl_3)(S)-2-(benzyloxy)-3,3-dimethylbutanal (**41d**). $^1\text{H-NMR}$ (CDCl_3)

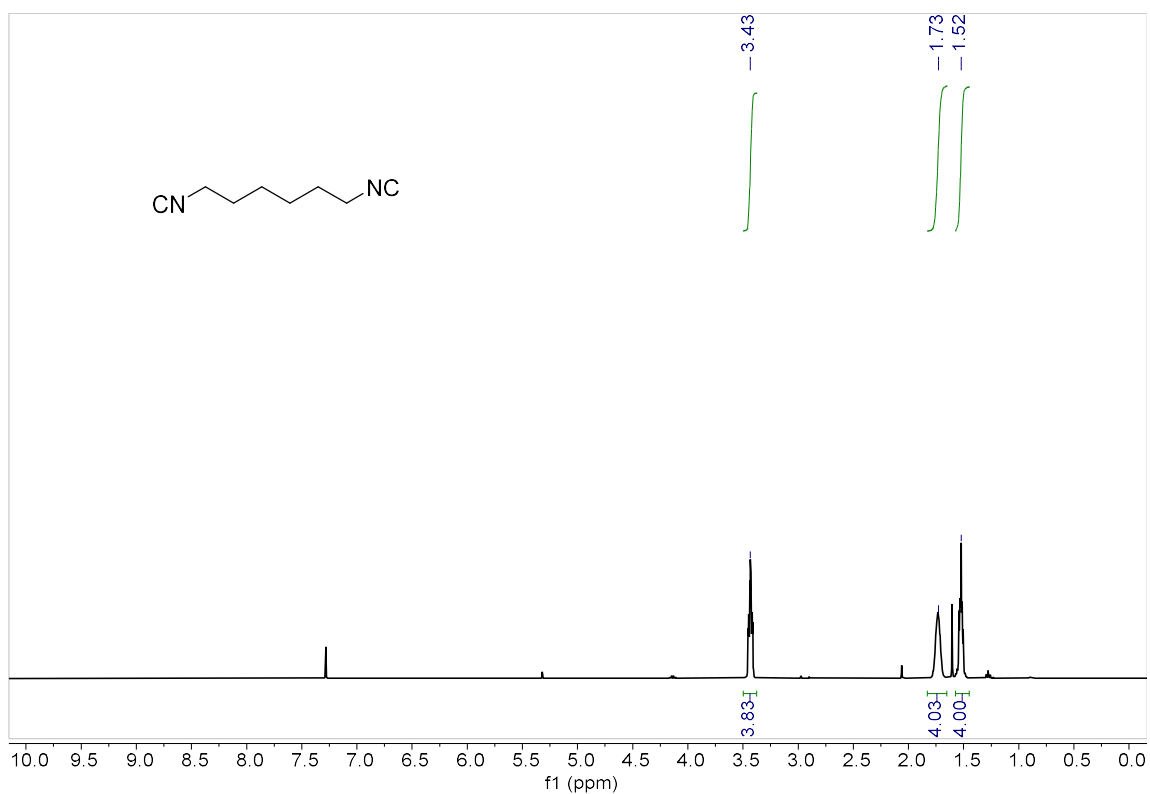
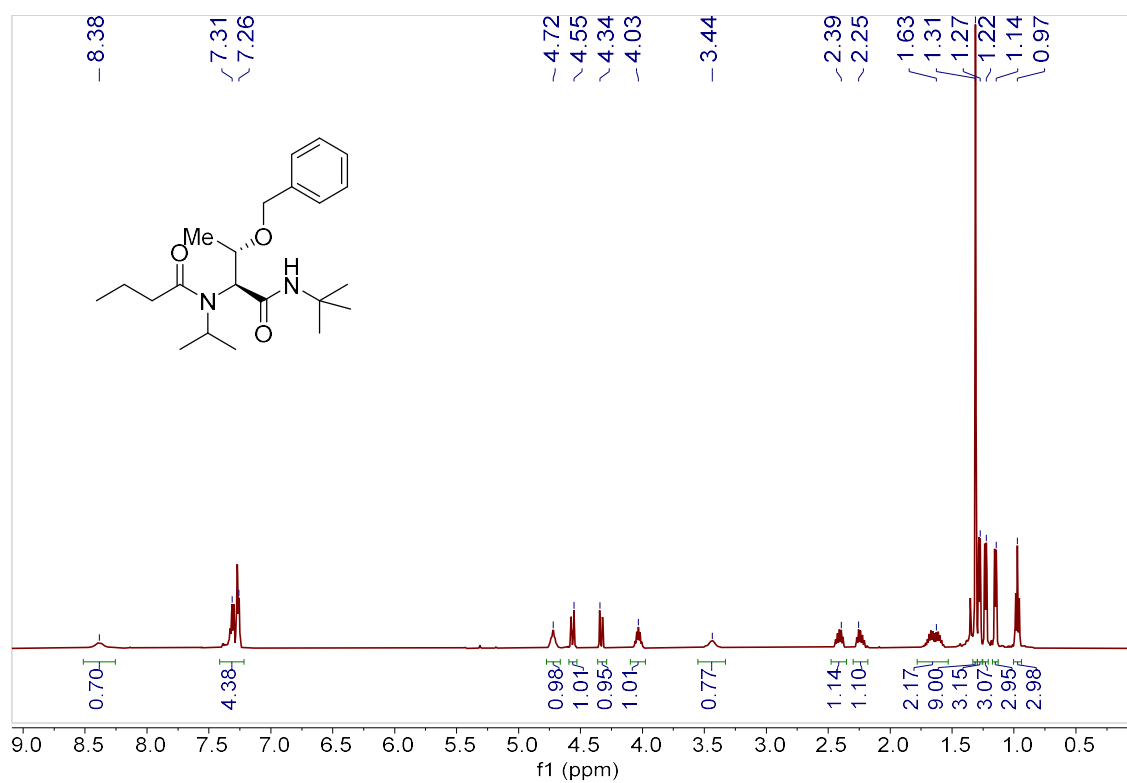
(S)-2-(benzyloxy)-3,3-dimethylbutanal (**41d**). ^{13}C -NMR (CDCl_3)



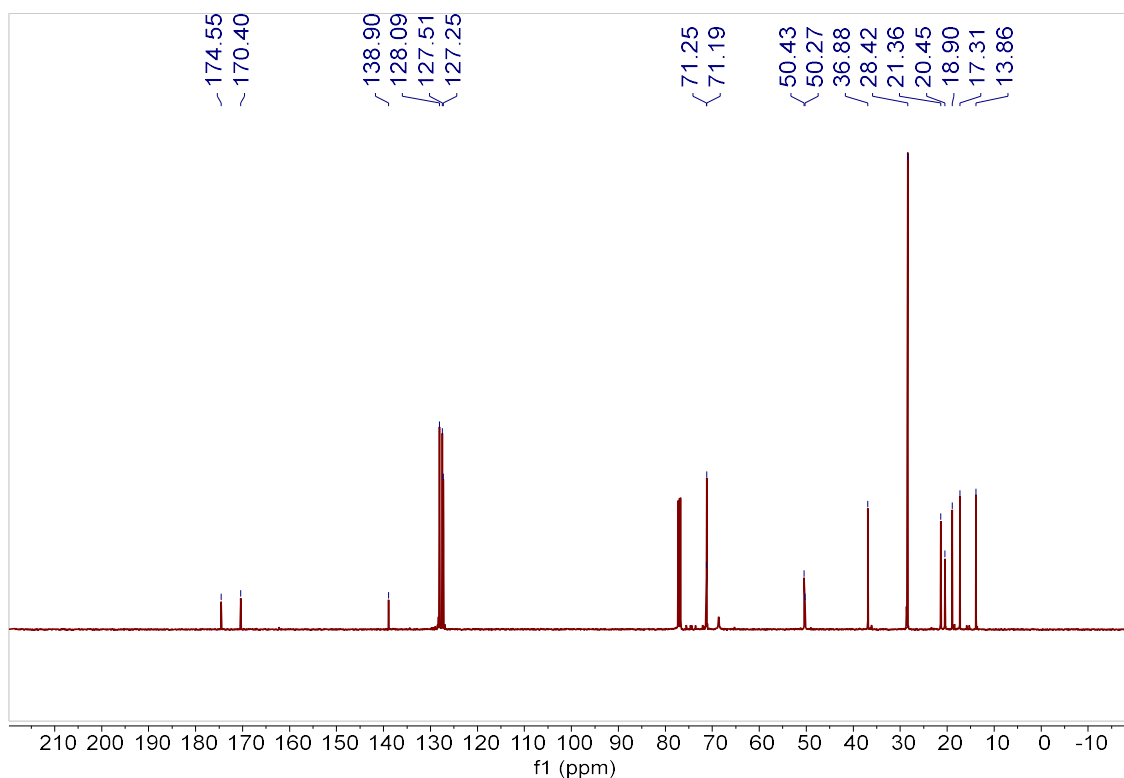
(S)-2-(benzyloxy)-3,3-dimethylbutanal (**41d**). g-COSY (CDCl_3)



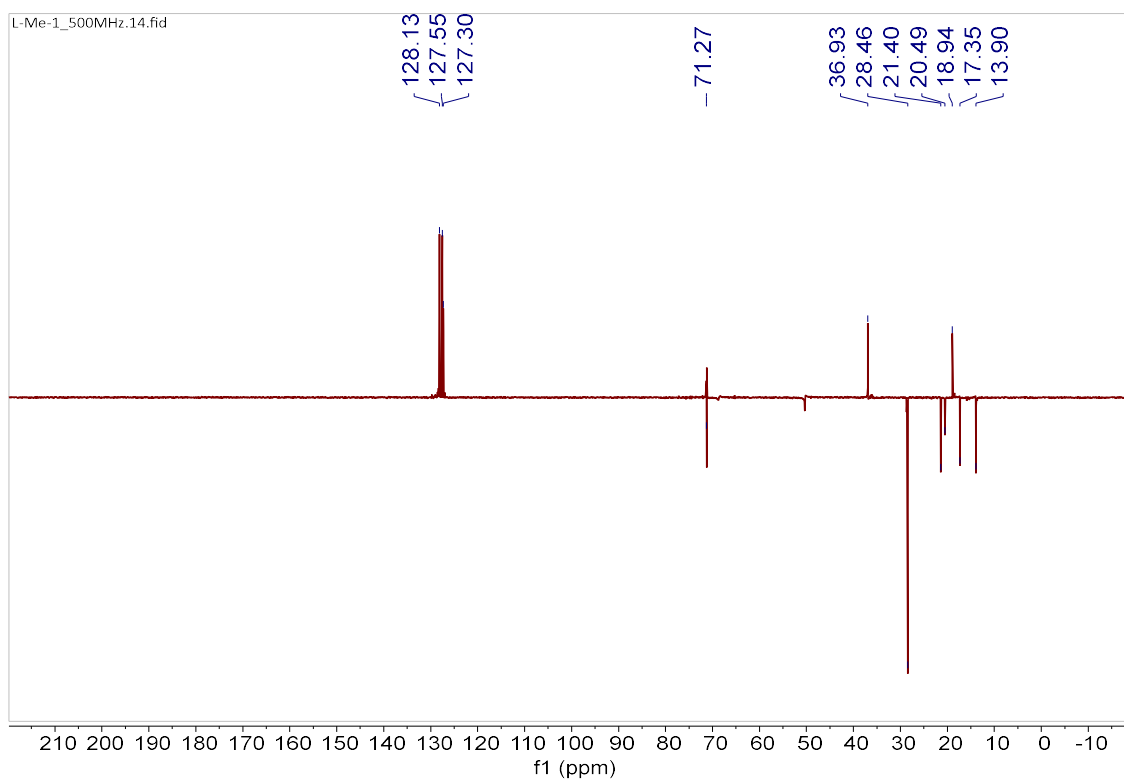
(S)-2-(benzyloxy)-3,3-dimethylbutanal (**41d**). g-HSQC(CDCl₃)N,N'-(hexane-1,6-diyl)diformamide. ¹H-NMR (CDCl₃)

1,6-diisocyanohexane (**47**). $^1\text{H-NMR}$ (CDCl_3)(2S,3S)-3-(benzyloxy)-N-(tert-butyl)-2-(N-isopropylbutyramido) butanamide (**45a-D1**). $^1\text{H-NMR}$ (CDCl_3)

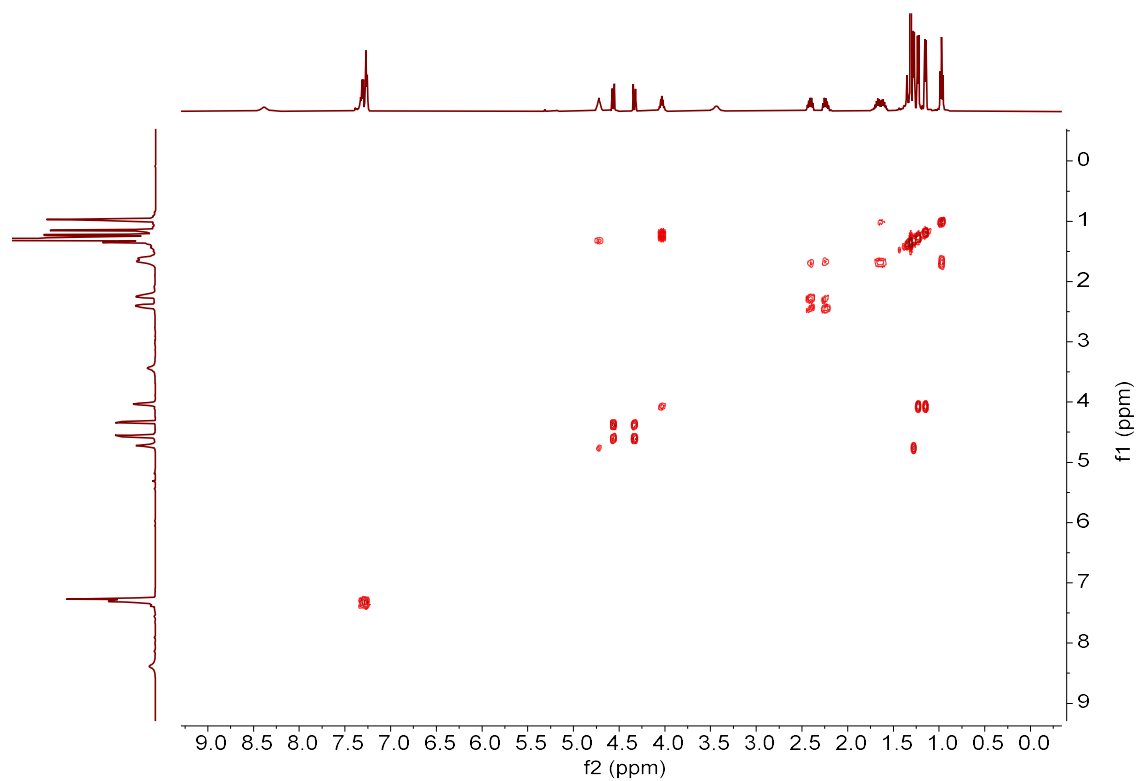
(2S,3S)-3-(benzyloxy)-N-(tert-butyl)-2-(N-isopropylbutyramido) butanamide (**45a-D1**).
¹³C-NMR (CDCl₃)



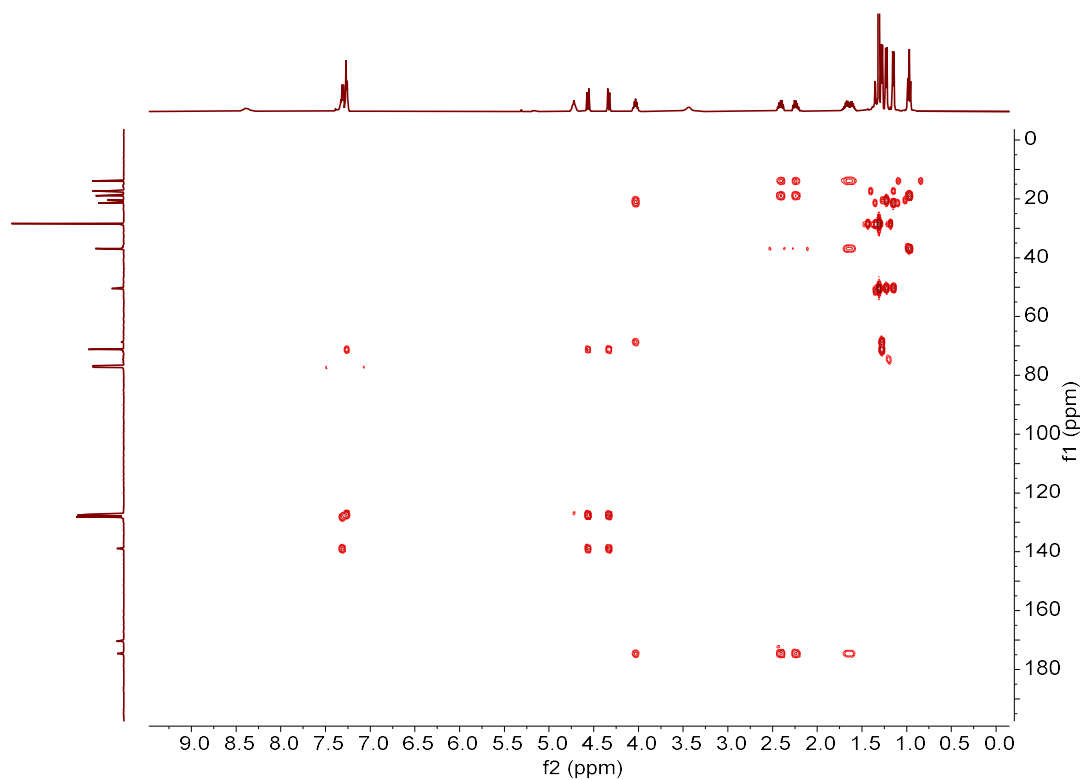
(2S,3S)-3-(benzyloxy)-N-(tert-butyl)-2-(N-isopropylbutyramido) butanamide (**45a-D1**).
DEPT 135 (CDCl₃)



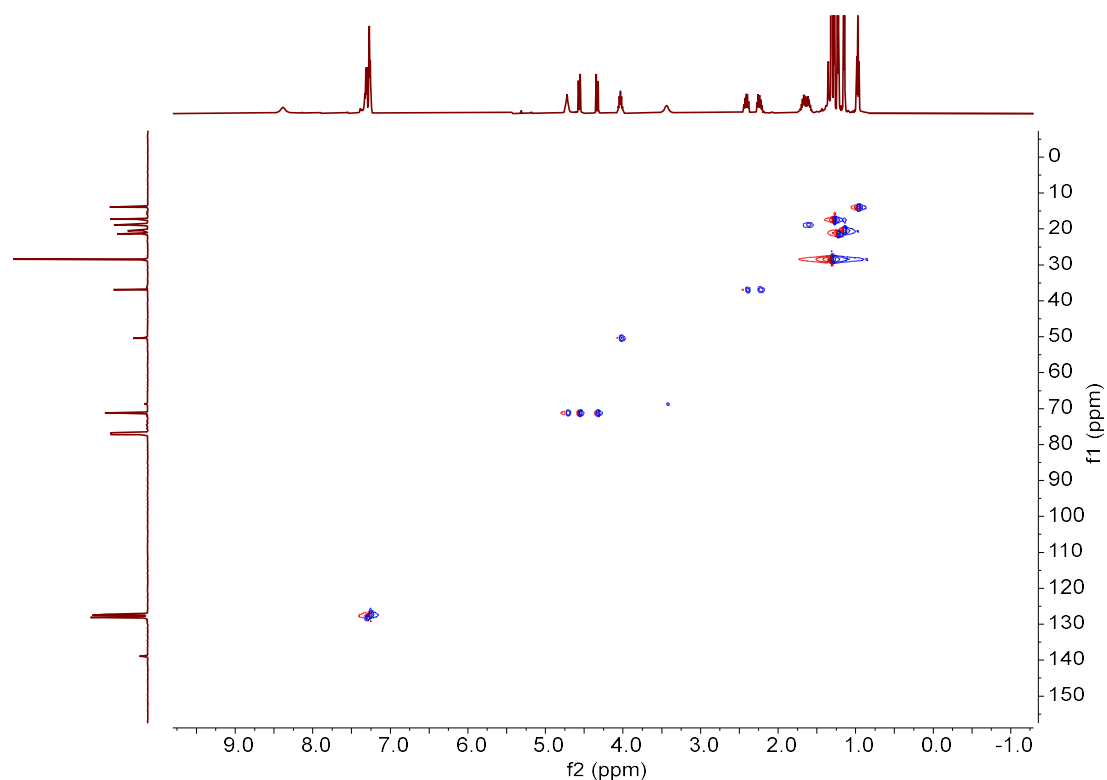
(2S,3S)-3-(benzyloxy)-N-(tert-butyl)-2-(N-isopropylbutyramido) butanamide (**45a-D1**).
g-COSY (CDCl₃)



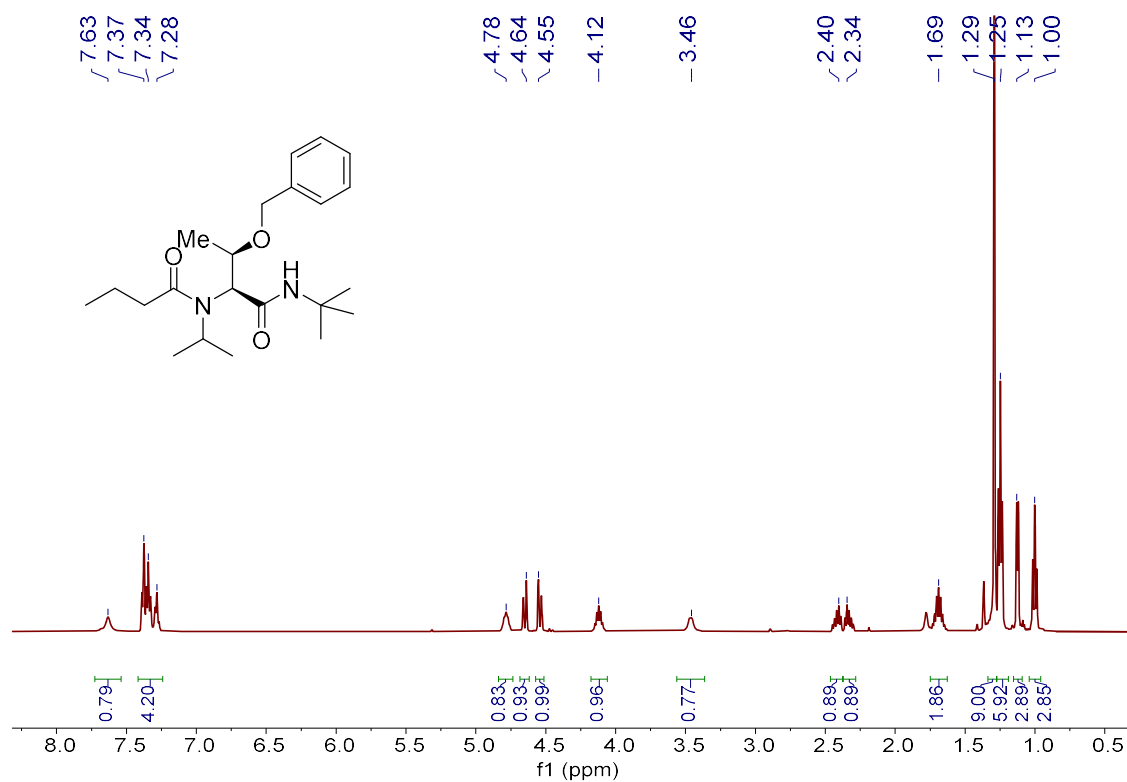
(2S,3S)-3-(benzyloxy)-N-(tert-butyl)-2-(N-isopropylbutyramido) butanamide (**45a-D1**).
g-HSQC (CDCl₃)



(2S,3S)-3-(benzyloxy)-N-(tert-butyl)-2-(N-isopropylbutyramido) butanamide (**45a-D1**).
g-HMBC (CDCl₃)

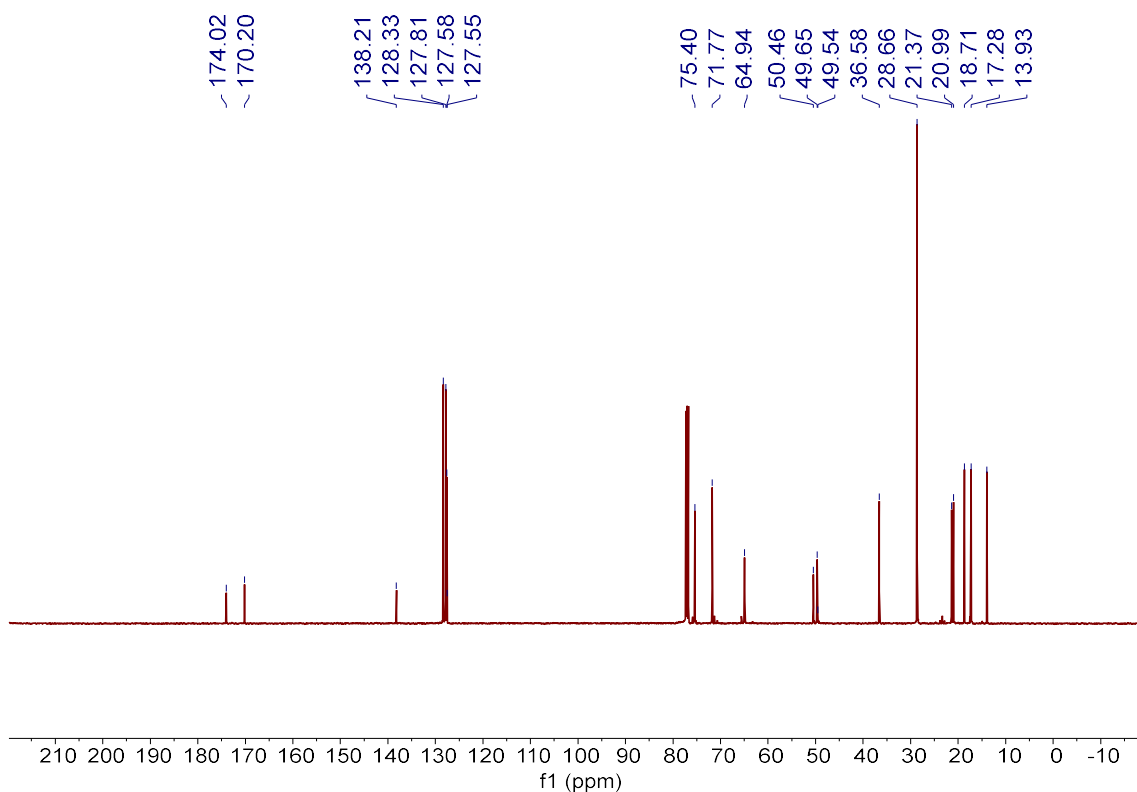


(2S,3R)-3-(benzyloxy)-N-(tert-butyl)-2-(N-isopropylbutyramido) butanamide (**45a-D2**).
¹H-NMR (CDCl₃)

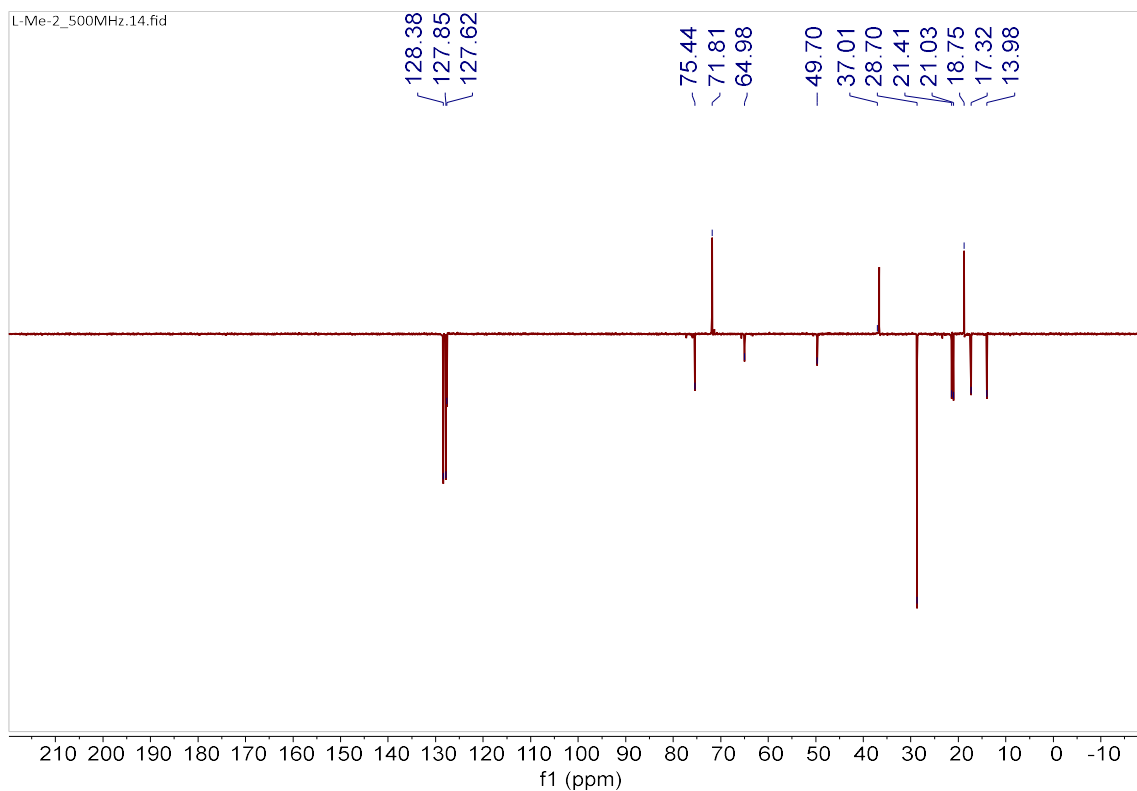


ANNEX IV

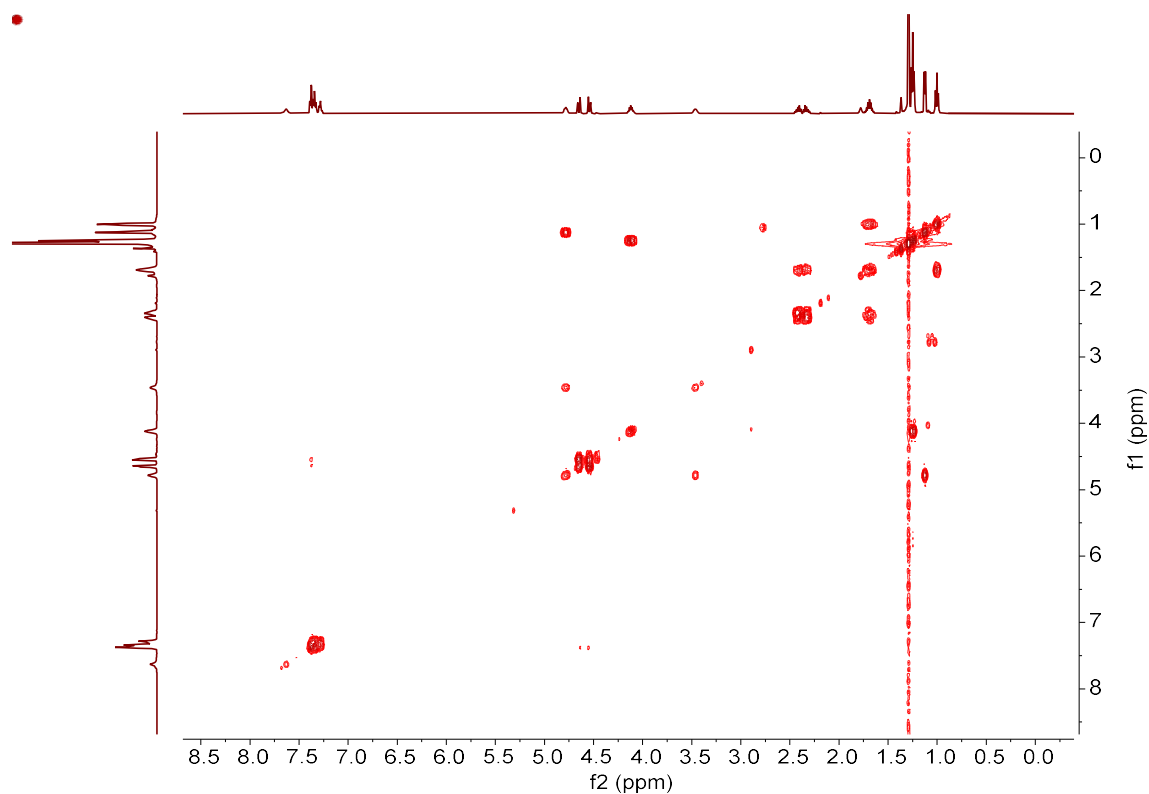
(2S,3R)-3-(benzyloxy)-N-(tert-butyl)-2-(N-isopropylbutyramido) butanamide (**45a-D2**).
 ^{13}C -NMR (CDCl_3)



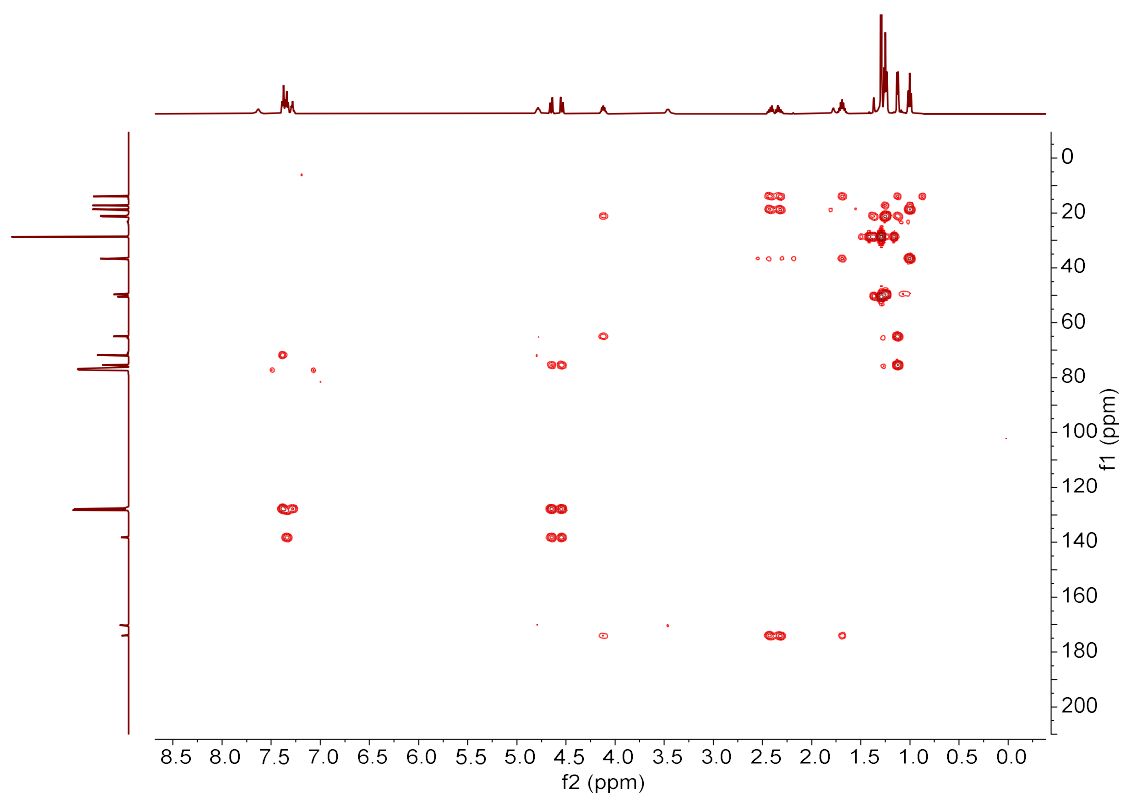
(2S,3R)-3-(benzyloxy)-N-(tert-butyl)-2-(N-isopropylbutyramido) butanamide (**45a-D2**).
DEPT 135 (CDCl_3)



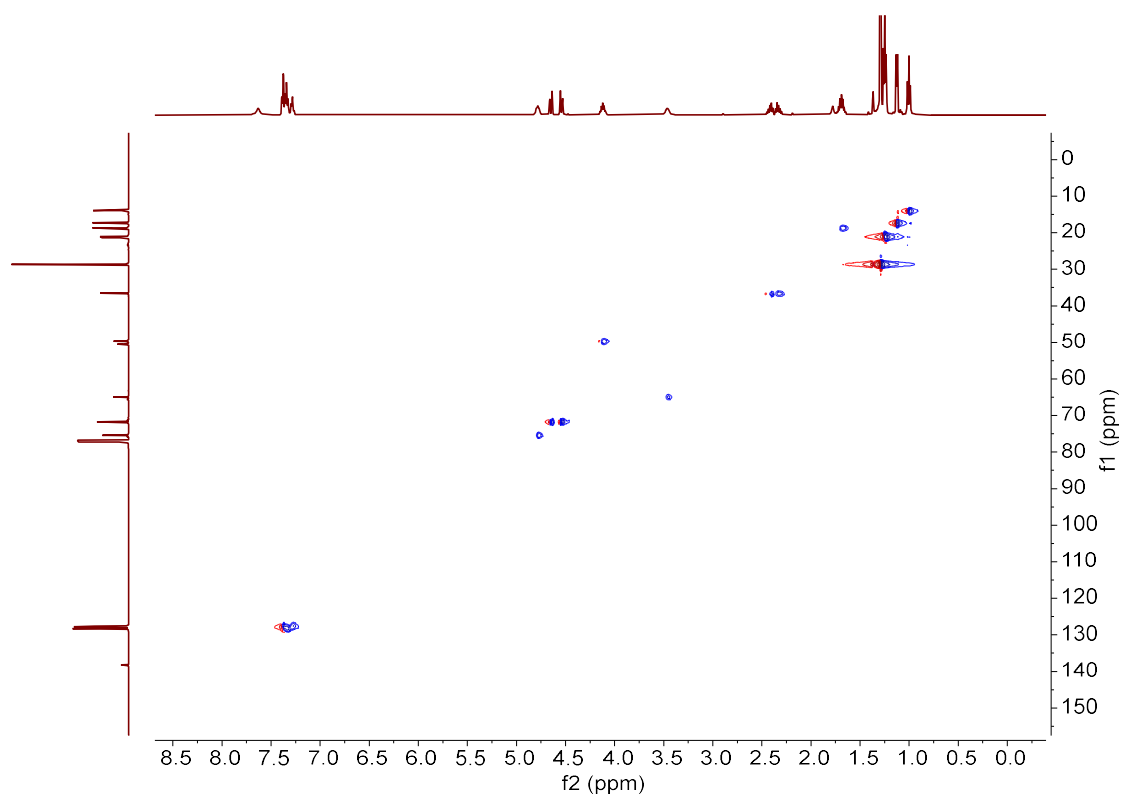
(2S,3R)-3-(benzyloxy)-N-(tert-butyl)-2-(N-isopropylbutyramido) butanamide (**45a-D2**).
g-COSY (CDCl₃)



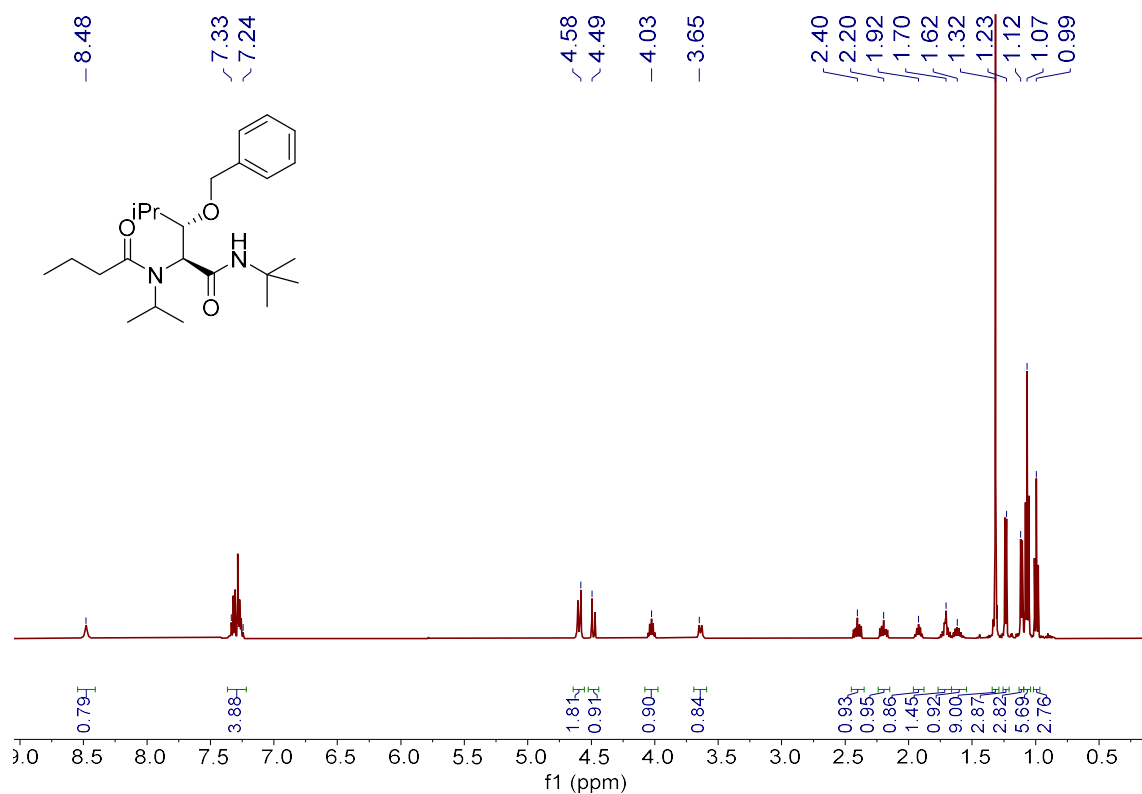
(2S,3R)-3-(benzyloxy)-N-(tert-butyl)-2-(N-isopropylbutyramido) butanamide (**45a-D2**).
g-HSQC (CDCl₃)



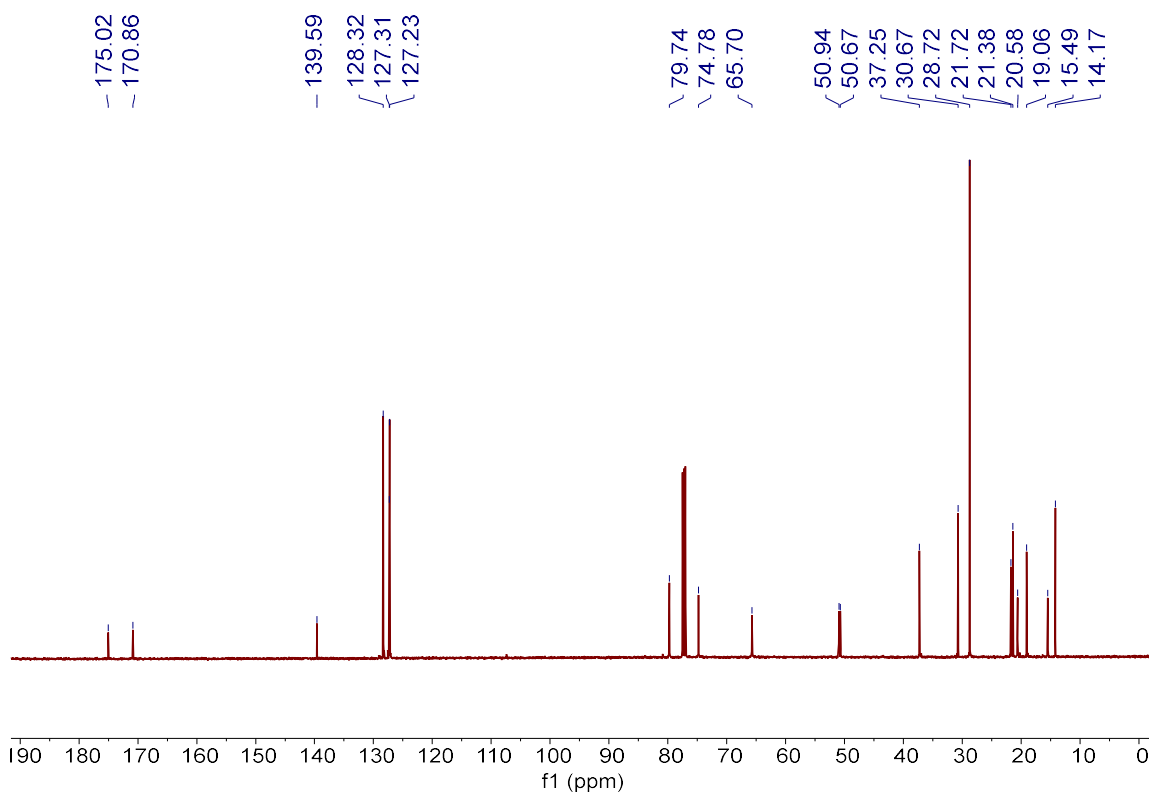
(2S,3R)-3-(benzyloxy)-N-(tert-butyl)-2-(N-isopropylbutyramido) butanamide (**45a-D2**).
g-HMBC (CDCl₃)



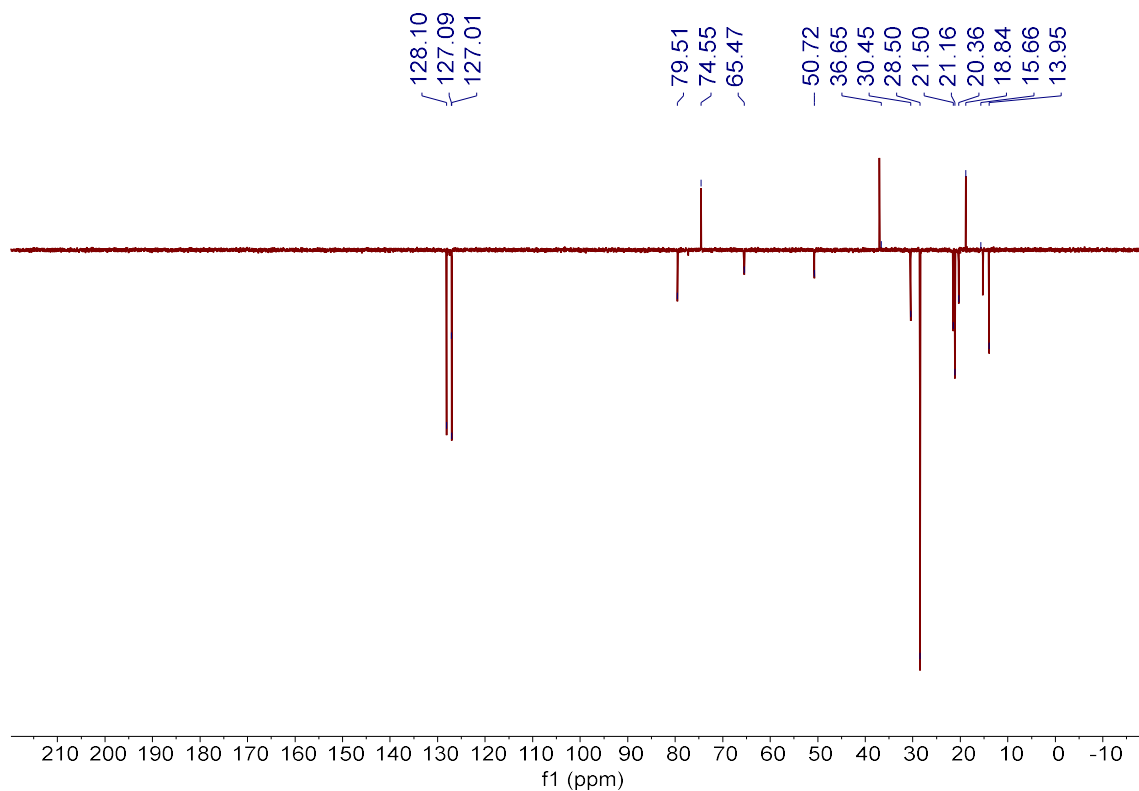
(2S,3S)-3-(benzyloxy)-N-(tert-butyl)-2-(N-isopropylbutyramido)-4-methylpentanamide (**45b-D1**). ¹H-NMR (CDCl₃)



(2S,3S)-3-(benzyloxy)-N-(tert-butyl)-2-(N-isopropylbutyramido)-4-methylpentanamide
(45b-D1). ^{13}C -NMR (CDCl_3)

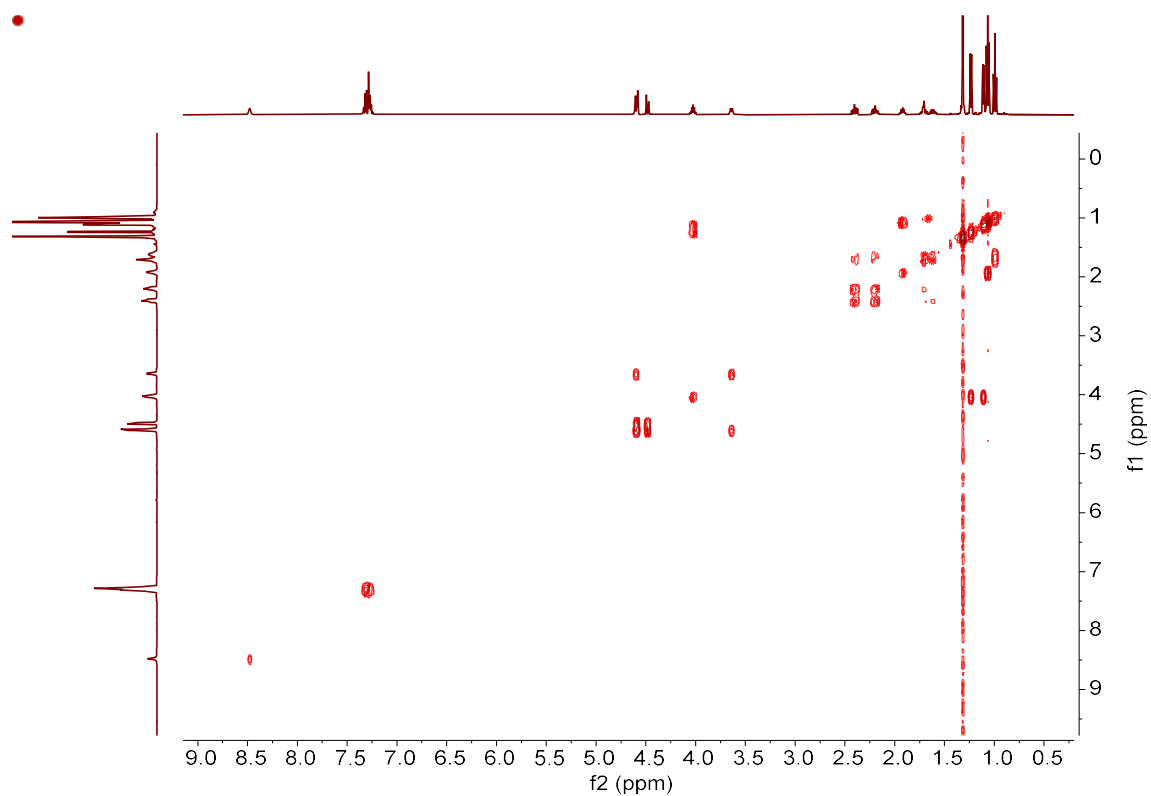


(2S,3S)-3-(benzyloxy)-N-(tert-butyl)-2-(N-isopropylbutyramido)-4-methylpentanamide
(45b-D1). DEPT 135 (CDCl_3)

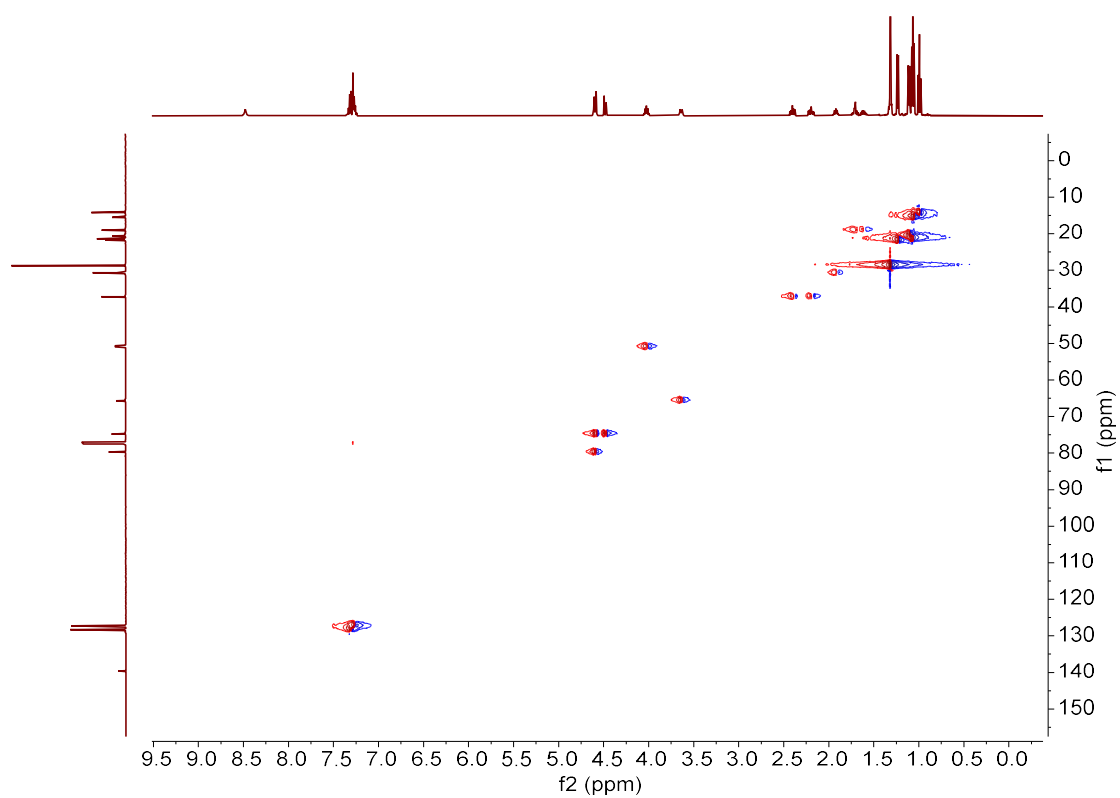


ANNEX IV

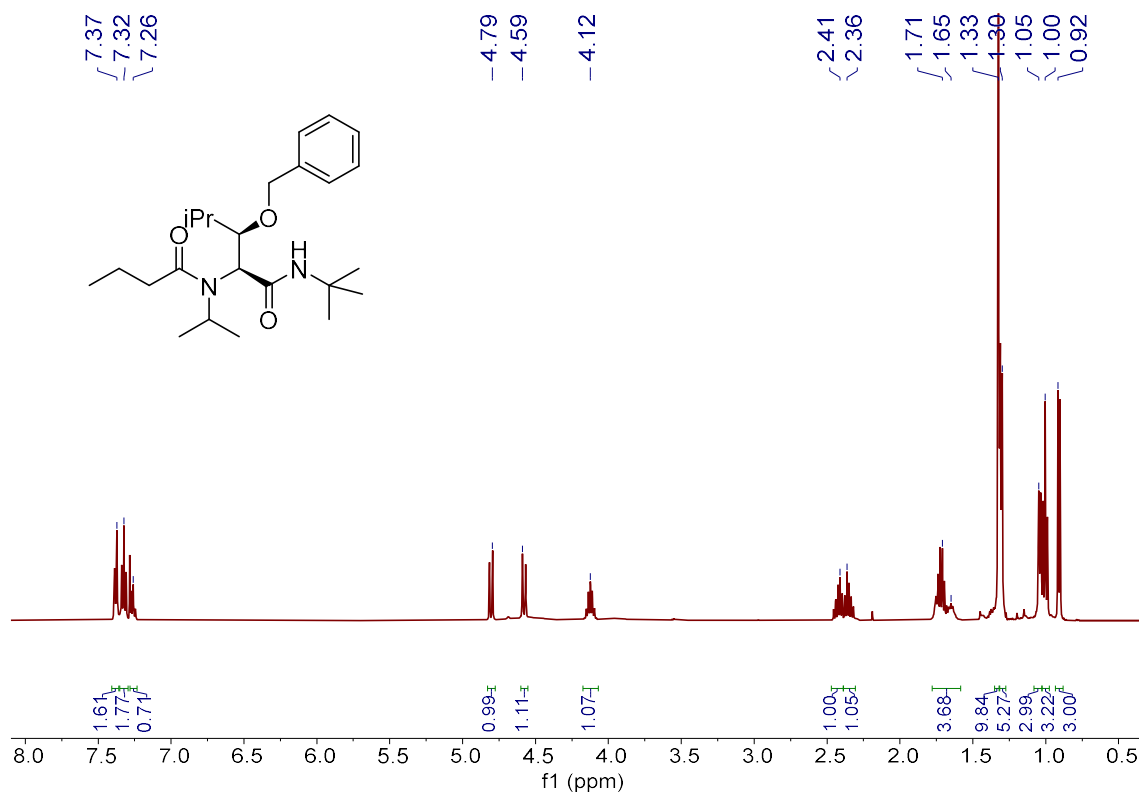
(2S,3S)-3-(benzyloxy)-N-(tert-butyl)-2-(N-isopropylbutyramido)-4-methylpentanamide
(45b-D1). g-COSY (CDCl₃)



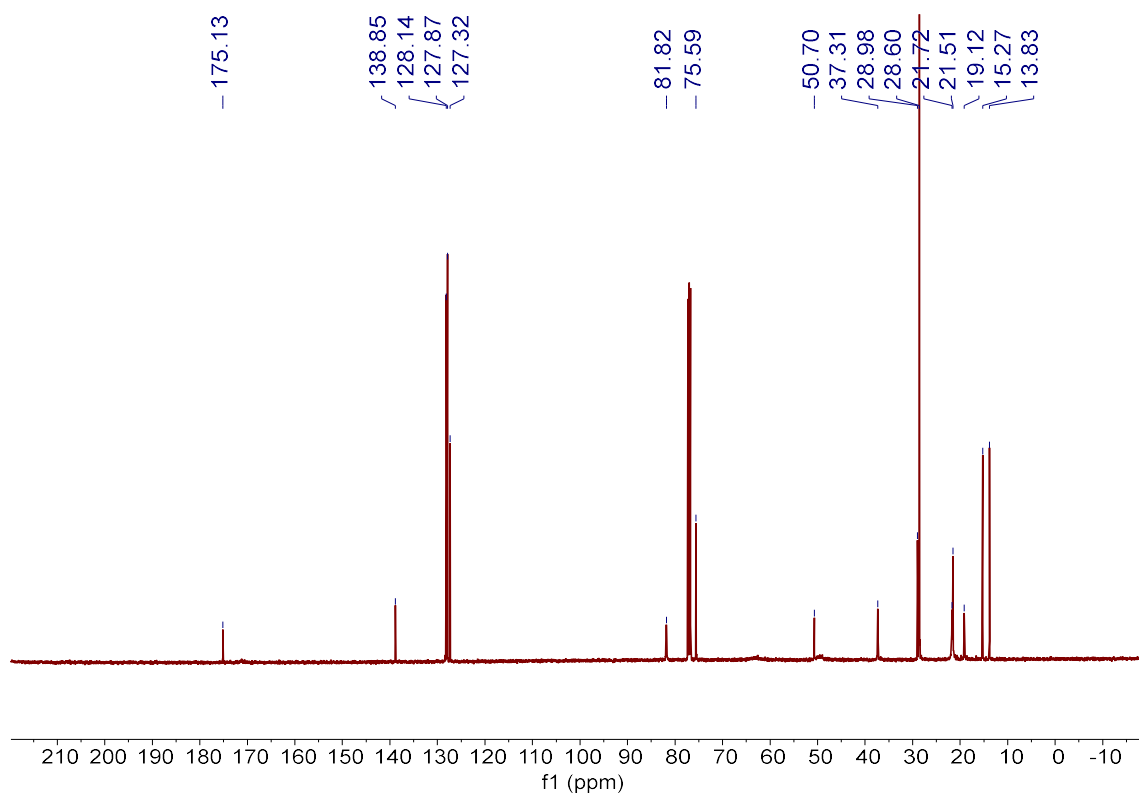
(2S,3S)-3-(benzyloxy)-N-(tert-butyl)-2-(N-isopropylbutyramido)-4-methylpentanamide
(45b-D1). g-HMBC (CDCl₃)



(2S,3R)-3-(benzyloxy)-N-(tert-butyl)-2-(N-isopropylbutyramido)-4-methylpentanamide
(45b-D2). ¹H-NMR (CDCl₃)

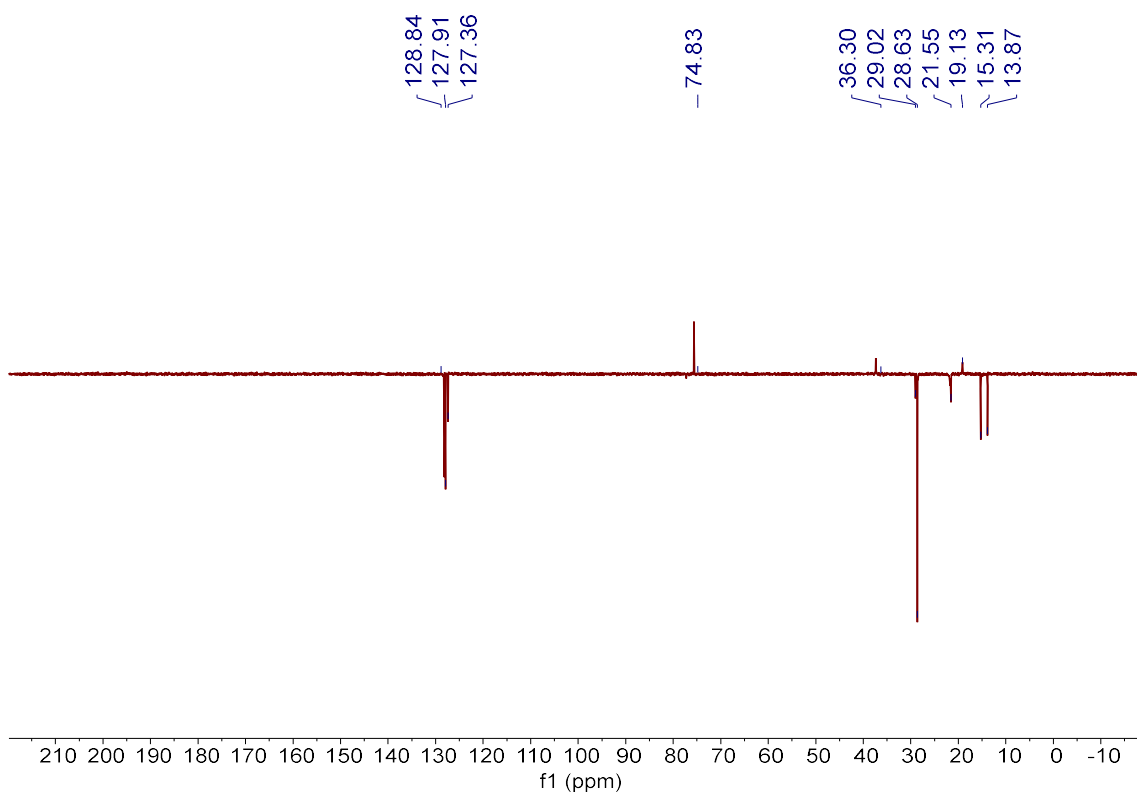


(2S,3R)-3-(benzyloxy)-N-(tert-butyl)-2-(N-isopropylbutyramido)-4-methylpentanamide
(45b-D2). ¹³C-NMR (CDCl₃)

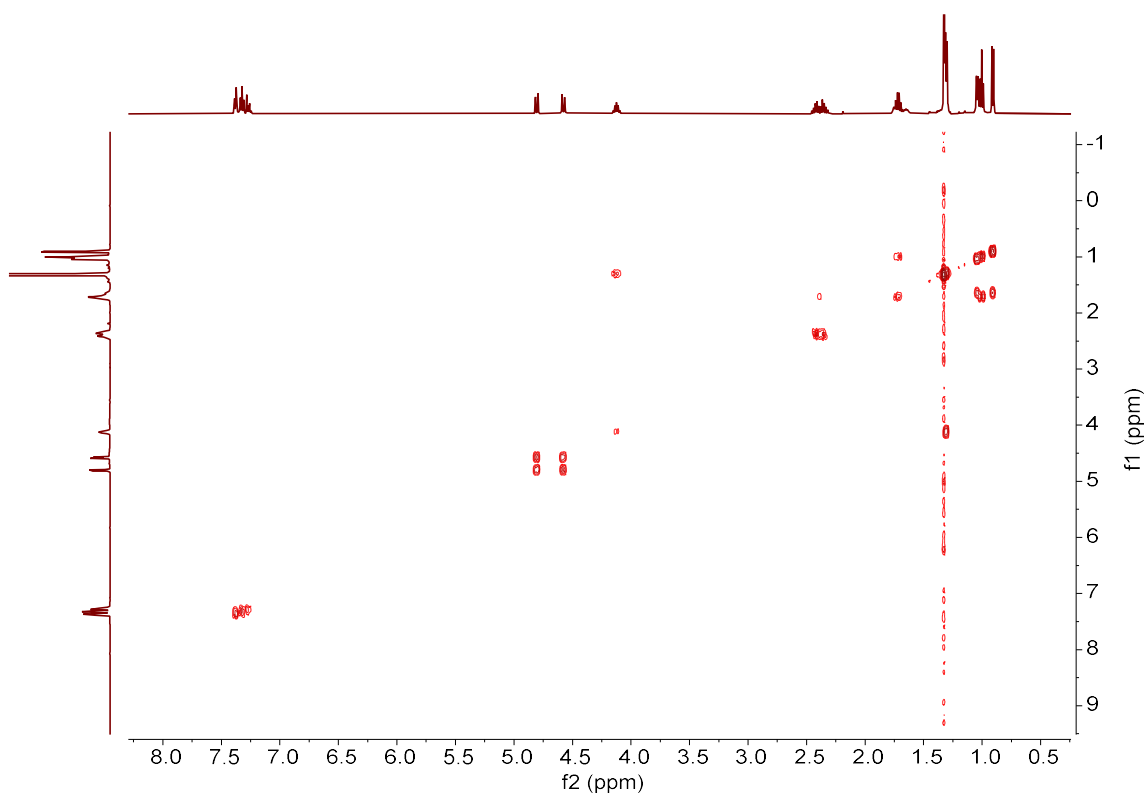


ANNEX IV

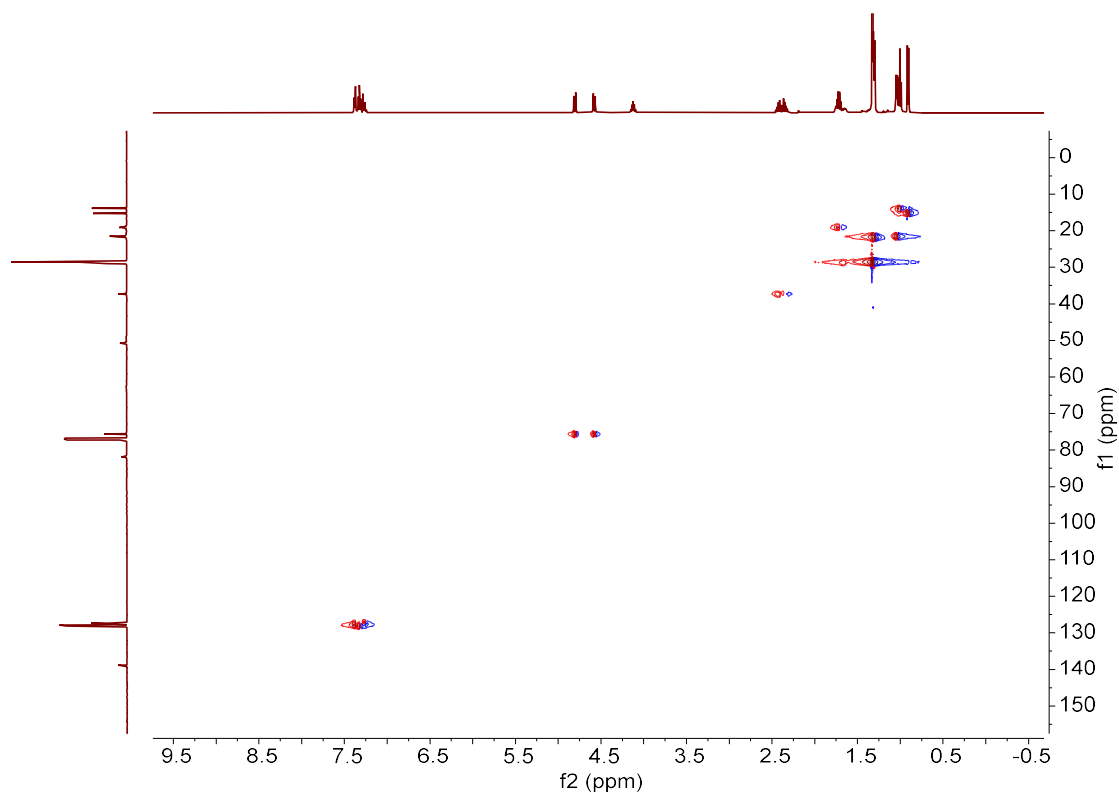
(2S,3R)-3-(benzyloxy)-N-(tert-butyl)-2-(N-isopropylbutyramido)-4-methylpentanamide
(45b-D2). DEPT 135 (CDCl₃)



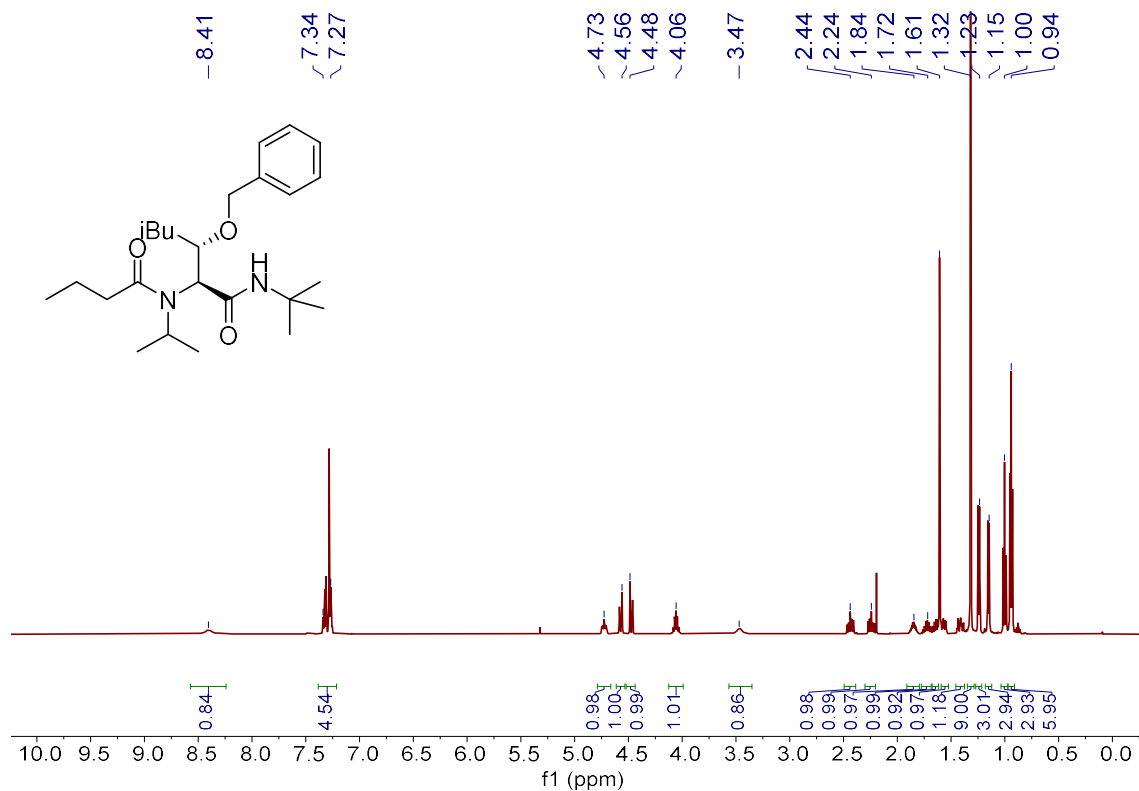
(2S,3R)-3-(benzyloxy)-N-(tert-butyl)-2-(N-isopropylbutyramido)-4-methylpentanamide
(45b-D2). g-COSY (CDCl₃)



(2S,3R)-3-(benzyloxy)-N-(tert-butyl)-2-(N-isopropylbutyramido)-4-methylpentanamide
(45b-D2). g-HMBC (CDCl₃)

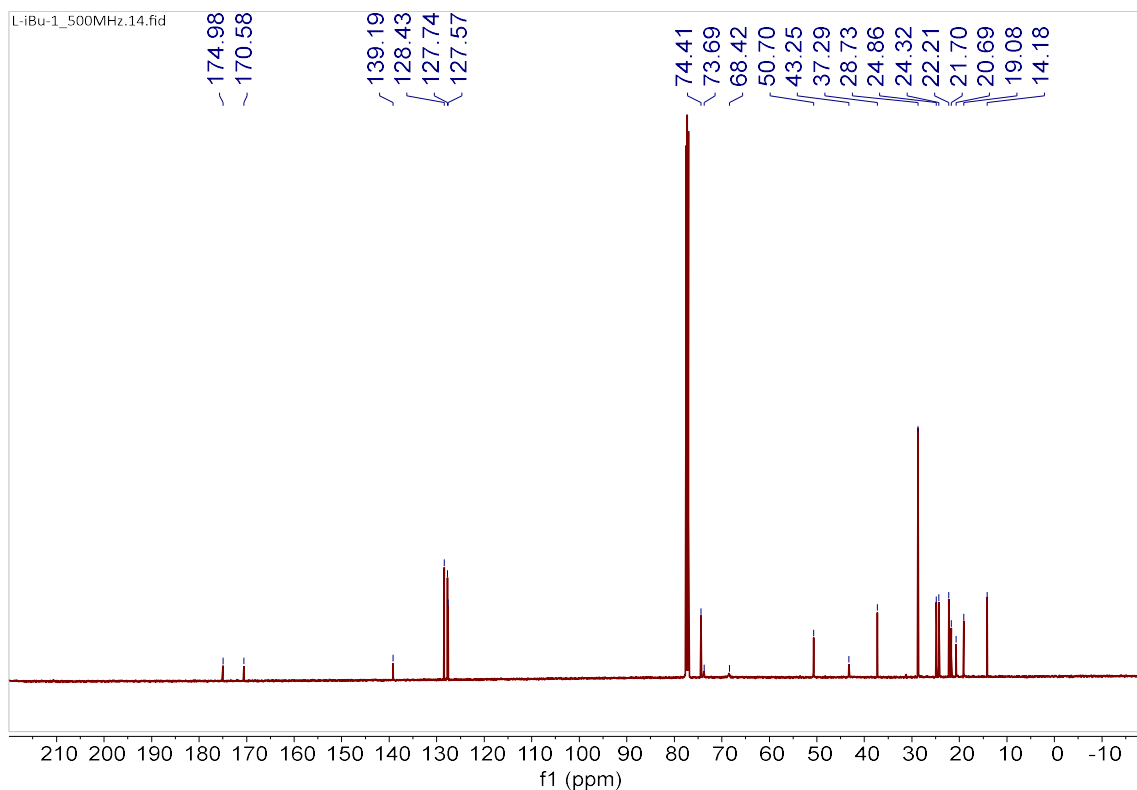


(2S,3S)-3-(benzyloxy)-N-(tert-butyl)-2-(N-isopropylbutyramido)-5-methylhexanamide
(45c-D1). ¹H-NMR (CDCl₃)

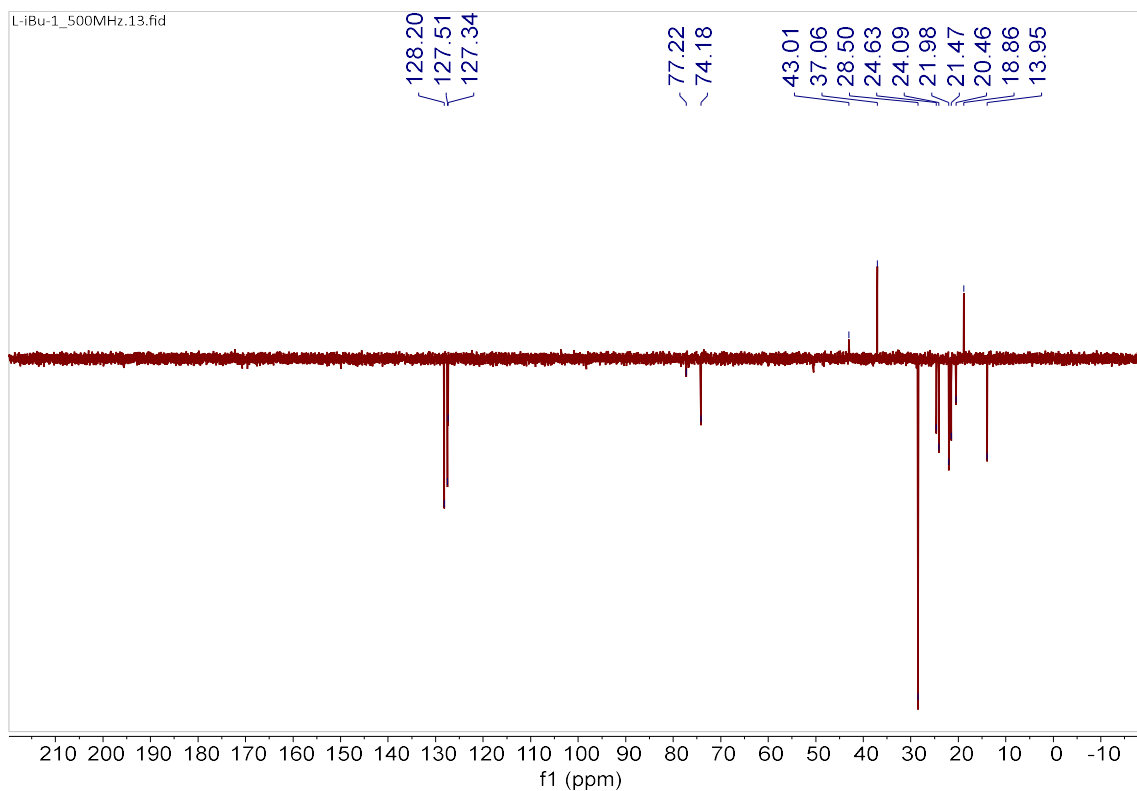


ANNEX IV

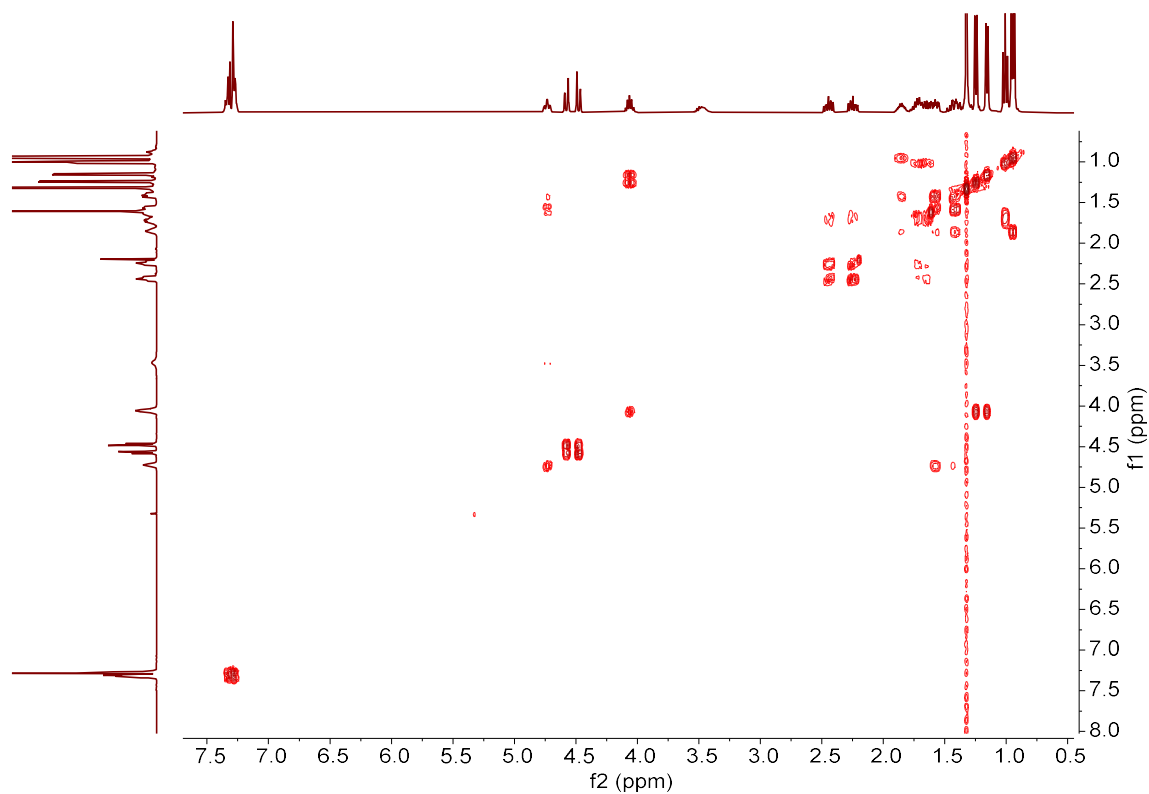
(2S,3S)-3-(benzyloxy)-N-(tert-butyl)-2-(N-isopropylbutyramido)-5-methylhexanamide
(45c-D1). ¹³C-NMR (CDCl₃)



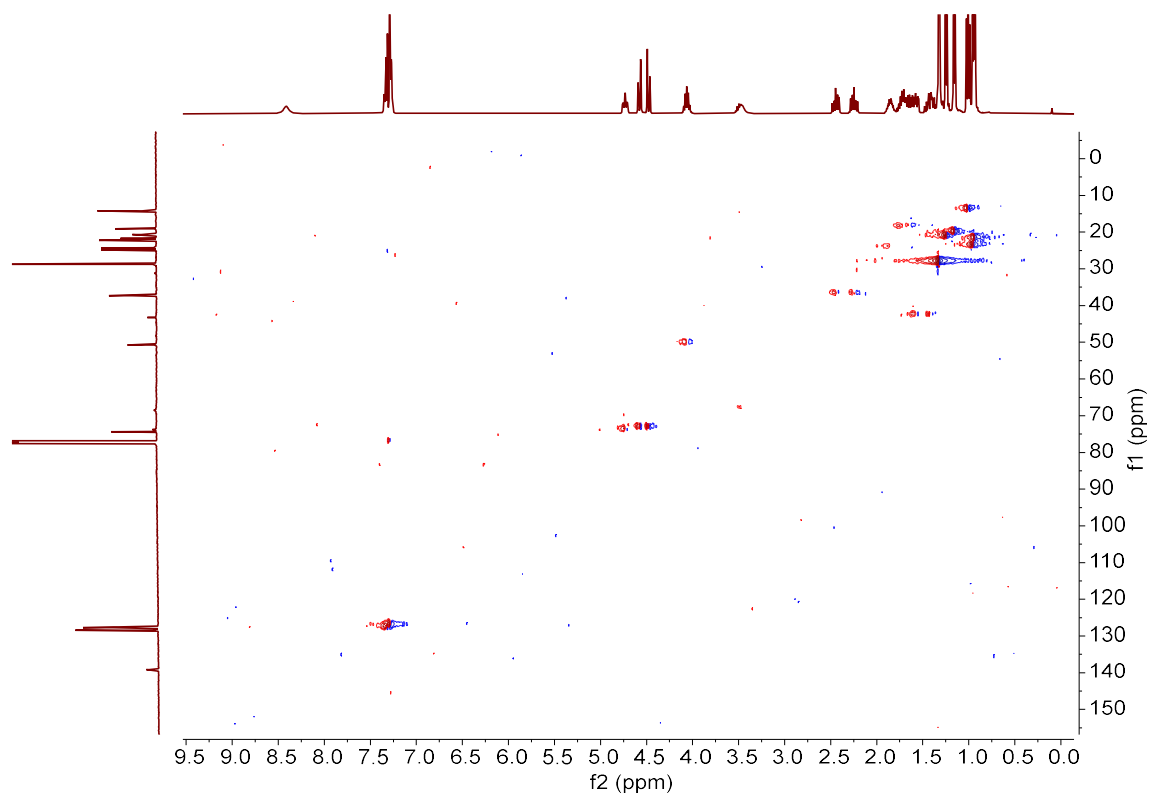
(2S,3S)-3-(benzyloxy)-N-(tert-butyl)-2-(N-isopropylbutyramido)-5-methylhexanamide
(45c-D1). DEPT 135 (CDCl₃)



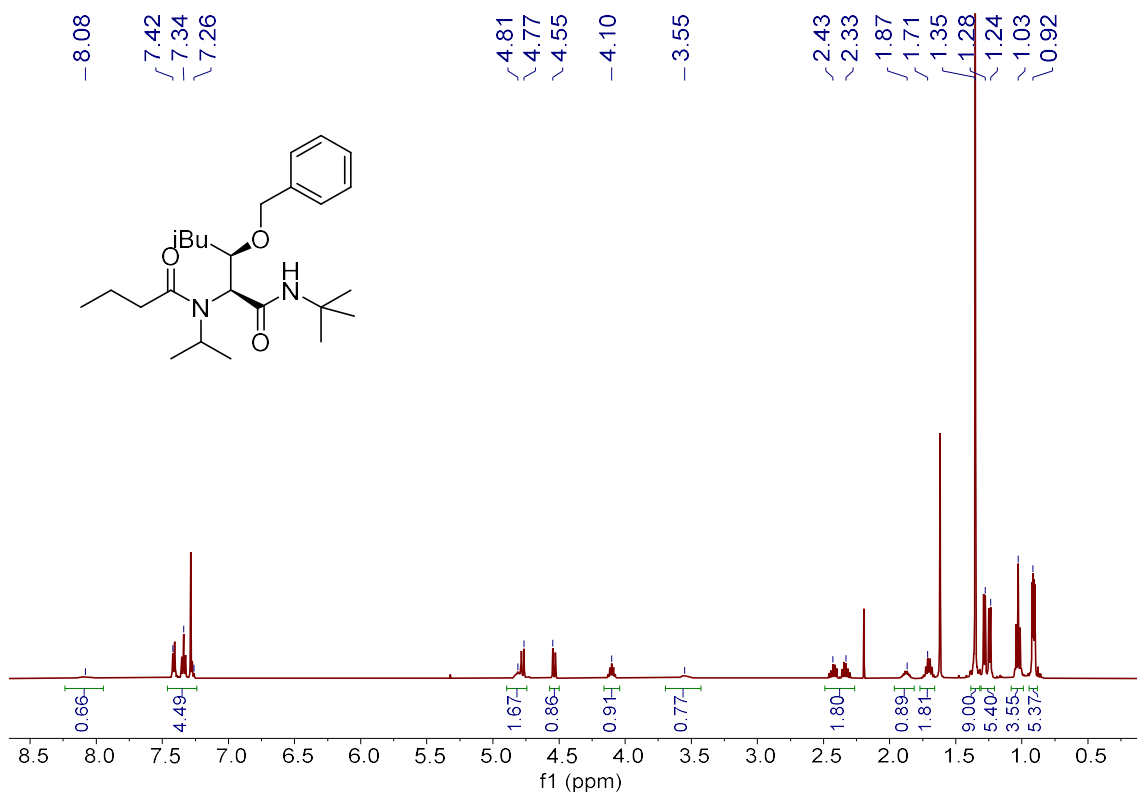
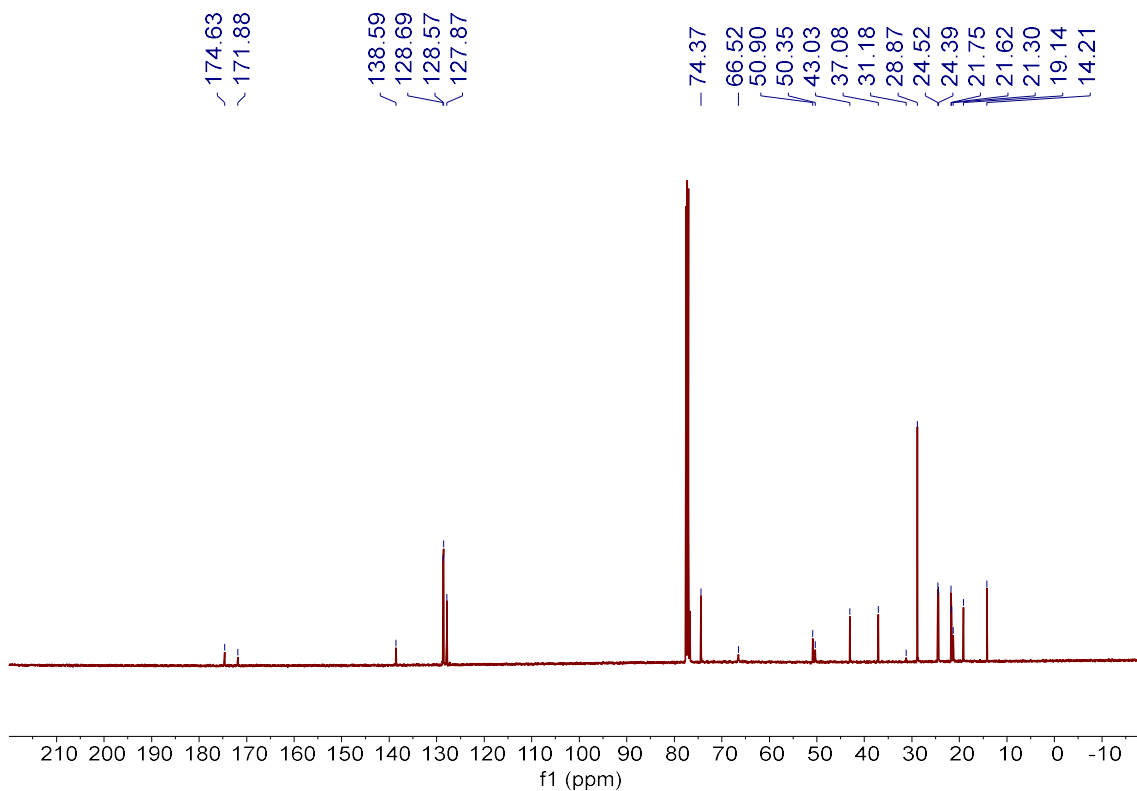
(2S,3S)-3-(benzyloxy)-N-(tert-butyl)-2-(N-isopropylbutyramido)-5-methylhexanamide
(45c-D1). g-COSY (CDCl₃)



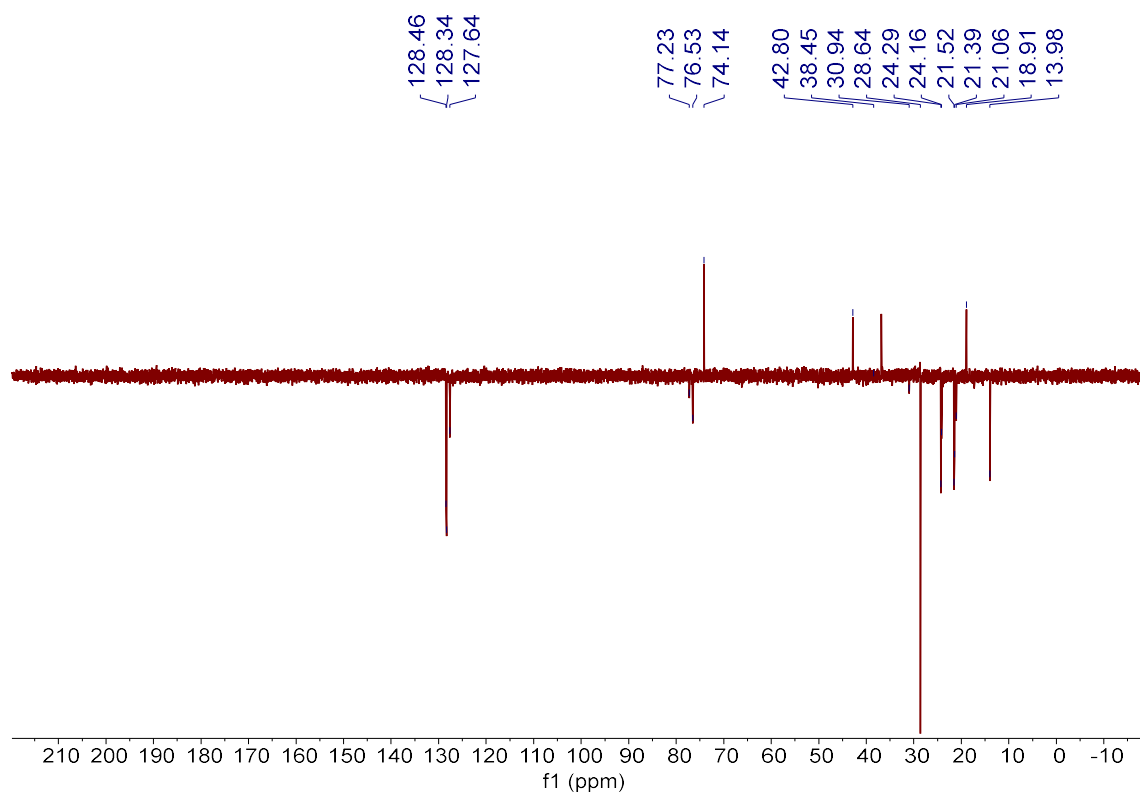
(2S,3S)-3-(benzyloxy)-N-(tert-butyl)-2-(N-isopropylbutyramido)-5-methylhexanamide
(45c-D1). g-HMBC (CDCl₃)



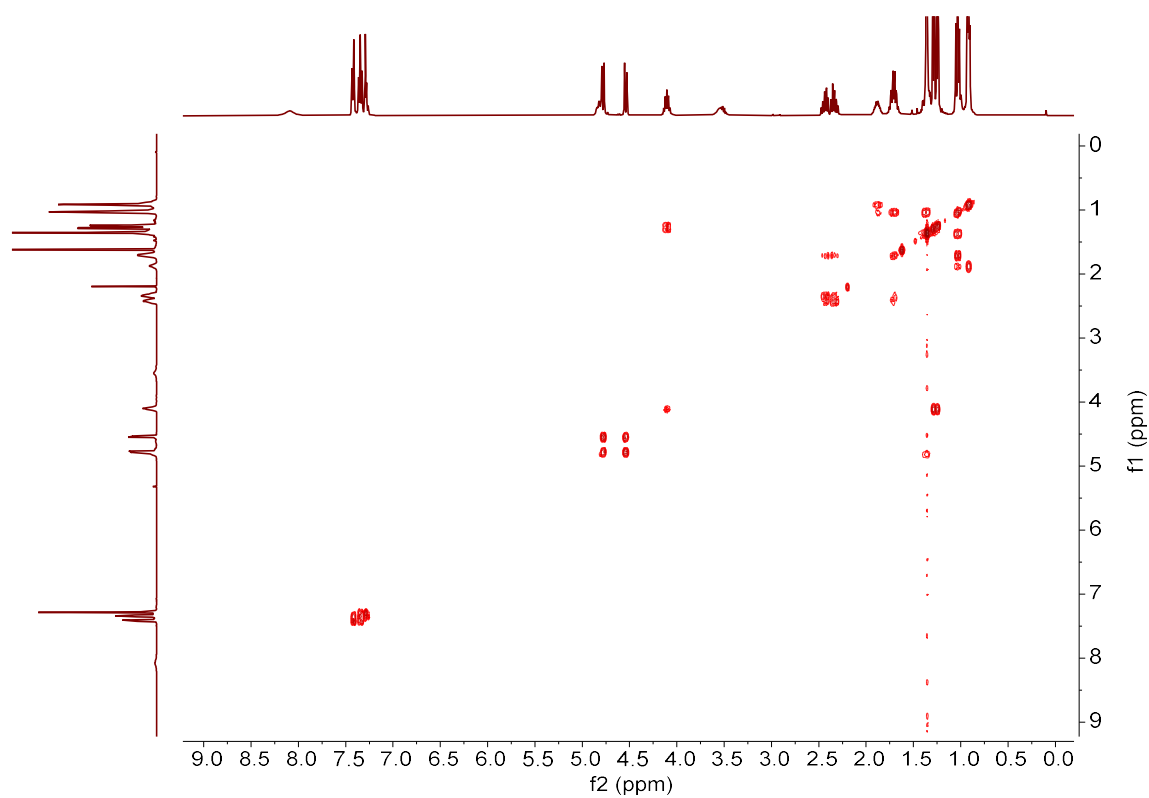
ANNEX IV

(2S,3R)-3-(benzyloxy)-N-(tert-butyl)-2-(N-isopropylbutyramido)-5-methylhexanamide
(45c-D2). ¹H-NMR (CDCl₃)(2S,3R)-3-(benzyloxy)-N-(tert-butyl)-2-(N-isopropylbutyramido)-5-methylhexanamide
(45c-D2). ¹³C-NMR (CDCl₃)

(2S,3R)-3-(benzyloxy)-N-(tert-butyl)-2-(N-isopropylbutyramido)-5-methylhexanamide
(45c-D2). DEPT 135 (CDCl₃)

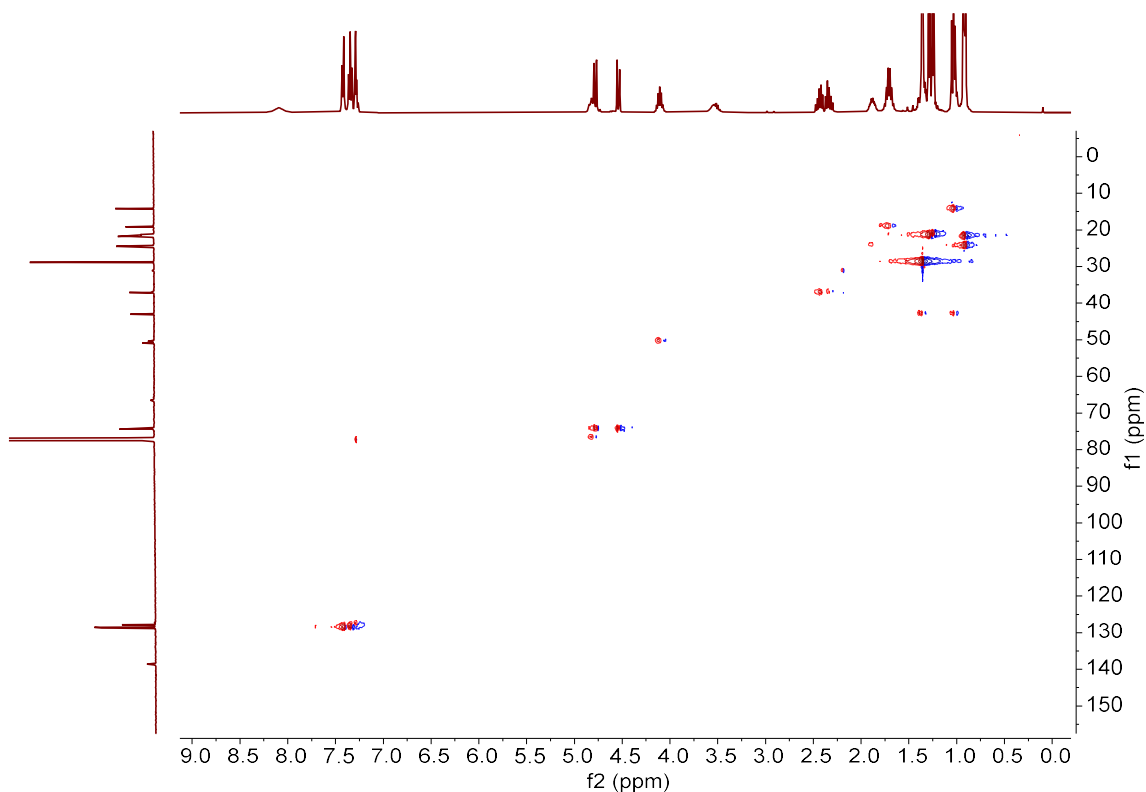


(2S,3R)-3-(benzyloxy)-N-(tert-butyl)-2-(N-isopropylbutyramido)-5-methylhexanamide
(45c-D2). g-COSY (CDCl₃)

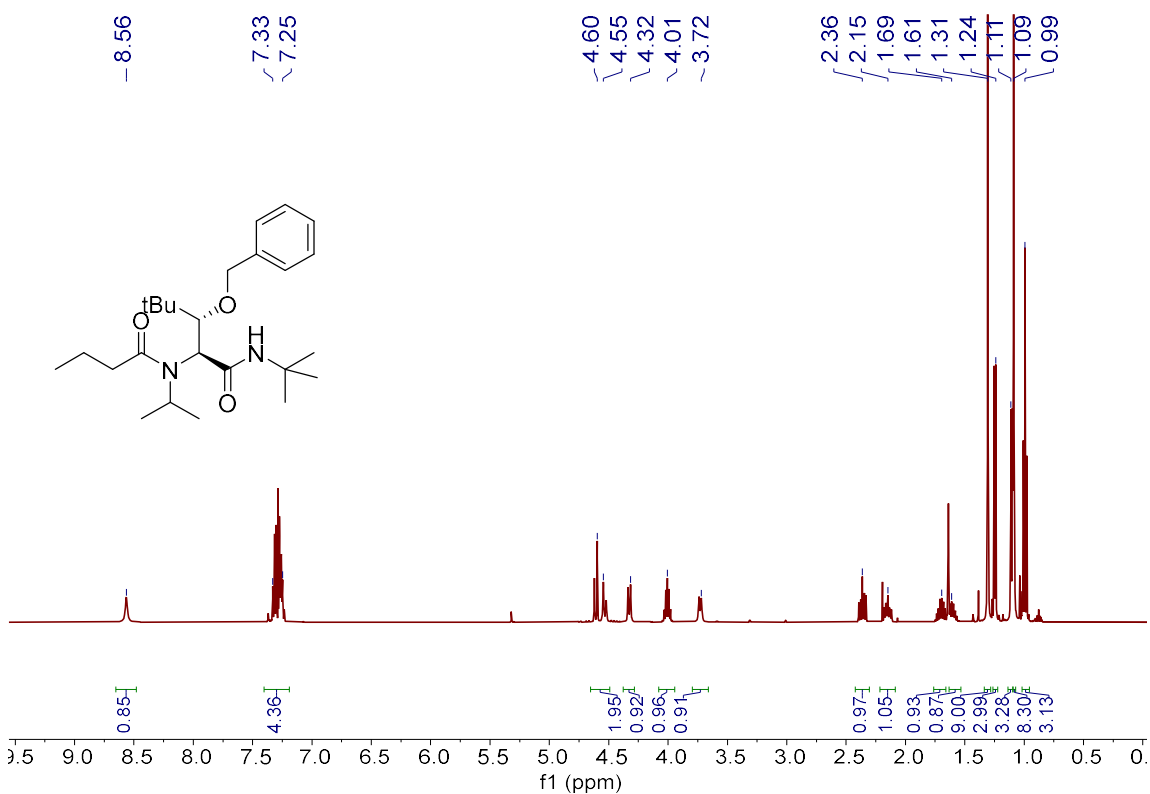


ANNEX IV

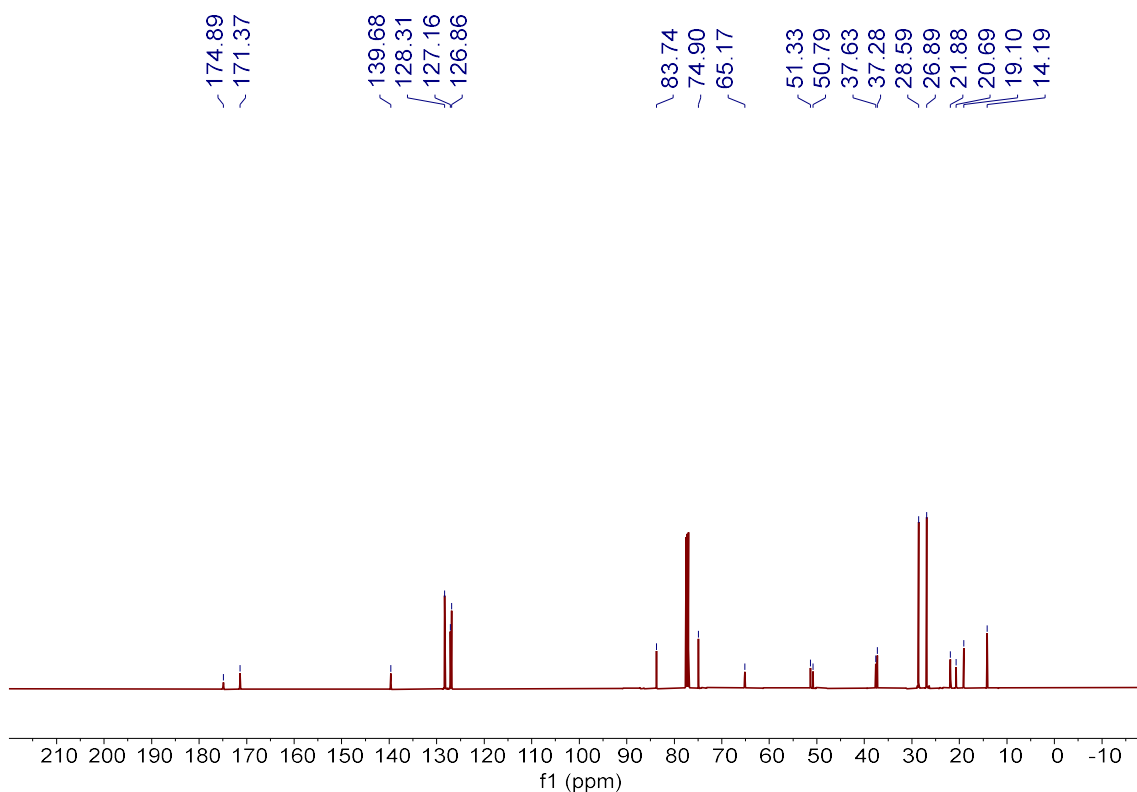
(2S,3R)-3-(benzyloxy)-N-(tert-butyl)-2-(N-isopropylbutyramido)-5-methylhexanamide (**45c-D2**). g-HMBC (CDCl₃)



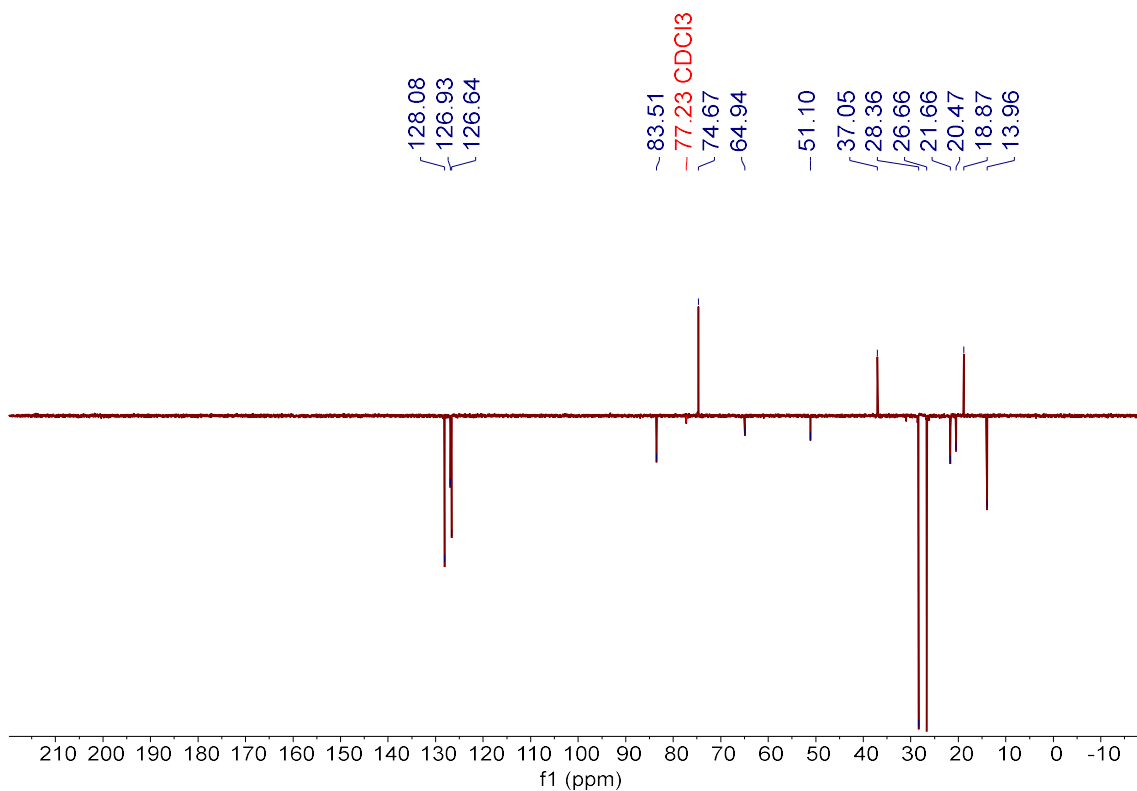
(2S,3S)-3-(benzyloxy)-N-(tert-butyl)-2-(N-isopropylbutyramido)-4,4-dimethylpentanamide (**45d-D1**). ¹H-NMR (CDCl₃)



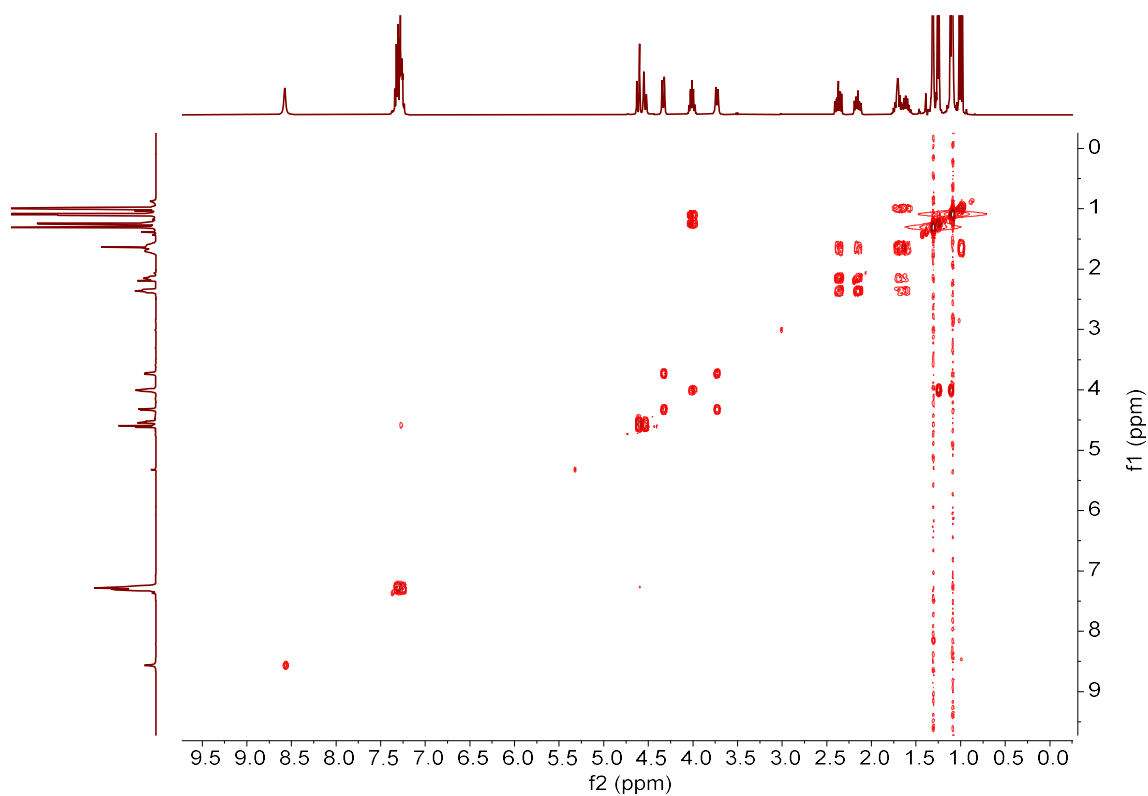
(2S,3S)-3-(benzyloxy)-N-(tert-butyl)-2-(N-isopropylbutyramido)-4,4-dimethylpentanamide (**45d-D1**). ^{13}C -NMR (CDCl_3)



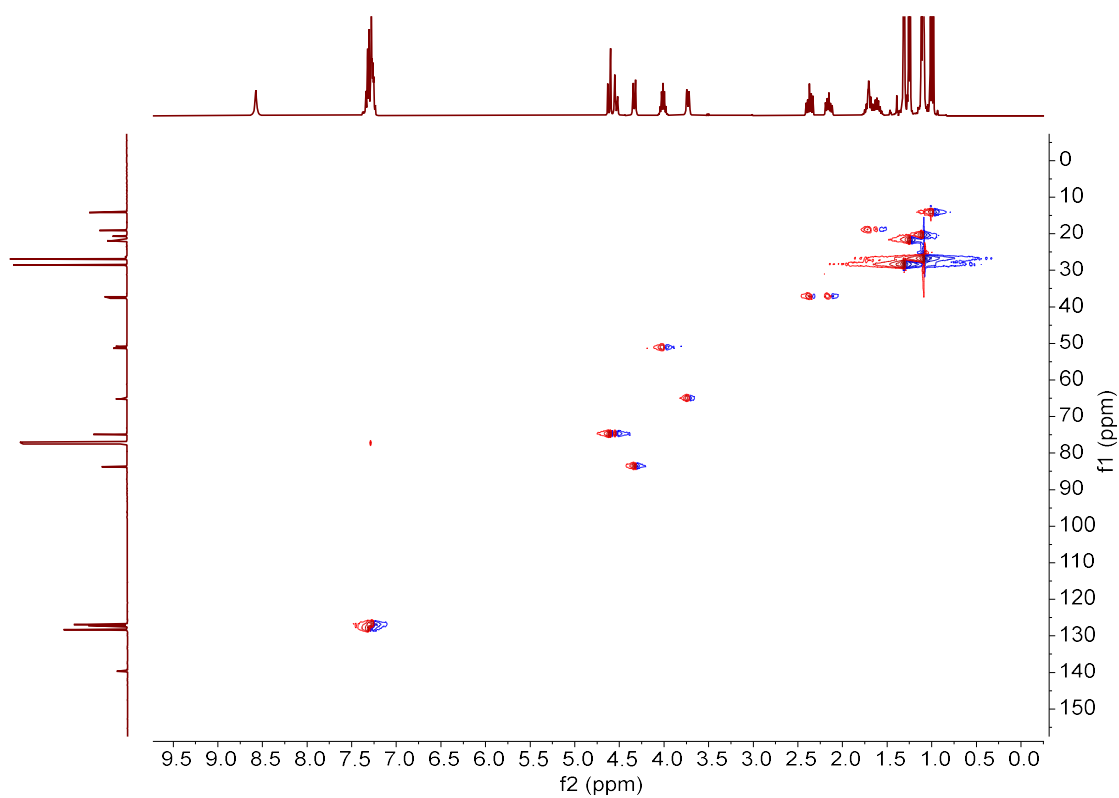
(2S,3S)-3-(benzyloxy)-N-(tert-butyl)-2-(N-isopropylbutyramido)-4,4-dimethylpentanamide (**45d-D1**). DEPT 135 (CDCl_3)



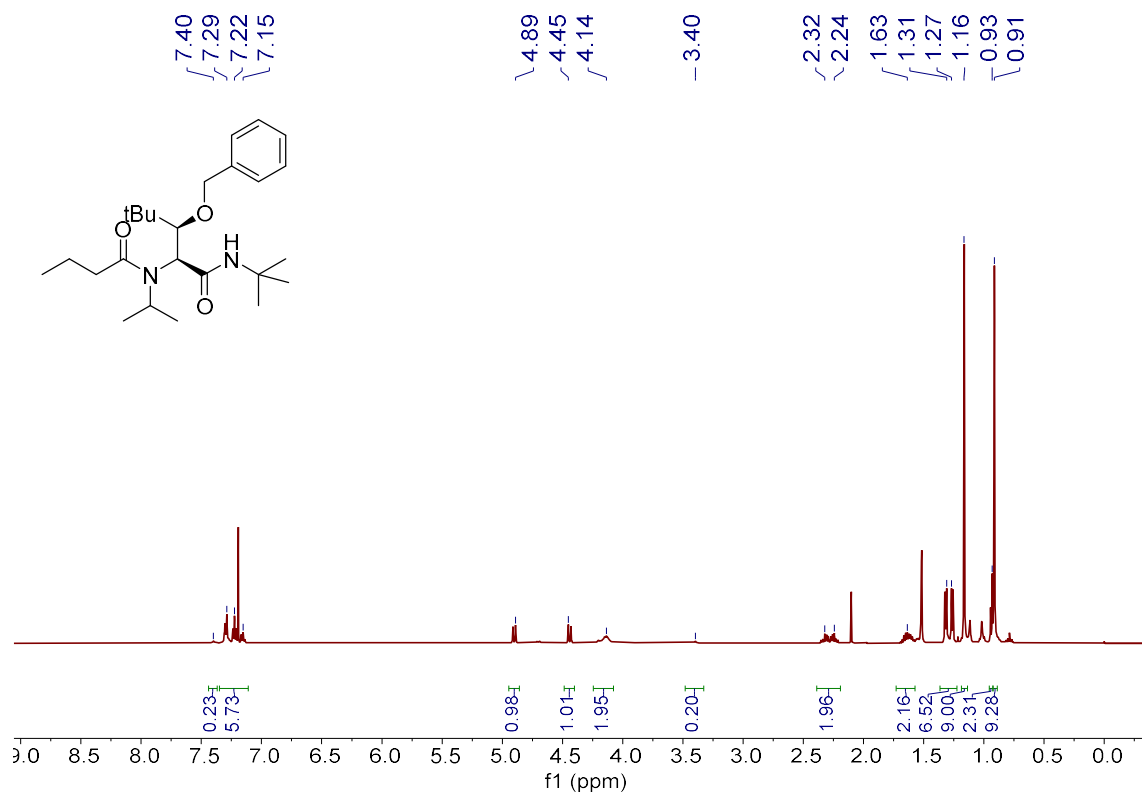
(2S,3S)-3-(benzyloxy)-N-(tert-butyl)-2-(N-isopropylbutyramido)-4,4-dimethylpentanamide (**45d-D1**). g-COSY (CDCl₃)



(2S,3S)-3-(benzyloxy)-N-(tert-butyl)-2-(N-isopropylbutyramido)-4,4-dimethylpentanamide (**45d-D1**). g-HMBC (CDCl₃)

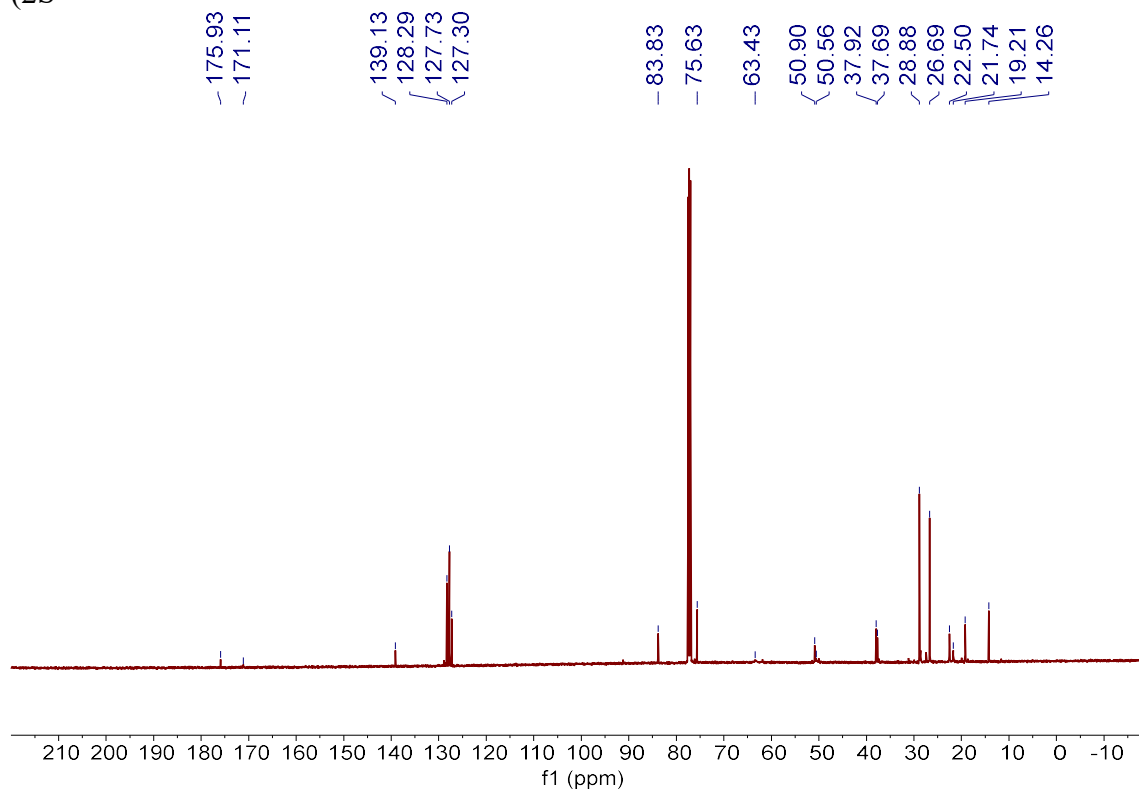


(2S,3R)-3-(benzyloxy)-N-(tert-butyl)-2-(N-isopropylbutyramido)-4,4-dimethylpentanamide (**45d-D2**). $^1\text{H-NMR}$ (CDCl_3)



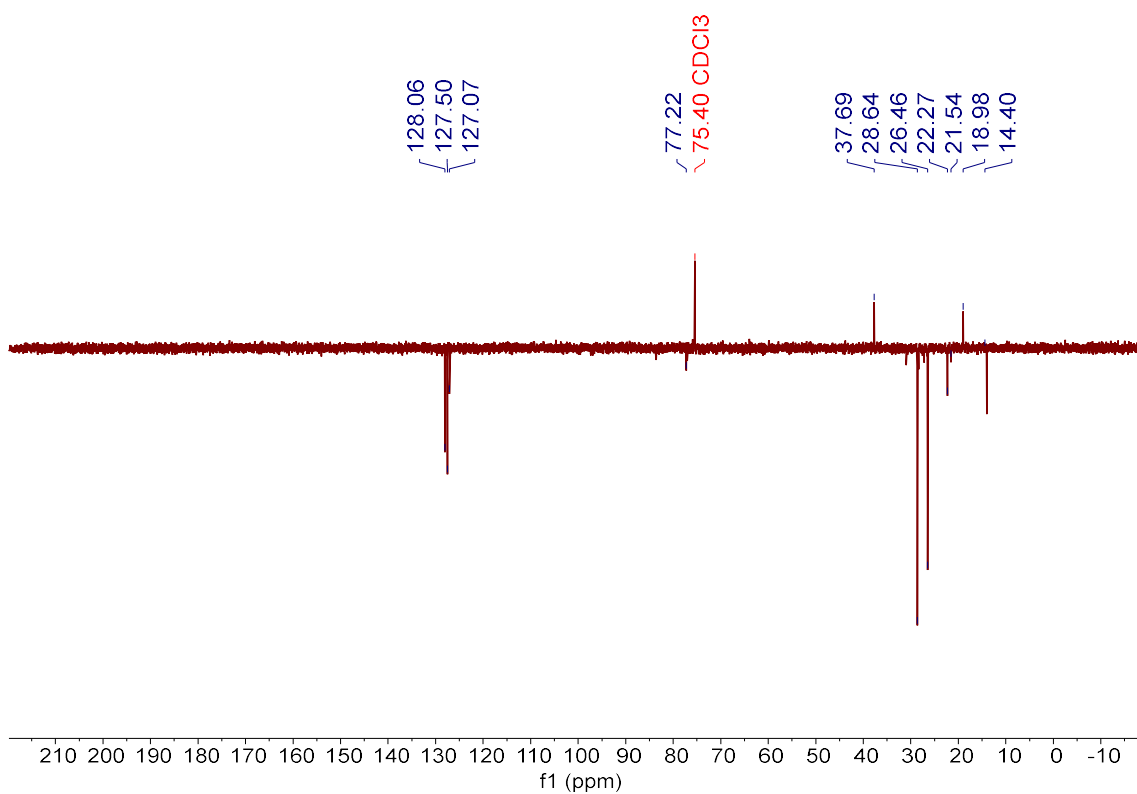
(2S,3R)-3-(benzyloxy)-N-(tert-butyl)-2-(N-isopropylbutyramido)-4,4-dimethylpentanamide (**45d-D2**). $^{13}\text{C-NMR}$ (CDCl_3)

(2S

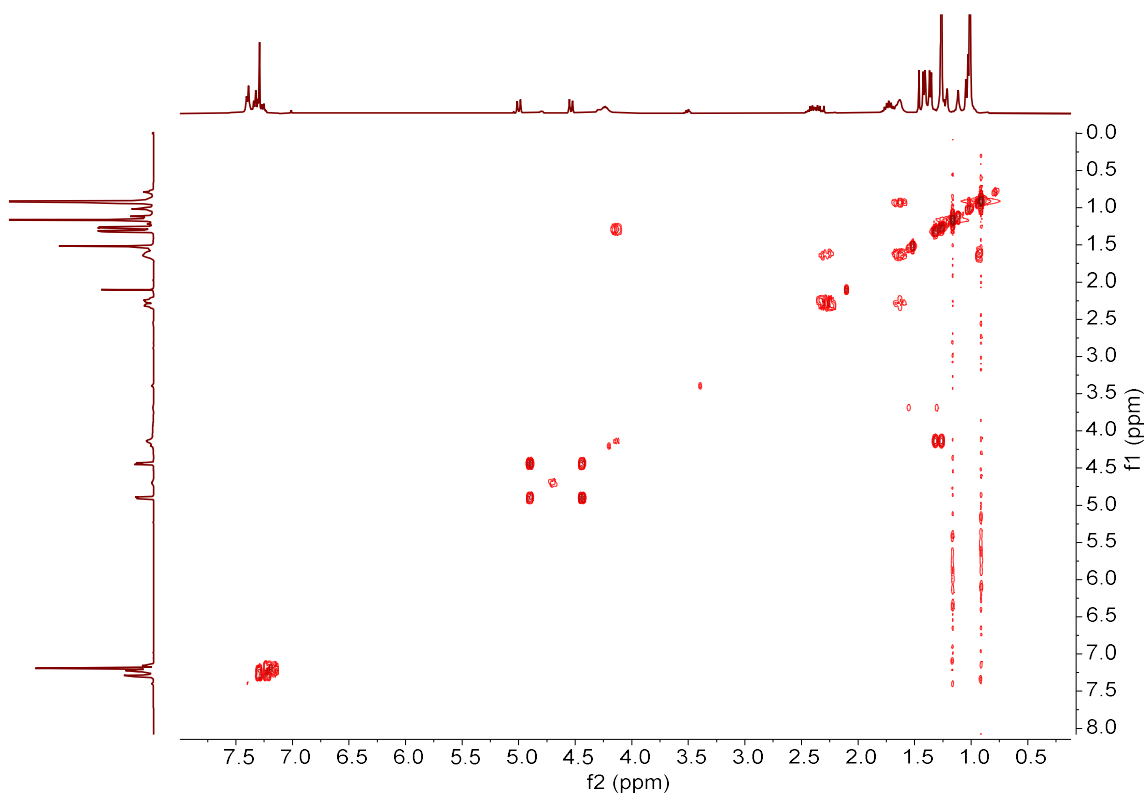


ANNEX IV

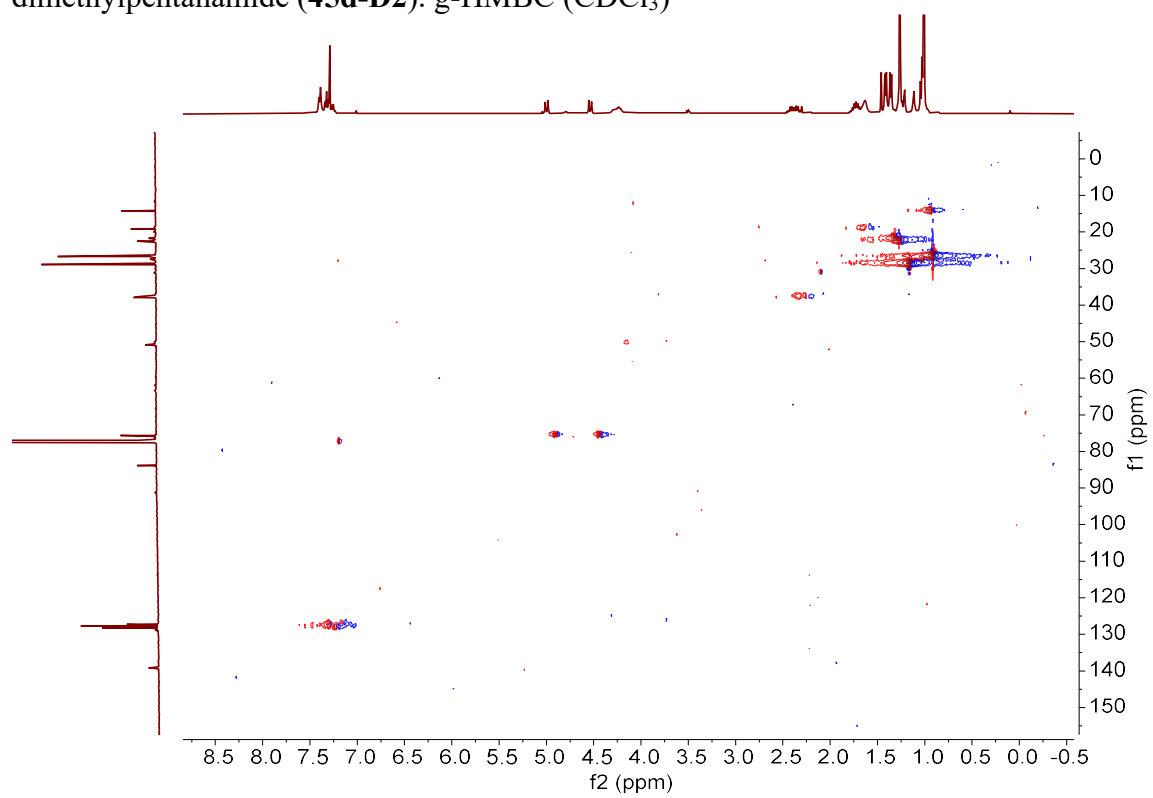
,3R)-3-(benzyloxy)-N-(tert-butyl)-2-(N-isopropylbutyramido)-4,4-dimethylpentanamide (**45d-D2**). DEPT 135 (CDCl₃)



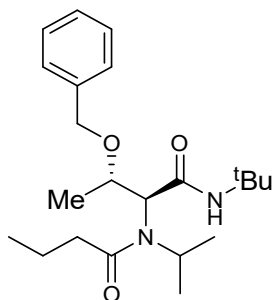
(2S,3R)-3-(benzyloxy)-N-(tert-butyl)-2-(N-isopropylbutyramido)-4,4-dimethylpentanamide (**45d-D2**). g-COSY (CDCl₃)



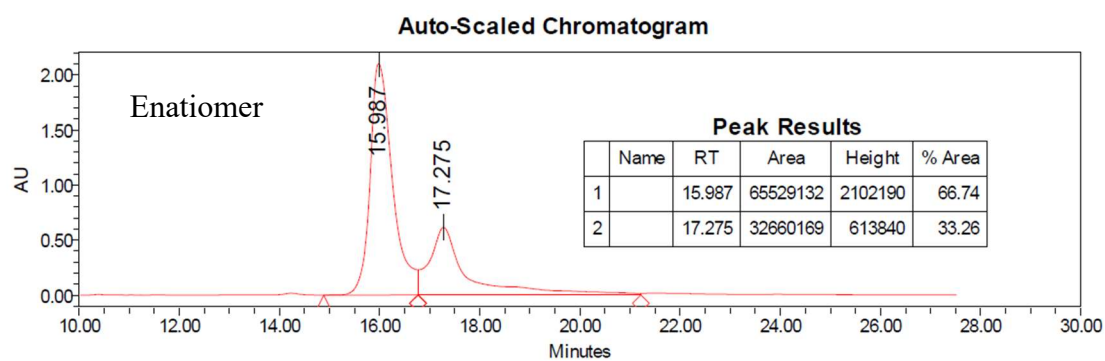
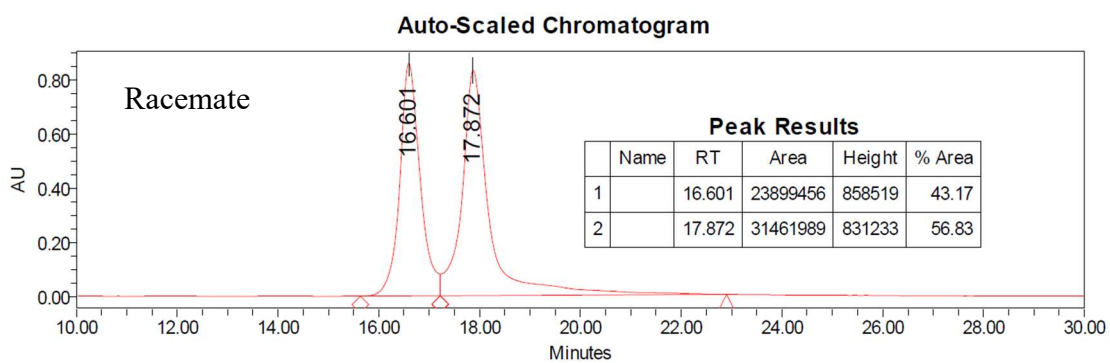
(2S,3R)-3-(benzyloxy)-N-(tert-butyl)-2-(N-isopropylbutyramido)-4,4-dimethylpentanamide (**45d-D2**). g-HMBC (CDCl₃)

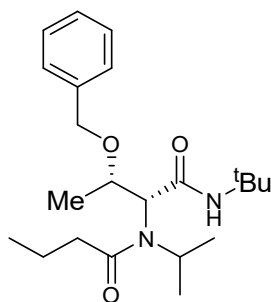


V. HPLC DATA

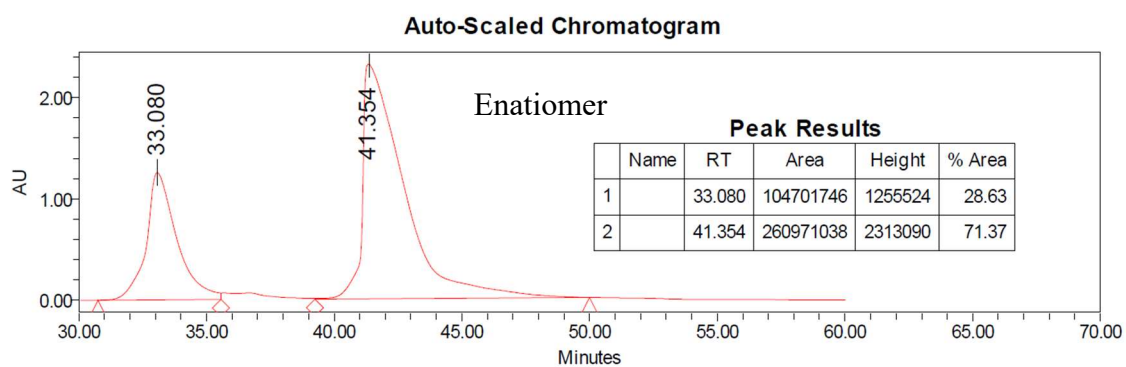
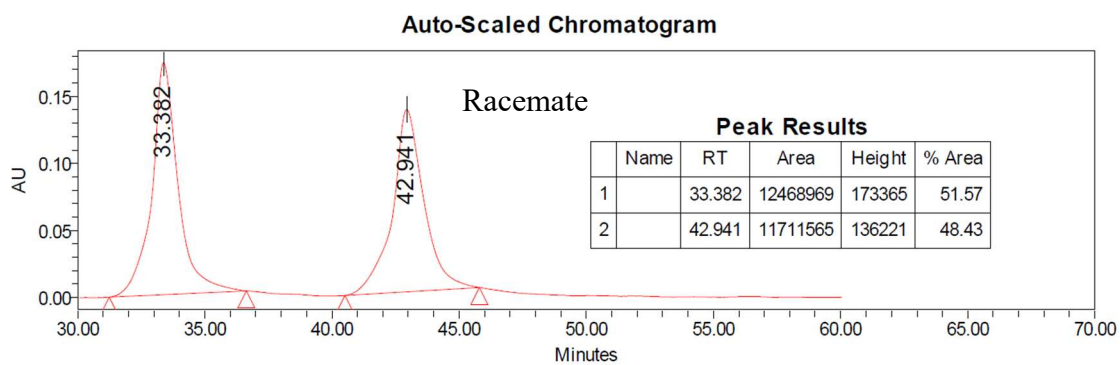


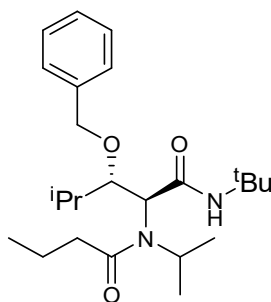
(2S,3S)-3-(benzyloxy)-N-(tert-butyl)-2-(N-isopropylbutanamide) butanamide (45a-D1).



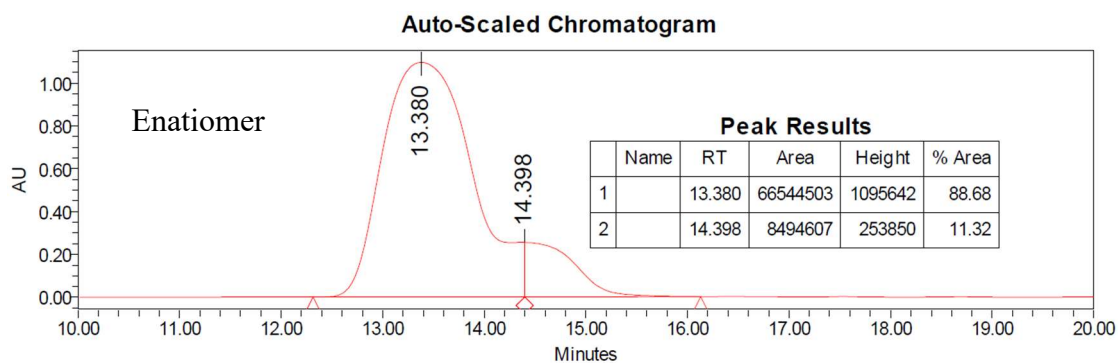
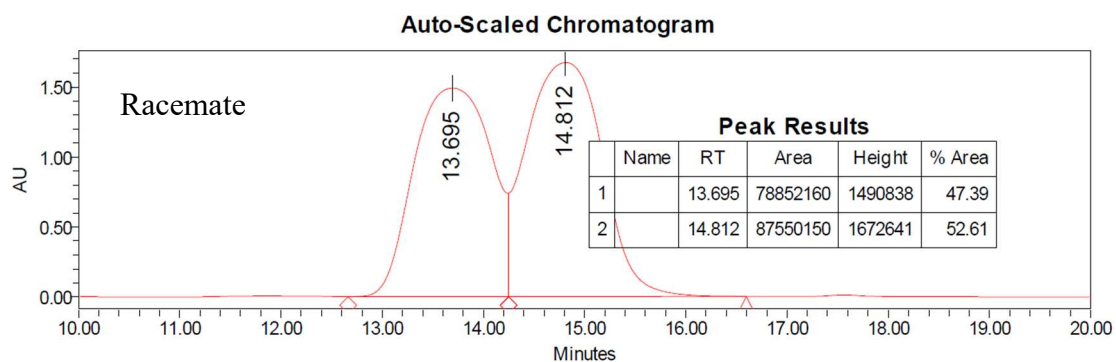


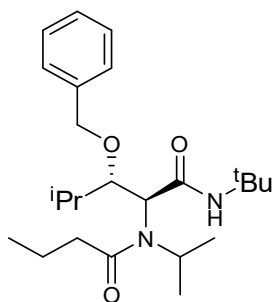
(2S,3R)-3-(benzyloxy)-N-(tert-butyl)-2-(N-isopropylbutyramido)-4,4-dimethylpentanamide (45a-D2).



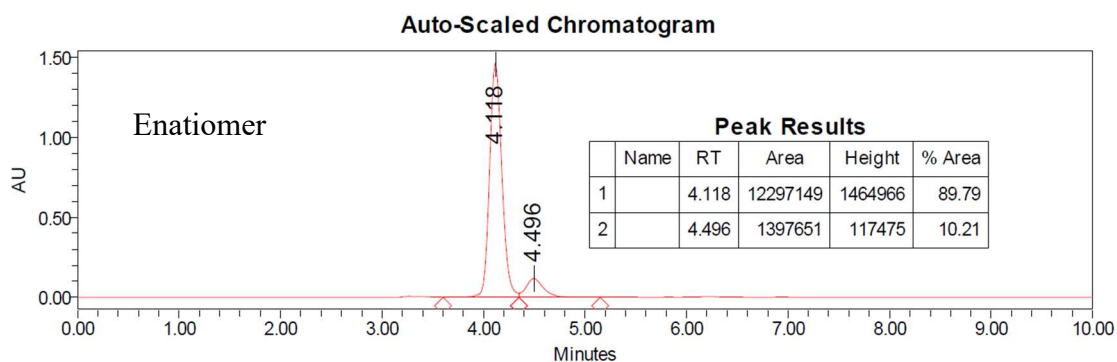
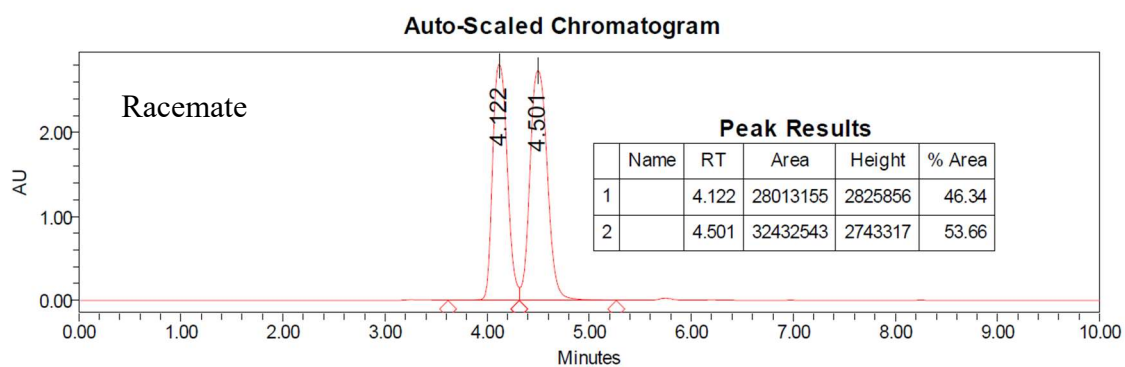


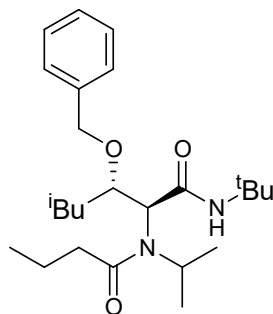
(2S,3S)-3-(benzyloxy)-N-(tert-butyl)-2-(N-isopropylbutyramido)-4-methylpentanamide (45b-D1).



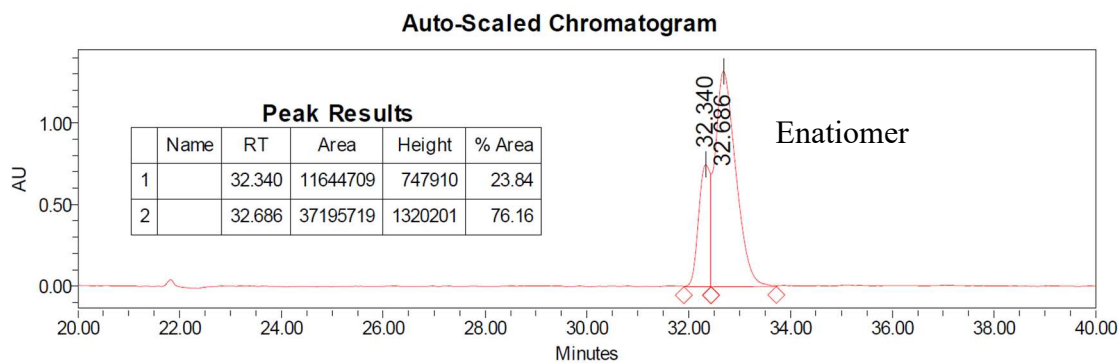
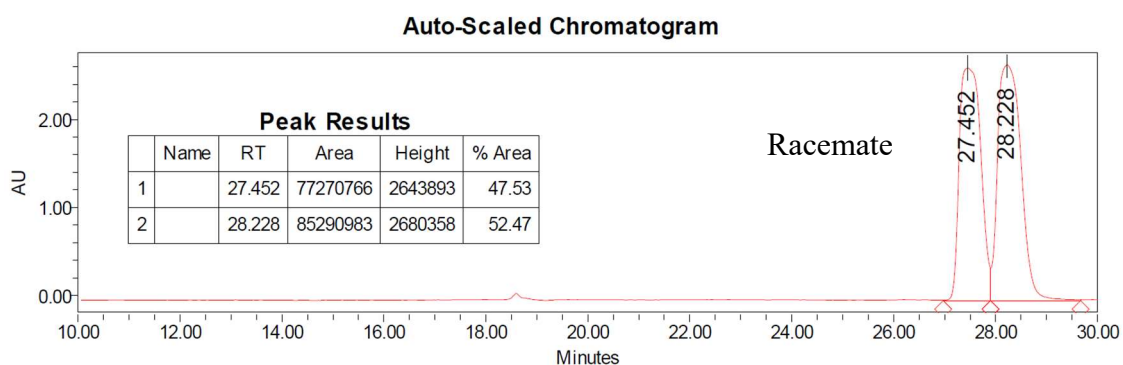


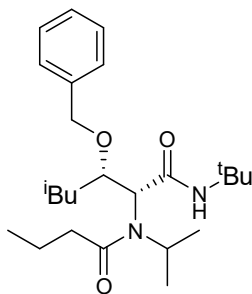
(2S,3R)-3-(benzyloxy)-N-(tert-butyl)-2-(N-isopropylbutyramido)-4-methylpentanamide (45b-D2).



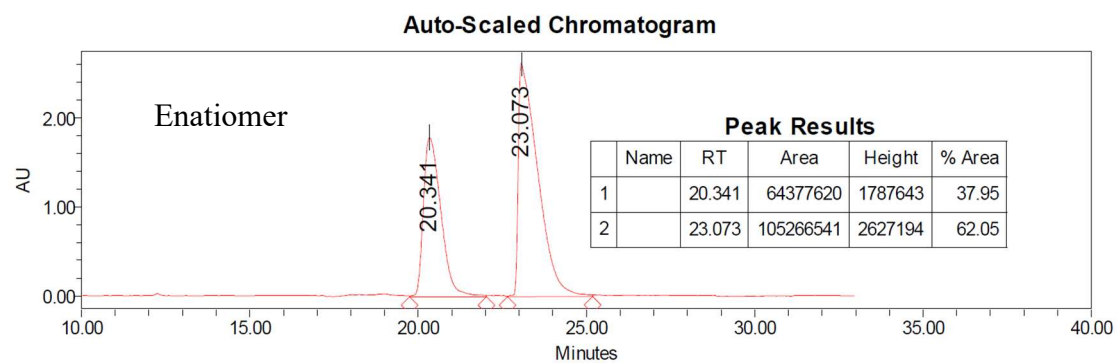
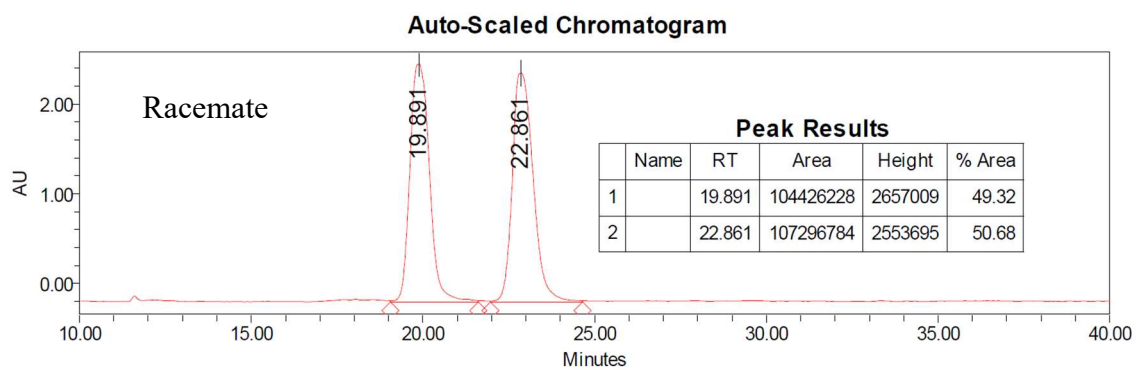


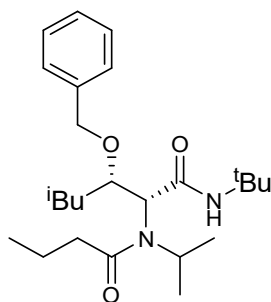
(2S,3S)-3-(benzyloxy)-N-(tert-butyl)-2-(N-isopropylbutyramido)-5-methylhexanamide (45c-D1). The retention time varies because of the room temperature changes and the HPLC system is too old, both samples were injected on the same day and same conditions.



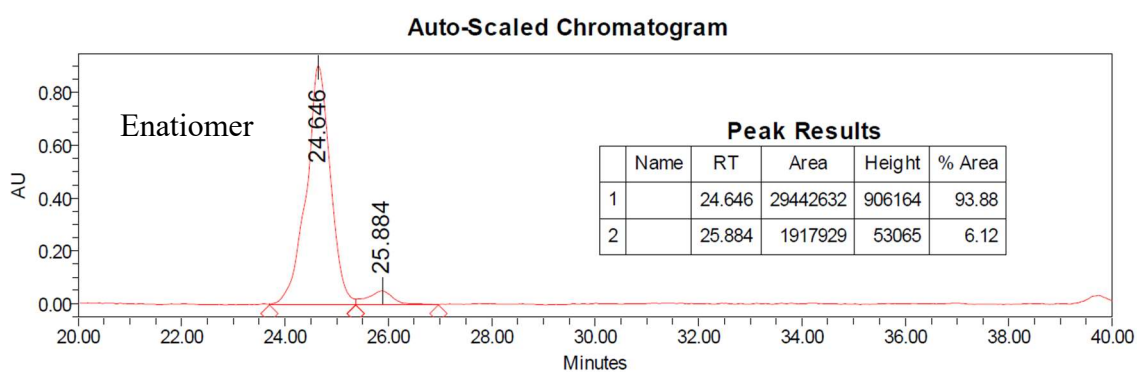
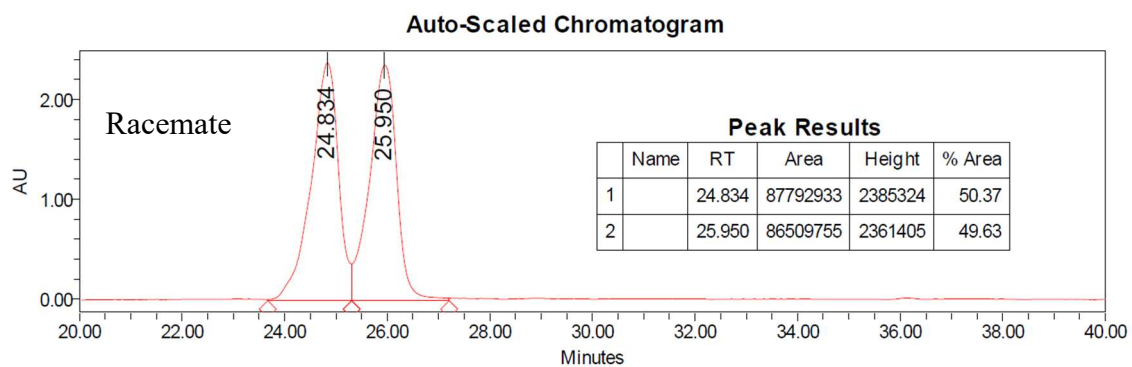


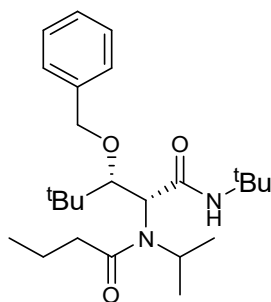
(2S,3R)-3-(benzyloxy)-N-(tert-butyl)-2-(N-isopropylbutyramido)-5-methylhexanamide (45c-D2).



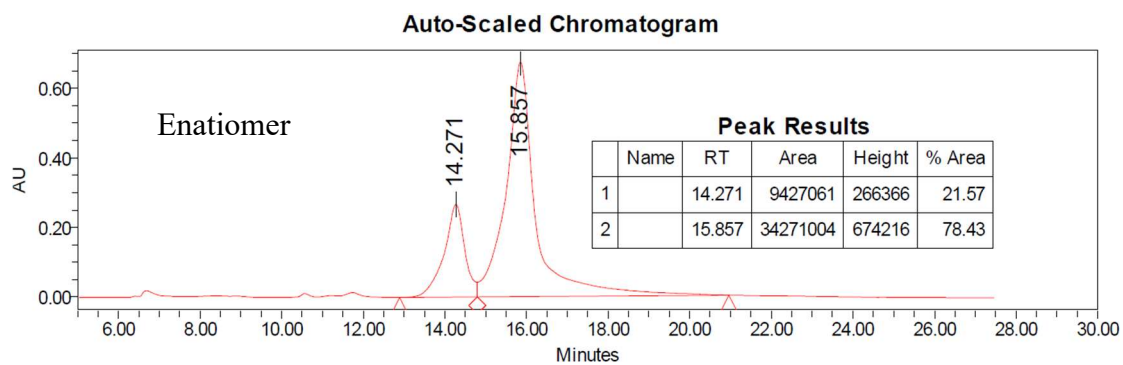
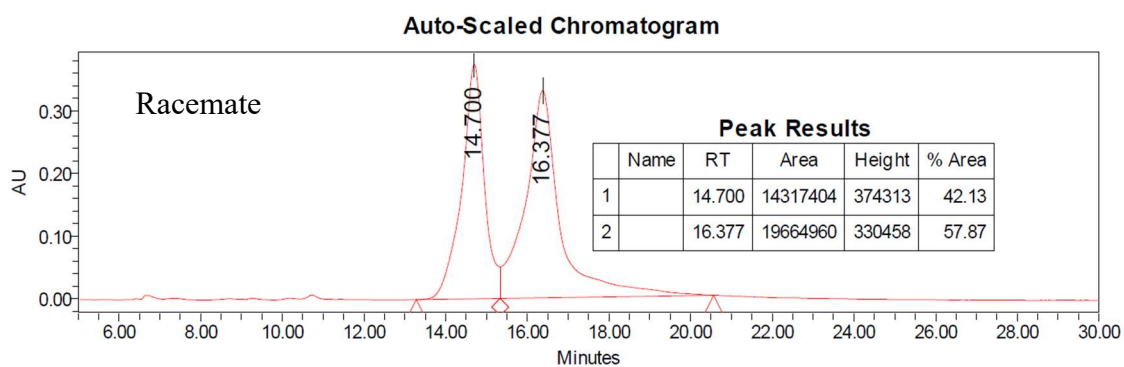


(2S,3S)-3-(benzyloxy)-N-(tert-butyl)-2-(N-isopropylbutyramido)-4,4-dimethylpentanamide (45d-D1).

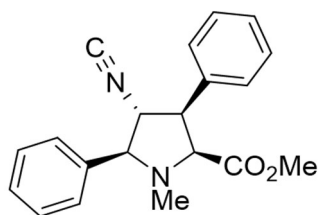




(2S,3R)-3-(benzyloxy)-N-(tert-butyl)-2-(N-isopropylbutyramido)-4,4-dimethylpentanamide (45d-D2).



VI. CRYSTAL XRD



23


SERVICIO GENERAL RAYOS X
Unidad de Moléculas y Materiales

✉ Servicios Generales de Investigación (SGIker)
 Facultad de Ciencia y Tecnología, Edificio CD3
 UPV/EHU,
 Eº Sarriena, s/n - 48940 Leioa (Bizkaia)



☎ 946013488
 Fax: 946013500
 ✉ leire.sanfelices@ehu.es

a20180200_JIX1pr

Comentario:

El usuario envió una muestra del compuesto **JIX1pr** (prismas incoloros) para determinar su estructura molecular. Se selecciona uno de ellos de tamaño aproximado $0.548 \times 0.301 \times 0.214 \text{ mm}^3$ para realizar la toma de datos.

Se confirma la estructura molecular coincidente con la propuesta por el usuario. La estructura cristalina determinada no es centrosimétrica (grupo espacial $P2_1$), en principio solo un enantiómero está presente en la estructura

Table 1 Crystal data and structure refinement for a20180200_JIX1pr.

Identification code	a20180200_JIX1pr
Empirical formula	$C_{20}H_{21}N_2O_2$
Formula weight	321.39
Temperature/K	150.00(10)
Crystal system	monoclinic
Space group	$P2_1$
a/Å	7.51325(10)
b/Å	10.65517(11)
c/Å	10.93651(14)
$\alpha/^\circ$	90.0
$\beta/^\circ$	99.3703(12)
$\gamma/^\circ$	90.0
Volume/Å ³	863.840(18)
Z	2
$\rho_{\text{calc}}/\text{cm}^{-3}$	1.236
μ/mm^{-1}	0.641
F(000)	342.0
Crystal size/mm ³	$0.548 \times 0.301 \times 0.214$
Radiation	CuK α ($\lambda = 1.54184$)
2 θ range for data collection/ $^\circ$	11.672 to 137.902
Index ranges	$-8 \leq h \leq 9, -12 \leq k \leq 12, -13 \leq l \leq 13$
Reflections collected	7289
Independent reflections	3197 [$R_{\text{int}} = 0.0176, R_{\text{sigma}} = 0.0215$]
Data/restraints/parameters	3197/1/219
Goodness-of-fit on F^2	1.065
Final R indexes [$I \geq 2\sigma(I)$]	$R_1 = 0.0308, wR_2 = 0.0807$

Table 3 Anisotropic Displacement Parameters ($\text{\AA}^2 \times 10^3$) for a20180200_JIX1pr.
The Anisotropic displacement factor exponent takes the form: -
 $2\pi^2 [h^2 a^2 U_{11} + 2hka * b * U_{12} + \dots]$.

Atom	U ₁₁	U ₂₂	U ₃₃	U ₂₃	U ₁₃	U ₁₂
O1	43.2(9)	30.2(7)	39.9(9)	3.5(7)	1.9(7)	-10.3(7)
O2	27.4(7)	34.2(8)	30.6(7)	-0.8(6)	-2.4(5)	0.9(6)
N1	27.0(8)	32.0(9)	23.0(8)	2.8(7)	5.2(6)	-1.6(7)
N2	24.6(8)	33.8(9)	24.2(8)	-0.9(7)	2.0(6)	0.2(7)
C1	25.0(9)	24.3(8)	23.7(9)	0.4(7)	4.5(7)	1.1(7)
C2	24.4(9)	22.2(9)	24.9(9)	1.0(7)	3.3(7)	-1.4(7)
C3	25.2(9)	26.1(9)	24.0(9)	-1.4(8)	3.4(7)	-2.1(8)
C4	28.4(9)	24.8(9)	23.9(9)	-0.6(8)	3.3(7)	0.5(8)
C5	36.1(11)	50.5(13)	27.7(10)	3.9(10)	10.1(8)	-0.9(10)
C6	23.4(9)	31.3(10)	26.4(9)	-0.8(8)	7.3(7)	0.3(7)
C7	36.7(12)	51.6(15)	37.9(12)	-4.5(11)	-7.2(9)	-6.2(10)
C8	18.8(8)	31.6(10)	23.1(9)	0.5(8)	1.0(7)	-2.1(7)
C9	26.8(10)	32.5(10)	25.0(10)	-0.2(8)	3.0(8)	-1.2(8)
C10	31.8(11)	39.1(11)	31.0(11)	-8.4(9)	2.2(8)	0.6(9)
C11	39.3(12)	60.4(15)	22.5(10)	-7.9(10)	3.6(8)	-0.7(11)
C12	44.8(13)	52.4(14)	24.2(10)	8.0(10)	1.0(9)	-5.5(11)
C13	33.4(11)	36.4(11)	29.6(11)	5.8(8)	2.0(8)	-2.8(9)
C14	29.0(10)	45.0(12)	36.2(12)	-5.2(9)	4.9(9)	-7.0(10)
C15	30.3(10)	33.0(10)	22.1(9)	0.5(8)	5.0(8)	4.3(8)
C16	37.6(12)	40.1(12)	28.6(10)	-0.2(9)	1.4(9)	-0.4(9)
C17	39.3(12)	62.6(16)	29.1(11)	-2.3(11)	-3.1(9)	2.0(12)
C18	52.0(15)	63.6(18)	28.6(12)	4.7(11)	-1.2(11)	23.4(12)
C19	70.2(19)	39.7(13)	37.9(14)	2.7(10)	4.9(12)	21.1(13)
C20	48.9(14)	34.5(12)	29.8(11)	-3.4(9)	2.3(10)	8.2(10)

Table 4 Bond Lengths for a20180200_JIX1pr.

Atom	Atom	Length/\AA	Atom	Atom	Length/\AA
O1	C6	1.200(3)	C4	C15	1.509(3)
O2	C6	1.336(2)	C8	C9	1.389(3)
O2	C7	1.441(3)	C8	C13	1.391(3)
N1	C1	1.460(2)	C9	C10	1.398(3)
N1	C4	1.461(2)	C10	C11	1.386(3)
N1	C5	1.459(2)	C11	C12	1.387(4)
N2	C3	1.436(2)	C12	C13	1.388(3)
N2	C14	1.147(3)	C15	C16	1.390(3)
C1	C2	1.569(3)	C15	C20	1.387(3)
C1	C6	1.511(3)	C16	C17	1.386(3)
C2	C3	1.547(3)	C17	C18	1.380(4)
C2	C8	1.514(3)	C18	C19	1.378(4)
C3	C4	1.537(3)	C19	C20	1.390(3)

Final R indexes [all data]	$R_1 = 0.0315$, $wR_2 = 0.0813$
Largest diff. peak/hole / e \AA^{-3}	0.13/-0.33
Flack parameter	0.07(8)
Bijvoet Pairs Coverage	99%
Hooft y	0.08(7)
P3 false	$\leq 10^{-38}$

[a] Esquema de pesado: $1/(\sigma^2(F_o^2) + (0.0723P)^2 + 0.1002P)$ donde $P = [\text{Max}(F_o^2, 0) + 2F_c^2]/3$.

[b] Expresión de extinción secundaria tipo SHELXL: $F_c^* = kF_c[1 + 0.001F_c^2\lambda^3/\text{sen}(2\theta)]^{-1/4}$

Table 2 Fractional Atomic Coordinates ($\times 10^4$) and Equivalent Isotropic Displacement Parameters ($\text{\AA}^2 \times 10^3$) for a20180200_JIX1pr. U_{eq} is defined as 1/3 of the trace of the orthogonalised U_{ij} tensor.

Atom	x	y	z	U_{eq}
O1	-6809(2)	-4488.5(15)	-5642.0(15)	38.3(4)
O2	-7670.1(19)	-2793.6(13)	-6792.4(13)	31.5(3)
N1	-4460(2)	-3090.3(16)	-3973.6(14)	27.2(4)
N2	-553(2)	-1658.7(16)	-4890.3(15)	27.7(4)
C1	-5293(2)	-2511.4(18)	-5137.6(17)	24.3(4)
C2	-3702(2)	-2142.8(17)	-5835.4(18)	23.9(4)
C3	-2040(3)	-2501.0(18)	-4868.0(17)	25.2(4)
C4	-2723(3)	-2463.3(18)	-3617.5(18)	25.8(4)
C5	-5619(3)	-3045(2)	-3025.7(19)	37.5(5)
C6	-6650(3)	-3393.8(19)	-5857.6(18)	26.7(4)
C7	-8956(3)	-3584(2)	-7555(2)	43.5(6)
C8	-3703(2)	-2725.1(18)	-7098.3(17)	24.8(4)
C9	-3580(3)	-4015(2)	-7248.2(19)	28.3(4)
C10	-3535(3)	-4530(2)	-8418(2)	34.3(5)
C11	-3606(3)	-3754(3)	-9441(2)	40.9(5)
C12	-3755(3)	-2467(3)	-9300(2)	41.0(5)
C13	-3803(3)	-1959(2)	-8137(2)	33.5(5)
C14	606(3)	-951(2)	-4836(2)	36.7(5)
C15	-1460(3)	-3110(2)	-2595.8(17)	28.4(4)
C16	-249(3)	-2397(2)	-1783(2)	35.9(5)
C17	1028(3)	-2971(3)	-902(2)	44.6(6)
C18	1090(4)	-4263(3)	-816(2)	48.9(7)
C19	-126(4)	-4976(3)	-1605(2)	49.7(7)
C20	-1402(3)	-4408(2)	-2497(2)	38.2(5)

Table 5 Bond Angles for a20180200_JIX1pr.

Atom	Atom	Atom	Angle/°	Atom	Atom	Atom	Angle/°
C6	O2	C7	114.18 (17)	O1	C6	C1	125.65 (18)
C1	N1	C4	106.05 (14)	O2	C6	C1	110.81 (17)
C5	N1	C1	112.63 (16)	C9	C8	C2	121.54 (17)
C5	N1	C4	113.95 (16)	C9	C8	C13	118.71 (19)
C14	N2	C3	175.4 (2)	C13	C8	C2	119.74 (18)
N1	C1	C2	106.11 (14)	C8	C9	C10	120.6 (2)
N1	C1	C6	110.40 (15)	C11	C10	C9	120.1 (2)
C6	C1	C2	113.91 (15)	C10	C11	C12	119.6 (2)
C3	C2	C1	101.50 (15)	C11	C12	C13	120.2 (2)
C8	C2	C1	117.00 (15)	C12	C13	C8	120.9 (2)
C8	C2	C3	113.77 (15)	C16	C15	C4	119.4 (2)
N2	C3	C2	112.19 (15)	C20	C15	C4	121.40 (18)
N2	C3	C4	111.83 (15)	C20	C15	C16	119.1 (2)
C4	C3	C2	104.64 (15)	C17	C16	C15	120.7 (2)
N1	C4	C3	99.42 (14)	C18	C17	C16	120.0 (2)
N1	C4	C15	114.52 (16)	C19	C18	C17	119.7 (2)
C15	C4	C3	112.71 (16)	C18	C19	C20	120.7 (2)
O1	C6	O2	123.54 (19)	C15	C20	C19	119.9 (2)

Table 6 Torsion Angles for a20180200_JIX1pr.

A	B	C	D	Angle/°	A	B	C	D	Angle/°
N1	C1	C2	C3	-4.08 (19)	C4	N1	C1	C6	156.31 (15)
N1	C1	C2	C8	120.35 (17)	C4	C15	C16	C17	-174.5 (2)
N1	C1	C6	O1	-12.8 (3)	C4	C15	C20	C19	174.9 (2)
N1	C1	C6	O2	167.67 (15)	C5	N1	C1	C2	157.71 (17)
N1	C4	C15	C16	149.08 (18)	C5	N1	C1	C6	-78.4 (2)
N1	C4	C15	C20	35.1 (3)	C5	N1	C4	C3	171.03 (17)
N2	C3	C4	N1	164.76 (15)	C5	N1	C4	C15	68.6 (2)
N2	C3	C4	C15	-73.5 (2)	C6	C1	C2	C3	125.74 (17)
C1	N1	C4	C3	-46.56 (18)	C6	C1	C2	C8	-1.3 (2)
C1	N1	C4	C15	166.95 (16)	C7	O2	C6	O1	-1.8 (3)
C1	C2	C3	N2	145.24 (15)	C7	O2	C6	C1	177.74 (17)
C1	C2	C3	C4	-23.80 (18)	C8	C2	C3	N2	88.18 (19)
C1	C2	C8	C9	-62.0 (2)	C8	C2	C3	C4	150.37 (15)
C1	C2	C8	C13	119.0 (2)	C8	C9	C10	C11	0.2 (3)

C2C1C6 O1	106.5(2)	C9 C8 C13C12	-0.9(3)
C2C1C6 O2	-73.1(2)	C9 C10C11C12	-1.1(4)
C2C3C4 N1	43.08(17)	C10C11C12C13	1.0(4)
C2C3C4 C15	164.78(16)	C11C12C13C8	0.0(4)
C2C8C9 C10	178.28(17)	C13C8 C9 C10	0.8(3)
C2C8C13C12	178.17(19)	C15C16C17C18	-0.8(4)
C3C2C8 C9	56.0(2)	C16C15C20C19	-1.0(3)
C3C2C8 C13	123.07(19)	C16C17C18C19	-0.2(4)
C3C4C15C16	98.2(2)	C17C18C19C20	0.7(4)
C3C4C15C20	-77.7(2)	C18C19C20C15	-0.1(4)
C4N1C1 C2	32.43(19)	C20C15C16C17	1.4(3)

Table 7 Hydrogen Atom Coordinates ($\text{\AA} \times 10^4$) and Isotropic Displacement Parameters ($\text{\AA}^2 \times 10^3$) for a20180200_JIX1pr.

Atom	x	y	z	U(eq)
H1	-5930.08	-1729.33	-4946.54	29
H2	-3710.69	-1209.74	-5934.46	29
H3	-1656.57	-3375.33	-5031.85	30
H4	-2917.74	-1573.76	-3379.18	31
H5A	-5008.87	-3455.5	-2270.08	56
H5B	-6753.82	-3481.79	-3326.43	56
H5C	-5871.72	-2168.83	-2843.8	56
H7A	-9732.81	-3067.47	-8163.34	65
H7B	-9697.34	-4024.3	-7031.71	65
H7C	-8313.66	-4199.13	-7987.17	65
H9	-3526.1	-4551.32	-6549.39	34
H10	-3454.41	-5414	-8511.18	41
H11	-3553.82	-4101.52	-10234.62	49
H12	-3823.99	-1931.16	-10000.58	49
H13	-3906.31	-1075.71	-8049	40
H14	1566.99	-363.95	-4791.38	44
H16	-296.23	-1507.14	-1831.5	43
H17	1860.53	-2475.98	-358.09	54
H18	1965.99	-4659.43	-215.53	59
H19	-91.36	-5864.96	-1539.8	60
H20	-2233.83	-4907.04	-3036.94	46

Experimental

Single crystals of $\text{C}_{20}\text{H}_{21}\text{N}_2\text{O}_2$ [a20180200_JIX1pr] were [1]. A suitable crystal was selected and [1] on a **SuperNova, Single source at offset/far, Atlas** diffractometer. The crystal was kept at 150.00(10) K during data collection. Using Olex2 [1], the structure was solved with the ShelXS [2] structure solution program using Direct Methods and refined with the ShelXL [3] refinement package using Least Squares minimisation.

1. Dolomanov, O.V., Bourhis, L.J., Gildea, R.J., Howard, J.A.K. & Puschmann, H. (2009), *J. Appl. Cryst.* 42, 339-341.
2. Sheldrick, G.M. (2008). *Acta Cryst.* A64, 112-122.
3. Sheldrick, G.M. (2015). *Acta Cryst.* C71, 3-8.

Crystal structure determination of [a20180200_JIX1pr]

Crystal Data for $C_{20}H_{21}N_2O_2$ ($M=321.39$ g/mol): monoclinic, space group $P2_1$ (no. 4), $a = 7.51325(10)$ Å, $b = 10.65517(11)$ Å, $c = 10.93651(14)$ Å, $\beta = 99.3703(12)^\circ$, $V = 863.840(18)$ Å³, $Z = 2$, $T = 150.00(10)$ K, $\mu(\text{CuK}\alpha) = 0.641$ mm⁻¹, $D_{\text{calc}} = 1.236$ g/cm³, 7289 reflections measured ($11.672^\circ \leq 2\theta \leq 137.902^\circ$), 3197 unique ($R_{\text{int}} = 0.0176$, $R_{\text{sigma}} = 0.0215$) which were used in all calculations. The final R_1 was 0.0308 ($I > 2\sigma(I)$) and wR_2 was 0.0813 (all data).

Refinement model description

Number of restraints - 1, number of constraints - unknown.

Details:

1. Fixed Uiso
 - At 1.2 times of:
 - All C(H) groups
 - At 1.5 times of:
 - All C(H,H,H) groups
- 2.a Ternary CH refined with riding coordinates:
 - C1(H1), C2(H2), C3(H3), C4(H4)
- 2.b Aromatic/amide H refined with riding coordinates:
 - C9(H9), C10(H10), C11(H11), C12(H12), C13(H13), C16(H16), C17(H17), C18(H18), C19(H19), C20(H20)
- 2.c Idealised Me refined as rotating group:
 - C5(H5A,H5B,H5C), C7(H7A,H7B,H7C)
- 2.d :
 - C14(H14)

This report has been created with Olex2, compiled on 2018.05.29 svn.r3508 for OlexSys. Please [let us know](#) if there are any errors or if you would like to have additional features.

ANALISIS CONFIGURACION ABSOLUTA

Puesto que se requería la determinación de la configuración absoluta, se ha realizado una toma de datos incluyendo pares de Friedel, consiguiendo una cobertura del 100% de los mismos. El *parámetro de Flack* (x) tiene un valor 0.08(8). El valor de la incertidumbre (0.08) está al límite de ser lo suficientemente pequeña para distinguir si el espécimen es de un enantiómero ($x = 0$), del opuesto ($x = 1$), o una macla racémica ($x = 0.5$),¹ algo que era de esperar por la ausencia de átomos pesados. El resultado se confirma con un análisis de los pares de Friedel usando estadística bayesiana² utilizando el programa PLATON³. Dados los datos de difracción con una cobertura de los pares de Friedel del 99%, este análisis indica que *la probabilidad de que la configuración absoluta se haya asignado correctamente es esencialmente del 100%*. De hecho, *la probabilidad de que la asignación sea incorrecta es menor de 10^{-38}* . Y el *parámetro de estructura absoluta* (equivalente a Flack) resulta ser de 0.08(7), confirmando la asignación.⁴

¹ H. D. Flack & G. Bernardinelli, *Acta Cryst.* 1999, A55, 908-915; H. D. Flack & G. Bernardinelli, *J. Appl. Cryst.* 2000, 33, 1143-1148.

² R. W. W. Hooft, L. H. Straver & A. L. Spek, *J. Appl. Cryst.* 2008, 41, 96-103

³ A. L. Spek (2010) PLATON, A Multipurpose Crystallographic Tool, Utrecht University, Utrecht, The Netherlands; A. L. Spek, *J. Appl. Cryst.* 2003, 36, 7-13.

⁴ A. L. Thompson & D. J. Watkin, *Tetrahedron: Asymmetry* 2009, 20, 712-717

En resumen, el cristal contiene un solo enantiómero, cuya configuración absoluta ha sido determinada con una certeza cercana al 100%: la probabilidad de que la asignación sea incorrecta es menor de 10^{-38} .

Texto sugerido en inglés⁵: Analysis of the absolute structure using likelihood methods (Hooft, Straver & Spek, 2008 [4]) was performed using PLATON (Spek, 2010[5]). The Friedel pair coverage of the experiment is almost complete (99%). The results indicated that the absolute structure had been correctly assigned. The method calculated that the probability that the structure is inverted is smaller than 10^{-38} . The absolute structure parameter γ (Hooft, Straver & Spek, 2008[4]) was calculated using PLATON (Spek, 2010[5]). The resulting value was $\gamma=0.08(7)$, which together with Flack parameter value, indicate that the absolute structure has probably been determined correctly.

1. R. W. W. Hooft, L. H. Straver & A. L. Spek, J. Appl. Cryst. 2008, 41, 96-103.
2. A. L. Spek (2010) PLATON, A Multipurpose Crystallographic Tool, Utrecht University, Utrecht, The Netherlands; A. L. Spek, J. Appl. Cryst. 2003, 36, 7-13.

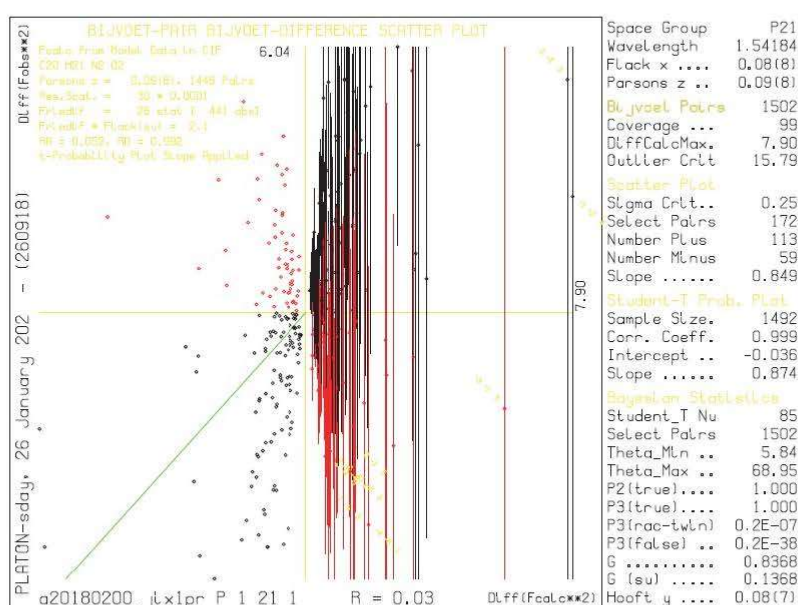


Figura 1. Análisis de la estructura absoluta mediante estadística bayesiana usando el programa Platon.

Es importante recordar que siempre que se determina la configuración absoluta mediante difracción de RX sobre monocristal, es imprescindible que se confirme la pureza enantiomérica en la disolución (RMN, HPLC quiral,...), ya que sólo se determina la estructura de un cristal (a lo sumo unos pocos), por lo que no se puede asegurar que todos los cristales contengan el mismo enantiómero debido a la posible resolución espontánea de una disolución racémica.

⁵ <http://www.absolutestructure.com/> (accedido el 27 de abril de 2022)

checkCIF/PLATON report

Structure factors have been supplied for datablock(s) a20180200_jix1pr

THIS REPORT IS FOR GUIDANCE ONLY. IF USED AS PART OF A REVIEW PROCEDURE FOR PUBLICATION, IT SHOULD NOT REPLACE THE EXPERTISE OF AN EXPERIENCED CRYSTALLOGRAPHIC REFEREE.

No syntax errors found. CIF dictionary Interpreting this report

Datablock: a20180200_jix1pr

Bond precision: C-C = 0.0032 Å Wavelength=1.54184

Cell: a=7.51325(10) b=10.65517(11) c=10.93651(14)
 alpha=90 beta=99.3703(12) gamma=90

Temperature: 150 K

	Calculated	Reported
Volume	863.840(19)	863.840(18)
Space group	P 21	P 1 21 1
Hall group	P 2yb	P 2yb
Moiety formula	C20 H21 N2 O2	C20 H21 N2 O2
Sum formula	C20 H21 N2 O2	C20 H21 N2 O2
Mr	321.39	321.39
Dx, g cm ⁻³	1.236	1.236
Z	2	2
Mu (mm ⁻¹)	0.640	0.641
F000	342.0	342.0
F000'	342.99	
h, k, lmax	9, 12, 13	9, 12, 13
Nref	3212[1700]	3197
Tmin, Tmax	0.793, 0.872	0.814, 0.901
Tmin'	0.704	

Correction method= # Reported T Limits: Tmin=0.814 Tmax=0.901
 AbsCorr = ANALYTICAL

Data completeness= 1.88/1.00 Theta(max)= 68.951

R(reflections)= 0.0308 (3142) wR2(reflections)=
 S = 1.065 Npar= 219 0.0813 (3197)

The following ALERTS were generated. Each ALERT has the format
test-name_ALERT_alert-type_alert-level.
Click on the hyperlinks for more details of the test.

Alert level C

PLAT411_ALERT_2_C	Short Inter H...H Contact	H3	..H14	.	2.13 Ang.
		-x,-1/2+y,-1-z =			2_544 Check
PLAT411_ALERT_2_C	Short Inter H...H Contact	H9	..H14	.	2.09 Ang.
		-x,-1/2+y,-1-z =			2_544 Check
PLAT790_ALERT_4_C	Centre of Gravity not Within Unit Cell: Resd. #				1 Note
	C20 H21 N2 O2				
PLAT911_ALERT_3_C	Missing FCF Refl Between Thmin & STh/L=		0.600		5 Report
PLAT913_ALERT_3_C	Missing # of Very Strong Reflections in FCF				5 Note
PLAT977_ALERT_2_C	Check Negative Difference Density on H14				-0.34 eA-3

Alert level G

PLAT791_ALERT_4_G	Model has Chirality at C1	(Sohnke SpGr)			S Verify
PLAT791_ALERT_4_G	Model has Chirality at C2	(Sohnke SpGr)			S Verify
PLAT791_ALERT_4_G	Model has Chirality at C3	(Sohnke SpGr)			R Verify
PLAT791_ALERT_4_G	Model has Chirality at C4	(Sohnke SpGr)			S Verify
PLAT910_ALERT_3_G	Missing # of FCF Reflection(s) Below Theta(Min).				1 Note
PLAT941_ALERT_3_G	Average HKL Measurement Multiplicity				4.3 Low
PLAT967_ALERT_5_G	Note: Two-Theta Cutoff Value in Embedded .res ..				138.0 Degree
PLAT978_ALERT_2_G	Number C-C Bonds with Positive Residual Density.				5 Info

0 **ALERT level A** = Most likely a serious problem - resolve or explain
0 **ALERT level B** = A potentially serious problem, consider carefully
6 **ALERT level C** = Check. Ensure it is not caused by an omission or oversight
8 **ALERT level G** = General information/check it is not something unexpected

0 ALERT type 1 CIF construction/syntax error, inconsistent or missing data
4 ALERT type 2 Indicator that the structure model may be wrong or deficient
4 ALERT type 3 Indicator that the structure quality may be low
5 ALERT type 4 Improvement, methodology, query or suggestion
1 ALERT type 5 Informative message, check

It is advisable to attempt to resolve as many as possible of the alerts in all categories. Often the minor alerts point to easily fixed oversights, errors and omissions in your CIF or refinement strategy, so attention to these fine details can be worthwhile. In order to resolve some of the more serious problems it may be necessary to carry out additional measurements or structure refinements. However, the purpose of your study may justify the reported deviations and the more serious of these should normally be commented upon in the discussion or experimental section of a paper or in the "special_details" fields of the CIF. checkCIF was carefully designed to identify outliers and unusual parameters, but every test has its limitations and alerts that are not important in a particular case may appear. Conversely, the absence of alerts does not guarantee there are no aspects of the results needing attention. It is up to the individual to critically assess their own results and, if necessary, seek expert advice.

Publication of your CIF in IUCr journals

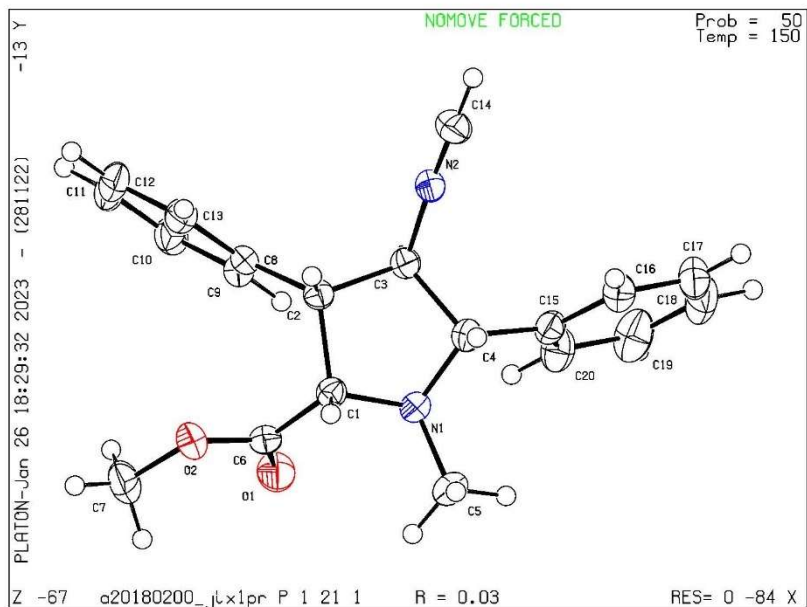
A basic structural check has been run on your CIF. These basic checks will be run on all CIFs submitted for publication in IUCr journals (*Acta Crystallographica*, *Journal of Applied Crystallography*, *Journal of Synchrotron Radiation*); however, if you intend to submit to *Acta Crystallographica Section C* or *E* or *IUCrData*, you should make sure that full publication checks are run on the final version of your CIF prior to submission.

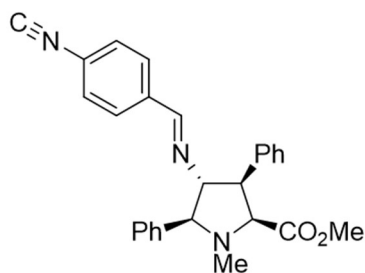
Publication of your CIF in other journals

Please refer to the *Notes for Authors* of the relevant journal for any special instructions relating to CIF submission.

PLATON version of 28/11/2022; check.def file version of 28/11/2022

Datablock a20180200_jlx1pr - ellipsoid plot





35-XL


SERVICIO GENERAL RAYOS X
Unidad de Moléculas y Materiales


✉ Servicios Generales de Investigación (SGIker)
 Facultad de Ciencia y Tecnología, Edificio CD3
 UPV/EHU.
 Bº Sarriena, s/n - 48940 Leioa (Bizkaia)

☎ 946013488
 Fax: 946013500
 ✉ leire.sanfclces@ehu.es

a20200322_JX115IremCA2

Comentario:

El usuario envió una muestra del compuesto **JX115I** (prismas incoloros) para determinar su estructura molecular. Se selecciona uno de ellos de tamaño aproximado $0.295 \times 0.243 \times 0.048 \text{ mm}^3$ para realizar la toma de datos.

Se confirma la estructura molecular coincidente con la propuesta por el usuario. La estructura cristalina determinada no es centrosimétrica (grupo espacial $P2_1$), en principio solo un enantiómero está presente en la estructura

Table 1 Crystal data and structure refinement for a20200322_JX115IremCA2.

Identification code	a20200322_JX115IremCA2
Empirical formula	$C_{28}H_{26}N_2O_2$
Formula weight	422.51
Temperature/K	150.01(10)
Crystal system	monoclinic
Space group	$P2_1$
a/Å	9.91367(12)
b/Å	8.94300(7)
c/Å	14.82969(12)
$\alpha/^\circ$	90.0
$\beta/^\circ$	91.7101(10)
$\gamma/^\circ$	90.0
Volume/Å ³	1314.18(2)
Z	2
$\rho_{\text{calc}}/\text{cm}^3$	1.068
μ/mm^{-1}	0.531
F(000)	448.0
Crystal size/mm ³	$0.295 \times 0.243 \times 0.048$
Radiation	CuK α ($\lambda = 1.54184$)
2 θ range for data collection/ $^\circ$	10.59 to 137.998
Index ranges	$-11 \leq h \leq 12$, $-10 \leq k \leq 10$, $-17 \leq l \leq 17$
Reflections collected	24246

C12	5043(3)	4924(3)	6549.5(18)	38.3(6)
C25	1987(3)	8885(3)	1670.9(19)	38.7(6)
C11	3967(3)	5705(3)	6894.8(17)	40.4(7)
C26	1245(3)	9698(3)	2270.1(19)	39.6(7)
C10	2784(3)	5879(3)	6371.8(17)	38.6(6)
C22	10782(3)	5815(4)	-285(2)	55.6(9)

Table 3 Anisotropic Displacement Parameters ($\text{\AA}^2 \times 10^3$) for a20200322_JX115IremCA2. The Anisotropic displacement factor exponent takes the form: $-2\pi^2[h^2a^2U_{11}+2hka^*b^*U_{12}+\dots]$.

Atom	U ₁₁	U ₂₂	U ₃₃	U ₂₃	U ₁₃	U ₁₂
O22	25.9(9)	22.5(8)	34.5(8)	10.0(6)	4.3(7)	-0.3(6)
O21	25.3(10)	38.1(10)	48.2(10)	13.8(8)	12.9(8)	7.3(8)
N1	17.9(10)	17.4(8)	28.3(8)	4.1(7)	1.7(7)	-0.4(7)
N2	18.7(10)	25.9(9)	30.9(9)	3.8(7)	6.8(8)	0.3(7)
C21	16.9(12)	45.2(13)	24.9(10)	-7.3(9)	8.4(9)	-13.1(10)
C23	18.9(12)	21.2(10)	27.6(10)	3.2(8)	-1.6(8)	-1.1(8)
C6	22.9(12)	20.6(10)	26.5(10)	1.3(8)	1.3(9)	0.3(8)
C14	21.0(12)	27.2(11)	29.4(10)	2.9(9)	4.2(9)	-1.0(9)
C3	18.3(12)	21.1(9)	28.6(10)	2.1(8)	4.6(9)	0.7(8)
C1	22.4(12)	16.0(9)	26.2(9)	1.3(7)	2.3(9)	1.1(8)
C8	22.0(12)	18.7(9)	29.3(10)	5.7(8)	0.9(9)	-4.1(9)
C18	21.7(13)	42.6(14)	26.0(10)	-2.1(9)	3.1(9)	-10.4(11)
C4	19.6(12)	19.3(10)	27.1(9)	1.1(8)	3.2(8)	-0.3(8)
C2	18.0(12)	19.4(9)	32.3(10)	3.1(8)	5.5(9)	3.8(8)
C15	17.1(12)	32.7(11)	28.2(10)	3.7(9)	0.3(9)	-4.0(9)
C28	30.1(14)	21.4(10)	31.4(11)	-1.2(9)	0.2(10)	2.2(9)
C16	22.5(12)	30.6(12)	30.3(10)	-1.5(9)	0.9(9)	-8.1(10)
C24	29.0(14)	30.4(12)	31.3(11)	6.9(9)	0.7(10)	-1.8(10)
C13	26.0(13)	25.7(11)	39.4(11)	9.3(9)	-5.5(10)	-1.7(10)
C5	22.9(13)	21.6(10)	34.5(11)	0.5(8)	-1.8(9)	-2.5(9)
C19	28.2(14)	37.0(13)	37.9(12)	-0.9(10)	7.5(10)	-10.0(11)
C20	30.1(14)	28.1(12)	38.9(12)	-2.6(10)	7.6(10)	-8.2(10)
C9	27.4(14)	34.1(12)	34.2(11)	-3.2(10)	-0.2(10)	4.9(10)
C27	39.0(16)	21.9(11)	43.7(13)	-6.6(9)	-8.2(12)	4.6(10)
C7	34.5(15)	32.2(12)	34.4(11)	13.1(10)	1.2(11)	-7.0(11)
C17	23.6(13)	39.7(13)	33.8(11)	-5.6(10)	2.6(10)	-8.7(11)
C12	38.5(16)	34.4(13)	41.2(13)	8.5(10)	-12.0(11)	-11.2(11)
C25	43.7(17)	29.6(12)	42.1(13)	12.4(10)	-9.0(12)	-7.1(11)
C11	55.3(19)	32.2(13)	33.1(12)	-1.7(10)	-7.8(12)	-8.8(12)
C26	47.5(17)	18.7(11)	51.3(14)	4.6(10)	-21.0(13)	-1.7(11)
C10	45.1(17)	35.6(13)	34.9(12)	-4.4(10)	0.9(12)	3.1(12)
C22	52(2)	67(2)	48.8(16)	-13.9(15)	17.3(15)	-22.2(18)

Independent reflections	4860 [R _{int} = 0.0347, R _{sigma} = 0.0275]
Data/restraints/parameters	4860/4/294
Goodness-of-fit on F ²	1.052
Final R indexes [I >= 2σ (I)]	R ₁ = 0.0384, wR ₂ = 0.1052
Final R indexes [all data]	R ₁ = 0.0405, wR ₂ = 0.1071
Largest diff. peak/hole / e Å ⁻³	0.45/-0.38
Flack parameter	0.11(10)
Bijvoet Pairs Coverage	100%
Hooft y	0.16(9)
P3 false	≤ 10 ⁻⁹⁹
[a] Esquema de pesado: 1/[σ ² (F _o ²) + (0.0723P) ² + 0.1002P] donde P = [Max(F _o ² , 0) + 2F _c ²]/3.	
[b] Expresión de extinción secundaria tipo SHELXL: F _c * = kF _c [1 + 0.001F _c ² λ ³ /sen(2θ)] ^{-1/4}	

Table 2 Fractional Atomic Coordinates (×10⁴) and Equivalent Isotropic Displacement Parameters (Å²×10³) for a20200322_JX115IremCA2. U_{eq} is defined as 1/3 of of the trace of the orthogonalised U_{ij} tensor.

Atom	x	y	z	U(eq)
O22	2444.9(17)	1217.0(17)	4904.8(11)	27.6(4)
O21	521.7(19)	2524(2)	4782.2(13)	37.0(4)
N1	1622.0(19)	4401(2)	3470.7(12)	21.2(4)
N2	5027(2)	4938(2)	2916.2(13)	25.0(4)
C21	9949(2)	5801(3)	262.3(14)	28.9(5)
C23	2099(2)	6803(2)	2708.2(14)	22.6(5)
C6	1663(2)	2304(2)	4561.4(14)	23.3(5)
C14	5828(2)	6020(3)	2781.8(15)	25.8(5)
C3	3919(2)	5215(2)	3511.8(14)	22.6(4)
C1	2413(2)	3170(2)	3852.6(14)	21.5(4)
C8	3765(2)	4486(2)	5151.5(14)	23.3(4)
C18	8951(3)	5830(3)	906.5(15)	30.0(5)
C4	2581(2)	5246(2)	2937.0(14)	21.9(4)
C2	3744(2)	3909(2)	4195.4(15)	23.2(5)
C15	6939(2)	5917(3)	2141.2(15)	26.0(5)
C28	1348(3)	7633(2)	3313.6(15)	27.6(5)
C16	7230(2)	4586(3)	1704.2(15)	27.8(5)
C24	2416(3)	7443(3)	1885.2(16)	30.3(5)
C13	4938(3)	4324(3)	5686.8(17)	30.5(5)
C5	463(2)	3935(2)	2905.6(16)	26.4(5)
C19	8697(3)	7161(3)	1343.7(17)	34.2(6)
C20	7693(3)	7185(3)	1968.9(17)	32.2(5)
C9	2691(3)	5278(3)	5508.4(17)	31.9(5)
C27	924(3)	9069(3)	3092.4(18)	35.1(6)
C7	1805(3)	267(3)	5556.1(17)	33.7(6)
C17	8232(3)	4530(3)	1080.8(16)	32.3(5)

Table 4 Bond Lengths for a20200322_JX115IremCA2.

Atom	Atom	Length/Å	Atom	Atom	Length/Å
O22	C6	1.335(3)	C8	C2	1.508(3)
O22	C7	1.447(3)	C8	C13	1.396(3)
O21	C6	1.203(3)	C8	C9	1.396(3)
N1	C1	1.456(3)	C18	C19	1.382(4)
N1	C4	1.465(3)	C18	C17	1.391(4)
N1	C5	1.463(3)	C15	C16	1.390(3)
N2	C14	1.271(3)	C15	C20	1.386(3)
N2	C3	1.451(3)	C28	C27	1.387(3)
C21	C18	1.397(3)	C16	C17	1.378(3)
C21	C22	1.1751(14)	C24	C25	1.392(4)
C23	C4	1.507(3)	C13	C12	1.389(4)
C23	C28	1.397(3)	C19	C20	1.381(4)
C23	C24	1.392(3)	C9	C10	1.389(4)
C6	C1	1.518(3)	C27	C26	1.388(4)
C14	C15	1.478(3)	C12	C11	1.386(5)
C3	C4	1.556(3)	C25	C26	1.377(4)
C3	C2	1.559(3)	C11	C10	1.395(4)
C1	C2	1.548(3)			

Table 5 Bond Angles for a20200322_JX115IremCA2.

Atom	Atom	Atom	Angle/°	Atom	Atom	Atom	Angle/°
C6	O22	C7	114.90(19)	C17	C18	C21	119.3(2)
C1	N1	C4	104.46(17)	N1	C4	C23	113.08(19)
C1	N1	C5	114.33(17)	N1	C4	C3	104.54(16)
C5	N1	C4	110.42(16)	C23	C4	C3	113.54(18)
C14	N2	C3	116.95(19)	C1	C2	C3	102.52(17)
C22	C21	C18	178.3(4)	C8	C2	C3	110.89(17)
C28	C23	C4	121.16(19)	C8	C2	C1	116.25(19)
C24	C23	C4	119.9(2)	C16	C15	C14	121.5(2)
C24	C23	C28	118.9(2)	C20	C15	C14	118.9(2)
O22	C6	C1	110.20(19)	C20	C15	C16	119.6(2)
O21	C6	O22	123.7(2)	C27	C28	C23	120.2(2)
O21	C6	C1	126.1(2)	C17	C16	C15	120.6(2)
N2	C14	C15	122.3(2)	C25	C24	C23	120.3(2)
N2	C3	C4	108.56(17)	C12	C13	C8	121.5(3)
N2	C3	C2	111.67(18)	C20	C19	C18	118.3(2)
C4	C3	C2	105.07(18)	C19	C20	C15	121.0(2)
N1	C1	C6	112.71(18)	C10	C9	C8	121.0(2)
N1	C1	C2	104.40(17)	C28	C27	C26	120.4(3)

C6	C1	C2	114.88(18)	C16	C17	C18	118.5(2)
C13	C8	C2	119.1(2)	C11	C12	C13	119.8(3)
C13	C8	C9	118.0(2)	C26	C25	C24	120.5(2)
C9	C8	C2	122.7(2)	C12	C11	C10	119.6(2)
C19	C18	C21	118.6(2)	C25	C26	C27	119.6(2)
C19	C18	C17	122.1(2)	C9	C10	C11	120.0(3)

Table 6 Torsion Angles for a20200322_JX115IremCA2.

A	B	C	D	Angle/°	A	B	C	D	Angle/°
O22	C6	C1	N1	178.39(17)	C4	C3	C2	C8	-116.6(2)
O22	C6	C1	C2	-59.0(2)	C2	C3	C4	N1	17.9(2)
O21	C6	C1	N1	2.9(3)	C2	C3	C4	C23	141.56(19)
O21	C6	C1	C2	122.4(3)	C2	C8	C13	C12	175.5(2)
N1	C1	C2	C3	-31.8(2)	C2	C8	C9	C10	-175.6(2)
N1	C1	C2	C8	89.3(2)	C15	C16	C17	C18	0.6(4)
N2	C14	C15	C16	-5.2(3)	C28	C23	C4	N1	35.2(3)
N2	C14	C15	C20	174.2(2)	C28	C23	C4	C3	-83.7(3)
N2	C3	C4	N1	137.46(18)	C28	C23	C24	C25	-0.2(4)
N2	C3	C4	C23	-98.8(2)	C28	C27	C26	C25	0.2(4)
N2	C3	C2	C1	-109.4(2)	C16	C15	C20	C19	2.5(4)
N2	C3	C2	C8	125.9(2)	C24	C23	C4	N1	-145.5(2)
C21	C18	C19	C20	179.0(2)	C24	C23	C4	C3	95.6(2)
C21	C18	C17	C16	-178.6(2)	C24	C23	C28	C27	0.2(4)
C23	C28	C27	C26	-0.2(4)	C24	C25	C26	C27	-0.1(4)
C23	C24	C25	C26	0.1(4)	C13	C8	C2	C3	-101.8(2)
C6	C1	C2	C3	155.76(18)	C13	C8	C2	C1	141.7(2)
C6	C1	C2	C8	-34.6(3)	C13	C8	C9	C10	-0.4(4)
C14	N2	C3	C4	109.5(2)	C13	C12	C11	C10	0.1(4)
C14	N2	C3	C2	-135.1(2)	C5	N1	C1	C6	-69.1(2)
C14	C15	C16	C17	177.2(2)	C5	N1	C1	C2	165.61(17)
C14	C15	C20	C19	-176.9(2)	C5	N1	C4	C23	73.8(2)
C3	N2	C14	C15	-175.6(2)	C5	N1	C4	C3	162.22(17)
C1	N1	C4	C23	162.84(17)	C19	C18	C17	C16	0.6(4)
C1	N1	C4	C3	-38.8(2)	C20	C15	C16	C17	-2.1(4)
C8	C13	C12	C11	0.0(4)	C9	C8	C2	C3	73.4(3)
C8	C9	C10	C11	0.5(4)	C9	C8	C2	C1	-43.2(3)
C18	C19	C20	C15	-1.3(4)	C9	C8	C13	C12	0.2(3)
C4	N1	C1	C6	170.14(17)	C7	O22	C6	O21	1.8(3)
C4	N1	C1	C2	44.8(2)	C7	O22	C6	C1	176.92(18)
C4	C23	C28	C27	179.5(2)	C17	C18	C19	C20	-0.2(4)

C4 C23 C24 C25 -179.4 (2) C12 C11 C10 C9 -0.3 (4)
 C4 C3 C2 C1 8.1 (2)

Table 7 Hydrogen Atom Coordinates ($\text{\AA} \times 10^4$) and Isotropic Displacement Parameters ($\text{\AA}^2 \times 10^3$) for a20200322_JX115IremCA2.

Atom	x	y	z	U(eq)
H14	5708.84	6926.33	3104.2	31
H3	4054.44	6183.56	3838.65	27
H1	2629.1	2466.97	3353.1	26
H4	2724.58	4693.08	2361.81	26
H2	4500.38	3181.96	4129.46	28
H28	1126.15	7213.01	3878.65	33
H16	6735.23	3707.97	1836.56	33
H24	2928.64	6891.84	1467.73	36
H13	5680.55	3790.54	5455.68	37
H5A	779.37	3394.16	2377.59	40
H5B	-49.52	4818.8	2707	40
H5C	-119	3279.28	3253.75	40
H19	9200.81	8035.86	1217.36	41
H20	7516.19	8084.06	2285.59	39
H9	1883.92	5408.34	5155.34	38
H27	410.22	9625.95	3506.2	42
H7A	1048.56	-266.33	5261.81	51
H7B	1469.66	881.82	6048.65	51
H7C	2462.07	-457.4	5799.09	51
H17	8427.54	3624.62	776.6	39
H12	5851.47	4800.65	6902.18	46
H25	2207.33	9311.92	1107.48	46
H11	4033.95	6119.32	7484.31	48
H26	955.77	10682.28	2121.66	48
H10	2041.22	6409.06	6606.39	46
H22	11330 (30)	5720 (50)	-834 (18)	67

Table 8 Solvent masks information for a20200322_JX115IremCA2.

Number	X	Y	Z	Volume	Electron count	Content
1	0.500	-0.374	0.000	256.2	51.3?	

Experimental

Single crystals of $\text{C}_{28}\text{H}_{26}\text{N}_2\text{O}_2$ [a20200322_JX115IremCA2]. A suitable crystal was selected and mounted on a SuperNova, Single source at offset/far, Atlas diffractometer. The crystal was kept at 150.01(10) K during data collection. Using Olex2 [1], the structure was solved with the ShelXT [2] structure solution program using Intrinsic Phasing and refined with the ShelXL [3] refinement package using Least Squares minimisation.

1. Dolomanov, O.V., Bourhis, L.J., Gildea, R.J., Howard, J.A.K. & Puschmann, H. (2009), *J. Appl. Cryst.* 42, 339-341.
2. Sheldrick, G.M. (2015). *Acta Cryst.* A71, 3-8.
3. Sheldrick, G.M. (2015). *Acta Cryst.* C71, 3-8.

Crystal structure determination of [a20200322_JX115IremCA2]

Crystal Data for $C_{28}H_{26}N_2O_2$ ($M=422.51$ g/mol): monoclinic, space group $P2_1$ (no. 4), $a = 9.91367(12)$ Å, $b = 8.94300(7)$ Å, $c = 14.82969(12)$ Å, $\beta = 91.7101(10)^\circ$, $V = 1314.18(2)$ Å³, $Z = 2$, $T = 150.01(10)$ K, $\mu(\text{CuK}\alpha) = 0.531$ mm⁻¹, $D_{\text{calc}} = 1.068$ g/cm³, 24246 reflections measured ($10.59^\circ \leq 2\theta \leq 137.998^\circ$), 4860 unique ($R_{\text{int}} = 0.0347$, $R_{\text{sigma}} = 0.0275$) which were used in all calculations. The final R_1 was 0.0384 ($I > 2\sigma(I)$) and wR_2 was 0.1071 (all data).

Refinement model description

Number of restraints - 4, number of constraints - unknown.

Details:

1. Fixed Uiso
 - At 1.2 times of:
 - All C(H) groups
 - At 1.5 times of:
 - All C(H,H,H) groups
2. Restrained distances
 - H22-C22
 - 0.89 with sigma of 0.01
 - C21-C22
 - 1.18 with sigma of 0.001
 - C21-H22
 - 2.25 with sigma of 0.01
- 3.a Ternary CH refined with riding coordinates:
 - C3(H3), C1(H1), C4(H4), C2(H2)
- 3.b Aromatic/amide H refined with riding coordinates:
 - C14(H14), C28(H28), C16(H16), C24(H24), C13(H13), C19(H19), C20(H20), C9(H9), C27(H27), C17(H17), C12(H12), C25(H25), C11(H11), C26(H26), C10(H10)
- 3.c Idealised Me refined as rotating group:
 - C5(H5A,H5B,H5C), C7(H7A,H7B,H7C)

This report has been created with Olex2, compiled on 2018.05.29 svn.r3508 for OlexSys. Please [let us know](#) if there are any errors or if you would like to have additional features.

ANALISIS CONFIGURACION ABSOLUTA

Puesto que se requería la determinación de la configuración absoluta, se ha realizado una toma de datos incluyendo pares de Friedel, consiguiendo una cobertura del 100% de los mismos. El *parámetro de Flack* (x) tiene un valor 0.11(10). El valor de la incertidumbre (0.10) está al límite de ser lo suficientemente pequeña para distinguir si el espécimen es de un enantiómero ($x = 0$), del opuesto ($x = 1$), o una macla racémica ($x = 0.5$),¹ algo que era de esperar por la ausencia de átomos pesados. El resultado se confirma con un análisis de los pares de Friedel usando estadística bayesiana² utilizando el programa PLATON³. Dados los datos de difracción con una cobertura de los pares de Friedel del 100%, este análisis indica que *la probabilidad de que la configuración absoluta se haya asignado correctamente es esencialmente del 100%*. De hecho, *la probabilidad de que la asignación sea incorrecta es menor de 10^{-16}* . Y el *parámetro de estructura absoluta* (equivalente a Flack) resulta ser de 0.16(9), confirmando la asignación.⁴

¹ H. D. Flack & G. Bernardinelli, *Acta Cryst.* 1999, A55, 908-915; H. D. Flack & G. Bernardinelli, *J. Appl. Cryst.* 2000, 33, 1143-1148.

² R. W. W. Hooft, L. H. Straver & A. L. Spek, *J. Appl. Cryst.* 2008, 41, 96-103

³ A. L. Spek (2010) PLATON, A Multipurpose Crystallographic Tool, Utrecht University, Utrecht, The Netherlands; A. L. Spek, *J. Appl. Cryst.* 2003, 36, 7-13.

⁴ A. L. Thompson & D. J. Watkin, *Tetrahedron: Asymmetry* 2009, 20, 712-717

En resumen, el cristal contiene un solo enantiómero, cuya configuración absoluta ha sido determinada con una certeza cercana al 100%: la probabilidad de que la asignación sea incorrecta es menor de 10^{-18} .

Texto sugerido en inglés⁵: Analysis of the absolute structure using likelihood methods (Hooft, Straver & Spek, 2008 [4]) was performed using PLATON (Spek, 2010[5]). The Friedel pair coverage of the experiment is almost complete (100%). The results indicated that the absolute structure had been correctly assigned. The method calculated that the probability that the structure is inverted is smaller than 10^{-18} . The absolute structure parameter γ (Hooft, Straver & Spek, 2008[4]) was calculated using PLATON (Spek, 2010[5]). The resulting value was $\gamma=0.16(9)$, which together with Flack parameter value, indicate that the absolute structure has probably been determined correctly.

1. R. W. W. Hooft, L. H. Straver & A. L. Spek, J. Appl. Cryst. 2008, 41, 96-103.
2. A. L. Spek (2010) PLATON, A Multipurpose Crystallographic Tool, Utrecht University, Utrecht, The Netherlands; A. L. Spek, J. Appl. Cryst. 2003, 36, 7-13.

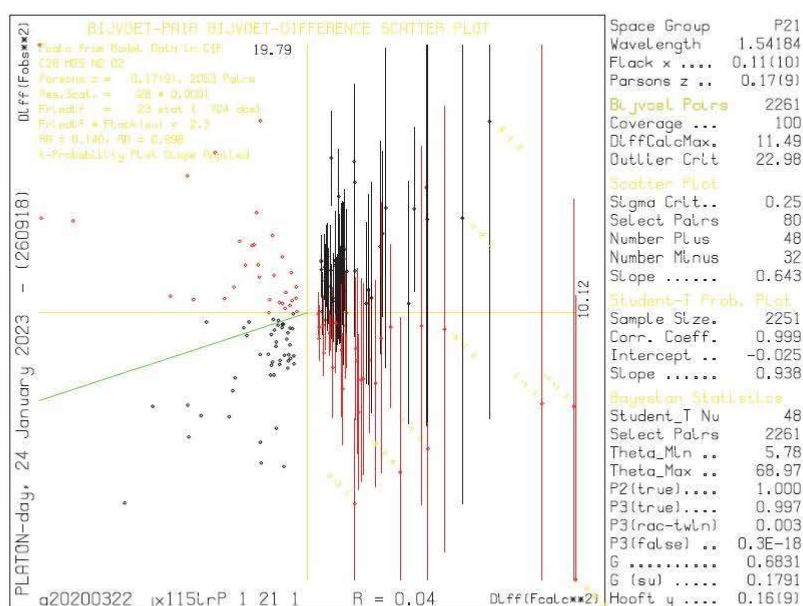


Figura 1. Análisis de la estructura absoluta mediante estadística bayesiana usando el programa Platon.

Es importante recordar que siempre que se determina la configuración absoluta mediante difracción de RX sobre monocristal, es imprescindible que se confirme la pureza enantiomérica en la disolución (RMN, HPLC quiral,...), ya que sólo se determina la estructura de un cristal (a lo sumo unos pocos), por lo que no se puede asegurar que todos los cristales contengan el mismo enantiómero debido a la posible resolución espontánea de una disolución racémica.

⁵ <http://www.absolutestructure.com/> (accedido el 27 de abril de 2022)

The following ALERTS were generated. Each ALERT has the format
test-name_ALERT_alert-type_alert-level.
 Click on the hyperlinks for more details of the test.

Alert level C

PLAT977_ALERT_2_C Check Negative Difference Density on H22 . -0.36 eA-3

Alert level G

PLAT002_ALERT_2_G	Number of Distance or Angle Restraints on AtSite	3	Note
PLAT142_ALERT_4_G	s.u. on b - Axis Small or Missing	0.00007	Ang.
PLAT143_ALERT_4_G	s.u. on c - Axis Small or Missing	0.00012	Ang.
PLAT172_ALERT_4_G	The CIF-Embedded .res File Contains DFIX Records	2	Report
PLAT173_ALERT_4_G	The CIF-Embedded .res File Contains DANG Records	1	Report
PLAT230_ALERT_2_G	Hirshfeld Test Diff for C18 --C21 .	5.1	s.u.
PLAT230_ALERT_2_G	Hirshfeld Test Diff for C21 --C22 .	10.5	s.u.
PLAT605_ALERT_4_G	Largest Solvent Accessible VOID in the Structure	237	A**3
PLAT791_ALERT_4_G	Model has Chirality at C1 (Sohnke SpGr)	S	Verify
PLAT791_ALERT_4_G	Model has Chirality at C2 (Sohnke SpGr)	S	Verify
PLAT791_ALERT_4_G	Model has Chirality at C3 (Sohnke SpGr)	R	Verify
PLAT791_ALERT_4_G	Model has Chirality at C4 (Sohnke SpGr)	S	Verify
PLAT860_ALERT_3_G	Number of Least-Squares Restraints	4	Note
PLAT910_ALERT_3_G	Missing # of FCF Reflection(s) Below Theta (Min).	2	Note
PLAT912_ALERT_4_G	Missing # of FCF Reflections Above STh/L= 0.600	1	Note
PLAT933_ALERT_2_G	Number of HKL-OMIT Records in Embedded .res File	2	Note
PLAT967_ALERT_5_G	Note: Two-Theta Cutoff Value in Embedded .res ..	138.0	Degree
PLAT978_ALERT_2_G	Number C-C Bonds with Positive Residual Density.	0	Info

0 **ALERT level A** = Most likely a serious problem - resolve or explain
 0 **ALERT level B** = A potentially serious problem, consider carefully
 1 **ALERT level C** = Check. Ensure it is not caused by an omission or oversight
 18 **ALERT level G** = General information/check it is not something unexpected

0 ALERT type 1 CIF construction/syntax error, inconsistent or missing data
 6 ALERT type 2 Indicator that the structure model may be wrong or deficient
 2 ALERT type 3 Indicator that the structure quality may be low
 10 ALERT type 4 Improvement, methodology, query or suggestion
 1 ALERT type 5 Informative message, check

It is advisable to attempt to resolve as many as possible of the alerts in all categories. Often the minor alerts point to easily fixed oversights, errors and omissions in your CIF or refinement strategy, so attention to these fine details can be worthwhile. In order to resolve some of the more serious problems it may be necessary to carry out additional measurements or structure refinements. However, the purpose of your study may justify the reported deviations and the more serious of these should normally be commented upon in the discussion or experimental section of a paper or in the "special_details" fields of the CIF. checkCIF was carefully designed to identify outliers and unusual parameters, but every test has its limitations and alerts that are not important in a particular case may appear. Conversely, the absence of alerts does not guarantee there are no aspects of the results needing attention. It is up to the individual to critically assess their own results and, if necessary, seek expert advice.

Publication of your CIF in IUCr journals

A basic structural check has been run on your CIF. These basic checks will be run on all CIFs submitted for publication in IUCr journals (*Acta Crystallographica*, *Journal of Applied Crystallography*, *Journal of Synchrotron Radiation*); however, if you intend to submit to *Acta Crystallographica Section C* or *E* or *IUCrData*, you should make sure that full publication checks are run on the final version of your CIF prior to submission.

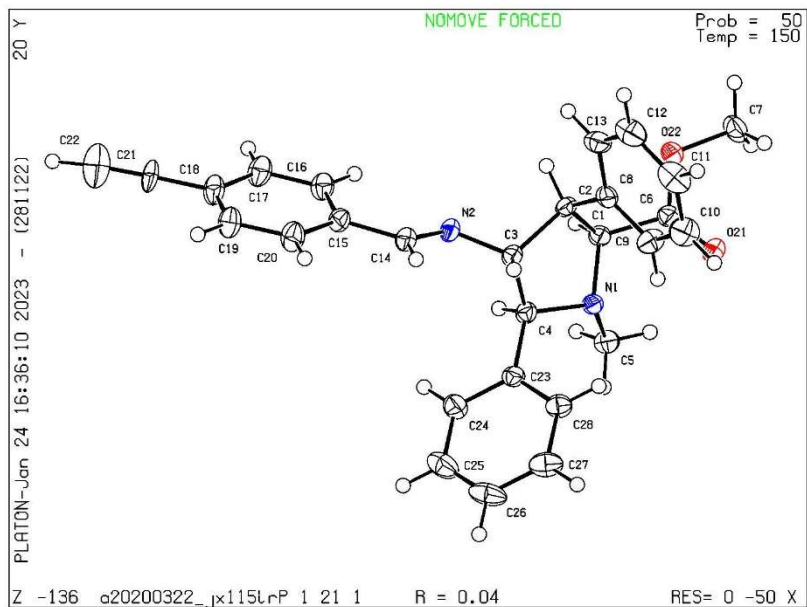
Publication of your CIF in other journals

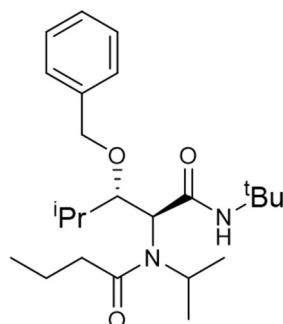
Please refer to the *Notes for Authors* of the relevant journal for any special instructions relating to CIF submission.

PLATON version of 28/11/2022; check.def file version of 28/11/2022

ANNEX VI

Datablock a20200322_jx115fremca2 - ellipsoid plot





45b-D1


**SERVICIO GENERAL RAYOS X
Unidad de Moléculas y Materiales**


✉ Servicios Generales de Investigación (SGIker)
Facultad de Ciencia y Tecnología, Edificio CD3
UPV/EHU.
Eº Sarriena, s/n - 48940 Leioa (Bizkaia)

☎ 946013488
Fax: 946013500
✉ leire.sanfelicis@ehu.es

a20200324_JX84

Comentario:

El usuario envió una muestra del compuesto *JX84* (prismas amarillos) para determinar su estructura molecular. Se selecciona uno de ellos de tamaño aproximado $0.331 \times 0.073 \times 0.052 \text{ mm}^3$ para realizar la toma de datos.

Se confirma la estructura molecular coincidente con la propuesta por el usuario. La estructura cristalina determinada es centrosimétrica (grupo espacial P-1).

Detalles técnicos:

La toma de datos se ha realizado en el difractómetro Agilent SuperNova Cu, equipado con detector de tipo CCD modelo Atlas, a una temperatura de 150.7(3)K, usando un Cryostream 700 de Agilent Cryosystems alimentado con nitrógeno líquido. Los datos se han procesado (determinación de celda unidad, corrección de absorción analítica empleando las caras indexadas, integración de intensidad de los datos y la corrección de Lorentz y de los efectos de polarización de los mismos), utilizando el paquete de software CrysAlis. La estructura se ha resuelto utilizando SHELXT y se ha refinado empleando la matriz completa de mínimos cuadrados con SHELXL-97(version2017). Los cálculos geométricos finales se llevaron a cabo con el Mercury y PLATON integrados en el paquete WinGX. Todos los átomos de hidrógeno se han localizado en el mapa de densidad residual y se han refinado con el modelo riding de SHELXL97(version2017).

Texto en inglés: "Intensity data were collected on an Agilent Technologies SuperNova diffractometer, wich was equipped with monochromated Cu $k\alpha$ radiation ($\lambda=1.54184 \text{ \AA}$) and Atlas CCD detector. Measurement was carried out at 150.7(3)K with the help of an Oxford Cryostream 700 PLUS temperature device. Data frames were processed (united cell detemination, analytical absorption correction with face indexing, intensity data integration and correction for Lorentz and polarization effects) using the CrysAlis software package.¹ The structure was solved using SHELXT² and refined by

¹ CrysAlisPro, Agilent Technologies, Version 1.171.37.31 (release 14-01-2014 CrysAlis171.NET)(compiled Jan 14 2014, 18:38:05).

² Sheldrick, G.M. (2015). Acta Cryst. A71, 3-8..

O3	6406.6(15)	5102.0(14)	8106.1(12)	28.6(3)
N1	3489.2(18)	6803.7(16)	6313.8(16)	29.2(4)
N2	3994.6(17)	3528.1(16)	7216.5(15)	26.5(4)
C1	3623(2)	5801(2)	7272.0(18)	26.7(5)
C2	4706(2)	4509.7(19)	7258.7(18)	24.7(4)
C3	5791(2)	4042.2(19)	8265.6(19)	27.1(5)
C4	6952(2)	2776(2)	8336(2)	33.8(5)
C5	7910(3)	2987(3)	7368(2)	44.5(6)
C6	9125(5)	1815(4)	7387(5)	43.2(15)
C6B	8847(8)	951(6)	9746(7)	73(2)
C7	7752(3)	2256(3)	9511(3)	57.5(8)
C8	2423(2)	8102(2)	6032(2)	34.6(5)
C9	992(3)	7906(3)	5892(3)	49.6(7)
C10	2787(3)	8940(2)	4915(2)	48.0(7)
C11	2441(3)	8757(2)	6941(3)	50.9(7)
C12	3162(2)	3078(2)	8186(2)	35.7(5)
C13	3645(3)	1588(3)	8782(2)	52.2(7)
C14	1587(3)	3616(3)	7908(3)	49.5(7)
C15	4128(2)	3146(2)	6270.5(19)	28.7(5)
C16	3412(3)	2175(2)	6111(2)	37.6(6)
C17	2690(20)	2690(20)	4856(16)	39(3)
C17B	3010(30)	2400(20)	4919(19)	45(3)
C18	1490(20)	3920(20)	4670(20)	61(5)
C18B	1780(30)	3700(30)	4480(18)	58(4)
C19	6181(2)	5739(2)	8963(2)	33.4(5)
C20	7064(2)	6660(2)	8736.0(19)	30.8(5)
C21	6477(3)	8012(2)	8342(2)	40.9(6)
C22	7321(3)	8852(3)	8108(3)	50.5(7)
C23	8742(3)	8342(3)	8271(2)	48.6(7)
C24	9351(3)	6995(3)	8661(2)	46.0(6)
C25	8511(2)	6164(2)	8893(2)	40.0(6)

Table 3 Anisotropic Displacement Parameters ($\text{\AA}^2 \times 10^3$) for a20200324_JX84. The Anisotropic displacement factor exponent takes the form: -

$2\pi^2[h^2a^2U_{11}+2hka*b*U_{12}+...]$.

Atom	U ₁₁	U ₂₂	U ₃₃	U ₂₃	U ₁₃	U ₁₂
O1	36.4(8)	35.2(8)	30.0(9)	-9.9(7)	8.0(7)	-4.6(7)
O2	51.6(10)	47.6(10)	36.3(10)	-22.3(8)	16.2(8)	-27.0(8)
O3	34.5(8)	27.9(7)	27.9(8)	-10.6(6)	4.5(6)	-14.0(6)
N1	29.9(9)	24.4(9)	30.2(11)	-7.5(8)	5.9(8)	-4.7(7)
N2	27.7(9)	25.6(9)	27.1(10)	-8.0(7)	2.9(7)	-9.5(7)
C1	25.9(10)	27.5(10)	27.0(12)	-8.8(9)	1.4(9)	-7.8(8)
C2	25.6(10)	23.3(10)	25.0(11)	-6.4(8)	3.2(8)	-7.8(8)
C3	29.6(11)	24.2(10)	28.6(12)	-6.8(9)	2.2(9)	-11.0(8)

C4	32.1(11)	26.0(11)	39.8(14)	-6.2(10)	-8.5(10)	-6.6(9)
C5	32.7(12)	40.8(13)	52.1(16)	-15.4(12)	3.4(11)	2.1(10)
C6	37(3)	31(2)	55(3)	-13(2)	0(2)	-2(2)
C6B	85(5)	49(4)	71(5)	-13(3)	-36(4)	1(3)
C7	59.9(17)	45.6(15)	49.5(18)	-6.5(13)	-19.7(14)	4.0(13)
C8	32.2(12)	27.1(11)	37.7(14)	-7.7(10)	1.3(10)	-0.8(9)
C9	35.1(13)	45.1(15)	56.0(18)	-6.4(13)	-4.2(12)	-2.1(11)
C10	49.5(15)	27.0(12)	50.2(17)	0.4(11)	6.0(13)	1.7(11)
C11	57.5(16)	31.3(13)	57.5(19)	-18.4(12)	-2.6(14)	2.3(12)
C12	40.9(13)	42.3(13)	31.6(13)	-12.7(10)	10.8(10)	-23.2(11)
C13	68.8(18)	49.9(16)	40.3(16)	-2.9(12)	8.7(14)	-33.5(14)
C14	42.1(14)	65.1(18)	57.2(19)	-31.0(15)	18.5(13)	-28.1(13)
C15	31.6(11)	25.3(10)	28.4(12)	-8.6(9)	1.4(9)	-6.9(9)
C16	46.6(14)	32.7(12)	38.4(15)	-13.3(10)	3.6(11)	-16.6(10)
C17	42(6)	40(7)	41(4)	-17(4)	-6(4)	-13(5)
C17B	48(7)	37(6)	54(5)	-17(5)	-3(5)	-15(5)
C18	59(8)	56(7)	58(8)	2(6)	-29(6)	-17(6)
C18B	61(8)	70(9)	55(6)	-25(6)	6(6)	-31(7)
C19	37.9(12)	36.4(12)	32.9(13)	-16.9(10)	7.5(10)	-15.3(10)
C20	34.6(12)	36.1(12)	27.0(12)	-15.1(10)	6.3(9)	-13.3(10)
C21	36.9(13)	37.6(13)	49.8(16)	-17.5(12)	6.1(11)	-9.3(10)
C22	60.7(17)	33.7(13)	60.0(19)	-15.3(12)	13.3(14)	-18.0(12)
C23	54.9(16)	54.3(16)	52.3(18)	-22.2(13)	16.4(13)	-35.1(14)
C24	37.3(13)	55.7(16)	50.0(17)	-17.5(13)	5.0(12)	-20.2(12)
C25	37.1(13)	36.1(13)	45.7(16)	-11.1(11)	2.0(11)	-10.7(10)

Table 4 Bond Lengths for a20200324_JX84.

Atom	Atom	Length/Å	Atom	Atom	Length/Å
O1	C1	1.233(3)	C8	C10	1.522(3)
O2	C15	1.232(3)	C8	C11	1.525(4)
O3	C3	1.440(2)	C12	C13	1.531(3)
O3	C19	1.433(3)	C12	C14	1.524(3)
N1	C1	1.340(3)	C15	C16	1.516(3)
N1	C8	1.477(3)	C16	C17	1.60(2)
N2	C2	1.477(3)	C16	C17B	1.47(2)
N2	C12	1.492(3)	C17	C18	1.50(2)
N2	C15	1.361(3)	C17B	C18B	1.56(2)
C1	C2	1.540(3)	C19	C20	1.496(3)
C2	C3	1.536(3)	C20	C21	1.382(3)
C3	C4	1.531(3)	C20	C25	1.390(3)
C4	C5	1.527(4)	C21	C22	1.394(4)
C4	C7	1.545(4)	C22	C23	1.367(4)
C5	C6	1.505(4)	C23	C24	1.380(4)

C6B C7	1.498(6)	C24 C25	1.383(3)
C8 C9	1.529(3)		

Table 5 Bond Angles for a20200324_JX84.

Atom Atom Atom	Angle/°	Atom Atom Atom	Angle/°
C19 O3 C3	115.55(16)	C10 C8 C9	110.0(2)
C1 N1 C8	126.02(18)	C10 C8 C11	109.8(2)
C2 N2 C12	117.67(17)	C11 C8 C9	110.8(2)
C15 N2 C2	116.38(17)	N2 C12 C13	113.8(2)
C15 N2 C12	125.92(18)	N2 C12 C14	113.7(2)
O1 C1 N1	124.64(19)	C14 C12 C13	112.8(2)
O1 C1 C2	121.27(19)	O2 C15 N2	120.53(19)
N1 C1 C2	114.08(18)	O2 C15 C16	118.0(2)
N2 C2 C1	110.12(16)	N2 C15 C16	121.42(19)
N2 C2 C3	114.23(16)	C15 C16 C17	109.9(7)
C3 C2 C1	109.31(17)	C17BC16 C15	113.2(8)
O3 C3 C2	105.00(16)	C18 C17 C16	111.7(13)
O3 C3 C4	108.74(17)	C16 C17BC18B	109.5(16)
C4 C3 C2	114.60(18)	O3 C19 C20	107.15(18)
C3 C4 C7	108.7(2)	C21 C20 C19	121.5(2)
C5 C4 C3	111.77(19)	C21 C20 C25	118.4(2)
C5 C4 C7	112.7(2)	C25 C20 C19	120.1(2)
C6 C5 C4	116.0(3)	C20 C21 C22	120.6(2)
C6B C7 C4	114.9(4)	C23 C22 C21	120.0(2)
N1 C8 C9	108.41(19)	C22 C23 C24	120.4(2)
N1 C8 C10	106.30(18)	C23 C24 C25	119.4(2)
N1 C8 C11	111.3(2)	C24 C25 C20	121.2(2)

Table 6 Torsion Angles for a20200324_JX84.

A B C D	Angle/°	A B C D	Angle/°
O1C1 C2 N2	69.2(3)	C3 C4 C5 C6	177.5(3)
O1C1 C2 C3	-57.0(3)	C3 C4 C7 C6B	174.9(4)
O2C15C16C17	-46.2(9)	C5 C4 C7 C6B	-60.7(5)
O2C15C16C17B	-32.4(12)	C7 C4 C5 C6	54.8(4)
O3C3 C4 C5	-49.3(2)	C8 N1 C1 O1	-6.6(4)
O3C3 C4 C7	75.7(2)	C8 N1 C1 C2	172.23(19)
O3C19C20C21	109.1(2)	C12N2 C2 C1	-62.5(2)
O3C19C20C25	-69.3(3)	C12N2 C2 C3	60.9(2)
N1C1 C2 N2	-109.6(2)	C12N2 C15 O2	-179.3(2)
N1C1 C2 C3	124.16(19)	C12N2 C15 C16	-0.3(3)
N2C2 C3 O3	176.66(16)	C15N2 C2 C1	115.6(2)
N2C2 C3 C4	57.4(2)	C15N2 C2 C3	-121.0(2)

N2C15C16C17	134.8(9)	C15N2 C12 C13	60.6(3)
N2C15C16C17B	148.6(11)	C15N2 C12 C14	-70.5(3)
C1N1 C8 C9	-67.1(3)	C15C16C17 C18	-67.3(14)
C1N1 C8 C10	174.6(2)	C15C16C17BC18B	-70.2(17)
C1N1 C8 C11	55.0(3)	C19O3 C3 C2	116.31(19)
C1C2 C3 O3	-59.5(2)	C19O3 C3 C4	-120.6(2)
C1C2 C3 C4	178.71(17)	C19C20C21 C22	-178.4(2)
C2N2 C12C13	-121.5(2)	C19C20C25 C24	178.3(2)
C2N2 C12C14	107.4(2)	C20C21C22 C23	-0.1(4)
C2N2 C15O2	2.8(3)	C21C20C25 C24	-0.1(4)
C2N2 C15C16	178.17(19)	C21C22C23 C24	0.3(4)
C2C3 C4 C5	67.9(2)	C22C23C24 C25	-0.4(4)
C2C3 C4 C7	-167.2(2)	C23C24C25 C20	0.3(4)
C3O3 C19C20	171.95(17)	C25C20C21 C22	0.0(4)

Table 7 Hydrogen Atom Coordinates ($\text{\AA} \times 10^4$) and Isotropic Displacement Parameters ($\text{\AA}^2 \times 10^3$) for a20200324_JX84.

Atom	x	y	z	U(eq)
H1	4092.33	6676.6	5805.29	35
H2	5205.92	4708.5	6550.88	30
H3	5306.4	3918.77	8985.26	33
H4	6501.18	2102.67	8273.36	41
H5A	7348.66	3356.83	6644.06	67
H5B	8581.77	2141.01	7397.51	67
H5C	8414.3	3598.84	7439.51	67
H6A	9687.44	2061.12	6746.95	65
H6B	8776.42	1096.24	7329.36	65
H6C	9703.56	1522.75	8095.97	65
H6BA	9610.55	1048.82	9252.17	110
H6BB	8433.9	309.56	9602.74	110
H6BC	9210.79	641.16	10538.32	110
H7A	8297.48	2845.46	9559.07	86
H7B	8383.04	1368.35	9619.56	86
H7C	7084.45	2223.34	10099.04	86
H9A	985.1	7537.96	5270.97	74
H9B	269.42	8757.24	5719.91	74
H9C	805.88	7298.3	6593.73	74
H10A	3699.3	9070.03	5015.06	72
H10B	2072.69	9798.48	4665.79	72
H10C	2822.53	8492.38	4343.64	72
H11A	2191.95	8220.51	7655.89	76
H11B	1763.79	9636.78	6709.91	76

H11C	3378	8835.14	7042.57	76
H12	3358.06	3480.71	8759.98	43
H13A	3191.46	1383.24	9493.69	78
H13B	4661.22	1294.61	8940.39	78
H13C	3390.42	1132.46	8293.22	78
H14A	1334.25	4570.85	7535.3	74
H14B	1106.23	3430.9	8607.57	74
H14C	1307.57	3192.17	7402.61	74
H16A	4047.7	1269.91	6427.9	45
H16B	2564.26	2237.61	6540.25	45
H16C	2698.29	2075.6	6667.8	45
H16D	4107.36	1302.11	6239.33	45
H17A	3386.52	2872.41	4303.46	47
H17B	2343.87	1992.16	4722.31	47
H17C	2719.35	1650.89	4848.05	54
H17D	3822.84	2474.64	4459.32	54
H18A	1096	4223.03	3889.05	92
H18B	1819.87	4600.99	4823.01	92
H18C	767.2	3723.46	5187.16	92
H18D	1548.1	3875.26	3676.18	88
H18E	2067.68	4436.49	4578.82	88
H18F	967.34	3605.87	4908.72	88
H19A	6451.28	5077.45	9721.58	40
H19B	5182.19	6233.67	8935.6	40
H21	5489.85	8371.13	8229.35	49
H22	6907.7	9780.24	7836.23	61
H23	9313.33	8917.35	8115.14	58
H24	10339.12	6641.7	8768.61	55
H25	8930.91	5237.11	9164.95	48

Table 8 Atomic Occupancy for a20200324_JX84.

Atom	Occupancy	Atom	Occupancy	Atom	Occupancy
H5A	0.493 (6)	H5B	0.493 (6)	H5C	0.493 (6)
C6	0.507 (6)	H6A	0.507 (6)	H6B	0.507 (6)
H6C	0.507 (6)	C6B	0.493 (6)	H6BA	0.493 (6)
H6BB	0.493 (6)	H6BC	0.493 (6)	H7A	0.507 (6)
H7B	0.507 (6)	H7C	0.507 (6)	H16A	0.48 (5)
H16B	0.48 (5)	H16C	0.52 (5)	H16D	0.52 (5)
C17	0.52 (5)	H17A	0.52 (5)	H17B	0.52 (5)
C17B	0.48 (5)	H17C	0.48 (5)	H17D	0.48 (5)
C18	0.52 (5)	H18A	0.52 (5)	H18B	0.52 (5)
H18C	0.52 (5)	C18B	0.48 (5)	H18D	0.48 (5)
H18E	0.48 (5)	H18F	0.48 (5)		

Experimental

Single crystals of $C_{25}H_{40}N_2O_3$ [a20200324_JX84]. A suitable crystal was selected and mounted on a SuperNova, Single source at offset/far, Atlas diffractometer. The crystal was kept at 150.7(3) K during data collection. Using Olex2 [1], the structure was solved with the ShelXT [2] structure solution program using Intrinsic Phasing and refined with the ShelXL [3] refinement package using Least Squares minimisation.

1. Dolomanov, O.V., Bourhis, L.J., Gildea, R.J., Howard, J.A.K. & Puschmann, H. (2009), *J. Appl. Cryst.* 42, 339-341.
2. Sheldrick, G.M. (2015). *Acta Cryst.* A71, 3-8.
3. Sheldrick, G.M. (2015). *Acta Cryst.* C71, 3-8.

Crystal structure determination of [a20200324_JX84]

Crystal Data for $C_{25}H_{40}N_2O_3$ ($M=416.59$ g/mol): triclinic, space group P-1 (no. 2), $a=10.0034(4)$ Å, $b=11.1308(3)$ Å, $c=12.4488(5)$ Å, $\alpha=72.231(3)^\circ$, $\beta=88.757(3)^\circ$, $\gamma=73.519(3)^\circ$, $V=1262.56(8)$ Å³, $Z=2$, $T=150.7(3)$ K, $\mu(\text{CuK}\alpha)=0.563$ mm⁻¹, $D_{\text{calc}}=1.096$ g/cm³, 19025 reflections measured ($7.476^\circ \leq 2\theta \leq 137.986^\circ$), 4679 unique ($R_{\text{int}}=0.0425$, $R_{\text{sigma}}=0.0371$) which were used in all calculations. The final R_1 was 0.0593 ($I > 2\sigma(I)$) and wR_2 was 0.1381 (all data).

Refinement model description

Number of restraints - 50, number of constraints - unknown.

Details:

1. Fixed Uiso
At 1.2 times of:
All C(H) groups, All C(H,H) groups, All C(H,H,H,H) groups, All N(H) groups
At 1.5 times of:
All C(H,H,H) groups
2. Restrained distances
C6B-C7 = C6-C5
1.5 with sigma of 0.01
3. Uiso/Uanis restraints and constraints
Uanis(C17B) * Ueq, Uanis(C17) * Ueq, Uanis(C18B) * Ueq, Uanis(C18)
* Ueq: with sigma of 0.01 and sigma for terminal atoms of 0.02
Uanis(C5) * Ueq, Uanis(C6) * Ueq, Uanis(C6B) * Ueq, Uanis(C7) * Ueq: with sigma of 0.005 and sigma for terminal atoms of 0.01
4. Others
Sof(H16C)=Sof(H16D)=Sof(C17)=Sof(H17A)=Sof(H17B)=Sof(C18)=Sof(H18A)=Sof(H18B)=
Sof(H18C)=1-FVAR(1)
Sof(H16A)=Sof(H16B)=Sof(C17B)=Sof(H17C)=Sof(H17D)=Sof(C18B)=Sof(H18D)=
Sof(H18E)=Sof(H18F)=FVAR(1)
Sof(H5A)=Sof(H5B)=Sof(H5C)=Sof(C6B)=Sof(H6BA)=Sof(H6BB)=Sof(H6BC)=1-FVAR(2)
Sof(C6)=Sof(H6A)=Sof(H6B)=Sof(H6C)=Sof(H7A)=Sof(H7B)=Sof(H7C)=FVAR(2)
- 5.a Ternary CH refined with riding coordinates:
C2(H2), C3(H3), C4(H4), C12(H12)
- 5.b Secondary CH2 refined with riding coordinates:
C16(H16A,H16B), C16(H16C,H16D), C17(H17A,H17B), C17B(H17C,H17D),
C19(H19A,H19B)
- 5.c Aromatic/amide H refined with riding coordinates:
N1(H1), C21(H21), C22(H22), C23(H23), C24(H24), C25(H25)
- 5.d Idealised Me refined as rotating group:
C5(H5A,H5B,H5C), C6(H6A,H6B,H6C), C6B(H6BA,H6BB,H6BC), C7(H7A,H7B,H7C),
C9(H9A,H9B,H9C), C10(H10A,H10B,H10C), C11(H11A,H11B,H11C),
C13(H13A,H13B,H13C),
C14(H14A,H14B,H14C), C18(H18A,H18B,H18C), C18B(H18D,H18E,H18F)

This report has been created with Olex2, compiled on 2018.05.29 svn.r3508 for OlexSys. Please [let us know](#) if there are any errors or if you would like to have additional features.

checkCIF/PLATON report

Structure factors have been supplied for datablock(s) a20200324_jx84

THIS REPORT IS FOR GUIDANCE ONLY. IF USED AS PART OF A REVIEW PROCEDURE FOR PUBLICATION, IT SHOULD NOT REPLACE THE EXPERTISE OF AN EXPERIENCED CRYSTALLOGRAPHIC REFEREE.

No syntax errors found. CIF dictionary Interpreting this report

Datablock: a20200324_jx84

Bond precision:	C-C = 0.0036 A	Wavelength=1.54184
Cell:	a=10.0034 (4)	b=11.1308 (3) c=12.4488 (5)
	alpha=72.231 (3)	beta=88.757 (3) gamma=73.519 (3)
Temperature:	151 K	

	Calculated	Reported
Volume	1262.56(9)	1262.56(8)
Space group	P -1	P -1
Hall group	-P 1	-P 1
Moiety formula	C25 H40 N2 O3	C25 H40 N2 O3
Sum formula	C25 H40 N2 O3	C25 H40 N2 O3
Mr	416.59	416.59
Dx, g cm-3	1.096	1.096
Z	2	2
Mu (mm-1)	0.559	0.563
F000	456.0	456.0
F000'	457.26	
h, k, lmax	12, 13, 15	12, 13, 15
Nref	4690	4679
Tmin, Tmax	0.952, 0.971	0.899, 0.978
Tmin'	0.830	

Correction method= # Reported T Limits: Tmin=0.899 Tmax=0.978
AbsCorr = ANALYTICAL

Data completeness= 0.998 Theta(max)= 68.993

R(reflections)= 0.0593 (3881)	wR2(reflections)= 0.1381 (4679)
S = 1.136	Npar= 311

The following ALERTS were generated. Each ALERT has the format

test-name_ALERT_alert-type_alert-level.

Click on the hyperlinks for more details of the test.

Alert level C

PLAT329_ALERT_4_C	Carbon Atom Hybridisation Unclear for	C5	Check
PLAT329_ALERT_4_C	Carbon Atom Hybridisation Unclear for	C7	Check
PLAT906_ALERT_3_C	Large K Value in the Analysis of Variance	9.654	Check
PLAT906_ALERT_3_C	Large K Value in the Analysis of Variance	2.210	Check
PLAT911_ALERT_3_C	Missing FCF Refl Between Thmin & STh/L= 0.600	3	Report

Alert level G

PLAT002_ALERT_2_G	Number of Distance or Angle Restraints on AtSite	4	Note
PLAT003_ALERT_2_G	Number of Uiso or Uij Restrained non-H Atoms ...	8	Report
PLAT007_ALERT_5_G	Number of Unrefined Donor-H Atoms	1	Report
PLAT154_ALERT_1_G	The s.u.'s on the Cell Angles are Equal ..(Note)	0.003	Degree
PLAT172_ALERT_4_G	The CIF-Embedded .res File Contains DFIX Records	1	Report
PLAT186_ALERT_4_G	The CIF-Embedded .res File Contains ISOR Records	2	Report
PLAT301_ALERT_3_G	Main Residue Disorder	(Resd 1)	10% Note
PLAT367_ALERT_2_G	Long? C(sp?)-C(sp?) Bond C4 - C5 .	1.53	Ang.
PLAT367_ALERT_2_G	Long? C(sp?)-C(sp?) Bond C4 - C7 .	1.54	Ang.
PLAT412_ALERT_2_G	Short Intra XH3 .. XHn H13C ..H16C .		2.01 Ang.
		x,y,z =	1_555 Check
PLAT412_ALERT_2_G	Short Intra XH3 .. XHn H14C ..H16C .		1.99 Ang.
		x,y,z =	1_555 Check
PLAT412_ALERT_2_G	Short Intra XH3 .. XHn H14C ..H16B .		1.93 Ang.
		x,y,z =	1_555 Check
PLAT720_ALERT_4_G	Number of Unusual/Non-Standard Labels	3	Note
PLAT793_ALERT_4_G	Model has Chirality at C2 (Centro SPGR)		R Verify
PLAT793_ALERT_4_G	Model has Chirality at C3 (Centro SPGR)		R Verify
PLAT860_ALERT_3_G	Number of Least-Squares Restraints	50	Note
PLAT912_ALERT_4_G	Missing # of FCF Reflections Above STh/L= 0.600		9 Note
PLAT933_ALERT_2_G	Number of OMIT Records in Embedded .res File ...	1	Note
PLAT941_ALERT_3_G	Average HKL Measurement Multiplicity	4.1	Low
PLAT978_ALERT_2_G	Number C-C Bonds with Positive Residual Density.	5	Info

0 **ALERT level A** = Most likely a serious problem - resolve or explain
 0 **ALERT level B** = A potentially serious problem, consider carefully
 5 **ALERT level C** = Check. Ensure it is not caused by an omission or oversight
 20 **ALERT level G** = General information/check it is not something unexpected

1 ALERT type 1 CIF construction/syntax error, inconsistent or missing data
 9 ALERT type 2 Indicator that the structure model may be wrong or deficient
 6 ALERT type 3 Indicator that the structure quality may be low
 8 ALERT type 4 Improvement, methodology, query or suggestion
 1 ALERT type 5 Informative message, check

It is advisable to attempt to resolve as many as possible of the alerts in all categories. Often the minor alerts point to easily fixed oversights, errors and omissions in your CIF or refinement strategy, so attention to these fine details can be worthwhile. In order to resolve some of the more serious problems it may be necessary to carry out additional measurements or structure refinements. However, the purpose of your study may justify the reported deviations and the more serious of these should normally be commented upon in the discussion or experimental section of a paper or in the "special_details" fields of the CIF. checkCIF was carefully designed to identify outliers and unusual parameters, but every test has its limitations and alerts that are not important in a particular case may appear. Conversely, the absence of alerts does not guarantee there are no aspects of the results needing attention. It is up to the individual to critically assess their own results and, if necessary, seek expert advice.

Publication of your CIF in IUCr journals

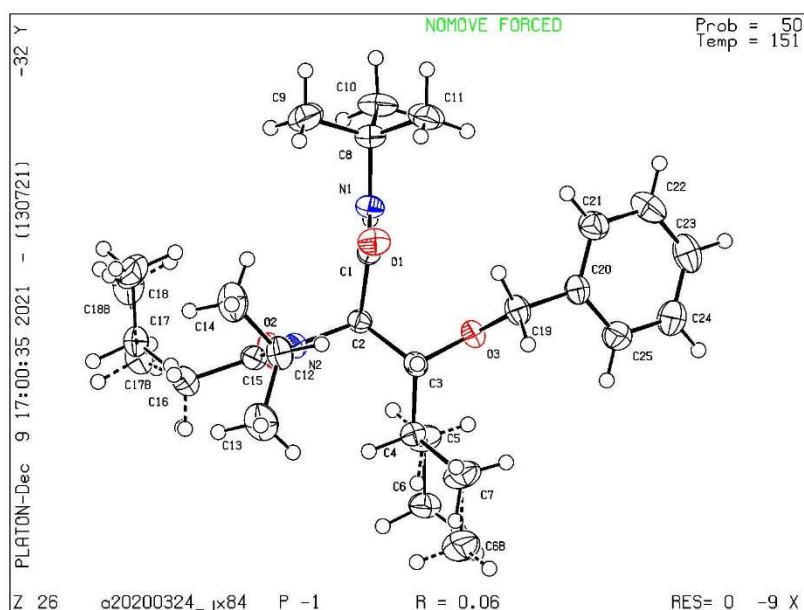
A basic structural check has been run on your CIF. These basic checks will be run on all CIFs submitted for publication in IUCr journals (*Acta Crystallographica*, *Journal of Applied Crystallography*, *Journal of Synchrotron Radiation*); however, if you intend to submit to *Acta Crystallographica Section C* or *E* or *IUCrData*, you should make sure that full publication checks are run on the final version of your CIF prior to submission.

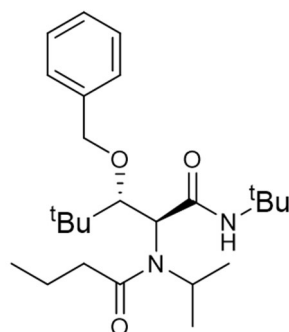
Publication of your CIF in other journals

Please refer to the *Notes for Authors* of the relevant journal for any special instructions relating to CIF submission.

PLATON version of 13/07/2021; check.def file version of 13/07/2021

Datablock a20200324_jx84 - ellipsoid plot





45d-D1


SERVICIO GENERAL RAYOS X
Unidad de Moléculas y Materiales

✉ Servicios Generales de Investigación (SGIker)
 Facultad de Ciencia y Tecnología, Edificio CD3
 UPV/EHU.
 Eº Sarriena, s/n - 48940 Leioa (Bizkaia)



☎ 946013488
 Fax: 946013500
 ✉ leire.sanfelicis@ehu.es

a20200323_JX941
Comentario:

El usuario envió una muestra del compuesto *JX941* (placas incoloras) para determinar su estructura molecular. Se selecciona uno de ellos de tamaño aproximado $0.455 \times 0.287 \times 0.081 \text{ mm}^3$ para realizar la toma de datos.

Se confirma la estructura molecular coincidente con la propuesta por el usuario. La estructura cristalina determinada es quiral (grupo espacial $P2_12_12_1$), con lo que en principio un solo enantiomero está presente en la estructura.

Detalles técnicos:

La toma de datos se ha realizado en el difractómetro Agilent SuperNova Cu, equipado con detector de tipo CCD modelo Atlas, a una temperatura de 150.95(10)K, usando un Cryostream 700 de Agilent Cryosystems alimentado con nitrógeno líquido. Los datos se han procesado (determinación de celda unidad, corrección de absorción analítica empleando las caras indexadas, integración de intensidad de los datos y la corrección de Lorentz y de los efectos de polarización de los mismos), utilizando el paquete de software CrysAlis. La estructura se ha resuelto utilizando SHELXT y se ha refinado empleando la matriz completa de mínimos cuadrados con SHELXL-97(version2017). Los cálculos geométricos finales se llevaron a cabo con el Mercury. y PLATON integrados en el paquete WinGX. Todos los átomos de hidrógeno se han localizado en el mapa de densidad residual y se han refinado con el modelo riding de SHELXL97(version2017).

Texto en inglés: "Intensity data were collected on an Agilent Technologies SuperNova diffractometer, wich was equipped with monochromated Cu $k\alpha$ radiation ($\lambda = 1.54184 \text{ \AA}$) and Eos CCD detector. Measurement was carried out at 150.95(10) K with the help of an Oxford Cryostream 700 PLUS temperature device. Data frames were processed (united cell detemination, analytical absorption correction with face indexing, intensity data integration and correction for Lorentz and polarization effects) using the CrysAlis software package.¹ The structure was solved using SHELXT² and refined by

¹ CrysAlisPro, Agilent Technologies, Version 1.171.37.31 (release 14-01-2014 CrysAlis171 .NET)(compiled Jan 14 2014, 18:38:05).

² Sheldrick, G.M. (2015). Acta Cryst. A71, 3-8..

full-matrix least-squares with SHELXL-97.³ Final geometrical calculations were carried out with Mercury⁴. and PLATON⁵ as integrated in WinGX.⁶

Puesto que se requería la determinación de la configuración absoluta, se ha realizado una toma de datos incluyendo pares de Friedel, consiguiendo una cobertura del 100% de los mismos. El *parámetro de Flack* (x) tiene un valor -0.1(2). El valor de la incertidumbre (0.02) no es lo suficientemente pequeña para distinguir si el espécimen es de un enantiómero ($x = 0$), del opuesto ($x = 1$), o una macla racémica ($x = 0.5$),⁷ algo que era de esperar por la ausencia de átomos pesados. El resultado se confirma con un análisis de los pares de Friedel usando estadística bayesiana⁸ utilizando el programa PLATON⁹. Dados los datos de difracción con una cobertura de los pares de Friedel del 100%, este análisis indica que *la probabilidad de que la configuración absoluta se haya asignado correctamente es esencialmente del 100%*. De hecho, *la probabilidad de que la asignación sea incorrecta es menor de $0.9 \cdot 10^{-9}$* . Y el *parámetro de estructura absoluta* (equivalente a Flack) resulta ser de -0.09(18), confirmando la asignación.¹⁰

En resumen, el cristal contiene un solo enantiómero, cuya configuración absoluta ha sido determinada con una certeza cercana al 100%: la probabilidad de que la asignación sea incorrecta es menor de 10^{-9} .

Texto sugerido en inglés¹¹: "Analysis of the absolute structure using likelihood methods (Hooft, Straver & Spek, 2008) was performed using PLATON (Spek, 2010). The results indicated that the absolute structure had been correctly assigned. The method calculated that the probability that the structure is inverted is smaller than 10^{-9} . The absolute structure parameter γ (Hooft, Straver & Spek, 2008) was calculated using PLATON (Spek, 2010). The resulting value was $\gamma = -0.09(18)$, which together with Flack parameter value, indicate that the absolute structure has probably been determined correctly".

Es importante recordar que siempre que se determina la configuración absoluta mediante difracción de RX sobre monocristal, es imprescindible que se confirme la pureza enantiomérica en la disolución (RMN, HPLC quiral,...), ya que sólo se determina la estructura de un cristal (a lo sumo unos pocos), por lo que no se puede asegurar que todos los cristales contengan el mismo enantiómero debido a la posible resolución espontánea de una disolución racémica.

³ Sheldrick, G. M. (2008). Acta Cryst. A64,112.; Sheldrick, G.M. (2015). Acta Cryst. C71, 3-8.

⁴ Macrae, C. F., J. Appl. Cryst. 2008, 41, 466

⁵ A. L. Spek (2010) PLATON, A Multipurpose Crystallographic Tool, Utrecht University, Utrecht, The Netherlands; A. L. Spek, J. Appl. Cryst. 2003, 36, 7

⁶ Farrugia, L. J., J. Appl. Cryst. 1999, 32, 837

⁷ H. D. Flack & G. Bernardinelli, Acta Cryst. 1999, A55, 908-915; H. D. Flack & G. Bernardinelli, J. Appl. Cryst. 2000, 33, 1143-1148.

⁸ R. W. W. Hooft, L. H. Straver & A. L. Spek, J. Appl. Cryst. 2008, 41, 96-103

⁹ A. L. Spek (2010) PLATON, A Multipurpose Crystallographic Tool, Utrecht University, Utrecht, The Netherlands; A. L. Spek, J. Appl. Cryst. 2003, 36, 7-13.

¹⁰ A. L. Thompson & D. J. Watkin, Tetrahedron: Asymmetry 2009, 20, 712-717

¹¹ <http://www.absolutestructure.com/> (accedido el 27 de abril de 2019)

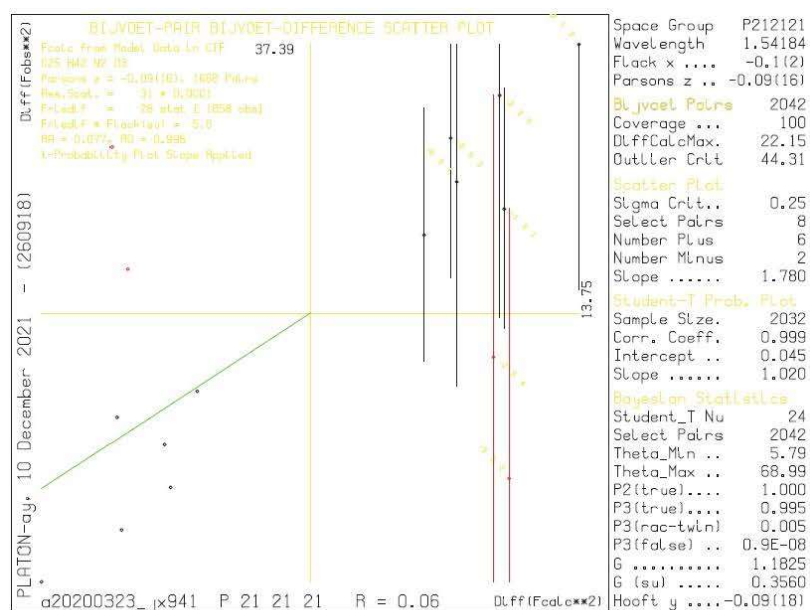


Figura 1. Análisis de la estructura absoluta mediante estadística bayesiana usando el programa Platon.

Table 1 Crystal data and structure refinement for a20200323_JX941.

Identification code	a20200323_JX941
Empirical formula	C ₂₅ H ₄₂ N ₂ O ₃
Formula weight	418.60
Temperature/K	150.95(10)
Crystal system	orthorhombic
Space group	P2 ₁ 2 ₁ 2 ₁
a/Å	11.5072(5)
b/Å	17.4570(5)
c/Å	12.6163(4)
α/°	90.0
β/°	90.0
γ/°	90.0
Volume/Å ³	2534.38(15)
Z	4
ρ _{calc} /cm ³	1.097
μ/mm ⁻¹	0.557
F(000)	920.0
Crystal size/mm ³	0.455 × 0.287 × 0.081
Radiation	CuKα (λ = 1.54184)

2 θ range for data collection/ $^{\circ}$	8.648 to 137.984
Index ranges	-13 \leq h \leq 13, -21 \leq k \leq 21, -15 \leq l \leq 15
Reflections collected	46581
Independent reflections	4708 [R _{int} = 0.1125, R _{sigma} = 0.0477]
Data/restraints/parameters	4708/96/369
Goodness-of-fit on F ²	1.071
Final R indexes [I \geq 2 σ (I)]	R ₁ = 0.0636, wR ₂ = 0.1603
Final R indexes [all data]	R ₁ = 0.0678, wR ₂ = 0.1638
Largest diff. peak/hole / e \AA^{-3}	0.24/-0.21
Flack parameter	-0.1(2)

[a] Esquema de pesado: $1/[\sigma^2(F_o^2) + (0.0339 P)^2 + 0.9563 P]$ donde $P = [\text{Max}(F_o^2, 0) + 2F_c^2]/3$.

[b] Expresión de extinción secundaria tipo SHELXL: $F_c^* = kF_c[1 + 0.001F_c^2\lambda^3/\text{sen}(2\theta)]^{-1/4}$

Table 2 Fractional Atomic Coordinates ($\times 10^4$) and Equivalent Isotropic Displacement Parameters ($\text{\AA}^2 \times 10^3$) for a20200323_JX941. U_{eq} is defined as 1/3 of the trace of the orthogonalised U_{ij} tensor.

Atom	x	y	z	U(eq)
O1	5319 (3)	3627.4 (16)	4802 (2)	40.9 (7)
O2	7970 (2)	3587.9 (16)	7421 (2)	40.1 (7)
O3	4441 (2)	3689.5 (14)	7141 (2)	33.1 (6)
N1	6811 (3)	4207.9 (19)	5649 (3)	39.8 (8)
N2	7155 (3)	2623.9 (17)	6468 (3)	33.4 (7)
C0BA	1144 (8)	4825 (5)	7241 (9)	56 (3)
C00O	3128 (10)	5317 (7)	6250 (8)	40 (3)
C00P	2067 (9)	5636 (8)	5994 (9)	54 (3)
C00Q	7840 (20)	2382 (15)	4620 (20)	45 (5)
C00S	6382 (15)	1497 (12)	5400 (20)	50 (6)
C1	6009 (3)	3659 (2)	5533 (3)	31.5 (8)
C2	6021 (3)	3022.6 (19)	6393 (3)	30.3 (8)
C3	5493 (3)	3310 (2)	7452 (3)	32.4 (8)
C4	5169 (4)	2692 (3)	8291 (3)	41.7 (10)
C4AA	7620 (40)	4460 (30)	3890 (20)	58 (9)
C5	4513 (5)	3099 (3)	9180 (4)	55.7 (12)
C5AA	7840 (40)	5385 (16)	5530 (30)	63 (7)
C6	4362 (5)	2077 (3)	7812 (4)	56.0 (12)
C6AA	5980 (30)	5290 (30)	4630 (40)	59 (11)
C7	6252 (5)	2312 (3)	8771 (4)	59.6 (14)
C8	7083 (4)	4823 (2)	4880 (4)	48.5 (11)
C9	6068 (13)	5381 (10)	4831 (19)	50 (4)
C9AA	2224 (7)	4517 (6)	7508 (9)	46 (3)
C10	8213 (16)	5206 (11)	5255 (15)	64 (4)
C11	7280 (20)	4500 (10)	3766 (10)	56 (4)
C12	8046 (4)	2942 (2)	7019 (3)	34.9 (8)
C13	9147 (4)	2474 (3)	7178 (3)	43.2 (10)
C14	10015 (4)	2858 (3)	7883 (4)	53.5 (12)
C15	11065 (4)	2351 (3)	8104 (4)	57.0 (13)

C16	7375 (4)	1987 (3)	5712 (4)	45.7 (11)
C17	6486 (18)	1332 (8)	5940 (20)	77 (6)
C18	7420 (20)	2205 (11)	4636 (16)	64 (5)
C19	4411 (4)	4492 (2)	7375 (4)	44.5 (10)
C20	3239 (4)	4797 (2)	7089 (4)	43.0 (10)
C21	2986 (13)	5014 (9)	6093 (9)	58 (4)
C22	1935 (11)	5343 (9)	5837 (11)	68 (5)
C23	1104 (5)	5422 (3)	6566 (5)	67.6 (15)
C24	1352 (11)	5264 (9)	7660 (9)	83 (4)
C25	2436 (10)	4944 (8)	7942 (9)	64 (4)

Table 3 Anisotropic Displacement Parameters ($\text{\AA}^2 \times 10^3$) for a20200323_JX941. The Anisotropic displacement factor exponent takes the form: - $2\pi^2 [h^2 a^2 U_{11} + 2hka \cdot b \cdot U_{12} + \dots]$.

Atom	U ₁₁	U ₂₂	U ₃₃	U ₂₃	U ₁₃	U ₁₂
O1	49.0 (17)	39.2 (14)	34.7 (14)	2.9 (12)	-8.2 (13)	-6.4 (13)
O2	37.9 (15)	36.2 (14)	46.1 (15)	-8.7 (12)	-8.2 (12)	2.3 (12)
O3	33.5 (14)	28.1 (12)	37.6 (13)	-3.7 (11)	-6.8 (11)	4.7 (11)
N1	48 (2)	32.9 (16)	38.5 (17)	4.3 (14)	-4.9 (16)	-7.3 (15)
N2	33.9 (18)	29.0 (14)	37.3 (16)	-4.0 (13)	-3.5 (14)	3.9 (13)
C0BA	35 (5)	45 (5)	87 (8)	-9 (5)	7 (5)	-8 (4)
C00O	43 (6)	51 (7)	27 (5)	-14 (5)	-3 (4)	4 (5)
C00P	59 (8)	50 (7)	53 (6)	-6 (5)	-19 (5)	15 (6)
C00Q	47 (10)	49 (11)	38 (7)	-13 (7)	1 (7)	16 (7)
C00S	52 (8)	44 (8)	55 (11)	-29 (7)	-11 (7)	10 (6)
C1	36 (2)	29.0 (17)	30.0 (17)	-3.3 (14)	-1.0 (15)	2.1 (15)
C2	34 (2)	23.2 (15)	33.8 (18)	-1.7 (14)	-4.3 (16)	1.2 (14)
C3	30.2 (19)	32.5 (17)	34.3 (18)	-1.7 (15)	-5.5 (16)	1.9 (15)
C4	38 (2)	47 (2)	40 (2)	12.4 (18)	-0.6 (18)	3.5 (18)
C4AA	59 (14)	63 (13)	51 (11)	10 (9)	13 (9)	1 (10)
C5	52 (3)	77 (3)	38 (2)	10 (2)	7 (2)	5 (3)
C5AA	52 (12)	54 (10)	83 (12)	17 (8)	6 (9)	-13 (9)
C6	55 (3)	45 (2)	68 (3)	17 (2)	1 (3)	-8 (2)
C6AA	79 (14)	52 (15)	47 (14)	14 (10)	-2 (9)	3 (10)
C7	54 (3)	74 (3)	51 (3)	32 (3)	3 (2)	14 (3)
C8	54 (3)	40 (2)	52 (2)	8 (2)	-1 (2)	-12 (2)
C9	74 (7)	28 (4)	49 (7)	6 (4)	5 (5)	-4 (4)
C9AA	46 (6)	32 (5)	60 (6)	1 (5)	1 (5)	-4 (4)
C10	56 (6)	58 (6)	78 (7)	15 (5)	4 (5)	-27 (5)
C11	64 (8)	50 (5)	55 (5)	17 (4)	16 (5)	6 (6)
C12	34 (2)	38.8 (19)	31.8 (17)	-3.1 (16)	-1.1 (16)	3.4 (16)
C13	37 (2)	52 (2)	41 (2)	-2.7 (18)	-1.6 (18)	11.2 (18)
C14	41 (3)	65 (3)	54 (3)	-7 (2)	-7 (2)	11 (2)
C15	42 (3)	84 (4)	45 (2)	0 (2)	0 (2)	16 (3)

C16	49(3)	37(2)	51(2)	-14.2(19)	-4(2)	15.8(19)
C17	107(10)	39(5)	84(11)	-26(7)	31(9)	-13(6)
C18	91(13)	52(7)	51(6)	-14(5)	12(9)	9(8)
C19	45(2)	30.7(18)	58(3)	-12.0(18)	-2(2)	3.8(17)
C20	42(2)	26.8(17)	60(3)	-5.2(19)	0(2)	4.2(17)
C21	66(8)	58(8)	51(7)	-25(6)	-17(5)	7(7)
C22	68(5)	66(6)	70(5)	-2(4)	-10(4)	7(4)
C23	54(3)	56(2)	93(3)	-5(2)	-10(3)	7(2)
C24	77(5)	81(5)	91(5)	-3(4)	13(4)	5(4)
C25	61(7)	65(8)	66(7)	18(6)	11(6)	13(6)

Table 4 Bond Lengths for a20200323_JX941.

Atom	Atom	Length/Å	Atom	Atom	Length/Å
O1	C1	1.219(5)	C4	C7	1.536(6)
O2	C12	1.239(5)	C4AAC8		1.533(13)
O3	C3	1.435(5)	C5AAC8		1.551(13)
O3	C19	1.431(4)	C6AAC8		1.539(13)
N1	C1	1.338(5)	C8	C9	1.522(9)
N1	C8	1.481(5)	C8	C10	1.535(9)
N2	C2	1.482(5)	C8	C11	1.532(9)
N2	C12	1.357(5)	C9AAC20		1.373(8)
N2	C16	1.487(5)	C12	C13	1.521(6)
C0BAC9AA		1.395(10)	C13	C14	1.496(7)
C0BAC23		1.346(9)	C14	C15	1.524(6)
C00O C00P		1.381(10)	C16	C17	1.560(14)
C00O C20		1.400(10)	C16	C18	1.41(2)
C00P C23		1.375(11)	C19	C20	1.495(6)
C00Q C16		1.63(3)	C20	C21	1.344(10)
C00S C16		1.481(18)	C20	C25	1.441(9)
C1	C2	1.553(5)	C21	C22	1.377(11)
C2	C3	1.551(5)	C22	C23	1.335(11)
C3	C4	1.557(5)	C23	C24	1.436(11)
C4	C5	1.526(7)	C24	C25	1.412(11)
C4	C6	1.544(7)			

Table 5 Bond Angles for a20200323_JX941.

Atom	Atom	Atom	Angle/°	Atom	Atom	Atom	Angle/°
C19	O3	C3	114.5(3)	C4AAC8	C6AA		112(2)
C1	N1	C8	126.4(4)	C6AAC8	C5AA		104(2)
C2	N2	C16	117.4(3)	C9	C8	C10	112.6(10)
C12	N2	C2	120.4(3)	C9	C8	C11	108.3(10)
C12	N2	C16	120.4(3)	C11	C8	C10	108.4(9)

C23	C0BAC9AA	118.8(8)	C20	C9AAC0BA	121.9(8)
C00P	C00O C20	121.3(10)	O2	C12 N2	121.9(4)
C23	C00P C00O	118.7(10)	O2	C12 C13	119.6(4)
O1	C1 N1	124.4(4)	N2	C12 C13	118.4(3)
O1	C1 C2	120.1(3)	C14	C13 C12	113.1(4)
N1	C1 C2	115.5(3)	C13	C14 C15	112.2(4)
N2	C2 C1	112.9(3)	N2	C16 C00Q	106.3(10)
N2	C2 C3	116.2(3)	N2	C16 C17	108.6(6)
C3	C2 C1	111.5(3)	C00S	C16 N2	118.2(8)
O3	C3 C2	104.2(3)	C00S	C16 C00Q	105.8(11)
O3	C3 C4	107.7(3)	C18	C16 N2	114.9(8)
C2	C3 C4	117.1(3)	C18	C16 C17	113.5(9)
C5	C4 C3	107.2(4)	O3	C19 C20	108.7(3)
C5	C4 C6	108.3(4)	C00O	C20 C19	119.8(6)
C5	C4 C7	108.2(4)	C9AAC20	C00O	116.4(7)
C6	C4 C3	111.1(4)	C9AAC20	C19	123.2(5)
C7	C4 C3	111.9(4)	C21	C20 C19	121.5(7)
C7	C4 C6	110.0(4)	C21	C20 C25	120.5(8)
N1	C8 C4AA	108.3(19)	C25	C20 C19	117.5(6)
N1	C8 C5AA	103.3(11)	C20	C21 C22	121.9(13)
N1	C8 C6AA	110(2)	C23	C22 C21	120.7(13)
N1	C8 C9	109.2(8)	C0BA	C23 C00P	121.0(8)
N1	C8 C10	107.0(5)	C22	C23 C24	120.0(9)
N1	C8 C11	111.5(8)	C25	C24 C23	119.6(10)
C4AAC8	C5AA	118(2)	C24	C25 C20	116.7(9)

Table 6 Torsion Angles for a20200323_JX941.

A	B	C	D	Angle/°	A	B	C	D	Angle/°
O1	C1	C2	N2	120.6(4)	C2	N2	C16	C17	-64.0(13)
O1	C1	C2	C3	-106.4(4)	C2	N2	C16	C18	64.3(14)
O2	C12	C13	C14	3.2(6)	C2	C3	C4	C5	-171.9(4)
O3	C3	C4	C5	-55.0(4)	C2	C3	C4	C6	-53.8(5)
O3	C3	C4	C6	63.1(4)	C2	C3	C4	C7	69.6(5)
O3	C3	C4	C7	-173.6(4)	C3	O3	C19	C20	-175.6(3)
O3	C19	C20	C00O	-113.0(8)	C8	N1	C1	O1	-6.1(7)
O3	C19	C20	C9AA	57.6(8)	C8	N1	C1	C2	172.0(4)
O3	C19	C20	C21	-84.4(9)	C9AAC0BA	C23	C00P		12.1(15)
O3	C19	C20	C25	103.4(8)	C12	N2	C2	C1	80.9(4)
N1	C1	C2	N2	-57.6(4)	C12	N2	C2	C3	-49.7(5)
N1	C1	C2	C3	75.3(4)	C12	N2	C16	C00Q	-80.9(10)
N2	C2	C3	O3	178.0(3)	C12	N2	C16	C00S	160.5(13)
N2	C2	C3	C4	-63.3(4)	C12	N2	C16	C17	131.3(13)
N2	C12	C13	C14	-174.5(4)	C12	N2	C16	C18	-100.3(14)

C0BAC9AAC20C00O	-10.4(14)	C12	C13	C14	C15	175.3(4)
C0BAC9AAC20C19	178.7(8)	C16	N2	C2	C1	-83.7(4)
C00O C00P C23C0BA	-10.9(17)	C16	N2	C2	C3	145.7(4)
C00P C00O C20C9AA	11.6(15)	C16	N2	C12	O2	159.9(4)
C00P C00O C20C19	-177.2(9)	C16	N2	C12	C13	-22.5(6)
C1 N1 C8 C4AA	-67(2)	C19	O3	C3	C2	-117.1(4)
C1 N1 C8 C5AA	167(2)	C19	O3	C3	C4	117.9(4)
C1 N1 C8 C6AA	56(2)	C19	C20	C21	C22	-175.6(11)
C1 N1 C8 C9	69.1(11)	C19	C20	C25	C24	177.3(10)
C1 N1 C8 C10	-168.8(12)	C20	C00O	C00P	C23	-1.4(18)
C1 N1 C8 C11	-50.5(12)	C20	C21	C22	C23	-3(2)
C1 C2 C3 O3	46.8(4)	C21	C20	C25	C24	5.0(16)
C1 C2 C3 C4	165.5(3)	C21	C22	C23	C24	8.8(19)
C2 N2 C12O2	-4.3(6)	C22	C23	C24	C25	-7.1(18)
C2 N2 C12C13	173.3(3)	C23	C0BAC9AAC20			-1.1(16)
C2 N2 C16C00Q	83.8(10)	C23	C24	C25	C20	0.2(19)
C2 N2 C16C00S	-34.9(14)	C25	C20	C21	C22	-3.7(18)

Table 7 Hydrogen Atom Coordinates ($\text{\AA}\times 10^4$) and Isotropic Displacement Parameters ($\text{\AA}^2\times 10^3$) for a20200323_JX941.

Atom	x	y	z	U(eq)
H1	7217.48	4202.4	6239.94	48
H0BA	450.1	4617.45	7530.49	67
H00O	3795.76	5453.51	5849.6	48
H00P	2003.15	5997.15	5433.41	65
H00A	7227.25	2706.52	4323.58	67
H00B	8045.64	1981.43	4110.93	67
H00C	8526.23	2694.7	4776.37	67
H00D	5976.3	1317.64	6036.03	75
H00E	6667.85	1055.01	4997.23	75
H00F	5844.31	1793.19	4958.29	75
H2	5465.25	2625.47	6130.21	36
H3	6032.22	3692.05	7779.75	39
H4AA	8379.62	4240.99	4066.31	87
H4AB	7705.6	4844.27	3335.38	87
H4AC	7105.94	4045.88	3634.42	87
H5A	4992.85	3514.37	9463.37	84
H5B	4337.65	2731.91	9745.66	84
H5C	3785.98	3310.27	8899.85	84
H5AA	7424.57	5539.05	6173.6	95
H5AB	8017.97	5838.67	5103.94	95
H5AC	8572.02	5130.96	5732.2	95
H6A	3703.37	2326.67	7460.65	84
H6B	4074.63	1741.82	8376.87	84

H6C	4795.6	1772.28	7292.98	84
H6AA	5336.52	4932.22	4478.21	89
H6AB	6118.63	5607.87	4002.72	89
H6AC	5778.62	5609.08	5232.69	89
H7A	6622.3	1985.85	8237.39	89
H7B	6023.62	1999.81	9382.14	89
H7C	6799.8	2708.72	9000.51	89
H9A	5377.53	5115.12	4564.76	75
H9B	6262.93	5805.66	4355.25	75
H9C	5910.78	5581.49	5542.52	75
H9AA	2256.89	4101.87	7994.04	55
H10A	8117.28	5384.08	5986.21	96
H10B	8390.7	5642.75	4795.11	96
H10C	8850.41	4834.51	5222.27	96
H11A	7966.35	4164.72	3771.89	85
H11B	7412.65	4922.84	3268.34	85
H11C	6599.61	4206.37	3544.53	85
H13A	8937.64	1971.69	7488.65	52
H13B	9509.99	2377.65	6479.16	52
H14A	9636.56	2993.1	8562.96	64
H14B	10278.64	3339.3	7544.5	64
H15A	11431.37	2205.87	7432.2	86
H15B	10814.13	1888.87	8480.85	86
H15C	11625.13	2632.32	8541.07	86
H16	8003.97	1653.19	6005.56	55
H16A	8159.32	1776.95	5891.22	55
H17A	6433.85	1245.4	6704.43	115
H17B	6745.22	860.54	5588.74	115
H17C	5720.87	1478.2	5664.07	115
H18A	7740.16	1783.34	4214.44	97
H18B	7918.56	2657.39	4560.61	97
H18C	6635.77	2326.48	4386.28	97
H19A	5019.13	4761.54	6964.49	53
H19B	4562.57	4575.43	8138.89	53
H21	3547	4938.52	5551.48	70
H22	1800.91	5515.79	5133.23	82
H23A	398.57	5698.69	6483.92	81
H23	347.21	5582.3	6361.7	81
H24	790.66	5373.62	8190.76	100
H25	2626.84	4831.39	8657.57	77

Table 8 Atomic Occupancy for a20200323_JX941.

Atom	Occupancy	Atom	Occupancy	Atom	Occupancy
------	-----------	------	-----------	------	-----------

C0BA	0.484 (13)	H0BA	0.484 (13)	C00O	0.484 (13)
H00O	0.484 (13)	C00P	0.484 (13)	H00P	0.484 (13)
C00Q	0.40 (4)	H00A	0.40 (4)	H00B	0.40 (4)
H00C	0.40 (4)	C00S	0.40 (4)	H00D	0.40 (4)
H00E	0.40 (4)	H00F	0.40 (4)	C4AA	0.32 (5)
H4AA	0.32 (5)	H4AB	0.32 (5)	H4AC	0.32 (5)
C5AA	0.32 (5)	H5AA	0.32 (5)	H5AB	0.32 (5)
H5AC	0.32 (5)	C6AA	0.32 (5)	H6AA	0.32 (5)
H6AB	0.32 (5)	H6AC	0.32 (5)	C9	0.68 (5)
H9A	0.68 (5)	H9B	0.68 (5)	H9C	0.68 (5)
C9AA	0.484 (13)	H9AA	0.484 (13)	C10	0.68 (5)
H10A	0.68 (5)	H10B	0.68 (5)	H10C	0.68 (5)
C11	0.68 (5)	H11A	0.68 (5)	H11B	0.68 (5)
H11C	0.68 (5)	H16	0.40 (4)	H16A	0.60 (4)
C17	0.60 (4)	H17A	0.60 (4)	H17B	0.60 (4)
H17C	0.60 (4)	C18	0.60 (4)	H18A	0.60 (4)
H18B	0.60 (4)	H18C	0.60 (4)	C21	0.516 (13)
H21	0.516 (13)	C22	0.516 (13)	H22	0.516 (13)
H23A	0.484 (13)	H23	0.516 (13)	C24	0.516 (13)
H24	0.516 (13)	C25	0.516 (13)	H25	0.516 (13)

Experimental

Single crystals of $C_{25}H_{42}N_2O_3$ [**a20200323_JX941**]. A suitable crystal was selected and **mounted** on a **SuperNova, Single source at offset/far, Atlas** diffractometer. The crystal was kept at 150.95(10) K during data collection. Using Olex2 [1], the structure was solved with the ShelXT [2] structure solution program using Intrinsic Phasing and refined with the ShelXL [3] refinement package using Least Squares minimisation.

1. Dolomanov, O.V., Bourhis, L.J., Gildea, R.J., Howard, J.A.K. & Puschmann, H. (2009), *J. Appl. Cryst.* 42, 339-341.
2. Sheldrick, G.M. (2015). *Acta Cryst.* A71, 3-8.
3. Sheldrick, G.M. (2015). *Acta Cryst.* C71, 3-8.

Crystal structure determination of [a20200323_JX941]

Crystal Data for $C_{25}H_{42}N_2O_3$ ($M=418.60$ g/mol): orthorhombic, space group $P2_12_12_1$ (no. 19), $a = 11.5072(5)$ Å, $b = 17.4570(5)$ Å, $c = 12.6163(4)$ Å, $V = 2534.38(15)$ Å³, $Z = 4$, $T = 150.95(10)$ K, $\mu(\text{CuK}\alpha) = 0.557$ mm⁻¹, $D_{\text{calc}} = 1.097$ g/cm³, 46581 reflections measured ($8.648^\circ \leq 2\theta \leq 137.984^\circ$), 4708 unique ($R_{\text{int}} = 0.1125$, $R_{\text{sigma}} = 0.0477$) which were used in all calculations. The final R_1 was 0.0636 ($I > 2\sigma(I)$) and wR_2 was 0.1638 (all data).

Refinement model description

Number of restraints - 96, number of constraints - unknown.

Details:

1. Fixed Uiso

At 1.2 times of:

All C(H) groups, All C(H,H) groups, All N(H) groups

At 1.5 times of:

All C(H,H,H) groups

2. Restrained distances

$C5AA-C8 = C10-C8 = C4AA-C8 = C11-C8 = C9-C8 = C6AA-C8$

1.54 with sigma of 0.01

$C00O-C20 = C22-C21 = C00P-C00O$

1.39 with sigma of 0.01

$C22-C23 = C00P-C23 = C24-C23 = C0BA-C9AA = C24-C25 = C25-C20 = C9AA-C20$

1.39 with sigma of 0.01

C21-C20 = C0BA-C23
 1.38 with sigma of 0.01
 3. Uiso/Uanis restraints and constraints
 Uanis(C18) * Ueq, Uanis(C00Q) * Ueq, Uanis(C00S) * Ueq, Uanis(C17)
 * Ueq: with sigma of 0.01 and sigma for terminal atoms of 0.02
 Uanis(C10) * Ueq, Uanis(C5AA) * Ueq, Uanis(C9) * Ueq, Uanis(C6AA)
 * Ueq, Uanis(C4AA) * Ueq, Uanis(C11) * Ueq: with sigma of 0.005 and
 sigma for terminal atoms of 0.01
 Uanis(C22) * Ueq, Uanis(C23) * Ueq, Uanis(C24) * Ueq: with sigma of
 0.003 and sigma for terminal atoms of 0.006
 4. Others
 Sof(C0BA)=Sof(H0BA)=Sof(C00O)=Sof(H00O)=Sof(C00P)=Sof(H00P)=Sof(C9AA)=
 Sof(H9AA)=Sof(H23A)=1-FVAR(1)
 Sof(C21)=Sof(H21)=Sof(C22)=Sof(H22)=Sof(H23)=Sof(C24)=Sof(H24)=Sof(C25)=
 Sof(H25)=FVAR(1)

 Sof(H16A)=Sof(C17)=Sof(H17A)=Sof(H17B)=Sof(H17C)=Sof(C18)=Sof(H18A)=Sof(H18B)=
 Sof(H18C)=1-FVAR(2)
 Sof(C00Q)=Sof(H00A)=Sof(H00B)=Sof(H00C)=Sof(C00S)=Sof(H00D)=Sof(H00E)=
 Sof(H00F)=Sof(H16)=FVAR(2)
 Sof(C9)=Sof(H9A)=Sof(H9B)=Sof(H9C)=Sof(C10)=Sof(H10A)=Sof(H10B)=Sof(H10C)=
 Sof(C11)=Sof(H11A)=Sof(H11B)=Sof(H11C)=1-FVAR(3)
 Sof(C4AA)=Sof(H4AA)=Sof(H4AB)=Sof(H4AC)=Sof(C5AA)=Sof(H5AA)=Sof(H5AB)=
 Sof(H5AC)=Sof(C6AA)=Sof(H6AA)=Sof(H6AB)=Sof(H6AC)=FVAR(3)
 5.a Ternary CH refined with riding coordinates:
 C2(H2), C3(H3), C16(H16), C16(H16A)
 5.b Secondary CH2 refined with riding coordinates:
 C13(H13A,H13B), C14(H14A,H14B), C19(H19A,H19B)
 5.c Aromatic/amide H refined with riding coordinates:
 N1(H1), C0BA(H0BA), C00O(H00O), C00P(H00P), C9AA(H9AA), C21(H21), C22(H22),
 C23(H23A), C23(H23), C24(H24), C25(H25)
 5.d Idealised Me refined as rotating group:
 C00Q(H00A,H00B,H00C), C00S(H00D,H00E,H00F), C4AA(H4AA,H4AB,H4AC), C5(H5A,H5B,
 H5C), C5AA(H5AA,H5AB,H5AC), C6(H6A,H6B,H6C), C6AA(H6AA,H6AB,H6AC),
 C7(H7A,H7B,
 H7C), C9(H9A,H9B,H9C), C10(H10A,H10B,H10C), C11(H11A,H11B,H11C),
 C15(H15A,H15B,
 H15C), C17(H17A,H17B,H17C), C18(H18A,H18B,H18C)

This report has been created with Olex2, compiled on 2018.05.29 svn.r3508 for OlexSys. Please [let us know](#) if there are any errors or if you
 would like to have additional features

checkCIF/PLATON report

Structure factors have been supplied for datablock(s) a20200323_jx941

THIS REPORT IS FOR GUIDANCE ONLY. IF USED AS PART OF A REVIEW PROCEDURE FOR PUBLICATION, IT SHOULD NOT REPLACE THE EXPERTISE OF AN EXPERIENCED CRYSTALLOGRAPHIC REFEREE.

No syntax errors found. CIF dictionary Interpreting this report

Datablock: a20200323_jx941

Bond precision: C-C = 0.0063 Å Wavelength=1.54184

Cell: a=11.5072(5) b=17.4570(5) c=12.6163(4)
 alpha=90 beta=90 gamma=90
 Temperature: 151 K

	Calculated	Reported
Volume	2534.38(15)	2534.38(15)
Space group	P 21 21 21	P 21 21 21
Hall group	P 2ac 2ab	P 2ac 2ab
Moiety formula	C25 H42 N2 O3	C25 H42 N2 O3
Sum formula	C25 H42 N2 O3	C25 H42 N2 O3
Mr	418.61	418.60
Dx, g cm ⁻³	1.097	1.097
Z	4	4
Mu (mm ⁻¹)	0.558	0.557
F000	920.0	920.0
F000'	922.51	
h, k, lmax	13, 21, 15	13, 21, 15
Nref	4707[2666]	4708
Tmin, Tmax	0.825, 0.956	0.833, 0.964
Tmin'	0.776	

Correction method= # Reported T Limits: Tmin=0.833 Tmax=0.964
 AbsCorr = ANALYTICAL

Data completeness= 1.77/1.00 Theta(max)= 68.992

R(reflections)= 0.0636(4371) wR2(reflections)=
 0.1638(4708)
 S = 1.071 Npar= 369

The following ALERTS were generated. Each ALERT has the format
test-name_ALERT_alert-type_alert-level.
Click on the hyperlinks for more details of the test.

Alert level C

PLAT089_ALERT_3_C	Poor Data / Parameter Ratio (Zmax < 18)	7.22	Note
PLAT234_ALERT_4_C	Large Hirshfeld Difference C24 --C25 .	0.16	Ang.
PLAT340_ALERT_3_C	Low Bond Precision on C-C Bonds	0.0063	Ang.
PLAT906_ALERT_3_C	Large K Value in the Analysis of Variance	2.396	Check

Alert level G

PLAT002_ALERT_2_G	Number of Distance or Angle Restraints on AtSite	17	Note
PLAT003_ALERT_2_G	Number of Uiso or Uij Restrained non-H Atoms ...	13	Report
PLAT007_ALERT_5_G	Number of Unrefined Donor-H Atoms	1	Report
PLAT172_ALERT_4_G	The CIF-Embedded .res File Contains DFIX Records	4	Report
PLAT186_ALERT_4_G	The CIF-Embedded .res File Contains ISOR Records	3	Report
PLAT301_ALERT_3_G	Main Residue Disorder(Resd 1)	30%	Note
PLAT410_ALERT_2_G	Short Intra H...H Contact H13B ..H16A .	2.02	Ang.
	x,y,z =	1_555	Check
PLAT412_ALERT_2_G	Short Intra XH3 .. XHn H2 ..H17C .	2.11	Ang.
	x,y,z =	1_555	Check
PLAT412_ALERT_2_G	Short Intra XH3 .. XHn H2 ..H00F .	2.12	Ang.
	x,y,z =	1_555	Check
PLAT720_ALERT_4_G	Number of Unusual/Non-Standard Labels	28	Note
PLAT791_ALERT_4_G	Model has Chirality at C2 (Sohnke SpGr)	S	Verify
PLAT791_ALERT_4_G	Model has Chirality at C3 (Sohnke SpGr)	S	Verify
PLAT811_ALERT_5_G	No ADDSYM Analysis: Too Many Excluded Atoms ...	!	Info
PLAT860_ALERT_3_G	Number of Least-Squares Restraints	96	Note
PLAT933_ALERT_2_G	Number of OMIT Records in Embedded .res File ...	1	Note
PLAT978_ALERT_2_G	Number C-C Bonds with Positive Residual Density.	2	Info

0 **ALERT level A** = Most likely a serious problem - resolve or explain
0 **ALERT level B** = A potentially serious problem, consider carefully
4 **ALERT level C** = Check. Ensure it is not caused by an omission or oversight
16 **ALERT level G** = General information/check it is not something unexpected

0 ALERT type 1 CIF construction/syntax error, inconsistent or missing data
7 ALERT type 2 Indicator that the structure model may be wrong or deficient
5 ALERT type 3 Indicator that the structure quality may be low
6 ALERT type 4 Improvement, methodology, query or suggestion
2 ALERT type 5 Informative message, check

It is advisable to attempt to resolve as many as possible of the alerts in all categories. Often the minor alerts point to easily fixed oversights, errors and omissions in your CIF or refinement strategy, so attention to these fine details can be worthwhile. In order to resolve some of the more serious problems it may be necessary to carry out additional measurements or structure refinements. However, the purpose of your study may justify the reported deviations and the more serious of these should normally be commented upon in the discussion or experimental section of a paper or in the "special_details" fields of the CIF. checkCIF was carefully designed to identify outliers and unusual parameters, but every test has its limitations and alerts that are not important in a particular case may appear. Conversely, the absence of alerts does not guarantee there are no aspects of the results needing attention. It is up to the individual to critically assess their own results and, if necessary, seek expert advice.

Publication of your CIF in IUCr journals

A basic structural check has been run on your CIF. These basic checks will be run on all CIFs submitted for publication in IUCr journals (*Acta Crystallographica*, *Journal of Applied Crystallography*, *Journal of Synchrotron Radiation*); however, if you intend to submit to *Acta Crystallographica Section C* or *E* or *IUCrData*, you should make sure that full publication checks are run on the final version of your CIF prior to submission.

Publication of your CIF in other journals

Please refer to the *Notes for Authors* of the relevant journal for any special instructions relating to CIF submission.

PLATON version of 13/07/2021; check.def file version of 13/07/2021

Datablock a20200323_jx941 - cllipsoid plot

